STUDIES ON TRANSITION METAL

MACROCYCLIC COMPLEXES

Gillian Reid

Ph.D Thesis

University of Edinburgh

1989

To my family

Declaration

Except where specific reference is made to other sources, the work presented in this thesis is the original work of the author. It has not been submitted, in whole or in part, for any other degree. Certain of the results have already been published.

Gillian Reid

Acknowledgements

The author wishes to thank Dr. Martin Schröder for his advice, encouragement and exceptional enthusiasm throughout the course of this work. I am also very grateful to Dr. A.J. Blake for his help and invaluable advice in the crystallographic determinations. My thanks also to Dr. R.O.Gould for his assistance with the disorder model in the structure solution for $[Cu(Me_2[18]aneN_2S_4)](PF_6)_2$.

I also wish to thank Drs. L.J. Yellowlees, A.J. Holder and T.I. Hyde for their invaluable contributions to this study.

In addition I am indebted to Dr. D. Reed, Mr. J.R.A. Millar and Miss H. Grant for recording ^{13}C and ^{1}H n.m.r. spectra, to Mrs E. MacDougall for performing microanalytical measurements and to Mr. A.T. Taylor and Miss E. Bell for recording all mass spectral data.

I would also like to thank Dr. S.G.D. Henderson and Mr. E.P. Morton for their advice and assistance during the production of this thesis, and everybody else who contributed to this project. Finally, I am very grateful to the S.E.R.C. for funding this work and to the University of Edinburgh for the use of their facilities.

Abstract

Chapter 1

An introduction to macrocyclic chemistry is given. The relevance of transition metal macrocycles and porphyrins to biological systems and substrate binding and activation is described. The general aims of the project are introduced.

Chapter 2

The synthesis, characterisation and electrochemistry of the mixed N- and S-donor macrocyclic complexes, $[M([18]aneN_2S_4)]^{2+}$, (M= Cu, Ni, Fe), and $[M'(Me_2[18]aneN_2S_4)]^{2+}$, (M'= Cu, Ni), are described. Single crystal X-ray structures of $[Ni([18]aneN_2S_4)]^{2+}$ and $[Fe([18]aneN_2S_4)]^{2+}$ each reveal octahedral stereochemistry at the metal ion with co-ordination to all six donor atoms in a rac-configuration (Ni-S= 2.40-2.43, Ni-N= 2.07-2.13, Fe-S= 2.26-2.27, Fe-N= 2.02-2.04Å). The single crystal structure of $[Cu(Me_2[18]aneN_2S_4)]^{2+}$ shows a tetragonally elongated octahedral stereochemistry for Cu(II) in a meso-configuration (Cu-S= 2.50, Cu-N= 2.20Å). This contrasts the X-ray structure of $[Cu([18]aneN_2S_4)]^{2+}$ which shows a tetragonally compressed stereochemistry in a rac-configuration. This structural difference is reflected in the redox propertiess of the Cu(II) complexes. $[Cu(Me_2[18]aneN_2S_4)]^{2+}$ exhibits a reversible Cu(II)/(I) couple at $E_{1/2}$ = +0.06V *vs.* Fc/Fc^+, while

$[Cu([18]aneN_2S_4)]^{2+}$ shows a reversible Cu(II)/(I) couple at a more negative potential ($E_{1/2}$= -0.31V *vs.* Fc/Fc^+). The single crystal structure of the binuclear cation, $[Cu_2(Me_2[18]aneN_2S_4)(NCMe)_2]^{2+}$ shows tetrahedral co-ordination of each Cu(I) centre to one N- and two S-donors of the macrocycle, (Cu-S= 2.29-2.32, Cu-N= 2.17Å), and one NCMe solvent molecule (Cu-N= 1.92Å).

Electrochemical studies on $[Ni([18]aneN_2S_4)]^{2+}$ show a reversible Ni(II)/(III) couple ($E_{1/2}$= +0.98V *vs.* Fc/Fc^+), and Ni(II)/(I) couple ($E_{1/2}$= -1.51V *vs.* Fc/Fc^+). A red e.s.r.-active solution containing the Ni(III) cation, $[Ni([18]aneN_2S_4)]^{3+}$, can be obtained by controlled potential electrolysis (+1.15V), (g_1= 2.129, g_2= 2.104, g_3= 2.027) or chemical oxidation (60% $HClO_4$). $[Ni(Me_2[18]aneN_2S_4)]^{2+}$ exhibits a reversible one-electron reduction at $E_{1/2}$= -1.13V *vs.* Fc/Fc^+, indicating a greater interaction with the soft S-donors in the latter species compared to the former.

Chapter 3

The synthesis and electrochemistry of $[Co([18]aneN_2S_4)]^{2+}$ and $[Rh([18]aneN_2S_4)]^{3+}$ are described. Single crystal X-ray structures of $[M([18]aneN_2S_4)]^{3+}$, (M= Co, Rh), each show octahedral co-ordination to the macrocycle with a rac-configuration, (Co-S= 2.25-2.27, Co-N= 2.20, Rh-S= 2.33-2.34, Rh-N= 2.08-2.10Å). Electrochemical studies on

$[Co([18]aneN_2S_4)]^{2+}$ in MeCN, show a reversible one-electron reduction ($E_{1/2}$= -1.30V *vs.* Fc/Fc^+) and oxidation ($E_{1/2}$= -0.07V *vs.* Fc/Fc^+), assigned to Co(II)/(I) and Co(II)/(III) couples respectively. Electrochemical studies on $[Rh([18]aneN_2S_4)]^{3+}$ show an irreversible two-electron reduction (E_{pc}= -1.34V *vs.* Fc/Fc^+). The reduction product is tentatively assigned as the Rh(I) species $[Rh([18]aneN_2S_4)]^+$.

The synthesis and characterisation of the deprotonated complex, $[Rh([18]aneS_6\text{-}H)]^{2+}$, are also described. Deprotonation of the co-ordinated hexathia macrocycle, [18]aneS$_6$, results in ring-opening to form a vinyl species.

Chapter 4

The synthesis, structure and electrochemistry of $[Pd([18]aneN_2S_4)]^{2+}$ and $[Pd(Me_2[18]aneN_2S_4)]^{2+}$ are described. A single crystal diffraction study of $[Pd([18]aneN_2S_4)]^{2+}$ shows an unusual distorted octahedral stereochemistry, due to long-range interaction of two S-donors, (Pd...S'= 2.95-3.00Å), to the equatorial N_2S_2 co-ordination plane, (Pd-N= 2.07-2.12, Pd-S= 2.31-2.36Å). This contrasts the single crystal structure of $[Pd(Me_2[18]aneN_2S_4)]^{2+}$ which shows square planar tetrathia co-ordination to Pd(II), (Pd-S= 2.32-2.34Å), with the N-Me groups directed away from the metal and not interacting, (Pd...N= 3.74-3.76Å). This structural difference has a marked effect on the redox properties of these Pd(II) complexes. $[Pd([18]aneN_2S_4)]^{2+}$ exhibits a

chemically reversible one-electron oxidation ($E_{1/2}$= +0.57V *vs.* Fc/Fc^+) in MeCN. Controlled potential electrolysis in MeCN leads to the formation of the d^7 $[Pd([18]aneN_2S_4)]^{3+}$ cation, which is characterised by e.s.r. (g_1= 2.064, g_2= 2.052, g_3= 2.019) and <u>in situ</u> UV/vis spectroscopy. Electrochemical studies on $[Pd(Me_2[18]aneN_2S_4)]^{2+}$ in MeCN show a one-electron reduction ($E_{1/2}$= -0.74V *vs.* Fc/Fc^+). Controlled potential electrolysis in MeCN leads to the formation of the d^9 $[Pd(Me_2[18]aneN_2S_4)]^{+}$ cation, which is characterised by e.s.r. (g_{11}= 2.155, $g_{\perp}$= 2.049, A_{11}= 48G, $A_{\perp}$= 43G) and <u>in situ</u> UV/vis spectroscopy.

The synthesis, characterisation and electrochemistry of the Pt(II) analogues, $[Pt([18]aneN_2S_4)]^{2+}$ and $[Pt(Me_2[18]aneN_2S_4)]^{2+}$ are also discussed.

The preparation of the binuclear complexes, $[M_2Cl_2([18]aneN_2S_4)]^{2+}$, (M= Pd, Pt) is reported. The single crystal structure of $[Pd_2Cl_2([18]aneN_2S_4)]^{2+}$ shows each Pd(II) ion bound to a square planar arrangement of two S- and one N-donor of the macrocycle and one terminal Cl^- ligand, (Pd-S= 2.31, Pd-N= 2.05, Pd-Cl= 2.30Å).

<u>Chapter 5</u>

The synthesis and structures of the tetrathia macrocyclic complexes, $[Pd([12]aneS_4)]^{2+}$ and $[Pd([16]aneS_4)]^{2+}$ are reported. Each of these cations adopts a square planar stereochemistry, with Pd(II) bound to four thioether-donor atoms. ($[Pd([12]aneS_4)]^{2+}$:

Pd-S= 2.28-2.31, $[Pd([16]aneS_4)]^{2+}$: Pd-S= 2.30-2.32Å). The metal ion is displaced out of the S_4 co-ordination plane by 0.3116A in $[Pd([12]aneS_4)]^{2+}$, reflecting an incompatibility between the macrocyclic cavity-size and the radius of the Pd(II) ion. The synthesis and characterisation of $[Pt([16]aneS_4)]^{2+}$ and the binuclear complexes, $[M_2([28]aneS_8)]^{4+}$, (M= Pd, Pt), are also described.

Electrochemical studies on all of these complexes are reported. The Pd(II) tetrathia complexes each undergo an irreversible one-electron reduction at similar potentials (E_{pc} *ca.* -0.8V *vs.* Fc/Fc^+), yielding orange diamagnetic complexes. This is attributed to generation of a transient Pd(I) monomer, followed by rapid dimerisation via formation of an unsupported metal-metal bond. $[Pd_2([28]aneS_8)]^{4+}$ undergoes an irreversible two-electron reduction (E_{pc}= -0.74V *vs.* Fc/Fc^+) in MeCN. The orange reduction product is assigned as the Pd(I)/Pd(I) dimer, $[Pd_2([28]aneS_8)]^{2+}$. These reduction products are each characterised by coulometry, e.s.r. and in situ UV/vis spectroscopy. In each case the Pd(II) precursor can be regenerated quantitatively from the reduction products.

Chapter 6

The synthesis and characterisation of $[RhCl_2([12]aneS_4)]^+$, $[MCl_2([14]aneS_4)]^+$, (M= Rh, Ir), $[RhCl_2([16]aneS_4)]^+$, and $[RhCl([15]aneS_5)]^{2+}$ are described. Single crystal X-ray diffraction studies on $[MCl_2([14]aneS_4)]^+$ each show octahedral co-ordination via four S-donors of a folded macrocycle, and mutually cis-dichloro ligands, (Rh-S= 2.29-2.33, Rh-Cl= 2.38, Ir-S= 2.27-2.34, Ir-Cl= 2.38-2.39Å). A single crystal X-ray study of $[RhCl_2([16]aneS_4)]^+$ also reveals octahedral geometry around the Rh(III) ion. However, in this case the macrocycle occupies four equatorial co-ordination sites, with mutually trans-dichloro ligands occupying the apical sites, reflecting the larger cavity-size of the 16-membered ring, (Rh-S= 2.35, Rh-Cl= 2.34Å). $[RhCl_2([12]aneS_4)]^+$ is assigned as the cis-dichloro isomer on the basis of UV/vis and ^{13}C n.m.r. spectroscopy.

Preliminary electrochemical studies on $[RhCl_2([14]aneS_4)]^+$ in MeCN show an irreversible one-electron reduction (E_{pc}= -1.10V *vs.* Fc/Fc^+), yielding a transient Rh(II) monomer. The reduction product is characterised by e.s.r. and <u>in situ</u> UV/vis spectroscopy, and the irreversibility is attributed to loss of Cl^- ligand upon reduction. The other tetrathia complexes exhibit similar redox properties.

Chapter 7

The synthesis, structure and electrochemistry of $[RhCl_2(Me_4[14]aneN_4)]^+$ are described. A single crystal structure of this complex shows $Me_4[14]aneN_4$ occupying the four equatorial sites, with mutually trans-chlorides completing the octahedral co-ordination, (Rh-N= 2.11, Rh-Cl= 2.36Å). The complex adopts the RRSS-configuration.

The complex shows a quasi-reversible reduction in MeCN ($E_{1/2}$= -0.99V *vs.* Fc/Fc^+). Reduction to form the Rh(II) monomer (g_1= 2.110, g_2= 2.015, g_3= 1.996) is accompanied by loss of Cl^-.

Chapter 8

The synthesis and characterisation of the mixed thia/oxa donor macrocyclic complexes $[MCl_2([15]aneS_2O_3)]$, $[M([15]aneS_2O_3)_2]^{2+}$, (M= Pd, Pt), $[M'([15]aneS_2O_3)_2Cl_2]^+$, (M'= Rh, Ir) and $[RuCl(PPh_3)([15]aneS_2O_3)_2]^+$ are described. The single crystal structure of $[Pd([15]aneS_2O_3)_2]^{2+}$ reveals Pd(II) bound to a square planar arrangement of four thioether-donor atoms, (Pd-S= 2.30-2.31Å). The possibility of binding alkali metal ions to oxa-donors is discussed.

List of Figures

List of Tables

Table of Contents

CHAPTER 1

Introduction

1.1: General

The co-ordination chemistry of macrocyclic ligands has been the subject of much attention in recent years [1]. This interest has been due to the enhanced stability of transition metal macrocyclic complexes relative to their open-chain analogues, and the ability of macrocyclic ligands to modify their mode of co-ordination to meet the stereochemical demands of a wide range of metal oxidation states [2-4]. The increased kinetic inertness and thermodynamic stability of macrocyclic complexes was first recognised by Cabbiness and Margerum during a study on a series of Cu(II) tetra-amine complexes [2], and was termed the "macrocyclic effect". Consequently, the macrocycle may be regarded as a protecting group for the metal ion centre, controlling its stereochemical and redox properties, and thus, enabling stabilisation of unusual oxidation states. The magnitude of the macrocyclic effect depends critically upon the particular complex in question. Several factors can lead to a diminished macrocyclic effect being observed. For example, incompatibility between the metal ion centre and the donor atom type, or ligand pre-organisation (see below) [5], or where the bad size-match between the macrocyclic cavity and the metal ion radius forces the complex to adopt a strained stereochemistry, e.g. in $[Cu([12]aneN_4)]^{2+}$ [6].

The kinetic stability of tetra-aza macrocyclic complexes has been well established, with both formation

and particularly dissociation rate constants (k_f and k_d respectively) being considerably lower than for the analogous non-macrocyclic systems [7]. Busch attributed this to the difference in flexibility of the co-ordinative bonds in these systems. Dissociation necessitates elongation and cleavage of the metal-donor bonds. This is inhibited in a macrocyclic complex since M-L bond cleavage leads to a distortion throughout the whole ring (1). In contrast, metal-donor bond cleavage in an open-chain system is more straightforward, involving an "unzipping" mechanism from one end of the chain to the other (2) [8]. Thus, for the equilibrium:

$$M^{2+}_{(aq)} + L \rightleftharpoons ML^{2+}$$

where the stability constant, $K = k_f/k_d$, lowering k_d, as occurs in macrocyclic complexes, leads to an increase in K [9].

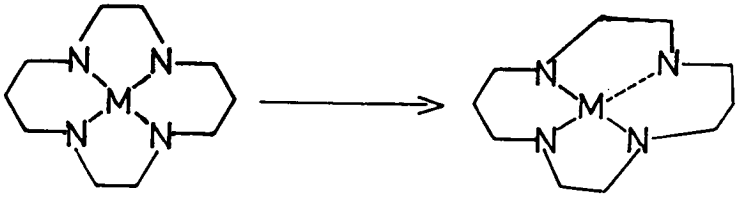

(1)

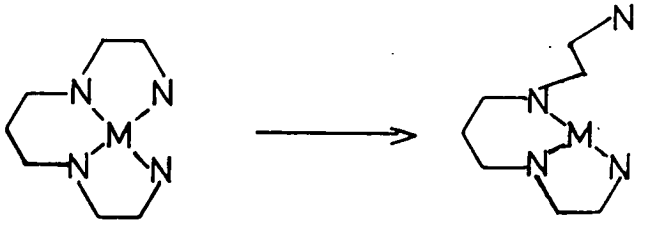

(2)

The purely thermodynamic rationale for the macrocyclic effect is rather more complex, and is still the focus of controversy. The macrocyclic effect is a consequence of the Gibb's free energy term

($\Delta G_f = \Delta H_f - T\Delta S_f$) for the metathetical reaction:

$$[ML]^{n+} + L^m \longrightarrow [ML^m]^{n+} + L$$

where L= non-cyclic ligand and L^m= macrocyclic ligand. While it has been established that both entropic and enthalpic contributions to the thermodynamics are important, there is still much uncertainty over the origin of the enthalpic term [10].

The entropic effect is usually favourable, since it is derived from an increase in the number of degrees of freedom in releasing the ligand from complexation. In a macrocyclic free-ligand there are considerably fewer internal degrees of freedom compared to an open-chain ligand. Co-ordination to a metal diminishes these in both systems. However, the net gain in entropy in releasing the free open chain ligand from complexation is higher than for the macrocyclic system.

Assessment of the importance of the enthalpic contribution is a more difficult task. This arises predominantly from the difference in solvation terms for L and L^m, and hence, the magnitude of this effect will be critically dependent on the ring size of the macrocycle, solvent and metal ion to be complexed. Margerum and co-workers have established the large difference in stability constants for Ni(II) complexes of [14]aneN_4 (3) and 2-3-2-tet, (4), arises mainly from enthalpic contributions. This is attributed to the differences in ligand solvation energies [9]. The same authors have shown that the magnitude of the macrocyclic effect in the

tetrathia complex, $[Ni([14]aneS_4)]^{2+}$, (5), versus its open chain analogue, $[Ni(TTT)]^{2+}$, (6), is substantially lower than for the tetra-aza systems above [11]. This diminished macrocyclic effect is attributed to the small difference in solvation terms for the two thioether ligands, which reflects the absence of hydrogen-bonding between these ligands and the solvent. In this case the macrocyclic effect is attributed predominantly to the difference in configurational entropy of the free ligands.

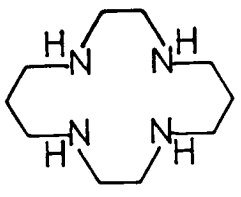

(3)

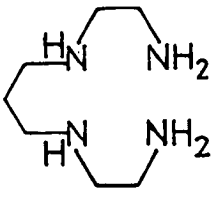

(4)

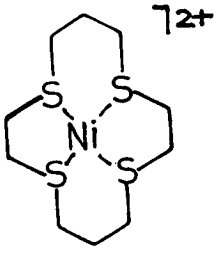

(5)

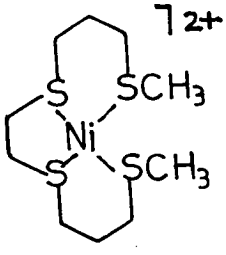

(6)

A further important factor contributing to the enhanced stability of some macrocyclic systems is ligand pre-organisation [5]. Structural studies on many macrocyclic polythioethers have shown that they prefer to adopt exo-conformations, in which the sulphur-donor atom lone-pairs are directed away from the macrocyclic cavity, e.g. $[14]aneS_4$ [12], $[18]aneS_6$ [13]. Co-ordination of a transition metal ion within the macrocyclic cavity, therefore, necessitates a conformational rearrangement to the endo-form (7). Therefore the macrocyclic effect for

certain thioethers may be weak or non-existant [11]. In contrast, the solid state structure of the small ring trithia macrocycle [9]aneS_3 shows that the preferred conformation of the free-ligand has the sulphur atom lone-pairs in an ideal orientation for facial co-ordination to a metal centre (8) [14]. Thus, for complexation this macrocycle is not required to undergo an energetically unfavourable conformational reorganisation. Similarly, the uncomplexed tetra-aza macrocycle, [14]aneN_4 adopts an endo-conformation with the nitrogen atom lone-pairs directed into the cavity and, is therefore ideally suited for equatorial co-ordination to a metal [15]. These systems are therefore pre-organised for metal complexation, although H-bonding in the solvated free ligand may also be an important factor.

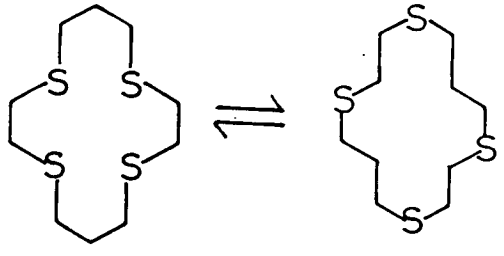

(7)

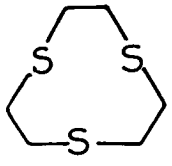

(8)

1.2: Biological Systems

The earliest known examples of transition metal macrocyclic complexes were those incorporating the tetrapyrrole unit, found in naturally occurring, biologically-active substances, e.g. haemoglobin (9) [16], chlorophyll (10) [17] and vitamin B_{12} (11) [18,19], containing Fe, Mg and Co respectively. In these metalloproteins the four equatorial co-ordination sites are taken up by the macrocyclic ligand, leaving the two remaining axial sites available for the binding and activation of substrate molecules.

One of the major reasons for the interest in the co-ordination chemistry of synthetic macrocycles is their potential as simple model molecules for complex biological systems [20]. The design of accurate metal complex models requires the introduction of the correct steric and electronic features into the ligand system. Synthetic macrocyclic ligands are ideally suited to this type of study since they can be tailored to meet the specific requirements by variation of the cavity size, number and type of donor atoms, degree of alkylation and unsaturation.

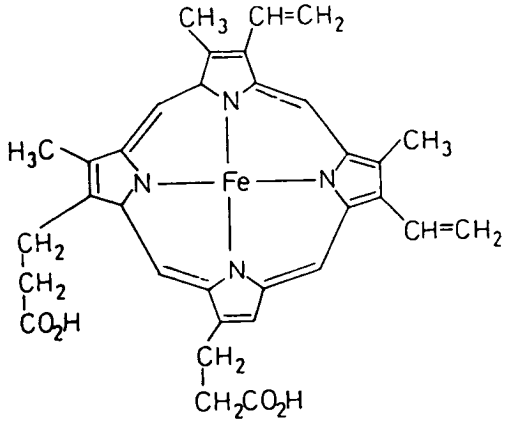

(9)

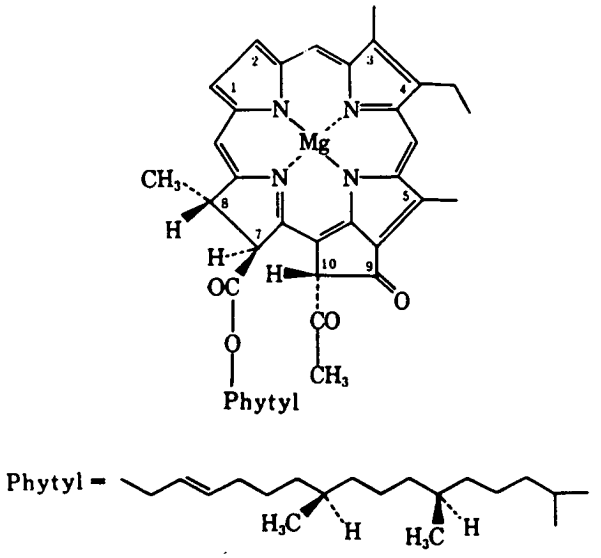

(10)

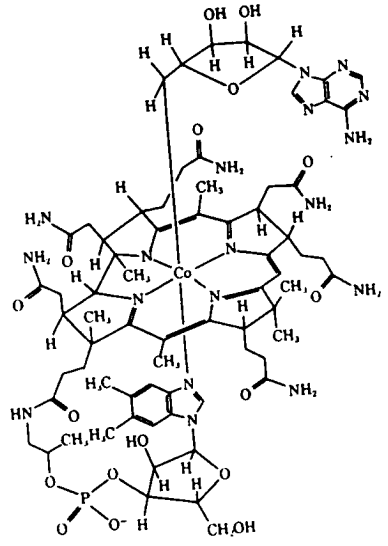

(11)

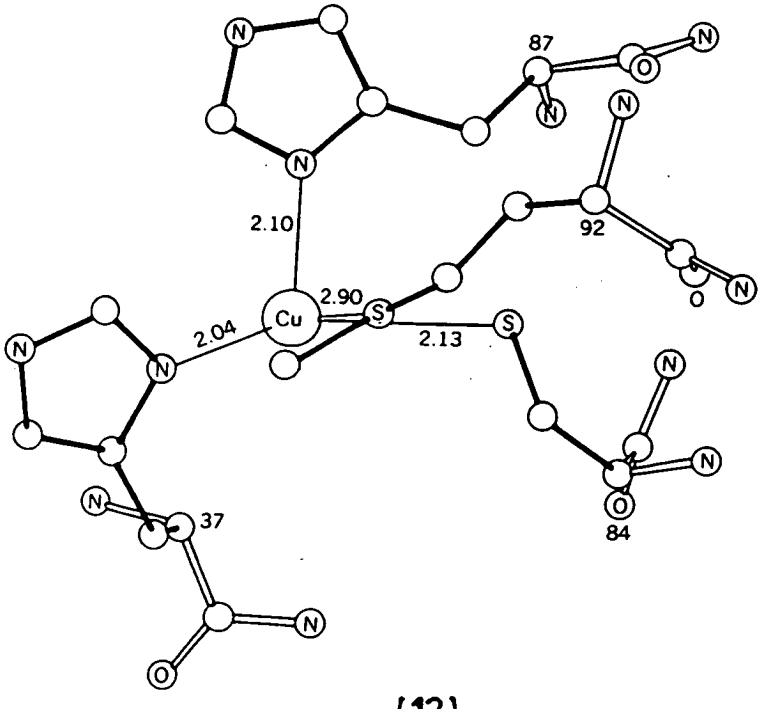

(12)

Transition metal centres are known to be present at the active site of many other enzymes which mediate vital processes *in vivo*. For example, nickel has been found at the active site of four general types of enzymes; urease, methyl coenzyme M reductase, carbon monoxide dehydrogenase and several hydrogenase enzymes [21]. Recent evidence has identified two distinct classes of hydrogenases which catalyse the reaction:

$$2H^+ + 2\bar{e} \longrightarrow H_2$$

1. enzymes containing trivalent nickel as well as one or more Fe-S clusters, and
2. enzymes containing only Fe-S clusters.

The evidence suggests that Ni is the site of interaction of H_2 in nickel hydrogenases, and e.s.r. spectroscopy has confirmed that Ni-S co-ordination is crucial for their activity. Furthermore, both the nature of the co-ordinating ligands and the stereochemical constraints appear to control the rate of electron-transfer within these systems [22].

The copper ion occupying the active site in the blue copper proteins, plastocyanin and azurin, is co-ordinated to two nitrogen (his-87 and his-37) and two sulphur-donors (cis-84 and met-92) in a distorted tetrahedral geometry (12) [23]. Copper adopts this entatic (strained) state to facilitate rapid electron-transfer.

1.3: Catalysis

The design of electroactive complexes incorporating one or two labile co-ordination sites is of major importance in the design of effective new catalysts. In view of the ability of the macrocyclic ligands to protect the metal centres, macrocyclic complexes have been the focus of considerable interest regarding their potential in the catalytic and electrocatalytic reduction of small molecule substrates, such as CO_2 [24-28] and O_2 [29-31], and the activation of species such as NO, NO_3^-, CO, N_2 and H_2 [32-35]. Electrocatalysts which mediate CO_2 reduction at low potentials are important for the preparation of fuels or chemicals from this inexpensive and abundant carbon source. Fischer and Eisenberg produced the first convincing results using various tetra-aza macrocyclic complexes of Ni and Co, (13-17), and showed CO and H_2 as the major reduction products [24]. More recently, $[Ni([14]aneN_4)]^{2+}$ has been reported to mediate the reduction of CO_2 to CO in aqueous solution, at around 0.5V below the thermodynamic value, without the generation of significant amounts of H_2 from the competing reaction of the electro-reduction of water [26,27]. Other macrocyclic complexes which facilitate the electrocatalytic reduction of CO_2 include Co and Ni phthalocyanines [25], and Ag(II) and Pd(II) complexes of OEP^{2-} and TPP^{2-} [36]. In the latter cases CO is not

detected as a reduction product, but rather oxalic acid and H_2.

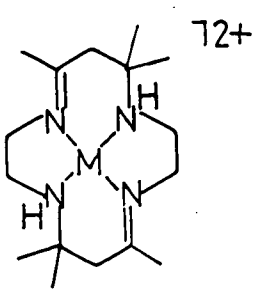

(13): M=Co
(14): M=Ni

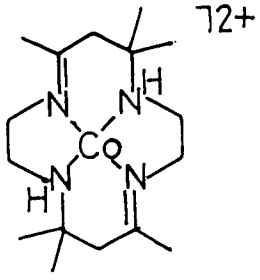

(15)

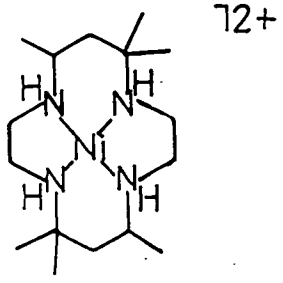

(16)

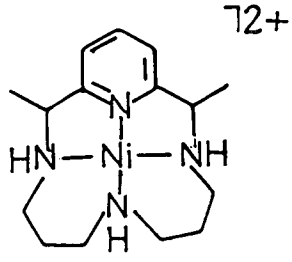

(17)

Catalysts which mediate the reduction of dioxygen are of considerable interest in the design of efficient fuel cells. Collman and co-workers have reported an elegant process for the four-electron reduction of O_2 to H_2O using a cofacial dimeric Co/Co porphyrin [30] (see also Chapter 3). The same authors have illustrated the application of several platinum metal porphyrin dimers, (M_2P_2, M= Ru, Ir, Os, Rh, P= OEP^{2-}, TTP^{2-}), for binding and insertion of small molecules such as CO and H_2 [37] (see also Chapter 5). The first example of a monomeric macrocyclic complex which catalyses the direct four-electron reduction of O_2 in acidic solution is Ir(OEP)H adsorbed on graphite electrodes. The proposed mechanism for the reduction is illustrated in Fig. 1.1. A major advantage of this system is that reduction occurs without production of significant H_2O_2 concentrations [31].

Fig. 1.1: Proposed mechanism for the catalytic reduction of O_2 by Ir(OEP)H

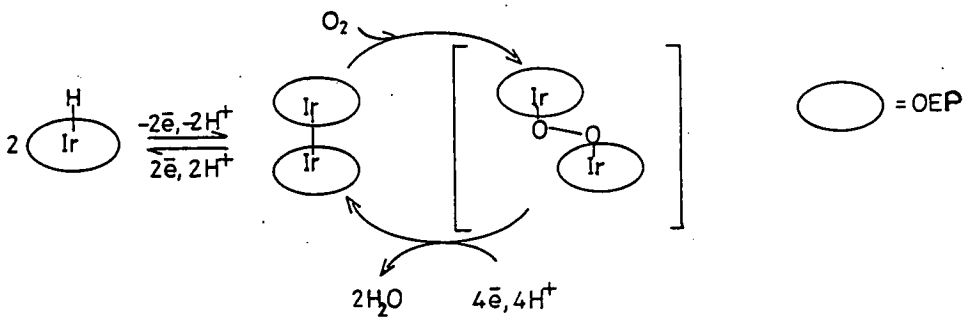

Wayland and co-workers have utilised $[Rh(OEP)]_2$ for the catalytic generation of methanol and formaldehyde from H_2 and CO by irradiation at 350nm [38].

Using tetra-aza and tetrathia macrocycles as protecting groups, complexes such as $[Rh(18)(C_3H_6Br)I]$, $[Rh(19)(C_6H_5CO)Cl]^+$ and $[Ni(20)CH_3]^+$ can be produced by oxidative addition of alkyl or acyl halides to the low-valent Rh(I) of Ni(I) precursor complexes [39-41].

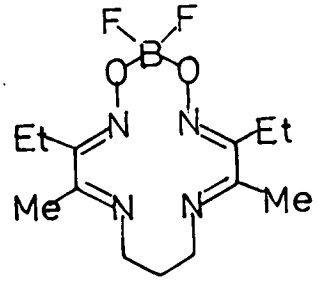

(18)

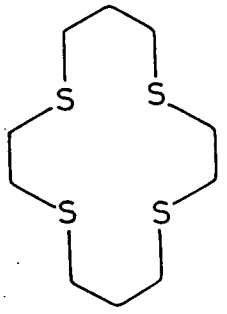

(19)

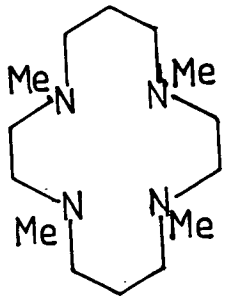

(20)

1.4: Aims of Work

Although thioethers are generally considered to be very poor ligands to transition metal centres [42], recent studies have established that macrocyclic thioethers are very effective ligands, with σ-donor, π-donor and π-acceptor properties being of relevance to metal-ligand binding. In contrast, saturated nitrogen ligands can participate only in σ-bonding. However, N-alkylation can impart both steric and electronic effects upon a polyaza macrocyclic complex . All of these features have been utilised for the stabilisation of a wide range of unusual transition metal oxidation states by macrocyclic ligands [3,4]. However, although the factors influencing the stability of homoleptic metal macrocyclic complexes are quite well established, fewer studies on mixed donor macrocyclic species have been undertaken. Consequently, a study of the co-ordination chemistry of the mixed sulphur- and nitrogen-donor macrocycles, [18]aneN_2S_4 and Me_2[18]aneN_2S_4, with a series of transition metal centres was initiated. Particular emphasis was placed upon structural characterisation of the complexes, in order to assess the co-ordinative flexibility of these potentially haxadentate 18-membered ring macrocycles, and investigation of the redox characteristics of the resulting metal complexes (Chapters 2, 3 and 4). We proposed also, that first row transition metal complexes of these macrocycles,

(particularly Cu, Ni, Fe and Co), may be of relevance as models for *in vivo* complexes, since they exhibit similar co-ordination spheres to those known to be present at the active site [43].

The multi-redox and catalytic properties exhibited by second and third row transition metal porphyrin complexes have been studied extensively by other workers [29,37,44]. However, there remains a general paucity of low-valent complexes incorporating these metals, [Pd(I), Pt(I), Rh(II), Ir(II)]. This is attributed mainly to the tendency for these species to undergo facile dimerisation reactions, via formation of a direct metal-metal bond [45,46]. Following the recent stabilisation of monomeric Pd(I) centres by tetra-aza ionophores by the group in Edinburgh [47], we proposed that stabilisation of Pd(I) could also be achieved by tetrathia co-ordination. Also, importantly, the Pd(II)/(I) redox potentials would be made more accessible by incorporation of the softer sulphur-donor atoms rather than nitrogen-donors. The second area of work was therefore concerned with a study of the synthesis and electrochemical properties of palladium and platinum complexes containing a series of tetrathia macrocyclic ligands, (Chapter 5). The importance of the platinum group metals in catalytic applications [48] led to this study being extended to rhodium and iridium systems involving these tetrathia macrocycles, (Chapter 6), and also the tetra-aza macrocycle, $Me_4[14]aneN_4$, (Chapter 7).

The resulting Rh and Ir complexes are ideally suited for catalytic investigation, since four co-ordination sites are taken up by the macrocycle, leaving two labile sites potentially available for binding and activation of small substrate molecules.

The final area of study was concerned with the co-ordination chemistry of macrocyclic ligands containing receptor sites potentially capable of binding both hard and soft metal guest ions. Chapter 8 describes the co-ordination of the mixed thia/oxa donor macrocycle, [15]aneS_2O_3, to platinum metal centres, and preliminary investigations into the utilisation of these systems for monitoring alkali metal cation concentrations in solution.

Fig. 1.2: Principle macrocyclic ligands discussed in this work

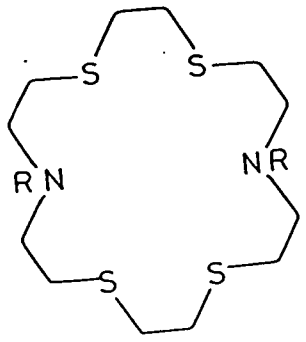

[18]aneN$_2$S$_4$: R=H

Me$_2$[18]aneN$_2$S$_4$: R=Me

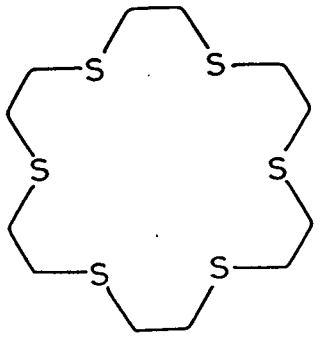

[18]aneS$_6$

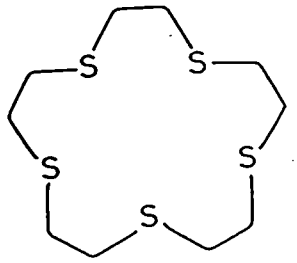

[15]aneS$_5$

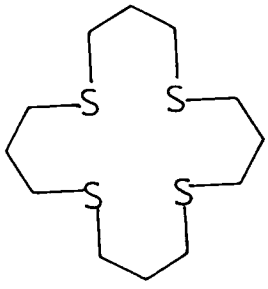

[16]aneS$_4$

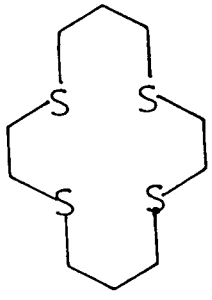

[14]aneS$_4$

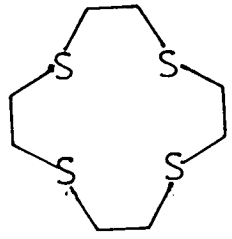

[12]aneS$_4$

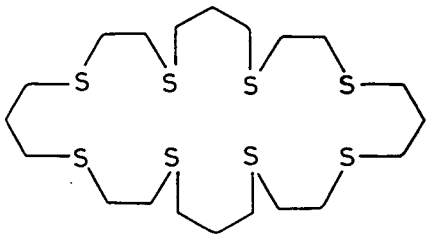

[28]aneS$_8$

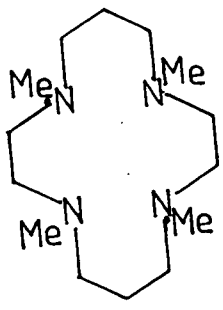

Me$_4$[14]aneN$_4$

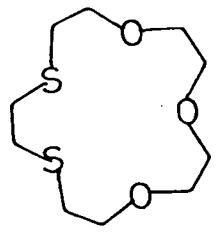

[15]aneS$_2$O$_3$

CHAPTER 2

Cu, Ni and Fe Complexes of

[18]aneN$_2$S$_4$ and Me$_2$[18]aneN$_2$S$_4$

2.1: Introduction

Transition metal centres are present at the active site of many enzymes which perform vital biological processes e.g. plastocyanin and azurin (Cu), vitamin B_{12} (Co), cytochromes (Fe) and hydrogenase enzymes (Ni) [16,18,19,23]. The need for simple metal complex models to assist our understanding of these systems provided the impetus for a study of the binding and redox properties of the 18-membered macrocycles, [18]aneN_2S_4 and Me_2[18]aneN_2S_4 with first row transition metals. The co-ordination chemistry of these macrocyclic ligands is of particular interest due to the incorporation of both hard and soft donor atoms in a co-ordinatively restricted environment.

Since the first synthesis of [18]aneN_2S_4 by Black and co-workers [49-51], very little work has been reported on its metal complexation. In their original report, Black and co-workers defined two possible conformations for a hexadentate ligand in octahedral geometry (Fig. 2.1):

1. meso, in which two S-N-S donor sets each bind facially to the metal centre, or,
2. racemic, where two S-N-S donor sets bind meridionally to the metal.

Fig. 2.1:

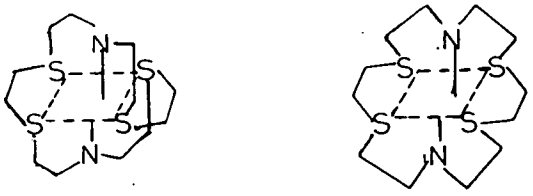

Subsequently, Lindoy and Busch reported the synthesis of another mixed N_2S_4 donor macrocycle, L (1) [52]. They proposed that the incorporation of the aromatic conjugation in this ligand would necessitate each S-N-S portion to be planar, and thus preclude the formation of a meso-isomer on co-ordination in an octahedral field.

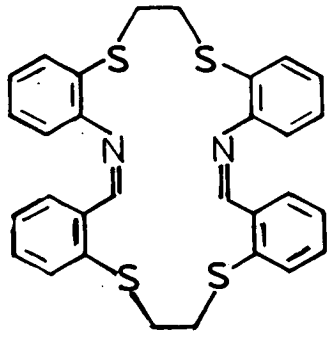

(1)

A range of octahedral complexes incorporating the homoleptic hexathia macrocycle, [18]aneS_6 have been structurally characterised. Without exception, in $[M([18]aneS_6)]^{x+}$ (M= Ru(II) [53], Pd(III) [54], Ni(II) [55], Cu(II) [56], Co(II) [57]), the macrocycle adopts a meso-conformation, thereby maximising the number of *gauche* placements at the C-S bonds. No metal complexes incorporating [18]aneN_2S_4 or Me_2[18]aneN_2S_4 have been structurally characterised previously. We therefore undertook a study of the co-ordination chemistry of these ligands with copper, nickel and iron centres.

Ligand Synthesis

The first preparation of [18]aneN_2S_4 was achieved by reaction of equimolar amounts of

1,5-dibromo-3-azapentane and the disodium salt of ethane-1,2-dithiol in ethanol. High dilution techniques were employed to encourage [2+2] cyclisation over linear polymerisation. This gave the free ligand as colourless needles in 4.6% yield [49-51]. An alternative synthesis later reported by Lehn *et al* [59], gives [18]aneN_2S_4 in 45% yield, via high dilution cyclisation of the appropriate dithia-dicarboxylic acid dichloride and -diamine, followed by diborane reduction of the resulting diamide.

The crystal structure of free [18]aneN_2S_4 shows the molecule sitting on a crystallographic inversion centre, in a conformation resembling a figure-eight [60]. The torsion angles at all four C-N bonds adopt an *anti*-placement, while all eight C-S linkages are *gauche*. Interestingly, the molecule does not participate in any significant H-bonding, and the S atoms, unlike the homoleptic thioether macrocycles described in Chapter 6 are neither exo- or endodentate. Rather, the C-S-C triangle is essentially perpendicular to the macrocycle plane.

Me_2[18]aneN_2S_4 can be obtained in almost quantitative yield by methylation of [18]aneN_2S_4 using formic acid/formaldehyde [61]. The reaction mechanism for methylation is a two-stage process [62], involving i. initial attack by formaldehyde, followed by ii. reduction with formic acid (2).

$$H^{\bullet} + \rangle HN + HCOH \xrightarrow{i} H_2O + \rangle \dot{N}{=}CH_2 \xrightarrow{ii} N{-}CH_3 \qquad (2)$$

2.2: Results and Discussion

2.2.1: $[Cu([18]aneN_2S_4)](PF_6)_2$

The paucity of low molecular weight models exhibiting similar spectral and redox properties to the blue copper proteins, has prompted a number of people to investigate the co-ordination of Cu(II) to polythioether macrocycles [63-68]. Rorabacher and co-workers have demonstrated that Cu(II) thioether macrocyclic complexes exhibit an intense absorption band in the 600nm region, a feature characteristic of blue copper proteins [65-68]. Contrary to original proposals, the appearance of such spectral features for simple square planar and octahedral Cu(II) thioether complexes confirms that distortion from tetragonal symmetry is not a prime requirement for producing these absorption bands. Furthermore, many of the model systems studied exhibit Cu(II)/(I) redox couples close to the characteristically positive potentials observed in nature (+0.2 to +0.8V *vs.* SHE at pH~7) [69,70].

Treatment of $Cu(NO_3)_2.6H_2O$ with one molar equivalent of $[18]aneN_2S_4$ in refluxing $EtOH/H_2O$ produced a bright green solution. Addition of excess PF_6^- counterion yielded a green precipitate which was recrystallised from H_2O to afford the product as green crystals.

The I.R. spectrum of the product shows bands confirming the presence of co-ordinated $[18]aneS_2S_4$ at 3270 and 3160cm^{-1} corresponding to N-H stretching

vibrations (υ(N-H)), 2920 and 1420cm^{-1} due to C-H stretching vibrations and C-H deformations (υ(C-H) and δ(C-H) respectively). Strong absorptions at 840 and 555cm^{-1} are characteristic of PF_6^- counterion. F.a.b. mass spectrometry reveals molecular ion peaks with the correct isotopic distributions at M^+= 535 and 389. These are assigned to $[^{63}Cu([18]aneN_2S_4+H)PF_6]^+$ and $[^{63}Cu([18]aneN_2S_4)]^+$ respectively. This, together with microanalytical data indicates the formulation $[Cu([18]aneN_2S_4)](PF_6)_2$. The UV/vis spectrum of the complex exhibits two intense charge-transfer transitions at λ_{max}= 395nm (ε_{max}= 2,460M^{-1}cm^{-1}) and 302 (1,970). A weaker absorption at 612 (202) can also be discerned, which is assigned tentatively to a d-d transition.

The single crystal X-ray structure of the ClO_4^- salt of this complex-cation has been determined in collaboration with Dr Michael G.B. Drew (of the University of Reading) [71]. The structure shows the cation adopting an unusual tetragonally compressed stereochemistry. The Cu(II) ion is bound to all six donor atoms with the complex taking up the rac-configuration (Fig. 2.2).

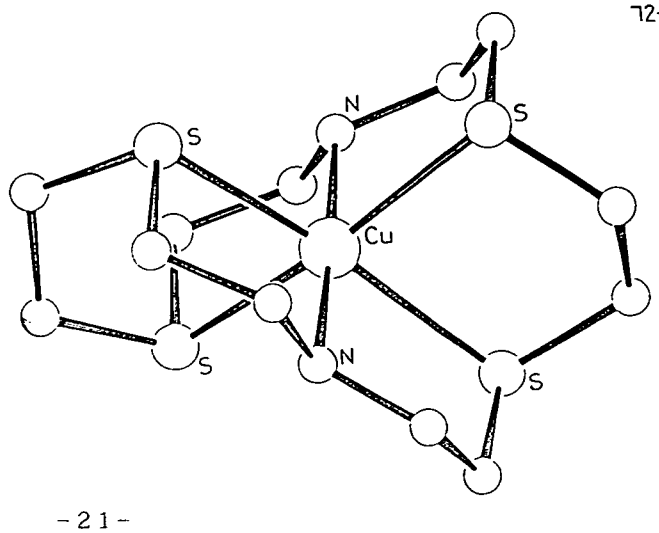

Fig. 2.2:
Single crystal structure of $[Cu([18]aneN_2S_4)]^{2+}$

This contrasts with $[Cu([18]aneS_6)]^{2+}$ which exhibits a tetragonally elongated stereochemistry with a meso-conformation [56], while the X-ray structure of $[Cu([9]aneS_3)_2]^{2+}$ shows the Cu(II) ion in an almost perfect octahedral geometry with each tridentate macrocycle binding facially [102]. The tetragonal compression in $[Cu([18]aneN_2S_4)]^{2+}$ occurs along the N-Cu-N axis [Cu-N= 2.007(13), 2.036(12)Å] and results in the four equatorial S-donors being pushed away from the Cu centre due to the conformational rigidity of the macrocycle [Cu-S= 2.577(5), 2.487(5), 2.528(5), 2.578(5)Å]. These Cu-S bond lengths are considerably longer than in related thioether crown complexes, e.g. $[Cu([18]aneS_6)]^{2+}$ [$Cu-S_{eq}$= 2.323(1), 2.402(1)A, $Cu-S_{ap}$= 2.635(1)Å] [56], $[Cu([9]aneS_3)_2]^{2+}$ [Cu-S= 2.419(3) to 2.459(3)Å] [102], $[Cu([14]aneS_4)]^{2+}$ [Cu-S= 2.297(1) to 2.308(1)Å] [153] and $[Cu([15]aneS_5)]^{2+}$ [Cu-S= 2.289(2) to 2.398(2)Å] [207]. The rac-configuration adopted by $[Cu([18]aneN_2S_4)]^{2+}$ reflects the preference for torsion angles incorporating secondary amine functions to adopt *anti*-placements, thus minimising 1,4-dipolar interactions.

2.2.2: $[Cu(Me_2[18]aneN_2S_4)](PF_6)_2$

Treatment of $Cu(NO_3)_2.6H_2O$ with one molar equivalent of $Me_2[18]aneN_2S_4$ in refluxing $EtOH/H_2O$ gave a green solution. Addition of excess NH_4PF_6 counterion afforded a green solid which was recrystallised from H_2O.

The I.R. spectrum of this product shows bands

assigned to C-H stretching vibrations, (υ(C-H) 2920, 2860cm^{-1}) and C-H deformations (δ(C-H) 1465, 1435cm^{-1}), as well as intense bands at 840 and 555cm^{-1} due to PF_6^- counterion. F.a.b. mass spectroscopy reveals molecular ion peaks at M^+= 563, 433 and 417 corresponding to

$$[^{63}Cu([Me_2[18]aneN_2S_4+H)PF_6]^+,$$

$$[^{63}Cu(Me_2[18]aneN_2S_4)H_2O-2H]^+ \text{ and}$$

$[^{63}Cu(Me_2[18]aneN_2S_4)]^+$ respectively. This, together with microanalytical and UV/vis spectral data, confirms the product to be $[Cu(Me_2[18]aneN_2S_4)](PF_6)_2$.

Interestingly, recrystallisation of this complex from EtOH/MeCN gives a near colourless solution, from which pale green crystals of $[Cu_2(Me_2[18]anN_2S_4)(NCMe)_2](PF_6)_2$ can be isolated. The I.R. spectrum of this binuclear Cu(I) species is very similar to the mononuclear Cu(II) complex, except for the appearance of a sharp peak at 2280cm^{-1} indicative of co-ordinated MeCN. The complex is stable to aerial oxidation in MeCN at room temperature, reflecting the net π-acceptor properties of the thioether-donor set. A single crystal structure determination of this complex was undertaken to elucidate the stereochemistry at Cu(I). Binuclear Cu(I) complexes incorporating an N_2S_2 donor set may be potential models for the blue copper proteins plastocyanin and azurin [23].

2.2.3: Single Crystal Structure of

$[Cu_2(Me_2[18]aneN_2S_4)(NCMe)_2](PF_6)_2$

Details of the structure solution are given in the Experimental Section. Lists of the relevant bond lengths, angles and torsions are presented in Tables 2.1, 2.2 and 2.3 respectively, and an ORTEP plot showing the stereochemistry of the cation is presented in Fig. 2.3.

The structure determination of this binuclear Cu(I) complex reveals a centrosymmetric structure with each Cu(I) centre bound tetrahedrally to two S-donors and one-N donor of the macrocycle [Cu-S(4)= 2.317(4), Cu-S(10)= 2.286(4), Cu-N(7)= 2.165(7)Å], and one MeCN molecule [Cu-N(1S)= 1.924(9)Å]. The Cu...Cu separation is 4.283(2)A, with each Cu(I) ion bound by an N_2S_2 donor set, similar to that found in Type 1 copper proteins. A very similar structure has been determined previously by the Edinburgh group [72] for $[Cu_2([18]aneS_6)(NCMe)_2]^{2+}$, which shows NS_3 co-ordination to each Cu(I) centre.

Fig. 2.3: View of the single crystal structure of $[Cu_2(Me_2[18]aneN_2S_4)(NCMe)_2]^{2+}$

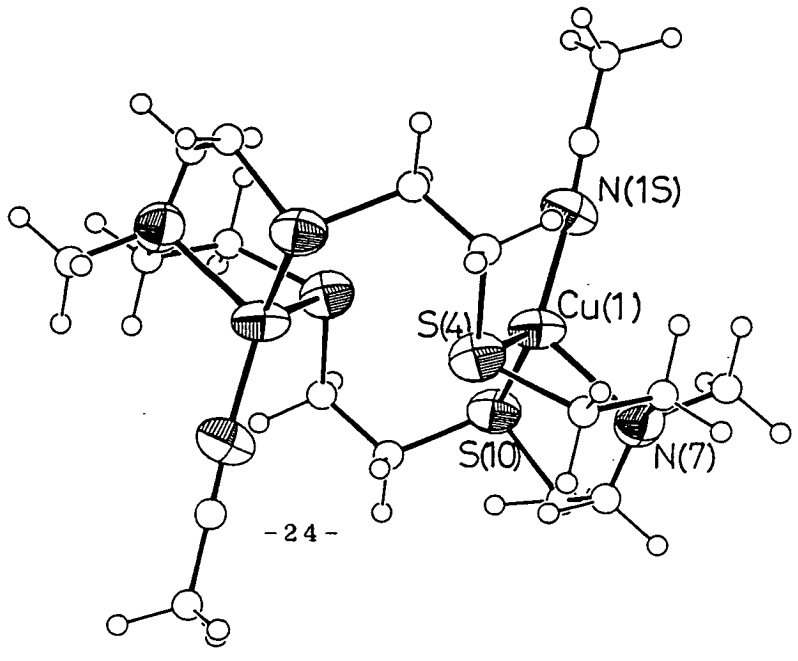

Single Crystal Structure of

$[Cu_2(Me_2[18]aneN_2S_4)(NCMe)_2](PF_6)_2$

Table 2.1: Selected Bond Lengths(Å) with e.s.d.'s

Cu(1)	- S(4)	2.317(4)	S(10)	- C(9)	1.807(8)
Cu(1)	-S(10)	2.286(4)	S(10)	-C(11)	1.804(11)
Cu(1)	- N(7)	2.165(7)	C(3D)	-C(11)	1.487(15)
Cu(1)	-N(1S)	1.924(9)	N(7)	-C(7N)	1.437(14)
S(4)	- C(3)	1.846(11)	N(1S)	-C(1S)	1.127(13)
S(4)	- C(5)	1.860(8)	C(1S)	-C(2S)	1.424(14)

Table 2.2: Selected Angles(^{o}) with e.s.d.'s

S(4)-Cu(1) -S(10)	118.90(13)	Cu(1) - N(7) - C(8)	106.4(5)
S(4)-Cu(1) - N(7)	89.10(21)	Cu(1) - N(7) -C(6')	110.4(5)
S(4)-Cu(1) -N(1S)	115.8(3)	Cu(1) - N(7) -C(8')	108.9(5)
S(10)-Cu(1) - N(7)	88.30(21)	Cu(1) - N(7) -C(7N)	113.2(6)
S(10)-Cu(1) -N(1S)	118.5(3)	C(6) - N(7) - C(8)	123.7(6)
N(7)-Cu(1) -N(1S)	118.7(3)	C(6) - N(7) -C(7N)	80.7(6)
Cu(1)- S(4) - C(3)	106.4(4)	C(8) - N(7) -C(7N)	130.1(8)
Cu(1)- S(4) - C(5)	92.5(3)	C(6') - N(7) -C(8')	117.5(6)
C(3)- S(4) - C(5)	99.5(4)	C(6') - N(7) -C(7N)	116.5(7)
Cu(1)-S(10) - C(9)	95.7(3)	C(8') - N(7) -C(7N)	88.9(7)
Cu(1)-S(10) -C(11)	109.4(4)	S(10) - C(9) - C(8)	114.3(5)
C(9)-S(10) -C(11)	101.2(4)	S(10) - C(9) -C(8')	113.7(5)
C(11)-C(3D) -S(4D)	111.1(7)	S(10) -C(11) -C(3D)	110.1(7)
S(4)- C(5) - C(6)	114.4(5)	Cu(1) -N(1S) -C(1S)	174.9(9)
S(4)- C(5) -C(6')	112.9(5)	N(1S) -C(1S) -C(2S)	177.4(11)
Cu(1)- N(7) - C(6)	97.2(4)		

Table 2.3: Selected Torsion angles(^{o}) with e.s.d.'s

C(3)	-	S(4)	-	C(5)	-	C(6)	-92.7(6)
C(5)	-	C(6)	-	N(7)	-	C(7N)	177.2(7)
C(3)	-	S(4)	-	C(5)	-	C(6')	-145.4(6)
C(6)	-	N(7)	-	C(8)	-	C(9)	162.0(6)
C(11)	-	S(10)	-	C(9)	-	C(8)	-99.0(6)
C(7N)	-	N(7)	-	C(8)	-	C(9)	-90.2(10)
C(11)	-	S(10)	-	C(9)	-	C(8')	-148.3(6)
C(8')	-	N(7)	-	C(6')	-	C(5)	-159.0(6)
C(9)	-	S(10)	-	C(11)	-	C(3D)	-173.4(7)
C(7N)	-	N(7)	-	C(6')	-	C(5)	97.4(9)
S(4D)	-	C(3D)	-	C(11)	-	S(10)	-62.1(8)
C(6')	-	N(7)	-	C(8')	-	C(9)	82.5(8)
S(4)	-	C(5)	-	C(6)	-	N(7)	-56.5(7)
C(7N)	-	N(7)	-	C(8')	-	C(9)	-157.9(7)
S(4)	-	C(5)	-	C(6')	-	N(7)	52.4(8)
N(7)	-	C(8)	-	C(9)	-	S(10)	-45.1(8)
C(5)	-	C(6)	-	N(7)	-	C(8)	-50.4(9)
S(10)	-	C(9)	-	C(8')	-	N(7)	56.9(7)

2.2.4: Electrochemical Study of $[Cu([18]aneN_2S_4)]^{2+}$ and $[Cu(Me_2[18]aneN_2S_4)]^{2+}$

We were interested to determine whether di-N-methylation would invoke a significant difference in the redox properties of the Cu(II) complexes, hence an electrochemical study of $[Cu([18]aneN_2S_4)]^{2+}$ and $[Cu(Me_2[18]aneN_2S_4)]^{2+}$ was initiated.

The cyclic voltammogram of $[Cu([18]aneN_2S_4)]^{2+}$ measured in MeCN (0.1M $NBu^n_4PF_6$ supporting electrolyte) at platinum electrodes reveals a reversible Cu(II)/(I) redox couple at $E_{1/2}$= -0.31V *vs.* Fc/Fc^+ (ΔE_p= 80mV at a scan rate of $100mVs^{-1}$). In contrast, the di-methylated complex, $[Cu(Me_2[18]aneN_2S_4)]^{2+}$, exhibits a reversible Cu(II)/(I) couple at $E_{1/2}$= +0.06V *vs.* Fc/Fc^+ (ΔE_p= 100mV at a scan rate of $150mVs^{-1}$). Coulometric measurements on both complexes in MeCN (0.1M $NBu^n_4PF_6$ supporting electrolyte) at a platinum basket confirm that each of these processes corresponds to a one-electron reduction, generating a colourless solution. The reduction products are e.s.r silent, consistent with the formation of d^{10} Cu(I) complexes. The large difference in Cu(II)/(I) couples for $[Cu([18]aneN_2S_4)]^{2+}$ and $[CuMe_2[18]aneN_2S_4)]^{2+}$ is remarkable considering that the complexes differ only in the degree of alkylation of the macrocyclic aza-functions, with N-H being replaced by N-Me. Furthermore, methylation of N-donors would be expected to stabilise the higher Cu(II) oxidation state, rather than

Cu(I). These results suggest that the stereochemistry at the Cu(II) centre in $[Cu(Me_2[18]aneN_2S_4)]^{2+}$ may be substantially different from the non-methylated species.

Molecular mechanics calculations on $[Cu(Me_2[18]aneN_2S_4)]^{2+}$ have been performed by Drew and Forsyth [71,73]. These involve computer-simulated replacement of the N-H protons by methyl groups in the structure obtained for $[Cu([18]aneN_2S_4)]^{2+}$. Several unfavourable steric interactions became apparent at the co-ordinated N-donors. This strain could be partially relieved by an increase of the Cu-N bond length to 2.12Å. In order to assess any structural differences between the two Cu(II) complexes a single crystal structure determination of $[CuMe_2[18]aneN_2S_4)]^{2+}$ was undertaken.

2.2.5: Single Crystal Structure of $[Cu(Me_2[18]aneN_2S_4)](PF_6)_2$

Details of the structure solution and refinement are given in the Experimental Section. Bond lengths are listed in Table 2.4, bond angles in Table 2.5 and torsion angles in Table 2.6. Two ORTEP plots illustrating the geometry of the cation are presented in Figs. 2.4 and 2.5.

The structure shows the cation disordered on a site of D_{3d} symmetry, the 1/3 occupied N-Me function being superimposed on the 2/3 occupied S. Thus, the Cu(II) ion is co-ordinated to all six macrocyclic donor atoms in a distorted octahedral environment,

[Cu-S= 2.496(5), Cu-N= 2.191(17)Å]. Notwithstanding the disorder identified, the cation is clearly a meso-isomer. Furthermore the evidence from the X-ray study strongly suggests that the stereochemistry around the Cu(II) ion is tetragonally elongated along the N-C-N axis. This geometry is fully consistent with the observed redox properties, since it allows a closer interaction between the metal centre and the four soft sulphur-donor atoms compared to its non-methylated analogue, thus providing greater stability of the Cu(I) species.

Interestingly, the hexathia Cu(II) analogue, $[Cu([18]aneS_6)]^{2+}$, shows a reversible one-electron reduction to the tetrahedral $[Cu([18]aneS_6)]^{+}$ cation at the even more anodic potential of +0.24V *vs.* Fc/Fc^{+} [56], reflecting the net π-acidity of six thioether donors. The reversibility of each of these Cu(II)/(I) redox couples suggests that Cu-S bond cleavage/formation is faster than electron-transfer.

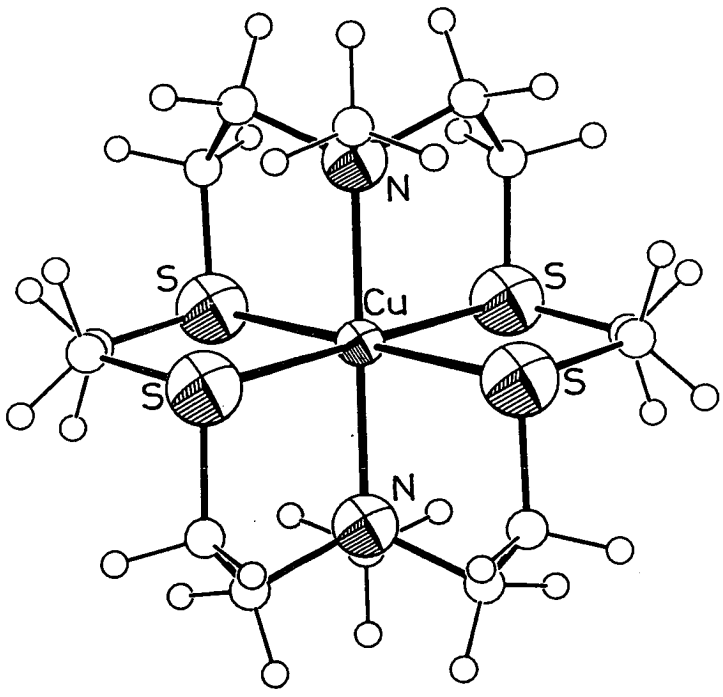

Fig. 2.4: View of the single crystal structure of $[Cu(Me_2[18]aneN_2S_4)]^{2+}$

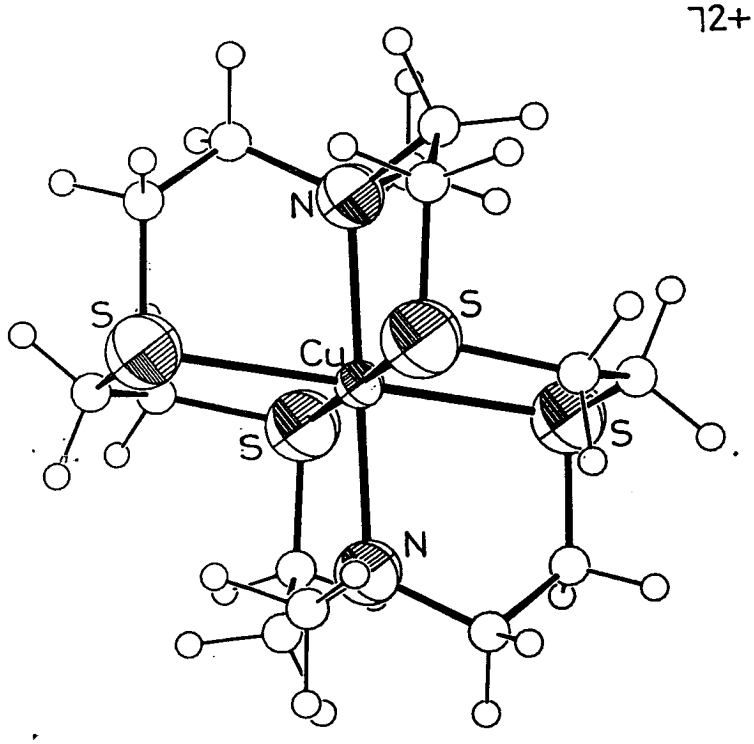

Fig. 2.5: Alternative view of the single crystal structure of $[Cu(Me_2[18]aneN_2S_4)]^{2+}$

Single Crystal Structure of

$[Cu(Me_2[18]aneN_2S_4)](PF_6)_2$

Table 2.4: Selected Bond Lengths(Å) with e.s.d.'s

Cu - S	2.496(5)	S - C	1.759(10)
Cu - N	2.191(17)	N - C	1.564(19)
C - C	1.427(11)	N - Me	1.42 (4)

Table 2.5: Selected Angles(°) with e.s.d.'s

S - Cu- S	89.79(2)	S - C - C	124.7(6)
S - Cu- N	78.4 (5)	C - S - C	99.8(4)
C - N - C	118.8 (11)	C - N - Me	94.7(17)

Table 2.6: Selected Torsion Angles(°) with e.s.d.'s

C - S - C - C	-78.1(8)
S - C - C - S	-32.5(11)
S - C - C - N	43.2(11)
C - C - N - C	106.6(12)

2.2.6: $[Ni([18]aneN_2S_4)](PF_6)_2$

Treatment of $Ni(NO_3)_2.6H_2O$ with one molar equivalent of $[18]aneN_2S_4$ in refluxing $EtOH/H_2O$ affords a bright purple solution. Addition of excess NH_4PF_6 and recrystallisation from H_2O led to the isolation of purple crystals.

The f.a.b. mass spectrum shows molecular ion peaks at $M^+ = 529$ and 383. These are assigned to $[^{58}Ni([18]aneN_2S_4)PF_6]^+$ and $[^{58}Ni([18]aneN_2S_4-H)]^+$ respectively. The product was assigned the formulation $[Ni([18]aneN_2S_4)](PF_6)_2$ on the basis of this evidence together with microanalytical and I.R. spectroscopic data.

In view of the paucity of structurally characterised complexes incorporating $[18]aneN_2S_4$, and in order to confirm the stereochemistry at Ni(II), a single crystal structure determination was undertaken.

2.2.7: Single Crystal Structure of

$[Ni(18]aneN_2S_4)](PF_6)_2.1/3H_2O$

Details of the structure solution are given in the Experimental Section. Selected bond lengths, angles and torsions are listed in Tables 2.7, 2.8 and 2.9 respectively. An ORTEP plot revealing the geometry of the cation is presented in Fig. 2.6.

The structure shows Ni(II) binding to an octahedral arrangement of all six donor atoms of the

macrocycle, [Ni-S(1)= 2.407(5), Ni-S(4)= 2.430(5), Ni-S(10)= 2.403(6), Ni-S(13)= 2.416(7), Ni-N(7)= 2.126(13) and Ni-N(16)= 2.065(13)Å]. These Ni-S bond lengths accord well with the sum of the covalent radii of Ni^{2+} and S^{2-} (2.44Å) [42]. Like the Cu(II) analogue discussed above, the complex cation adopts a rac-configuration, with S(4)-N(7)-S(10) and S(1)-N(16)-S(13) binding meridionally to the metal centre.

By contrast, the single crystal structure of $[Ni([18]aneS_6)]^{2+}$ adopts a meso-configuration, with compressed Ni-S bond lengths ranging from 2.376(1) to 2.397(1)Å [55]. A similar compression is observed in the related bis-macrocyclic species, $[Ni([9]aneS_3)_2]^{2+}$, where each ligand binds facially to Ni(II) [Ni-S range from 2.377(1) to 2.400(1)Å] [55]. Interestingly, however, Ni(II) co-ordinates to $[24]aneS_6$ to give the rac-isomer, with all Ni-S bond lengths in the range 2.415(1) to 2.445(1)Å, i.e. uncompressed [58]. The meridional stereochemistry in this large ring complex results in only eight out of twelve C-S bonds adopting *gauche* placements. These results suggest that in $[Ni([18]aneS_6)]^{2+}$ the importance of *gauche* placement of C-S linkages over-rides the energetically unfavourable compression of Ni-S bonds, while with $[24]aneS_6$ the reverse is true, probably since the remaining S lone-pairs interact to a lesser extent in the larger ring macrocycle.

Unlike $[Ni([18]aneS_6)]^{2+}$, which is

centrosymmetric, $[Ni([18]aneN_2S_4)]^{2+}$ shows a tetrahedral distortion out of the least-squares S(1), S(4), S(10), S(13) co-ordination plane, with S(1) and S(13) lying above by +0.2268 and +0.2253Å respectively, and S(4) and S(10) lying below by -0.2238 and -0.2283Å respectively. This distortion is a result of the small bite angle of the S N S portions.

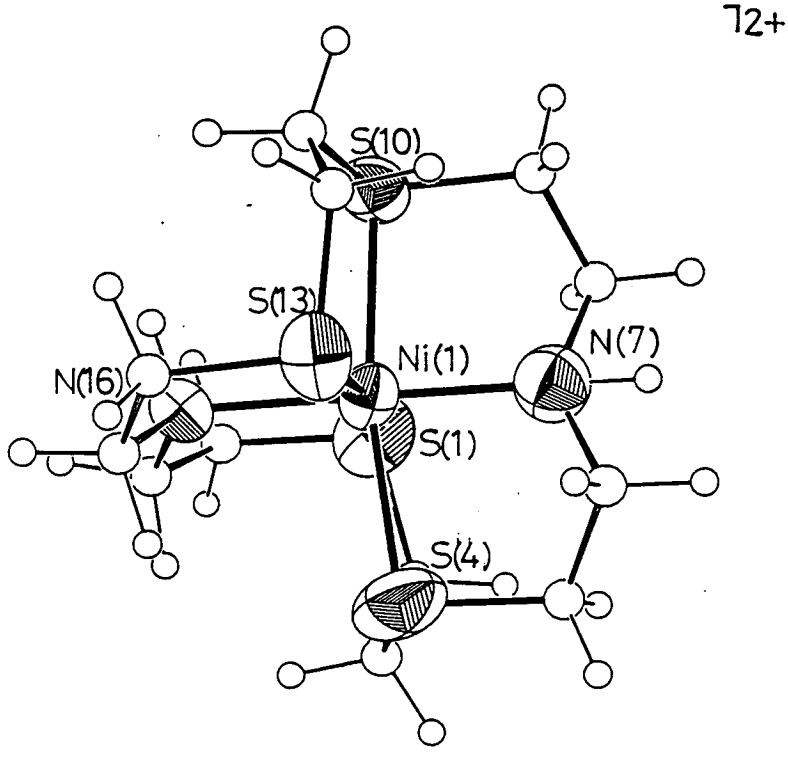

Fig. 2.6: View of the single crystal structure of $[Ni([18]aneN_2S_4)]^{2+}$

Single Crystal Structure of

$[Ni([18]aneN_2S_4)](PF_6)_2 \cdot 1/3H_2O$

Table 2.7: Selected Bond Lengths(Å) with e.s.d.'s

Ni(1)	- S(1)	2.407(5)	N(7)	-C(6)	1.488(21)
Ni(1)	- S(4)	2.430(5)	N(7)	-C(8)	1.408(23)
Ni(1)	-S(10)	2.403(6)	N(16)	-C(15)	1.500(20)
Ni(1)	-S(13)	2.416(7)	N(16)	-C(15')	1.500(20)
Ni(1)	- N(7)	2.126(13)	N(16)	-C(17)	1.500(18)
Ni(1)	-N(16)	2.065(13)	N(16)	- C(17')	1.500(19)
S(1)	- C(2)	1.793(20)	C(2)	-C(3)	1.45(3)
S(1)	-C(18)	1.830(12)	C(5)	-C(6)	1.51(3)
S(4)	- C(3)	1.846(19)	C(8)	-C(9)	1.54(3)
S(4)	- C(5)	1.814(19)	C(11)	-C(12)	1.50(3)
S(10)	- C(9)	1.839(19)	C(14)	-C(15)	1.500(20)
S(10)	-C(11)	1.853(23)	C(14)	-C(15')	1.500(20)
S(13)	-C(12)	1.818(24)	C(17)	-C(18)	1.500(17)
S(13)	-C(14)	1.830(15)	C(17')	-C(18)	1.500(18)

Table 2.8: Selected Angles(°) with e.s.d.'s

S(1)-Ni(1)- S(4)	87.81(18)	C(12) -S(13) -C(14)	103.2(9)
S(1)-Ni(1)-S(10)	92.91(19)	Ni(1) - N(7) - C(6)	110.0(10)
S(1)-Ni(1)-S(13)	170.39(21)	Ni(1) - N(7) - C(8)	113.3(10)
S(1)-Ni(1)- N(7)	94.0(4)	C(6) - N(7) - C(8)	111.4(13)
S(1)-Ni(1)-N(16)	85.4(4)	Ni(1) -N(16) -C(15)	111.6(9)
S(4)-Ni(1)-S(10)	168.05(20)	Ni(1) -N(16) -C(15')	108.1(9)
S(4)-Ni(1)-S(13)	93.90(20)	Ni(1) -N(16) -C(17)	110.1(9)
S(4)-Ni(1)- N(7)	83.6(4)	Ni(1) -N(16) -C(17')	108.5(9)
S(4)-Ni(1)-N(16)	94.8(4)	C(15) -N(16) -C(17)	138.2(12)
S(10)-Ni(1)-S(13)	87.37(21)	C(15')-N(16) -C(17')	143.3(12)
S(10)-Ni(1)- N(7)	84.4(4)	S(1) - C(2) - C(3)	117.2(14)
S(10)-Ni(1)-N(16)	97.2(4)	S(4) - C(3) - C(2)	115.5(13)
S(13)-Ni(1)- N(7)	95.6(4)	S(4) - C(5) - C(6)	111.3(12)
S(13)-Ni(1)-N(16)	85.0(4)	N(7) - C(6) - C(5)	110.4(14)
N(7)-Ni(1)-N(16)	178.3(5)	N(7) - C(8) - C(9)	112.7(15)
Ni(1)- S(1)- C(2)	101.8(6)	S(10) - C(9) - C(8)	110.9(12)
Ni(1)- S(1)-C(18)	96.1(4)	S(10) -C(11) -C(12)	115.1(16)
C(2)- S(1)-C(18)	103.6(7)	S(13) -C(12) -C(11)	115.7(17)
Ni(1)- S(4)- C(3)	101.2(6)	S(13) -C(14) -C(15)	109.8(10)
Ni(1)- S(4)- C(5)	97.7(6)	S(13) -C(14) -C(15')	109.8(10)
C(3)- S(4)- C(5)	101.5(8)	N(16) -C(15) -C(14)	109.6(12)
Ni(1)-S(10)- C(9)	97.5(6)	N(16) -C(15')-C(14)	109.5(12)
Ni(1)-S(10)-C(11)	103.8(7)	N(16) -C(17) -C(18)	109.6(10)
C(9)-S(10)-C(11)	102.8(9)	N(16) -C(17')-C(18)	109.5(11)
Ni(1)-S(13)-C(12)	103.6(8)	S(1) -C(18) -C(17)	109.8(8)

Table 2.9: Selected Torsion angles(°) with e.s.d.'s

C(18)	- S(1)	- C(2)	- C(3)	-62.1(15)
C(17)	-N(16)	-C(15)	-C(14)	-121.1(17)
C(2)	- S(1)	-C(18)	-C(17)	134.4(10)
C(17')	-N(16)	-C(15')	-C(14)	123.6(19)
C(2)	- S(1)	-C(18)	-C(17')	75.7(11)
C(15)	-N(16)	-C(17)	-C(18)	-128.0(16)
C(5)	- S(4)	- C(3)	- C(2)	-68.4(15)
C(15')	-N(16)	-C(17')	-C(18)	115.9(19)
C(3)	- S(4)	- C(5)	- C(6)	128.9(13)
S(1)	- C(2)	- C(3)	- S(4)	-49.3(18)
C(11)	-S(10)	- C(9)	- C(8)	79.9(14)
S(4)	- C(5)	- C(6)	- N(7)	-54.7(16)
C(9)	-S(10)	-C(11)	-C(12)	-70.6(18)
N(7)	- C(8)	- C(9)	-S(10)	50.8(18)
C(14)	-S(13)	-C(12)	-C(11)	-65.3(18)
S(10)	-C(11)	-C(12)	-S(13)	-45.3(22)
C(12)	-S(13)	-C(14)	-C(15)	137.8(12)
S(13)	-C(14)	-C(15)	-N(16)	-57.7(13)
C(12)	-S(13)	-C(14)	-C(15')	79.4(13)
S(13)	-C(14)	-C(15')	-N(16)	57.7(13)
C(8)	- N(7)	- C(6)	- C(5)	-177.0(14)
N(16)	-C(17)	-C(18)	- S(1)	-58.2(12)
C(6)	- N(7)	- C(8)	- C(9)	-174.2(14)
N(16)	-C(17')	-C(18)	- S(1)	58.3(12)

2.2.8: $[Ni(Me_2[18]aneN_2S_4)](PF_6)_2$

$[Ni(Me_2[18]aneN_2S_4)](PF_6)_2$ was prepared using the same method as for the non-methylated analogue, and isolated as a blue solid.

The f.a.b. mass spectrum of this product shows peaks with the correct isotopic distributions at M^+ = 557, 431 and 412, which are assigned to

$$[^{58}Ni(Me_2[18]aneN_2S_4)PF_6]^+,$$

$$[^{58}Ni(Me_2[18]aneN_2S_4)H_2O+H]^+ \text{ and}$$

$$[^{58}Ni(Me_2[18]aneN_2S_4)]^+ \text{ respectively.}$$

Microanalytical and I.R. spectroscopic data are also consistent with the above formulation.

2.2.9: Electronic Spectra

The UV/vis spectrum of $[Ni([18]aneN_2S_4)]^{2+}$ reveals, in addition to two intense charge-transfer bands, two much weaker d-d transitions at λ_{max} = 824nm (ε_{max} = $68M^{-1}cm^{-1}$) and 546 (68). The di-methylated complex, $[Ni(Me_2[18]aneN_2S_4)]^{2+}$, also shows two intense charge-transfer bands and two d-d bands at 903 (59) and 574 (53). For a d^8 transition metal in an octahedral field, three d-d transitions are predicted. The highest energy transition, corresponding to $^3A_2 \longrightarrow {}^3T_1$, is probably obscured beneath the intense charge-transfer bands. The lowest energy transition corresponds to $^3A_{2g} \longrightarrow {}^3T_{2g}$ = 10Dq. This enables a comparison of ligand field splitting parameters for a series of nitrogen and sulphur-donor macrocycles in an octahedral field (Table

2.10). As expected, the ligand field exerted on Ni(II) by [18]aneN_2S_4 is intermediate between that of the related 18-membered ring homoleptic hexa-aza and hexathia systems, and higher than that of its di-methylated analogue, reflecting the weaker ligand field exerted by tertiary aza-functions over secondary [5]. Furthermore, the intensities of the d-d transitions in $[Ni([18]aneN_2S_4)]^{2+}$ and $[Ni(Me_2[18]aneN_2S_4)]^{2+}$ are higher than for any of the homoleptic systems, particularly those which are rigorously centrosymmetric, reflecting the lower symmetry imposed by the incorporation of mixed donors.

Table 2.10: Electronic Spectral Data for Octahedral Ni(II) N- and S-Donor Macrocyclic Complexes

Complex	λ_{max} (nm)	(ε_{max}) ($M^{-1}cm^{-1}$)	10Dq (cm^{-1})	Ref.
$[Ni([9]aneN_3)_2]^{2+}$	816	(107)	12500	74
	549	(97)		
$[Ni([18]aneN_6)]^{2+}$	893	(21)	11200	75
	552	(64)		
$[Ni([18]aneN_2S_4)]^{2+}$	824	(21)	12135	this work
	546	(68)		
$[Ni(Me_2[18]aneN_2S_4)]^{2+}$	903	(59)	11075	this work
	574	(53)		
$[Ni([9]aneS_3)_2]^{2+}$	790	(30)	12755	99
	530	(30)		
$[Ni([12]aneS_3)_2]^{2+}$	890	(25)	11240	76
	570	(34)		
$[Ni([18]aneS_6)]^{2+}$	815	(25)	12290	58
	520	(27)		
$[Ni([24]aneS_6)]^{2+}$	905	(100)	11050	58
	590	(70)		

2.2.10: Electrochemical Study of $[Ni([18]aneN_2S_4]^{2+}$ and $[Ni(Me_2[18]aneN_2S_4)]^{2+}$

Cyclic voltammetry of $[Ni([18]aneN_2S_4)](PF_6)_2$ measured in MeCN (0.1M $NBu^n_4PF_6$ supporting electrolyte) at platinum electrodes reveals two chemically reversible redox processes at $E_{1/2}$= +0.98V (Fig. 2.7) and -1.51V *vs.* Fc/Fc^+ (Fig. 2.8). The former process is assigned to a one-electron oxidation generating the corresponding Ni(III) species, on the grounds that a 1:1 peak-to-peak ratio is obtained upon addition of an equimolar quantity of ferrocene. However, coulometric measurements performed to confirm the nature of this oxidative process consistently gave n> 1-electron, and provided clear evidence for some subsequent process occurring in solution. We therefore suggest that generation of the Ni(III) complex is followed by either ligand deprotonation at an N-H function, or alternatively, a process similar to that observed recently in $[Rh([9]aneS_3)_3]^{3+}$ [77]. This Rh(III) complex readily undergoes deprotonation at a C-H function, which is accompanied by C-S bond cleavage yielding the 2+ cation, $[Rh([9]aneS_3)([9]aneS_3-H)]^{2+}$, incorporating a vinyl function (Chapter 3).

Fig. 2.7:

Oxidative cyclic voltammogram of

$[Ni([18]aneN_2S_4)]^{2+}$ (MeCN/0.1M $NBu^n_4PF_6$)

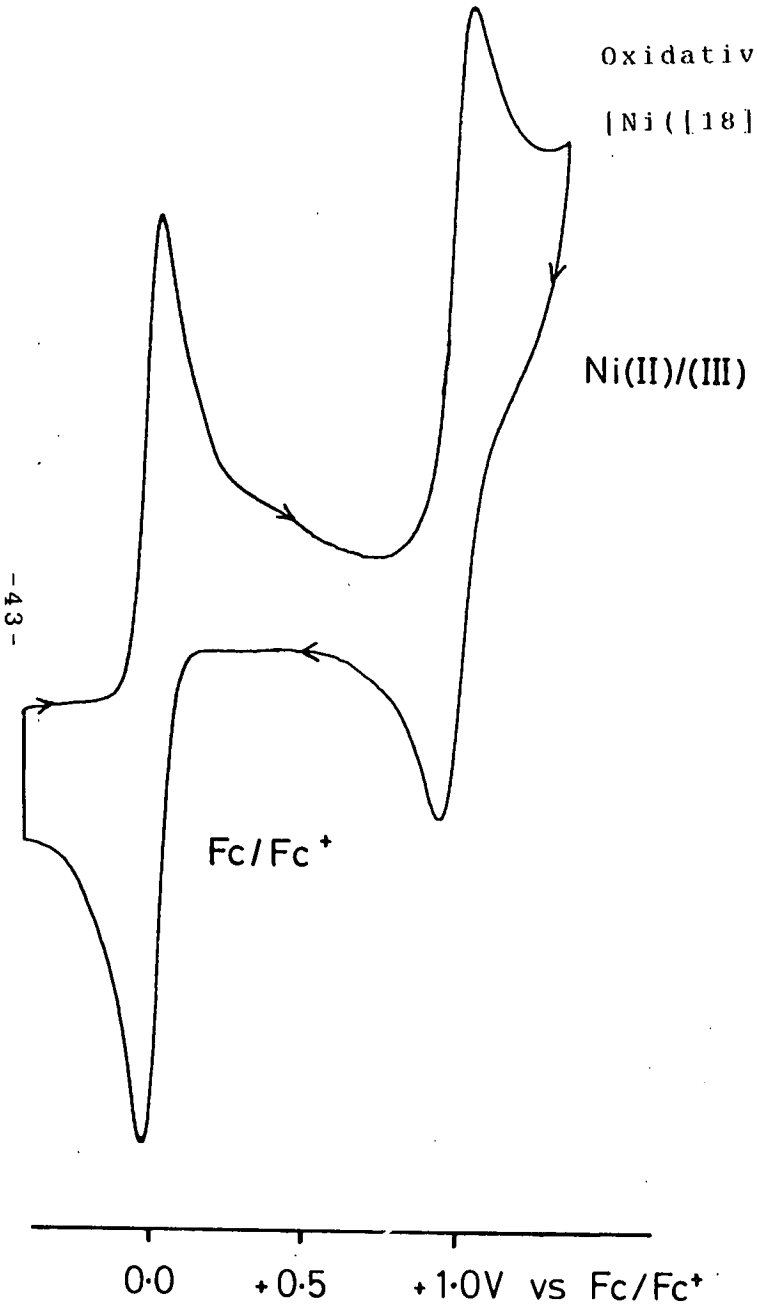

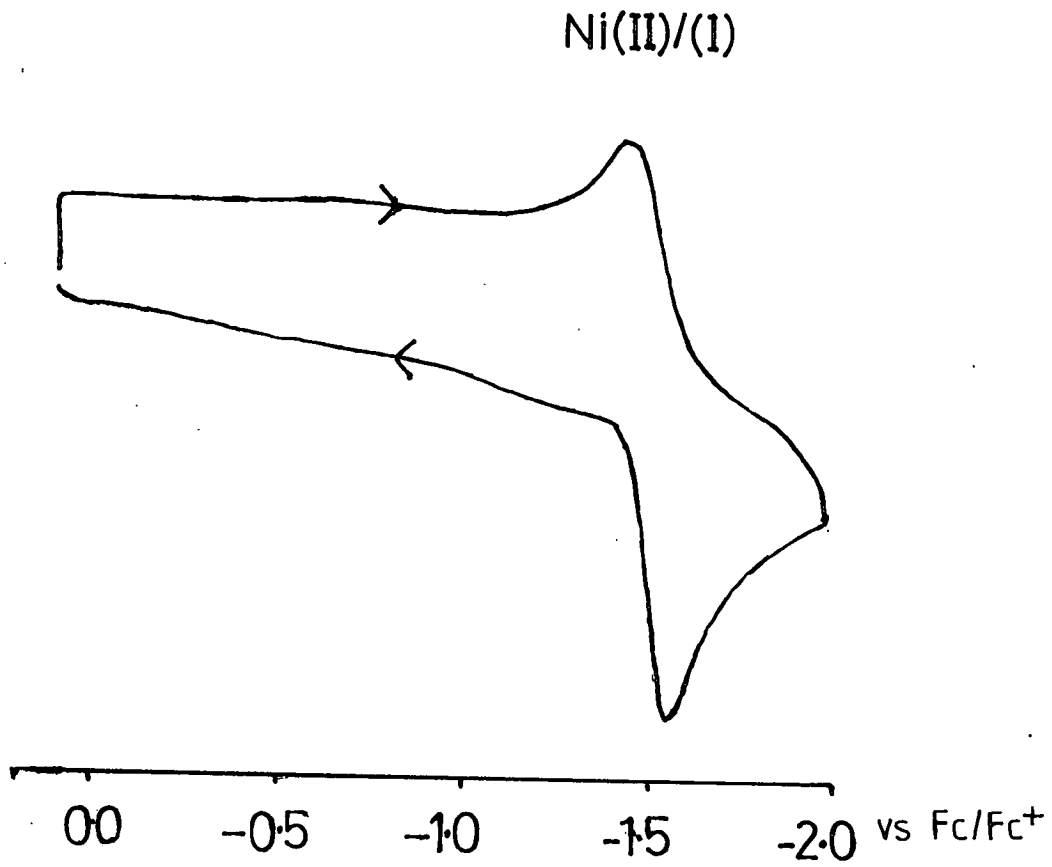

Fig. 2.8: Reductive cyclic voltammogram of

$[Ni([18]aneN_2S_4)]^{2+}$ (MeCN/0.1M $NBu^n_4PF_6$)

Controlled potential electrolysis of $[Ni([18]aneN_2S_4)]^{2+}$ at +1.15V in MeCN at a platinum basket generates a deep red paramagnetic solution initially. The e.s.r. spectrum (Fig. 2.9) of this product (measured at 77K as an MeCN glass) shows a strong anisotropic signal with g_1= 2.129, g_2= 2.104, g_3= 2.027, consistent with the formation of a d^7 Ni(III) species [78-80].

A very similar spectrum is obtained by chemical oxidation using 60% $HClO_4$, giving g_1= 2.108, g_2= 2.071, g_3= 2.037. The enhanced stability of this $[Ni([18]aneN_2S_4)]^{3+}$ in acidic media is consistent with the proposed occurrence of a deprotonation process during electrochemical oxidation.

The latter redox process is attributed to a Ni(II)/(I) couple. However, no stable Ni(I) species could be detected during bulk electrolysis. This may be due to the highly cathodic reduction potential.

The related bis-trithia system, $[Ni([9]aneS_3)_2]^{2+}$, shows a reversible Ni(II)/(III) couple at $E_{1/2}$= +0.97V *vs.* Fc/Fc^+ [98]. A quasi-reversible Ni(II)/(I) couple is also apparent at $E_{1/2}$= -1.11V *vs.* Fc/Fc^+ at -25°C. This reduction potential is more anodic compared to $[Ni([18]aneN_2S_4)]^{2+}$, reflecting the softer hexathia donor set.

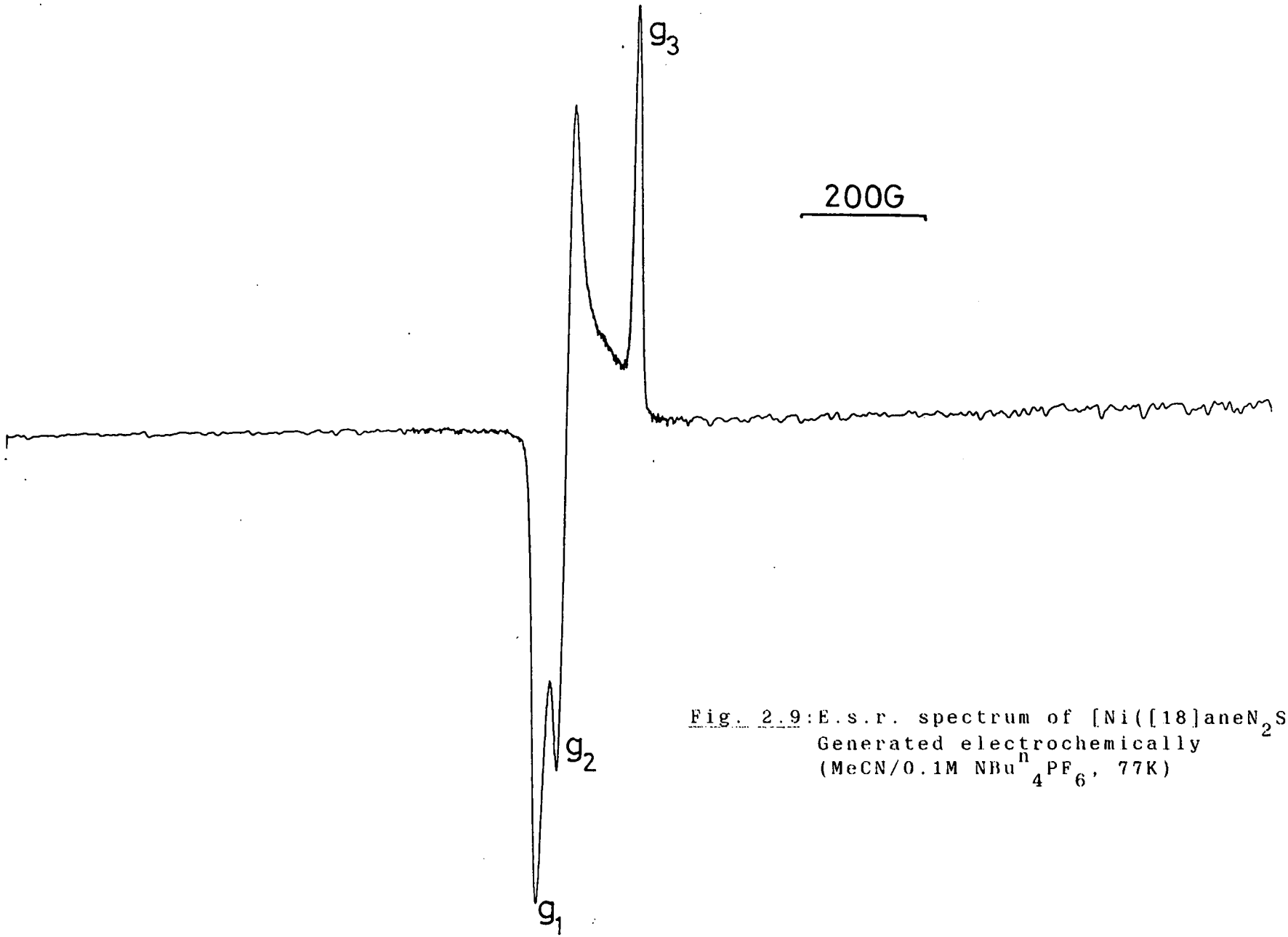

Fig. 2.9: E.s.r. spectrum of $[Ni([18]aneN_2S_4)]^{3+}$. Generated electrochemically ($MeCN/0.1M\ NBu^n_4PF_6$, 77K)

The cyclic voltammogram of $[Ni(Me_2[18]aneN_2S_4)](PF_6)_2$ measured under the same conditions as above exhibits a reversible reduction at $E_{1/2}$= -1.13V *vs.* Fc/Fc^+ (ΔE_p= 70mV at a scan rate of $100mVs^{-1}$). Coulometric measurements performed in MeCN at -1.3V, 298K gave n= 1.08 electrons, suggesting that this corresponds to a Ni(II)/(I) redox couple. No oxidative process could be clearly discerned in the range of the solvent (up to +2.0V). The more anodic Ni(II)/(I) couple for the di-methylated compared to $[Ni([18]aneN_2S_4)]^{2+}$ is in accord with results obtained for the Cu analogues, where the Cu(II)/(I) redox couple is also more accessible for the di-methylated complex. This suggests that that the complexes have similar stereochemical characteristics. In order to confirm the stereochemistry of $[Ni(Me_2[18]aneN_2S_4)]^{2+}$ a single crystal structure determination was undertaken.

2.2.11: Single Crystal Structure of $[Ni(Me_2[18]aneN_2S_4)](PF_6)_2$

Details of the X-ray structural analysis are given in the Experimental Section. Unfortunately, the diffraction data collected showed crystallographically imposed 3-fold symmetry, suggesting severe disorder of the macrocyclic S and N-Me functions, as identified previously in $[Cu(Me_2[18]aneN_2S_4)](PF_6)_2$ (2.2.6). In the Ni(II) complex, however, the quality of the data was

poorer, with the result that full structure solution and refinement was not possible.

The X-ray structure determination on $[Ni(Me_2[18]aneN_2S_4)](PF_6)_2$ shows that this complex crystallises with very similar diffraction symmetry to its Cu(II) analogue ($P\bar{3}m1$). Furthermore, the unit cell parameters are very similar. This evidence strongly suggests that the two complexes exhibit similar stereochemistries. Thus, Ni(II) is also co-ordinated to an octahedral arrangement of all six macrocyclic donor atoms, with the complex probably adopting a meso-configuration (Fig. 2.10).

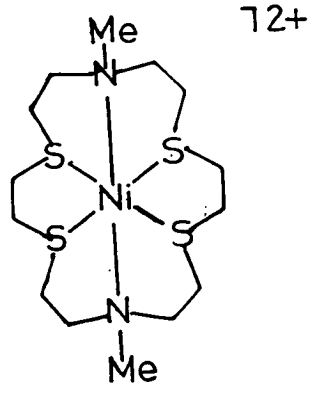

Fig. 2.10: Proposed structure of $[Ni(Me_2[18]aneN_2S_4)]^{2+}$

2.2.12: $[Fe([18]aneN_2S_4)](BPh_4)_2$

Treatment of $FeCl_2.4H_2O$ with one molar equivalent of $[18]aneN_2S_4$ in refluxing dry, degassed MeCN for 1h afforded a deep blue precipitate. After cooling, this solid was collected, washed with MeCN and diethyl ether, and dried *in vacuo*.

The I.R. spectrum of this complex shows a band at $3130cm^{-1}$ corresponding to an N-H stretching vibration (υ(N-H)). Other bands observed are indicative of the presence of co-ordinated macrocycle, with the exception of a strong peak at $280cm^{-1}$, which is assigned to a Fe-Cl stretching vibration (υ(Fe-Cl)). The f.a.b. mass spectrum shows molecular ion peaks at M^+= 417 and 382, which are assigned to $[^{56}Fe([18]aneN_2S_4)Cl]^+$ and $[^{56}Fe([18]aneN_2S_4-H)]^+$ respectively. These data indicate the formulation $[Fe([18]aneN_2S_4)Cl_2]$.

Metathesis of this dichloro-species with $NaBPh_4$, yielded the complex $[Fe([18]aneN_2S_4)](BPh_4)_2$ as a blue solid. Recrystallisation from $MeCN/H_2O$ afforded blue crystals as well as some decomposition product.

There is no evidence for co-ordinated Cl^- in the I.R. spectrum of this product. F.a.b. mass spectroscopy reveals a molecular ion peak at M^+= 381, corresponding to $[^{56}Fe([18]aneN_2S_4-H)]^+$. Both the $[Fe([18]aneN_2S_4)]^{2+}$ cation and the dichloride salt readily hydrolyse in solution. For this reason we were unable to obtain good microanalytical data for either of these species.

2.2.13: Single Crystal Structure of

$[Fe([18]aneN_2S_4)](BPh_4)_2.2MeCN.1/2MeOH$

The single crystal structure of this complex was determined in order to elucidate the stereochemistry and macrocyclic conformation adopted around Fe(II).

Details of the structure solution are given in the Experimental Section. Selected bond lengths, angles and torsions are listed in Tables 2.11, 2.12 and 2.13 respectively. An ORTEP plot showing the geometry of the cation is presented in Fig. 2.11.

The structure confirms a rac-configuration for $[Fe([18]aneN_2S_4)]^{2+}$, with all six macrocyclic donor atoms bound to the Fe(II) centre [Fe-S(1)= 2.2674(15), Fe-S(4)= 2.2673(16), Fe-S(10)= 2.2578(17), Fe-S(13)= 2.2588(16), Fe-N(7)= 2.037(5), Fe-N(16)= 2.022(4)Å]. The overall stereochemistry of the cation, therefore, is very similar to that observed for $[Ni([18]aneN_2S_4)]^{2+}$, and confirms a preference for this macrocycle to adopt a rac-configuration. A significant tetrahedral distortion of the sulphur-donor atoms out of the least-squares S(1), S(4), S(10), S(13) plane is evident, with S(1) and S(13) lying above the plane by +0.1372 and +0.1387Å respectively, and S(4) and S(10) lying below the plane by -0.1368 and -0.1391Å respectively. The magnitude of the distortion is less than that of the Ni(II) analogue, presumably reflecting the smaller ionic radius of low spin Fe(II) over Ni(II) (0.75 and 0.83Å respectively [80]).

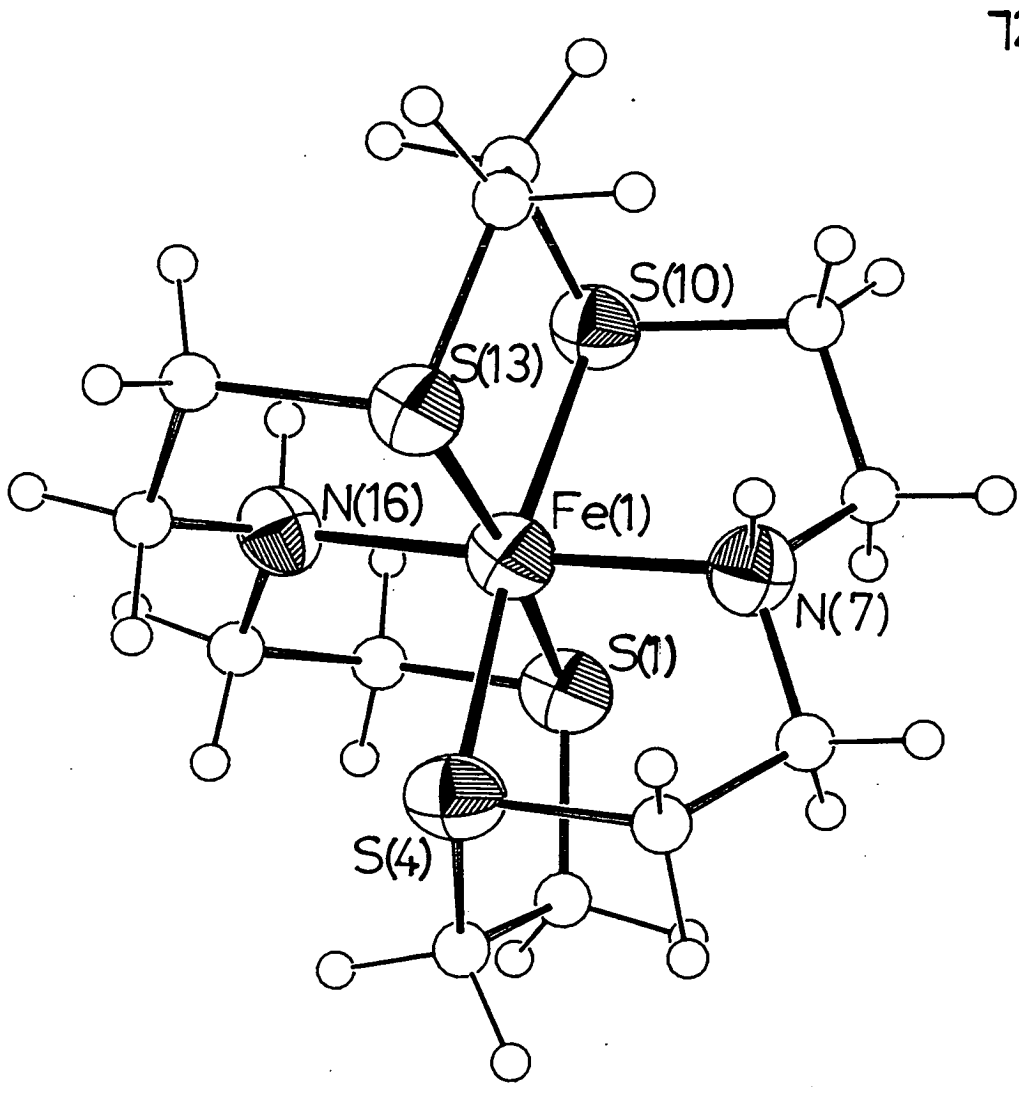

Fig. 2.11: View of the single crystal structure of $[Fe([18]aneN_2S_4)]^{2+}$

Single Crystal Structure of

$[Fe([18]aneN_2S_4)](BPh_4)_2.2MeCN.1/2MeOH$

Table 2.11: Selected Bond Lengths(Å) with e.s.d.'s

Fe(1) - S(1)	2.2674(15)	C(6) - N(7)	1.485(7)
Fe(1) - S(4)	2.2673(16)	N(7) - C(8)	1.498(8)
Fe(1) - N(7)	2.037(5)	C(8) - C(9)	1.524(9)
Fe(1) -S(10)	2.2578(17)	C(9) -S(10)	1.819(7)
Fe(1) -S(13)	2.2588(16)	S(10) -C(11)	1.822(6)
Fe(1) -N(16)	2.022(4)	C(11) -C(12)	1.526(9)
S(1) - C(2)	1.826(6)	C(12) -S(13)	1.817(6)
S(1) -C(18)	1.826(6)	S(13) -C(14)	1.804(6)
C(2) - C(3)	1.503(8)	C(14) -C(15)	1.532(9)
C(3) - S(4)	1.823(6)	C(15) -N(16)	1.477(8)
S(4) - C(5)	1.843(6)	C(16) -C(17)	1.503(7)
C(5) - C(6)	1.528(8)	C(17) -C(18)	1.518(8)

Table 2.12: Selected Angles(^{o}) with e.s.d.'s

S(1)-Fe(1) - S(4)	90.66(5)	S(4) - C(5) - C(6)	108.6(4)
S(1)-Fe(1) - N(7)	92.50(13)	C(5) - C(6) - N(7)	108.2(5)
S(1)-Fe(1) -S(10)	90.16(6)	Fe(1) - N(7) - C(6)	112.1(3)
S(1)-Fe(1) -S(13)	172.77(6)	Fe(1) - N(7) - C(8)	114.0(4)
S(1)-Fe(1) -N(16)	86.02(13)	C(6) - N(7) - C(8)	111.2(4)
S(4)-Fe(1) - N(7)	85.61(13)	N(7) - C(8) - C(9)	108.0(5)
S(4)-Fe(1) -S(10)	173.20(6)	C(8) - C(9) -S(10)	112.1(4)
S(4)-Fe(1) -S(13)	90.46(6)	Fe(1) -S(10) - C(9)	98.06(21)
S(4)-Fe(1) -N(16)	91.94(13)	Fe(1) -S(10) -C(11)	106.55(20)
N(7)-Fe(1) -S(10)	87.62(13)	C(9) -S(10) -C(11)	104.0(3)
N(7)-Fe(1) -S(13)	94.71(13)	S(10) -C(11) -C(12)	114.5(4)
N(7)-Fe(1) -N(16)	177.13(18)	C(11) -C(12) -S(13)	114.7(4)
S(10)-Fe(1) -S(13)	89.56(6)	Fe(1) -S(13) -C(12)	106.68(20)
S(10)-Fe(1) -N(16)	94.85(13)	Fe(1) -S(13) -C(14)	98.99(21)
S(13)-Fe(1) -N(16)	86.80(13)	C(12) -S(13) -C(14)	103.3(3)
Fe(1)- S(1) - C(2)	103.46(20)	S(13) -C(14) -C(15)	110.5(4)
Fe(1)- S(1) -C(18)	100.00(19)	C(14) -C(15) -N(16)	108.7(5)
C(2)- S(1) -C(18)	101.4(3)	Fe(1) -N(16) -C(15)	114.4(4)
S(1)- C(2) - C(3)	112.8(4)	Fe(1) -N(16) -C(17)	112.1(3)
C(2)- C(3) - S(4)	113.5(4)	C(15) -N(16) -C(17)	111.4(4)
Fe(1)- S(4) - C(3)	103.29(20)	N(16) -C(17) -C(18)	108.7(4)
Fe(1)- S(4) - C(5)	99.95(19)	S(1) -C(18) -C(17)	109.3(4)
C(3)- S(4) - C(5)	101.3(3)		

Table 2.13: Selected Torsion Angles(°) with e.s.d.'s

C(18)	- S(1)	- C(2)	- C(3)	-68.8(5)
C(8)	- C(9)	-S(10)	-C(11)	79.1(5)
C(2)	- S(1)	-C(18)	-C(17)	130.8(4)
C(9)	-S(10)	-C(11)	-C(12)	-78.3(5)
S(1)	- C(2)	- C(3)	- S(4)	-46.8(5)
S(10)	-C(11)	-C(12)	-S(13)	-32.6(6)
C(2)	- C(3)	- S(4)	- C(5)	-69.1(5)
C(11)	-C(12)	-S(13)	-C(14)	-79.6(5)
C(3)	- S(4)	- C(5)	- C(6)	130.7(4)
C(12)	-S(13)	-C(14)	-C(15)	79.8(5)
S(4)	- C(5)	- C(6)	- N(7)	-50.8(5)
S(13)	-C(14)	-C(15)	-N(16)	49.2(6)
C(5)	- C(6)	- N(7)	- C(8)	-175.9(5)
C(14)	-C(15)	-N(16)	-C(17)	-174.2(5)
C(6)	- N(7)	- C(8)	- C(9)	-172.7(5)
C(15)	-N(16)	-C(17)	-C(18)	-177.0(5)
N(7)	- C(8)	- C(9)	-S(10)	49.2(6)
N(16)	-C(17)	-C(18)	- S(1)	-49.6(5)

2.3: Conclusions

The mixed N_2S_4 donor macrocycles, [18]aneN_2S_4 and Me_2[18]aneN_2S_4, can readily encapsulate a series of first row transition metal ions, (Cu(II), Ni(II) and Fe(II)), in an octahedral field. [18]aneN_2S_4 exhibits a clear preference for the chiral (±) racemic-configuration in which two S-N-S donor sets bind meridionally to the central metal. In contrast, octahedral Cu(II) and Ni(II) complexes incorporating the di-N-methylated analogue, Me_2[18]aneN_2S_4 prefer to adopt a meso-configuration involving facial co-ordination of two S-N-S donor sets to the metal centre. These represent the first structurally characterised complexes of these ligands. [18]aneN_2S_4 stabilises Ni in the +1, +2 and +3 oxidation states and Cu in the +1 and +2 states. The low-valent (+1) species can be stabilised further by di-N-methylation of the macrocycle. This stabilisation is attributed to the difference in stereochemistry between the parent M(II) complexes.

These complexes may therefore be potentially useful models for biological systems. Indeed, the crystal structure of a stable binuclear Cu(I) complex, $[Cu_2(Me_2[18]aneN_2S_4)(NCMe)_2]^{2+}$, shows Cu(I) bound tetrahedrally to an N_2S_2 donor set similar to that found in Type 1 blue copper proteins.

2.4: Experimental

2.4.1: Methylation of [18]aneN_2S_4 [61]

[18]aneN_2S_4 (100mg, 0.306mmol) was heated for 24h at 96°C in 98% formic acid (1.5ml)/formaldehyde (4ml) under N_2. On cooling to room temperature, 15% NaOH (8.5ml) was added giving pH= 10. Extracting with $CHCl_3$ (8x5ml), drying ($MgSO_4$), removal of solvent and recrystallisation from $CHCl_3$/hexane gave colourless needles (Yield: 87mg, 80%). Mol. wt. 354.64. Elemental analysis: found C= 42.6, H= 8.68, N= 7.00%; calculated for $[C_{14}H_{30}N_2S_4].2H_2O$: C= 43.0, H= 8.77, N= 7.17%. F.a.b. mass spectrum (3-NOBA matrix): found M^+= 355; calculated for $[C_{14}H_{30}N_2S_4]$ M^+= 354. ^1H n.m.r. spectrum (80.13MHz, $CDCl_3$, 298K): δ= 2.76 (s, $NC\underline{H}_2$, 8H), 2.63 (s, $SC\underline{H}_2$, 16H), 2.25ppm (s, $C\underline{H}_3$, 6H). ^{13}C DEPT n.m.r. spectrum (50.32MHz, $CDCl_3$, 298K): δ= 57.20 ($N\underline{C}H_2$), 42.30 ($\underline{C}H_3$), 32.27 and 29.73ppm (2x$S\underline{C}H_2$).

2.4.2: [Cu([18]aneN_2S_4)]$(PF_6)_2$

$Cu(NO_3)_2.6H_2O$ (36mg, 0.123mmol) was added to a refluxing solution of [18]aneN_2S_4 (40mg, 0.123mmol) in EtOH/H_2O (1:1 v.v., 40ml). The resulting mixture was refluxed for 1h under N_2 yielding a bright green solution. Addition of excess NH_4PF_6 gave a green precipitate which was recrystallised from aqueous solution to give green crystals (Yield: 70mg, 84%). Mol. wt. 680.055. Elemental analysis: found C= 20.5, H= 3.84, N= 4.05, S= 19.1%; calculated for

$[C_{12}H_{26}N_2S_4Cu](PF_6)_2$: C= 21.2, H= 3.85, N= 4.12, S= 18.9%. F.a.b. mass spectrum (3-NOBA matrix): found M^+= 535, 389; calculated for

$[^{63}Cu([18]aneN_2S_4)PF_6]^+$ M^+= 534,

$[^{63}Cu([18]aneN_2S_4)]^+$ M^+= 389.

UV/vis spectrum (MeCN): λ_{max}= 612nm (ε_{max}= 202$M^{-1}cm^{-1}$), 395 (2,460), 302 (1,970). I.R. spectrum (KBr disc): 3270m, 3160w, 2920w, 2840w, 1465m, 1425m, 1410m, 1320w, 1300w, 1280w, 1260w, 1090w, 1070m, 1020w, 1000w, 970m, 840vs, 780w, 740w, 640w, 555vs, 445w cm^{-1}.

2.4.3: $[Cu(Me_2[18]aneN_2S_4)](PF_6)_2$

Method as for 2.4.2 above, using $Cu(NO_3)_2.6H_2O$ (34mg, 0.113mmol) and $Me_2[18]aneN_2S_4$ (40mg, 0.113mmol). The product was isolated as deep green crystals (Yield: 70mg, 84%). Mol. wt. 708.11. Elemental analysis: found C= 24.0, H= 4.28, N= 3.97, S= 16.9%; calculated for $[C_{14}H_{30}N_2S_4Cu](PF_6)_2$: C= 23.8, H= 4.27, N= 3.96, S= 18.1%. F.a.b. mass spectrum (3-NOBA matrix): found M^+= 563, 433 and 417; calculated for

$[^{63}Cu(Me_2[18]aneN_2S_4)PF_6]^+$ M^+= 562,

$[^{63}Cu(Me_2[18]aneN_2S_4)H_2O]^+$ M^+= 435,

$[^{63}Cu(Me_2[18]aneN_2S_4)]^+$ M^+= 417.

UV/vis spectrum (MeCN): λ_{max}= 667nm (ε_{max}= 503$M^{-1}cm^{-1}$), 414 (9,060). I.R. spectrum (KBr disc): 2980w, 2920w, 2860w, 1465m, 1435m, 1320w, 1290w, 1280w, 1260w, 1225w, 1210w, 1160w, 1135w, 1090w, 1070w, 1050w, 1015m, 1000w, 980m, 840vs, 740w, 720w, 640w, 620w, 555vs, 460w cm^{-1}.

Single Crystal Structure Determinations

The following computer programs were used in the solution and refinement of the crystal structures; SHELX76 [82], SHELX86 [83], CALC [84], DIRDIF [85], DIFABS [86]. The learnt-profile method used was that of Ref.87. The scattering factor curves for elements not inlaid in SHELX76 were taken from Ref.88. The graphics programs ORTEP [89] and PLUTO [90] were used to obtain plots of the molecules.

2.4.4: Single Crystal Structure of

$[Cu(Me_2[18]aneN_2S_4)](PF_6)_2$

Blue needles of this complex were obtained by recrystallisation from MeCN.

Crystal Data:

$[C_{14}H_{30}N_2S_4Cu](PF_6)_2$, M= 708.0. Trigonal, space group $P\bar{3}m1$, a= 10.5140(4), c= 6.6604(5)Å, V= 637.6Å^3 (by least-squares refinement on diffraction angles for 35 centred reflections measured at $\pm\omega$ [$28<2\theta<30^o$, λ= 0.71073Å]), Z= 1, D_c= 1.84gcm^{-3}. Crystal dimensions 0.72x0.12x0.12mm, μ(Mo-Kα)=13.9cm^{-1}, F(000)= 359.

Data Collection and Processing:

Stoe STADI-4 four-circle diffractometer, $\omega/2\theta$ scan mode with ω scan-width $(1.05+0.347\tan\theta)^o$. Graphite-monochromated Mo-Kα radiation; 1261 data collected (two asymmetric units), 728 unique ($2\theta_{max}$= 60^o,

h $-12 \longrightarrow 12$, k $0 \longrightarrow 14$, l $0 \longrightarrow 9$) giving 447 with $\underline{F} > 6\sigma(\underline{F})$. No significant crystal decay, no absorption correction.

Structure Analysis and Refinement:

The Cu atom was fixed at the origin, and a Patterson function located the phosphorus and partial sulphur atom. Other non-H atoms were located by successive least-squares refinements and difference Fourier syntheses. The cation was found to be disordered on a site of D_{3d} symmetry, the 1/3 occupied N-Me function being superimposed on the 2/3 occupied S, with N-S= 0.73 and S-Me= 0.68Å. A single carbon in a general position refined well for all twelve methylene atoms. The PF_6^- anion also exhibited severe disorder, with a four-fold axis of the ion coincident with a three-fold axis of the crystal. Hydrogen atoms were placed in fixed, calculated positions. Anisotropic thermal parameters were refined for all non-H atoms except for the methyl carbon. The high thermal parameters indicate that the e.s.d.'s of the derived parameters are somewhat underestimated, but it is clear that the cation adopts a meso-configuration. The weighting scheme $\underline{w}^{-1} = \sigma^2(\underline{F}) + 0.00034\underline{F}^2$ gave satisfactory agreement analyses. At final convergence $\underline{R}$= 0.052, $\underline{R}_w$= 0.058, $\underline{S}$= 1.25 for 57 independent parameters, and the final difference Fourier synthesis showed no feature above 0.37 or below -0.30eÅ^{-3}.

2.4.5: Single Crystal Structure of

$[Cu_2(Me_2[18]aneN_2S_4)(NCMe)_2](PF_6)_2$

Pale green crystals of this complex were obtained by recrystallisation of $[Cu(Me_2[18]aneN_2S_4)](PF_6)_2$ from MeCN/EtOH. The crystal selected was mounted in a 0.5mm capillary to prevent solvent loss.

Crystal Data:

$[C_{18}H_{36}N_2S_4Cu_2](PF_6)_2$, M= 853.79. Triclinic, space group P1, a= 7.3435(18), b= 11.0562(26), c= 11.824(3)Å, α= 62.298(10), β= 81.904(15), γ= 82.764(16), V= 839.5Å^3 (by least-squares refinement on diffraction angles for 22 centred reflections measured at $\pm\omega$ [$22<2\theta<24^o$, λ= 0.71073Å]), Z= 1, D_c= 1.526gcm^{-3}. Crystal dimensions 1.35x0.12x0.08mm, μ(Mo-Kα)= 10.17cm^{-1}, F(000)= 359.

Data Collection and Processing:

Stöe STADI-4 four-circle diffractometer, $\omega/2\theta$ scan mode, with ω scan-width $(1.20+0.347\tan\theta)^o$, graphite-monochromated Mo-Kα radiation; 2187 reflections measured ($2\theta_{max}$= 45^o, h $-7\longrightarrow7$, k $-10\longrightarrow11$, l $0\longrightarrow12$) giving 1208 with $F>4\sigma(F)$. No significant crystal decay, no absorption correction.

Structure Analysis and Refinement:

The Cu position was deduced from a Patterson synthesis. Iterative cycles of least-squares refinement

and difference Fourier syntheses revealed the positions of all other non-hydrogen atoms. During refinement, some disorder of the C atoms adjacent to the aza-functions of the macrocycle became apparent. This was modelled successfully by refining the C-C-N units as rigid groups with idealised bond lengths (1.50Å) and tetrahedral angles around each of these atoms; this identified two equally occupied sites for each C adjacent to N. The PF_6^- counterions also exhibited some disorder which was modelled using partially occupied F atoms, such that the total number of F atoms per P atom summed to six. Macrocyclic H atoms were included in fixed, calculated positions, while the methyl group in CH_3CN was refined as a rigid group. Anisotropic thermal parameters were refined for all non-hydrogen atoms, except for the disordered C atoms. The weighting scheme $\underline{w}^{-1} = \sigma^2(\underline{F}) + 0.009748\underline{F}^2$ gave satisfactory agreement analyses. At final convergance $\underline{R}$= 0.0715, $\underline{R}_w$= 0.0839, $\underline{S}$= 1.105 for 218 independent parameters, and the final difference Fourier synthesis showed no feature above 0.88 or below -0.45eÅ.

2.4.6: $[Ni([18]aneN_2S_4)](PF_6)_2$

Method as for 2.4.2 above, using $Ni(NO_3)_2.6H_2O$ (36mg, 0.123mmol) and $[18]aneN_2S_4$ (40mg, 0.123mmol). The product was isolated as purple crystals (Yield: 70mg, 85%). Mol. wt. 675.22. Elemental analysis: found C= 20.7, H= 4.83, N= 4.32, S= 18.8%; calculated for

$[C_{12}H_{26}N_2S_4Ni](PF_6)_2$: C= 21.3, H= 3.88, N= 4.15, S= 19.0%. F.a.b. mass spectrum (3-NOBA matrix): found M^+= 529 and 383; calculated for

$[^{58}Ni([18]aneN_2S_4)PF_6]^+$ M^+= 529,

$[^{58}Ni([18]aneN_2S_4)]^+$ M^+= 384.

UV/vis spectrum (MeCN): λ_{max}= 824nm (ε_{max}= $68M^{-1}cm^{-1}$), 546 (68), 303 (9,200), 262 (3,350). I.R. spectrum (KBr disc): 3280m, 3180w, 2920m, 2880w, 1555m, 1470m, 1430m, 1420m, 1380w, 1320m, 1290w, 1265w, 1240w, 1210w, 1150w, 1135w, 1090m, 1050w, 1020m, 1000w, 970m, 840vs, 790w, 740m, 640w, 555vs, 460w cm^{-1}.

2.4.7: Single Crystal Structure of

$[Ni([18]aneN_2S_4)](PF_6)_2.1/3H_2O$

Purple crystals of this complex were obtained by recrystallisation from a 1:1 v.v. mixture of MeCN/EtOH. The crystal selected was mounted in a 0.5mm capillary to prevent solvent loss.

Crystal Data:

$[C_{12}H_{26}N_2S_4Ni](PF_6)_2.1/3H_2O$, M= 681.22. Orthorhombic, space group P_{cab}, a= 12.8260(20), b= 18.0825(27), c= 22.200(4)Å, V= 5148.8Å^3 (by least-squares refinement on diffraction angles for 52 centred reflections measured at $\pm\omega$ [$10<2\theta<11^o$, λ= 0.71073Å]). Z= 8, D_c= 1.76gcm^{-3}. Crystal dimensions 0.20x0.20x0.40mm, μ(Mo-Kα)= 17.54cm^{-1}, F(000)= 3280.

Data Collection and Processing:

Stöe STADI-4 four-circle diffractometer, $\omega/2\theta$ scan mode, with learnt profiles, graphite-monochromated Mo-Kα radiation; 3182 reflections measured ($2\theta_{max} = 45^{o}$, h $0 \longrightarrow 12$, k $0 \longrightarrow 19$, l $0 \longrightarrow 23$) giving 1454 with $\underline{F} > 4\sigma(\underline{F})$. No significant crystal decay, no absorption correction.

Structure Analysis and Refinement:

The Ni position was deduced from a Patterson synthesis. Iterative cycles of least-squares refinement and difference Fourier syntheses revealed the positions of all other non-hydrogen atoms. During refinement, some disorder of the C atoms adjacent to the aza-functions of the macrocycle became apparent. This was modelled successfully by refining the C-C-N units as rigid groups with idealised bond lengths (1.50Å) and tetrahedral angles around each of these atoms; this identified two alternative sites for each C adjacent to N, in a ratio 2:3. One of the PF_6^- counterions also showed significant disorder. This was modelled reasonably well by using partially occupied F atoms, such that the total number of F atoms per P atom summed to six. A partially occupied H_2O solvent molecule was found to be associated per cation. H atoms were included in fixed, calculated positions. Anisotropic thermal parameters were refined for Ni, S, P, N, all fully occupied C atoms and all F atoms with greater than 50% occupancy. The weighting scheme $\underline{w}^{-1} = \sigma^2(\underline{F}) + 0.002170\underline{F}^2$ gave satisfactory agreement

analyses. At final convergance $\underline{R}$= 0.0794, $\underline{R}_w$= 0.0976, $\underline{S}$= 1.167 for 285 independent parameters, and the final difference Fourier synthesis showed no feature above 0.98 or below -0.58e$\mathring{A}^{-3}$.

2.4.8: $[Ni(Me_2[18]aneN_2S_4)](PF_6)_2$

Method as for 2.4.2 above, using $Ni(NO_3)_2.6H_2O$ (36mg, 0.123mmol) and $Me_2[18]aneN_2S_4$ (40mg, 0.123mmol). The product was isolated as a blue microcrystalline solid (Yield: 60mg, 70%). Mol. wt. 702.37. Elemental analysis: found C= 24.3, H= 4.24, N= 4.17, S= 18.2%; calculated for $[C_{14}H_{30}N_2S_4Ni](PF_6)_2$: C= 23.9, H= 4.31, N= 3.99, S= 18.3%. F.a.b. mass spectrum (3-NOBA matrix): found M^+= 557, 431 and 412; calculated for

$[^{58}Ni(Me_2[18]aneN_2S_4)PF_6]^+$ M^+= 557,

$[^{58}Ni(Me_2[18]aneN_2S_4)H_2O]^+$ M^+= 430,

$[^{58}Ni(Me_2[18]aneN_2S_4)]^+$ M^+= 412.

UV/vis spectrum (MeCN): λ_{max}= 903nm (ε_{max}= 59$M^{-1}cm^{-1}$), 574 (53), 312 (5,230), 273 (2,960). I.R. spectrum (KBr disc): 3010w, 2940w, 1470m, 1430m, 1380w, 1320m, 1270w, 1230w, 1210w, 1160w, 1140w, 1070w, 1030w, 1005w, 990m, 840vs, 745m, 685w, 640w, 620w, 555vs, 460w cm^{-1}.

2.4.9: Single Crystal Structure of

$[Ni(Me_2[18]aneN_2S_4)](PF_6)_2$

Recrystallisation of this complex from a 1:1 v.v. mixture of MeCN/EtOH yielded pale blue crystals suitable for an X-ray crystallographic study. A single crystal was

selected and sealed in a 0.5mm capillary to prevent solvent loss.

Crystal Data:

$[C_{14}H_{30}N_2S_4Ni](PF_6)_2$. M= 702.7. Trigonal, space group $P\bar{3}m1$, a= 10.408(12), c= 6.777(5)Å, V= 635.77Å^3 (by least-squares refinement on diffraction angles for 8 centred reflections measured at $\pm\omega$ [λ= 0.71073Å]), Z= 1, D_c= 1.83gcm^{-3}.

Data Collection and Processing:

Stöe STADI-4 four-circle diffractometer, $\omega/2\theta$ scan mode, with ω scan-width $(1.05+0.347\tan\theta)^o$. Graphite-monochromated Mo-Kα radiation; 606 reflections measured ($2\theta_{max}$= 60^o, h -9⟶10, k 0⟶11, l 0⟶7). No significant crystal decay.

Structure Analysis and Refinement:

The Ni position was located from a Patterson synthesis, however, development of the structure was hampered by extreme disorder of the macrocyclic S and N-Me atoms.

2.4.10: $[Fe([18]aneN_2S_4)Cl_2]$

Reaction of $FeCl_2.4H_2O$ (22mg, 0.107mmol) and $[18]aneN_2S_4$ (35mg, 0.107mmol) in refluxing dry, degassed MeCN (35ml) for 1h under N_2 afforded a deep blue precipitate, which was filtered, washed with MeCN and

diethyl ether and dried *in vacuo* (Yield: 40mg, 83%). Mol. wt. 453.34. F.a.b. mass spectrum (3-NOBA matrix): found M^+= 417 and 381; calculated for

$[^{56}Fe([18]aneN_2S_4)^{35}Cl]^+$ M^+= 417,

$[_{56}Fe([18]aneN_2S_4)]^+$ M^+= 382.

I.R. spectrum (KBr disc): 3130m, 2960w, 2920w, 2860w, 1465m, 1430m, 1315m, 1290w, 1250w, 1230w, 1200w, 1110m, 1070m, 1015m, 995w, 930w, 850w, 820w, 790m, 680w, 630w, 450w, 360w, 280m cm^{-1}.

2.4.11: $[Fe([18]aneN_2S_4)](BPh_4)_2$

Metathesis of the dichloro species above, with $NaBPh_4$ in $MeCN/H_2O$ yielded a blue precipitate. Recrystallisation from MeCN/EtOH gave the product as blue crystals. Mol. wt. 1020.89. F.a.b. mass spectrum (3-NOBA matrix): found M^+= 381; calculated for $[^{56}Fe([18]aneN_2S_4)]^+$ M^+= 382. I.R. spectrum (KBr disc): 3180m, 3040m, 2980w, 2920w, 1575m, 1475m, 1460m, 1420m, 1405m, 1380w, 1305w, 1260w, 1170w, 1120w, 1080w, 1060w, 1030w, 990w, 970w, 920w, 840w, 820w, 785w, 755m, 735vs, 710vs, 610vs, 470w cm^{-1}.

2.4.12: Single Crystal Structure of

$[Fe([18]aneN_2S_4)](BPh_4)_2.2MeCN.1/2CH_3OH$

Recrystallisation of the complex from a 1:1 v.v. mixture of MeCN/EtOH gave deep blue columnar crystals. A single crystal was selected and sealed in a 0.5mm capillary to prevent solvent loss.

Crystal Data:

$[C_{12}H_{26}N_2S_4Fe](C_{24}H_{20}B)_2.2CH_3CN.1/2CH_3OH$,

M= 1143.0. Triclinic, space group $P\bar{1}$, a= 11.8615(8), b= 15.4285(12), c= 17.9412(13)Å, α= 67.301(3), β= 78.542(4), γ= 76.696(3)°, V= 2925.6Å^3 (by least-squares refinement on diffraction angles for 27 centred reflections measured at $\pm\omega$ [$32<2\theta<35°$, λ= 0.71073Å]), Z= 2, D_c= 1.297gcm^{-3}. Crystal dimensions 0.69x0.27x0.27mm, μ(Mo-Kα)= 19.64cm^{-1}, F(000)= 1188.

Data Collection and Processing:

Stöe STADI-4 four-circle diffractometer, $\omega/2\theta$ scan mode using the learnt-profile method. Graphite-monochromated Mo-Kα radiation; 8245 reflections measured ($2\theta_{max}$= 60°, h -13⟶12, k -15⟶17, l -18⟶20) giving 6110 with $F>6\sigma(F)$. No significant crystal decay.

Structure Analysis and Refinement:

The Fe position was deduced from a Patterson synthesis. Iterative cycles of least-squares refinement and difference Fourier synthesis revealed the positions of all other non-hydrogen atoms. Absorption correction was made using 14 ψ-scans (maximum correction= 0.356, minimum= 0.171). Two fully occupied MeCN molecules and one half-occupied MeOH solvent molecule were found to be associated per cation. H atoms were included in fixed, calculated positions, and the phenyl rings of the BPh_4^-

counter-anion were refined as rigid groups. Anisotropic thermal parameters were refined for Fe, S, N, B and C atoms. The weighting scheme $\underline{w}^{-1} = \sigma^2(\underline{F}) + 0.000509\underline{F}^2$ gave satisfactory agreement analyses. At final convergance $\underline{R} = 0.0668$, $\underline{R}_w = 0.0947$, $\underline{S} = 1.232$ for 591 independent parameters, and the final difference Fourier synthesis showed no feature above 0.60 or below $-0.61 e\text{Å}^{-3}$.

CHAPTER 3

Cobalt and Rhodium Complexes of

[18]aneN$_2$S$_4$

3.1: Introduction

The octahedral macrocyclic complexes, $[M([18]aneN_2S_4)]^{x+}$ (M= Fe(II), Ni(II), Cu(II)) have been discussed in Chapter 2, and their redox properties related to the electronic and stereochemical characteristics of the macrocycle. In the course of this work, the ability of this macrocycle to stabilise a range of metal oxidation states has been demonstrated. This is largely attributed to the flexibility of the ligand, enabling it to modify its mode of co-ordination to conform to the preferred stereochemical requirements of each d^n-configuration. These results have prompted an investigation of the co-ordination of this ligand to cobalt and rhodium centres. These metals are of particular interest since they exhibit multi-electron redox behaviour, with the +1, +2 and +3 oxidation states being available.

This has resulted in extensive application of Co and Rh complexes in catalytic processes. For example, Collman *et al* have reported [30] the electrocatalytic four-electron reduction of oxygen to water by a dicobalt cofacial porphyrin, (1). The major advantage of this system is that the catalysed reduction produces water almost exclusively at exceptionally positive potentials, with only trace quantities of H_2O_2 being generated. Schrock and co-workers have demonstrated the use of Rh(I) systems as highly active hydrogenation catalysts[91,92].

Wilkinson's catalyst, $[RhCl(PPh_3)_3]$, mediates a wide range of reactions, including the catalytic hydrogenation of olefins under very mild conditions, and the catalytic decarbonylation of aldehydes and acyl halides [93]. Rhodium complexes have also been shown to mediate C-C bond cleavage in strained alkanes [48]. For example, bicyclo[2.1.0]pentanes are rearranged to cyclopentenes by Rh(I) according to the scheme, (2) [94,95]. Similar behaviour is observed for bicyclo[3.1.0]hexanes [96] and bicyclo[4.1.0]heptanes [97].

(1)

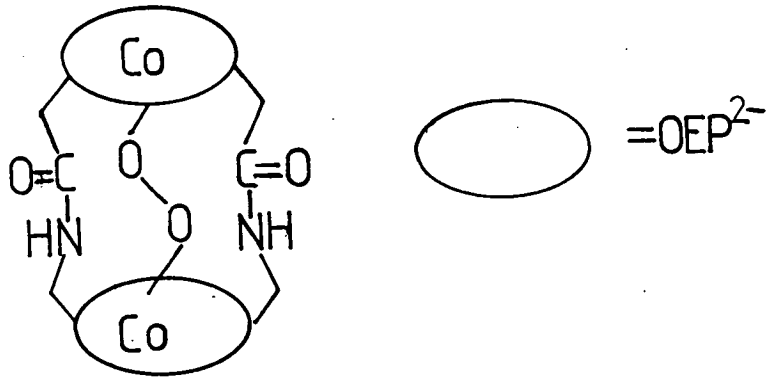

(2)

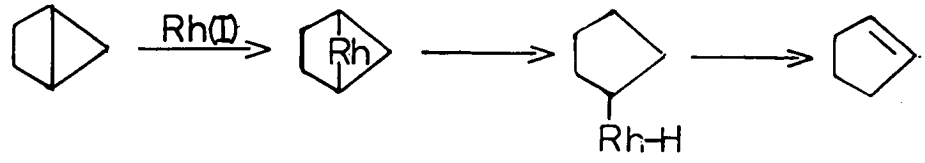

3.2: Results and Discussion

This chapter describes the synthesis and characterisation of Co(II), Co(III) and Rh(III) complexes incorporating [18]aneN_2S_4. An investigation into the electrochemical characteristics of the products is discussed. Finally, a description of the attempt to synthesise the related rhodium hexathia complex, $[Rh([18]aneS_6)]^{3+}$ is given, and the characterisation of an unusual deprotonated species, $[Rh([18]aneS_6\text{-}H)]^{2+}$ is mentioned.

3.2.1: Cobalt

Reaction of $Co(NO_3)_2.6H_2O$ with one molar equivalent of [18]aneN_2S_4 in refluxing $EtOH/H_2O$ afforded a purple solution. Addition of excess PF_6^- counterion gave a purple precipitate, which was recrystallised from acetone, yielding the product as a purple solid.

The f.a.b. mass spectrum of the complex shows molecular ion peaks at M^+= 530 and 384, corresponding to $[^{59}Co([18]aneN_2S_4)PF_6]^+$ and $[^{59}Co([18]aneN_2S_4\text{-}H)]^+$ respectively. This evidence combined with microanalytical and I.R. spectroscopic data confirms the formulation $[Co([18]aneN_2S_4)](PF_6)_2$.

The UV/vis spectrum of $[Co([18]aneN_2S_4)](PF_6)_2$ exhibits two d-d transitions at λ_{max}= 593nm (ε_{max}= $68M^{-1}cm^{-1}$) and 534 (73) in addition to two much more intense S⟶Co charge-transfer absorptions at 298nm (2,390) and 247 (4,795). The energies of the d-d

transitions and the magnitudes of the extinction coefficients are in accord with low-spin Co(II) in an octahedral field [98,99]. The generation of a low-spin Co(II) species with an N_2S_4 donor set reflects the strong ligand field imparted by the thioether-donor atoms. The electronic spectra and magnetic measurements of the related complexes $[Co([9]aneS_3)_2]^{2+}$ and $[Co([9]aneN_3)_2]^{2+}$ are consistent with low- and high-spin Co(II) respectively [99,100]. Sargeson and co-workers have shown that low-spin Co(II) is preferred when encapsulated by a caging N_3S_3 donor ligand [101].

The single crystal X-ray structures of the $[M([18]aneN_2S_4)]^{2+}$, (M= Ni(II), Cu(II) and Fe(II)) discussed in Chapter 2 each shows the central metal ion co-ordinated to an octahedral arrangement of all six donor atoms of the macrocycle, with two S-N-S portions binding meridionally to the metal, generating a rac-configuration for the complex. It therefore seems highly likely that a similar geometry would be observed for $[Co([18]aneN_2S_4)]^{2+}$. A tetragonal distortion similar to that observed in low-spin $[Co([18]aneS_6)]^{2+}$ [$Co-S_{eq}$= 2.251(1), 2.292(1)A, $Co-S_{ap}$= 2.479(1)Å] [57] might be expected, although the hexathia species exhibits a rather more pronounced elongation than is usually observed for low-spin d^7 Co(II). The stereochemistry of the related complex, $[Co(3)_2]^{2+}$ is also severely distorted [57]. However, this cation is probably best described as square planar, with two apical

sulphur-donors interacting weakly at long range [Co-S_{eq}= 2.253(3), 2.253(3), 2.254(3), 2.258(3), Co-S_{ap}= 2.580(3), 2.635(3)Å]. The tetragonal elongation in $[Co([9]aneS_3)_2]^{2+}$ is much smaller, [Co-S= 2.356(6), 2.240(7), 2.367(5)Å] [102].

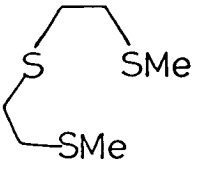

(3)

3.2.2: Single Crystal Structure of $[Co([18]aneN_2S_4)](PF_6)_3.3H_2O$

Aerial oxidation of an aqueous solution of $[Co([18]aneN_2S_4)](PF_6)_2$ gave dark orange crystals which were assigned to the Co(III) complex, $[Co([18]aneN_2S_4)](PF_6)_3$. In order to confirm that this product was a genuine Co(III) complex, and to elucidate the stereochemistry, a single crystal structure determination was undertaken. Furthermore, the synthesis of $[Co([18]aneN_6)]^{3+}$ has been reported [103], but the structures of the Co(III) and Co(II) species have not been determined.

Details of the structure solution and refinement are given in the Experimental Section. Relevant bond lengths, angles and torsions are given in Tables 3.1, 3.2 and 3.3 respectively. Two ORTEP plots illustrating the geometry of the cation are presented in Figs. 3.1 and 3.2.

The structure shows Co(III) bound to all six

macrocyclic donor atoms in a near octahedral geometry. Co-S= 2.2682(13), 2.2488(13), 2.2524(13), 2.2539(13)Å and Co-N= 1.993(4), 1.994(4)Å. The complex adopts a rac-configuration as observed for all other first row complexes with this ligand. There is a tetrahedral distortion of the S-donor atoms out of the least-squares S_4 co-ordination plane. The extent of this distortion is intermediate between that observed in $[Fe([18]aneN_2S_4)]^{2+}$ and $[Ni([18]aneN_2S_4)]^{2+}$ (Chapter 2), with S(1) and S(10) lying above the plane by +0.1204 and +0.1199Å respectively and S(4) and S(13) lying below the plane by -0.1196 and -0.1207Å respectively in $[Co([18]aneN_2S_4)]^{3+}$.

Extensive H-bonding is also evident from the structure determination (Table 3.4). This occurs between the three H_2O solvent molecules, the N-H functions of the $[Co([18]aneN_2S_4)]^{3+}$ cation and the PF_6^- anions.

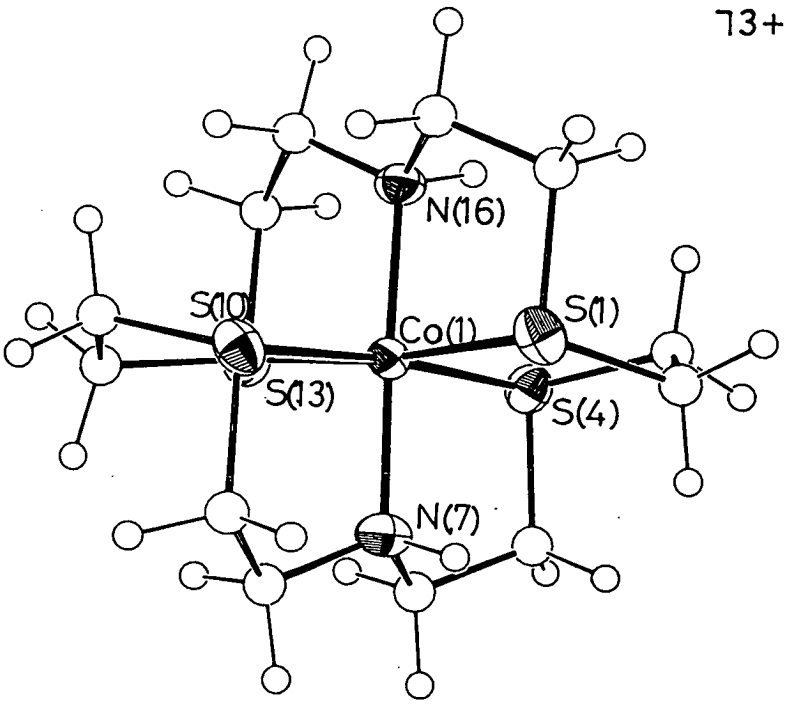

Fig. 3.1: View of the single crystal structure of $[Co([18]aneN_2S_4)]^{3+}$

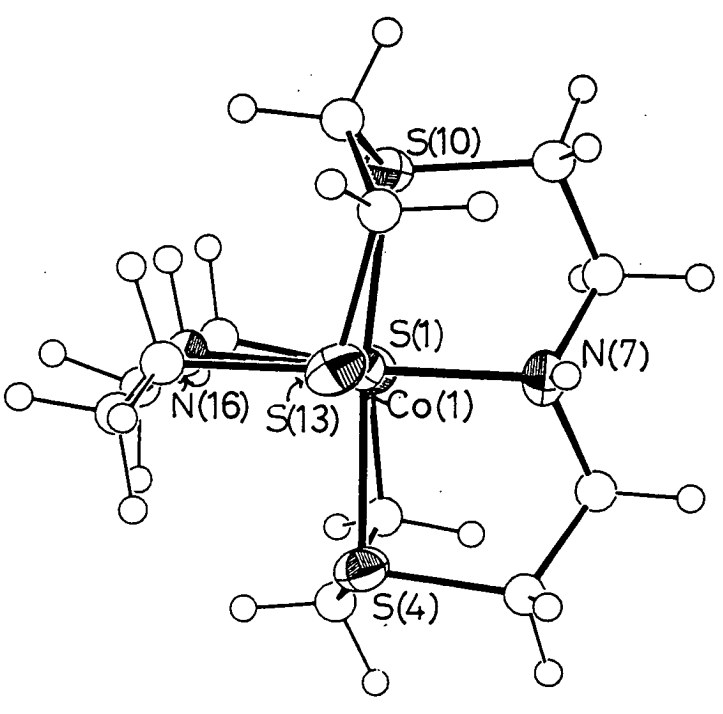

Fig. 3.2: Alternative view of the single crystal structure of $[Co([18]aneN_2S_4)]^{3+}$

Single Crystal Structure of

$[Co([18]aneN_2S_4)](PF_6)_3 \cdot 3H_2O$

Table 3.1: Selected Bond Lengths(Å) with e.s.d.'s

Co(1) - S(1)	2.2682(13)	C(6) - N(7)	1.494(6)
Co(1) - S(4)	2.2488(13)	N(7) - C(8)	1.494(6)
Co(1) - N(7)	1.993(4)	C(8) - C(9)	1.514(7)
Co(1) -S(10)	2.2524(13)	C(9) -S(10)	1.830(5)
Co(1) -S(13)	2.2539(13)	S(10) -C(11)	1.811(5)
Co(1) -N(16)	1.994(4)	C(11) -C(12)	1.499(7)
S(1) - C(2)	1.817(5)	C(12) -S(13)	1.821(5)
S(1) -C(18)	1.831(5)	S(13) -C(14)	1.821(5)
C(2) - C(3)	1.519(7)	C(14) -C(15)	1.496(7)
C(3) - S(4)	1.810(5)	C(15) -N(16)	1.490(6)
S(4) - C(5)	1.828(5)	N(16) -C(17)	1.493(6)
C(5) - C(6)	1.504(7)	C(17) -C(18)	1.495(7)

Table 3.2: Selected Angles(^{o}) with e.s.d.'s

S(1)-Co(1)- S(4)	90.43(5)	S(4) - C(5) - C(6)	108.7(4)
S(1)-Co(1)- N(7)	93.17(12)	C(5) - C(6) - N(7)	108.5(4)
S(1)-Co(1)-S(10)	89.29(5)	Co(1) - N(7) - C(6)	112.2(3)
S(1)-Co(1)-S(13)	173.85(5)	Co(1) - N(7) - C(8)	114.5(3)
S(1)-Co(1)-N(16)	86.21(11)	C(6) - N(7) - C(8)	111.1(4)
S(4)-Co(1)- N(7)	86.26(12)	N(7) - C(8) - C(9)	108.3(4)
S(4)-Co(1)-S(10)	173.88(5)	C(8) - C(9) -S(10)	111.0(4)
S(4)-Co(1)-S(13)	90.48(5)	Co(1) -S(10) - C(9)	98.13(17)
S(4)-Co(1)-N(16)	91.41(11)	Co(1) -S(10) -C(11)	104.45(16)
N(7)-Co(1)-S(10)	87.65(12)	C(9) -S(10) -C(11)	104.37(23)
N(7)-Co(1)-S(13)	92.96(12)	S(10) -C(11) -C(12)	114.9(3)
N(7)-Co(1)-N(16)	177.59(15)	C(11) -C(12) -S(13)	114.3(3)
S(10)-Co(1)-S(13)	90.45(5)	Co(1) -S(13) -C(12)	105.06(16)
S(10)-Co(1)-N(16)	94.67(11)	Co(1) -S(13) -C(14)	97.58(16)
S(13)-Co(1)-N(16)	87.68(11)	C(12) -S(13) -C(14)	104.02(22)
Co(1)- S(1)- C(2)	103.55(17)	S(13) -C(14) -C(15)	111.0(3)
Co(1)- S(1)-C(18)	98.67(16)	C(14) -C(15) -N(16)	109.0(4)
C(2)- S(1)-C(18)	102.16(23)	Co(1) -N(16) -C(15)	114.7(3)
S(1)- C(2)- C(3)	112.1(3)	Co(1) -N(16) -C(17)	111.9(3)
C(2)- C(3)- S(4)	112.9(3)	C(15) -N(16) -C(17)	112.4(3)
Co(1)- S(4)- C(3)	103.91(16)	N(16) -C(17) -C(18)	108.2(4)
Co(1)- S(4)- C(5)	99.65(17)	S(1) -C(18) -C(17)	109.6(3)
C(3)- S(4)- C(5)	102.36(23)		

Table 3.3: Selected Torsion Angles(°) with e.s.d.'s

C(18)	- S(1)	- C(2)	- C(3)	-67.1(4)
C(8)	- C(9)	-S(10)	-C(11)	79.0(4)
C(2)	- S(1)	-C(18)	-C(17)	130.7(3)
C(9)	-S(10)	-C(11)	-C(12)	-71.9(4)
S(1)	- C(2)	- C(3)	- S(4)	-47.7(4)
S(10)	-C(11)	-C(12)	-S(13)	-38.1(5)
C(2)	- C(3)	- S(4)	- C(5)	-68.1(4)
C(11)	-C(12)	-S(13)	-C(14)	-76.3(4)
C(3)	- S(4)	- C(5)	- C(6)	131.8(4)
C(12)	-S(13)	-C(14)	-C(15)	76.0(4)
S(4)	- C(5)	- C(6)	- N(7)	-50.2(5)
S(13)	-C(14)	-C(15)	-N(16)	49.3(4)
C(5)	- C(6)	- N(7)	- C(8)	-176.2(4)
C(14)	-C(15)	-N(16)	-C(17)	-173.1(4)
C(6)	- N(7)	- C(8)	- C(9)	-174.9(4)
C(15)	-N(16)	-C(17)	-C(18)	-174.1(4)
N(7)	- C(8)	- C(9)	-S(10)	48.2(5)
N(16)	-C(17)	-C(18)	- S(1)	-50.6(4)

Table 3.4: Hydrogen-Bonding Parameters for

$[Co([18]aneN_2S_4)](PF_6)_3.3H_2O$

Bond Lengths(Å) with e.s.d.'s

H(7)	- O(2S)	1.756(6)	H(16)	- O(1S)	1.929(5)
H(1SA)	- F(26)	2.48 (4)	H(1SB)	- F(36)	2.11 (4)
H(2SA)	- F(16)	2.18 (4)	H(2SB)	- O(1S)	2.53 (5)
H(3SA)	- F(25)	2.30 (5)	H(3SB)	- O(2S)	1.92 (5)

Bond Angles(°) with e.s.d.'s

N(7)-H(7)···O(2S)	162.5	(4)
H(2SA)-O(2S)···H(7)	98.9	(27)
H(2SB)-O(2S)···H(7)	87.7	(27)
N(16)-H(16)···O(1S)	158.9	(4)
H(1SA)-O(1S)···H(16)	99.6	(26)
H(1SB)-O(1S)···H(16)	111.6	(26)
O(1S)-H(1SA)···F(26)	159	(4)
O(1S)-H(1SB)···F(36)	165	(4)
O(2S)-H(2SA)···F(16)	133	(4)
O(2S)-H(2SB)···O(1S)	140	(4)
H(1SA)-O(1S)···H(2SB)	116.1	(28)
H(1SB)-O(1S)···H(2SB)	112.9	(28)
O(3S)-H(3SA)···F(25)	133	(4)
O(3S)-H(3SB)···O(2S)	142	(4)
H(2SA)-O(2S)···H(3SB)	89	(3)
H(2SB)-O(2S)···H(3SB)	138	(3)

3.2.3: Electrochemical Study on $[Co([18]aneN_2S_4)]^{2+}$

The redox couples for a series of cobalt poly-thia and -aza macrocyclic complexes are presented in Table 3.5.

A study of the electrochemical characteristics of $[Co([18]aneN_2S_4)]^{2+}$ would allow an assessment to be made of the influence of mixed S and N-donation upon the cobalt ion.

Cyclic voltammetry of $[Co([18]aneN_2S_4)](PF_6)_2$ measured in MeCN (0.1M $NBu^n_4PF_6$ supporting electrolyte) at platinum electrodes reveals two reversible redox processes; an oxidation occurring at $E_{1/2}$= -0.07V *vs.* Fc/Fc^+ (ΔE_p= 100mV at a scan rate of $230mVs^{-1}$), and a reduction at $E_{1/2}$= -1.30V *vs.* Fc/Fc^+ (ΔE_p= 75mV at a scan rate of $230mVs^{-1}$) as shown in Fig. 3.3. Coulometric measurements performed in MeCN (0.1M $NBu^n_4PF_6$ supporting electrolyte) at a platinum basket electrode, confirm that the former process corresponds to a one-electron oxidation, generating an orange solution containing the complex-cation $[Co([18]aneN_2S_4)]^{3+}$, while the latter corresponds to a one-electron reduction, yielding a pale green solution of $[Co([18]aneN_2S_4)]^{+}$. The larger peak separation for the Co(II)/(III) couple suggests that a significant stereochemical change occurs at the metal centre on oxidation. This may reflect the inertness of the low-spin d^6 centre and high M-S bond strength. In contrast, cleavage of M-S to give a square planar Co(I)

species is rapid relative to the rate of electron-transfer.

The oxidation potential for $[Co([18]aneN_2S_4)]^{2+}$ is only slightly less anodic than that reported for $[Co([18]aneS_6)]^{2+/3+}$, while the reduction is more cathodic. This reflects the incorporation of two nitrogen donor atoms which have no π-bonding facility.

The reversibility of the Co(II)/(I) redox couple for $[Co([18]aneN_2S_4)]^{2+}$ contrasts with $[Co([18]aneS_6)]^{2+}$, suggesting a slower rate of Co-L bond cleavage/formation in the latter case.

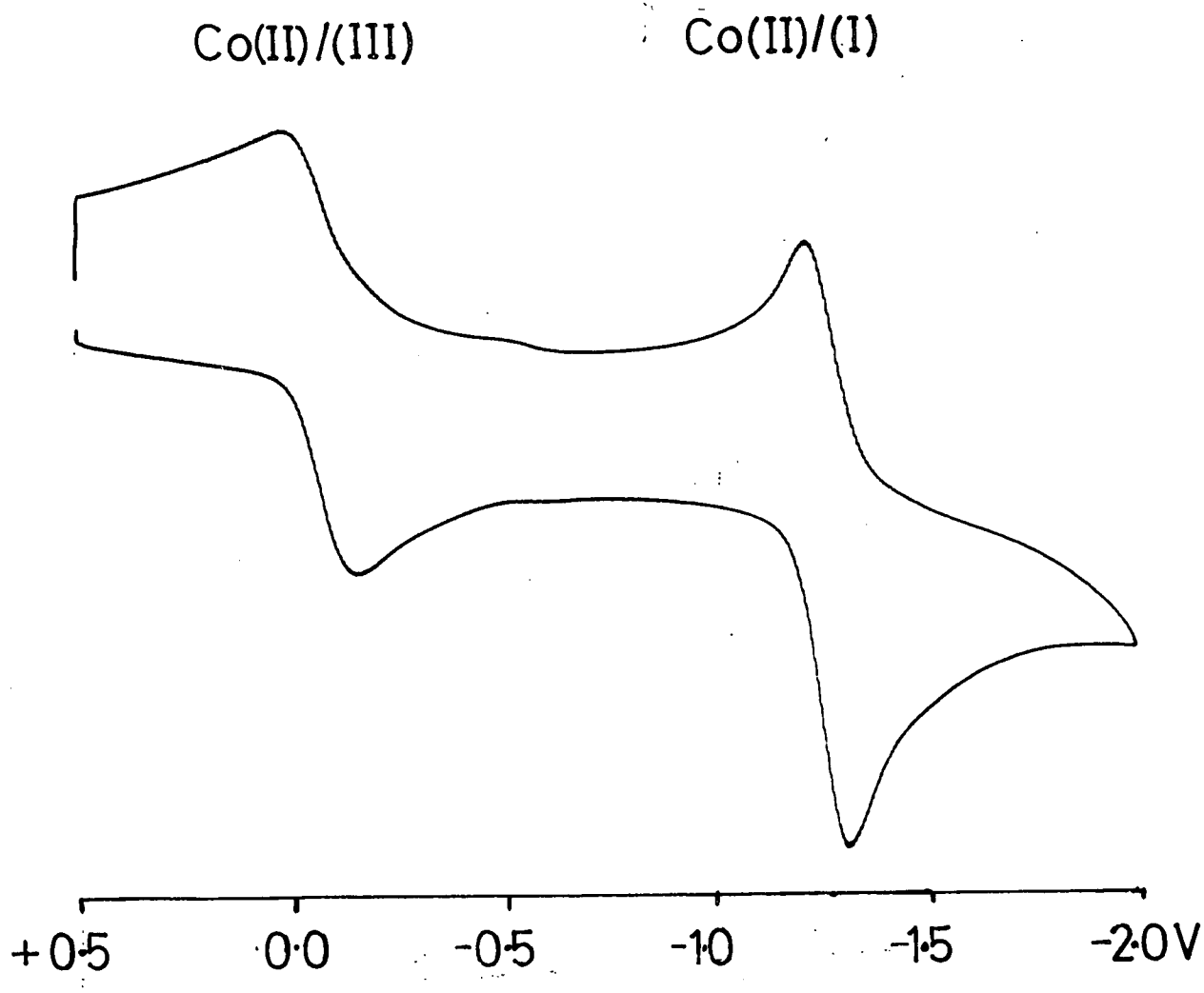

Fig. 3.3: Oxidative and reductive cyclic voltmmograms of $[Co([18]aneN_2S_4)]^{2+}$ ($MeCN/0.1M\ NBu^n_4PF_6$)

Table 3.5: Redox Couples For Selected Cobalt Macrocyclic Complexes

Complex	$E_{1/2}{}^{a}$ $Co^{II/III}$	$E_{1/2}{}^{a}$ $Co^{II/I}$	Ref.
$[Co([18]aneN_6)]^{2+}$	-1.13	-	103
$[Co([9]aneN_3)_2]^{2+}$	-0.868	-	99
$[Co([18]aneN_2S_4)]^{2+}$	-0.07	-1.30	this work
$[Co([9]aneS_3)_2]^{2+}$	-0.013	-0.86	99
$[Co([18]aneS_6)]^{2+}$	+0.124	-0.88 [b]	57

a= in volts *vs.* Fc/Fc^{+}, b= irreversible

3.2.4: Rhodium

Treatment of $RhCl_3.3H_2O$ with 3.2 equivalents of $TlPF_6$ in refluxing MeCN afforded a yellow solution and copious amounts of greyish/white TlCl precipitate, which was removed by filtration. Subsequent reaction of the yellow filtrate with one molar equivalent of $[18]aneN_2S_4$ yielded a pale yellow solution. The product was isolated by removal of solvent and recrystallisation from MeCN/EtOH. Removal of Cl^{-} by Tl^{+} was required as a driving force for the reaction, since d^6 metals are

notoriously inert to substitution [104].

The I.R. spectrum of the complex shows no peaks in the Rh-Cl stretching region (250-400cm^{-1}), suggesting encapsulation of Rh(III) by the macrocycle. The f.a.b. mass spectrum is in accord with this, revealing molecular ion peaks with the correct isotopic distributions at M^+= 719, 573 and 427. These are assigned respectively to

$$[^{103}Rh([18]aneN_2S_4)(PF_6)_2]^+,$$

$$[^{103}Rh([18]aneN_2S_4\text{-}H)PF_6]^+ \text{ and}$$

$$[^{103}Rh([18]aneN_2S_4\text{-}2H)]^+.$$

No peaks of the correct mass for chloro-containing species are apparent. This evidence combined with microanalytical data confirms our assignment of the complex as $[Rh([18]aneN_2S_4)](PF_6)_3$.

The synthesis of $[Rh([18]aneN_2S_4)]^{3+}$ can also be achieved in good yield via reaction of an aqueous solution of $[Rh(H_2O)_6](NO_3)_3$ with one molar equivalent of $[18]aneN_2S_4$ in refluxing MeOH, to afford a bright yellow solution. The complex can be isolated as an orange BPh_4^- salt by addition of an excess of $NaBPh_4$, followed by recrystallisation from MeCN.

The I.R. spectrum of the BPh_4^- salt reveals υ(N-H) at 3200cm^{-1}. Other characteristic bands corresponding to co-ordinated macrocycle and BPh_4^- counterion are also apparent. F.a.b. mass spectral data is in agreement with this, revealing a molecular ion peak at M^+= 427, assigned to $[^{103}Rh([18]aneN_2S_4\text{-}2H)]^+$. The ^{1}H n.m.r. spectrum indicates a ratio of $3BPh_4^-$ counterions

(d= 6.8-8.0ppm, m, 60H) to one macrocycle (2.0-3.9ppm, br. m, $C\underline{H}_2$, 24H). This evidence confirms our assignment as $[Rh([18]aneN_2S_4)](BPh_4)_3$.

In order to deduce the stereochemistry and conformation of the macrocycle in $[Rh([18]aneN_2S_4)]^{3+}$, a single crystal X-ray structural determination was undertaken.

3.2.5: Single Crystal Structure of $[Rh([18]aneN_2S_4)](PF_6)_3.3H_2O$

Details of the structure solution and refinement are given in the Experimental Section. Tables 3.6, 3.7 and 3.8 list relevant bond lengths, angles and torsions respectively. Two ORTEP plots revealing the stereochemical arrangement of the macrocyclic ligand around the rhodium ion are presented in Figs. 3.4 and 3.5.

The single crystal structure of $[Rh([18]aneN_2S_4)]^{3+}$ is very similar to its Co(III) analogue, and shows Rh(III) co-ordinated to all six donor atoms of the macrocycle, with the N-donors occupying mutually trans-positions. The Rh-S and Rh-N bond lengths [Rh-S(1)= 2.3289(14), Rh-S(4)= 2.3416(14), Rh-S(10)= 2.3353(14), Rh-S(13)= 2.3349(14), Rh-N(7)= 2.083(4), Rh-N(16)= 2.101(5)Å] are in close agreement with those observed in related macrocyclic complexes, e.g. $[Rh([9]aneS_3)_2]^{3+}$ [Rh-S= 2.3316(14), 2.3335(12), 2.3335(12)Å] [105] and $[Rh([9]aneN_3)_2]^{3+}$

[Rh-N= 2.065(19), 2.073(21), 2.058(18)Å] [106]. In $[Rh([18]aneN_2S_4)]^{3+}$ the angles around S are lower than the tetrahedral value, as normally observed in thiacrown complexes. The complex adopts a rac-configuration, as observed for each of the first row metal complexes incorporating this ligand. There is no evidence for the presence of a meso-isomer. Angles around the Rh(III) ion deviate considerably from octahedral, and indeed, calculations reveal a large tetrahedral distortion of the thioether-donor atoms out of the least-squares S(1), S(4), S(10), S(13) co-ordination plane, with S(4) and S(10) lying above the plane by +0.1754 and +0.1748Å respectively, and S(1) and S(13) lying below by -0.1743 and -0.1759Å respectively. No such distortion has ever been observed for $[M([18]aneS_6)]^{n+}$, (M= Co(II), Cu(II), Ni(II)), where the structures are rigorously centrosymmetric with any strain being accommodated by a constriction of the M-S bond lengths [53-58].

Significant H-bonding is also apparent from the crystal structure. As in the isoelectronic and isostructural Co(III) complex, $[Co([18]aneN_2S_4)]^{3+}$, this occurs between the N-H functions of the macrocycle, H_2O solvent molecules and F atoms of the PF_6^- counterions, H(7)...O(1S)= 1.888(7)Å, angle N(7)-H(7)···O(1S)= 166.9(5)°, H(16)···O(2S)= 1.726(8)Å, angle N(16)-H(16)···O(2S)= 170.9(5)°, F(28)···O(3S)= 2.822(15)Å and O(2S)···O(3S)= 2.655(11)Å.

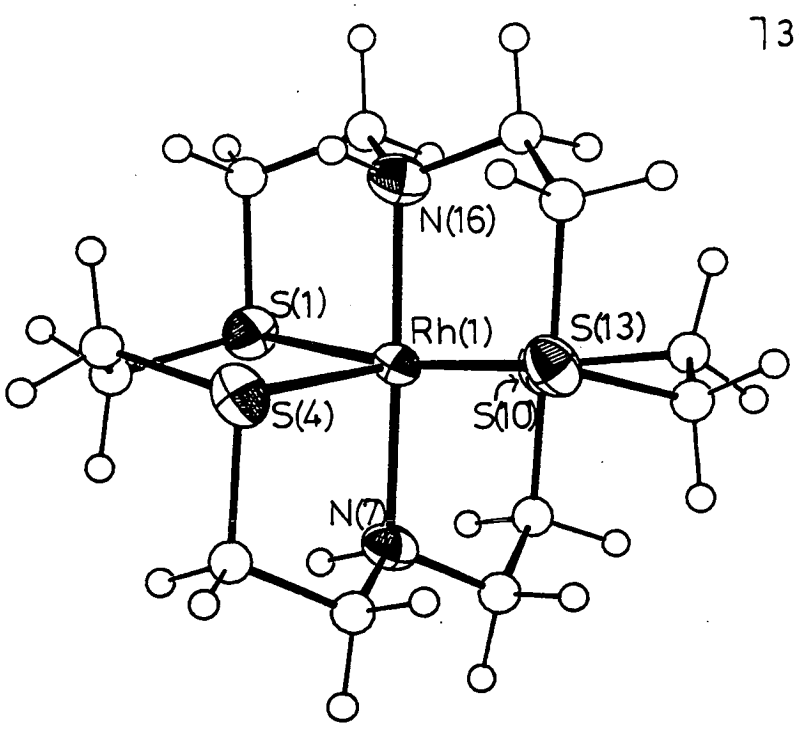

Fig. 3.4: View of the single crystal structure of $[Rh([18]aneN_2S_4)]^{3+}$

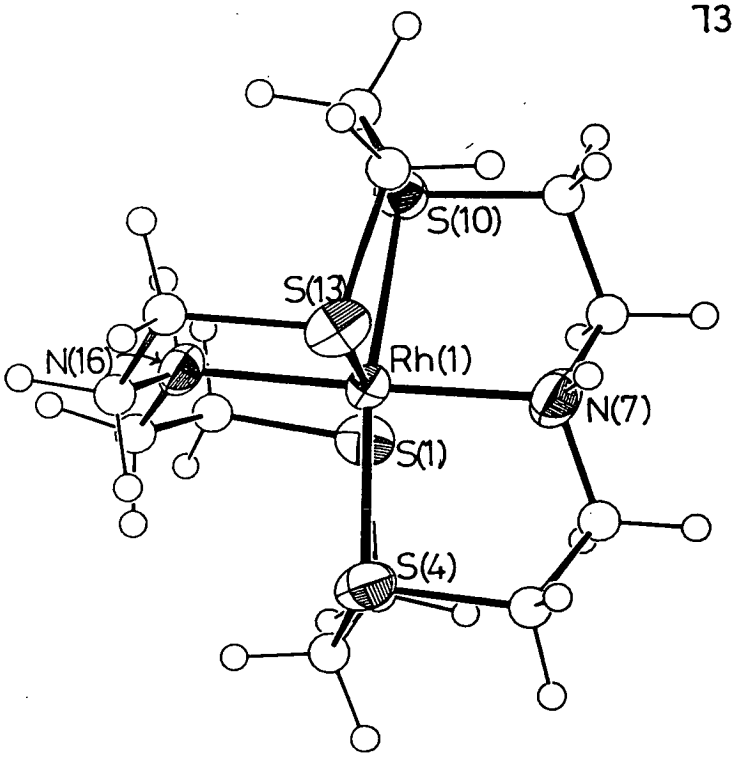

Fig. 3.5: Alternative view of the single crystal structure of $[Rh([18]aneN_2S_4)]^{3+}$

Single Crystal Structure of

$[Rh([18]aneN_2S_4)](PF_6)_3.3H_2O$

Table 3.6: Selected Bond Lengths(Å) with e.s.d.'s

Rh(1)	- S(1)	2.3289(14)	C(6)	- N(7)	1.488(7)
Rh(1)	- S(4)	2.3416(14)	N(7)	- C(8)	1.498(8)
Rh(1)	- N(7)	2.083(4)	C(8)	- C(9)	1.497(8)
Rh(1)	-S(10)	2.3353(14)	C(9)	-S(10)	1.834(6)
Rh(1)	-S(13)	2.3349(14)	S(10)	-C(11)	1.833(6)
Rh(1)	-N(16)	2.101(5)	C(11)	-C(12)	1.482(8)
S(1)	- C(2)	1.811(6)	C(12)	-S(13)	1.821(6)
S(1)	-C(18)	1.826(7)	S(13)	-C(14)	1.833(6)
C(2)	- C(3)	1.500(8)	C(14)	-C(15)	1.514(9)
C(3)	- S(4)	1.826(6)	C(15)	-N(16)	1.507(8)
S(4)	- C(5)	1.821(6)	N(16)	-C(17)	1.486(8)
C(5)	- C(6)	1.507(8)	C(17)	-C(18)	1.505(10)

Table 3.7: Selected Angles(^{o}) with e.s.d.'s

S(1)-Rh(1) - S(4)	88.83(5)	S(4)- C(5) - C(6)	111.2(4)
S(1)-Rh(1) - N(7)	92.59(12)	C(5)- C(6) - N(7)	109.2(5)
S(1)-Rh(1) -S(10)	92.49(5)	Rh(1)- N(7) - C(6)	110.7(3)
S(1)-Rh(1) -S(13)	171.43(5)	Rh(1)- N(7) - C(8)	113.2(3)
S(1)-Rh(1) -N(16)	85.29(13)	C(6)- N(7) - C(8)	114.1(4)
S(4)-Rh(1) - N(7)	85.25(12)	N(7)- C(8) - C(9)	109.9(5)
S(4)-Rh(1) -S(10)	171.33(5)	C(8)- C(9) -S(10)	111.6(4)
S(4)-Rh(1) -S(13)	91.44(5)	Rh(1)-S(10) - C(9)	97.31(19)
S(4)-Rh(1) -N(16)	94.70(13)	Rh(1)-S(10) -C(11)	104.56(20)
N(7)-Rh(1) -S(10)	86.13(12)	C(9)-S(10) -C(11)	104.9(3)
N(7)-Rh(1) -S(13)	95.97(12)	S(10)-C(11) -C(12)	115.1(4)
N(7)-Rh(1) -N(16)	177.88(17)	C(11)-C(12) -S(13)	115.5(4)
S(10)-Rh(1) -S(13)	88.52(5)	Rh(1)-S(13) -C(12)	103.96(19)
S(10)-Rh(1) -N(16)	93.95(13)	Rh(1)-S(13) -C(14)	98.20(19)
S(13)-Rh(1) -N(16)	86.15(13)	C(12)-S(13) -C(14)	104.7(3)
Rh(1)- S(1) - C(2)	103.65(19)	S(13)-C(14) -C(15)	111.9(4)
Rh(1)- S(1) -C(18)	98.11(21)	C(14)-C(15) -N(16)	109.8(5)
C(2)- S(1) -C(18)	103.3(3)	Rh(1)-N(16) -C(15)	111.8(4)
S(1)- C(2) - C(3)	114.1(4)	Rh(1)-N(16) -C(17)	109.1(4)
C(2)- C(3) - S(4)	113.8(4)	C(15)-N(16) -C(17)	112.8(5)
Rh(1)- S(4) - C(3)	103.04(21)	N(16)-C(17) -C(18)	108.8(5)
Rh(1)- S(4) - C(5)	98.07(19)	S(1)-C(18) -C(17)	109.9(5)
C(3)- S(4) - C(5)	102.0(3)		

Table 3.8: Selected Torsion Angles(^{o}) with e.s.d.'s

C(18)	- S(1)	- C(2)	- C(3)	-67.1(5)
C(8)	- C(9)	-S(10)	-C(11)	75.0(5)
C(2)	- S(1)	-C(18)	-C(17)	134.2(5)
C(9)	-S(10)	-C(11)	-C(12)	-74.6(5)
S(1)	- C(2)	- C(3)	- S(4)	-47.8(5)
S(10)	-C(11)	-C(12)	-S(13)	-41.3(6)
C(2)	- C(3)	- S(4)	- C(5)	-66.9(5)
C(11)	-C(12)	-S(13)	-C(14)	-69.6(5)
C(3)	- S(4)	- C(5)	- C(6)	131.1(4)
C(12)	-S(13)	-C(14)	-C(15)	79.1(5)
S(4)	- C(5)	- C(6)	- N(7)	-52.8(5)
S(13)	-C(14)	-C(15)	-N(16)	50.9(6)
C(5)	- C(6)	- N(7)	- C(8)	-176.4(5)
C(14)	-C(15)	-N(16)	-C(17)	-172.6(5)
C(6)	- N(7)	- C(8)	- C(9)	-173.9(5)
C(15)	-N(16)	-C(17)	-C(18)	-178.1(5)
N(7)	- C(8)	- C(9)	-S(10)	52.2(6)
N(16)	-C(17)	-C(18)	- S(1)	-56.4(6)

3.2.6: Electrochemical Study on $[Rh([18]aneN_2S_4)]^{3+}$

Since co-ordination of $[18]aneN_2S_4$ to Cu(II), Ni(II) and Co(II) enables generation of unusual oxidation states, we were interested to investigate the redox activity of the d^6 Rh(III) system, to determine whether this complex could be activated electrochemically to afford a mononuclear d^7 Rh(II) species. A further impetus for this work comes from the recent reports revealing the effectiveness of the trithia macrocycle, $[9]aneS_3$, in stabilising both the d^7 Rh(II) and d^8 Rh(I) complexes, $[Rh([9]aneS_3)_2]^{2+}$ (Rh(III)/(II): $E_{1/2}$= -0.71V *vs.* Fc/Fc^+) and $[Rh([9]aneS_3)_2]^{+}$ (Rh(II)/(I): $E_{1/2}$= -1.08V *vs.* Fc/Fc^+) [105,107]. Interestingly, such stabilisation cannot be achieved by the analogous bis(tri-aza) complex, $[Rh([9]aneN_3)_2]^{3+}$. This system shows two irreversible reductions at the considerably more cathodic potentials, E_{pc}= -1.93 and -2.32V *vs.* Fc/Fc^+ [108]. An investigation of the electrochemical properties of $[Rh([18]aneN_2S_4)]^{3+}$ provides a means of assessing the effect which mixed sulphur and nitrogen-donation has on the stability of Rh(III)/(II)/(I). Although the systems are not strictly analogous, the former two being bis-macrocyclic species incorporating 9-membered rings, as opposed to the 18-membered N_2S_4 system, a qualitative measure of the influence of mixed donor co-ordination should be possible.

Electrochemical measurements could not be

performed on. $[Rh([18]aneN_2S_4)](PF_6)_3$, due to the very low solubility of the PF_6^- salt in MeCN. Thus, all measurements were performed on the much more soluble BPh_4^- salt.

Cyclic voltammetry of $[Rh([18]aneN_2S_4)](BPh_4)_3$ measured in MeCN (0.1M $NBu^n{}_4PF_6$ supporting electrolyte) at platinum electrodes reveals only one irreversible reduction. At 298K, this occurs at E_{pc}= -1.34V *vs.* Fc/Fc^+ (scan rate= $180mVs^{-1}$). Upon lowering the temperature to 238K and increasing the scan rate to $400mVs^{-1}$, this reduction shifts cathodically to -2.02V *vs.* Fc/Fc^+ but remains irreversible. Coulometric measurements performed on the reduction by controlled potential electrolysis of the complex at -1.35V *vs.* Ag/AgCl in MeCN (0.1M $NBu^n{}_4BPh_4$ supporting electrolyte) at a platinum basket electrode, gives a value for n of *ca.* 2.2 electrons, generating a yellow solution. This strongly suggests that this reduction corresponds to a two-electron process, giving a d^8 Rh(I) species. It is highly likely that a Rh(I) product generated by the two-electron reduction of $[Rh([18]aneN_2S_4)]^{3+}$ would involve co-ordination of the d^8 ion to a square planar arrangement of four thioether donor atoms of the macrocycle, with the N-H functions either non-interacting or only interacting weakly at long-range. Indeed the π-acidity of the sulphurs would be expected to provide enhanced stability of the low-valent species.

This reduced species may be active towards

oxidative addition reactions of substrates. The conformation of the macrocycle in the Rh(III) precursor may be responsible for the fact that no d^7 Rh(II) intermediate could be identified, and, furthermore, a square planar Rh(I) tetrathia macrocyclic complex, $[Rh([14]aneS_4)]^+$, has been reported previously [109,110].

3.2.7: Reaction of $RhCl_3$ With $[18]aneS_6$

A wide range of transition metal complexes incorporating the hexathia macrocycle $[18]aneS_6$ have been reported [53-58]. In view of the successful synthesis of the octahedral cation, $[Rh([18]aneN_2S_4)]^{3+}$ described above, we attempted the synthesis of the related homoleptic hexathia complex, $[Rh([18]aneS_6)]^{3+}$, by a similar method.

Treatment of $[Rh(H_2O)_6]^{3+}$ with one molar equivalent of $[18]aneS_6$ in refluxing $MeOH/H_2O$ for 5h afforded a bright red solution. Addition of excess NH_4PF_6 yielded a red precipitate which was recrystallised from MeCN.

The f.a.b. mass spectrum of this product shows a molecular ion peak at $M^+ = 462$, corresponding to $[^{103}Rh([18]aneS_6-H)]^+$. We were intrigued by the intense colouration exhibited by this complex, [$\lambda_{max} = 475nm$, ($\varepsilon_{max} = 271M^{-1}cm^{-1}$)] ,since very recently the deprotonated complex, $[Rh([9]aneS_3)([9]aneS_3-H)]^{2+}$ has been structurally characterised (Fig. 3.6) [111]. This species is formed by deprotonation of a methylene group adjacent

to S, followed by ring opening, and exhibits a similar intense red colouration in solution (λ_{max} = 474nm).

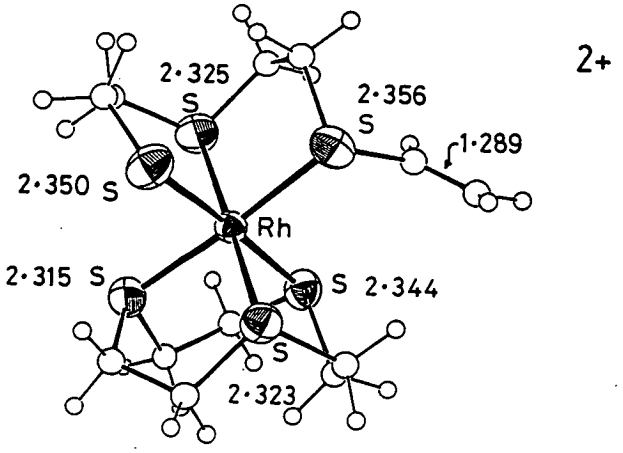

Fig. 3.6: Single crystal structure of $[Rh([9]aneS_3)([9]aneS_3\text{-}H)]^{2+}$

We proposed that a similar reaction occurs for $[Rh([18]aneS_6)]^{3+}$. This was confirmed by an n.m.r. study. The ^1H n.m.r. spectrum of the red product obtained from the reaction of Rh(III) with $[18]aneS_6$ is second order, with δ= 6.69-6.37 (vinyl C<u>H</u>, 1H), 6.18-5.95 (vinyl C<u>H</u>$_2$, 2H) and 3.88-2.63ppm (C<u>H</u>$_2$, 20H) (Fig. 3.7). The ^{13}C DEPT n.m.r. spectrum is consistent with this, showing eleven distinct methylene carbon resonances at δ= 127.28 (vinyl <u>C</u>H$_2$, 1C), 45.07, 43.70, 41.85, 40.89, 39.91, 39.33, 38.30, 36.94, 36.15 and 30.84ppm (S<u>C</u>H$_2$<u>C</u>H$_2$S, 10C), as well as one vinyl <u>C</u>H resonance at 124.71ppm (Fig. 3.8). There is no evidence for the presence of other isomers or products such as $[Rh([18]aneS_6)]^{3+}$ in solution. This evidence, together with microanalytical and I.R. spectroscopic data, is consistent with the formulation $[Rh([18]aneS_6\text{-}H)](PF_6)_2$. The proposed mechanism for the deprotonation of $[Rh([18]aneS_6)]^{3+}$ is illustrated in Fig. 3.9.

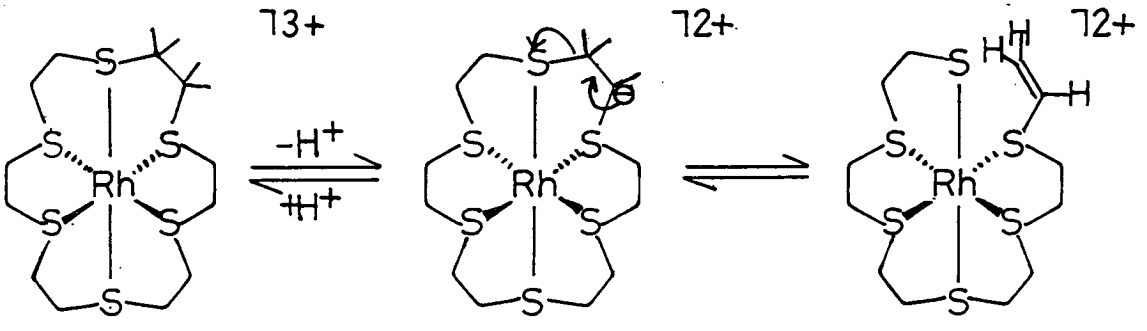

Fig. 3.9: Proposed mechanism for the deprotonation of $[Rh([18]aneS_6)]^{3+}$

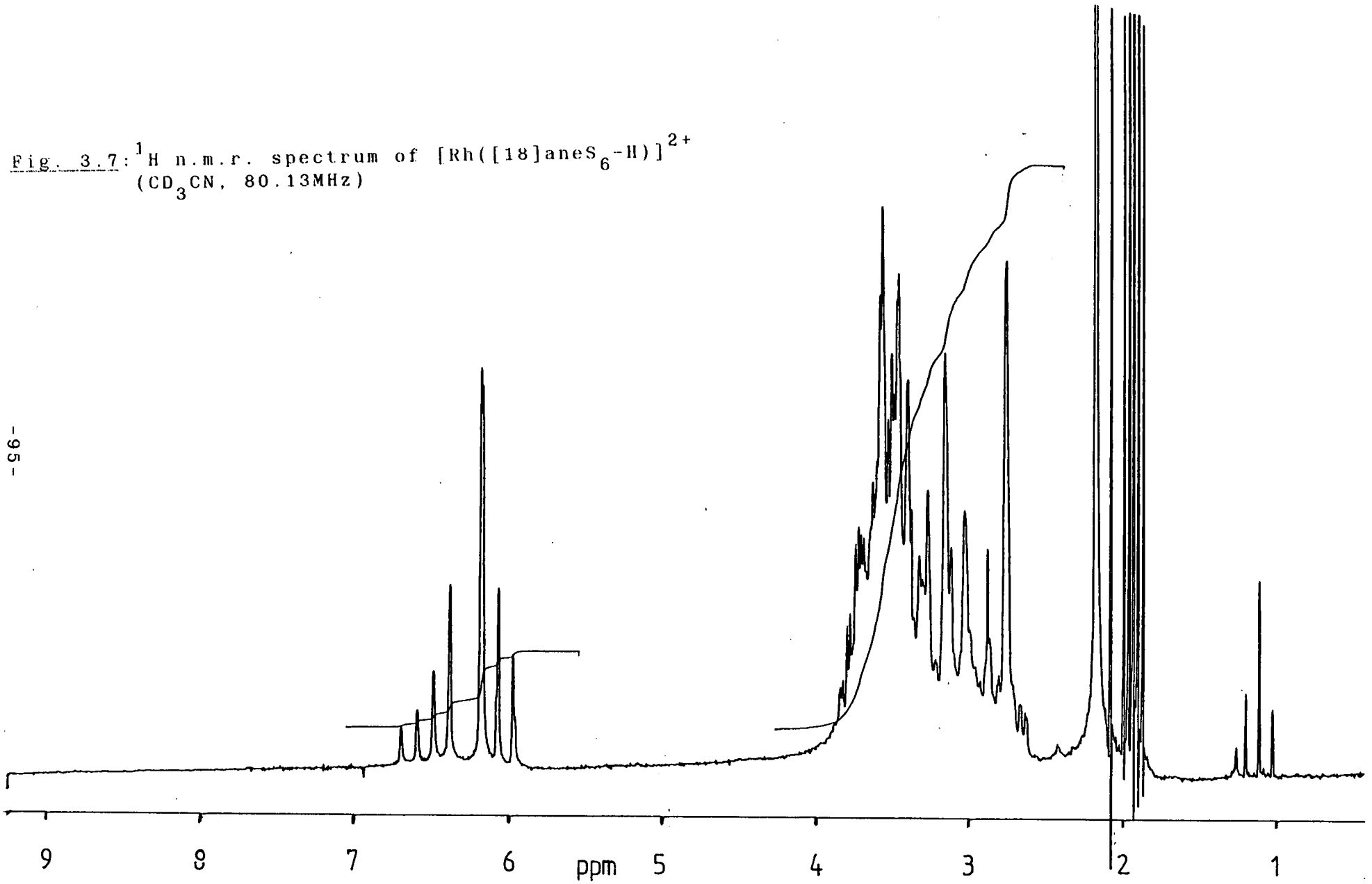

Fig. 3.7: ^{1}H n.m.r. spectrum of $[Rh([18]aneS_6-H)]^{2+}$ (CD_3CN, 80.13MHz)

Fig. 3.8: ^{13}C DEPT n.m.r. spectrum of $[Rh([18]aneS_6-H)]^{2+}$ (CD_3CN, 50.32MHz)

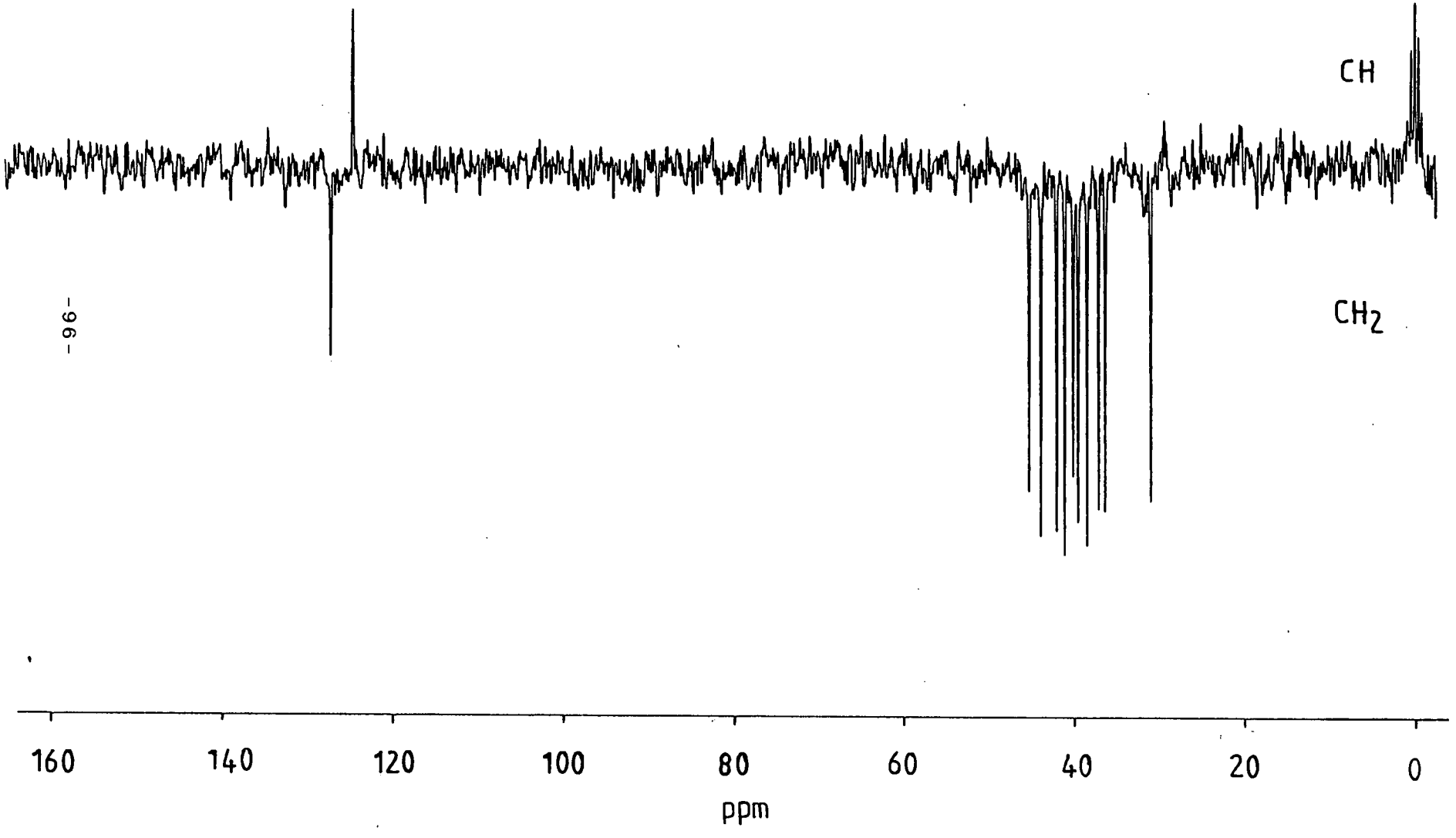

3.3: Conclusions

This chapter has described the synthesis of $[Co([18]aneN_2S_4)]^{2+}$. Electrochemical studies on this species reveal that this macrocycle enables stabilisation of Co in the +1, +2 and +3 oxidation states.

The preparation of $[Rh([18]aneN_2S_4)]^{3+}$ has also been achieved. This species represents the first example of Rh(III) encapsulated by octahedral co-ordination to an 18-membered ring macrocycle. Preliminary electrochemical studies suggest that generation of a d^8 Rh(I) species can be achieved upon reduction of the Rh(III) precursor. This species may undergo oxidative addition reactions.

Finally, the synthesis of the deprotonated species $[Rh([18]aneS_6\text{-}H)]^{2+}$ has been achieved, and this product has been characterised by n.m.r. spectroscopy. Interestingly, at present we have no evidence for the occurrence of a similar deprotonation reaction in $[Rh([18]aneN_2S_4)]^{3+}$. This may be attributed to the low solubility of the PF_6^- salt in aqueous solution.

3.4: Experimental

3.4.1: $[Co([18]aneN_2S_4)](PF_6)_2$

Reaction of $Co(NO_3)_2.6H_2O$ (36mg, 0.123mmol) with $[18]aneN_2S_4$ (40mg, 0.123mmol) in refluxing $EtOH/H_2O$ (1:1 v.v., 30ml) under N_2 for 1h yielded a purple solution. After cooling, excess NH_4PF_6 was added to afford a purple precipitate. Recrystallisation from aqueous solution gave a deep purple crystalline material (Yield: 60mg, 73%). Mol. wt. 675.45. Elemental analysis: found C= 20.8, H= 3.90, N= 4.17, S= 19.4%; calculated for $[C_{12}H_{26}N_2S_4Co](PF_6)_2$: C= 21.3, H= 3.85, N= 4.15, S= 19.0%. F.a.b. mass spectrum (3-NOBA matrix): found M^+= 530 and 384; calculated for

$[^{59}Co([18]aneN_2S_4)PF_6]^+$ M^+= 530,

$[^{59}Co([18]aneN_2S_4)]^+$ M^+= 385.

UV/vis spectrum (MeCN): λ_{max}= 593nm (ε_{max}= $68M^{-1}cm^{-1}$), 534 (73), 298 (2,390), 247 (4,795). I.R. spectrum (KBr disc): 3260m, 3160m, 2920w, 2880w, 1470m, 1430m, 1415m, 1385w, 1320w, 1300w, 1285w, 1260w, 1240w, 1210w, 1145w, 1100w, 1070w, 1025w, 1010m, 980w, 840vs, 790m, 640w, 555vs cm^{-1}.

3.4.2: Single Crystal Structure of $[Co([18]aneN_2S_4)](PF_6)_3.3H_2O$

Recrystallisation of $[Co([18]aneN_2S_4)](PF_6)_2$ from aqueous solution resulted in aerial oxidation to the corresponding Co(III) complex. This product was isolated as dark red crystals. A suitable single dark red tablet

was selected for a crystallographic study.

Crystal Data:

$[C_{12}H_{26}N_2S_4Co](PF_6)_3.3H_2O$ M= 874.45. Monoclinic, space group $P2_1/n$, a= 11.5485(3), b= 13.9779(2), c= 19.1378(4)Å, β= 106.561(2)°, V= 2961.1Å^3 (by least-squares refinement on diffraction angles for 38 reflections measured at $\pm\omega$ [$30<2\theta<32°$, λ= 0.71073Å]), Z= 4, D_c= 1.96gcm^{-3}. Crystal dimensions 0.70x0.45x0.25mm, μ(Mo-Kα)= 10.84cm^{-1}, F(000)= 1760.

Data Collection and Processing:

Stöe STADI-4 four-circle diffractometer, $\omega/2\theta$ scan mode with ω scan-width $(1.05+0.347\tan\theta)°$. Graphite-monochromated Mo-Kα radiation, 4079 reflections measured ($2\theta_{max}$= 45°, h -12⟶11, k 0⟶15, l 0⟶20) giving 3297 with $F>6\sigma(F)$. No significant crystal decay, no absorption correction.

Structure Analysis and Refinement:

The Co atom was located using a Patterson synthesis, and successive cycles of least-squares refinement and difference Fourier synthesis identified the positions of all other non-H atoms. The cation and the three PF_6^- anions were well ordered. Three fully occupied H_2O solvent molecules were found to be associated per cation. These were refined with the O-H bond lengths fixed at 0.96Å and the H-O-H angle

tetrahedral. Anisotropic thermal parameters were refined for all non-H atoms. H-atoms were included in fixed, calculated positions. The weighting scheme $\underline{w}^{-1} = \sigma^2(\underline{F}) + 0.000257\underline{F}^2$ gave satisfactory agreement analyses. At final convergence, $\underline{R} = 0.0397$, $\underline{R}_w = 0.0549$, $\underline{S} = 1.234$ for 406 independent parameters, and the final difference Fourier synthesis showed no feature above 0.73 or below $0.37 e\text{Å}^{-3}$.

3.4.3: $[Rh([18]aneN_2S_4)](PF_6)_3$

$RhCl_3.3H_2O$ (40mg, 0.152mmol) and $TlPF_6$ (175mg, 0.501mmol)were refluxed for 3h under N_2 to give a yellow solution and a white precipitate. After cooling, the TlCl precipitate was removed by filtration. $[18]aneN_2S_4$ (45mg, 0.138mmol) was added to the yellow filtrate, and the resulting mixture was refluxed under N_2 for a further 18h, to give a pale yellow solution. Removal of the MeCN and recrystallisation from MeCN/EtOH yielded the product as orange crystals (Yield: 71mg, 54%). Mol. wt. 864.38. Elemental analysis: found C= 16.4, H= 2.89, N= 3.37%; calculated for $[C_{12}H_{26}N_2S_4Rh](PF_6)_3$: C= 16.7, H= 3.03, N= 3.24%. F.a.b. mass spectrum (3-NOBA matrix): found M^+= 719, 573 and 427; calculated for

$[^{103}Rh([18]aneN_2S_4)(PF_6)_2]^+$ $M^+ = 719$,

$[^{103}Rh([18]aneN_2S_4)PF_6]^+$ $M^+ = 574$,

$[^{103}Rh([18]aneN_2S_4)]^+$ $M^+ = 429$.

I.R. spectrum (KBr disc): 3240m, 3080w, 2980w, 2880w,

1465m, 1420m, 1380w, 1290w, 1230w, 1210w, 1175w, 1140m, 1065w, 1020w, 1000w, 970w, 840vs, 740m, 555vs, 495w cm^{-1}.

3.4.4: $[Rh([18]aneN_2S_4)](BPh_4)_3$

Treatment of $RhCl_3.3H_2O$ with three equivalents of $AgNO_3$ in refluxing H_2O for 5h under N_2 affords a bright yellow solution of $[Rh(H_2O)_6](NO_3)_3$ and AgCl precipitate which can be removed by filtration.

Reaction of $[Rh(H_2O)_6](NO_3)_3$ (0.13mmol in 5ml H_2O) with $[18]aneN_2S_4$ (40mg, 0.123mmol) in refluxing MeOH (40ml) for 2h under N_2 afforded a bright yellow solution. After cooling, excess $NaBPh_4$ in H_2O was added to give a yellow precipitate. Recrystallisation from acetone/H_2O in the presence of $NaBPh_4$ and then from MeCN/H_2O gave the product as an orange precipitate (116mg, 68%). Mol. wt. 1387.2. F.a.b. mass spectrum (3-NOBA matrix): found M^+= 427; calculated for $[^{103}Rh([18]aneN_2S_4)]^+$ M^+= 429. ^1H n.m.r. spectrum (80.13MHz, CD_3NO_2, 298K): δ= 2.0-3.9 (br. m, CH_2, 24H), 6.8-8.0ppm (m, BPh_4^-, 60H). I.R. spectrum (KBr disc): 3200vs, 3020m, 3010w, 2990m, 2970w, 2960w, 2910w, 1950w, 1900w, 1820w, 1570m, 1470m, 1420m, 1385m, 1300w, 1260w, 1180m, 1145m, 1120w, 1060w, 1020m, 990w, 910m, 860w, 840m, 740vs, 710vs, 705vs, 620m, 590m, 485m, 460m cm^{-1}.

3.4.5: Single Crystal Structure of $[Rh([18]aneN_2S_4)](PF_6)_3.3H_2O$

Recrystallisation of the complex from aqueous

solution yielded orange plates suitable for a crystallographic study.

Crystal Data:

$[C_{12}H_{26}N_2S_4Rh](PF_6)_3.3H_2O$ M= 918.42. Monoclinic, space group $\underline{P}2_1/n$, $\underline{a}$= 11.7097(12), $\underline{b}$= 13.9470(11), $\underline{c}$= 19.1954(17)Å, β= 107.048(6)°, $\underline{V}$= 2997.1Å^3 (by least-squares refinement on diffraction angles for 35 reflections measured at $\pm\omega$ [$34<2\theta<35°$, λ= 0.71073Å]), $\underline{Z}$= 4, $\underline{D}_c$= 2.035gcm^{-3}. Crystal dimensions 0.62x0.62x0.15mm, μ(Mo-Kα)= 10.62cm^{-1}, $\underline{F}$(000)= 1832.

Data Collection and Processing:

Stöe STADI-4 four-circle diffractometer, $\omega/2\theta$ scan mode using the learnt-profile method. Graphite-monochromated Mo-Kα radiation, 4424 reflections measured ($2\theta_{max}$= 45°, h -12⟶12, k 0⟶14, l 0⟶20) giving 4125 with $\underline{F}>6\sigma(\underline{F})$. No significant crystal decay, no absorption correction.

Structure Analysis and Refinement:

The Rh atom was located using a Patterson synthesis, and successive cycles of least-squares refinement and difference Fourier synthesis identified the positions of all other non-H atoms. During refinement some disorder of one of the PF_6^- counterions was observed. This was modelled successfully using partial F atoms, such that there was a total of six F atoms

associated with the P atom. Three fully occupied H_2O solvent molecules were found to be associated per cation, however, the protons on these could not be located. Anisotropic thermal parameters were refined for Rh, S, P, O, N and all fully occupied F atoms. Macrocyclic H atoms were included in fixed, calculated positions. The weighting scheme $\underline{w}^{-1} = \sigma^2(\underline{F}) + 0.007342\underline{F}^2$ gave satisfactory agreement analyses. At final convergence, $\underline{R} = 0.0618$, $\underline{R}_w = 0.0978$, $\underline{S} = 1.460$ for 384 independent parameters, and the final difference Fourier synthesis showed no feature above 1.39 or below 1.14e$\mathring{A}^{-3}$.

3.4.5: $[Rh([18]aneS_6-H)](PF_6)_2$

$RhCl_3.3H_2O$ (0.152mmol) in H_2O (6ml) was added to a refluxing solution containing $[18]aneS_6$ (55mg, 0.152mmol) in MeOH (40ml). The reaction mixture was refluxed for 10h under N_2, to give a bright red solution. Addition of excess NH_4PF_6 afforded a red precipitate which was recrystallised from MeCN (Yield: 65mg, 57%). Mol. wt. 752.50. Elemental analysis: found C= 19.3, H= 3.08%; calculated for $[C_{12}H_{23}S_6Rh](PF_6)_2$: C= 19.2, H= 3.08%. F.a.b. mass spectrum (3-NOBA matrix): found M^+= 462; calculated for $[^{103}Rh([18]aneS_6-H)]^+$ M^+= 462. ^1H n.m.r. spectrum (80.13MHz, CD_3CN, 298K): δ= 6.69-6.37 (m, C$\underline{H}$, 1H), 6.18-5.95 (m, C$\underline{H}_2$, 2H), 3.88-2.63ppm (C$\underline{H}_2$, 20H). ^{13}C DEPT n.m.r. spectrum (50.32MHz, CD_3CN, 298K): δ= 127.28 (C$\underline{H}_2$, 1C), 124.71 (C$\underline{H}$, 1C), 45.07, 43.70, 41.85, 40.89, 39.91,

39.33, 38.30, 36.94, 36.15, 30.84ppm ($\underline{C}H_2$, 10C). UV/vis spectrum (MeCN): λ_{max}= 475nm (ε_{max}= 271$M^{-1}cm^{-1}$), 268 (300,004). I.R. spectrum (KBr disc): 3000m, 2950m, 1435m, 1410w, 1380m, 1280w, 960w, 930w, 925w, 840vs, 745w, 670w, 600w, 555vs, 425w cm^{-1}.

CHAPTER 4

Stereochemical and Redox Properties of Palladium and Platinum Complexes of [18]aneN$_2$S$_4$ and Me$_2$[18]aneN$_2$S$_4$

4.1: Introduction

Pd and Pt are particularly useful metal centres with which to monitor the co-ordinative flexibility of macrocyclic ligand systems, since they have the potential to exhibit multi-electron redox behaviour with widely differing stereochemical requirements. The preferred geometries for the 0, +2, +3 and +4 oxidation states are tetrahedral, square planar, tetragonally-elongated and octahedral respectively.

The chemistry of Pd and Pt is dominated by the d^8 +2 oxidation state. A few examples of Pd(I) and Pd(III) complexes have been reported. However, these species occur almost exclusively as metal-metal bonded dimers (Chapter 5). The literature relating to genuine monomeric M(I) and M(III) species (M= Pd, Pt) is extremely sparse [112-119]. As a result, the design of ligand systems capable of stabilising these unusual oxidation states has become a major synthetic target. Connelly and co-workers [117,118] have recently reported Pd(I) mononuclear species which have been electrogenerated from π-complexes of the type $[Pd(C_5Ph_5)(L)]$, (L= cyclooctadiene, norbornadiene or dibenzocyclooctatetraene).

The effectiveness of homoleptic polythia and polyaza macrocyclic co-ordination in stabilising Pd(III) [115,120,121] and Pt(III) [122] has been demonstrated

recently by the Edinburgh group. $[Pd([9]aneN_3)_2]^{2+}$ exhibits a reversible Pd(II)/(III) redox couple at $E_{1/2}$= +0.07V *vs.* Fc/Fc^+. The single crystal X-ray structure of the air-stable oxidation product, $[Pd([9]aneN_3)_2]^{3+}$ has been obtained (Fig. 4.1). It shows two tridentate macrocycles binding facially to the Pd(III) ion via all six nitrogen-donor atoms, to give a tetragonally elongated geometry, [Pd-N(1)= 2.180(9), Pd-N(4)= 2.118(9), Pd-N(7)= 2.111(9)Å] [121]. A similar stereochemistry has been observed for the thia analogue, $[Pd([9]aneS_3)_2]^{3+}$, [Pd-S(1)= 2.5448(15), Pd-S(4)= 2.3558(14), Pd-S(7)= 2.3692(15)Å], confirming a preference for Pd(III) to adopt a Jahn-Teller elongated geometry [115]. The Pd(II)/(III) oxidation potential for $[Pd([9]aneS_3)_2]^{2+}$, ($E_{1/2}$= +0.605V *vs.* Fc/Fc^+) [120], is rather more anodic than for the tri-aza system. This is attributed to the softness of the sulphur-donors over nitrogen. The analogous Pt(II) complex, $[Pt([9]aneS_3)_2]^{2+}$ exhibits a reversible Pt(II)/(III) redox couple at $E_{1/2}$= +0.39V *vs.* Fc/Fc^+ [122]. Stabilisation of Pd(III), Pt(III) and Pt(IV) can also be achieved by the related hexathia macrocycle, $[18]aneS_6$ [123]. The accessibility of the +3 and +4 oxidation states in these systems is attributed to the structurally accommodating nature of these ligands, which enables them to modify their binding mode to conform to the stereochemical requirements of each different d^n-configuration.

Fig. 4.1: Single crystal structure of $[Pd([9]aneN_3)_2]^{3+}$

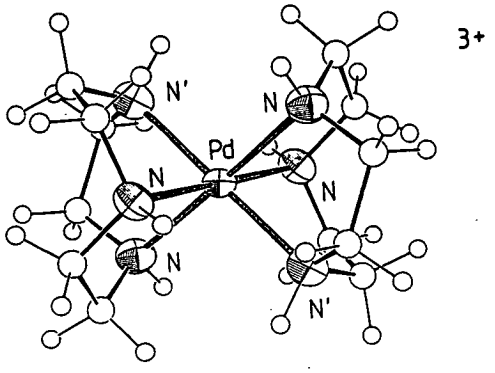

Generation of mononuclear Pd(I) has been achieved by incorporation of tetra-aza ionophores. $[Pd(L)]^{2+}$ complexes exhibit reversible Pd(II)/(I) redox couples at $E_{1/2}$= -2.10, -1.53 and -1.27V *vs.* Fc/Fc^+ for L= $[14]aneN_4$, $Me_4[14]aneN_4$ and $Bz_4[14]aneN_4$ respectively [119] (see also Chapter 7). These redox couples all occur at rather negative potentials.

In view of these results, we undertook a study of the co-ordination of the potentially hexadentate, mixed sulphur and nitrogen-donor 18-membered ring macrocycles, $[18]aneN_2S_4$ and $Me_2[18]aneN_2S_4$, with Pd(II) and Pt(II). We were particularly interested in monitoring the co-ordinative flexibility of these large ring systems, especially since the stereochemical requirements of the ligands and metal(II) species are not mutually compatible. The co-ordination chemistry of these mixed donor macrocycles with Pd(II) and Pt(II) has not been explored previously. A discussion of the literature relating to these systems is given in Chapter 2.

A few examples of mixed N and S-donor macrocyclic complexes incorporating Pd(II) have been reported [124,125]. However, most of these bind two metal

centres within the macrocyclic cavity to give binuclear species [124]. The Pd(II) complex, (1), represents one of only a few mononuclear complexes in which Pd(II) is bound to a mixed N and S-donor macrocycle. The single crystal X-ray structure of this cation shows Pd(II) on an inversion centre and co-ordinated in a distorted square planar arrangement of the two S and two N-donor atoms [Pd-S= 2.307(1), Pd-N= 2.047(4)Å] [125].

This chapter describes the synthesis and characterisation of mononuclear and binuclear Pd(II) and Pt(II) complexes incorporating [18]aneN_2S_4 and Me_2[18]aneN_2S_4. A full electrochemical study of the mononuclear Pd species is also presented.

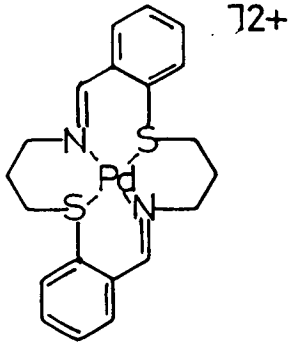

(1)

4.2: Results and Discussion

4.2.1: $[Pd([18]aneN_2S_4)](PF_6)_2$

Reaction of $PdCl_2$ with one molar equivalent of $[18]aneN_2S_4$ in refluxing MeCN in the presence of *ca* 2.2 molar equivalents of $TlPF_6$ gave a purple solution and white TlCl precipitate which was removed by filtration. Removal of the solvent from the filtrate yielded a blue solid which was recrystallised from H_2O to afford a dark blue product.

The f.a.b. mass spectrum of the complex shows peaks with the appropriate isotopic distribution at M^+= 577 and 431 due to $[^{106}Pd([18]aneN_2S_4)PF_6]^+$ and $[^{106}Pd([18]aneN_2S_4-H)]^+$ respectively. On the basis of this data together with microanalyses and I.R. spectroscopy, the product was assigned the formulation $[Pd([18]aneN_2S_4)](PF_6)_2$. The ^{13}C DEPT n.m.r. spectrum measured at 298K, exhibits broad, ill-resolved resonances indicative of an averaging process in solution. Cooling to 208K does not freeze out this process sufficiently to enable its characterisation. The ^1H n.m.r. spectrum at 298K is also broad. The second order multiplet at δ= 3.56-2.70ppm, corresponds to the macrocyclic methylene protons, and the resonance at δ= 5.00ppm is assigned to the N-H functions, on the basis of its disappearance after a D_2O shake. Cooling this sample to 243K leads to sharpening of the methylene proton signals. [δ= 3.41-2.75ppm]. The UV/vis spectrum of

$[Pd([18]aneN_2S_4)](PF_6)_2$ shows several intense charge-transfer transitions at λ_{max}= 322nm (ε_{max}= 2,815$M^{-1}cm^{-1}$), 266 (7,910) and 233 (12,140). In addition, a low-intensity transition is observed at 514nm (124), assigned to a d-d transition. This band occurs at much lower energy than is usual for Pd(II) bound to nitrogen or sulphur. Furthermore, the nature of this band is similar to that observed for $[Pd([9]aneS_3)_2]^{2+}$ (λ_{max}= 615nm (ε_{max}= 54$M^{-1}cm^{-1}$)). The single crystal structure of $[Pd([9]aneS_3)_2]^{2+}$ shows a very unusual geometry for the d^8 Pd(II) centre (Fig. 4.2) [120], with the cation adopting a distorted octahedral stereochemistry, [Pd-S_{eq}= 2.332(3), 2.311(3) and Pd-S_{ap}= 2.952(4)Å]. The low energy of the d-d transition in this species is attributed to the interaction of the axial sulphur-donor atoms with the metal centre. The availability of up to six donor atoms in $[Pd([18]aneN_2S_4)]^{2+}$ led us to suggest that a similar unusual stereochemistry may account for its electronic spectrum. In order to elucidate the stereochemistry and co-ordination sphere around the Pd(II) centre, a single crystal X-ray structural determination was undertaken.

Fig. 4.2: Single crystal structure of $[Pd([9]aneS_3)_2]^{2+}$

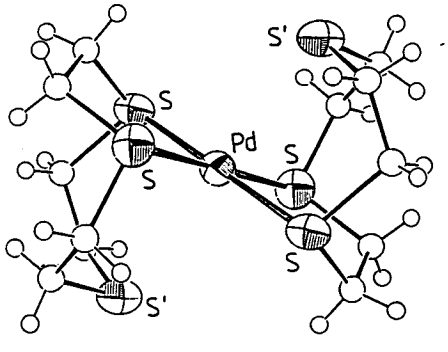

4.2.2: Single Crystal Structure of

$[Pd([18]aneN_2S_4)](BPh_4)_2$.

Details of the structure solution are given in the Experimental Section. Selected bond lengths, angles and torsions are presented in Tables 4.1, 4.2 and 4.3 respectively. ORTEP plots showing the structure of the cation are shown in Figs. 4.3 and 4.4.

Green columnar crystals were obtained by metathesis of the PF_6^- salt of the complex with $NaBPh_4$ in H_2O, followed by recrystallisation from $MeNO_2$. The structure shows the Pd(II) ion co-ordinated to an N_2S_2 donor-set in a square planar configuration, [Pd-S(1)= 2.311(3), Pd-N(7)= 2.123(7), Pd-S(13)= 2.357(3), Pd-N(16)= 2.068(7)Å], with S(1), N(16), S(13) binding meridionally to the metal centre, as found for the octahedral complexes with this macrocycle (Chapters 2 and 3). The two remaining thioether-donors interact at long-range with the metal centre, [Pd...S(10)= 2.954(4), Pd...S(4)= 3.000(3)Å], and are displaced from the least-squares Pd-S(1)-N(7)-S(13)-N(16) plane by +2.863 and -2.901Å respectively. The S(4)-Pd-S(10) angle is 158.94(9)°. The stereochemistry at Pd(II) is therefore distorted octahedral, with a formal $N_2S_2 + S_2$ co-ordination sphere. The approach of the two thioether-donors at long-range is probably responsible for the difference in Pd-N bond lengths (0.055(10)Å). Elongation of the Pd-N(7) bond length may provide a mechanism for the averaging process observed in solution.

Interestingly, $[Pd([18]aneS_6)]^{2+}$ exhibits a different stereochemistry [126], with the macrocycle adopting an S-shaped double boat conformation involving a long-range, weak interaction of the two apical S-donors as illustrated in Fig. 4.5, [$Pd-S_{ap}$= 3.2730(17)Å, $Pd-S_{eq}$= 2.3114(14), 2.3067(15)Å].

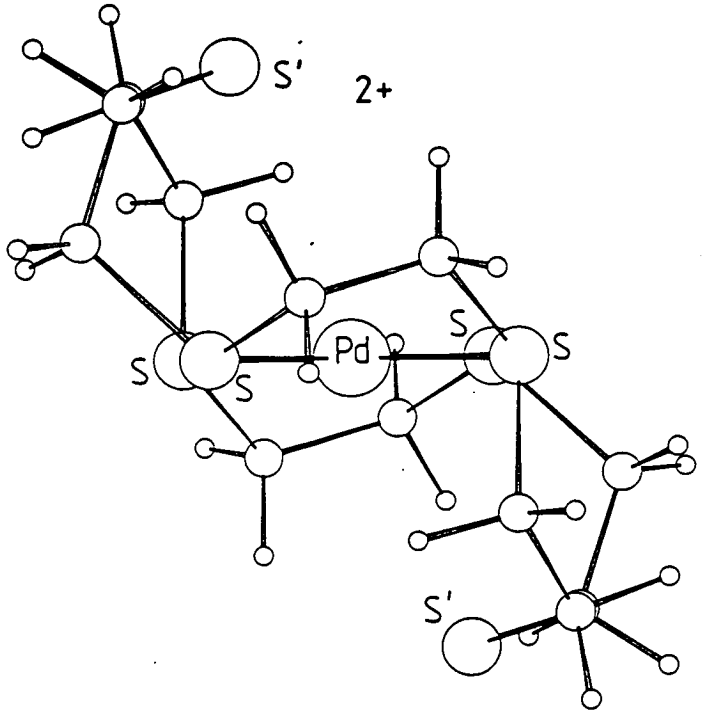

Fig. 4.5: Single crystal structure of $[Pd([18]aneS_6)](BPh_4)_2$

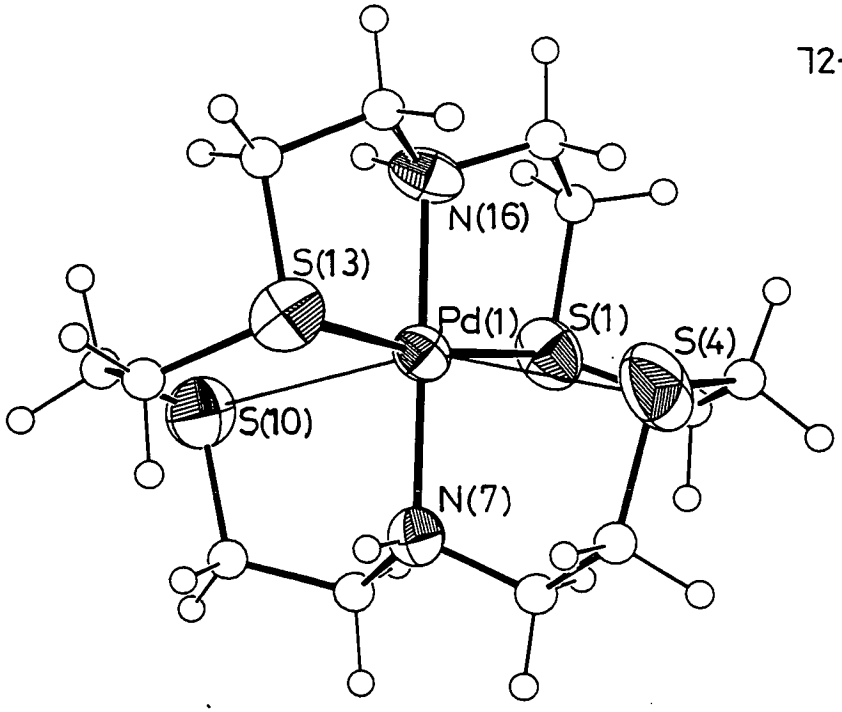

Fig. 4.3: View of the single crystal structure of $[Pd([18]aneN_2S_4)]^{2+}$

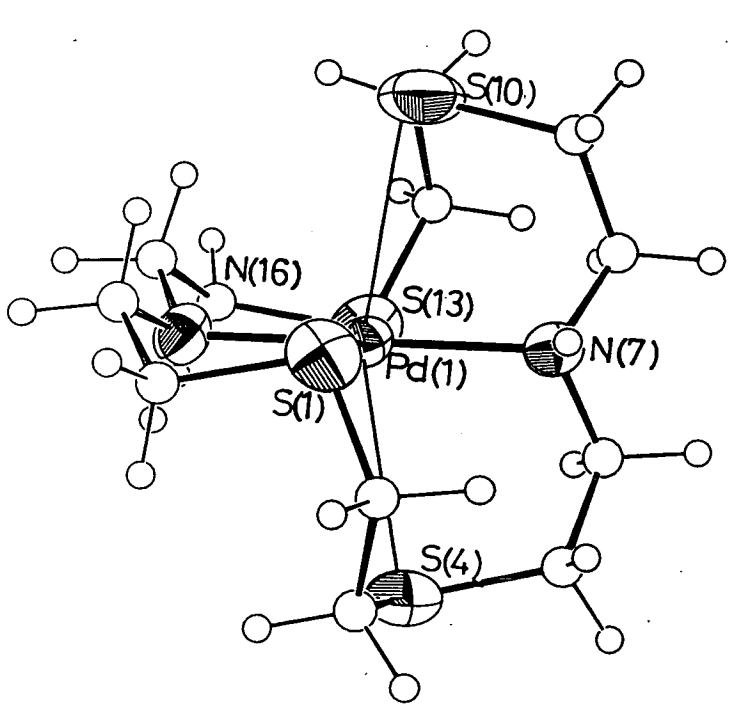

Fig. 4.4: Alternative view of the single crystal structure of $[Pd([18]aneN_2S_4)]^{2+}$

Single Crystal Structure of

$[Pd([18]aneN_2S_4)](BPh_4)_2$

Table 4.1: Selected Bond Lengths(Å) with e.s.d.'s

Pd(1)	- S(1)	2.311(3)	S(13)	-C(12)	1.815(14)
Pd(1)	- S(4)	3.000(3)	S(13)	-C(14)	1.810(11)
Pd(1)	-S(10)	2.954(4)	N(7)	- C(6)	1.472(12)
Pd(1)	-S(13)	2.357(3)	N(7)	- C(8)	1.481(12)
Pd(1)	- N(7)	2.123(7)	N(16)	-C(15)	1.487(13)
Pd(1)	-N(16)	2.068(7)	N(16)	-C(17)	1.463(14)
S(1)	- C(2)	1.778(11)	C(2)	- C(3)	1.545(16)
S(1)	-C(18)	1.835(12)	C(5)	- C(6)	1.523(14)
S(4)	- C(3)	1.798(12)	C(8)	- C(9)	1.512(15)
S(4)	- C(5)	1.806(11)	C(11)	-C(12)	1.493(20)
S(10)	- C(9)	1.795(12)	C(14)	-C(15)	1.506(16)
S(10)	-C(11)	1.788(15)	C(17)	-C(18)	1.497(16)

Table 4.2: Selected Angles(°) with e.s.d.'s

S(1)-Pd(1) - S(4)	81.55(9)	C(9)-S(10)-C(11)	104.2(6)
S(1)-Pd(1) -S(10)	101.52(10)	Pd(1)-S(13)-C(12)	110.6(4)
S(1)-Pd(1) -S(13)	169.54(10)	Pd(1)-S(13)-C(14)	98.5(4)
S(1)-Pd(1) - N(7)	93.93(19)	C(12)-S(13)-C(14)	102.8(6)
S(1)-Pd(1) -N(16)	85.16(21)	Pd(1)- N(7) -C(6)	112.7(5)
S(4)-Pd(1) -S(10)	158.94(9)	Pd(1)- N(7) -C(8)	115.0(5)
S(4)-Pd(1) -S(13)	100.05(9)	C(6)- N(7) -C(8)	108.7(7)
S(4)-Pd(1) - N(7)	78.68(19)	Pd(1)-N(16)-C(15)	109.4(6)
S(4)-Pd(1) -N(16)	101.29(20)	Pd(1)-N(16)-C(17)	112.1(6)
S(10)-Pd(1) -S(13)	80.75(9)	C(15)-N(16)-C(17)	113.2(8)
S(10)-Pd(1) - N(7)	80.31(19)	S(1)- C(2) -C(3)	118.7(8)
S(10)-Pd(1) -N(16)	99.73(21)	S(4)- C(3) -C(2)	117.9(8)
S(13)-Pd(1) - N(7)	96.51(19)	S(4)- C(5) -C(6)	115.8(7)
S(13)-Pd(1) -N(16)	84.39(21)	N(7)- C(6) -C(5)	114.3(8)
N(7)-Pd(1) -N(16)	179.1(3)	N(7)- C(8) -C(9)	114.3(8)
Pd(1)- S(1) - C(2)	110.5(4)	S(10)- C(9) -C(8)	119.4(8)
Pd(1)- S(1) -C(18)	97.0(4)	S(10)-C(11)-C(12)	120.7(10)
C(2)- S(1) -C(18)	101.6(5)	S(13)-C(12)-C(11)	118.2(10)
Pd(1)- S(4) - C(3)	94.8(4)	S(13)-C(14)-C(15)	111.3(8)
Pd(1)- S(4) - C(5)	87.4(3)	N(16)-C(15)-C(14)	110.2(9)
C(3)- S(4) - C(5)	101.6(5)	N(16)-C(17)-C(18)	108.6(9)
Pd(1)-S(10) - C(9)	86.7(4)	S(1)-C(18)-C(17)	105.8(8)
Pd(1)-S(10) -C(11)	96.9(5)		

Table 4.3: Selected Torsion Angles(^{o}) with e.s.d.'s

C(18)	- S(1)	- C(2)	- C(3)	61.4(9)
C(6)	- N(7)	- C(8)	- C(9)	179.6(8)
C(2)	- S(1)	-C(18)	-C(17)	-153.2(8)
C(17)	-N(16)	-C(15)	-C(14)	-176.7(9)
C(5)	- S(4)	- C(3)	- C(2)	59.1(9)
C(15)	-N(16)	-C(17)	-C(18)	-176.6(9)
C(3)	- S(4)	- C(5)	- C(6)	-123.1(8)
S(1)	- C(2)	- C(3)	- S(4)	50.5(11)
C(11)	-S(10)	- C(9)	- C(8)	-65.7(10)
S(4)	- C(5)	- C(6)	- N(7)	63.8(10)
C(9)	-S(10)	-C(11)	-C(12)	63.2(12)
N(7)	- C(8)	- C(9)	-S(10)	-59.2(11)
C(14)	-S(13)	-C(12)	-C(11)	67.4(11)
S(10)	-C(11)	-C(12)	-S(13)	44.0(15)
C(12)	-S(13)	-C(14)	-C(15)	-94.8(9)
S(13)	-C(14)	-C(15)	-N(16)	-49.3(10)
C(8)	- N(7)	- C(6)	- C(5)	168.9(8)
N(16)	-C(17)	-C(18)	- S(1)	62.0(10)

4.2.3: $[Pt([18]aneN_2S_4)](PF_6)_2$

The yellow complex, $[Pt([18]aneN_2S_4)](PF_6)_2$ has been prepared by the same method as for the Pd analogue. This species shows peaks in the f.a.b. mass spectrum with the correct isotopic distribution at M^+= 667 and 521, assigned to $[^{195}Pt([18]aneN_2S_4+H)PF_6]^+$ and $[^{195}Pt([18]aneN_2S_4)]^+$ respectively. The complex was assigned on the basis of this data together with I.R. and microanalytical data. The ^1H n.m.r. spectrum exhibits an N-H resonance at δ= 5.68ppm, as well as a broad, second-order multiplet due to the macrocyclic methylene protons in the range δ= 2.84-3.42ppm. The ^{13}C DEPT n.m.r. spectrum measured at 298K, 50.32MHz, shows six broadened methylene carbon resonances at δ= 55.39 (two overlapping $N\underline{C}H_2$ resonances), 53.11 ($N\underline{C}H_2$), 36.84, 34.74 and 28.08ppm ($3xS\underline{C}H_2$). Remeasuring the sample using a higher field strength, (90.56MHz, in $(CD_3)_2CO$), clarifies the spectrum, revealing methylene carbon resonances at δ= 56.1 (2C, $N\underline{C}H_2$), 53.8 (2C, $N\underline{C}H_2$), 46.6, 42.0, 38.3; 37.3, 35.3 (2C), 28.2 and 26.3ppm (total of 8C, $S\underline{C}H_2$). These data are consistent with a distorted 5-co-ordinate square-based pyramidal stereochemistry around Pt(II), involving primary N_2S_2 co-ordination, with one axial S-donor and the other S-donor dangling (Fig. 4.6). A single crystal X-ray structural determination of $[Pt([18]aneN_2S_4)]^{2+}$ would be required to confirm this. An elongated square-based pyramidal geometry has been observed for $[Pt([9]aneS_3)_2]^{2+}$ (Fig. 4.7) [122],

[Pt-S_{eq}= 2.25-2.30Å, Pt-S_{ap}= 2.88Å]. The sixth thioether-donor atom is not co-ordinated to the metal centre [Pt···S'= 4.04Å].

Fig. 4.7: Single crystal structure of $[Pt([9]aneS_3)_2]^{2+}$

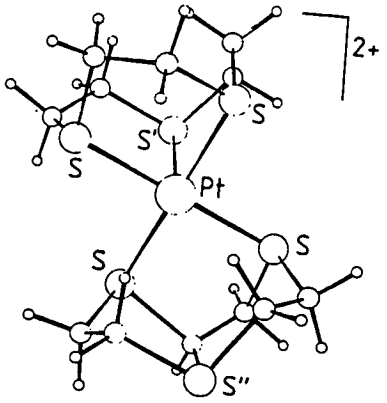

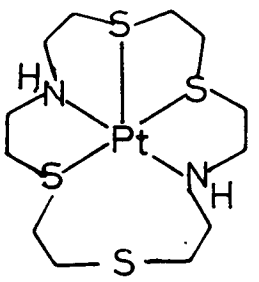

Fig. 4.6: Proposed structure of $[Pt([18]aneN_2S_4)]^{2+}$

4.2.4: $[Pd(Me_2[18]aneN_2S_4)](PF_6)_2$

Treatment of $PdCl_2$ with one molar equivalent of $Me_2[18]aneN_2S_4$ in refluxing $MeCN/H_2O$ affords an orange solution. Addition of excess NH_4PF_6 gave an orange product which was recrystallised from MeCN.

The f.a.b. mass spectrum of the product exhibits molecular ion peaks at M^+= 604 and 460 corresponding to $[^{106}Pd(Me_2[18]aneN_2S_4-H)PF_6]^+$ and $[^{106}Pd(Me_2[18]aneN_2S_4)]^+$ respectively. These data together with microanalyses and I.R. spectroscopy confirm the formulation $[Pd(Me_2[18]aneN_2S_4)](PF_6)_2$. The ^1H n.m.r. spectrum of the complex shows a singlet at δ= 2.48ppm due to the methyl protons. A complex, second-order multiplet is apparent in the range δ= 2.68-3.50ppm arising from the methylene protons. ^{13}C DEPT n.m.r. spectroscopy of $[Pd(Me_2[18]aneN_2S_4)]^{2+}$ shows four distinct resonances at δ= 49.87, 40.31, 39.40 ($\underline{C}H_2$) and 41.57ppm ($\underline{C}H_3$). These

data confirm the presence of only one isomer in solution, and are consistent with a square planar stereochemistry around the Pd(II) centre. In view of the unusual geometry observed for $[Pd([18]aneN_2S_4)]^{2+}$, it was important to confirm the stereochemistry adopted by this di-N-methylated analogue, and also to determine the precise donor-set to the Pd(II) ion. A single crystal X-ray structural determination was therefore undertaken.

4.2.5: Single Crystal Structure of

$[Pd(Me_2[18]aneN_2S_4)](PF_6)_2.Me_2CO$

Details of the structure solution are given in the Experimental Section. Bond lengths, angles and torsions are listed in Tables 4.4, 4.5 and 4.6 respectively, and two ORTEP plots showing the cationic geometry are presented in Figures 4.8 and 4.9.

The structure of $[Pd(Me_2[18]aneN_2S_4)](PF_6)_2.Me_2CO$ is markedly different from that determined for the non-methylated analogue. It shows square planar co-ordination of the four thioether-donors of the macrocycle to the Pd(II) ion, [Pd-S(1)= 2.3399(22), Pd-S(4)= 2.3331(22), Pd-S(10)= 2.3261(22), Pd-S(13)= 2.3239(21)Å]. The two N-Me functions are orientated away from, and do not interact with, the metal centre, [Pd···N(7)= 3.744(7), Pd···N(16)= 3.760(6)Å]. The macrocycle, therefore, co-ordinates to the Pd(II) centre as a simple tetradentate thioether-donor.

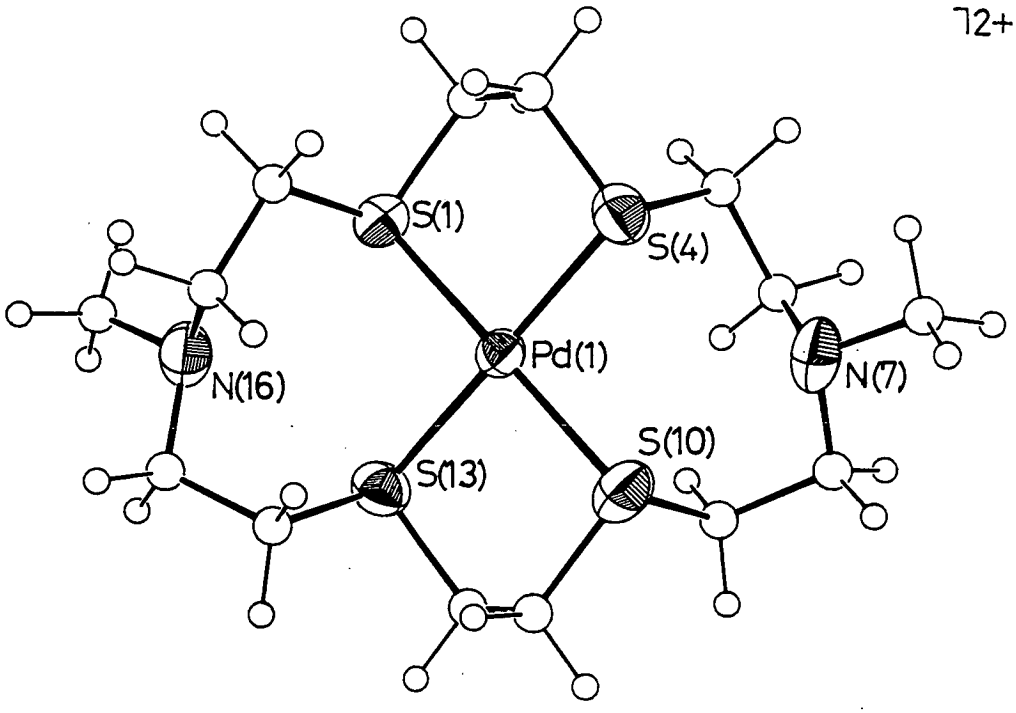

Fig. 4.8: View of the single crystal structure of $[Pd(Me_2[18]aneN_2S_4)]^{2+}$

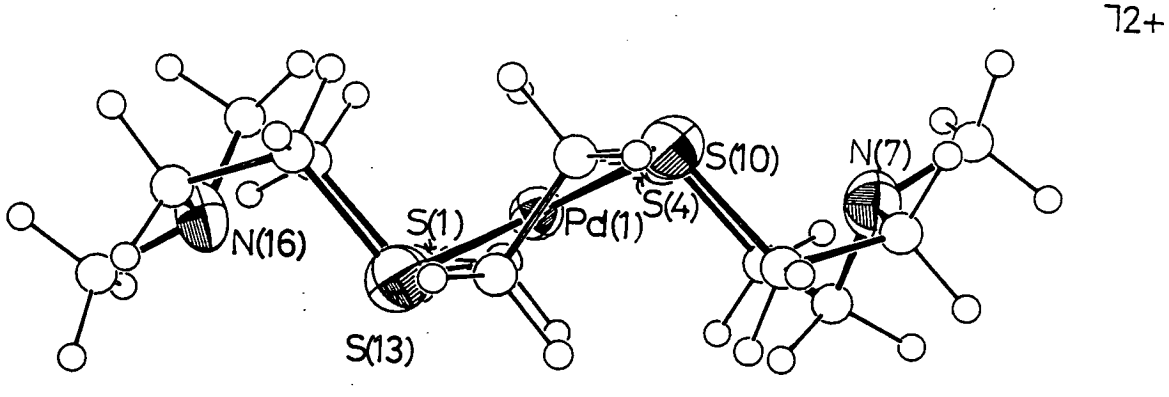

Fig. 4.9: Alternative view of the single crystal structure of $[Pd(Me_2[18]aneN_2S_4)]^{2+}$

Single Crystal Structure of

$[Pd(Me_2[18]aneN_2S_4)](PF_6)_2.(CH_3)_2CO$

Table 4.4: Selected Bond Lengths(Å) with e.s.d.'s

Pd - S(1)	2.3399(22)	N(7) -C(7N')	1.467(24)
Pd -S(13)	2.3239(21)	N(16) -C(15)	1.450(12)
Pd - S(4)	2.3331(22)	N(16) -C(15')	1.47(3)
Pd -S(10)	2.3261(22)	N(16) -C(17)	1.467(11)
S(1) - C(2)	1.810(10)	N(16) -C(17')	1.47(3)
S(1) -C(18)	1.816(8)	N(16) -C(16N)	1.462(14)
S(13)-C(12)	1.818(9)	N(16) -C(16')	1.47(4)
S(13)-C(14)	1.827(9)	C(2) - C(3)	1.515(13)
S(4) - C(3)	1.809(9)	C(5) - C(6)	1.533(15)
S(4) - C(5)	1.842(9)	C(5) -C(6')	1.557(20)
S(10)- C(9)	1.840(9)	C(8) - C(9)	1.547(14)
S(10)-C(11)	1.815(10)	C(8') - C(9)	1.537(20)
N(7) - C(6)	1.469(14)	C(11) -C(12)	1.488(13)
N(7) -C(6')	1.468(19)	C(14) -C(15)	1.535(13)
N(7) - C(8)	1.455(13)	C(14) -C(15')	1.53(3)
N(7) -C(8')	1.482(19)	C(17) -C(18)	1.521(12)
N(7) -C(7N)	1.469(18)	C(17')-C(18)	1.55(3)

Table 4.5: Selected Angles(°) with e.s.d.'s

S(1) - Pd -S(13)	90.59(7)	C(15) -N(16) -C(16N)	115.2(7)
S(1) - Pd - S(4)	89.21(8)	C(15')-N(16) -C(17')	115.5(16)
S(1) - Pd -S(10)	179.43(8)	C(15')-N(16) -C(16')	101.4(19)
S(13)- Pd - S(4)	179.52(8)	C(17) -N(16) -C(17')	51.1(12)
S(13)- Pd -S(10)	89.00(8)	C(17) -N(16) -C(16N)	109.2(7)
S(4) - Pd -S(10)	91.21(8)	C(17')-N(16) -C(16')	118.8(19)
Pd - S(1) - C(2)	101.1(3)	S(1) - C(2) - C(3)	111.6(7)
Pd - S(1) -C(18)	109.7(3)	S(4) - C(3) - C(2)	111.0(6)
C(2) - S(1) -C(18)	98.4(4)	S(4) - C(5) - C(6)	105.6(7)
Pd -S(13) -C(12)	101.8(3)	S(4) - C(5) -C(6')	108.4(8)
Pd -S(13) -C(14)	109.4(3)	N(7) - C(6) - C(5)	108.5(9)
C(12)-S(13) -C(14)	98.0(4)	N(7) -C(6') - C(5)	107.4(12)
Pd - S(4) - C(3)	101.2(3)	N(7) -C(6') - C(8)	59.2(8)
Pd - S(4) - C(5)	107.6(3)	N(7) - C(8) - C(9)	108.8(8)
C(3) - S(4) - C(5)	99.0(4)	N(7) -C(8') - C(9)	108.0(12)
Pd -S(10) - C(9)	107.8(3)	S(10) - C(9) - C(8)	110.9(6)
Pd -S(10) -C(11)	102.2(3)	S(10) -C(11) -C(12)	112.1(7)
C(9) -S(10) -C(11)	98.3(4)	S(13) -C(12) -C(11)	112.3(6)
C(6) - N(7) - C(8)	111.3(8)	S(13) -C(14) -C(15)	109.4(6)
C(6) - N(7) -C(7N)	107.0(9)	N(16) -C(15) -C(14)	110.1(8)
C(6')- N(7) -C(8')	114.1(11)	N(16) -C(15')-C(14)	108.8(17)
C(6')- N(7) -C(7N')	119.1(12)	N(16) -C(17) -C(18)	110.2(7)
C(8) - N(7) -C(7N)	115.6(9)	N(16) -C(17')-C(18)	108.6(18)
C(8')- N(7) -C(7N)	68.3(10)	S(1) -C(18) -C(17)	106.6(6)
C(8')- N(7) -C(7N')	107.1(12)	S(1) -C(18) -C(17')	108.2(11)

Table 4.6: Selected Torsion Angles(°) with e.s.d.'s

C(18)	-S(1)	- C(2)	-C(3)	-70.6(7)
C(7N')	-N(7)	- C(8')	-C(9)	-168.1(13)
C(2)	- S(1)	- C(18)	-C(17)	-150.8(6)
C(17)	-N(16)	- C(15)	-C(14)	157.7(7)
C(2)	- S(1)	- C(18)	-C(17')	157.9(12)
C(16N)	-N(16)	- C(15)	-C(14)	-76.2(10)
C(14)	-S(13)	- C(12)	-C(11)	71.4(7)
C(17')	-N(16)	- C(15')	-C(14)	57.9(22)
C(12)	-S(13)	- C(14)	-C(15)	-161.7(6)
C(16')	-N(16)	- C(15')	-C(14)	-172.2(20)
C(12)	-S(13)	- C(14)	-C(15')	146.5(11)
C(15)	-N(16)	- C(17)	-C(18)	-67.2(9)
C(5)	-S(4)	- C(3)	-C(2)	-67.1(7)
C(16N)	-N(16)	- C(17)	-C(18)	163.4(8)
C(3)	S(4)	- C(5)	-C(6)	-148.2(7)
C(15')	-N(16)	- C(17')	-C(18)	-158.8(16)
C(3)	-S(4)	- C(5)	-C(6')	159.8(9)
C(16')	-N(16)	- C(17')	-C(18)	80.4(25)
C(11)	-S(10)	- C(9)	-C(8)	-159.2(7)
S(1)	-C(2)	- C(3)	-S(4)	-59.1(8)
C(11)	-S(10)	- C(9)	-C(8')	147.0(8)

Table 4.6: continued

S(4)	-C(5)	- C(6)	-N(7)	-52.4(9)
C(9)	-S(10)	- C(11)	-C(12)	70.8(7)
S(4)	-C(5)	- C(6')	-N(7)	46.6(12)
C(8)	-N(7)	- C(6)	-C(5)	-66.2(10)
N(7)	-C(8)	- C(9)	-S(10)	-45.2(9)
C(7N)	-N(7)	- C(6)	-C(5)	166.7(9)
N(7)	-C(8')	- C(9)	-S(10)	60.0(11)
C(8')	-N(7)	- C(6')	-C(5)	-158.6(11)
S(10)	-C(11)	- C(12)	-S(13)	55.3(8)
C(7N')	-N(7)	- C(6')	-C(5)	73.2(16)
S(13)	-C(14)	- C(15)	-N(16)	-43.6(9)
C(6)	-N(7)	- C(8)	-C(9)	159.2(8)
S(13)	-C(14)	- C(15')	-N(16)	58.2(17)
C(7N)	-N(7)	- C(8)	-C(9)	-78.5(11)
N(16)	-C(17)	- C(18)	-S(1)	-51.0(8)
C(6')	-N(7)	- C(8')	-C(9)	57.8(15)
N(16)	-C(17')	- C(18)	-S(1)	48.3(18)

A comparison of the crystal structures of $[Pd([18]aneN_2S_4)]^{2+}$ and $[Pd(Me_2[18]aneN_2S_4)]^{2+}$ demonstrates that replacement of N-H by N-Me moieties has a remarkable influence on the stereochemistry around the Pd(II) ion. This difference is attributed to the steric bulk of the N-Me groups. Fig. 4.10 shows a space-filling model of $[Pd([18]aneN_2S_4)]^{2+}$, viewed along the N(7)-H(7) bond. It can be seen from this that the proton on N(7) fits neatly into the *niche* between the sulphur-donors. However, a methyl group is significantly larger, and therefore, replacement of this proton with a methyl group would necessitate a conformational change, as found in $[Pd(Me_2[18]aneN_2S_4)](PF_6)_2$.

Fig. 4.10: Space-filling diagram of $[Pd([18]aneN_2S_4)]^{2+}$

N2S4PD in P21/c

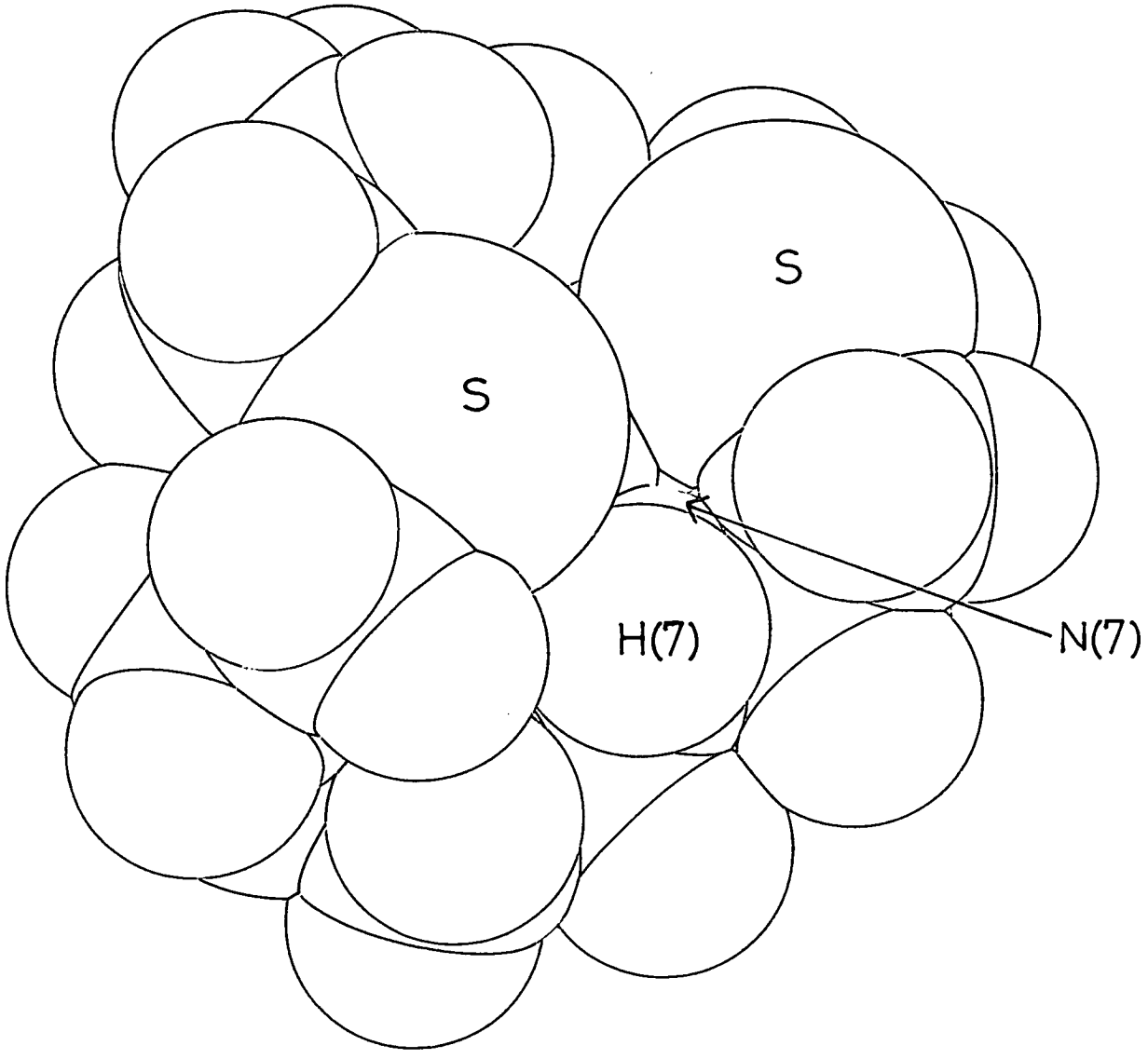

4.2.6: $[Pt(Me_2[18]aneN_2S_4)](PF_6)_2$

$[Pt(Me_2[18]aneN_2S_4)](PF_6)_2$ has also been prepared by an analogous route to the Pd system. The resulting cream solid has been characterised by f.a.b. mass spectroscopy, which exhibits molecular ion peaks at M^+= 694 and 549 ascribed to $[^{195}Pt(Me_2[18]aneN_2S_4)PF_6]^+$ and $[^{195}Pt(Me_2[18]aneN_2S_4)]^+$ respectively. I.R. spectroscopy and microanalytical data are consistent with this formulation. The ^1H n.m.r. spectrum of this complex, (Fig. 4.11), shows a singlet at δ= 2.46ppm due to the methyl protons. The second-order patterns at δ= 3.18-3.30 and 3.55-3.62ppm integrate to a total of sixteen protons, and, therefore, are assigned to the methylene protons adjacent to sulphur. These multiplets show ^{195}Pt satellites (I= 1/2, 33.7%), which are broadened due to chemical shift anisotropy relaxation. The multiplets at δ= 2.54-2.62 and 2.80-2.87ppm are assigned to the methylene protons adjacent to the N-donors. The ^{13}C DEPT n.m.r. spectrum of $[Pt(Me_2[18]aneN_2S_4)]^{2+}$ is almost identical to that of the Pd(II) complex, with one methyl carbon resonance at δ= 40.83ppm and three distinct methylene carbon resonances at δ= 49.18, 39.87 and 39.28ppm. This evidence suggests that $[Pt(Me_2[18]aneN_2S_4)](PF_6)_2$ is probably isostructural with its Pd analogue.

Fig. 4.11: ^{1}H n.m.r. spectrum of $[Pt(Me_2[18]aneN_2S_4)]^{2+}$ (CD_3CN, 360.13MHz)

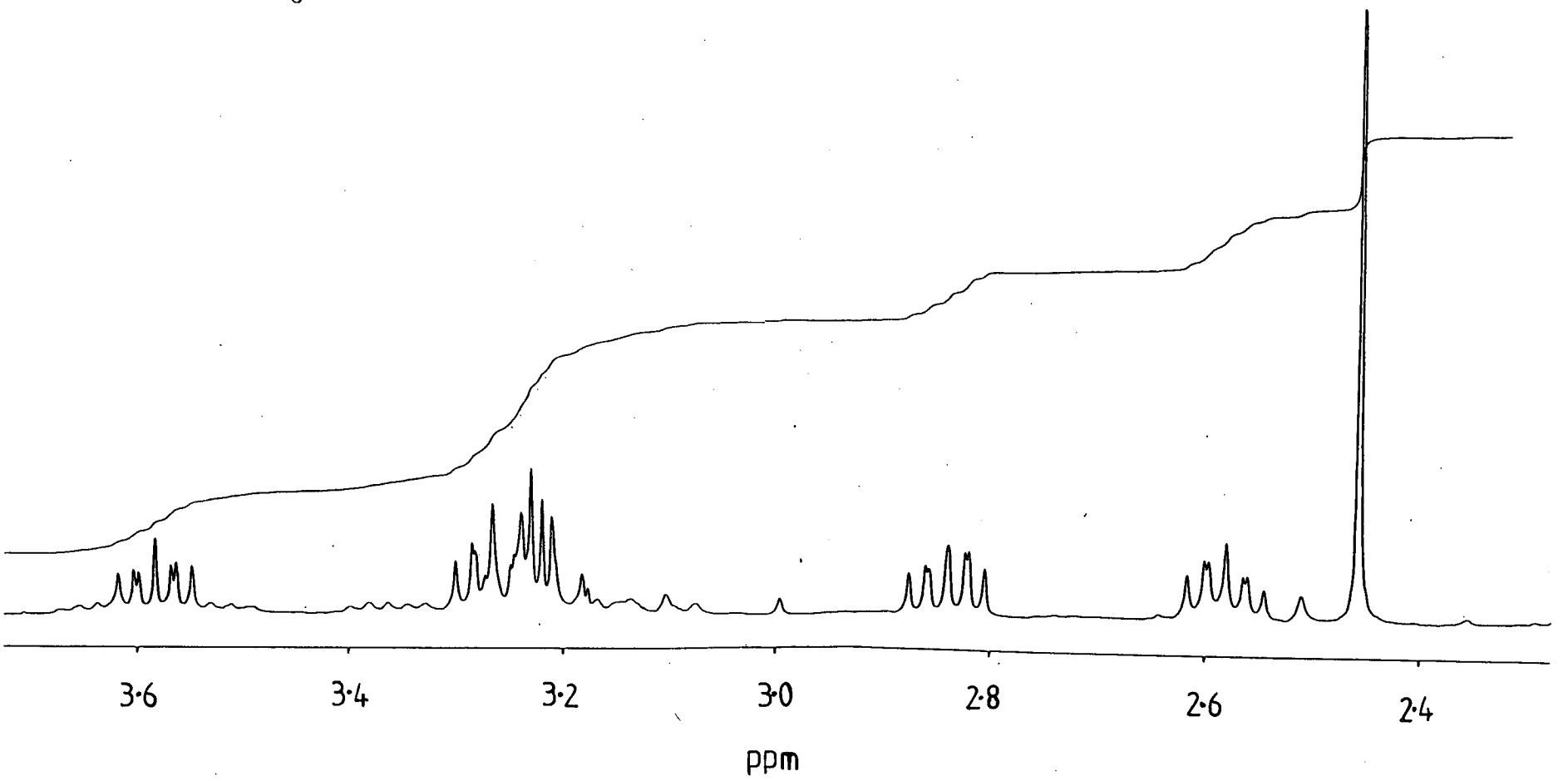

4.3: Electrochemical Study of $[M(L)]^{2+}$

(M= Pd, Pt, L= [18]aneN$_2$S$_4$, Me$_2$[18]aneN$_2$S$_4$)

In view of the paucity of literature relating to genuine d^7 or d^9 Pt and Pd monomeric species, and the recently reported successful stabilisation of these +1 and +3 metal oxidation states by polythia and polyaza macrocyclic ligands, we undertook an investigation of the redox and electronic properties of $[M([18]aneN_2S_4)]^{2+}$ and $[M(Me_2[18]aneN_2S_4)]^{2+}$, (M= Pd, Pt).

4.3.1: $[M([18]aneN_2S_4)]^{2+}$ (M= Pd, Pt)

Cyclic voltammetry of $[Pd([18]aneN_2S_4)](PF_6)_2$ in MeCN (0.1M $NBu^n{}_4PF_6$ supporting electrolyte) at platinum electrodes shows a chemically reversible oxidation at $E_{1/2}$= +0.57V *vs.* Fc/Fc^+ (ΔE_p= 195mV at a scan rate of 150mVs^{-1}), (Fig. 4.12). An irreversible reduction is also observed at E_{pc}= -1.53V *vs.* Fc/Fc^+. Coulometric measurements performed on the complex in MeCN at +0.75V *vs.* Fc/Fc^+, at a platinum basket electrode, give n= 0.95 electrons, for complete conversion to the bright-red oxidised species. Thus, this process corresponds to a one-electron oxidation. The e.s.r. spectrum of the oxidation product, measured at 77K as a frozen glass, shows a strong anisotropic signal with, g_1= 2.064, g_2= 2.052 and g_3= 2.019, (Fig. 4.13). These spectral features are consistent with the formation of the d^7 Pd(III) species, $[Pd([18]aneN_2S_4)]^{3+}$ [116,120,121,123].

Further verification for the process being predominantly metal-based comes from the appearance of some unresolved hyperfine coupling to ^{105}Pd (I= 5/2, 22.2%). Comparable spectral features have been observed for $[Pd([9]aneS_3)_2]^{3+}$ as well as for Pd(III)-dithiolene complexes [116,127,128].

Oxidation of Pd(II) to Pd(III) was monitored by <u>in situ</u> UV/vis spectroscopy using an O.T.T.L.E. system. Conversion of $[Pd([18]aneN_2S_4)]^{2+}$ to $[Pd([18]aneN_2S_4)]^{3+}$ occurs <u>reversibly</u> and <u>isosbestically</u> (λ_{iso}= 241nm), (Fig. 4.14). $[Pd([18]aneN_2S_4)]^{2+}$: λ_{max}= 514nm (ε_{max}= 124$M^{-1}cm^{-1}$), 332 (4,250), 166 (10,000), 233 (10,850); $[Pd([18]aneN_2S_4)]^{3+}$: λ_{max}= 488nm (ε_{max}= 3,180$M^{-1}cm^{-1}$), 341 (5,890), 264 (11,170).

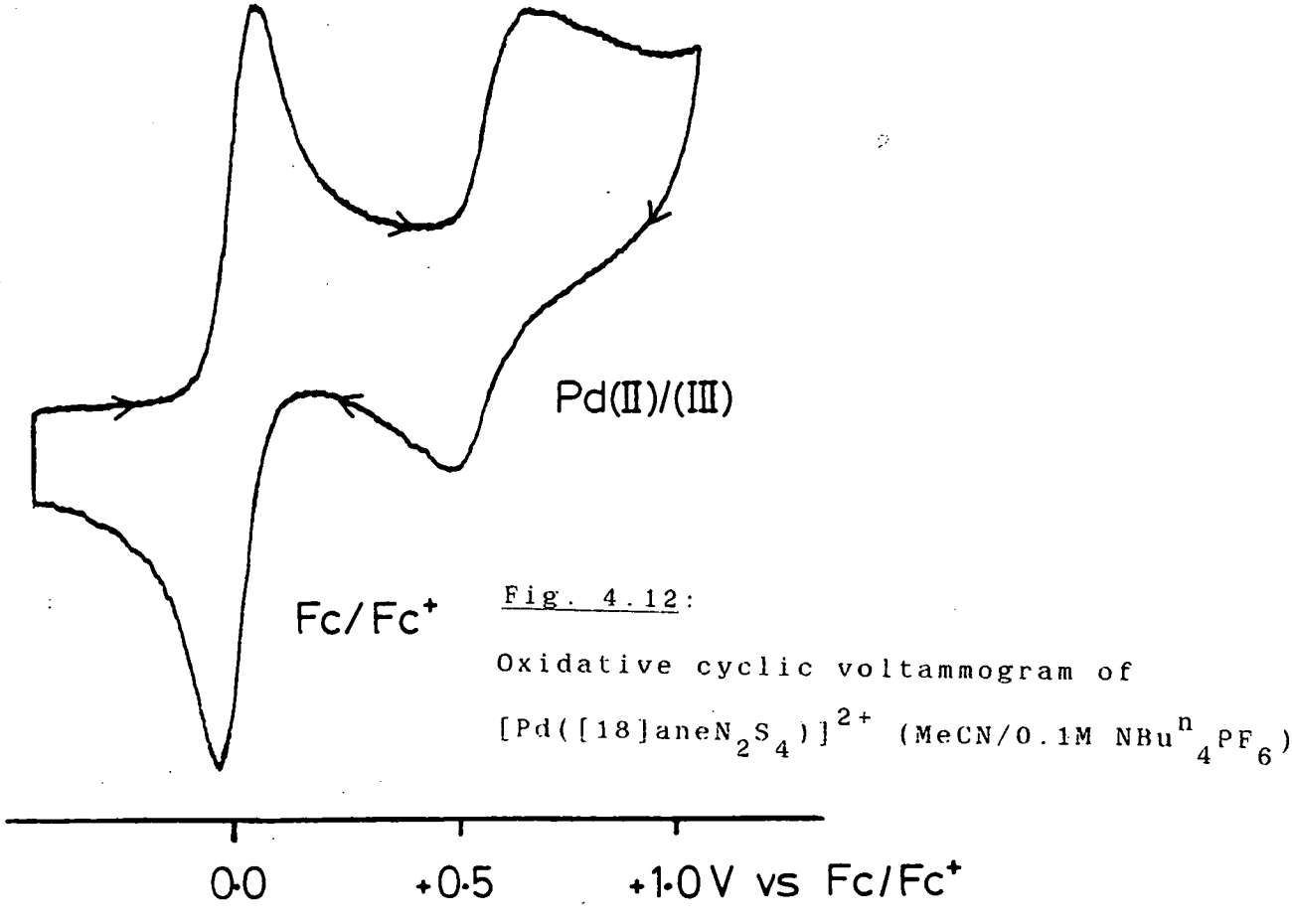

<u>Fig. 4.12</u>:
Oxidative cyclic voltammogram of $[Pd([18]aneN_2S_4)]^{2+}$ (MeCN/0.1M $NBu^n_4PF_6$)

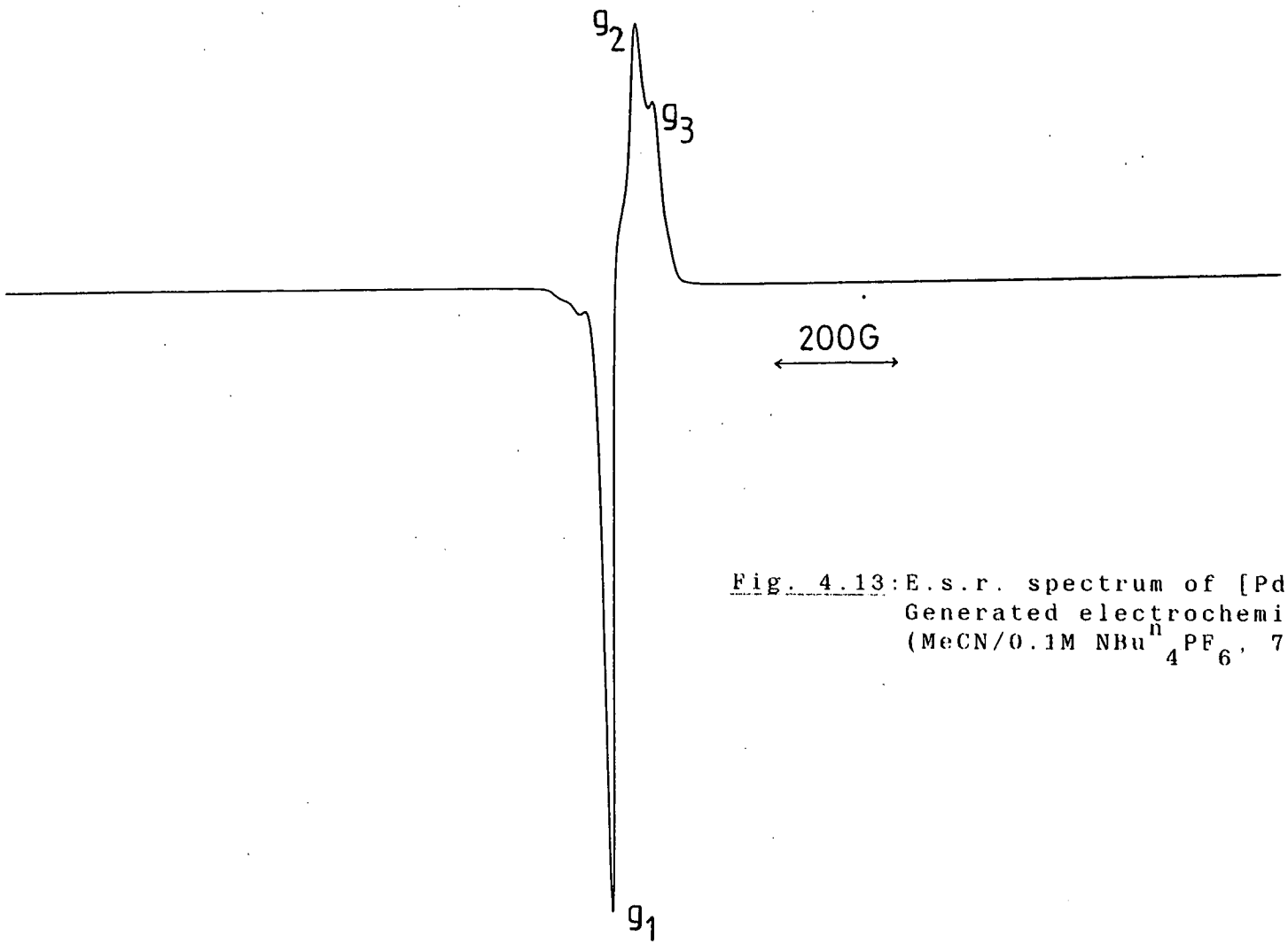

Fig. 4.13: E.s.r. spectrum of $[Pd([18]aneN_2S_4)]^{3+}$
Generated electrochemically
(MeCN/0.1M $NBu^n_4PF_6$, 77K)

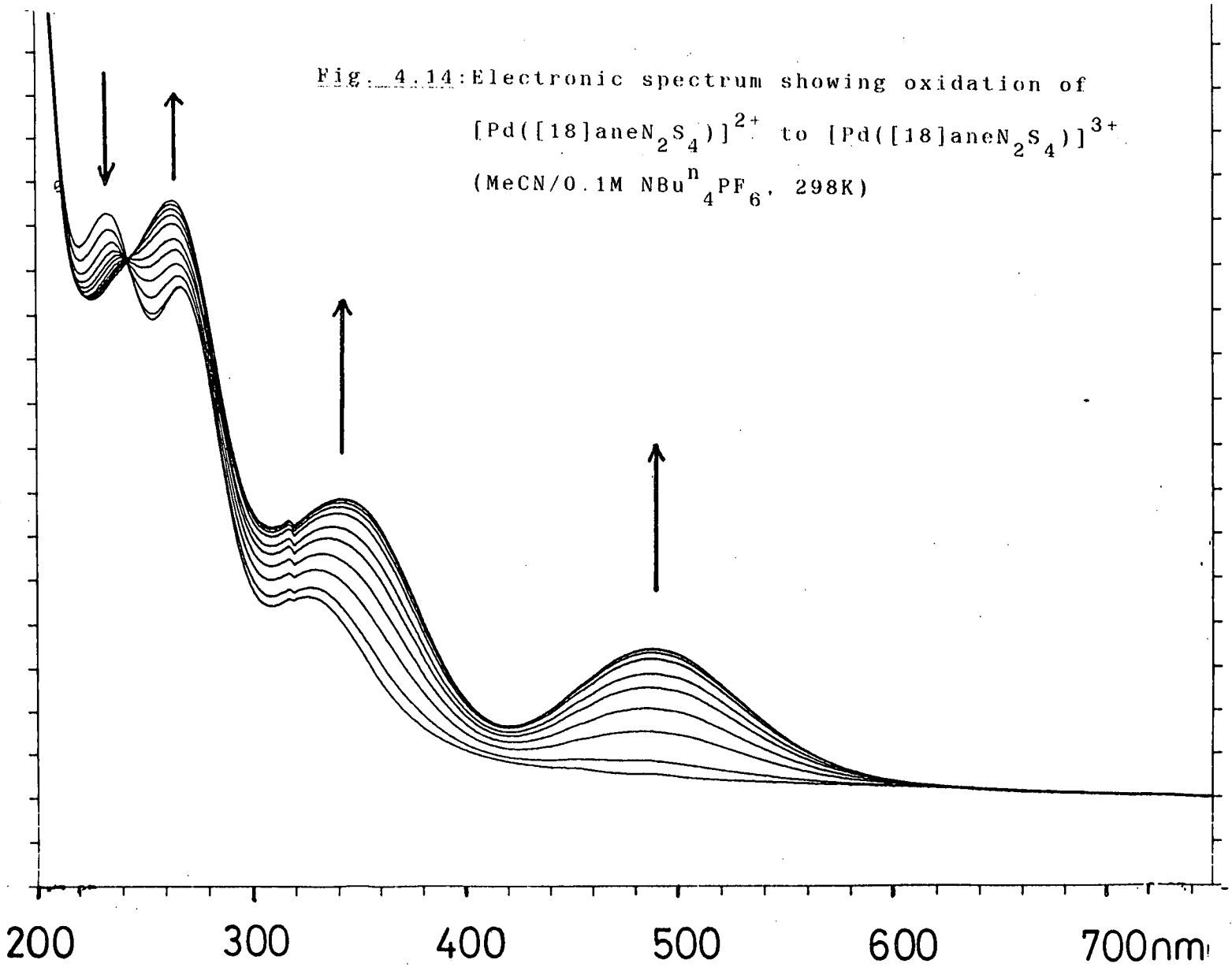

Fig. 4.14: Electronic spectrum showing oxidation of $[Pd([18]aneN_2S_4)]^{2+}$ to $[Pd([18]aneN_2S_4)]^{3+}$ (MeCN/0.1M $NBu^n_4PF_6$, 298K)

A preliminary electrochemical study of $[Pt([18]aneN_2S_4)](PF_6)_2$ was undertaken using the same conditions. The cyclic voltammogram of $[Pt([18]aneN_2S_4)]^{2+}$ shows a chemically reversible oxidation at E_{pa}= +1.07V, E_{pc}= -0.01V *vs.* Fc/Fc^+, (Fig. 4.15). This is an exceptionally broad wave, with ΔE_p= 1180mV at a scan rate of $330mVs^{-1}$. An irreversible reduction is also apparent at E_{pc}= -1.82V *vs.* Fc/Fc^+. Coulometric measurements performed at +1.75V *vs.* Ag/AgCl gave a yellow solution with n= 1.08 electrons. The e.s.r. spectrum (77K, MeCN glass) of the oxidation product shows a rhombic signal, g_1= 2.115, g_2= 2.049, g_3= 1.987, (Fig. 4.16). Hyperfine coupling to ^{195}Pt (I= 1/2, 33.7%) is difficult to discern due to the weakness of the signal. However, these data are consistent with the formation, in low yield, of a d^7 Pt(III) species [114,122]. We tentatively suggest that the low yield of $[Pt([18]aneN_2S_4)]^{3+}$ may be due to a C-H deprotonation reaction similar to that observed in the 3+ cations, $[Rh([9]aneS_3)_2]^{3+}$, (Chapter 3), and $[Rh([18]aneS_6)]^{3+}$. The exceptionally broad oxidation wave for $[Pt([18]aneN_2S_4)]^{2+/3+}$ suggests that a large stereochemical change at the metal centre occurs upon oxidation to Pt(III).

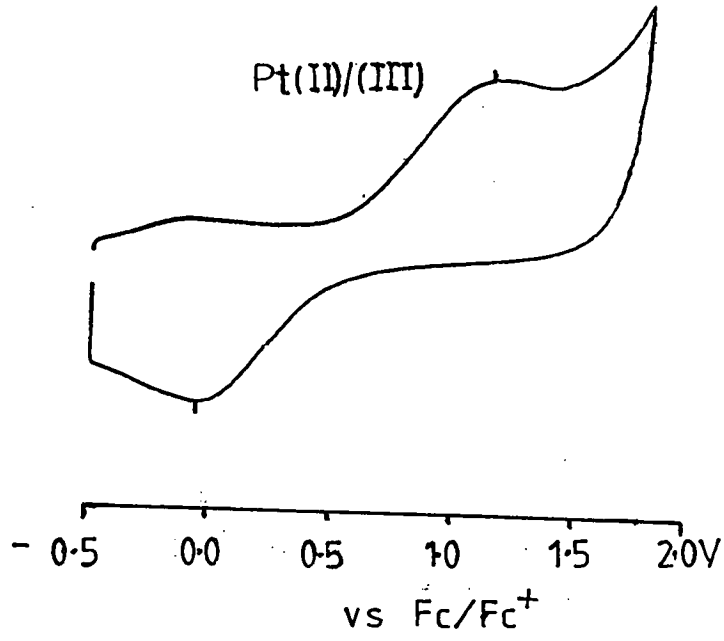

Fig. 4.15: Oxidative cyclic voltammogram of $[Pt([18]aneN_2S_4)]^{2+}$ ($MeCN/0.1M\ NBu^n_4PF_6$)

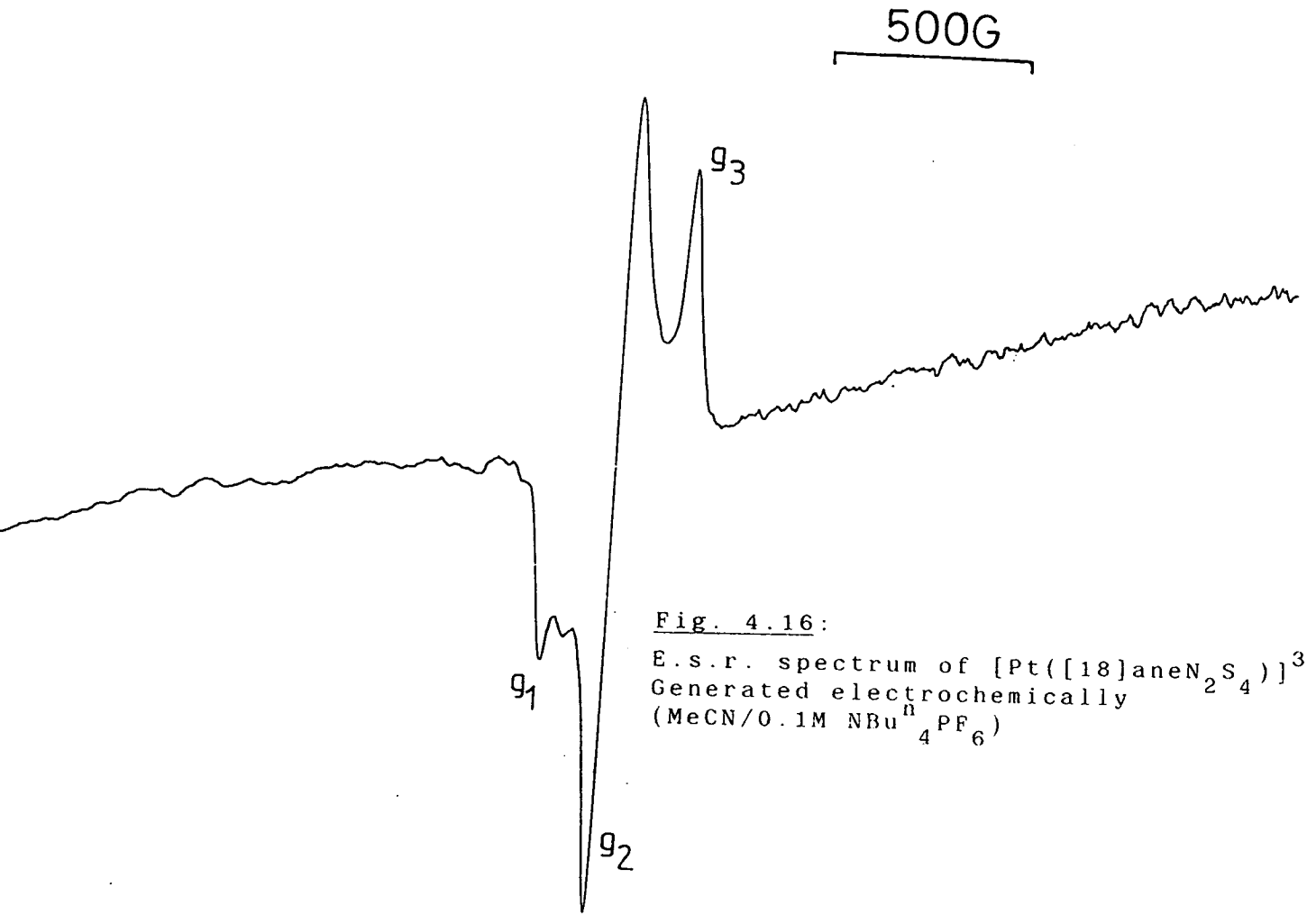

Fig. 4.16:
E.s.r. spectrum of $[Pt([18]aneN_2S_4)]^{3+}$ Generated electrochemically ($MeCN/0.1M\ NBu^n_4PF_6$)

4.3.2: $[M(Me_2[18]aneN_2S_4)]^{2+}$ (M= Pd, Pt)

Cyclic voltammetry of $[Pd(Me_2[18]aneN_2S_4)](PF_6)_2$, measured under the same conditions as described above, reveals a chemically reversible reduction occurring at $E_{1/2}$= -0.74V *vs.* Fc/Fc^+ (ΔE_p= 72mV at a scan rate of $100mVs^{-1}$) as shown in Fig. 4.17. No oxidative activity is observed within the range of the solvent up to +2.0V. Coulometry, measured by bulk electrogeneration of the complex at -0.90V *vs.* Fc/Fc^+, confirms that the reduction corresponds to a one-electron process (n= 1.08 electrons), giving a bright yellow paramagnetic species. The e.s.r. spectrum of this product shows (Fig. 4.18) a strong anisotropic signal with axial symmetry, g_{11}= 2.155, $g_{\perp}$= 2.049. In the $g_{\perp}$ region, the 1st, 2nd, 5th and 6th features of the hyperfine coupling to ^{105}Pd are evident, giving $A_{\perp}$= 34G. Similarly, close examination of the g_{11} region allows the 1st and 2nd features to be discerned, giving A_{11}= 48G. This data is consistent with the formation of a metal-based d^9 Pd(I) radical [117-119,129,130]. Interestingly, the g-values for this species are closer to the free-spin value of 2.0023 than those for the only other macrocyclic Pd(I) monomers reported, $[Pd(Me_4[14]aneN_4)]^+$ (g_{11}= 2.302, $g_{\perp}$= 2.076) and $[Pd(Bz_4[14]aneN_4)]^+$ (g_{11}= 2.320, $g_{\perp}$= 2.086), indicating a greater degree of covalency in $[Pd(Me_2[18]aneN_2S_4)]^+$. This can be attributed to the π-acidity of the

thioether-donors which allows some delocalisation of electron-density onto the S-donors.

The reduction of $[Pd(Me_2[18]aneN_2S_4)]^{2+}$ to $[Pd(Me_2[18]aneN_2S_4)]^{+}$ was also followed by <u>in situ</u> UV/vis spectroscopy using an O.T.T.L.E. system (Fig. 4.19). Importantly, the spectrum shows the process to occur both reversibly and isosbestically (λ_{iso}= 224, 274nm; $[Pd(Me_2[18]aneN_2S_4)]^{2+}$: λ_{max}= 373nm (ε_{max}= 3,004$M^{-1}cm^{-1}$), 298 (14,460), 232 (15,070); $[Pd(Me_2[18]aneN_2S_4)]^{+}$: λ_{max}= 290nm (ε_{max}= 9,300$M^{-1}cm^{-1}$), 235 (10,440)), thus precluding the formation of any long-lived intermediates during the one-electron reduction.

The cyclic voltammogram of $[Pt(Me_2[18]aneN_2S_4)](PF_6)_2$, measured under the same conditions to its Pd(II) analogue, shows an irreversible reduction occurring at E_{pc}= -1.52V *vs.* Fc/Fc^{+}, indicative of reduction to Pt(I) followed by rapid quenching of this species, possibly via the formation of a direct metal-metal bond. No examples of monomeric d^9 Pt(I) species have been reported.

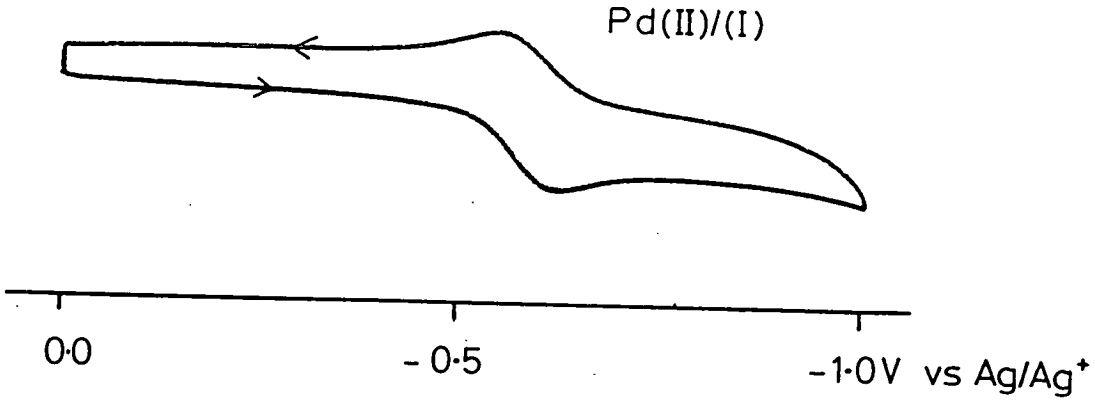

<u>Fig. 4.17</u>: Reductive cyclic voltammogram of $[Pd(Me_2[18]aneN_2S_4)]^{2+}$ (MeCN/0.1M $NBu^n_4PF_6$)

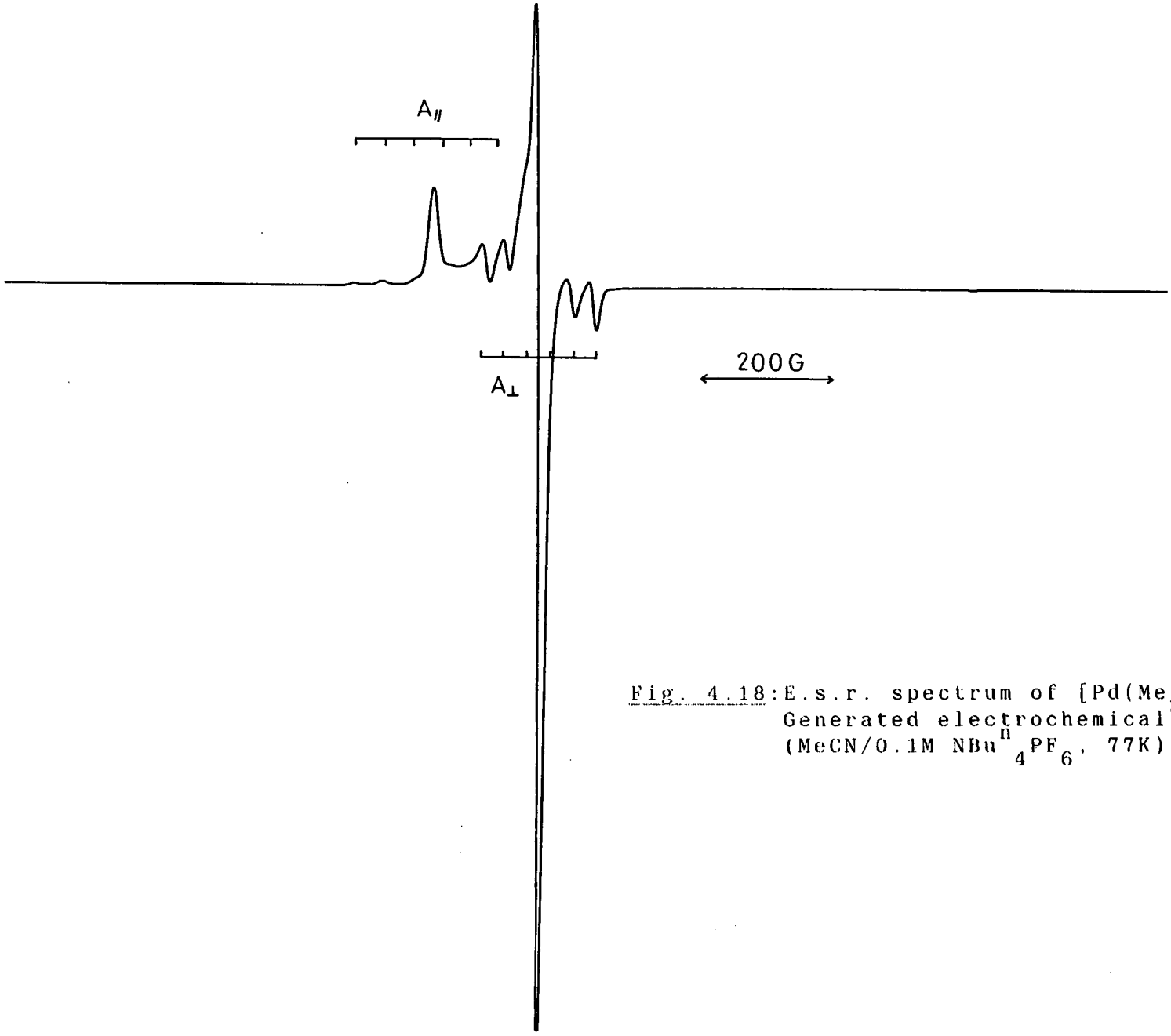

Fig. 4.18: E.s.r. spectrum of $[Pd(Me_2[18]aneN_2S_4)]^+$ Generated electrochemically (MeCN/0.1M $NBu^n_4PF_6$, 77K)

Fig. 4.19: Electronic spectrum showing reduction of $[Pd(Me_2[18]aneN_2S_4)]^{2+}$ to $[Pd(Me_2[18]aneN_2S_4)]^{+}$ (MeCN/0.1M $NBu^n_4PF_6$, 248K)

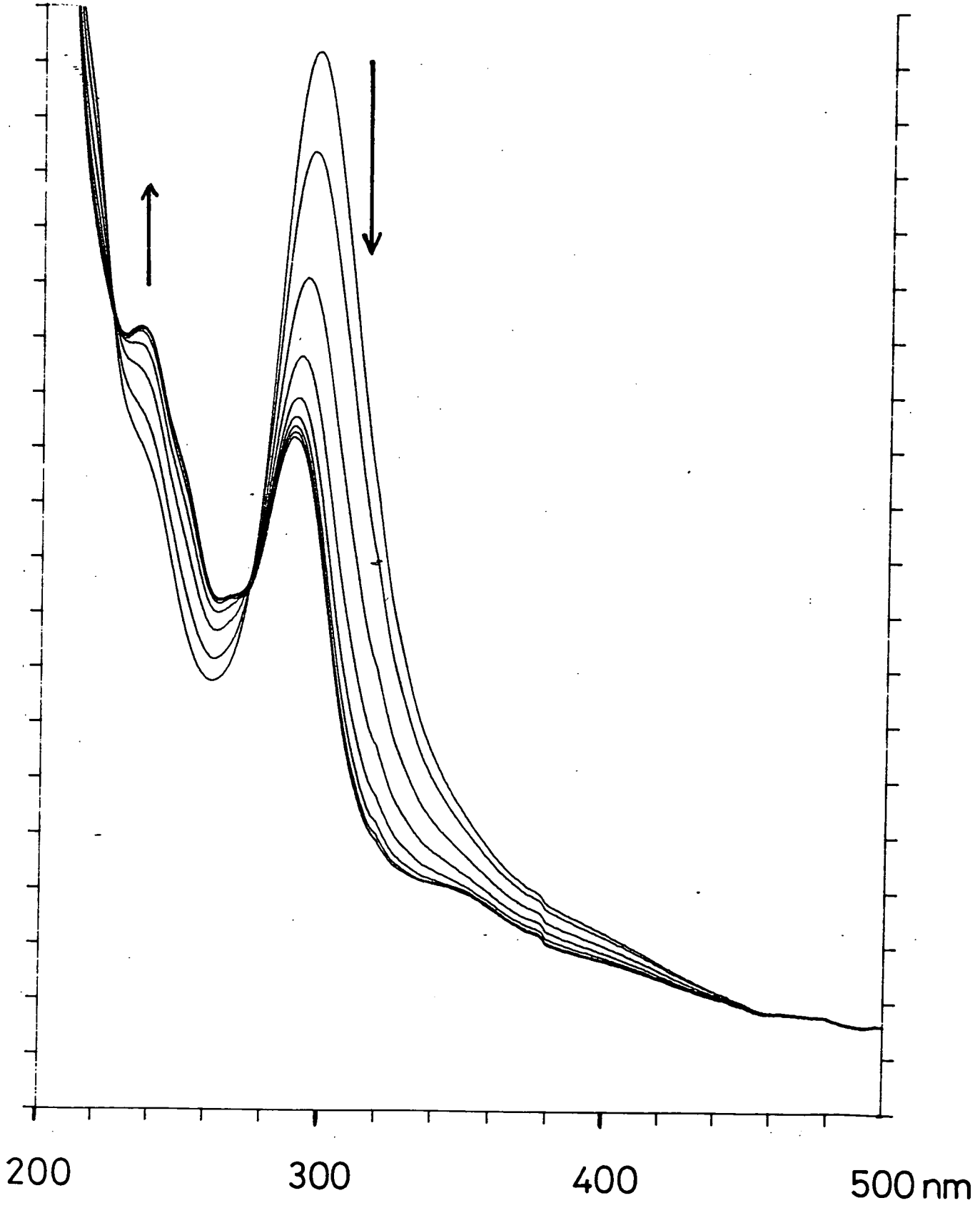

4.4: Binuclear Complexes Incorporating [18]aneN$_2$S$_4$

Metal dimers are critical to the function of a number of elaborately constructed biological systems, including hemerythrin superoxide dismutase, chlorophyll dimers in photosynthetic units, binuclear manganese complexes in the photosynthetic oxidation of H_2O to give O_2, cytochrome oxidase for the multi-electron reduction of O_2 and mono-oxygenases for the activation of O_2 by two-electron transfer [131].

In view of the co-ordinative versatility of [18]aneN$_2$S$_4$ in mononuclear Pd and Pt complexes already demonstrated, and the potential of binuclear platinum metal complexes in catalytic processes, an investigation of the ability of this macrocycle to function as a binucleating agent was initiated.

Reaction of two molar equivalents of $PdCl_2$ with one equivalent of [18]aneN$_2$S$_4$ in refluxing MeCN/H_2O yielded a golden yellow solution. Addition of PF_6^- counterion and recrystallisation from MeCN gave the product as yellow needles.

The I.R. spectrum of the complex exhibited bands characteristic of co-ordinated macrocycle, and PF_6^-. Additionally, the single absorption apparent at 330cm^{-1} is indicative of a terminal Pd-Cl stretching vibration, (υ(Pd-Cl)). F.a.b. mass spectrometry reveals molecular ion peaks at M^+= 609, 575, 539 and 431 which are assigned to

$[^{106}Pd_2{}^{35}Cl_2([18]aneN_2S_4+H)]^+$,

$[^{106}Pd_2{}^{35}Cl([18]aneN_2S_4+2H)]^+$,

$[^{106}Pd_2([18]aneN_2S_4+H)]^+$ and

$[^{106}Pd([18]aneN_2S_4-H)]^+$ respectively.

The ^1H n.m.r. spectrum of the product shows a complex second order multiplet in the range δ= 2.7-3.6 and 4.2-4.6ppm due to the macrocyclic methylene protons, while the ^{13}C DEPT n.m.r. spectrum shows three distinct methylene carbon resonances at δ= 54.77 ($N\underline{C}H_2$, 4C), 38.28 ($NCH_2\underline{C}H_2S$, 4C) and 30.44ppm ($S\underline{C}H_2\underline{C}H_2S$, 4C). This evidence combined with microanalyses confirms the assignment of the product as $[Pd_2Cl_2([18]aneN_2S_4)](PF_6)_2$.

The analogous binuclear Pt(II) complex, $[Pt_2Cl_2([18]aneN_2S_4)](PF_6)_2$ was prepared by the same method, and characterised by I.R. (υ(Pt-Cl)= 330cm^{-1}), ^1H n.m.r. and f.a.b. mass spectroscopy and microanalysis.

A single crystal X-ray structure determination of $[PdCl_2([18]aneN_2S_4)](PF_6)_2$ was undertaken to confirm the nature of the donor set to each Pd(II) centre, and to reveal the conformation of the co-ordinated macrocycle.

4.4.1: Single Crystal Structure of

$[Pd_2Cl_2([18]aneN_2S_4)](PF_6)_2.2MeCN$

Details of the structure solution are given in the Experimental Section. Relevant bond lengths, angles and torsions are presented in Tables 4.7, 4.8 and 4.9 respectively. Two ORTEP plots depicting the geometry of the cation are shown in Figs. 4.20 and 4.21.

The structure shows the cation sitting on a crystallographic inversion centre, with a 2-fold rotation axis relating adjacent molecules within the crystal lattice. Each Pd(II) centre is bound to a square planar co-ordination sphere comprising two sulphur-donors and one nitrogen-donor of the macrocycle, and a terminal Cl^- ligand, [Pd-S(1)= 2.317(4), Pd-S(7)= 2.316(4), Pd-N(4)= 2.049(13), Pd-Cl= 2.305(4)Å]. The Cl^- ligands are displaced out of the least-squares S(1)-N(4)-S(7)-Cl plane by 0.0712Å, due to the steric influence of the central methylene groups separating the S-donors. Interestingly, the closest non-bonded interaction, of 3.406(2)Å, is between two Pd atoms in adjacent molecules, related by the crystallographic 2-fold axis, as indicated on the packing diagram shown in Fig. 4.22. The intramolecular Pd...Pd distance is 4.196(2)Å indicating that the two metals are non-interacting.

Lehn and coworkers [124] have reported a similar NS_2Cl donor set for each Pd(II) centre in the binuclear complex, (2).

The ability of [18]aneN_2S_4 to perform as a binucleating agent for Pd(II) and Pt(II) further exemplifies the versatility of this mixed donor macrocycle.

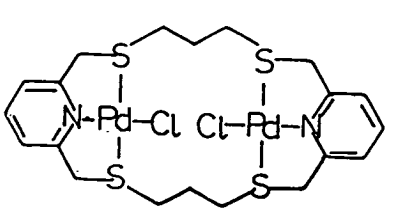

(2)

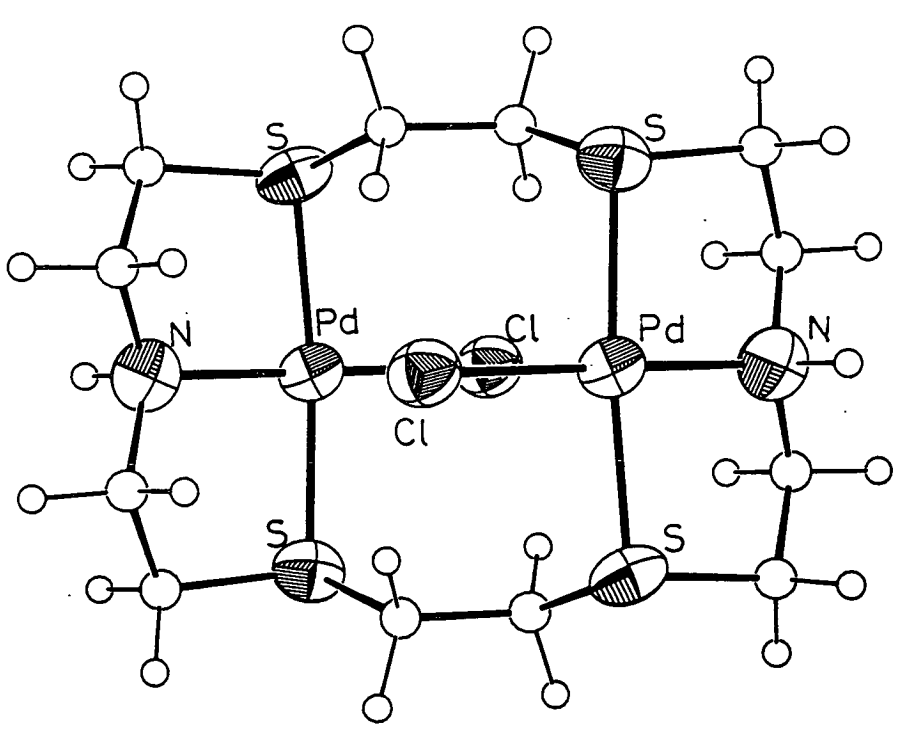

Fig. 4.20: View of the single crystal structure of $[Pd_2Cl_2([18]aneN_2S_4)]^{2+}$

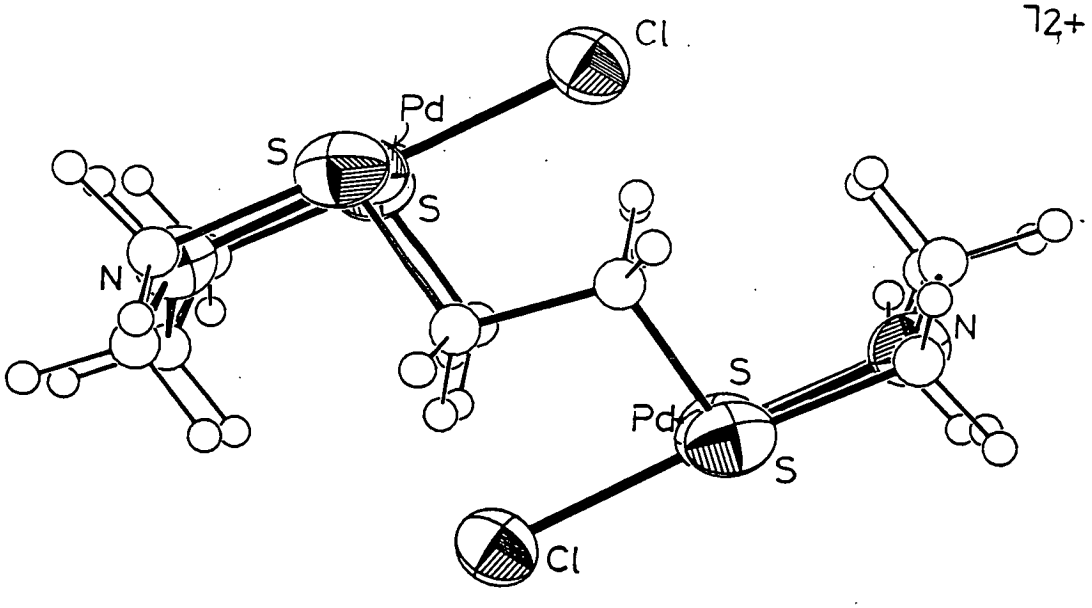

Fig. 4.21: Alternative view of the single crystal structure of $[Pd_2Cl_2([18]aneN_2S_4)]^{2+}$

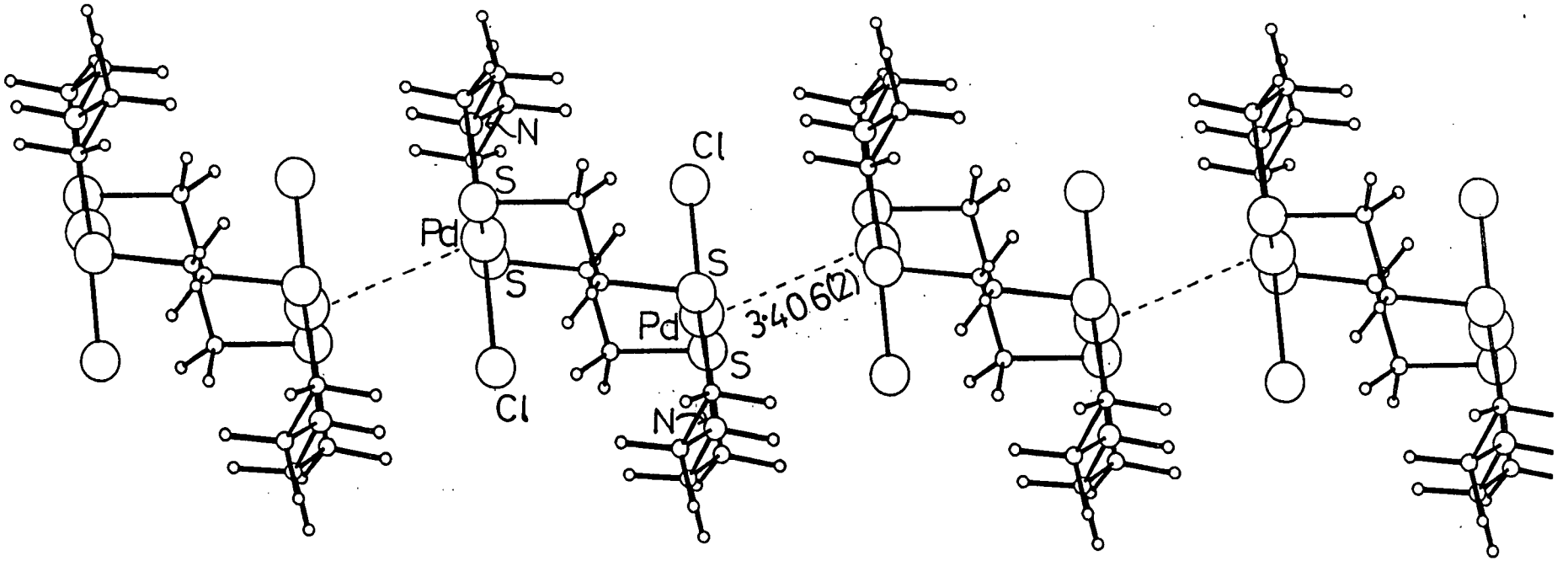

Fig. 4.22: Packing diagram of $[Pd_2Cl_2([18]aneN_2S_4)]^{2+}$

Single Crystal Structure of

$[Pd_2Cl_2([18]aneN_2S_4)](PF_6)_2.2CH_3CN$

Table 4.7: Selected Bond Lengths(Å) with e.s.d.'s

Pd(1) -Cl(1)	2.305(4)	C(3) - N(4)	1.549(20)
Pd(1) - S(1)	2.317(4)	N(4) - C(5)	1.479(21)
Pd(1) - N(4)	2.049(13)	C(5) - C(6)	1.486(24)
Pd(1) - S(7)	2.316(4)	C(6) - S(7)	1.847(18)
S(1) - C(2)	1.819(17)	C(17)- C(18)	1.509(22)
S(1) -C(18)	1.815(16)	C(17)- S(7')	1.856(16)
C(2) - C(3)	1.525(23)		

Table 4.8: Selected Angles(°) with e.s.d.'s

Cl(1) -Pd(1)- S(1)	93.16(14)	C(2) - C(3) - N(4)	106.6(12)
Cl(1) -Pd(1)- N(4)	178.8(4)	Pd(1) - N(4) - C(3)	110.7(9)
Cl(1) -Pd(1)- S(7)	93.38(14)	Pd(1) - N(4) - C(5)	112.8(10)
S(1) -Pd(1)- N(4)	87.4(4)	C(3) - N(4) - C(5)	112.3(12)
S(1) -Pd(1)- S(7)	173.41(15)	N(4) - C(5) - C(6)	109.1(13)
N(4) -Pd(1)- S(7)	86.1(4)	C(5) - C(6) - S(7)	111.1(12)
Pd(1) - S(1)- C(2)	97.1(6)	Pd(1) - S(7) - C(6)	97.2(6)
Pd(1) - S(1)-C(18)	106.5(5)	C(18)-C(17) -S(7')	108.5(10)
C(2) - S(1)-C(18)	100.3(7)	S(1) -C(18) -C(17)	108.5(10)
S(1) - C(2)- C(3)	111.3(11)	C(17)- S(7')-C(6')	99.3(8)

Table 4.9: Sele cted Torsion angles(^{o}) with e.s.d.'s

C(18)- S(1) - C(2) - C(3)	76.3(12)
N(4) - C(5) - C(6) - S(7)	-52.1(16)
C(2) - S(1) - C(18) -C(17)	178.2(11)
S(7')- C(17)- C(18)- S(1)	147.9(8)
S(1) - C(2) - C(3) - N(4)	55.6(14)
C(18)- C(17)- S(7')- C(6')	178.6(11)
C(2) - C(3) - N(4) - C(5)	-179.5(12)
C(17)- S(7')- C(6')- C(5')	76.9(13)
C(3) - N(4) - C(5) - C(6)	177.3(13)

4.5: Conclusions

The results show that $[Pd([18]aneN_2S_4)]^{2+}$ and its di-N-methylated analogue $[Pd(Me_2[18]aneN_2S_4)]^{2+}$ adopt completely different stereochemistries, the former preferring an $N_2S_2 + S_2$ donor set in a distorted octahedral geometry, while the latter prefers an S_4 donor set in a square planar geometry.

The stereochemical differences between the two complexes are also reflected in their electrochemical properties, with the non-methylated system facilitating stabilisation of Pd(III), and, the methylated system being particularly effective for stabilisation of Pd(I).

The generation of Pd(III) from the 4+2 co-ordinate $[Pd([18]aneN_2S_4)]^{2+}$ is consistent with the availability of a distorted octahedral stereochemistry in this system. Indeed, the large peak separation in the cyclic voltammogram (ΔE_p= 195mV at a scan rate of $150mVs^{-1}$) is representative of the stereochemical change occurring at the metal upon oxidation. Interestingly, cyclic voltammetry of the related hexathia system, $[Pd([18]aneS_6)]^{2+}$, under identical conditions, reveals no oxidative process in the range 0 to +2.0V. This is attributed to a kinetic barrier, since chemical oxidation in $HClO_4$ generates the red $[Pd([18]aneS_6)]^{3+}$ cation, which has been structurally characterised [53]. These results suggest that the ligand conformation is a crucial factor, and that there may be a significant conformational barrier to the formation of the

corresponding Pd(III) complex with [18]aneS$_6$.

The Pd(II)/(III) couple for the mixed-donor system is intermediate between that observed for $[Pd([9]aneN_3)_2]^{2+/3+}$ [121,204] and $[Pd([9]aneS_3)_2]^{2+/3+}$ [115,120], consistent with the presence of two hard N-donors and four softer S-donors.

Recently, Sauvage and coworkers [132] have shown that d^9 Ni(I) centres can be stabilised by tetrahedral co-ordination to catenand ligands (Fig. 4.23). Therefore, it seems likely that stabilisation of d^9 Pd(I) by $Me_2[18]aneN_2S_4$ would involve a similar tetrahedral distortion. This system represents the first thioether complex which exhibits a reversibie Pd(II)/(I) couple at 298K. The reduction potential for $[Pd(Me_2[18]aneN_2S_4)]^{2+/+}$ occurs at a considerably more anodic value compared to the tetra-aza complexes, $[Pd(L)]^{2+}$ (L= [14]aneN$_4$, Me_4[14]aneN$_4$ or Bz_4[14]aneN$_4$). This is attributed to the greater π-acidity of the thioether donors, and to the greater flexibility of the macrocycle, which enables the large Pd(I) centre to be accommodated more readily.

The results from this study also demonstrate the ability of [18]aneN$_2$S$_4$ to function both as a mono- and binucleating agent. Although the binuclear complex reported herein exhibits no metal-metal interaction, replacement of the terminal Cl^- ligands with a different potentially bridging species may shorten the metal-metal distance.

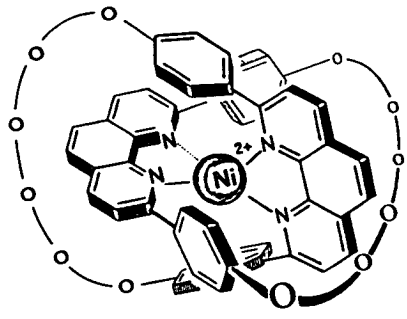

Fig. 4.23: Structure of [Ni(catenand)]$^{2+}$

$$E_{1/2}(Ni^{II/I}) = -0{\cdot}550V \text{ vs. } Fc/Fc^{+}$$

4.6: Experimental

4.6.1: $[Pd([18]aneN_2S_4)](PF_6)_2$

To a refluxing solution of $[18]aneN_2S_4$ (47mg, 0.144mmol) in MeCN (30ml) was added $PdCl_2$ (25mg, 0.141mmol) and $TlPF_6$ (110mg, 0.310mmol). The reaction mixture was refluxed for 3h under N_2 to yield a purple solution and fine white precipitate. After cooling, the precipitate (TlCl) was removed by filtration, to leave a purple solution. Removal of the solvent and recrystallisation from H_2O afforded a dark blue solid (Yield: 50mg, 49%). Mol. wt. 722.915. Elemental analysis; found C= 19.3, H= 3.61, N= 3.83, S= 17.8%; calculated for $[C_{12}H_{26}N_2S_4Pd](PF_6)_2$: C= 19.9, H= 3.62, N= 3.88, S= 17.7%. F.a.b. mass spectum (3-NOBA matrix): found M^+= 577, 431; calculated for

$[^{106}Pd([18]aneN_2S_4)PF_6]^+$ M^+= 577,

$[^{106}Pd([18]aneN_2S_4]^+$ M^+= 432.

^1H n.m.r. spectrum (360.13MHz, CD_3CN, 298K): δ= 3.7-2.56ppm (br, $C\underline{H}_2$), 5.0 (br, $N\underline{H}$), (360.13MHz, CD_3CN, 243K): δ= 5.16 (br, $N\underline{H}$), 2.3-3.6ppm (m, $C\underline{H}_2$). ^{13}C DEPT n.m.r. spectrum (50.32MHz, CD_3CN, 298K): resonances very broad, not easily distinguished from noise. Not significantly better resolved at 90.56MHz, 298K in $(CD_3)_2CO$: d= 56.28, 51.12, 47.26, 34.05, 31.88, 27.29ppm ($\underline{C}H_2$). UV/vis spectrum (MeCN): λ_{max}= 514nm (ε_{max}= $124M^{-1}cm^{-1}$), 322 (2.185), 266 (7.910), 233 (12.140). I.R. spectrum (KBr disc): 3260m, 3120m,

3000w, 2930m, 1460m, 1425m, 1300m, 1270w, 1230m, 1210w, 1150w, 1130w, 1105m, 1060w, 1030w, 1015w, 1000w, 980w, 840vs, 740m, 640w, 555vs cm^{-1}.

4.6.2: Single Crystal Structure of

$[Pd([18]aneN_2S_4)](BPh_4)_2$

Single crystals suitable for X-ray crystallography were obtained by metathesis of a small sample of $[Pd([18]aneN_2S_4)](PF_6)_2$ with $NaBPh_4$ in H_2O, which yielded a green precipitate. Recrystallisatiom from $MeNO_2$ afforded green columnar crystals. A single crystal was selected and sealed in a 0.5mm glass capillary to prevent solvent loss.

Crystal Data:

$[C_{12}H_{26}N_2S_4Pd](C_{24}H_{20}B)_2$, M= 1071.45. Monoclinic, space group $P2_1/c$, a= 16.8888(12), b= 16.5533(15), c= 18.5376(12)Å, β= 93.144(8)°, V= 5174.6Å^3 (by least-squares refinement on diffraction angles for 36 reflections measured at $\pm\omega$ [$15<2\theta<17°$, λ= 0.71073Å]), Z= 4, D_c= 1.375gcm^{-3}. Crystal dimensions 0.30x0.10x0.08mm, μ(Mo-Kα)= 0.52mm^{-1}, F(000)= 2240.

Data Collection and Processing:

Stöe STADI-4 four-circle diffractometer, $\omega/2\theta$ scan mode using the learnt profile method. Graphite-monochromated Mo-Kα radiation; 6815 reflections ($2\theta_{max}$= 45°, h -18⟶14, k 0⟶17, l 0⟶19) giving 4006

with $\underline{F}>4\sigma(\underline{F})$. No significant crystal decay, no absorption correction.

Structure Analysis and Refinement:

A Patterson synthesis located the Pd atom and this was input into DIRDIF which identified the positions of all non-H atoms except for one macrocyclic C atom. The structure was developed by least-squares refinement and difference Fourier synthesis. Anisotropic thermal parameters were refined for Pd, S, N, C and B atoms. Hydrogen atoms were included in fixed, calculated positions. The weighting scheme $\underline{w}^{-1}= \sigma^2(\underline{F})+0.001155\underline{F}^2$ gave satisfactory agreement analyses. At convergence $\underline{R}$, $\underline{R}_w= 0.0623$ and 0.0786 respectively, $\underline{S}= 1.110$ for 517 independent parameters, and the final difference Fourier synthesis showed no feature above 0.48 or below $-0.45 e\text{Å}^{-3}$.

4.6.3: $[Pt([18]aneN_2S_4)](PF_6)_2$

Method as for 4.6.1, using $PtCl_2$ (33mg, 0.123mmol), $TlPF_6$ (103mg, 0.294mmol) and $[18]aneN_2S_4$ (40mg, 0.123mmol). The product was isolated as a yellow solid (Yield: 80mg, 81%). Mol. wt. 811.515. Elemental analysis: found C= 17.1, H= 3.11, N= 3.43, S= 15.5%; calculated for $[C_{12}H_{26}N_2S_4Pt](PF_6)_2$: C= 17.8, H= 3.23, N= 3.45, S= 15.8%. F.a.b. mass spectrum (3-NOBA matrix): found M^+= 667, 521; calculated for

$[^{195}Pt([18]aneN_2S_4)PF_6]^+$ M^+= 666,

$[^{195}Pt([18]aneN_2S_4)]^+$ $M^+ = 521$.

^1H n.m.r. spectrum (360.13MHz, CD_3CN, 298K): δ= 5.68 (br, N$\underline{H}$, 1H), 3.76 (br, N$\underline{H}$, 1H), 2.84-3.42ppm (br, C$\underline{H}_2$, 24H), (360.13MHz, CD_3CN, 238K): δ= 5.75 (br, N$\underline{H}$, 1H), 3.75 (br, N$\underline{H}$, 1H), 2.74-3.22ppm (br m, C$\underline{H}_2$, 24H). ^{13}C DEPT n.m.r. spectrum (50.32MHz, CD_3CN, 298K): δ= 28.08, 34.74, 36.84, 53.11, 55.39ppm (two overlapping resonances) ($\underline{C}H_2$). ^{13}C DEPT n.m.r. spectrum (90.56MHz, $(CD_3)_2CO$, 298K): δ=56.1 (N$\underline{C}H_2$, 2C), 53.8 (N$\underline{C}H_2$, 2C), 46.6, 42.0, 38.3, 37.3, 35.3 (two overlapping resonances), 28.2, 26.3ppm (S$\underline{C}H_2$, total of 8C). I.R. spectrum (KBr disc): 3140m, 3000w, 2945w, 1460m, 1420m, 1410m, 1310m, 1270w, 1240w, 1220w, 1125m, 1055m, 1020m, 840vs, 720m, 555vs cm^{-1}.

4.6.4: $[Pd_2Cl_2([18]aneN_2S_4)](PF_6)_2$

Reaction of $PdCl_2$ (44mg, 0.245mmol) with $[18]aneN_2S_4$ (40mg, 0.123mmol) in refluxing $MeCN/H_2O$ (1:1 v.v.) for 4h under N_2 afforded a yellow solution. Addition of excess NH_4PF_6 gave a yellow precipitate which was recrystallised from MeCN to yield the product as yellow needles (105mg, 95%). Mol. Wt. 900.221. Elemental analysis: found C= 15.9, H= 2.79, N= 3.32, S= 14.4%; calculated for $[C_{12}H_{26}Cl_2N_2S_4Pd_2](PF_6)_2$ C= 16.0, H= 2.91, N= 3.11, S= 14.2%. F.a.b. mass spectrum (3-NOBA matrix): found M^+= 609, 575, 539, 431; calculated for

$[^{106}Pd_2{}^{35}Cl_2([18]aneN_2S_4)]^+$ $M^+ = 608$,

$[^{106}Pd_2{}^{35}Cl([18]aneN_2S_4)]^+$ $M^+ = 573$.

$[^{106}Pd_2([18]aneN_2S_4)]^+$ $M^+ = 538$,

$[^{106}Pd([18]aneN_2S_4)]^+$ $M^+ = 432$.

^1H n.m.r. spectrum (80.13MHz, CD_3CN, 298K): δ= 2.7-3.6 and 4.2-4.6 (m, $C\underline{H}_2$, 24H), 5.6ppm (br, $N\underline{H}$, 2H). ^{13}C DEPT n.m.r. spectrum (50.32MHz, CD_3CN, 298K): δ= 54.77 ($N\underline{C}H_2$, 4C), 38.28 ($NCH_2\underline{C}H_2S$, 4C), 30.44ppm ($S\underline{C}H_2\underline{C}H_2S$, 4C). UV/vis spectrum (MeCN): λ_{max}= 376nm (ε_{max}= 3,543$M^{-1}cm^{-1}$), 262 (17,330), 224 (22,200). I.R. spectrum (KBr disc): 3200m, 3060m, 3000w, 2965w, 1460m, 1420vs, 1330w, 1310m, 1270w, 1260m, 1225w, 1140w, 1120w, 1100m, 1060m, 1010m, 840vs, 740m, 650w, 555vs, 330m cm^{-1}.

4.6.5: Single Crystal Structure of

$[Pd_2Cl_2([18]aneN_2S_4)](PF_6)_2$

Recrystallisation of the complex from MeCN afforded yellow needles of crystallographic quality. A suitable crystal was selected and sealed in a glass capillary to prevent solvent loss.

Crystal Data:

$[C_{12}H_{26}Cl_2N_2S_4Pd_2](PF_6)_2.2CH_3CN$, M= 982.3. Monoclinic, space group C2/c, a= 18.617(13), b= 15.569(11), c= 14.323(14)Å, β= 113.59(5)°, V= 3804.6Å^3 (by least-squares refinement on diffraction angles for 32 reflections measured at $\pm\omega$ [24<2θ<25°, λ= 0.71073Å]), Z= 4, D_c= 1.715gcm^{-3}. Crystal dimensions 0.77x0.23x0.19mm, μ(Mo-Kα)= 13.96cm^{-1}, F(000)= 1936.

Data Collection and Processing:

Stöe STADI-4 four-circle diffractometer, $\omega/2\theta$ scan mode, with ω scan-width $(1.20+0.347\tan\theta)^{o}$. Graphite-monochromated Mo-Kα radiation: 2456 reflections measured ($2\theta_{max}= 45^{o}$, h -20⟶18, k -16⟶16, l 0⟶15) giving 1708 with $\underline{F}>6\sigma(\underline{F})$. No significant crystal decay.

Structure Analysis and Refinement:

A Patterson synthesis located the Pd atom and the structure was developed by least-squares refinement and difference Fourier synthesis to reveal all other non-H atom positions. Absorption correction was made using DIFABS (max transmission factor= 1.463, minimum= 0.744). During refinement some disorder of the PF_6^- counterion was identified. This was modelled successfully using partial F atoms, giving a total of six F atoms per P atom. Each binuclear cation was found to have two molecules of MeCN solvent associated. These too were found to be disordered, and were modelled by constraining the C-C and C-N bond lengths to be 1.50 and 1.23Å respectively, and constraining the N-C-C angle to be linear. Anisotropic thermal parameters were refined for Pd, Cl, S, P, F, N and C atoms except for those associated with the solvent molecules. Hydrogen atoms were included in fixed, calculated positions. The weighting scheme $\underline{w}^{-1}= \sigma^2(\underline{F})+0.002282\underline{F}^2$ gave satisfactory agreement analyses. At convergence $\underline{R}$, $\underline{R}_w= 0.0757$ and

0.1037 respectively, S= 1.201 for 177 independent parameters, and the final difference Fourier synthesis showed no feature above 0.97 or below -1.22eÅ^{-3}.

4.6.7: $[Pt_2Cl_2([18]aneN_2S_4)](PF_6)_2$

Method as for 4.6.4 above, using $PtCl_2$ (65mg, 0.246mmol) and $[18]aneN_2S_4$ (40mg, 0.123mmol). The product was isolated as a pale yellow solid (Yield:73mg, 55%). Mol. wt. 1077.42. Elemental analysis: found C= 13.8, H= 2.38, N= 2.84%; calculated for $[C_{12}H_{26}N_2S_4Cl_2Pt_2](PF_6)_2$: C= 13.4, H= 2.43, N= 2.60%. F.a.b. mass spectrum (dmf/glycerol matrix): found M^+= 786, 750, 555, 521; calculated for

$[^{195}Pt_2{}^{35}Cl_2([18]aneN_2S_4)]^+$ M^+= 786,

$[^{195}Pt_2{}^{35}Cl([18]aneN_2S_4)]^+$ M^+= 751,

$[^{195}Pt{}^{35}Cl([18]aneN_2S_4)]^+$ M^+= 556,

$[^{195}Pt([18]aneN_2S_4)]^+$ M^+= 521.

^1H n.m.r. spectrum (80.13MHz, CD_3CN, 298K): δ= 7.45 (br, NH). 2.2-3.6ppm (m, CH_2). I.R. spectrum (KBr disc): 3140m, 3000w, 2950w, 1460m, 1420m, 1410m, 1310m, 1270w, 1240w, 1220w, 1120m, 1055w, 1020m, 1000w, 840vs, 740m, 555vs, 330w cm^{-1}.

4.6.8: $[Pd(Me_2[18]aneN_2S_4)](PF_6)_2$

Reaction of $PdCl_2$ (15mg, 0.086mmol) with $Me_2[18]aneN_2S_4$ (31mg, 0.087mmol) in refluxing $MeCN/H_2O$ (3:1vv, 30ml) under N_2 for 5h afforded an orange

solution. Addition of excess NH_4PF_6 and removal of the MeCN gave an orange precipitate, which was recrystallised from MeCN (Yield: 40mg, 63%). Mol. wt. 750.97. Elemental analysis: found C= 21.7, H= 3.90, N= 3.74, S= 16.6%; calculated for $[C_{14}H_{30}N_2S_4Pd](PF_6)_2$: C= 22.4, H= 4.03, N= 3.73, S= 17.1%. F.a.b. mass spectrum (3-NOBA matrix): found M^+= 604, 460; calculated for

$[^{106}Pd(Me_2[18]aneN_2S_4)PF_6]^+$ M^+= 605,

$[^{106}Pd(Me_2[18]aneN_2S_4)]^+$ M^+= 460.

^1H n.m.r. spectrum (80.13MHz, CD_3CN, 298K): δ= 2.48ppm (s, $C\underline{H}_3$, 6H), 2.68-3.50ppm (m, $C\underline{H}_2$, 24H). ^{13}C DEPT n.m.r. spectrum (50.32MHz, CD_3CN, 298K): δ= 49.87, 40.31, 39.40 ($\underline{C}H_2$) and 41.57ppm ($\underline{C}H_3$). UV/vis spectrum (MeCN): λ_{max}= 373nm (ε_{max}= 3,004$M^{-1}cm^{-1}$), 298 (14,460), 232 (15,070). I.R. spectrum (KBr disc): 2950w, 2850w, 1420m, 1400m, 1370m, 1300w, 1260w, 1240m, 1210w, 1150w, 1120w, 1110w, 1060w, 1005w, 940m, 840vs, 740m, 730w, 670w, 555vs cm^{-1}.

4.6.9: Single Crystal Structure of

$[Pd(Me_2[18]aneN_2S_4)](PF_6)_2.Me_2CO$

Vapour diffusion of diethyl ether into a solution of the complex in Me_2CO gave yellow plates of crystallographic quality. A crystal was selected and mounted in a 0.5mm glass capillary to prevent solvent loss.

Crystal Data:

$[C_{14}H_{30}N_2S_4Pd](PF_6)_2.C_3H_6O$, M= 809.0. Orthorhombic, space group P_{cab}, a= 14.3369(15), b= 17.6915(7), c= 14.2952(11)Å, V= 6162Å^3 (by least-squares refinement on diffraction angles for 58 reflections measured at $\pm\omega$ [$24<2\theta<25^o$, λ= 0.71073Å]), Z= 8, D_c= 1.774gcm^{-3}. Crystal dimensions 0.92x0.08x0.15mm, μ(Mo-Kα)= 10.0cm^{-1}, F(000)= 3360.

Data Collection and Processing:

Stöe STADI-4 four-circle diffractometer, $\omega/2\theta$ scan mode using the learnt-profile method. Graphite-monochromated Mo-Kα radiation; 4527 reflections measured ($2\theta_{max}$= 45^o, h 0⟶15, k -0⟶16, l 0⟶24) giving 2693 with $F>6\sigma(F)$. No significant crystal decay, no absorption correction.

Structure Analysis and Refinement:

A Patterson synthesis located the Pd atom and the structure was developed by least-squares refinement and difference Fourier synthesis to reveal all other non-H atom positions. It was discovered that one PF_6^- counterion and both -C-N(Me)-C moieties were affected by disorder. This was modelled successfully using partial F and C atoms respectively, thus generating two alternative sites for the C atoms adjacent to the N-Me functions and giving a total of six F atoms per P atom. The crystal

lattice was found to contain one acetone molecule per cation. Anisotropic thermal parameters were refined for Pd, S, P, N, O and all fully occupied C and F atoms. H atoms were included in fixed, calculated positions. The weighting scheme $\underline{w}^{-1} = \sigma^2(\underline{F}) + 0.000843\underline{F}^2$ gave satisfactory agreement analyses. At convergence $\underline{R}$, $\underline{R}_w$ = 0.0450 and 0.0606 respectively, $\underline{S}$ = 1.186 for 375 independent parameters, and the final difference Fourier synthesis showed no feature above 0.84 or below -0.50e$\mathring{A}^{-3}$.

4.6.10: $[Pt(Me_2[18]aneN_2S_4)](PF_6)_2$

Reaction of $PtCl_2$ (30mg, 0.113mmol) with $Me_2[18]aneN_2S_4$ (40mg, 0.113mmol) under the same conditions as 4.6.8 above, gave a pale yellow product (Yield: 55mg, 58%). Mol. wt. 839.57. Elemental analysis: found C= 19.7, H= 3.57, N= 3.33, S= 15.3%; calculated for $[C_{14}H_{30}N_2S_4Pt](PF_6)_2$: C= 20.0, H= 3.60, N= 3.34, S= 15.3%. F.a.b. mass spectrum (3-NOBA matrix): found M^+ = 694, 549; calculated for

$[^{195}Pt(Me_2[18]aneN_2S_4)PF_6]^+$ M^+ = 694.

$[^{195}Pt(Me_2[18]aneN_2S_4)]^+$ M^+ = 549.

^1H n.m.r spectrum (300.13MHz, CD_3CN, 298K): δ= 2.46 (s, $C\underline{H}_3$, 6H), 2.54-2.62 and 2.80-2.87ppm (m, $NC\underline{H}_2$, 8H), 3.18-3.30 and 3.55-3.62ppm (m, $C\underline{H}_2SC\underline{H}_2$, 16H). ^{13}C DEPT n.m.r. spectrum (50.32MHz, CD_3CN, 298K): δ= 49.18 ($\underline{C}H_2N$), 39.87 ($S\underline{C}H_2CH_2N$), 39.28 ($S\underline{C}H_2\underline{C}H_2S$) and 40.83ppm ($\underline{C}H_3$). UV/vis spectrum (MeCN): λ_{max}= 243nm (ε_{max}= 22,800$M^{-1}cm^{-1}$). I.R. spectrum (KBr disc): 2950m,

2920w, 2840w, 1460m, 1420m, 1379w, 1310m, 1260w, 1240w, 1220w, 1110m, 1070m, 1030w, 1015w, 980w, 840vs, 745m, 555vs, 340m cm^{-1}.

CHAPTER 5

Structural and Redox Studies on

Palladium and Platinum Tetrathia Macrocyclic Complexes

5.1: Introduction

The Edinburgh group has recently reported the stabilisation of Pd(I) by tetra-aza ionophores [119]. However, the Pd(II)/(I) redox couples for these complexes occur at rather negative potentials (Chapter 4). We proposed that replacement of the tetra-aza ligand by a softer tetrathia ionophore would render the Pd(II)/(I) redox couple more accessible. This provided the impetus for a study of palladium and platinum thioether macrocyclic complexes. The macrocyclic ligands selected for this work were the three tetrathia macrocycles [12]aneS_4, [14]aneS_4 and [16]aneS_4, and the large ring 28-membered octathia macrocycle, [28]aneS_8.

Ligand Synthesis

The synthesis of macrocyclic thioether compounds was first reported by Tucker and Reid in 1933 [133]. Subsequently, several groups have endeavoured to develop systematic, high-yield routes to these cyclic species [134-138].

The prediction from Hard and Soft Acids and Bases Theory [139] that alkali metal ions will exhibit an affinity for oxygen atoms, has been used extensively in the template synthesis of numerous polyoxa crown ethers [140-144]. However, using alkali metals as templating agents to encourage cyclisation in preference to linear polymerisation is much less successful for

polythia crown ethers. In fact, no suitable templating agent has proven effective for the soft sulphur atoms, and this has inhibited the improvement of syntheses. Thus, the preparation of most polythia crowns requires long reaction times coupled with the employment of high dilution techniques, since only under these conditions is cyclisation kinetically favoured.

The preparation of [12]aneS_4 and [14]aneS_4 was reported by Rosen and Busch [134,135] [by reaction of the appropriate tetrathiaundecane and dibromoalkane, (1)]. Since then several higher yield syntheses have been reported. Buter and Kellog [138] have prepared a series of polythia and mixed polyoxa/thia macrocycles in much improved yields by utilising Cs^+ to promote ring closure, via deprotonation of the thiol functions. This approach is particularly applicable to systems which require S_N2 ring closure by attack of a thiolate anion on an activated carbon centre, (2). The authors do not suggest that the Cs^+ acts as a templating agent, although this is a possibility. More recently, Ochrymowycz and co-workers [136] have published a systematic approach to the synthesis of a range of macrocyclic polythia ethers of differing ring size and number of donors.

The ligands [12]aneS_4, [14]aneS_4, [16]aneS_4 and [28]aneS_8 are now readily available from a commercial supplier.

As an introduction, a survey of the chemistry of these ligands is given here.

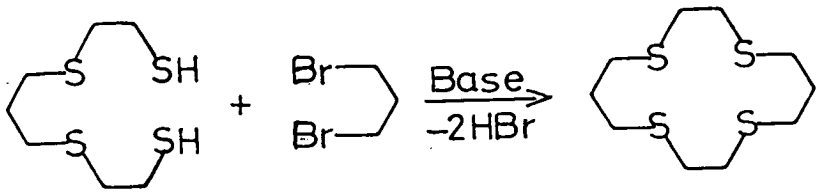

(1)

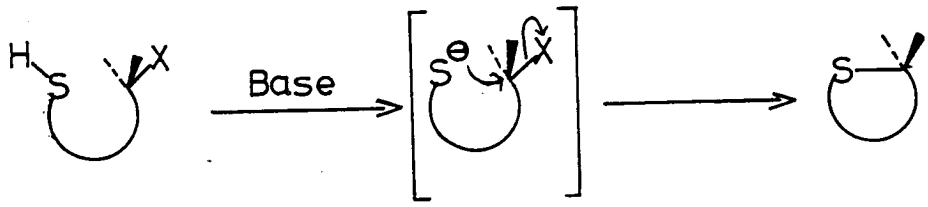

(2)

[14]aneS$_4$

The single crystal X-ray structure of [14]aneS$_4$ [12] shows two isomeric forms of the ligand, giving three independent molecules. In each case the ligand adopts a rectangular "exodentate" conformation with the sulphur atom lone-pairs directed outward, presumably to minimise lone-pair interactions, (3). A study of the torsion angles reveals eight *gauche* and six *anti* interactions in the exodentate conformer versus six *gauche* and eight *anti* interactions in the endodentate conformer. Thus, it is apparent that [14]aneS$_4$ adopts the configuration with the maximum number of *gauche* C-S linkages, in order to avoid unfavourable 1,4-interactions.

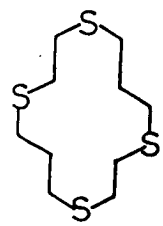

(3)

The conformation of the free ligand indicates a tendency toward exodentate binding of metal ions. Indeed, exodentate co-ordination of this ligand has been observed in several cases. The solid state structure of

$[Nb_2Cl_{10}([14]aneS_4)]$ [145] shows the macrocycle bridging two $NbCl_5$ fragments, functioning as a monodentate ligand to each metal centre, leaving two unco-ordinated sulphur atoms. The geometry at each Nb(V) centre is best described as square pyramidal to five chlorides, with a macrocyclic sulphur occupying the sixth site. The equatorial chlorides are bent over towards the macrocycle [angle Cl_{ap}-Nb-Cl_{ap}= 97.2(4)^{o}]. Tetrahedral geometry is achieved around each Hg(II) centre in the complex $[Hg_2Cl_4([14]aneS_4)]$ by exodentate co-ordination of two S-donors of the macrocycle and two Cl^- atoms, (4) [146]. A further example of exo-cyclic co-ordination to a metal is the extremely air-sensitive $[AlMe_3]_4[14]aneS_4$ [147], (5). Structural studies show a centrosymmetric molecule with one $AlMe_3$ fragment bonded to each S-donor, generating a tetrahedral environment for each Al centre. The Al-S bond lengths are in the range 2.512(2) to 2.531(2)Å, and are elongated compared to other Al-S bonds (e.g. $[Me_2AlSMe]_n$, Al-S= 2.348(2)Å [148], $K[Al_2Me_6SCN]$, Al-S= 2.489(2)Å [149]). Interestingly, two complexes incorporating platinum metals, $[M_2Cl_2(C_5Me_5)_2([14]aneS_4)]^{2+}$ (M= Rh, Ir) also exhibit exodentate co-ordination [4,150]. The single crystal structure of the binuclear Rh(III) complex, (6), is centrosymmetric with each Rh centre bound to two S-donors of the macrocycle and a chloride ion, with the C_5Me_5 ligand binding facially to complete the octahedral arrangement. The geometry is quite severely distorted in this case [angle Cl-Rh-S= 102.77(10)^{o}] and the propyl

linkages separate the two pairs of S-donors, leaving the metal centres 7.277(1)Å apart.

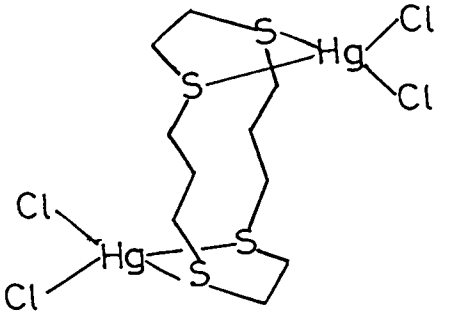

(4)

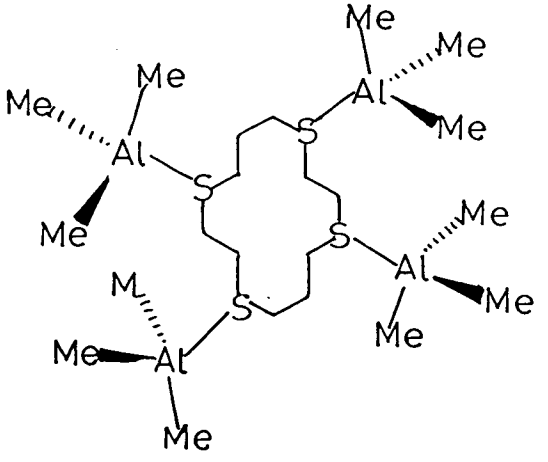

(5)

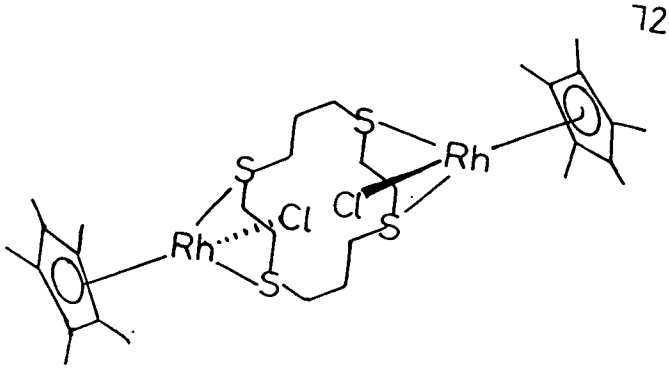

(6)

Endo-cyclic binding of metal ions by [14]aneS$_4$ has also been reported. Square planar co-ordination of [14]aneS4 to Ni(II) [151,152], Cu(II) [153], Pd(II) [154] and Rh(I) [109,110] has been reported. In the Cu(II) complex trans-$OClO_3^-$ ligands give a tetragonally elongated stereochemistry. There are generally five different isomers for a square planar or tetragonal complex of a tetradentate macrocycle, depending upon the orientation of the chelate rings, (Fig. 5.1).

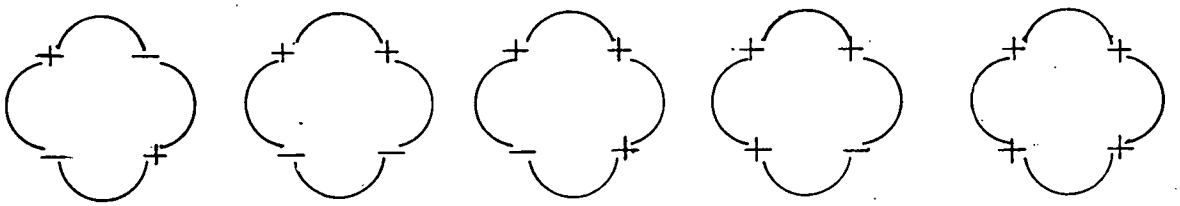

Fig. 5.1: Diagrammatic representation of the five main isomers for $[M(L)]^{n+}$, (L= tetrathia macrocycle), (+ and - refer to the orientation of the S atom lone-pairs above and below the plane)

Notably, [Rh([14]aneS$_4$)]Cl [109] crystallises in the cccc-configuration, with the metal in a distorted square planar environment, sitting 0.133(2)A above the S_4 co-ordination plane, (Fig. 5.2). This geometry is stabilised by weak intermolecular interactions, Rh...Rh= 3.313Å, Rh...S= 3.697(9)Å. Treatment of this species with $NaBPh_4$ in MeOH at room temperature generates the ctct-form.

The chain structure exhibited by the Cu(I) complex, $[Cu([14]aneS_4)]^+$, completes the known binding

modes of this ligand. Here, the tetrahedral structure around Cu(I) is achieved by binding of three S-donors of one ligand and one S-donor of another macrocycle [155].

Fig. 5.2: Single crystal structure of $[Rh([14]aneS_4)]^+$

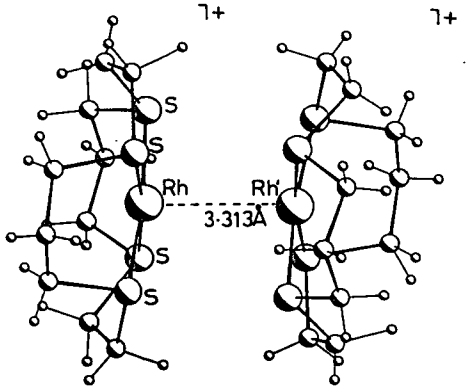

The solid state structure of $[RuCl_2([14]aneS_4)]$ reported by Poon and Lai [156] shows endo, tetradentate co-ordination of the ligand. The macrocycle is unable to accommodate the large Ru(II) ion within the cavity, and therefore adopts a folded configuration with mutually cis-chlorides. This complex converts into the trans-isomer in the presence of bulky iodide ligands. However, the reported pseudo-square planar complex $[Rh([14]aneS_4)]^+$ discussed above demonstrates that contrary to predictions based on hole-size calculations [156], this macrocycle can incorporate the large Rh(I) ion.

The insertion of Rh(III) into $[14]aneS_4$ has been reported previously by Travis and Busch [110]. The dichloro complex has been assigned as the cis-isomer on the basis of I.R. spectroscopy.

[12]aneS_4

The single crystal structure of the free ligand has been reported by Cooper et al [13], and shows, like [14]aneS_4, all four sulphur atoms are exodentate in a conformation which appears square in projection, with every C-S linkage adopting *gauche* placement.

Investigations of the co-ordination chemistry of this 12-membered ring, potentially tetradentate ligand have been very limited. [12]aneS_4 is reported to complex Ni(II) [157]. However, the cavity of the macrocycle is too small to allow it to accommodate the metal, and the Ni(II) complex has been formulated as $[Ni_2([12]aneS_4)_3](BF_4)_4$. Very recently the crystal structure of the chloro-bridged dimer, $[Ni_2Cl_2([12]aneS_4)_2]^{2+}$ has been determined in Edinburgh [158]. This shows each octahedral Ni(II) centre bound to all four thioether-donors of a folded macrocycle, with two Cl^- ligands bridging the metal centres as illustrated in Fig. 5.3. [Ni-S(1)= 2.412(3), Ni-S(4)= 2.4144(25), Ni-S(7)= 2.373(3), Ni-Cl= 2.411(3), 2.382(3)Å]. Rorabacher *et al* [67] have prepared the Cu(II) complex of this ligand, in an attempt to obtain a simple model for the blue copper proteins.

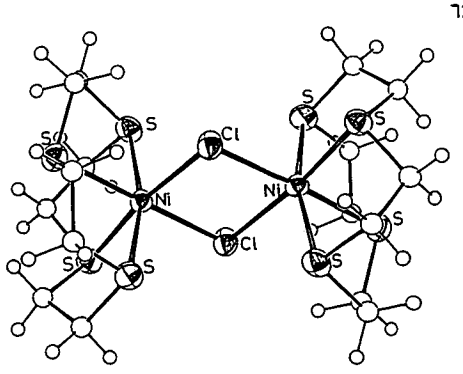

Fig. 5.3:
Single crystal structure of $[Ni_2Cl_2([12]aneS_4)_2]^{2+}$

Recently, $[PtMe_3([12]aneS_4)]Cl$, a Pt(IV) complex incorporating $[12]aneS_4$ has been reported [159]. The X-ray structure shows octahedral Pt(IV) bound facially to three Me groups and to three S-donors of the endodentate macrocycle, leaving one sulphur unco-ordinated, (7). This complex exhibits fluxional behaviour in solution, attributed to a ligand commutation involving exchange between metal-co-ordinated and unco-ordinated sulphur atoms of the macrocycle.

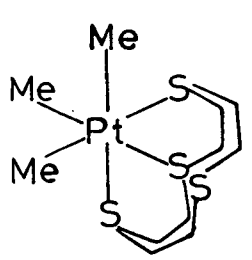

(7)

$[16]aneS_4$

Very few examples of transition metal complexes incorporating $[16]aneS_4$ have been reported [67,160,161]. Recently however, Yoshida and co-workers [162] have published the binding of Mo(0) and Mo(II) to a related 16-membered tetrathia macrocycle, (8). The complexes $[Mo(L)(CO)_2]$ and $[MoX_2(L)]$ (X= Cl, Br) exhibit trans-configurations. N.m.r. and single crystal X-ray diffraction confirm that $[Mo(L)(CO)_2]$ adopts a cccc-conformation, with all four six-membered chelate rings assuming the chair-form.

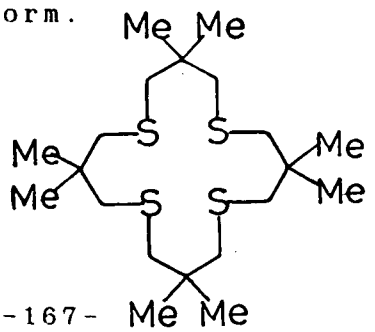

(8)

[28]aneS_8

The preparation of the large ring octathia macrocycle, [28]aneS_8 was first reported by Travis and Busch in 1970 [163]. The ligand was prepared by a [2+2] cyclisation between the dianion of 1,4,8,11-tetrathioundecane with 1,3-dibromopropane.

Travis and Busch have shown that [28]aneS_8 reacts with Ni(II) to give a binuclear complex, $[Ni_2([28]aneS_8)]^{4+}$. However, only insoluble metal complexes were obtained by reaction of this ligand with MCl_4^{2-}, (M= Pd, Pt). These products show a metal to ligand ratio of 4:1, and it was proposed that the ligand binds in a bidentate manner towards each metal ion, with Cl^- ligands completing the square planar metal co-ordination sphere [163]. No other metal complexes incorporating this macrocycle have been reported.

5.2: Results and Discussion

The approach adopted was based on synthesis of the Pd(II) precursors followed by electrochemical reduction and characterisation of the redox products.

5.2.1: $[Pd([12]aneS_4)](PF_6)_2$

Reaction of K_2PdCl_4 with one molar equivalent of $[12]aneS_4$ in refluxing $MeOH/H_2O$ afforded a bright yellow solution. Addition of excess PF_6^- counterion gave a yellow precipitate which was recrystallised from MeCN.

Importantly, the I.R. spectrum of the complex shows no bands in the range 250-400cm^{-1}, thus precluding the formation of any species involving Pd-Cl bonds. The f.a.b. mass spectrum of the complex exhibits molecular ion peaks at M^+= 491 and 345. On the basis of their isotopic distributions, these are assigned to $[^{106}Pd([12]aneS_4)PF_6]^+$ and $[^{106}Pd([12]aneS_4-H)]^+$ respectively. The ^1H n.m.r. spectrum of the complex shows an AA'BB' pattern at δ= 3.51-3.58 and 3.81-3.88ppm, due to the inequivalence of the axial and equatorial methylene protons, while the ^{13}C DEPT n.m.r. spectrum shows one methylene carbon resonance at δ= 39.05ppm, indicating square planar co-ordination of the Pd(II) centre to all four macrocyclic S-donors. This together with microanalytical and UV/vis spectral data confirms the formulation $[Pd([12]aneS_4)](PF_6)_2$. In order to confirm the stereochemistry and conformation adopted, and to determine the extent of displacement of the Pd(II) ion

out of the macrocyclic cavity, a single crystal X-ray analysis was undertaken.

5.2.2: Single Crystal Structure of $[Pd([12]aneS_4)](PF_6)_2.MeCN$

Details of the structure solution and refinement are given in the Experimental Section. Relevant bond lengths, angles and torsion angles are given in Tables 5.1, 5.2 and 5.3 respectively. Two ORTEP plots revealing the geometry of the cation are presented in Figs. 5.4 and 5.5.

The structure shows the Pd(II) ion occupying a crystallographic mirror plane and co-ordinated in a distorted square planar arrangement to all four macrocyclic S-donors [Pd-S(1)= 2.280(4), Pd-S(4)= 2.306(4)Å]. The angles around Pd(II) are close to 90^{o}. The complex adopts a cccc-conformation, with all four chelate rings directed to one face of the Pd atom. As a consequence of the bad size-match of the 12-membered ring macrocycle and the relatively large Pd(II) ion, the metal is displaced above the four precisely coplanar S-donors by 0.3116Å, in the opposite direction to the methylene chains, thereby leaving one face of the metal ion exposed.

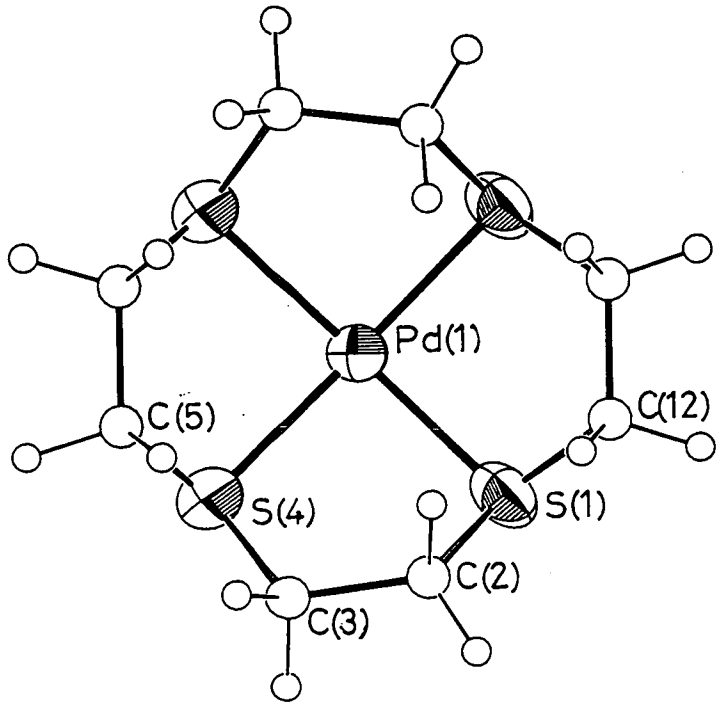

Fig. 5.4: View of the single crystal structure of $[Pd([12]aneS_4)]^{2+}$

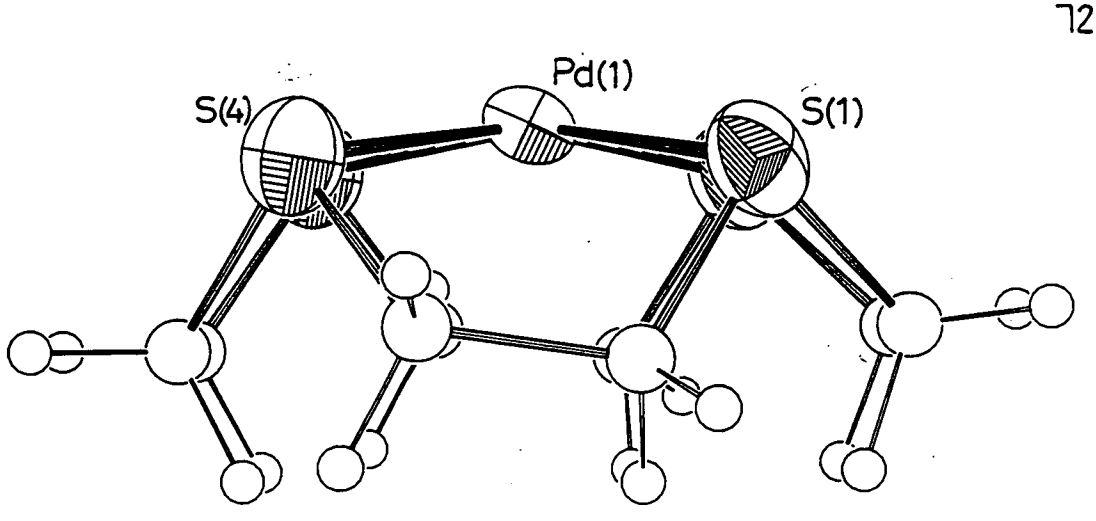

Fig. 5.5: Alternative view of the single crystal structure of $[Pd([12]aneS_4)]^{2+}$

Crystal Structure of

$[Pd([12]aneS_4)](PF_6)_2.MeCN$

Table 5.1: Selected Bond Lengths(Å) with e.s.d.'s

Pd(1) - S(1)	2.280(4)	Pd(1) - S(4)	2.307(4)

Table 5.2: Selected Angles(°) with e.s.d.'s

S(1)-Pd(1)- S(4)	88.59(14)	S(4)- C(3)-(C2')	111.4(10)
S(1)-Pd(1)- S(1D)	90.32(4)	Pd(1)- S(4)- C(3)	98.7(4)
S(4)-Pd(1)-S(4D)	88.28(14)	Pd(1)- S(4)- C(5)	96.3(6)
Pd(1)-S(1) - C(2)	96.7(6)	Pd(1)- S(4)- C(5')	106.4(6)
Pd(1)-S(1) -C(12)	100.6(5)	C(3)- S(4)- C(5)	90.2(7)
Pd(1)-S(1) -C82')	104.4(6)	C(3)- S(4)- C(5')	111.1(8)
C(2)-S(1) -C(12)	90.6(8)	S(4)- C(5)- C(5D)	117.5(12)
C(12)-S(1) -C(2')	116.0(7)	S(1)-C(12) -C(12D)	117.9(10)
S(1)-C(2) - C(3)	113.8(3)	S(4) -C(5) -C(5'D)	117.5(14)
C(2)-C(3) - S(4)	118.8(11)	S(1) -C(2')- C(3)	113.8(2)

Table 5.3: Selected Torsion Angles(^{o}) with e.s.d.'s

C(12)	- S(1)	- C(2)	- C(3)	-145.7(13)
C(2')	- C(3)	- S(4)	-C(5')	162.6(11)
C(2)	- S(1)	-C812)	-C(12D)	120.7(12)
S(4)	- C(3)	-C(2')	- S(1)	-45.4(14)
C(2')	- S(1)	-C(12)	-C(12D)	135.7(11)
C(3)	- S(4)	- C(5)	-C(5D)	-130.7(13)
C(12)	- S(1)	-C(2')	- C(3)	-94.8(13)
C(3)	- S(4)	-C(5')	-C(5'D)	-120.0(14)
S(1)	- C(2)	- C(3)	- S(4)	22.3(17)
S(4)	- C(5)	-C(5D)	-S(4D)	0.1(18)
C(2)	- C(3)	- S(4)	- C(5)	109.4(13)
S(1)	-C812)	-C(12D)	-S(1D)	0.1(15)
C(2)	- C(3)	- S(4)	-C(5')	124.3(13)
S(4)	-C(5')	-C(5'D)	-S(4D)	-0.1(21)
C(27)	- C(3)	- S(4)	- C(5)	147.7(12)

5.2.3: $[M([14]aneS_4)](PF_6)_2$, (M= Pd, Pt)

The Pd(II) and Pt(II) complexes of $[14]aneS_4$, $[M([14]aneS_4)]^{2+}$ have been prepared previously in Edinburgh [4,164]. The single crystal structure of $[Pd([14]aneS_4)]^{2+}$ shows Pd(II) bound in a square planar arrangement to all four macrocyclic S-donors, [Pd-S(1)= 2.292(10), Pd-S(4)= 2.242(9), Pd-S(8)= 2.308(8), Pd-S(11)= 2.278(10)Å], as illustrated in Fig. 5.6. It can be seen from this that like $[Pd([12]aneS_4)]^{2+}$, the complex adopts a cccc-conformation with all of the methylene chains directed to one face of the PdS_4 plane. In this case, the metal is displaced out of the least-squares S_4 plane by only 0.0381Å, reflecting the larger hole-size of this ligand.

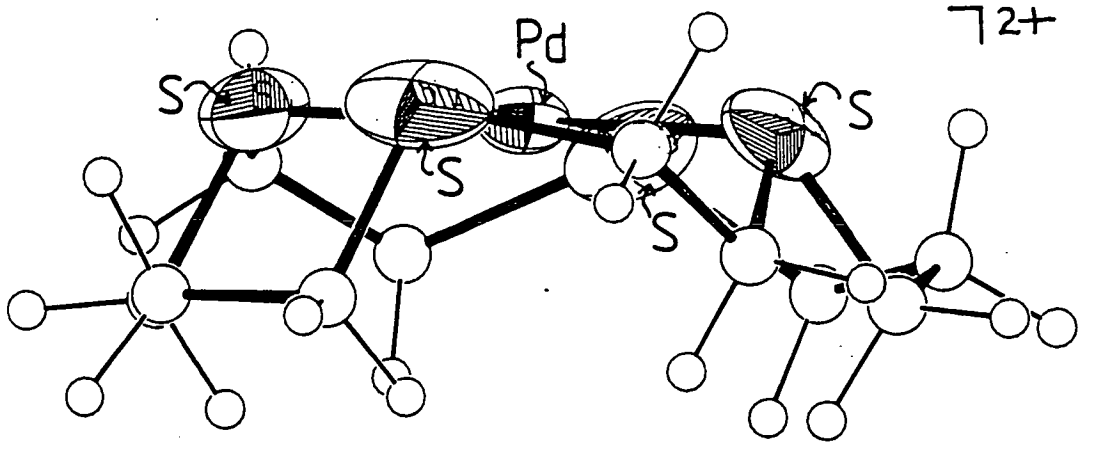

Fig. 5.6: Single crystal structure of $[Pd([14]aneS_4)]^{2+}$

5.2.4: $[M([16]aneS_4)](PF_6)_2$. (M= Pd, Pt)

Treatment of $PdCl_2$ with one molar equivalent of $[16]aneS_4$ under similar conditions to those employed for the synthesis of $[Pd([12]aneS_4)]^{2+}$, yielded a yellow crystalline solid.

The f.a.b. mass spectrum of the complex reveals molecular ion peaks at M^+= 547, 439, 419 and 401, corresponding to $[^{106}Pd([16]aneS_4)PF_6]^+$, $[^{106}Pd([16]aneS_4).2H_2O-H]^+$, $[^{106}Pd([16]aneS_4).H_2O-H]^+$ and $[^{106}Pd([16]aneS_4-H)]^+$ respectively. The ^1H n.m.r. spectrum of the product measured at 298K reveals two broadened second order resonances at δ= 3.19-3.33 and 2.50-2.69ppm. These integrate as 2:1, and thus, are assigned to $SC\underline{H}_2$ and $CH_2C\underline{H}_2CH_2$ respectively. The ^{13}C DEPT n.m.r. spectrum of the complex measured at 50.32MHz, 298K reveals two distinct methylene carbon resonances for the complex, at δ= 33.78 ($S\underline{C}H_2$, 8C) and 23.18ppm ($CH_2\underline{C}H_2CH_2$, 4C), corresponding to a fully symmetric conformation. Interestingly, the ^{13}C DEPT n.m.r. spectrum measured at 90.56MHz, 298K shows six distinct methylene resonances indicating the presence of two different isomers. The resonances at δ= 33.43 ($S\underline{C}H_2$, 8C) and 23.68ppm ($CH_2\underline{C}H_2CH_2$, 4C) are consistent with a symmetric isomer, while those at δ= 35.19 ($S\underline{C}H_2$, 4C), 31.86 ($S\underline{C}H_2$, 4C), 23.98 ($CH_2\underline{C}H_2CH_2$, 2C) and 21.62ppm ($CH_2\underline{C}H_2CH_2$, 2C) are consistent with a less symmetric isomer. These results show that in solution at 298K there are different

conformations rapidly interconverting via a ring-flipping mechanism, and at high-field the rate of interconversion is sufficiently low to observe two distinct sets of resonances (Fig. 5.7). This time averaging process is probably a consequence of the flexibility of the propyl linkages. These data, together with microanalyses and I.R. spectroscopy, confirm our assignment of the product as $[Pd([16]aneS_4)](PF_6)_2$.

In order to confirm the stereochemistry around the central metal ion, and to determine which conformation is preferred in the solid phase, a single crystal X-ray structural analysis was undertaken.

Fig. 5.7: ^{13}C DEPT n.m.r. spectrum of $[Pd([16]aneS_4)]^{2+}$ (CD_3CN, 90.56MHz)

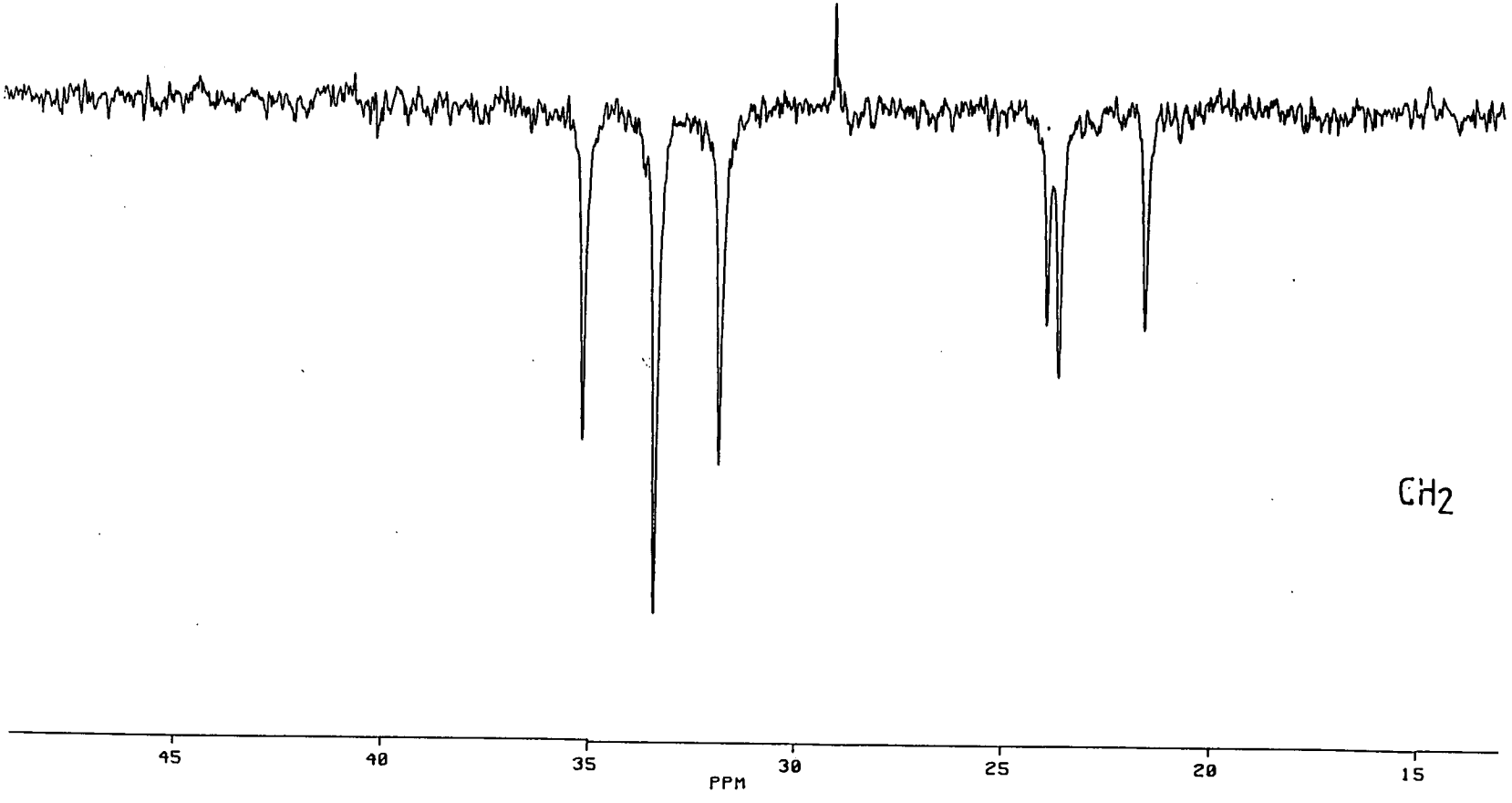

5.2.5: Single Crystal Structure of

$[Pd([16]aneS_4)](PF_6)_2$

Details of the structure solution and refinement are given in the Experimental Section. Lists of relevant bond lengths, angles and torsions are given in Tables 5.4, 5.5 and 5.6 respectively. Two ORTEP plots illustrating the geometry of the cation are presented in Figs. 5.8 and 5.9.

The structure shows two independent half-molecules per unit cell. Each Pd(II) ion occupies a crystallographic inversion centre, and is bound to all four S-donor atoms of the macrocycle in a square planar geometry [Pd-S(1)= 2.304(10), Pd-S(5)= 2.303(10)Å], with all angles around Pd(II) close to 90^{o}. The macrocyclic complex adopts a ctct-conformation in the solid state, with two adjacent six-membered chelate rings directed above the PdS_4 co-ordination plane, and the other two below. The Pd(II) ion lies precisely in the plane of the four S-donors as a direct consequence of the crystallographically imposed inversion centre at the Pd atom.

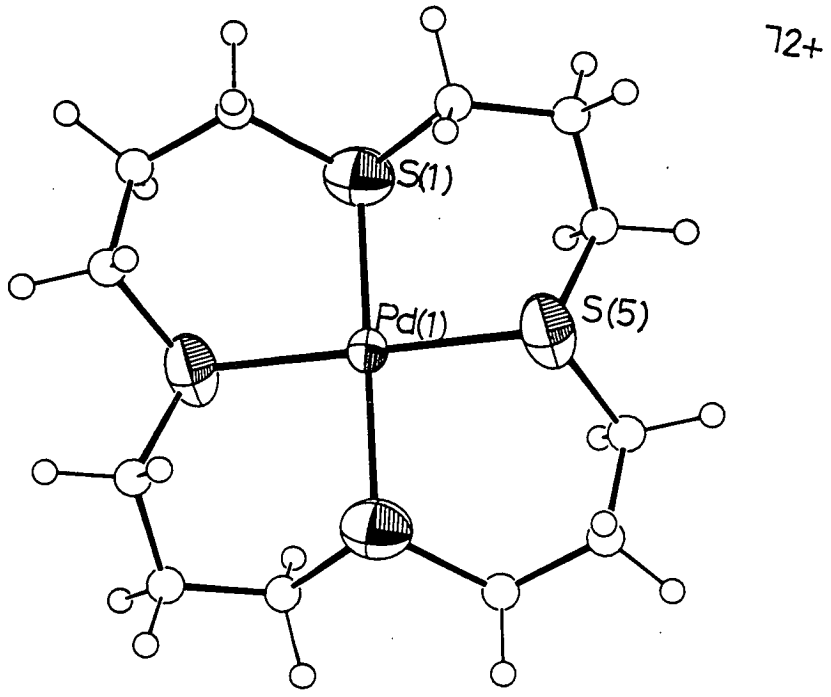

Fig. 5.8: View of the single crystal structure of $[Pd([16]aneS_4)]^{2+}$

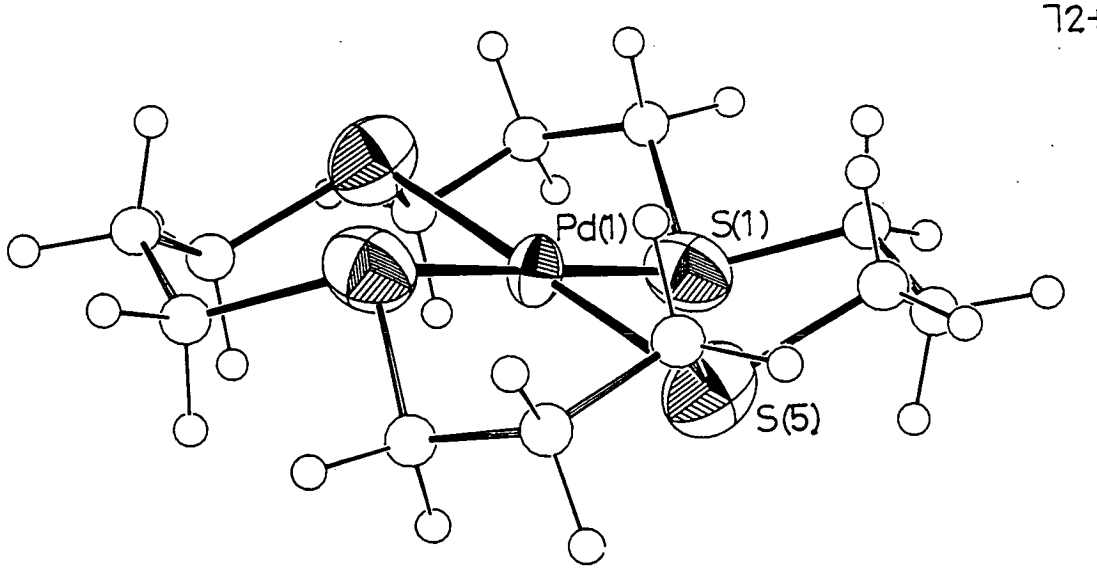

Fig. 5.9: Alternative view of the single crystal structure of $[Pd([16]aneS_4)]^{2+}$

Single Crystal Structure of

$[Pd([16]aneS_4)](PF_6)_2$

Table 5.4: Selected Bond Lengths(Å) with e.s.d.'s

Pd(1)-S(11)	2.304(10)	Pd(2)-S(21)	2.300(10)
Pd(1)-S(15)	2.303(10)	Pd(2)-S(25)	2.315(9)

Table 5.5: Selected Angles(°) with e.s.d.'s

S(11)-Pd(1) -S(11')	179.9(4)	S(21) -Pd(2) -S(21')	179.9(3)
S(11)-Pd(1) -S(15)	83.3(3)	S(21) -Pd(2) -S(25)	91.2(3)
Pd(1)-S(11) -C(12)	107.9(11)	Pd(2) -S(21) -C(22)	105.8(9)
Pd(1)-S(11')-C(18)	115.0(14)	Pd(2) -S(21')-C(28)	108.7(9)
C(18)-S(11')-C(12')	92.5(17)	C(28) -S(21')-C(22')	92.8(12)
Pd(1)-S(15) -C(14)	110.4(10)	Pd(2) -S(25) -C(24)	104.6(9)
Pd(1)-S(15) -C(16)	118.3(10)	Pd(2) -S(25) -C(26)	112.3(10)
C(14)-S(15) -C(16)	94.5(13)	C(24) -S(25) -C(26)	97.8(12)
S(11)-C(12) -C(13)	121.2(22)	S(21) -C(22) -C(23)	113.2(17)
C(12)-C(13) -C(14)	117.5(26)	C(22) -C(23) -C(24)	114.1(22)
S(15)-C(14) -C(13)	113.2(20)	S(25) -C(24) -C(23)	114.0(18)
S(15)-C(16) -C(17)	113.5(21)	S(25) -C(26) -C(27)	114.4(20)
C(16)-C(17) -C(18)	140.9(31)	S(11')-C(18) -C(17)	116.9(28)
C(26)-C(27) -C(28)	115.7(23)	S(21')-C(28) -C(27)	106.0(19)

Table 5.6: Selected Torsion Angles(°) with e.s.d.'s

C(12')	-S(11')	-C(18)	-C(17)	-160.8(29)
S(21)	-Pd(2)	-S(25)	-C(26)	-135.8(10)
C(18)	-S(11')	-C(12')	-C(13')	116.0(28)
Pd(2)	-S(21)	-C(22)	-C(23)	79.3(18)
C(16)	-S(15)	-C(14)	-C(13)	152.5(21)
Pd(2)	-S(21')	-C(28)	-C(27)	75.0(18)
C(14)	-S(15)	-C(16)	-C(17)	-137.8(22)
C(22')	-S(21')	-C(28)	-C(27)	-177.3(19)
S(11)	-C(12)	-C(13)	-C(14)	-65.5(34)
C(28)	-S(21')	-C(22')	-C(23')	170.3(19)
C(12)	-C(13)	-C(14)	-S(15)	44.6(33)
Pd(2)	-S(25)	-C(24)	-C(23)	79.6(19)
S(15)	-C(16)	-C(17)	-C(18)	4.9(56)
C(26)	-S(25)	-C(24)	-C(23)	-164.8(19)
C(16)	-C(17)	-C(18)	-S(11')	36.6(60)
Pd(2)	-S(25)	-C(26)	-C(27)	-54.8(22)
S(21')	-Pd(2)	-S(21)	-C(22)	36.6(60)
C(24)	-S(25)	-C(26)	-C(27)	-164.2(20)
S(25)	-Pd(2)	-S(21)	-C(22)	-27.7(9)
S(21)	-C(22)	-C(23)	-C(24)	-44.3(27)
S(21)	-Pd(2)	-S(21')	-C(28)	-27.7(9)
C(22)	-C(23)	-C(24)	-S(25)	-40.6(27)
S(25)	-Pd(2)	-S(21')	-C(28)	-53.7(10)
S(25)	-C(26)	-C(27)	-C(28)	72.4(28)
S(21)	-Pd(2)	-S(25)	-C(24)	-30.8(9)
C(26)	-C(27)	-C(28)	-S(21')	-81.7(25)

The Pt(II) analogue, $[Pt([16]aneS_4)](PF_6)_2$ was prepared by the same method as for the Pd(II) complex above. The I.R. spectrum of the resulting cream-coloured solid shows bands assigned to υ(C-H) (3000, 2920, 2845cm^{-1}) and δ(C-H) (1440, 1420). Bands characteristic of PF_6^- counterion are also apparent at 840 (υ(P-F)) and 555cm^{-1} (δ(P-F)). The f.a.b. mass spectrum of the complex shows molecular ion peaks at M^+= 636 and 490, assigned to $[^{195}Pt([16]aneS_4)PF_6]^+$ and $[^{195}Pt([16]aneS_4\text{-}H)]^+$ respectively. These data together with microanalyses confirm the formulation of this product as $[Pt([16]aneS_4)](PF_6)_2$. Furthermore, the data strongly indicate that this system is isostructural with its Pd(II) analogue. The ^1H n.m.r. spectrum of $[Pt([16]aneS_4)]^{2+}$ measured at 360.13MHz, 298K, like its Pd analogue, shows two very broad resonances. Temperature dependence is confirmed by a variable temperature study, and cooling to 238K, results in significant sharpening of each of these resonances, giving complex second order multiplets at δ= 3.06-3.28 ($SC\underline{H}_2$, 16H) and 2.31-2.55ppm ($CH_2C\underline{H}_2CH_2$, 8H), (Fig. 5.10). Interestingly both of these multiplets exhibit ^{195}Pt satellites (I=1/2, 33.0%), although $^3J_{Pt-H}$ and $^4J_{Pt-H}$ cannot be discerned accurately due to the complexity of the spectrum.

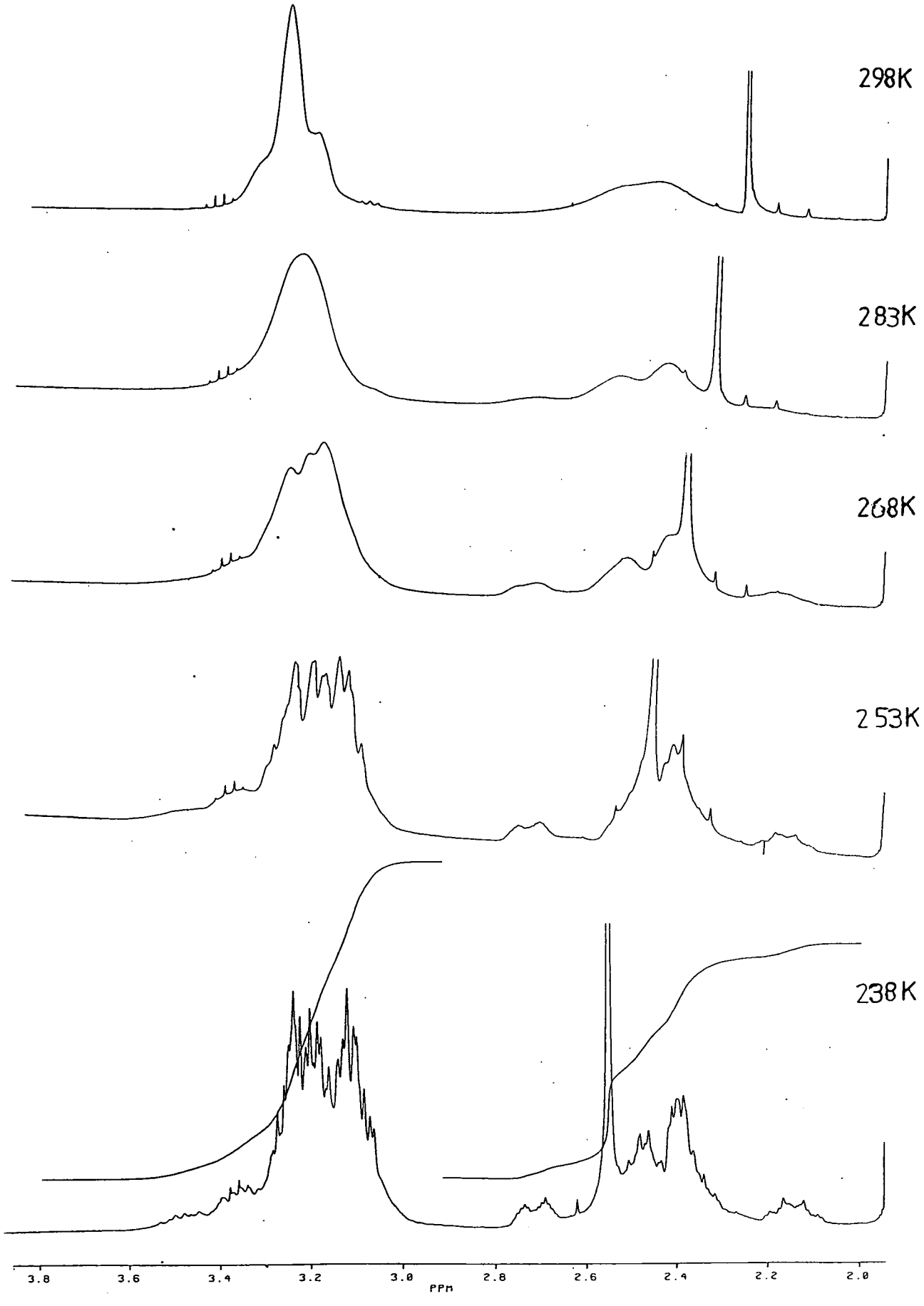

Fig. 5.10:

Variable temperature ^{1}H n.m.r. spectra of $[Pt([16]aneS_4)]^{2+}$

(CD_3CN, 360.13MHz)

The ^{13}C DEPT n.m.r. spectrum measured at 50.32MHz, 298K, is also broadened, with two resonances at δ= 32.96 and 24.26ppm, assigned to $S\underline{C}H_2$ and $CH_2\underline{C}H_2CH_2$ respectively. Measuring this spectrum at 90.56MHz, 298K results in significant sharpening of the signals. The spectrum shows methylene carbon resonances corresponding to several different conformations at δ= 33.12 ($S\underline{C}H_2$, 8C) and 23.79ppm ($CH_2\underline{C}H_2CH_2$, 4C) due to a symmetric isomer; δ= 35.61 ($S\underline{C}H_2$, 4C), 31.52 ($S\underline{C}H_2$, 4C), 24.05 ($CH_2\underline{C}H_2CH_2$, 2C) and 21.74ppm ($CH_2\underline{C}H_2CH_2$, 2C) due to an asymmetric isomer. Further weak resonances at δ= 33.81, 31.70, 22.67 and 20.55ppm are tentatively assigned to another asymmetric isomer, (Fig. 5.11). This evidence suggests that the Pt(II) and Pd(II) complexes of [16]aneS_4 exhibit similar characteristics in solution.

Fig. 5.11: ^{13}C DEPT n.m.r. spectrum of $[Pt([16]aneS_4)]^{2+}$ (CD_3CN, 90.56MHz)

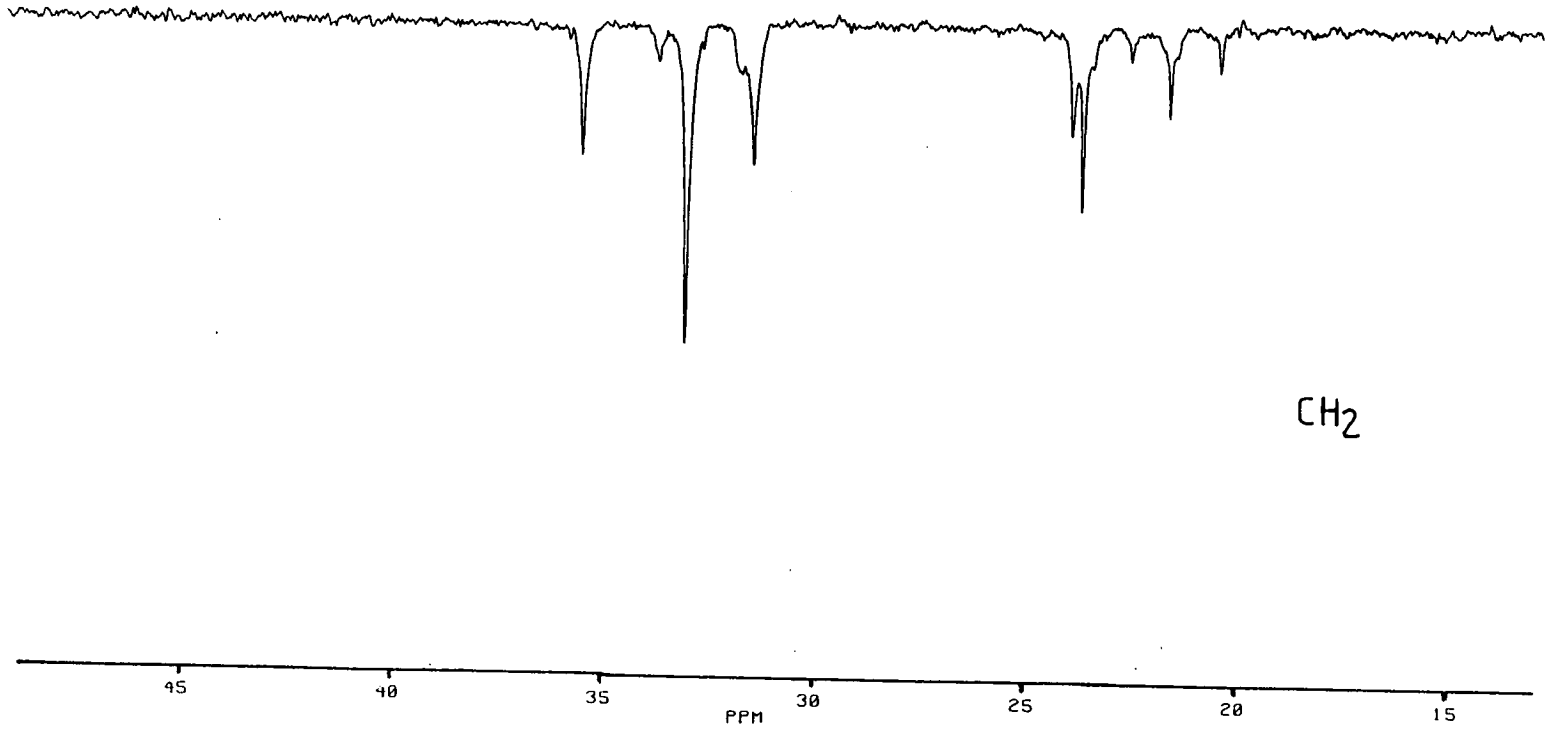

5.2.6: $[M_2([28]aneS_8)](PF_6)_4$, (M= Pd, Pt)

Reaction of two molar equivalents of $K_2[PdCl_4]$ with one molar equivalent of $[28]aneS_8$ in refluxing $MeOH/H_2O$ afforded a bright yellow precipitate probably corresponding to $[Pd_4Cl_8([28]aneS_8)]$ initially. Prolonged refluxing resulted in slow dissolution of this to give a bright yellow solution. Addition of excess PF_6^- counterion gave a yellow precipitate, which was recrystallised from $MeCN/H_2O$.

Importantly, the I.R. spectrum of this complex shows no Pd-Cl stretching vibrations in the range 400-250cm^{-1}. The f.a.b. mass spectrum of the complex reveals molecular ion peaks with the correct isotopic distributions at M^+= 1184, 1076, 1058, 1037, 928, 911, 892 and 749. These are assigned to

$[^{106}Pd_2([28]aneS_8+H)(PF_6)_3]^+$,

$[^{106}Pd_2([28]aneS_8)(PF_6)_2.2H_2O+2H]^+$,

$[^{106}Pd_2([28]aneS_8)(PF_6)_2.H_2O]^+$,

$[^{106}Pd_2([28]aneS_8-H)(PF_6)_2]^+$,

$[^{106}Pd_2([28]aneS_8).PF_6.2H_2O-H]^+$,

$[^{106}Pd_2([28]aneS_8).PF_6.H_2O]^+$,

$[^{106}Pd_2([28]aneS_8-H).PF_6]^+$ and

$[^{106}Pd_2([28]aneS_8+H)]^+$ respectively.

The ^1H n.m.r. spectrum of the complex, measured at 298K, shows two broad, second order multiplets due to the macrocyclic methylene protons, at δ= 2.7-4.0 ($SC\underline{H}_2$), and 2.2-2.5ppm ($CH_2C\underline{H}_2CH_2$). Recording the spectrum at

360.13MHz, 298K, results in significant sharpening of these multiplets, indicating an averaging process in solution. This probably corresponds to interconversion of different conformations in solution, as observed for $[M([16]aneS_4)]^{2+}$, (M= Pd, Pt). The ^{13}C DEPT n.m.r. spectrum of the complex, measured at 50.32MHz, 298K, reveals six major $\underline{C}H_2$ resonances at δ= 41.60, 39.62, 36.56, 35.73, 33.48 and 25.59ppm, consistent with a binuclear complex in which each Pd(II) centre is bound to four sulphur-donors in a square planar stereochemistry. Several other much less intense $\underline{C}H_2$ resonances are also apparent at δ= 37.28, 37.07, 24.18, 23.84 and 23.51ppm, consistent with the presence of a second isomer in solution. This is confirmed by measuring the ^{13}C DEPT n.m.r. spectrum at 90.56MHz, 298K, (Fig. 5.12). This spectrum provides clear evidence for two different conformations in solution, with δ= 41.26, 39.37, 36.14, 35.23 (4x$S\underline{C}H_2$, 16C) and 25.09ppm ($CH_2\underline{C}H_2CH_2$, 4C) due to the presence of a fully symmetrical conformation, and δ= 37.03, 36.82, 36.14 (overlapping), 35.88, 32.83, 32.69, 32.48, 32.33 (8x$S\underline{C}H_2$, 16C), 23.56 ($CH_2\underline{C}H_2CH_2$, 1C), 23.08 ($CH_2\underline{C}H_2CH_2$, 2C) and 22.59ppm ($CH_2\underline{C}H_2CH_2$, 1C) consistent with the presence of a less symmetrical isomer in which one six-membered chelate ring has flipped into the opposite configuration. These data, together with microanalytical and UV/vis spectral data, confirm our assignment of the product as $[Pd_2([28]aneS_8)](PF_6)_4$.

Fig. 5.12: ^{13}C DEPT n.m.r. spectrum of $[Pd_2([28]aneS_8)]^{4+}$ (CD_3CN, 90.56MHz)

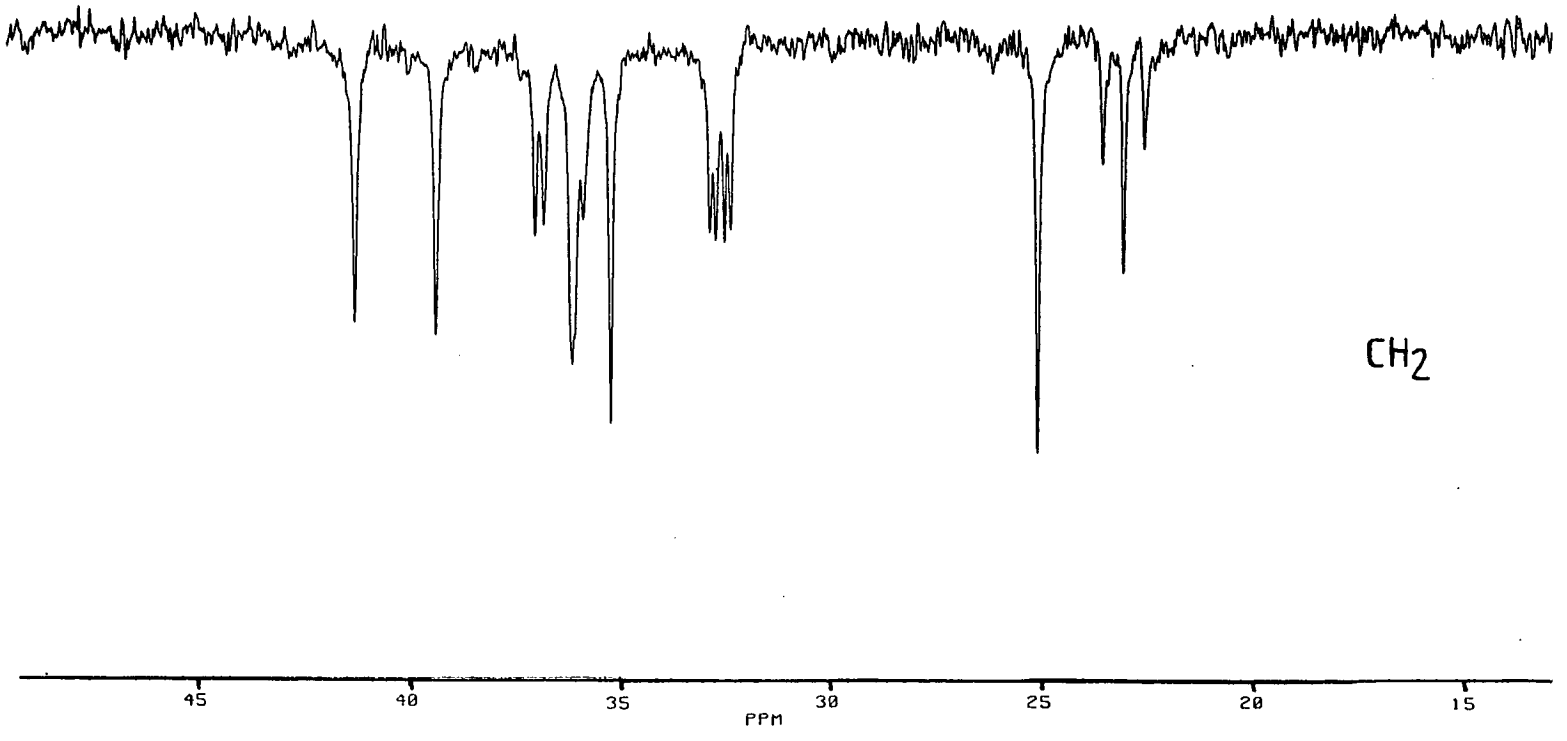

The analogous binuclear Pt(II) complex was prepared by a similar method. This product was confirmed to be $[Pt_2([28]aneS_8)](PF_6)_4$ on the basis of microanalytical data and I.R. spectroscopy, (υ(C-H) 2960, 2900, δ(C-H) 1420, υ(P-F) 840, δ(P-F) 555cm^{-1}). The f.a.b. mass spectrum is in accord with this, showing molecular ion peaks with the correct isotopic distributions at M^+= 1360, 1250, 1232, 1213, 1105, 189 and 1069. These are assigned to

$[^{195}Pt_2([28]aneS_8\text{-}H)(PF_6)_3]^+$,

$[^{195}Pt_2([28]aneS_8)(PF_6)_2.2H_2O\text{-}2H]^+$,

$[^{195}Pt_2([28]aneS_8)(PF_6)_2.H_2O\text{-}2H]^+$,

$[^{195}Pt_2([28]aneS_8\text{-}3H)(PF_6)_2]^+$,

$[^{195}Pt_2([28]aneS_8).PF_6.2H_2O\text{-}2H]^+$,

$[^{195}Pt_2([28]aneS_8).PF_6.H_2O]^+$ and

$[^{195}Pt_2([28]aneS_8\text{-}2H).PF_6]^+$ respectively.

The ^1H n.m.r. spectrum of the complex shows broad second order multiplets at δ= 3.46-2.96 ($SC\underline{H}_2$) and 2.22-1.96ppm ($CH_2C\underline{H}_2CH_2$). The ^{13}C DEPT n.m.r. spectrum of $[Pt_2([28]aneS_8)]^{4+}$ exhibits methylene carbon resonances at δ= 40.24, 38.46, 37.25, 36.73, 36.30, 35.67, 35.13, 33.83, 33.61, 25.29 and 23.28ppm. These data indicate the presence of more than one isomer in solution, interchanging rapidly, probably via a ring-flipping mechanism, as proposed for the Pd analogue above.

5.3: Electrochemical Study of $[M(L)]^{2+}$ and $[M_2([28]aneS_8)]^{4+}$, (M= Pd, Pt, L= $[12]aneS_4$. $[14]aneS_4$, $[16]aneS_4$)

5.3.1: Palladium

Table 5.7 lists the reduction products and UV/vis spectral data for all of the palladium complexes studied.

Table 5.7: UV/vis spectral data for Pd tetrathia and octathia macrocyclic complexes (in MeCN/0.1M $NBu^n_4PF_6$)

Complex	1st Red^n Product		2nd Red^n Product	
	λ_{max}	(ε_{max})	λ_{max}	(ε_{max})
$[Pd([12]aneS_4)]^{2+}$	384	(44,290)	-	
	272	(32,870)		
$[Pd([14]aneS_4)]^{2+}$	421	(6,445)	567	(8,200)
	376	(5,405)		
	268	(8,150)		
	218	(7,370)		
$[Pd([16]aneS_4)]^{2+}$	449	(3,770)	588	(8,530)
	369	(6,170)		
	273	(3,940)		
$[Pd_2([28]aneS_8)]^{4+}$	431	(8,870)	-	
	361	(8,770)		
	276	(12,850)		

Note: λ in nm, ε in $M^{-1}cm^{-1}$

[14]aneS$_4$

Cyclic voltammetry of [Pd([14]aneS$_4$)](PF$_6$)$_2$ measured at 298K in MeCN (0.1M NBu$^n_4$PF$_6$ supporting electrolyte) at platinum electrodes, shows two irreversible reductions at Ep_c= -0.90 and -1.69V *vs.* Fc/Fc$^+$ (scan rate= 160mVs^{-1}). No oxidative activity is observed within the solvent range (0 to +2.0V *vs.* Fc/Fc$^+$). Upon cooling to 238K, and increasing the scan rate to 10Vs^{-1}, the first reduction becomes fully reversible ($E_{1/2}$= -0.87V *vs.* Fc/Fc$^+$).

A quantitative investigation of the first reduction process was undertaken. Coulometry of [Pd([14]aneS$_4$)]$^{2+}$, measured at -1.0V, 298K in MeCN (0.1M NBu$^n_4$PF$_6$ supporting electrolyte) at a platinum basket, confirms that this reduction corresponds to a one-electron process (n= 1.03 electrons). Similar behaviour is observed in acetone. During bulk electrolysis the solution changes to an orange colour prior to giving a final intense-purple colour. Both the orange and the purple air-sensitive solutions were found to be e.s.r silent. Controlled potential electrolysis at -1.0V, 238K in the same medium gives a bright yellow solution initially. The e.s.r spectrum (measured at 77K, MeCN glass) of this bright yellow solution shows a weak anisotropic signal with axial symmetry, g_{11}= 2.092, $g_{\perp}$= 2.045. Hyperfine coupling to ^{105}Pd (I=1/2, 22.2%) is discernible in the $g_{\perp}$ region, giving $A_{\perp}$= 32G,

(Fig. 5.13). These spectral features are consistent with initial formation of a genuine d^9 Pd(I) monomeric species [117-119,129,130]. This paramagnetic species is rapidly quenched upon increasing its concentration, giving an e.s.r. silent orange material, and subsequently a purple solution. This behaviour is characteristic of a bimolecular process probably corresponding to a dimerisation via formation of a direct metal-metal bond. The orange solution is apparently redox inactive. However, this material is stable only at low temperature, and there may be a kinetic barrier at this temperature inhibiting oxidation. The cyclic voltammogram of the purple solution measured at 308K shows a rather broad and ill-defined oxidation at E_{pa} = +0.09V *vs.* Fc/Fc^+. Controlled potential electrolysis at 308K , +0.25V regenerates the original Pd(II) starting material quantitatively.

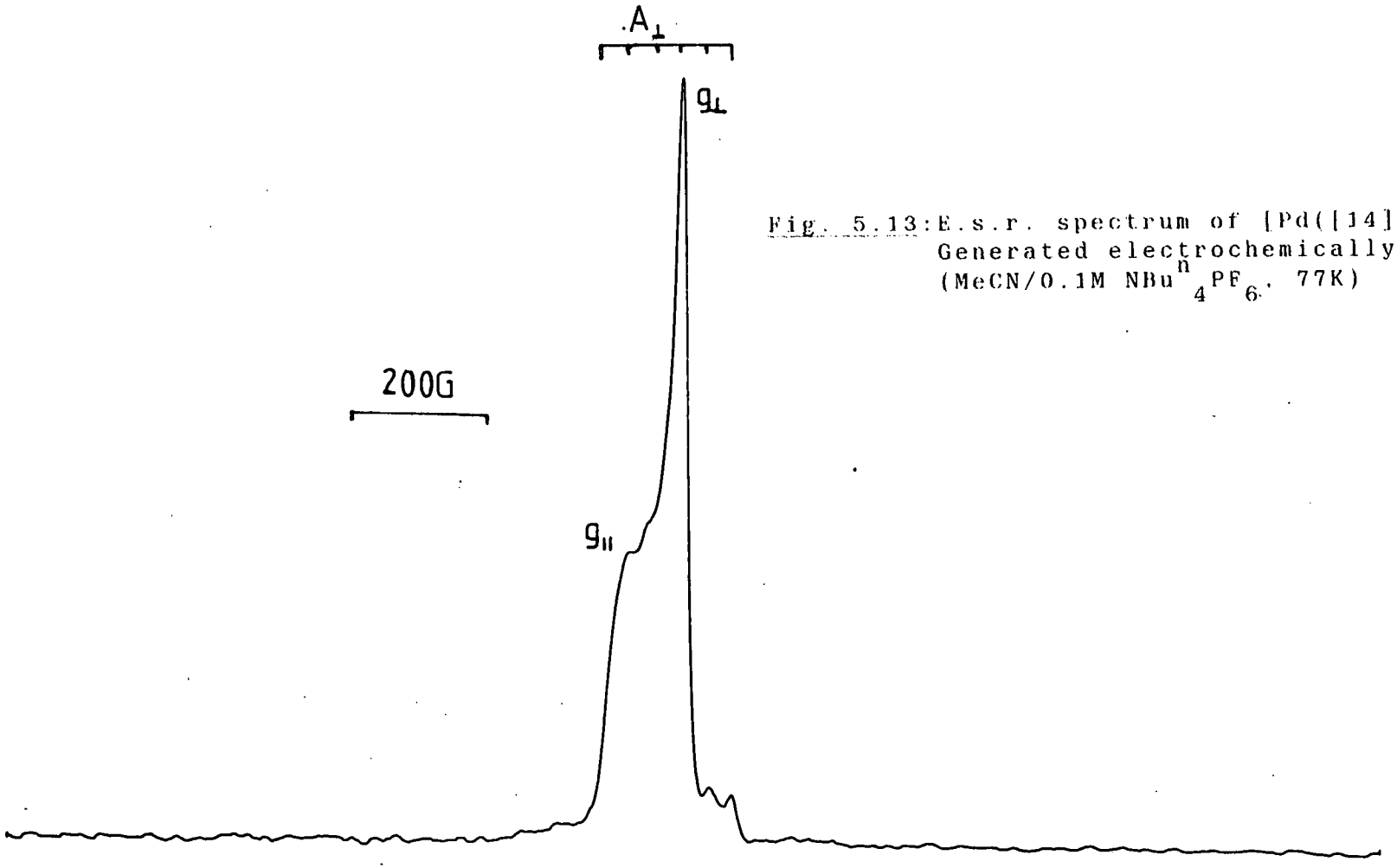

Fig. 5.13: E.s.r. spectrum of $[Pd([14]aneS_4)]^+$ Generated electrochemically ($MeCN/0.1M\ NBu^n_4PF_6$, 77K)

Facile dimerisation via formation of a direct metal-metal bond is characteristic of the second and third series transition metals. A number of platinum metal porphyrin complexes incorporating unsupported metal-metal bonds of the general type $[M_2P_2]$, (M= Ru(II), Os(II), Rh(II) and Ir(II), P= OEP^{2-} and TTP^{2-}) have been reported [165-169]. These act as precursors for highly reactive monomeric systems; for example, $[Rh_2P_2]$ acts as a source of the highly reactive [RhP]$^{\cdot}$ radical, which has been shown to effectively bind and activate small molecules such as NO and O_2 [37]. Wayland and co-workers have also shown that this dimer provides a source of Rh(OEP)H, which readily undergoes CO insertion into the Rh-H bond via a free radical mechanism, generating a formyl species:

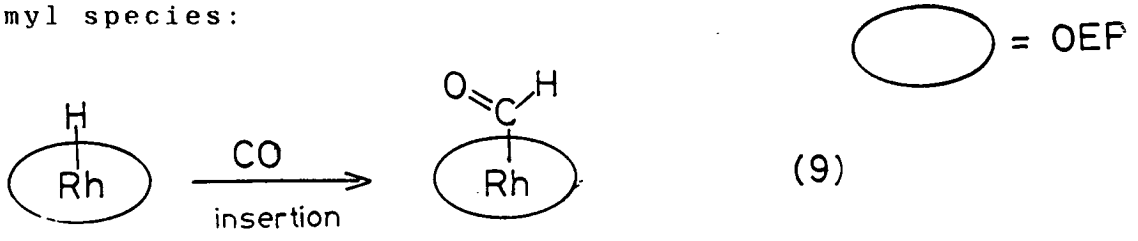

(9)

Interestingly, this process is the only example of an equilibrium between a metal hydride and CO where the formyl product is thermally favoured [32,38].

All of these metalloporphyrin dimers can undergo a large number of insertion and binding reactions. A representative summary of the chemistry of the diruthenium species $[Ru_2(OEP)_2]$ is illustrated in Fig. 5.14 [37].

In addition, highly nucleophilic M(I) porphyrin anions can be generated electrochemically (M= Fe, Co, Rh and Ir). These potent metal anions react with alkyl halides to give M(III) porphyrin alkyls, (10). In some cases, even C-C bonds in strained carbocyclic rings can be ruptured by these anions, generating organometallic porphyrin derivatives [37].

(10) 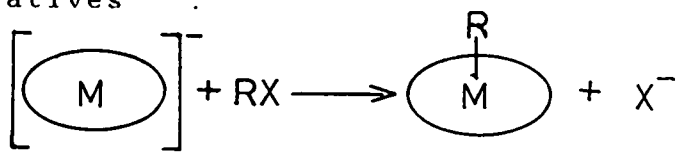

M=Fe, Co, Rh, Ir = porph

There are only three important examples of non-porphyrinoid metal-metal bonded macrocyclic complexes. These include the Ni(I)-Ni(I) dimer reported by Addison et al [170], incorporating the tetra-aza cyclops ligand, (11):

$2[Ni(cyclops)]^+ + 2e^- \longrightarrow 2[Ni(cyclops)] \longrightarrow [Ni(cyclops)]_2$

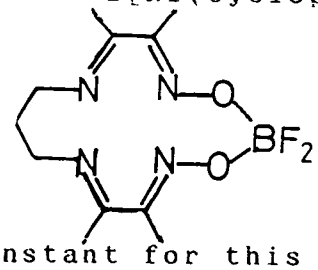

(11)

The dimerisation constant for this reaction, K_d, has been determined as 5900±200.

Both of the other examples, $[M_2L_2]$, [M= Rh(II), Ru(II)] [171] incorporate the di-anionic tetra-aza macrocycle, (12), and involve an unsupported metal-metal bond. The Rh(II)-Rh(II) and dimer has been characterised by X-ray crystallography [Rh-Rh bond length= 2.625(2)Å], and in each case the macrocycle adopts a saddle-shaped

conformation directed away from the metal-metal bond, as a consequence of the steric interactions between the methyl groups and the benzenoid rings. No other metal-metal bonded macrocyclic complexes have been reported.

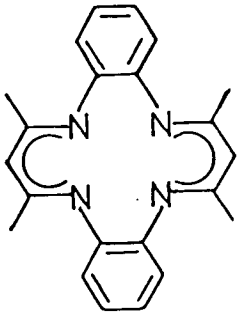

(12)

A few diamagnetic non-macrocyclic Pd complexes involving a Pd(I)-Pd(I) bond are known. The complex-cation $[Pd_2(CNMe)_6]^{2+}$ is probably the most extensively studied example [172,173]. This stable species has been shown by single crystal X-ray crystallography to have the staggered structure, (13), with an unsupported Pd(I)-Pd(I) bond of 2.5301(9)Å. In solution the cation is fluxional. This is thought to be due either to free rotation about the metal-metal bond, or an equilibrium between the Pd(I)-Pd(I) dimer and a Pd(II)-Pd(0) dimer.

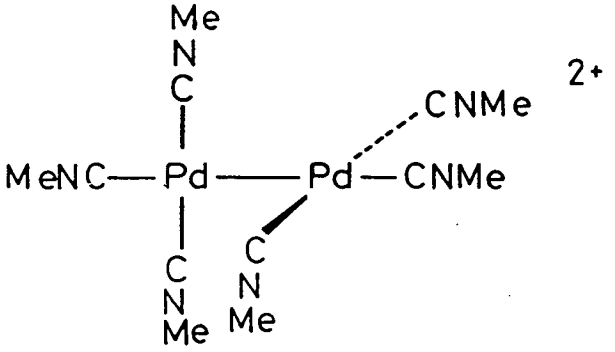

(13)

Fig. 5.14: Summary of Collman's work on reactions of $Ru_2(OEP)_2$

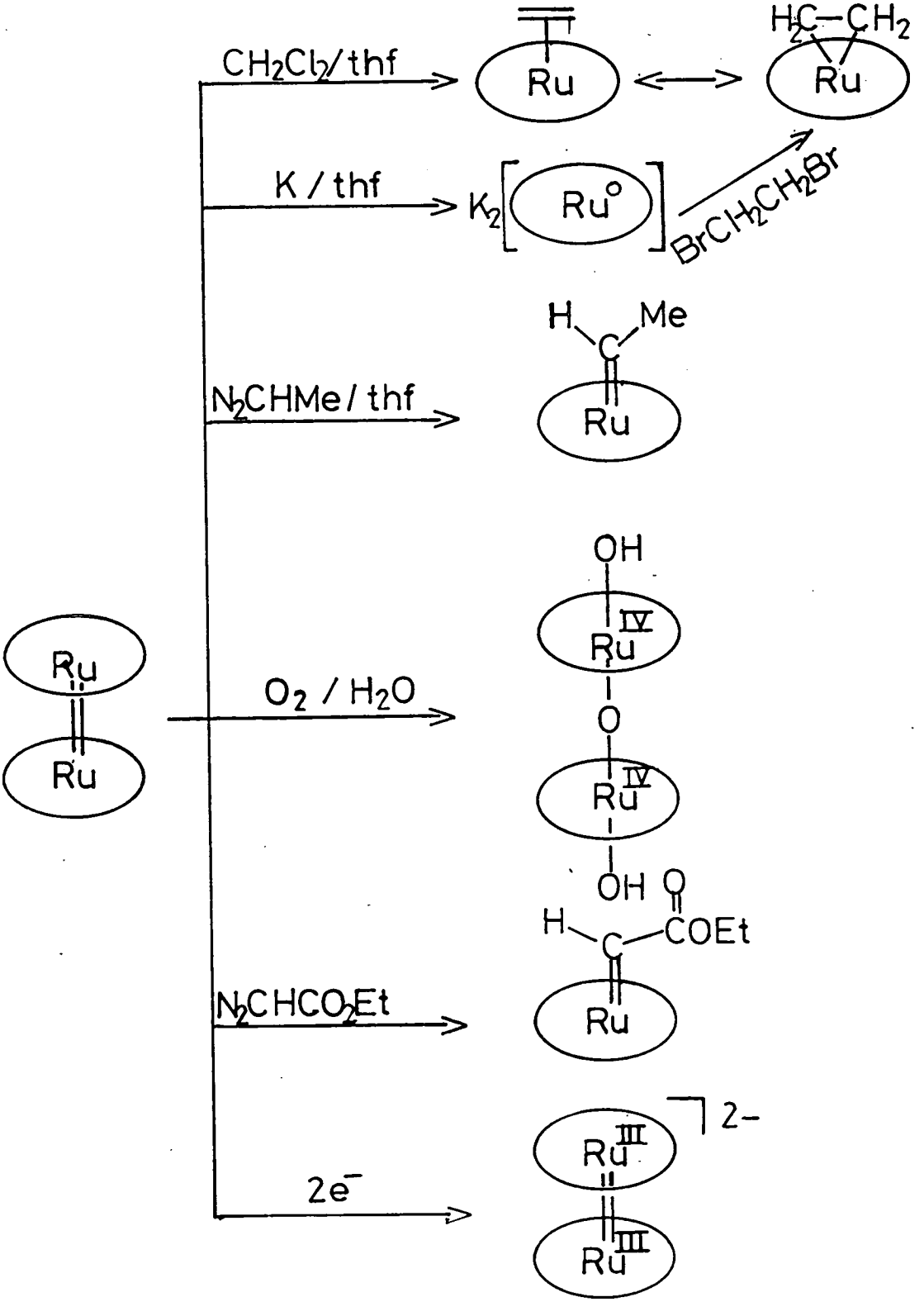

= OEP

Many of the Pd(I)-Pd(I) dimers reported require π-acceptor ligands to stabilise them, e.g. dppm, thiophosphide [174,175]. These species have metal-metal bonds in the range 2.6-3.5Å. In most cases the metal-metal bond is also highly reactive, especially towards insertion of small molecules [176-179], as illustrated for the bridged phosphine dimer in Fig. 5.14. The metal-metal bond can be ruptured in many instances by UV irradiation, generating a paramagnetic metal-based radical [180].

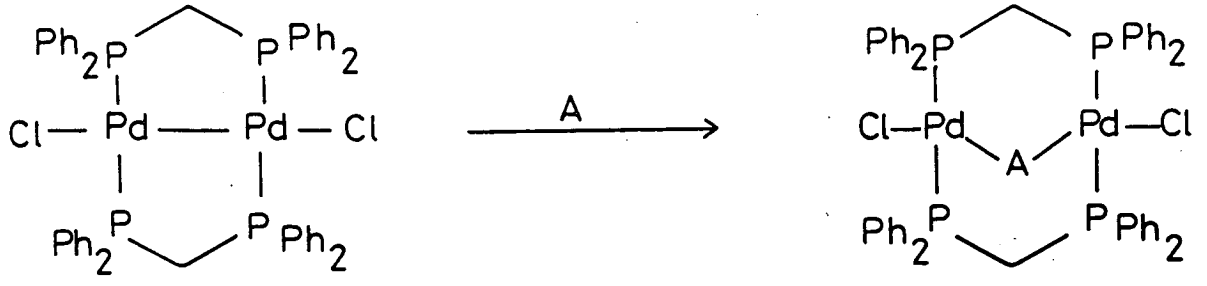

Fig. 5.15: Insertion reactions of $Pd_2Cl_2(dppm)_2$ A = CO, SO_2

In an effort to elucidate the nature of the products from the reduction of $[Pd([14]aneS_4)]^{2+}$, the one-electron reduction was followed at 243K by *in situ* UV/vis spectroscopy using an O.T.T.L.E. system. The reduction occurs isosbestically (λ_{iso} = 350, 241nm), with loss of intensity of the absorption bands at λ_{max} = 330 and 265nm. This is accompanied by the growth of three new absorption bands at λ_{max} = 421, 376 and 218nm as shown in Fig. 5.16. Maintaining the same reduction potential and warming the solution to 273K results in a further

conversion to the purple species. The spectrum of this latter species is essentially featureless, except for an intense band at λ_{max}= 567nm (ε_{max} *ca* 8,200$M^{-1}cm^{-1}$) as shown in Fig. 5.17. Importantly, no current is passed during conversion of the orange product to the purple species, and reoxidation at +0.25V, 298K regenerates the original Pd(II) complex quantitatively.

The results from this study indicate that the first reduction process involves formation of a transient metal-based radical species, $[Pd([14]aneS_4)]^+$, which is rapidly quenched to form an orange diamagnetic product. It is highly likely that this corresponds to the Pd(I)-Pd(I) metal-metal bonded species as proposed in Fig. 5.18.

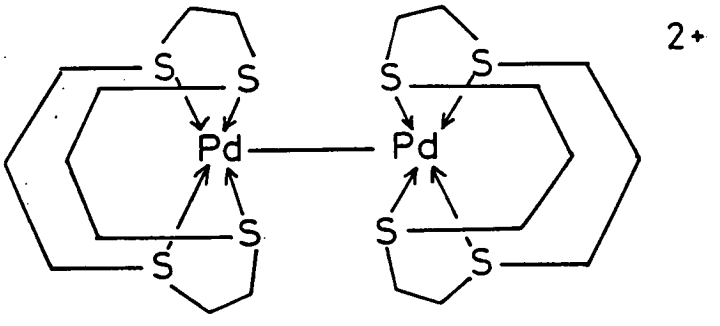

Fig. 5.18: Proposed structure of $[Pd_2([14]aneS_4)_2]^{2+}$ (orange dimer)

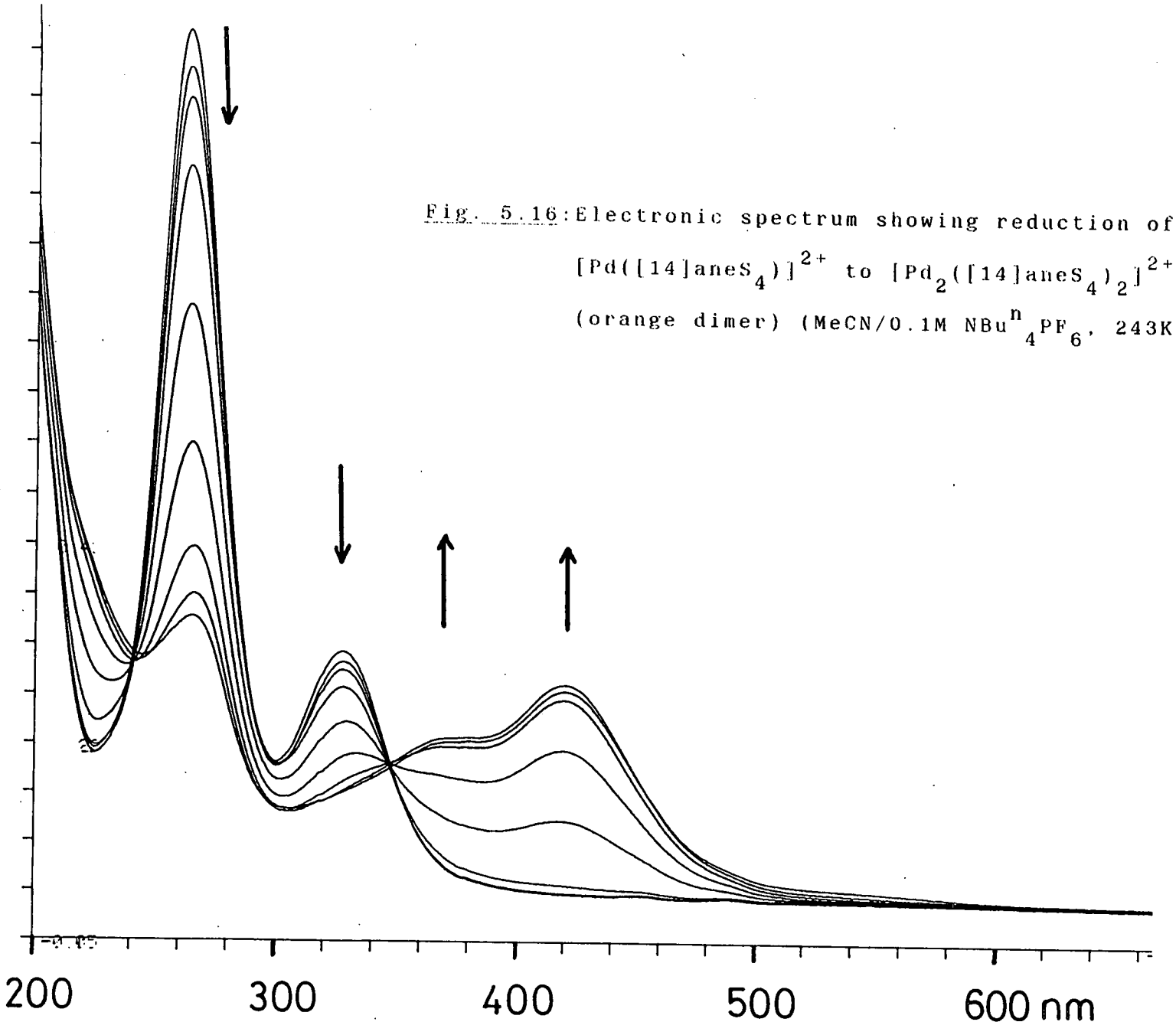

Fig. 5.16: Electronic spectrum showing reduction of $[Pd([14]aneS_4)]^{2+}$ to $[Pd_2([14]aneS_4)_2]^{2+}$ (orange dimer) (MeCN/0.1M $NBu^n_4PF_6$, 243K)

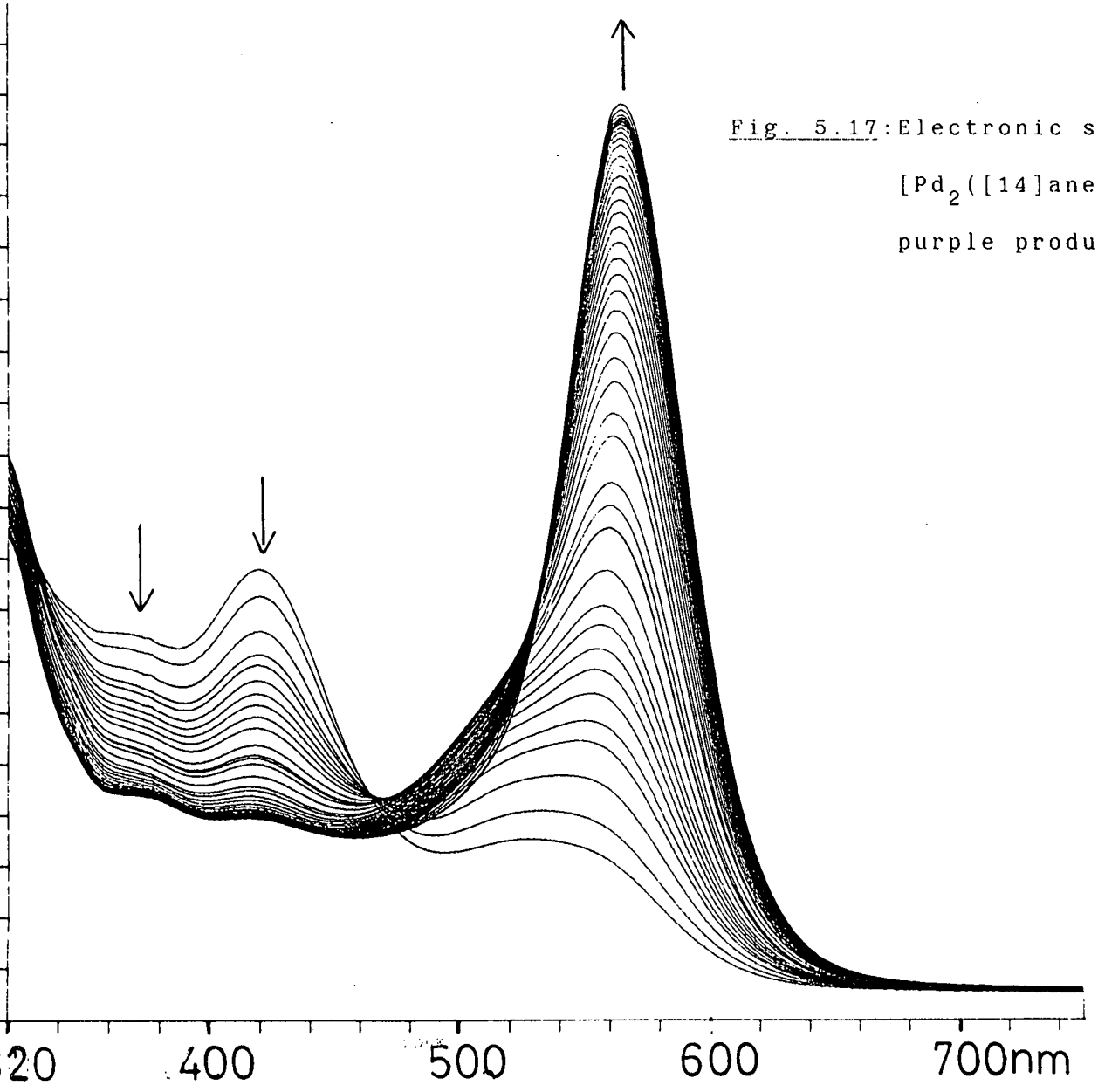

Fig. 5.17: Electronic spectrum showing conversion of $[Pd_2([14]aneS_4)_2]^{2+}$ (orange dimer) to purple product (MeCN/0.1M $NBu^n_4PF_6$, 273K)

Consideration of the stereochemistry and ligand conformation in the Pd(II) precursor suggests that this clipping together of two Pd(I) monomers might be extremely facile, due to the availability of one face of the central metal. The results show that this product undergoes a further change which is apparently kinetically controlled yielding a purple species. The nature of this species is not known. However, most of the Pd(I)-Pd(I) dimeric complexes reported are 16-electron species, where each metal ion is four co-ordinate with the metal-metal bond ocupying one of these sites [172-179]. The results from this study strongly suggest that the first diamagnetic species generated (orange) corresponds to $[Pd_2([14]aneS_4)_2]^{2+}$, in which each Pd(I) centre remains bound to all four thioether donors, with the metal-metal bond occupying a fifth co-ordination site, with each metal being formally an 18-electron centre. We tentatively suggest that the purple species formed upon warming may correspond to a different Pd(I)-Pd(I) dimer in which each metal has 16-electrons associated. It is likely that such a species would form by a simple rearrangement involving cleavage of one Pd-S bond on each metal ion, to give the complex proposed in Fig. 5.19, where each Pd(I) ion is four co-ordinate with one dangling S-donor. The formation of a Pd(II)-Pd(0) species, however, cannot be ruled out.

Fig. 5.19: Proposed structure of second reduction product (purple) from $[Pd([14]aneS_4)]^{2+}$

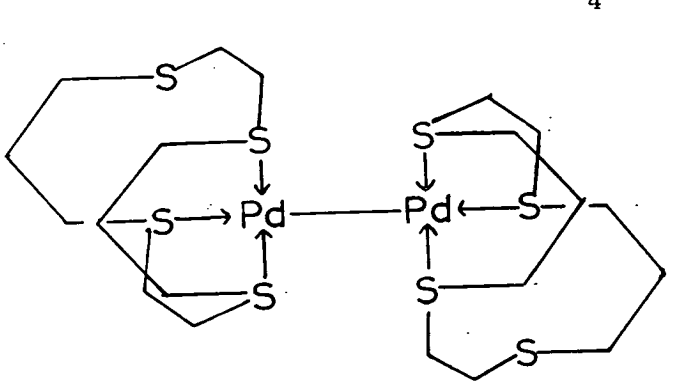

In order to determine the origin of the new absorption bands at λ_{max}= 376 and 421nm (orange product) and λ_{max}= 567nm (purple product), an *in situ* UV/vis spectroscopic study in acetone at 228K using an O.T.T.L.E. system was performed. The UV/vis spectrum of $[Pd([14]aneS_4)]^{2+}$ shows an absorption band at λ_{max}= 325nm (the second high energy band is obscured beneath the solvent front). This represents a 5nm shift upon changing the solvent, and such solvent dependence is characteristic of ligand⟶ metal charge-transfer transitions. In contrast, the bands corresponding to the orange and the purple solutions exhibit no solvent dependence, (λ_{max}= 376, 421 (orange), 567nm (purple). This behaviour suggests that these bands are a consequence of transitions within the metal-metal bonded framework - probably $\sigma \longrightarrow \sigma^*$ transitions. However, in order to confirm this, studies in solvents of more widely ranging dielectric constants are required. A fast-scan cyclic voltammetric study of the first reduction of $[Pd([14]aneS_4)]^{2+}$ was undertaken. The results (Table 5.8, Fig. 5.20) show that the reduction becomes more reversible at low temperature and fast scan-rate. This

confirms that a bimolecular process is responsible for the quenching of the Pd(I) monomer, $[Pd([14]aneS_4)]^+$.

Table 5.8: Variable Scan-Rate and Concentration Study of the Reductive Cyclic Voltammogram of $[Pd([14]aneS_4)]^{2+}$ ($MeCN/0.1M\ NBu^n_4PF_6$, 238K)

scan-rate[a] / Vs^{-1}	i_{pa}/i_{pc}	concentration[b] / $x10^3 moldm^{-3}$	i_{pa}/i_{pc}
0.10	0.364	12.87	0.404
0.50	0.373	6.44	0.412
1.00	0.404	3.40	0.638
2.00	0.523	1.70	0.687
5.00	0.600	1.13	0.750
10.00	0.688	0.85	0.800
20.00	0.698		
30.00	0.766		
40.00	0.810		

a) concentration= $1.287x10^{-2} moldm^{-3}$

b) scan-rate= $1.00Vs^{-1}$

A study of the electrochemistry of the related Pd(II) tetrathia complexes, $[Pd([12]aneS_4)]^{2+}$ and $[Pd([16]aneS_4)]^{2+}$ was undertaken to investigate whether these exhibit similar redox characteristics.

Fig. 5.20: Reductive cyclic voltammograms of $[Pd([14]aneS_4)]^{2+}$ ($MeCN/0.1M\ NBu^n_4PF_6$)

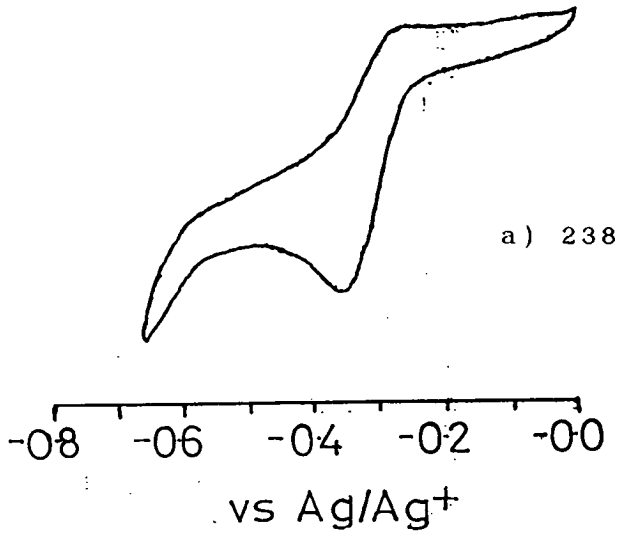

a) 238K, scan-rate= $100mVs^{-1}$

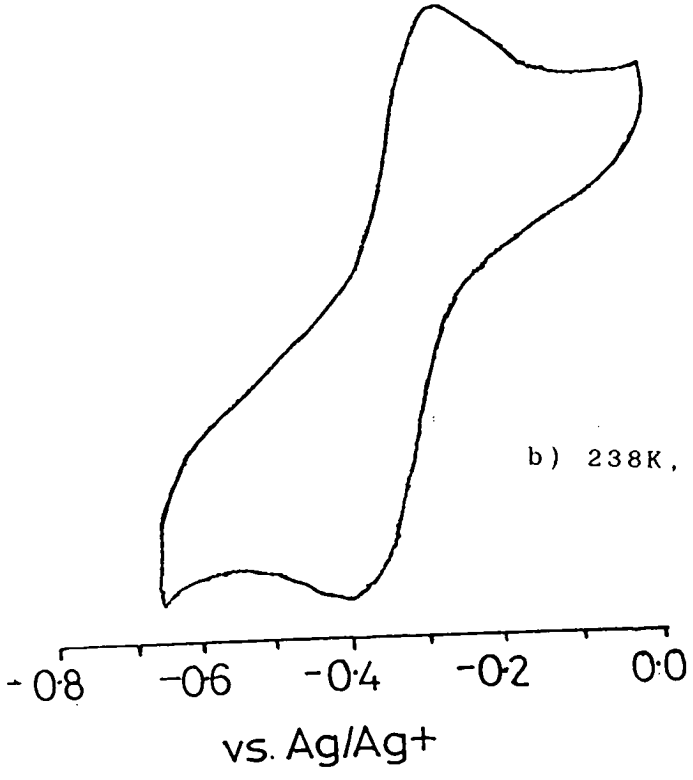

b) 238K, scan-rate= $1Vs^{-1}$

[12]aneS$_4$

Cyclic voltammetry of [Pd([12]aneS$_4$)](PF$_6$)$_2$ under analogous conditions to those for [Pd([14]aneS$_4$)]$^{2+}$, at 298K reveals an irreversible reduction at Ep$_c$= -0.57V *vs.* Fc/Fc$^+$ (scan rate= 270mVs^{-1}). No oxidative activity is observed in the range of the solvent. This reduction remains irreversible at 238K and high scan rate (30Vs^{-1}).

Coulometric measurements performed on this process at -0.75V *vs.* Fc/Fc$^+$, 298K gives n= 0.81 electrons. The resulting orange solution is e.s.r silent. During reduction plating out of metal is also observed, indicating some decomposition of the reduction product. This is consistent with the macrocyclic cavity size being too small to accommodate the large Pd(I) centre. The cyclic voltammogram of the orange reduction product shows a rather broad, irreversible oxidation at E$_{pa}$= +0.05V *vs.* Fc/Fc$^+$. Controlled potential electrolysis of the orange solution at +0.2V regenerates the original Pd(II) species, [Pd([12]aneS$_4$)]$^{2+}$ as measured by UV/vis spectroscopy

This reduction was also followed by <u>in situ</u> UV/vis spectroscopy using an O.T.T.L.E. system, at -0.75V, 273K. Importantly, the conversion occurs isosbestically, (λ_{iso}= 366, 330, 282, 240nm) (Fig. 5.21), with loss of intensity of the absorption band at λ_{max}= 370nm and a shift to lower energy of the band at 260nm. Re-oxidation at OV, 273K results in <u>quantitative</u>,

isosbestic regeneration of the Pd(II) starting material. Warming the reduced solution to 298K leads to decomposition, presumably via demetallation or disproportionation.

These results suggest that the reduction once again involves generation of an extremely transient Pd(I) monomer. These then clip together very rapidly to give a Pd(I)-Pd(I) dimer incorporating an unsupported metal-metal bond.

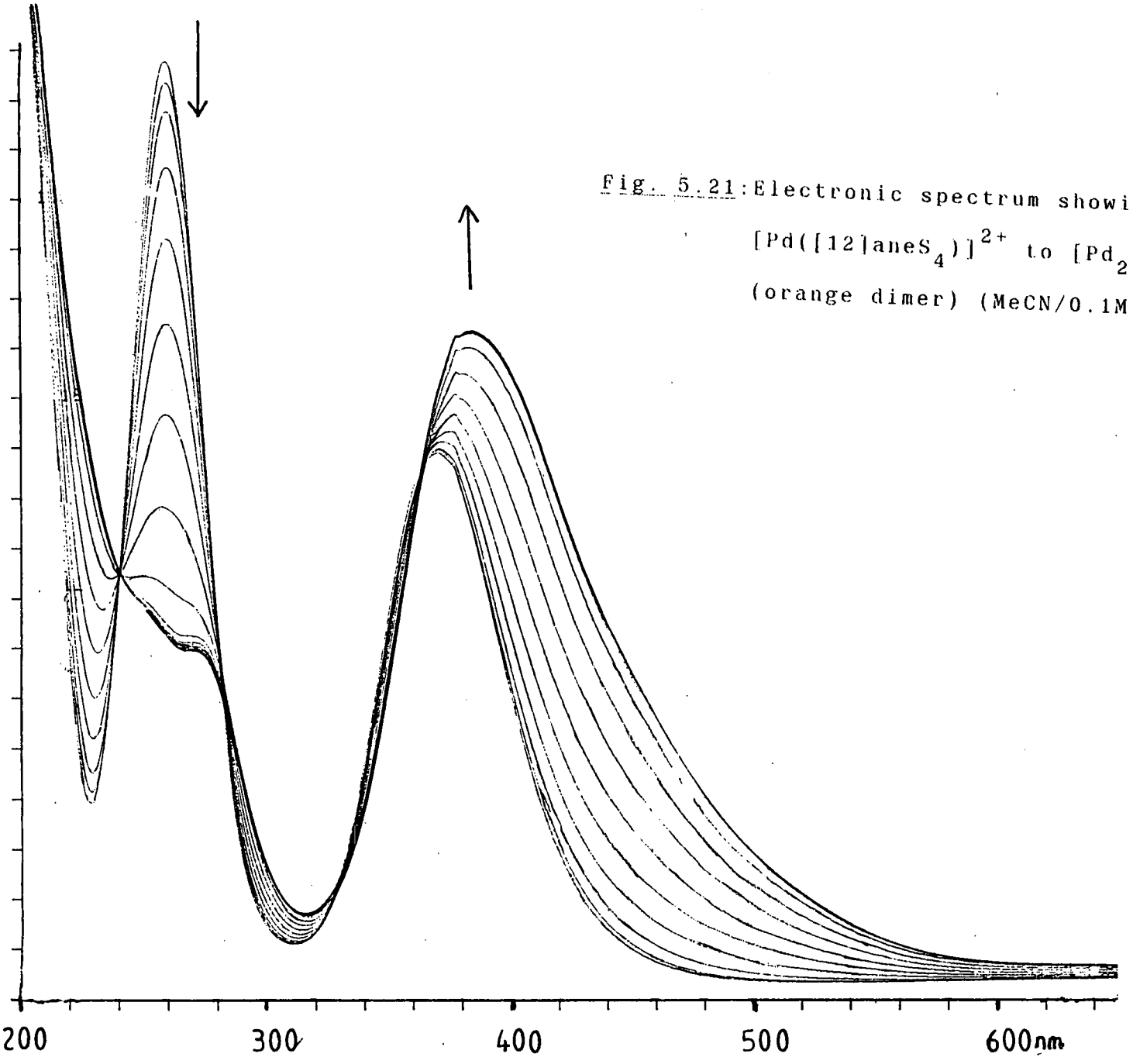

Fig. 5.21: Electronic spectrum showing reduction of $[Pd([12]aneS_4)]^{2+}$ to $[Pd_2([12]aneS_4)_2]^{2+}$ (orange dimer) (MeCN/0.1M $NBu^n{}_4PF_6$, 273K)

[16]aneS$_4$

Cyclic voltammetry of [Pd([16]aneS$_4$)](PF$_6$)$_2$ at 298K under similar conditions shows two irreversible reductions at Ep$_c$= -0.88 and -1.71V *vs.* Fc/Fc$^+$ (scan rate= 250mVs^{-1}). These processes remain irreversible even at 238K and high scan-rate (30Vs^{-1})

A quantitative measurement of the first reduction was performed. Coulometry at -1.0V, 298K confirms this to be a one-electron process (n= 1.03 electrons), giving an orange solution initially, which gradually converts to an intense green solution. This behaviour strongly resembles that of [Pd([14]aneS$_4$)]$^{2+}$ and [Pd([12]aneS$_4$)]$^{2+}$, thus, presumably similar processes occur in each case. The green solution shows no redox activity at 298K. However, controlled potential electrolysis at 0V, 298K results in slow oxidation, regenerating [Pd([16]aneS$_4$)]$^{2+}$ quantitatively. This indicates that there is a kinetic barrier inhibiting oxidation on the cyclic-voltammetric time-scale. This barrier may correspond to cleavage of the metal-metal bond and rearrangement to give the d^9 Pd(I) monomer, [Pd([16]aneS$_4$)]$^+$, transiently, which is then rapidly oxidised to give the Pd(II) starting material.

This reduction was also followed by <u>in situ</u> UV/vis spectroscopy using an O.T.T.L.E. system. At 248K the conversion occurs isosbestically, (λ_{iso}= 348, 250nm), with a substantial decrease in the intensity of the band at λ_{max}= 292nm and concommitant growth of new bands at

λ_{max}= 449 and 369nm, generating the orange solution, (Fig. 5.22). Maintaining the same potential and warming to 273K results in a further isosbestic conversion, with no current flowing, (λ_{iso}= 510, 263, 212nm), with loss of intensity of the bands at λ_{max}= 449, 369 and 273nm, and growth of an intense band at λ_{max}= 588nm (ε_{max}= 8,530$M^{-1}cm^{-1}$) which is responsible for the green colour, (Fig. 5.23).

Re-oxidation of the green solution at 298K, 0V results in quantitative regeneration of the Pd(II) monomeric starting material. The non-isosbestic nature of this oxidation is confirmation that this process is not just a simple one-electron transfer.

[28]aneS_8

The outcome of the electrochemical investigation carried out on the Pd(II) tetrathia macrocyclic complexes prompted a study of the redox characteristics of $[Pd_2([28]aneS_8)]^{4+}$.

Cyclic voltammetry of $[Pd_2([28]aneS_8)](PF_6)_4$ in MeCN (0.1M $NBu^n_4PF_6$ supporting electrolyte) at 293K shows two irreversible reductions (Fig. 5.24) at E_{pc}= -0.74 and -1.29V *vs.* Fc/Fc^+. These reductions remain irreversible even at low temperature (233K). No oxidation is observed in the range of the solvent (0 to +2.0V).

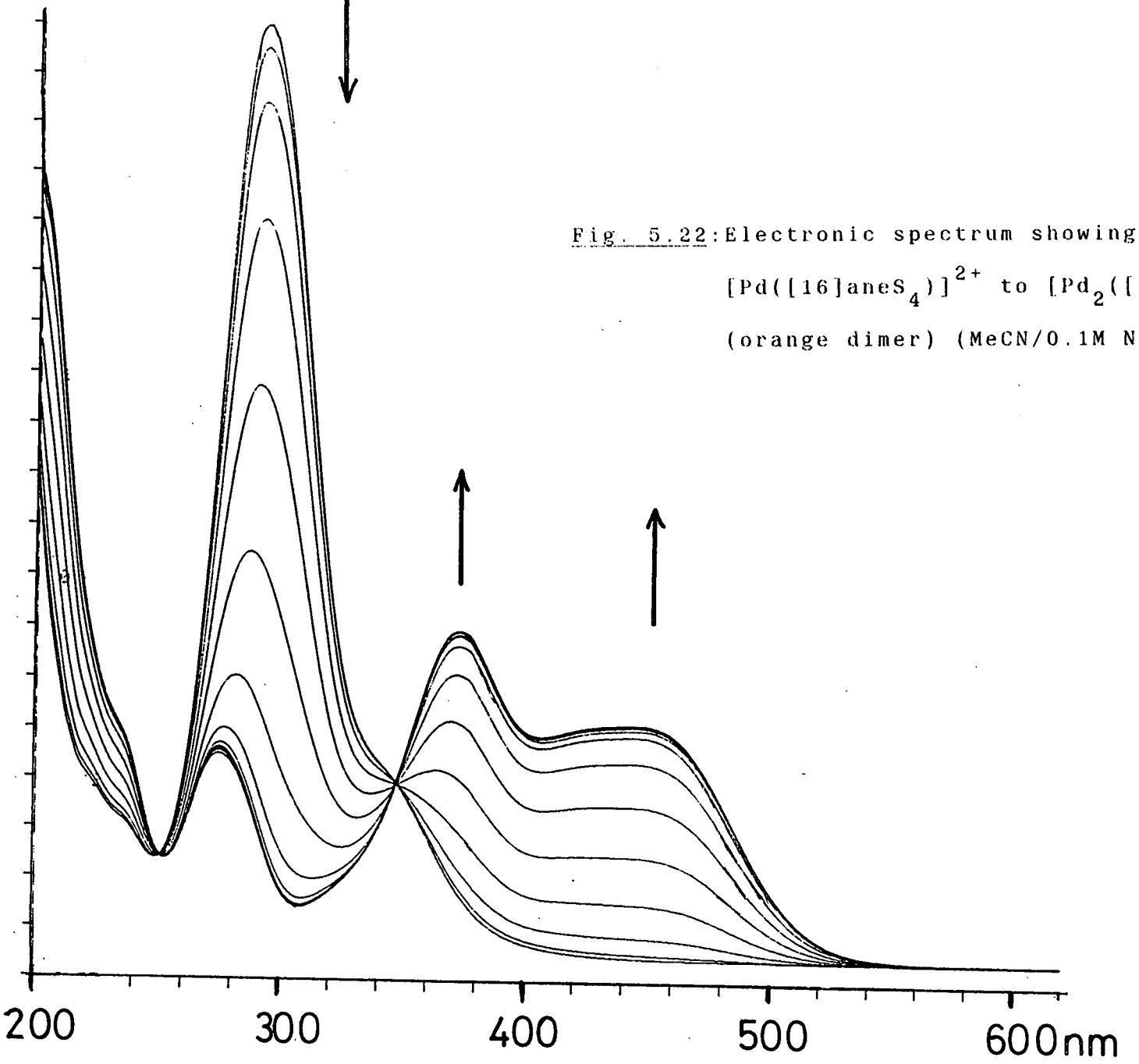

Fig. 5.22: Electronic spectrum showing reduction of $[Pd([16]aneS_4)]^{2+}$ to $[Pd_2([16]aneS_4)_2]^{2+}$ (orange dimer) (MeCN/0.1M $NBu^n_4PF_6$, 248K)

Fig. 5.23: Electronic spectrum showing conversion of $[Pd_2([16]aneS_4)_2]^{2+}$ (orange dimer) to green product (MeCN/ 0.1M $NBu^n_4PF_6$, 273K)

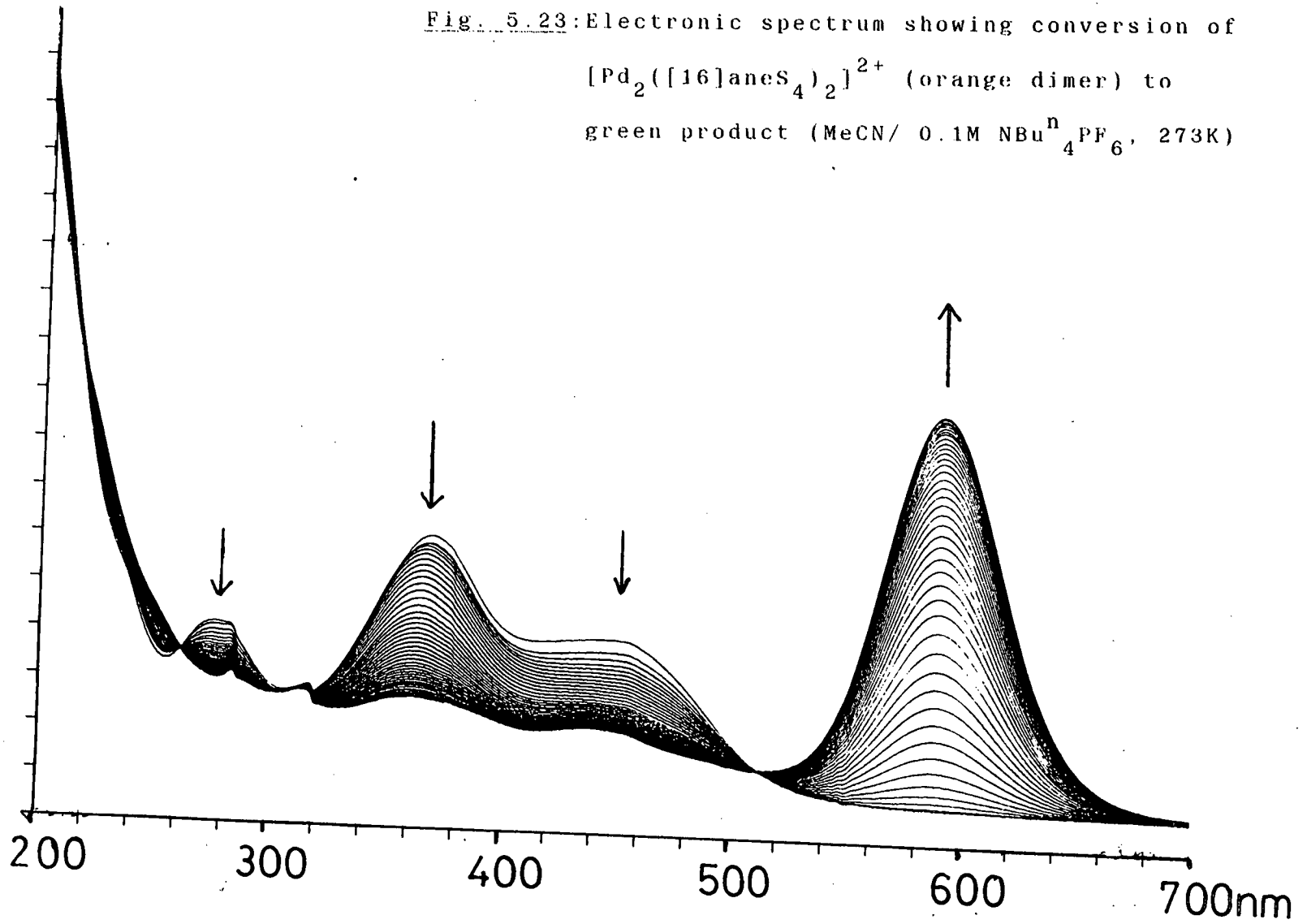

A quantitative investigation of the first reduction process was undertaken. Coulometry of the Pd(II)/(II) complex at -0.9V, 293K in MeCN (0.1M $NBu^n_4PF_6$ supporting electrolyte) at a platinum basket, confirms the reduction to be a two-electron process (n= 1.94 electrons). The orange solution produced was found to be e.s.r. silent; the ligand is redox inactive in this potential range. Cyclic voltammetry of the reduction product shows a broad, irreversible oxidation near +0.5V *vs.* Fc/Fc^+.

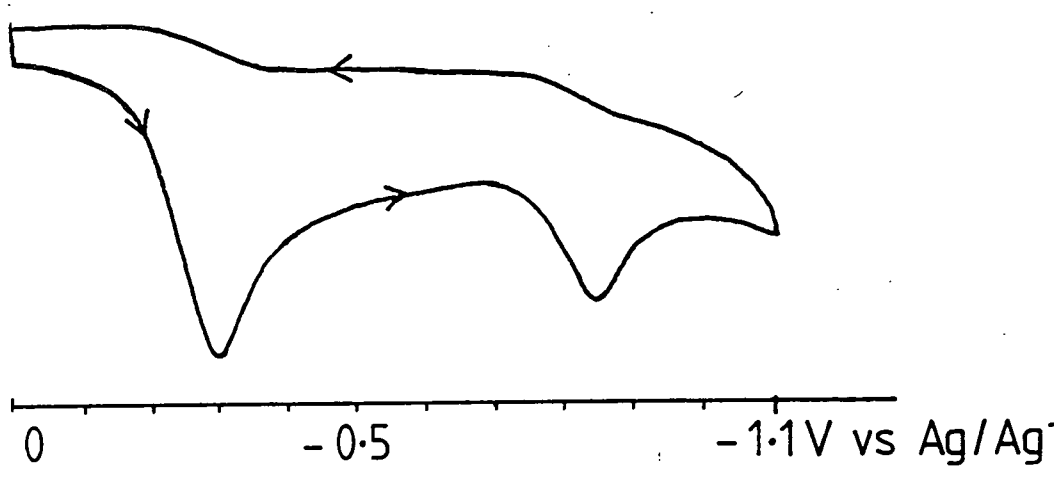

Fig. 5.24: Reductive cyclic voltammogram of $[Pd_2([28]aneS_8)]^{4+}$ ($MeCN/0.1M\ NBu^n_4PF_6$)

The reduction of $[Pd_2([28]aneS_8)](PF_6)_4$ was followed at 243K by <u>in situ</u> UV/vis spectroscopy using an O.T.T.L.E. system. The reduction occurs isosbestically, (λ_{iso}= 342, 242nm), with loss of intensity of the absorption band at λ_{max}= 274nm, with concommitant growth of bands at λ_{max}= 431 and 360nm (Fig. 5.25), giving a spectrum with features strongly resembling those obtained upon reduction of each of the Pd(II) tetrathia macrocyclic systems discussed above. Reoxidation at +0.6V at 293K regenerated the Pd(II)/(II) starting material <u>quantitatively</u>.

These results suggest that reduction of $[Pd_2([28]aneS_8)]^{4+}$ affords a diamagnetic complex which we tentatively assign to the metal-metal bonded Pd(I)-Pd(I) dimer, $[Pd_2([28]aneS_8)]^{2+}$, according to the scheme illustrated in Fig. 5.26. The relative stability of this product is attributed to a combination of the π-acidity of the thioether-donor set, and the nature of the cyclic ligand which will tend to support, and therefore stabilise, the metal-metal bond.

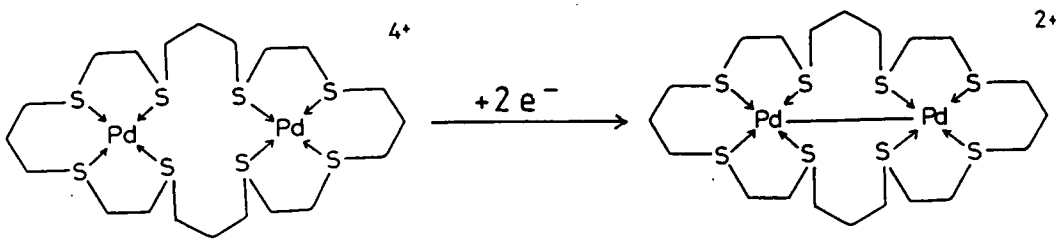

<u>Fig. 5.26</u>: Proposed scheme for reduction of $[Pd_2([28]aneS_8)]^{4+}$

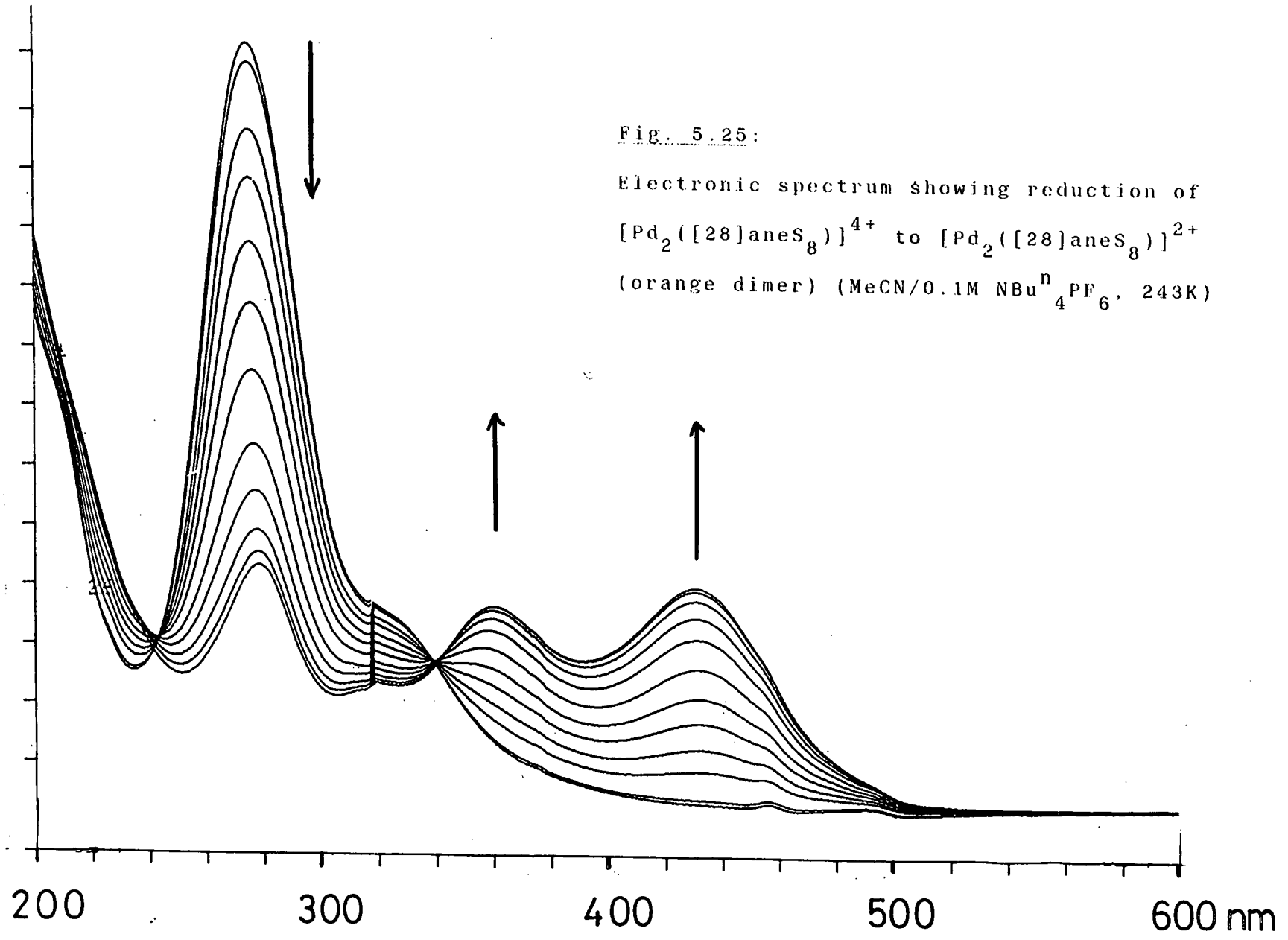

Fig. 5.25:

Electronic spectrum showing reduction of $[Pd_2([28]aneS_8)]^{4+}$ to $[Pd_2([28]aneS_8)]^{2+}$ (orange dimer) (MeCN/0.1M $NBu^n_4PF_6$, 243K)

5.3.2: Platinum

Cyclic voltammetry of $[Pt([14]aneS_4)](PF_6)_2$, and $[Pt([16]aneS_4)](PF_6)_2$ at 298K, under similar conditions to their Pd analogues, shows an irreversible reduction at Ep_c= -1.45V and -1.50V *vs.* Fc/Fc^+ respectively. Coulometric measurements confirm that these each correspond to a one-electron reduction (n= 0.92 and 1.02 electrons respectively), generating yellow solutions which are both e.s.r. silent.

5.4: Summary and Conclusions

The synthesis of a series of Pd(II) and Pt(II) tetrathia macrocyclic complexes has been achieved. Structural and spectroscopic techniques confirm all of these to be square planar, with all four sulphur-donors bound to the d^8 central metal ion. Binuclear Pd(II) and Pt(II) complexes incorporating the large ring macrocycle, [28]aneS_8, have also been prepared successfully.

The evidence accummulated from the electrochemical investigation has confirmed that all three tetrathia macrocyclic complexes studied exhibit very similar redox behaviour. The results strongly suggest in each case that a transient Pd(I) monomer is formed initially. However, this is rapidly quenched via a dimerisation process yielding an orange Pd(I)-Pd(I) dimer incorporating an unsupported metal-metal bond. Reduction of the related binuclear system, $[Pd_2([28]aneS_8)]^{4+}$, is a two-electron process, giving an orange diamagnetic solution, with spectral features closely resembling those of the tetrathia Pd(I)-Pd(I) dimers. These results are consistent with formation of a direct metal-metal bond upon reduction of the binuclear precursor. Interestingly, with the 14- and 16- membered ring macrocycles, the orange dimers undergo a further reaction, which is kinetically controlled, generating intense purple- and green-coloured solutions respectively. The nature of these products is not yet known. However, we tentatively suggest that the kinetic barrier corresponds to cleavage

of one Pd-S bond, giving a Pd(I)-Pd(I) dimer in which each metal has 16-electrons associated, and is therefore square planar to three thioether donors, with the metal-metal bond occupying the fourth site. This second process does not occur for the 28-membered ring system. This may be due to the enhanced stability of the orange dimer resulting from the large ring macrocycle which will tend to support the metal-metal bond. Similarly, the 12-membered ring dimer does not undergo a kinetically-controlled conversion. This may be attributed to the macrocyclic cavity being the correct size to stabilise the orange product, $[Pd_2([12]aneS_4)_2]^{2+}$, but too small to accommodate the tridentate chelation to the S-donors. In each case the original Pd(II) starting material can be re-oxidised quantitatively.

The Pd(I)-Pd(I) metal-metal bonded dimers reported herein represent the first thioether macrocyclic complexes incorporating platinum metals which involve a direct metal-metal bond.

Preliminary studies on the Pt(II) analogues indicate that these complexes also undergo an irreversible one-electron reduction, possibly generating analogous Pt(I)-Pt(I) metal-metal bonded dimers.

5.5: Experimental

5.5.1: $[Pd([12]aneS_4)](PF_6)_2$

Reaction of K_2PdCl_4 (68mg, 0.208mmol) with $[12]aneS_4$ (50mg, 0.208mmol) in refluxing $MeOH/H_2O$ (1:1 v.v., 100ml) under N_2 for 4h afforded a bright yellow solution. Addition of excess NH_4PF_6 gave a yellow precipitate which was collected by filtration. Recrystallisation from MeCN yielded the product as a bright yellow solid (Yield: 85mg, 65%). Mol. wt. 636.78. Elemental analysis: found C= 14.5, H= 2.49, S= 20.3%; calculated for $[C_8H_{16}S_4Pd](PF_6)_2$: C= 15.1, H= 2.53, S= 20.1%. F.a.b. mass spectrum (3-NOBA matrix): found M^+= 491 and 345. Calculated for $[^{106}Pd([12]aneS_4)PF_6]^+$ M^+= 491, $[^{106}Pd([12]aneS_4)]^+$ M^+= 346. ^1H n.m.r. spectrum (360.13MHz, CD_3CN, 298K): AA'BB' pattern, δ= 3.51-3.58 (m, 8H), 3.81-3.88ppm (m, 8H). ^{13}C DEPT n.m.r. spectrum (50.32MHz, CD_3CN, 298K): δ= 39.05ppm ($8x\underline{C}H_2$). UV/vis spectrum (MeCN): λ_{max}= 368nm (ε_{max}= 36,455$M^{-1}cm^{-1}$), 260 (92,330). I.R. spectrum (KBr disc): 2960w, 2920w, 1440m, 1410m, 1305w, 1130w, 1065m, 1030m, 930w, 840vs, 730m, 625w, 555vs, 520w cm^{-1}.

5.5.2: Single Crystal Structure of $[Pd([12]aneS_4)](PF_6)_2.MeCN$

Orange needles were obtained from vapour diffusion of diethyl ether into a solution of the complex in MeCN. A suitable single crystal was selected and

sealed in a 0.5mm glass capillary to prevent solvent loss.

Crystal Data:

$[C_8H_{16}S_4Pd](PF_6)_2.MeCN$. M= 677.83. Orthorhombic, space group P_{nma}, a= 16.8321(15), b= 9.3077(6), c= 14.2615(6)Å°, V= 2233.1Å^3 (by least-squares refinement on angles for 36 centred reflections measured at $\pm\omega$ [22.1<2θ<24.7°, λ= 0.71073Å]), Z= 4, D_c= 2.016gcm^{-3}. Crystal dimensions 0.25x0.10x0.08mm, μ(Mo-Kα)= 13.88cm^{-1}, F(000)= 1424.

Data Collection and Processing:

Stöe STADI-4 four-circle diffractometer, $\omega/2\theta$ scan mode using the learnt-profile method. Graphite-monochromated Mo-Kα radiation; 3074 reflections (two asymmetric units) ($2\theta_{max}$= 45°, h -10⟶10, k -15⟶15, l -18⟶18) giving 1106 with $F>4\sigma(F)$. No crystal decay, no absorption correction.

Structure Analysis and Refinement:

The Pd position was deduced from a Patterson synthesis. Iterative cycles of least-squares refinement and difference Fourier synthesis revealed the positions of all other non-hydrogen atoms. During refinement disorder of the cation became evident. This was modelled by using partial C-atoms and constraining all S-C and C-C bond lengths to be 1.83 and 1.52Å respectively, giving

two equally occupied conformations. The cation was found to have one fully occupied MeCN solvent molecule associated. Anistropic thermal parameters were refined for Pd, S, P, N and all fully occupied C and F atoms. Macrocyclic H atoms were placed in fixed, calculated positions, and the methyl group of the solvent molecule was refined as a rigid group. The weighting scheme $\underline{w}^{-1} = \sigma^2(\underline{F}) + 0.003855\underline{F}^2$ gave satisfactory agreement analyses. At final convergence $\underline{R} = 0.0777$, $\underline{R}_w = 0.1089$. $\underline{S} = 1.156$ for 152 independent parameters, and the final difference Fourier synthesis showed no feature above 1.40 or below $0.69 e\text{Å}^{-3}$.

5.5.3: $[Pd([16]aneS_4)](PF_6)_2$

Method as for 5.5.1, using K_2PdCl_4 (44mg, 0.135mmol) and $[16]aneS_4$ (40mg, 0.135mmol). The product was isolated as a yellow crystalline solid (Yield: 67mg, 72%). Mol. wt. 692.89. Elemental analysis: found C= 20.4, H= 3.46, S= 17.9%; calculated for $[C_{12}H_{24}S_4Pd](PF_6)_2$: C= 20.8, H= 3.49, S= 18.5%. F.a.b. mass spectrum (3-NOBA matrix): found M^+= 547, 439, 419 and 401. Calculated for

$[^{106}Pd([16]aneS_4).PF_6]^+$ M^+= 547,

$[^{106}Pd([16]aneS_4).2H_2O]^+$ M^+= 438,

$[^{106}Pd([16]aneS_4).H_2O]^+$ M^+= 420,

$[^{106}Pd([16]aneS_4)]^+$ M^+= 402.

^1H n.m.r. spectrum (80.13MHz, CD_3NO_2, 298K): δ= 3.19-3.33

(m, $SC\underline{H}_2$, 16H), 2.50-2.69ppm (m, b, $CH_2C\underline{H}_2CH_2$, 8H). ^{13}C DEPT n.m.r. spectrum (50.32MHz, CD_3NO_2, 298K): δ= 33.78 ($S\underline{C}H_2$, 8C), 23.18ppm ($CH_2\underline{C}H_2CH_2$, 4C). ^{13}C DEPT n.m.r. spectrum (360.13MHz, CD_3CN, 298K): δ= 33.43 ($S\underline{C}H_2$, 8C), 23.68ppm ($CH_2\underline{C}H_2CH_2$, 4C) (symmetric isomer), and 35.19 ($S\underline{C}H_2$, 4C), 31.86 ($S\underline{C}H_2$, 4C), 23.98 ($CH_2\underline{C}H_2CH_2$, 2C), 21.62ppm ($CH_2\underline{C}H_2CH_2$, 2C) (asymmetric isomer). UV/vis spectrum (MeCN): λ_{max}= 292nm (ε_{max}= 18,130$M^{-1}cm^{-1}$). I.R. spectrum (KBr disc): 2980w, 2920m, 2845w, 1430m, 1410m, 1305w, 1280w, 1245w, 1195w, 1130w, 1010w, 995w, 840vs, 740w, 555vs, 470w cm^{-1}.

5.5.4: Single Crystal Structure of $[Pd([16]aneS_4)](PF_6)_2$

Single crystals were obtained by recrystallisation of the complex from aqueous solution. A suitable crystal was selected and sealed in a 0.5mm glass capillary to prevent solvent loss.

Crystal Data:

$[C_{12}H_{24}S_4Pd](PF_6)_2$. M= 692.89. Triclinic, space group $P\bar{1}$, $\underline{a}$= 10.131(10), $\underline{b}$= 10.653(10). $\underline{c}$= 13.114(13)Å, α= 69.054(24), β= 69.91(5), γ= 63.77(4)°, $\underline{V}$= 1156.3Å^3 (by least-squares refinement on diffractometer angles for 23 centred reflections, λ= 0.71073Å), $\underline{Z}$= 2, $\underline{D}_c$= 1.990gcm^{-3}. Yellow needles. Crystal dimensions 0.39x0.16x0.16mm. μ(Mo-Kα)= 13.16cm^{-1}, $\underline{F}$(000)= 688.

Data Collection and Processing:

Stöe STADI-4 four-circle diffractometer, $\omega/2\theta$ mode with ω scan-width $(1.05+0.347\tan\theta)^{o}$, graphite-monochromated Mo-Kα radiation; 3155 reflections measured to $2\theta = 45^{o}$ (h $-8 \longrightarrow 10$, k $-9 \longrightarrow 11$, l $0 \longrightarrow 14$) giving 1190 with $\underline{F} > 4\sigma(\underline{F})$. No significant crystal decay, no absorption correction.

Structure Analysis and Refinement:

A Patterson synthesis located two half-occupied Pd atoms on crystallographic inversion centres. The structure was developed by successive cycles of least-squares refinement and difference Fourier synthesis. During refinement unrealistic C-C and C-S bond lengths were obtained. This is attributed to the weak diffraction data. These bonds were constrained to be 1.50 and 1.83Å respectively. Additionally, one of the PF_6^- counterions showed some disorder. This was modelled successfully by using partial F atoms, such that the P atom was associated with six F atoms. Anisotropic thermal parameters were refined for Pd, S, P and all fully occupied F atoms. H atoms were included in fixed, calculated positions. The weighting scheme, $\underline{w}^{-1} = \sigma^2\underline{F} + 0.000810\underline{F}^2$ gave satisfactory agreement analyses. At convergence, $\underline{R}$, $\underline{R}_w = 0.0869$ and 0.0911 respectively, $\underline{S} = 1.145$ for 219 independent parameters, and in the final difference Fourier synthesis the maximum and minimum

residuals were +0.84 and -0.81eÅ^{-3} respectively.

5.5.5: [Pt([16]aneS$_4$)](PF$_6$)$_2$

Method as for 5.5.1, using K_2PtCl_4 (56mg, 0.135mmol) and [16]aneS$_4$ (40mg, 0.135mmol). The product was isolated as a white microcrystalline solid (Yield: 77mg, 73%). Mol. wt. 781.58. Elemental analysis: found C= 18.5, H= 3.12, S= 16.3%; calculated for $[C_{12}H_{24}S_4Pt](PF_6)_2$: C= 18.4, H= 3.09, S= 16.4%. F.a.b. mass spectrum (3-NOBA matrix): found M^+= 636 and 490. Calculated for $[^{195}Pt([16]aneS_4).PF_6]^+$ M^+= 636, $[^{195}Pt([16]aneS_4)]^+$ M^+= 491. ^1H n.m.r. spectrum (360.13MHz, CD_3CN, 238K): δ= 3.06-3.28 (SCH_2, 16H) and 2.31-2.55ppm ($CH_2CH_2CH_2$, 8H). ^{13}C DEPT n.m.r. spectrum (360.13MHz, CD_3CN, 298K): δ= 33.12 (SCH_2, 8C), 23.79ppm ($CH_2CH_2CH_2$, 4C) (symmetric isomer), and δ= 35.61 (SCH_2, 4C), 31.52 (SCH_2, 4C), 24.05 ($CH_2CH_2CH_2$, 2C), 21.74ppm ($CH_2CH_2CH_2$, 2C) (asymmetric isomer), and δ= 33.81, 31.70, 22.67, 20.55ppm (asymmetric isomer). I.R. spectrum (KBr disc): 3000m, 2920w, 2845w, 1440m, 1420m, 1380w, 1300m, 1290w, 1260w, 1245w, 1200w, 1125w, 1025w, 840vs, 770m, 740w, 555vs cm^{-1}.

5.5.6: [Pd$_2$([28]aneS$_8$)](PF$_6$)$_4$

Reaction of K_2PdCl_4 (61mg, 0.186mmol) with [28]aneS$_8$ (50mg, 0.093mmol) in refluxing MeOH/H_2O (1:1 v.v., 50ml) for 1h under N_2 afforded a yellow precipitate of $[Pd_4Cl_8([28]aneS_8)]$. Refluxing for a further 2h give an orange solution. Addition of excess

NH_4PF_6 and recrystallisation from $MeCN/H_2O$ yielded the product as an orange solid. (Yield: 110mg, 89%). Mol. wt. 1329.70. Elemental analysis: found C= 18.2, H= 3.07, S= 19.8%; calculated for $[C_{20}H_{40}S_8Pd_2](PF_6)_4$: C= 18.1, H= 3.03, S= 19.3%. F.a.b. mass spectrum (3-NOBA matrix): found M^+= 1184, 1076, 1058, 1037, 928, 911, 892 and 749. Calculated for

$[^{106}Pd_2([28]aneS_8)(PF_6)_3]^+$ M^+= 1183,

$[^{106}Pd_2([28]aneS_8)(PF_6)_2.2H_2O]^+$ M^+= 1074,

$[^{106}Pd_2([28]aneS_8)(PF_6)_2.H_2O]^+$ M^+= 1058,

$[^{106}Pd_2([28]aneS_8)(PF_6)_2]^+$ M^+= 1038,

$[^{106}Pd_2([28]aneS_8).PF_6.2H_2O]^+$ M^+= 929,

$[^{106}Pd_2([28]aneS_8).PF_6.H_2O]^+$ M^+= 911,

$[^{106}Pd_2([28]aneS_8).PF_6]^+$ M^+= 893,

$[^{106}Pd_2([28]aneS_8)]^+$ M^+=748.

^1H n.m.r. spectrum (80.13MHz, CD_3CN, 298K): δ= 2.7-4.0ppm (br m, $SC\underline{H}_2$), 2.2-2.5ppm (br m, $CH_2C\underline{H}_2CH_2$). ^{13}C DEPT n.m.r. spectrum (50.32MHz, CD_3CN, 298K): δ= 41.60, 39.62, 36.56, 35.73, 33.48, 25.59ppm (6x$C\underline{H}_2$ of the major isomer) and 37.28, 37.07, 24.18, 23.84 and 23.51ppm (5x$C\underline{H}_2$ of a minor isomer). ^{13}C DEPT n.m.r. spectrum (360.13MHz, CD_3CN, 298K): δ= 41.26, 39.37, 36.14, 35.23 (4x$SC\underline{H}_2$, 16C) and 25.09ppm ($CH_2C\underline{H}_2CH_2$, 4C) (fully symmetrical isomer), and δ= 37.03, 36.82, 36.14, 35.88, 32.69, 32.48, 32.33 (8x$SC\underline{H}_2$, 16C),

23.56 ($CH_2C\underline{H}_2CH_2$, 1C), 23.08 ($CH_2C\underline{H}_2CH_2$, 2C),

22.59ppm ($CH_2C\underline{H}_2CH_2$, 1C) (less symmetrical isomer).

UV/vis spectrum (MeCN): λ_{max}= 274nm

(ε_{max}= 32,900$M^{-1}cm^{-1}$). I.R. spectrum (KBr disc): 3650m, 3580w, 2980m, 2940m, 2845w, 1640m, 1425m, 1410m, 1380w, 1350m, 1300m, 1280m, 1250m, 1195w, 1170w, 1120m, 1025w, 1000m, 840vs, 740m, 555vs, 465w cm^{-1}.

5.5.7: $[Pt_2([28]aneS_8)](PF_6)_4$

Method as for 5.5.6, using K_2PtCl_4 (155mg, 0.372mmol) and $[28]aneS_8$ (100mg, 0.186mmol). The product was isolated as a pale yellow solid (Yield: 136mg, 48%). Mol. wt. 1506.86. Elemental analysis: found C= 16.3, H= 2.73%; calculated for $[C_{20}H_{40}S_8Pt_2](PF_6)_4$: C= 15.9, H= 2.68%. F.a.b. mass spectrum (3-NOBA matrix): found M^+= 1360, 1250, 1232, 1212, 1105, 1089, 1069. Calculated for

$[^{195}Pt_2([28]aneS_8)(PF_6)_3]^+$ M^+= 1361,

$[^{195}Pt_2([28]aneS_8)(PF_6)_2.2H_2O]^+$ M^+= 1252,

$[^{195}Pt_2([28]aneS_8)(PF_6)_2.H_2O]^+$ M^+= 1234,

$[^{195}Pt_2([28]aneS_8)(PF_6)_2]^+$ M^+= 1216,

$[^{195}Pt_2([28]aneS_8).PF_6.2H_2O]^+$ M^+= 1107,

$[^{195}Pt_2([28]aneS_8).PF_6.H_2O]^+$ M^+= 1089,

$[^{195}Pt_2([28]aneS_8).PF_6]^+$ M^+= 1071.

^1H n.m.r. spectrum (360.13MHz, CD_3CN, 298K): δ= 3.46-2.96 (SCH_2, 32H) and 2.22-1.96ppm ($CH_2CH_2CH_2$, 8H). ^{13}C DEPT n.m.r. spectrum (360.13MHz, CD_3CN, 298K): δ= 40.24, 38.46, 37.25, 36.73, 36.49, 36.30, 35.67, 35.13, 33.83, 33.61, 33.12 (SCH_2), 25.29, 23.23ppm ($CH_2CH_2CH_2$). I.R. spectrum (KBr disc): 2960m, 2900w, 1500w, 1420m, 1300w, 1250m, 1200m, 1170m, 840vs, 555vs cm^{-1}.

CHAPTER 6

Rhodium and Iridium Thioether Macrocyclic Complexes

6.2: Results and Discussion

6.2.1: $[RhCl_2([14]aneS_4)]PF_6$

The solid state structure of $[14]aneS_4$ shows all four sulphurs are exodentate [12]. Therefore, the generation of a complex in which the metal is inserted into the macrocyclic cavity would necessitate a conformational change approximating a "pseudo-rotation", in which each *anti* interaction is rotated into a *gauche* interaction and *vice versa*.

$[14]aneN_4$, the tetra-aza analogue of $[14]aneS_4$, binds Rh(III) to afford cis- and trans-$[RhCl_2([14]aneN_4)]^+$ depending upon the reaction conditions [182-185]. Busch and co-workers have prepared $[RhCl_2([14]aneS_4)]^+$, and, on the basis of I.R. spectroscopy, assigned it as the cis-dichloro isomer [110,181]. In order to ascertain whether it might be possible to generate the complex trans-$[RhCl_2([14]aneS_4)]^+$, and in view of the potential of macrocyclic complexes incorporating two mutually cis labile sites to undergo, for example, carbonyl [186] and hydride [187] insertion reactions, the synthesis and full characterisation of $[RhCl_2([14]aneS_4)]^+$ was undertaken.

Reaction of $RhCl_3.3H_2O$ with one molar equivalent of $[14]aneS_4$ in refluxing methanol produced a bright yellow solution. Addition of excess NH_4PF_6 yielded a yellow, air-stable product. Recrystallisation from MeCN gave yellow crystals.

6.1: Introduction

The synthesis of polythioether macrocycles is now relatively straightforward (Chapter 5), but there still exist only a few reports of co-ordination complexes incorporating these ligands, the majority of which contain first-row transition metals [67,152-154,157,158,163,181].

As discussed in Chapter 1, examples of platinum metal polythioether macrocyclic complexes and genuine mononuclear Rh(II) species are extremely sparse. This Chapter outlines the preparation of a range of mononuclear d^6 Rh(III) and Ir(III) complexes incorporating the 12-, 14- and 16-membered ring tetrathia macrocycles, [12]aneS_4, [14]aneS_4 and [16]aneS_4, as well as the pentathioether, [15]aneS_5. These sulphur-donor ligands might be expected to exhibit some back-bonding capability which would favour stabilisation of low valent metal centres such as Rh(II). This provided the impetus for a preliminary investigation of the redox and electronic properties of the rhodium(III) precursors.

The I.R. spectrum of the complex shows several weak bands in the range 270-350cm^{-1}. These are in the correct region for either Rh-Cl or Rh-S stretching vibrations, υ(Rh-Cl) and υ(Rh-S), hence it was difficult to assign these exactly. The PF_6^- counterion exhibits characteristic strong bands at 840 and 555cm^{-1}.

F.a.b. mass spectrometry of the complex showed positive ion peaks with the correct isotopic distributions at M^+= 441, 406 and 370 corresponding to $[^{103}Rh^{35}Cl_2([14]aneS_4)]^+$, $[^{103}Rh^{35}Cl([14]aneS_4)]^+$ and $[^{103}Rh([14]aneS_4)]^+$ respectively via successive loss of chloride ligands. The ^{1}H n.m.r. spectrum of the BPh_4^- salt suggested a ratio of one BPh_4^- anion to one [14]aneS$_4$ ligand, while the ^{13}C DEPT n.m.r. spectrum in CD_3CN showed five macrocyclic methylene carbon resonances at δ= 38.31, 30.10, 29.95, 29.85 and 23.84ppm indicating the presence of only one isomer in solution involving cis-dichloro ligands (Fig. 6.1). The assignment of the cation as a cis-isomer is suggested also by UV/vis spectral data, which shows d-d absorption bands at λ_{max}= 362nm (ε_{max}= 949M^{-1}cm^{-1}), 319 (765) and a charge-transfer band at 260nm (ε_{max}= 10,370M^{-1}cm^{-1}). The magnitudes of the extinction coefficients for the d-d transitions are consistent with the lower symmetry cis-isomer; octahedral d^6 complexes tend to show lower extinction coefficients in trans-configurations[182,183]. This together with microanalytical data indicate the formulation cis-$[RhCl_2([14]aneS_4)]PF_6$.

Fig. 6.1: ^{13}C DEPT n.m.r. spectra of:

a) cis-$[RhCl_2([12]aneS_4)]^+$

b) cis-$[RhCl_2([14]aneS_4)]^+$

c) trans-$RhCl_2([16]aneS_4)]^+$

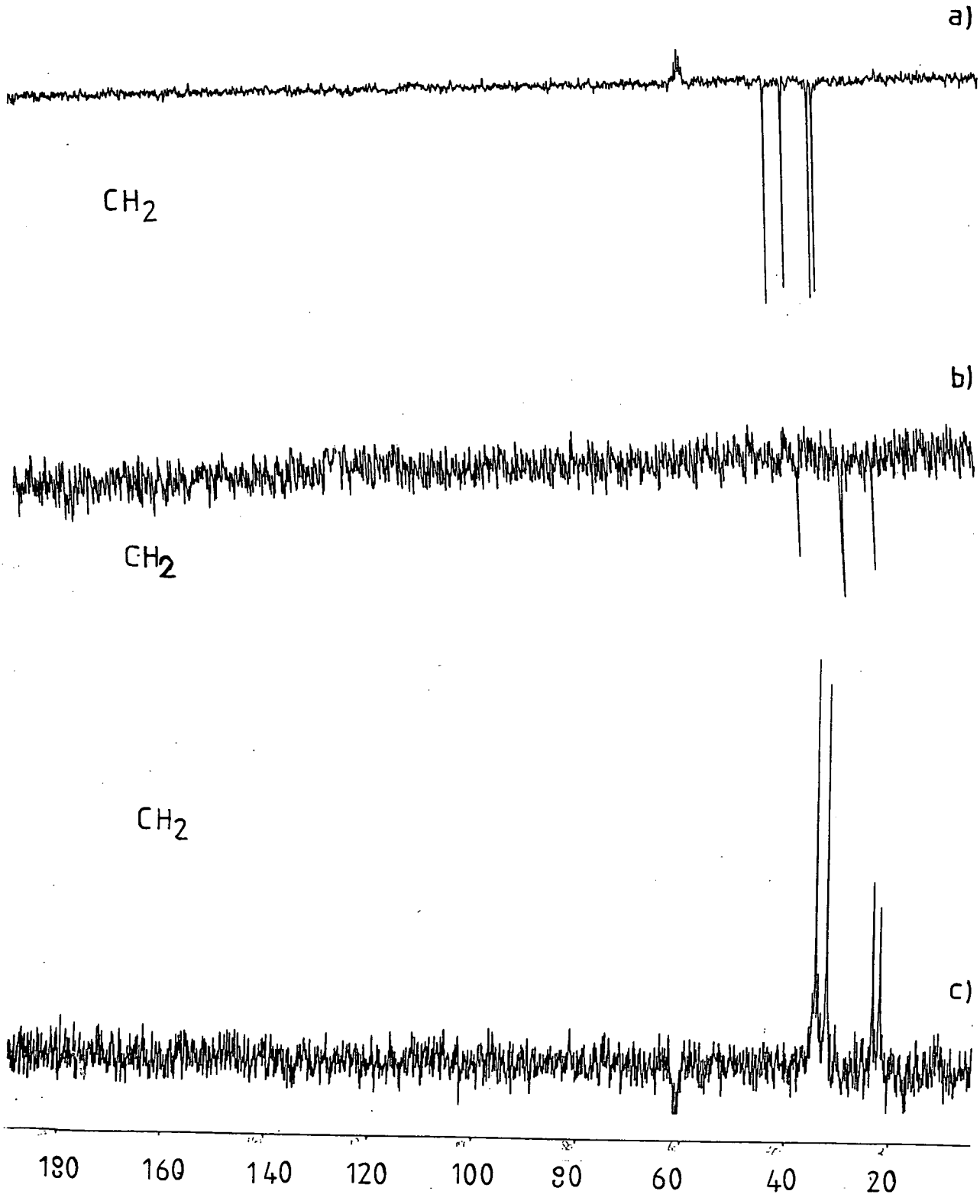

In order to deduce the stereochemistry and conformation of the complex, a single crystal X-ray structural determination was undertaken.

6.2.2: Single Crystal Structure of $[RhCl_2([14]aneS_4)]PF_6$

Details of the structure solution are given in the Experimental Section. Selected bond lengths are given in Table 6.1, bond angles in Table 6.2 and torsion angles in Table 6.3. An ORTEP plot showing the molecular structure of the cation is presented in Fig. 6.2.

The structural analysis confirms the cis-configuration of the complex [Rh-Cl= 2.3836(12), Rh-S(1)= 2.2870(12), Rh-S(4)= 2.3275(12)Å], with the Rh atom lying on a crystallographic 2-fold axis. The folded macrocycle is co-ordinated to the Rh(III) centre via all four S-donors, with the angles around the metal being close to octahedral. The conformation of the macrocycle in this complex is very similar to that observed in the related d^6 complex cis-$[RuCl_2([14]aneS_4)]$ [155] and the pattern of Rh-S bond lengths follows the same trend, with Rh-S(1) trans to Cl(1) being 0.040(2)Å shorter than Rh-S(4) trans to S(11). This is attributed to the trans-effect of S over Cl^-.

Both the cation and PF_6^- counteranion were ordered, with the P of PF_6^- occupying a crystallographic inversion centre.

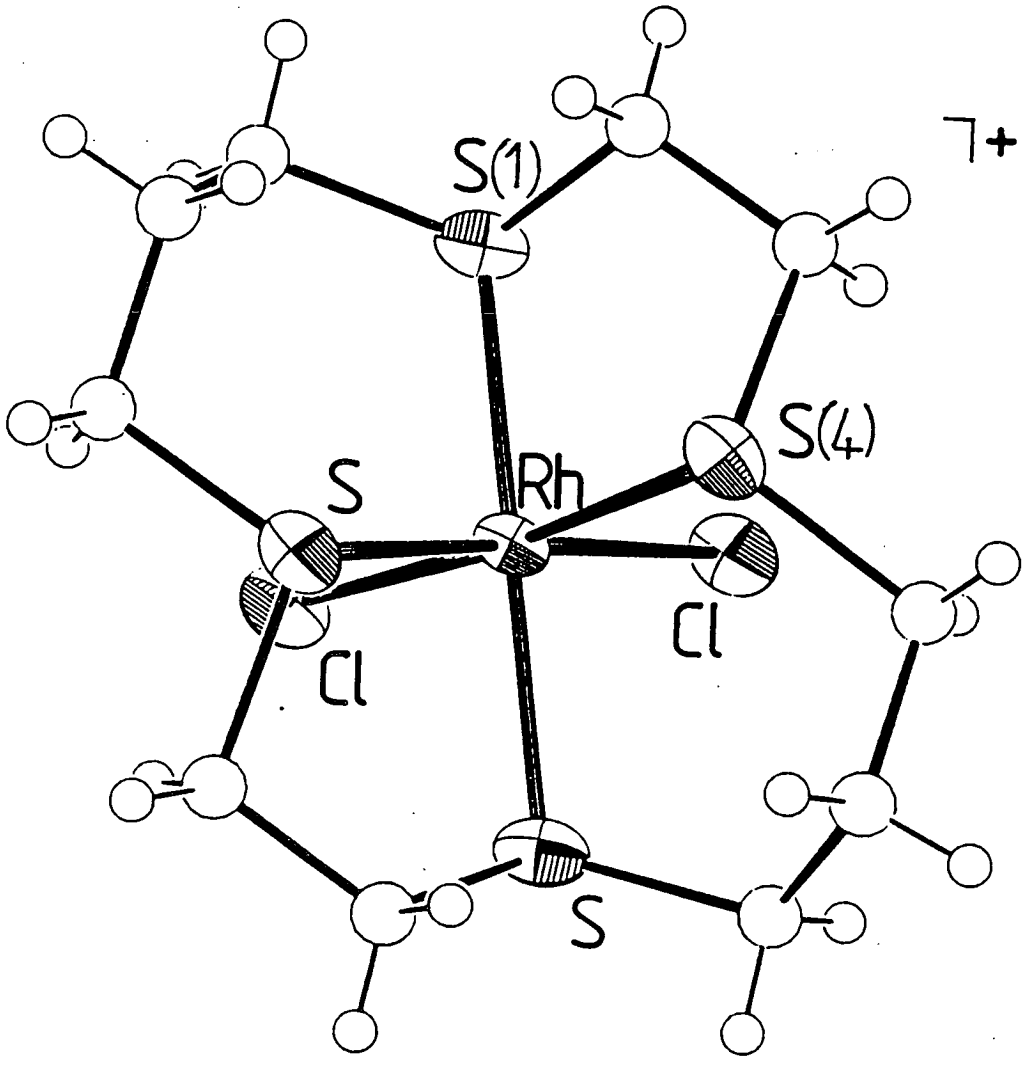

Fig. 6.2: View of the single crystal structure of $[RhCl_2([14]aneS_4)]^+$

Single Crystal Structure of

$[RhCl_2([14]aneS_4)]PF_6$

Table 6.1: Selected Bond Lengths(Å) with e.s.d.'s

Rh(1) -Cl(1)	2.3836(12)	C(2) - C(3)	1.509(8)
Rh(1) - S(1)	2.2870(12)	C(3) - S(4)	1.827(5)
Rh(1) - S(4)	2.3275(12)	S(4) - C(5)	1.816(6)
S(1) - C(2)	1.814(5)	C(5) - C(6)	1.525(8)
S(1) -C(14)	1.806(5)	C(6) - C(7)	1.510(8)

Table 6.2: Selected Angles(°) with e.s.d.'s

Cl(1)-Rh(1)- S(1)	92.00(4)	Rh(1)- S(1) -C(14)	108.96(18)
Cl(1)-Rh(1)- S(4)	86.51(4)	C(2)- S(1) -C(14)	105.32(25)
Cl(1)-Rh(1)-Cl(2)	92.01(4)	S(1)- C(2) - C(3)	107.7(4)
Cl(1)-Rh(1)- S(8)	174.25(4)	C(2)- C(3) - S(4)	109.3(4)
Cl(1)-Rh(1)-S(11)	88.72(4)	Rh(1)- S(4) - C(3)	103.19(17)
S(1)-Rh(1)- S(4)	87.40(4)	Rh(1)- S(4) - C(5)	111.43(19)
S(1)-Rh(1)- S(8)	84.32(4)	C(3)- S(4) - C(5)	103.1(3)
S(1)-Rh(1)-S(11)	97.71(4)	S(4)- C(5) - C(6)	118.2(4)
S(4)-Rh(1)- S(8)	97.71(4)	C(5)- C(6) - C(7)	115.9(5)
S(4)-Rh(1)-S(11)	173.13(4)	C(6)- C(7) - S(8)	108.7(4)
Rh(1)- S(1)- C(2)	100.37(18)		

Table 6.3: Selected Torsion Angles(^{o}) with e.s.d.'s

C(14)	- S(1)	- C(2)	- C(3)	169.0(4)
C(6)	- C(7)	- S(8)	- C(9)	-173.9(4)
C(2)	- S(1)	-C(14)	-C(13)	-173.9(4)
C(7)	- S(8)	- C(9)	-C(10)	169.0(4)
S(1)	- C(2)	- C(3)	- S(4)	-60.9(4)
S(8)	- C(9)	-C(10)	-S(11)	-60.9(4)
C(2)	- C(3)	- S(4)	- C(5)	150.6(4)
C(9)	-C(10)	-S(11)	-C(12)	150.6(4)
C(3)	- S(4)	- C(5)	- C(6)	-70.1(5)
C(10)	-S(11)	-C(12)	-C(13)	-70.1(5)
S(4)	- C(5)	- C(6)	- C(7)	-70.9(6)
S(11)	-C(12)	-C(13)	-C(14)	-70.9(6)
C(5)	- C(6)	- C(7)	- S(8)	85.1(5)
C(12)	-C(13)	-C(14)	- S(1)	85.1(5)

6.2.3: $[IrCl_2([14]aneS_4)]PF_6$

Very few non-porphyrin macrocyclic complexes of Ir have been reported to-date [4,186-190], and there are no examples of Ir complexation by $[14]aneS_4$ in the literature. This section outlines the synthesis and single crystal structural determination of the Ir(III) species, $[IrCl_2([14]aneS_4)]^+$.

$IrCl_3.3H_2O$ was treated with one molar equivalent of $[14]aneS_4$ in refluxing ethanol/H_2O under N_2 for 14h in the presence of excess $NaBPh_4$. On cooling, the yellow/brown precipitate was collected and recrystallised from $MeNO_2$ to afford a cream coloured product.

The I.R. spectrum of this complex shows, in addition to bands due to co-ordinated $[14]aneS_4$ and BPh_4^- counterion, two bands at 310 and 305cm^{-1} assigned to Ir-Cl stretching vibrations, υ(Ir-Cl), suggesting the formation of a cis-dichloro complex. The f.a.b. mass spectrum of the complex shows the main molecular ion peak at M^+= 531 corresponding to $[^{193}Ir^{35}Cl_2([14]aneS_4)]^+$, with the correct isotopic distribution. Daughter peaks at M^+= 496 and 461 correspond to $[^{193}Ir^{35}Cl([14]aneS_4)]^+$ and $[^{193}Ir([14]aneS_4)]^+$ respectively via successive loss of Cl^-. The ^1H n.m.r. spectrum of the product shows a complex second order multiplet in the range δ= 2.5-3.5ppm due to the non-equivalent macrocyclic protons. The electronic spectrum of the complex shows absorptions at λ_{max}= 348nm (ε_{max}= 113$M^{-1}cm^{-1}$)and 297 (1,400). On the basis of its extinction coefficient, we tentatively

assign the former band to a d-d transition. These data, together with microanalytical data suggest that the complex generated was cis-$[IrCl_2([14]aneS_4)]^+$.

In view of the paucity of structurally characterised Ir macrocyclic complexes, and in order to deduce the connectivity and conformation of the macrocyclic ligand, a single crystal X-ray structural determination was undertaken.

6.2.4: Single Crystal Structure of $[IrCl_2([14]aneS_4)]BPh_4$

Details of the structure solution are given in the Experimental Section. Selected bond lengths, angles and torsions are given in Tables 6.4, 6.5 and 6.6 respectively. An ORTEP plot showing the structure of the cation is presented in Figure 6.3.

The structural analysis confirms the cis-configuration of the Cl^- ligands, with Ir-Cl(1)= 2.389(5), Ir-Cl(2)= 2.385(5)Å. The macrocycle is co-ordinated to the Ir(III) centre as a tetradentate ligand, Ir-S(1)= 2.277(4), Ir-S(4)= 2.287(5), Ir-S(8)= 2.268(4), Ir-S(11)= 2.343(5)Å, and adopts a folded conformation with Cl(1) and Cl(2) lying trans to S(8) and S(1) respectively - generating an overall geometry and bond length distribution very similar to both cis-$[RuCl_2([14]aneS_4)]$ [155] and cis-$[RhCl_2([14]aneS_4)]^+$. This further substantiates the tendency for this macrocycle to bind larger metal ions to give cis octahedral complexes. The ^{13}C DEPT n.m.r.

spectrum of $[IrCl_2([14]aneS_4)]^+$ shows five resonances due to the secondary carbon centres of the co-ordinated macrocycle at δ= 37.99, 29.52, 28.96, 28.39 and 23.90ppm, confirming that in solution this complex retains the cis-stereochemistry.

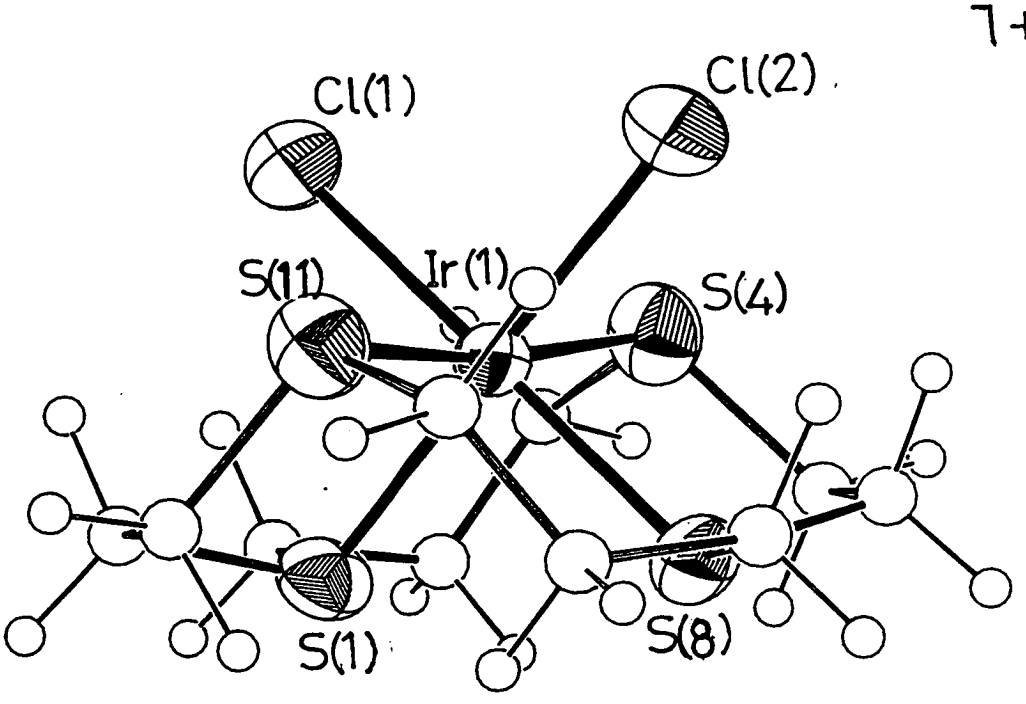

Fig. 6.3: View of the single crystal structure of $[IrCl_2([14]aneS_4)]^+$

Single Crystal Structure of

cis-$[IrCl_2([14]aneS_4)]BPh_4$

Table 6.4: Selected Bond Lengths(Å) with e.s.d.'s

Ir(1) - S(1)	2.277(4)	S(8) - C(7)	1.772(21)
Ir(1) - S(4)	2.287(5)	S(8) - C(9)	1.775(20)
Ir(1) - S(8)	2.268(4)	S(11)- C(10)	1.851(23)
Ir(1) - S(11)	2.343(5)	S(11)- C(12)	1.811(21)
Ir(1) -Cl(1)	2.389(5)	C(2) - C(3)	1.55(3)
Ir(1) -Cl(2)	2.385(5)	C(5) - C(6)	1.46(3)
S(1) - C(2)	1.855(21)	C(6) - C(7)	1.58(3)
S(1) - C(14)	1.809(17)	C(9) - C(10)	1.59(3)
S(4) - C(3)	1.781(20)	C(12)- C(13)	1.48(3)
S(4) - C(5)	1.755(24)	C(13)- C(14)	1.57(3)

Table 6.5: Selected Angles(°) with e.s.d.'s

S(1)-Ir(1)- S(4)	88.10(15)	Ir(1) -S(4) -C(5)	111.3(8)
S(1)-Ir(1)- S(8)	86.42(15)	C(3) -S(4) -C(5)	102.1(10)
S(1)-Ir(1)- S(11)	97.65(15)	Ir(1) -S(8) -C(7)	110.1(7)
S(1)-Ir(1)-Cl(1)	91.29(16)	Ir(1) -S(8) -C(9)	103.5(6)
S(1)-Ir(1)-Cl(2)	176.15(15)	C(7) -S(8) -C(9)	103.7(9)
S(4)-Ir(1)- S(8)	98.93(16)	Ir(1) -S(11)-C(10)	103.1(7)
S(4)-Ir(1)- S(11)	172.26(16)	Ir(1) -C(11)-C(12)	111.0(7)
S(4)-Ir(1)-Cl(1)	86.72(16)	C(10)-S(11)-C(12)	100.2(10)
S(4)-Ir(1)-Cl(2)	88.96(16)	S(1) -C(2) -C(3)	103.5(13)
S(8)-Ir(1)- S(11)	86.64(16)	S(4) -C(3) -C(2)	109.0(14)
S(8)-Ir(1)-Cl(1)	173.81(16)	S(4) -C(5) -C(6)	118.5(18)
S(8)-Ir(1)-Cl(2)	91.58(15)	C(5) -C(6) -C(7)	118.7(20)
S(11)-Ir(1)-Cl(1)	87.97(16)	S(8) -C(7) -C(6)	108.0(15)
S(11)-Ir(1)-Cl(2)	85.51(16)	S(8) -C(9) -C(10)	105.0(13)
Cl(1)-Ir(1)-Cl(2)	91.02(16)	S(11)-C(10)-C(9)	107.4(14)
Ir(1)-S(1) - C(2)	99.9(7)	S(11)-C(12)-C(13)	120.4(15)
Ir(1)-S(1) - C(14)	110.0(6)	C(12)-C(13)-C(14)	116.3(17)
C(2)-S(1) - C(14)	104.8(9)	S(1) -C(14)-C(13)	106.5(12)
Ir(1)-S(4) - C(3)	103.4(7)		

Table 6.6: Selected Torsion Angles(^{o}) with e.s.d.'s

C(14)- S(1) - C(2) - C(3)	-169.5(12)
C(2) - S(1) - C(14)- C(13)	173.6(12)
C(5) - S(4) - C(3) - C(2)	-156.3(14)
C(3) - S(4) - C(5) - C(6)	67.9(20)
C(9) - S(8) - C(7) - C(6)	170.7(14)
C(7) - S(8) - C(9) - C(10)	-171.7(13)
C(12)- S(11)- C(10)- C(9)	-151.8(14)
C(10)- S(11)- C(12)- C(13)	70.9(18)
S(1) - C(2) - C(3) - S(4)	64.7(14)
S(4) - C(5) - C(6) - C(7)	72.1(25)
C(5) - C(6) - C(7) - S(8)	-81.6(22)
S(8) - C(9) - C(10)- S(11)	62.1(15)
S(11)- C(12)- C(13)- C(14)	70.0(22)
C(12)- C(13)- C(14)- S(1)	-84.5(18)

6.2.5: $[RhCl_2([12]aneS_4)]PF_6$

The generation of a cis-dichloro complex upon reaction of $RhCl_3$ with the 14-membered ring macrocyclic ligand $[14]aneS_4$ (Section 6.2.1) suggested that reaction of Rh(III) with the smaller 12-membered ring macrocycle, $[12]aneS_4$, would also generate a cis-dichloro species.

Treatment of $RhCl_3.3H_2O$ with one molar equivalent of $[12]aneS_4$ in refluxing methanol for 2h under N_2 generates a bright yellow solution. Addition of excess NH_4PF_6 followed by recrystallisation from MeCN gives the bright yellow complex $[RhCl_2([12]aneS_4)]PF_6$ in excellent yield.

The I.R. spectrum of the complex shows a series of bands in the range 360-270cm^{-1} which correspond to Rh-Cl and/or Rh-S stretching vibrations (υ(Rh-Cl) and υ(Rh-S) respectively). F.a.b. mass spectroscopy shows peaks with the correct isotopic distributions at M^+= 413 and 378, which are assigned to $[^{103}Rh^{35}Cl_2([12]aneS_4)]^+$ and $[^{103}Rh^{35}Cl([12]aneS_4)]^+$ respectively. The UV/vis spectrum of the complex shows absorption bands at λ_{max}= 401nm (ε_{max}= 1,781$M^{-1}cm^{-1}$) and a shoulder at 300 (1,165) corresponding to d-d transitions, and a charge-transfer transition at 250 (21,920). The intensities of the d-d bands are comparable with those observed for cis-$[RhCl_2([14]aneS_4)]^+$, indicative of a cis-configuration for the chlorides. The ^1H n.m.r. spectrum of the product shows a complex second order multiplet in the range δ= 3.3-4.2ppm due to the methylene

protons of co-ordinated [12]aneS$_4$, while ^{13}C DEPT n.m.r. spectroscopy shows four distinct methylene carbon resonances at δ= 44.41, 41.03, 36.08 and 35.16ppm, (Fig. 6.1), which is consistent with Rh(III) binding to a folded macrocycle, with two mutually cis-Cl$^-$ ligands. This evidence, together with microanalytical data, is consistent with the formulation cis-[RhCl$_2$([12]aneS$_4$)]PF$_6$.

6.2.6: [RhCl$_2$([16]aneS$_4$)]PF$_6$

In view of the recent publication reporting trans-Mo(O) and Mo(II) complexes incorporating a 16-membered ring tetrathia macrocycle[162], we argued that [16]aneS$_4$ would be capable of binding Rh(III) to yield an octahedral complex with trans-configuration.

Reaction of RhCl$_3$.3H$_2$O with one molar equivalent of [16]aneS$_4$ in refluxing ethanol for 1h gives a bright yellow solution, from which the complex [RhCl$_2$([16]aneS$_4$)]PF$_6$ can be isolated upon addition of excess NH$_4$PF$_6$. Recrystallisation from MeCN affords bright yellow crystals of the product.

The f.a.b. mass spectrum of the complex shows molecular ion peaks with correct isotopic distributions at M$^+$= 469, 434 and 399 which are attributed to [^{103}Rh^{35}Cl$_2$([16]aneS$_4$)]$^+$ and successive loss of Cl$^-$ from this species. The UV/vis spectrum of this complex shows a d-d transition at λ_{max}= 369nm (ε_{max}= 151M^{-1}cm^{-1}). This

extinction coefficient is considerably lower than those observed for the related 12- and 14-membered ring complexes which both exhibit cis-configurations. This suggests a higher degree of symmetry at the Rh centre in $[RhCl_2([16]aneS_4)]^+$, and hence a trans-placement of the two chloro-ligands. The ^1H n.m.r. spectrum of the product shows a complex multiplet at δ= 2.28-3.65ppm due to the macrocyclic protons. These data, together with microanalyses and I.R. spectroscopy, confirm the formulation trans-$[RhCl_2([16]aneS_4)]PF_6$.

The geometry around the Rh(III) centre, and the conformation of the macrocycle were of particular interest to us; consequently, we undertook a single crystal X-ray structural determination of this complex.

6.2.7: Single Crystal Structure of $[RhCl_2([16]aneS_4)]PF_6$

Details of the structure solution are given in the Experimental Section. Selected bond lengths are given in Table 6.7, bond angles in Table 6.8 and torsion angles in Table 6.9. Two ORTEP plots showing the cationic geometry are presented in Figures 6.4 and 6.5.

The trans-configuration of the Cl^- ligands was confirmed by this study. The structure shows the Rh atom lying on a crystallographic inversion centre and the tetrathia ligand binding equatorially to the metal, with the six-membered chelate rings adopting alternate chair and twist-boat conformations. In this species the Rh-S bond lengths are exactly equivalent [Rh-S= 2.3483(27)Å],

indicating the absence of a similar trans-influence as observed for the Rh(III), Ir(III) and Ru(II) [14]aneS_4 analogues.[155] The PF_6^- counter-anion has crystallographically imposed 2-fold symmetry through the P atom and two F atoms.

^{13}C DEPT n.m.r. confirms retention of this stereochemistry in solution, showing four methylene-carbon resonances at δ= 34.42, 32.27, 23.26 and 21.85ppm (Fig. 6.1).

The geometry of this cation is therefore very similar to that of the complex $[Mo(CO)_2(L)]$ (L= 3,3,7,7,11,11,15,15-octamethyl-1,5,9,13-tetrathiacyclohexadecane), where the CO ligands occupy mutually trans co-ordination sites.[162]

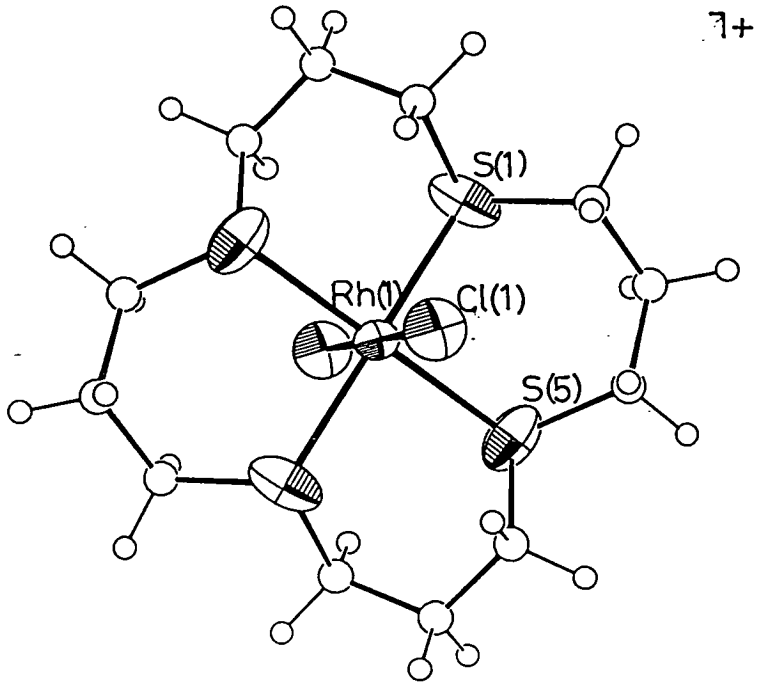

Fig. 6.4: View of the single crystal structure of $[RhCl_2([16]aneS_4)]^+$

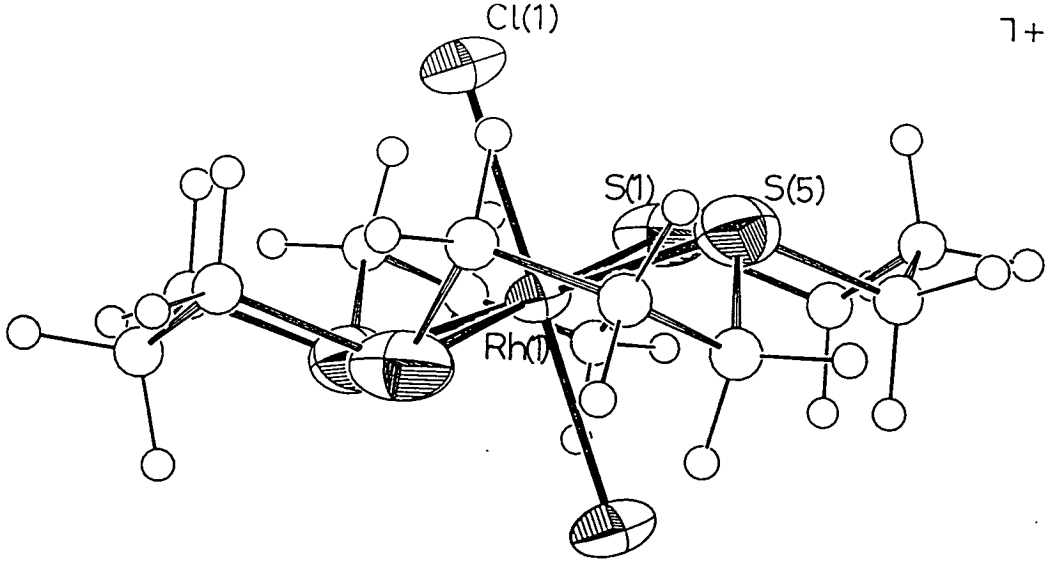

Fig. 6.5: Alternative view of the single crystal structure of $[RhCl_2([16]aneS_4)]^+$

Single Crystal Structure of

$[RhCl_2([16]aneS_4)]PF_6$

Table 6.7: Selected Bond Lengths(Å) with e.s.d.'s

Rh(1)-Cl(1)	2.3391(22)	S(5)- C(6)	1.800(14)
Rh(1)- S(1)	2.3483(25)	C(2)- C(3)	1.517(21)
Rh(1)- S(5)	2.3483(27)	C(3)- C(4)	1.514(22)
S(1)- C(2)	1.811(13)	C(6)- C(7)	1.507(22)
S(1)-C(8')	1.832(14)	C(7)- C(8)	1.501(22)
S(5)- C(4)	1.807(15)		

Table 6.8: Selected Angles(°) with e.s.d.'s

Cl(1)-Rh(1) - S(1)	92.88(8)	C(4)- S(5) - C(6)	97.2(6)
Cl(1)-Rh(1) - S(5)	92.72(8)	S(1)- C(2) - C(3)	112.1(10)
S(1)-Rh(1) - S(5)	90.31(9)	C(2)- C(3) - C(4)	114.8(13)
Rh(1)- S(1) - C(2)	110.1 (4)	S(5)- C(4) - C(3)	115.1(11)
Rh(1)- S(1) -C(8')	104.5 (5)	S(5)- C(6) - C(7)	111.8(10)
C(2)- S(1) -C(8')	97.1 (6)	C(6)- C(7) - C(8)	115.0(13)
Rh(1)- S(5) - C(4)	110.0 (5)	S(1')- C(8) - C(7)	112.4(10)
Rh(1)- S(5) - C(6)	105.1 (4)		

Table 6.9: Selected Torsion Angles(°) with e.s.d.'s

C(8')	S(1)	C(2)	C(3)	173.9(11)
S(1)	C(2)	C(3)	C(4)	-76.1(14)
C(2')	-S(1')	C(8)	C(7)	-166.6(11)
C(2)	C(3)	C(4)	S(5)	74.9(15)
C(6)	S(5)	C(4)	C(3)	-170.7(11)
S(5)	C(6)	C(7)	C(8)	-42.8(16)
C(4)	S(5)	C(6)	C(7)	-165.5(11)
C(6)	C(7)	C(8)	-S(1')	-44.0(16)

6.2.8: Electrochemical Study On $[RhCl_2(L)]^+$:

(L= $[12]aneS_4$, $[14]aneS_4$, $[16]aneS_4$)

The literature relating to Rh(II) species is dominated by dimeric complexes such as metalloporphyrins of the general type Rh_2P_2 (P= OEP^{2-}, TTP^{2-}) (Chapter 5). There are only a few examples of genuine mononuclear Rh(II) species [105,168,190-203], and reports of Rh(II) porphyrin intermediates [168,191-194] represent an important example.

In recent years, the Edinburgh group has directed a great deal of effort towards investigations of the electrochemical properties of platinum group metal complexes incorporating polythia and polyaza macrocycles, with particular emphasis on the stabilisation of unusual oxidation states. In the course of this study, a series of complexes have been prepared successfully in which the metal exists in an uncommon d^n-configuration, e.g. $[M([9]aneS_3)_2]^{3+}$ (M= Pd(III) [115,120], Pt(III) [122]), $[Pd([9]aneN_3)_2]^{3+}$ [121,204] and $[Pd(Me_4[14]aneN_4)]^+$ [119]. The results indicate that monomeric d^7 Rh(II) species may also be accessible via electrochemical reduction of the appropriate Rh(III) complexes incorporating N and S-donor macrocycles. A further impetus for this work has been the stabilisation of Rh(II) by homoleptic, hexathia co-ordination in $[Rh([9]aneS_3)_2]^{2+}$ (Chapter 2) [105,107].

Cyclic voltammetry of cis-$[RhCl_2(L)]^+$ (L= $[12]aneS_4$, $[14]aneS_4$) and trans-$[RhCl_2([16]aneS_4)]^+$ in MeCN (0.1M $^nBu_4NPF_6$ supporting electrolyte) at platinum

electrodes shows an irreversible reduction for each complex at E_{pc}= -1.10, -1.10 and -0.83V *vs.* Fc/Fc^+ respectively. No oxidation is observed in MeCN in the range 0 to 1.8V *vs.* Fc/Fc^+.

[12]aneS_4

Successive coulometric measurements performed on $[RhCl_2([12]aneS_4)]^+$ at -0.95V *vs.* Ag/AgCl, 298K yielded values for n of 1.44 and 1.83 electrons respectively, and in each case the generation of a golden yellow solution was accompanied by some plating out of rhodium metal. This is indicative of decomposition/disproportionation of the reduction product, and is consistent with the small 12-membered ring tetrathia ligand being unable to accommodate the large Rh(II) centre.

[14]aneS_4

Coulometric measurement of the reduction of $[RhCl_2([14]aneS_4)]^+$ at -1.1V *vs.* Ag/AgCl gives n= 1.06 electrons, and generates a pale yellow paramagnetic species which cannot be re-oxidised to generate the starting product. The e.s.r. spectrum of the reduction product, measured at 77K as a MeCN glass, shows a weak, rhombic signal with g_1= 2.230, g_2= 2.090, g_3= 2.003, consistent with the formation, in low yield, of a d^7 Rh(II) species [115].

The reduction was followed by in situ UV/vis spectroscopy at 248K using an O.T.T.L.E. system.

Reduction of Rh(III) to Rh(II) leads to collapse of the charge-transfer absorption at λ_{max}= 246nm, and growth of a new band at λ_{max}= 288nm (ε_{max} *ca* 4,600$M^{-1}cm^{-1}$) and a shoulder at 310nm (*ca* 2,200). This process is irreversible and is not isosbestic, indicating that the reduction is not a simple one-electron transfer, but also involves some chemical or co-ordinative change.

All of these data are consistent with reduction to d^7 Rh(II) followed by loss of Cl^- from the complex, generating a five-co-ordinate or solvated product. In each of these systems binding of Cl^- to the metal would be expected to be destabilised on reduction.

Cyclic voltametry of cis-[$IrCl_2$([14]aneS_4)]PF_6 in MeCN shows no oxidation in the range 0 to 2.0V. The complex exhibits an irreversible reduction at E_{pc}= -1.82V *vs*. Fc/Fc^+ at a scan rate of 200mVs^{-1}. Coulometric measurements performed at -2.0V under the same conditions as used for rhodium, gave n= 0.85 electrons, suggesting that this complex also undergoes a one-electron reduction accompanied by loss of chloride ligand. The reduction potential is relatively cathodic compared to those observed for the related Rh(III) tetrathia macrocyclic complexes. Larger ring thioether macrocycles would be more likely to afford trans-dichloro Ir(III) species, and to stabilise lower valent, electron-rich Ir centres [205].

[16]aneS_4

Coulometric measurements of the reduction of

$[RhCl_2([16]aneS_4)]^+$ at -1.0V gives n= 0.98 electrons. The bright yellow reduction product cannot be oxidised to regenerate the starting material, again suggesting that the reduction involves a one-electron reduction to a highly reactive Rh(II) complex combined with rapid loss of Cl^- ligand in a process similar to that proposed for the 14-membered tetrathia system above. Loss of Cl^- is confirmed by the observation of a $Cl^{-/0}$ couple at *ca* +0.8V *vs.* Fc/Fc^+ in the cyclic voltammogram of the reduced solution. The reduction product decomposes rapidly at room temperature.

These studies of the redox chemistry of the Rh(III) tetrathia macrocyclic complexes suggest that similar processes occur in each system. Further characterisation of the reduction products was inhibited by decomposition reactions in solution. The transient nature of the Rh(II) species may be due to further reduction and Cl^- loss, yielding a highly reactive, square planar Rh(I) tetrathia macrocyclic product. Such complexes have been isolated and characterised crystallographically [109], e.g. $[Rh([14]aneS_4)]^+$ which has been shown to undergo extremely facile oxidative addition reactions with a variety of substrates, including CH_3I, Cl_2 and even CH_2Cl_2 [109,110].

An alternative approach to Rh(II) species was also initiated. This involved attempting to substitute the Cl^- ligands (π-donors) in the Rh(III) precursor for

other species with back-bonding capability, so that the Rh-substituent bond would be strengthened rather than weakened upon reduction. Substitution reactions were attempted using pyridine, PPh_3, PEt_3 and $P(OMe)_3$. Unfortunately, even in the presence of Tl^+ (to remove the Cl^- as a TlCl insoluble precipitate in MeCN or $MeNO_2$) we were unable to generate pure compounds. F.a.b. mass spectroscopy of the isolated products showed peaks consistent with the presence of chloride-containing rhodium species. The failure of this approach is presumably attributable to the inertness of the d^6 Rh(III) centre to substitution, hampering complete displacement of Cl^- even under forcing conditions. Alternative routes to these phosphine complexes may be achieved by utilizing different Rh(III) starting compounds, such as $RhCl_3(PR_3)_3$ where one or more Rh-phosphine bonds may be retained in preference to Rh-Cl.

6.2.9: $[RhCl([15]aneS_5)](PF_6)_2$

The generation of transition metal complexes incorporating specific labile sites is of particular interest currently, due to the potential of such species for the activation of small substrate molecules via co-ordination to a metal centre. Binding and insertion reactions of this nature using metalloporphyrin dimers of the general type M_2P_2 (M= Rh, Ir, Ru, Os, and P= OEP^{2-}, TTP^{2-}) have received a great deal of attention in recent

years (Chapter 5).

We argued that co-ordination of a pentathia macrocyclic ligand to Rh(III) would occupy five co-ordination sites, leaving one vacant, and thus available for further reaction. Moreover, the thioether macrocycle would act as a protecting group for the metal centre while also possibly permitting some degree of stabilisation of unusual oxidation states. These complexes, therefore, have potential in electrocatalysis.

Very few transition metal complexes incorporating [15]aneS_5 have been reported. The single crystal structure of [15]aneS_5 [13] shows the ligand to adopt a rather irregular shape, in which all five sulphur-donor atoms are exodentate. In this species seven out of ten C-S bonds adopt a *gauche* placement. Although odd-membered rings generally show anomalous torsion angles due to significant ring strain [206], the majority of C-S torsions in [15]aneS_5 are *gauche*. This further consolidates the observation that crown thioethers have a strong affinity for *gauche* placements at the C-S bonds.

Rorabacher *et al* have reported the synthesis and single crystal X-ray structure of the Cu(II) complex, [Cu([15]aneS_5)]$(ClO_4)_2$ [207]. The structure shows the Cu(II) ion co-ordinated to all five sulphur-donors of the macrocycle, generating a quasi-square-pyramidal structure. It is interesting that the metal ion sits 0.41A° above the mean S_4 plane, and the Cu-S_{ap} bond length of 2.398(2)Å is only 0.08Å longer than the mean of

the four $Cu-S_{eq}$ distances. The Cu(I) complex, $[Cu([15]aneS_5)]^+$, adopts a tetrahedral geometry, with the Cu(I) ion binding to four S-donors with the fifth sulphur dangling.[207]

Schröder and co-workers have recently prepared the Pd(II) and Pt(II)[208] complexes, $[M([15]aneS_5)]^{2+}$. The solid state structure of the Pd(II) species (Fig. 6.6) shows a very unusual geometry , with the d^8 Pd(II) ion bound to all five sulphur-donors of the ligand, giving an irregular structure with three short Pd-S bonds [Pd-S= 2.294(12), 2.278(8), 2.336(11)Å] and two rather longer [Pd-S= 2.532(11), 2.540(11)Å]. Interestingly, the d^8 Pt(II) complex is not isostructural. In this case the metal is bound to a distorted square planar arrangement of the S – donors, with normal Pt-S bond lengths [Pt-S=2.283(7), 2.309(7), 2.301(8), 2.306(7)Å], leaving one sulphur atom interacting at long-range [Pt-S= 2.894(9)Å], (Fig. 6.7).

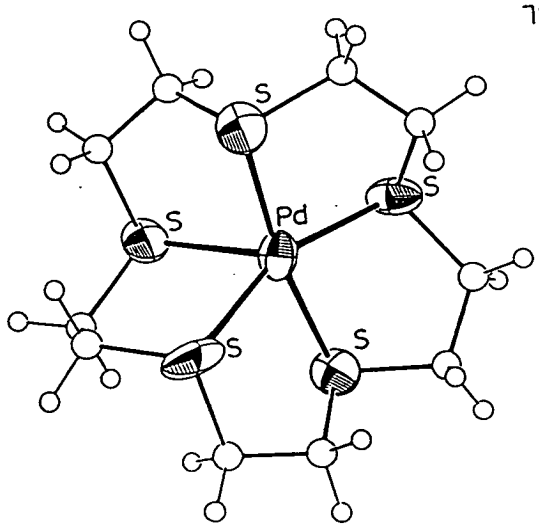

Fig. 6.6:Single crystal structure of $[Pd([15]aneS_5)]^{2+}$

Fig. 6.7: Single crystal structure of $[Pt([15]aneS_5)]^{2+}$

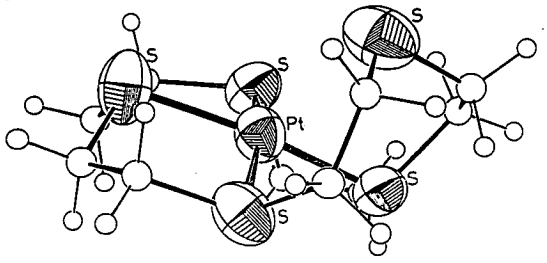

Reaction of $RhCl_3.3H_2O$ with one molar equivalent of $[15]aneS_5$ in refluxing methanol for 3h gave a pale yellow solution which yielded the complex $[RhCl([15]aneS_5)](PF_6)_2$ as a light yellow microcrystalline solid upon addition of excess NH_4PF_6, and recrystallisation from MeCN.

We were particularly interested to determine whether the macrocycle would be sufficiently flexible to allow the fifth sulphur to occupy an apical co-ordination site, while still binding to Rh(III) equatorially via the other four. Otherwise Cl^- ligands might be expected to occupy both apical sites. The f.a.b. mass spectrum of the product showed molecular ion peaks at M^+= 437, 403 which are assigned to $[^{103}Rh^{35}Cl([15]aneS_5)-H]^+$ and $[^{103}Rh([15]aneS_5)]^+$ on the basis of their isotopic distributions. No peaks are observed at higher mass units. ^1H n.m.r. spectroscopy in CD_3NO_2 shows a complex second order multiplet due to the methylene protons. ^{13}C DEPT n.m.r. exhibits five independent methylene-carbon resonances at δ= 36.20, 39.03, 39.89, 40.31 and 40.69ppm, consistent with pentadentate co-ordination of the macrocycle to Rh(III) with Cl^- accommodating the vacant site. The resonance at δ= 36.20ppm is assigned

tentatively to the CH_2 groups adjacent to the apical sulphur-donor. This evidence combined with microanalytical and I.R. spectroscopic data confirms the presence of only one Cl^- ligand, i.e. the complex can be assigned as $[RhCl([15]aneS_5)](PF_6)_2$

6.3: Conclusions

This investigation of Rh(III) and Ir(III) polythia macrocyclic complexes demonstrates that these d^6 metal centres readily co-ordinate to tetrathia macrocycles to generate highly stable octahedral complexes. This further exemplifies the observation that while thioethers (R_2S) are relatively weak donors to transition metals (Chapter 1)[42], binding is significantly enhanced if the sulphur atom is incorporated in a macrocycle. The hole-size in the 16-membered macrocycle, $[16]aneS_4$, is sufficiently large to enable complexation of Rh(III), with the four thioether-donors occupying equatorial sites. In contrast, the cavity-sizes of the 12- and 14-membered rings are too small to encircle the Rh(III) ion. Thus, while Rh(III) does bind to all four sulphur-donors, the latter two macrocycles are required to adopt a folded conformation, producing two mutually cis-co-ordination sites.

Preliminary electrochemical investigations indicate that monomeric Rh(II) species are accessible upon reduction of the 14- and 16-membered ring

macrocyclic Rh(III) precursors. However, the reduction products are extremely reactive and much less stable than $[Rh([9]aneS_3)_2]^{2+}$. The difference in stability may be attributed to several factors. Firstly, the hexathia co-ordination in the bis-$[9]aneS_3$ system will favour stabilisation of low-oxidation states due to the back-bonding capability of sulphur. In contrast, the complexes discussed in this Chapter incorporate two π-donor Cl^- ligands, and only four sulphur-donors. This is also reflected in the reduction potentials, which are significantly more cathodic. Secondly, d^7 Rh(II) species would be expected to exhibit a Jahn-Teller distorted geometry. In $[Rh([9]aneS_3)_2]^{2+}$, the 9-membered trithia macrocycles are sufficiently flexible to accommodate this stereochemical requirement, but still protect each co-ordination site. In contrast, reduction of $[RhCl_2([14]aneS_4)]^+$ will tend to destabilise the Rh-Cl bonds, resulting in rapid loss of Cl^- to form co-ordinatively unsaturated, and therefore reactive Rh centres.

6.4: Experimental

6.4.1: $[RhCl_2([12]aneS_4)]PF_6$

Reaction of $RhCl_3.3H_2O$ (43mg, 0.116mmol) in H_2O (5ml) with $[12]aneS_4$ (40mg, 0.116mmol) in refluxing MeOH (130ml) for 2h under N_2 afforded a bright yellow solution. Addition of excess NH_4PF_6 gave a yellow precipitate which was collected and recrystallised from MeCN (Yield: 75mg, 81%). Mol. wt. 559.23. Elemental analysis: found C= 17.2, H= 2.91, S= 23.1%; calculated for $[C_8H_{16}Cl_2S_4Rh]PF_6$: C= 17.2, H= 2.88, S= 22.9%. UV/vis spectrum (MeCN): λ_{max}= 401nm (ε_{max}= 1,781$M^{-1}cm^{-1}$), 300(sh) (1,165), 250 (21,920). F.a.b. mass spectrum (3-NOBA matrix): found M^+= 413, 378; calculated for

$[^{103}Rh^{35}Cl_2([12]aneS_4)]^+$ M^+= 413,

$[^{103}Rh^{35}Cl([12]aneS_4)]^+$ M^+= 378.

^1H n.m.r. spectrum (80MHz, CD_3CN, 298K): δ= 3.3-4.2ppm (16H, $C\underline{H}_2$, m). ^{13}C DEPT n.m.r. (50.32MHz, CD_3CN, 298K): δ= 44.41, 41.03, 36.08, 35.16ppm ($\underline{C}H_2$). I.R. spectrum (KBr disc): 2990m, 2925m, 1410vs, 1280m, 1265m, 1150w, 1120w, 1090m, 990w, 950w, 925m, 840vs, 555vs, 360m, 345m, 330m, 290m, 270w cm^{-1}.

6.4.2: $[RhCl_2([14]aneS_4)]PF_6$

To a refluxing solution of $[14]aneS_4$ (61mg, 0.228mmol) in MeOH (100ml) was added $RhCl_3.3H_2O$ (60mg, 0.228mmol) in H_2O (5ml) dropwise. The reaction mixture was refluxed under N_2 for 1h to yield a bright yellow solution which was filtered to remove insoluble

chloro-bridged polymer. Addition of excess NH_4PF_6 afforded a yellow precipitate, which was recrystallised from MeCN (Yield: 100mg, 75%). As reported by Busch [157], it is important that $RhCl_3$ is added to a refluxing solution of the ligand to minimise the formation of chloro-bridged polymer. Mol. wt. 587.28. Elemental analysis: found C= 20.4, H= 3.44, S= 21.4%; calculated for $[C_{10}H_{20}Cl_2S_4Rh]PF_6$: C= 20.4, H= 3.43, S= 21.8%. UV/vis spectrum (MeCN): λ_{max}= 362nm (ε_{max}= 949$M^{-}cm^{-1}$), 319 (765), 246 (10,370). I.R. spectrum (KBr disc): 3000m, 2940w, 1430vs, 1420vs, 1400m, 1360w, 1300w, 1280w, 1270m, 1240w, 1160w, 1130m, 1100w, 1020w, 1010w, 985m, 930m, 840vs, 555vs, 460w, 370w, 310m, 280m cm^{-1}.

6.4.3: $[RhCl_2([14]aneS_4)]BPh_4$

The BPh_4^- salt was prepared by the same method as 6.4.2, using $NaBPh_4$ in place of NH_4PF_6. Mol. wt. 761.55. Elemental analysis: found C= 53.4, H= 5.35, Cl= 9.67, S= 16.9%; calculated for $[C_{10}H_{20}Cl_2S_4Rh][C_{24}H_{20}B]$: C= 53.6, H= 5.29, Cl= 9.31, S= 16.8. F.a.b. mass spectrum (3-NOBA matrix): found M^+= 441, 406, 370; calculated for

$[^{103}Rh^{35}Cl_2([14]aneS_4)]^+$ M^+= 441,

$[^{103}Rh^{35}Cl([14]aneS_4)]^+$ M^+= 406,

$[^{103}Rh([14]aneS_4-H)]^+$ M^+= 370.

^1H n.m.r. spectrum (80MHz, CD_3CN, 298K): δ= 6.8-7.7 (20H, BPh_4^-, m), 2.5-3.6ppm (20H, $C\underline{H}_2$, m). ^{13}C DEPT n.m.r. spectrum (50.32MHz, CD_3CN, 333K): δ= 38.31, 30.10, 29.95, 29.85, 23.84ppm ($\underline{C}H_2$).

6.4.4: Single Crystal Structure of $[RhCl_2([14]aneS_4)]PF_6$

Yellow crystals suitable for a single crystal X-ray structure determination were obtained by recrystallisation of the complex from MeCN.

Crystal Data:

$[C_{10}H_{20}Cl_2S_4Rh]PF_6$, M= 587.28, monoclinic, space group C2/c, a= 10.746(8), b= 11.298(5), c= 15.708(8)Å, β= 92.00(5)°, V= 1905.9Å^3, (by least-squares refinement on diffractometer angles for 12 centred reflections, λ= 0.71073Å), Z= 4, D_c= 2.047gcm^{-3}. Crystal dimensions 0.50x0.50x0.30mm, μ(Mo-Kα)= 16.5cm^{-1}, F(000)= 1168.

Data Collection and Processing:

Stöe STADI-4 four-circle diffractometer, ω/θ mode with ω scan-width $(2.0+0.35\tan\theta)^o$, graphite-monochromated Mo-Kα radiation; 1320 reflections measured to $2\theta = 45^o$ (h -12⟶12, k 0⟶12, l 0⟶17), giving 1161 with $F>6\sigma(F)$. No significant crystal decay, no absorption correction.

Structure Analysis and Refinement:

A Patterson synthesis located the Rh atom and iterative cycles of least-squares refinement and difference Fourier synthesis located all remaining atoms, including H-atoms which were then refined positionally but with a fixed, isotropic thermal parameter (U=

0.08Å^2). All non-H atoms were refined anisotropically. The weighting scheme $\underline{w}^{-1} = \sigma^2(\underline{F}) + 0.000076\underline{F}^2$ gave satisfactory agreement analyses. At convergence $\underline{R}$, $\underline{R}_w = 0.0311$ and 0.0461 respectively for 141 parameters, $\underline{S} = 1.191$ and in the final difference Fourier synthesis the maximum and minimum residuals were 0.84 and $-0.50 e\text{Å}^{-3}$ respectively.

6.4.5: $[IrCl_2([14]aneS_4)]BPh_4$

To a refluxing solution of $[14]aneS_4$ (40mg, 0.149mmol) in refluxing ethanol (50ml) containing an excess of $NaBPh_4$ was added $IrCl_3.3H_2O$ (52mg, 0.147mmol) in H_2O (5ml). The reaction mixture was refluxed under N_2 for 14h, cooled and the yellow/brown precipitate collected. This was then dissolved in hot $MeNO_2$ and filtered to remove insoluble chloro-bridged polymer. The filtrate was cooled to afford a cream precipitate of $[IrCl_2([14]aneS_4)]BPh_4$ which was collected and dried *in vacuo* (Yield: 42mg, 33%). Mol. wt. 850.85. Elemental analysis: found C= 47.4, H= 4.78; calculated for $[C_{10}H_{20}Cl_2S_4Ir][C_{24}H_{20}B]$: C= 48.0, H= 4.74. F.a.b. mass spectrum (dmf/glycerol matrix): found M^+= 531, 496, 461; calculated for

$[^{193}Ir^{35}Cl_2([14]aneS_4)]^+$ M^+= 531,

$[^{193}Ir^{35}Cl([14]aneS_4)]^+$ M^+= 496,

$[^{193}Ir([14]aneS_4)]^+$ M^+= 461.

UV/vis spectrum (MeCN): λ_{max}= 348nm (ε_{max}= $113M^{-1}cm^{-1}$),

297 (1,400), 275 (2,760), 267 (3,370), 216 (29,400). I.R. spectrum (CsI disc): 3060m, 2980m, 2910m, 1580m, 1480m, 1430vs, 1300w, 1270m, 1190w, 1130w, 1030w, 860m, 850m, 810w, 740vs, 710vs, 610 vs, 530m, 310m, 305m cm^{-1}.

6.4.6: $[IrCl_2([14]aneS_4)]PF_6$

Replacement of $NaBPh_4$ with NH_4PF_6 in the above preparation (6.4.5) yielded the corresponding PF_6^- salt. Mol. wt. 676.58. Elemental analysis: found C= 18.1, H= 3.04, S= 18.8%; calculated for $[C_{10}H_{20}Cl_2S_4Ir]PF_6$: C= 17.8, H= 2.98, S= 18.9%. ^1H n.m.r. spectrum (200MHz, CD_3NO_2, 293K): δ= 2.5-3.5ppm ($C\underline{H}_2$, m). ^{13}C DEPT n.m.r. spectrum (50.32MHz, CD_3NO_2, 293K): δ= 37.99, 29.52, 28.96, 28.39, 23.90ppm.

6.4.7: Single Crystal Structure of $[IrCl_2([14]aneS_4)]BPh_4$

Colourless needles suitable for X-ray crystallography were obtained by vapour diffusion of diethyl ether into a solution of the complex in $MeNO_2$.

Crystal Data:

$[C_{10}H_{20}Cl_2S_4Ir][C_{24}H_{20}B]$, M= 850.85, monoclinic, space group $\underline{P}2_1$, $\underline{a}$= 12.6927(14), $\underline{b}$= 12.1361(20), $\underline{c}$= 14.4912(18)Å, β= 111.813(13), $\underline{V}$= 2072.4Å^3, (by least-squares refinement on diffractometer angles for 20 centred reflections, λ= 0.71073Å), $\underline{Z}$= 2, $\underline{D}_c$= 1.363gcm^{-3}. Crystal dimensions 0.46x0.15x0.15mm, μ(Mo-Kα)= 35.18cm^{-1}, $\underline{F}$(000)= 848.

Data Collection and Processing:

Stöe STADI-4 four-circle diffractometer, ω/θ mode with ω scan-width $(1.4+0.35\tan\theta)^{o}$, graphite monochromated Mo-Kα radiation; 2882 reflections measured to $2\theta = 45^{o}$ (h -13⟶12, k 0⟶13, l 0⟶14), giving 2508 with $\underline{F}>6\sigma(\underline{F})$. No significant crystal decay.

Structure Analysis and Refinement:

The Ir position was located from a Patterson synthesis and input to DIRDIF which located the Cl and S atoms. Iterative rounds of least-squares refinement and difference Fourier synthesis located all other non-H atoms. At isotropic convergence, final correction for absorption was made using DIFABS. Initial absorption correction was made using 48 ψ-scans (maximum transmission factor= 0.2382, minimum= 0.2022). Anisotropic thermal parameters were refined for Ir, S, Cl, and all macrocyclic C-atoms. H-atoms were included in fixed, calculated positions. The phenyl groups of the BPh_4^- counterion were refined as rigid groups. The absolute configuration of the structure was not easy to establish with certainty since both hands refined well to essentially the same $\underline{R}$-factors. The 20 reflections were selected with the greatest discrimination factor defined as $\underline{d} = \underline{F}_1\underline{F}_2\sin^2(T_1-T_2)/\underline{F}_0$, where subscripts 1 and 2 refer to structure factors calculated for the Ir atoms and for the other atoms respectively. For the fully refined data

sets, these 20 data gave $\underline{R}$= 0.032 for the hand chosen, and 0.049 for the opposite hand. More strikingly, bond lengths to Ir are much less consistent in the less favoured hand, the Ir-S lengths being more divergent, and the Ir-Cl lengths being much shorter. The weighting scheme $\underline{w}^{-1}= \sigma^2(\underline{F})+0.002572\underline{F}^2$ gave satisfactory agreement analyses. At final convergence $\underline{R}$, $\underline{R}_w$= 0.0363 and 0.0509 respectively, $\underline{S}$= 1.137 for 205 parameters, and in the final difference Fourier synthesis the maximum and minimum residuals were +0.67 and -0.64e$\mathring{A}^{-3}$ respectively.

6.4.8: $[RhCl_2([16]aneS_4)]PF_6$

Reaction of $RhCl_3.3H_2O$ (35mg, 0.135mmol) in H_2O (5ml) with [16]aneS_4 (40mg, 0.135mmol) in refluxing EtOH (150ml) for 1h under N_2 afforded a bright yellow solution. Addition of excess NH_4PF_6 gave a yellow precipitate which was collected and recrystallised from MeCN (Yield: 60mg, 72%). Mol. wt. 615.34. Elemental analysis: found C= 23.6, H= 3.90, S= 20.3%; calculated for $[C_{12}H_{24}Cl_2S_4Rh]PF_6$: C= 23.4, H= 3.93, S= 20.8%. F.a.b. mass spectrum (3-NOBA matrix): found M^+= 469, 434, 399; calculated for

$[^{103}Rh^{35}Cl_2([16]aneS_4)]^+$ M^+= 469,

$[^{103}Rh^{35}Cl([16]aneS_4)]^+$ M^+= 434,

$[^{103}Rh([16]aneS_4)]^+$ M^+= 399.

^1H n.m.r. spectrum (80MHz, CD_3CN, 298K): δ= 2.3-3.7ppm (24H, $C\underline{H}_2$, m). ^{13}C DEPT n.m.r. spectrum (50.32MHz, CD_3CN, 298K): δ= 34.42, 32.27, 23.26, 21.85ppm($\underline{C}H_2$). UV/vis

spectrum (MeCN): λ_{max}= 369nm (ε_{max}= 151$M^{-1}cm^{-1}$), 278 (38,290), 232 (18,930). I.R. spectrum (KBr disc): 2980w, 2920m, 2840w, 1430vs, 1405m, 1310m, 1290m, 1255w, 1240m, 1195w, 1160m, 1120w, 1080w, 1020m, 840vs, 555vs, 365m, 305m, 270w cm^{-1}.

6.4.9: Single Crystal Structure of $[RhCl_2([16]aneS_4)]PF_6$

Yellow crystals of suitable quality for an X-ray structural determination were obtained by recrystallisation of the complex from MeCN.

Crystal Data:

$[C_{12}H_{24}Cl_2S_4Rh]PF_6$, M= 615.34, monoclinic, space group C2/c, a= 11.9507(20), b= 11.1055(15), c= 16.2067(18)Å, β= 95.197(21)°, V= 2142.1Å^3, (by least-squares refinement on diffractometer angles for 30 centred reflections, λ= 0.71073Å), Z= 4, D_c= 1.908gcm^{-3}. Crystal dimensions 0.23x0.15x0.15mm, μ(Mo-Kα)= 14.72cm^{-1}, F(000)= 1232.

Data Collection and Processing:

Stöe STADI-4 four-circle diffractometer, $\omega/2\theta$ mode with ω scan-width $(1.20+0.347\tan\theta)^o$, graphite-monochromated Mo-Kα radiation; 1549 reflections measured to 2θ= 45° (h -12⟶12, k 0⟶11, l 0⟶17) giving 1067 with $F>6\sigma(F)$. No significant crystal decay, no absorption correction.

Structure Analysis and Refinement:

Analysis of intensity statistics clearly indicated the position of the Rh atom; using this information as input, DIRDIF successfully located the Cl, S and P atoms. Subsequent iterative cycles of least-squares refinement and difference Fourier synthesis located all other non-H atoms. H-atoms were included in fixed, calculated positions, and Rh, S, C, P, F atoms were refined anisotropically. Both the cation and PF_6^- anion were ordered. The weighting scheme $\underline{w}^{-1} = \sigma^2(\underline{F}) + 0.000475\underline{F}^2$ gave satisfactory agreement analyses. At convergence $\underline{R}$, $\underline{R}_w$ = 0.0396 and 0.0536 respectively for 121 parameters, $\underline{S}$ = 1.202 and in the final difference Fourier synthesis the maximum and minimum residuals were +0.80 and -0.51$e\text{Å}^{-3}$ respectively.

6.4.10: $[RhCl([15]aneS_5)](PF_6)_2$

Reaction of $RhCl_3.3H_2O$ (35mg, 0.133mmol) in H_2O (5ml) with $[15]aneS_5$ (40mg, 0.133mmol) in refluxing MeOH (30ml) for 3h under N_2 yielded a pale yellow solution. Addition of excess NH_4PF_6 afforded a yellow precipitate which was collected, recrystallised from MeCN and dried *in vacuo* (Yield: 77mg, 83%). Mol. wt. 693.40. Elemental analysis: found C= 17.0, H= 2.78, S= 23.6%; calculated for $[C_{10}H_{30}ClS_5Rh](PF_6)_2$: C= 17.3, H= 2.91, S= 23.1%. F.a.b. mass spectrum (3-NOBA matrix): found M^+= 437, 403; calculated for $[^{103}Rh^{35}Cl([15]aneS_5)]^+$ M^+= 438,

$[^{103}Rh([15]aneS_5)]^+$ M^+ = 403. ^1H n.m.r. spectrum (80MHz, CD_3NO_2, 298K): δ = 3.1-4.0ppm ($C\underline{H}_2$, m). ^{13}C DEPT n.m.r. spectrum (50.32MHz, CD_3NO_2, 298K): δ = 36.20, 39.03, 39.89, 40.31, 40.69ppm ($\underline{C}H_2$). I.R. spectrum (KBr disc): 3005m, 2940m, 2840w, 1430vs, 1290w, 1275w, 1160w, 1120w, 950w, 840vs, 555vs, 360w, 315w, 285w cm^{-1}.

CHAPTER 7

Structural and Electrochemical Studies

on $[RhCl_2(Me_4[14]aneN_4)]^+$

7.1: Introduction

The co-ordination chemistry of nitrogen-donor macrocyclic ligands with transition metal ions has been investigated extensively in recent years [209]. However, only a few complexes incorporating platinum group metals have been reported [19,182,183,187].

Electrochemical studies on a series of Rh(III) and Ir(III) tetrathia macrocyclic complexes showed that highly reactive Rh(II) monomeric species could be generated (Chapter 6). We proposed that more stable Rh(II) monomers may be generated by replacing the sulphur-donor atoms with nitrogen-donors. The macrocycle selected for this study was the 14-membered tetra-aza macrocycle, $Me_4[14]aneN_4$.

$Me_4[14]aneN_4$ binds to a wide variety of transition metal ions, and can be associated with a wide range of oxidation states, from d^2 Os(VI) and Ru(VI) [210,211] in the presence of oxo-ligands, to d^{10} Cu(I) and Ni(I) in aqueous solution [212,213]. Recently, Schröder and co-workers have shown that a d^9 Pd(I) centre can be stabilised by the tetra-aza ionophores, $Me_4[14]aneN_4$ and $Bz_4[14]aneN_4$, (1-3) [119], thus, further confirming that these ligands can stabilise low oxidation states.

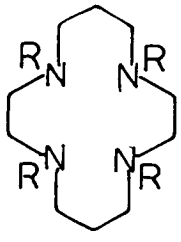

(1) R=H
(2) R=Me
(3) R=Bz

We reasoned, therefore, that the stabilisation of reduced Rh(II) and Rh(I) centres might be achieved using this redox-inactive tetra-aza macrocyclic ligand system.

There are few examples of monomeric Rh(II) centres. These include $[Rh([9]aneS_3)_2]^{2+}$ which shows a reversible Rh(III)/(II) redox couple at $E_{1/2}$= -0.71V *vs.* Fc/Fc^+ [105,107], [Rh(L')] (L'= porphyrinate^{2-}), which readily dimerises to $[\{Rh(L')\}_2]$ involving a direct Rh-Rh bond [168,191-194], and $[Rh(sepulchrate)]^{2+}$ (4) which show a Rh(III)/(II) couple at $E_{1/2}$= -1.71V *vs.* Fc/Fc^+ [190]. Both of these latter two incorporate polyaza macrocyclic derivatives, thus providing a further incentive for our study of the co-ordination of $Me_4[14]aneN_4$ with rhodium(III).

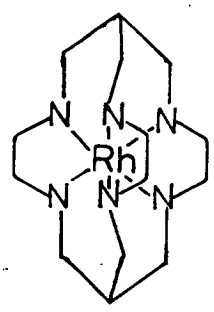

A further advantage of $Me_4[14]aneN_4$ is that it incorporates tertiary amine functions which are not susceptible to oxidative dehydrogenation on complexation to a metal centre. This is a decomposition process which is characteristic of complexes involving secondary amines to form α-imine products,(5). N-alkylation inhibits this reaction, as well as slowing down the rate of ligand exchange. Indeed, the stabilisation of Cu(I) and Ni(I) by

$Me_4[14]aneN_4$ is attributed to these two factors combined with the weaker ligand field exerted by the N-alkylated ligand, which also favours the low oxidation state [214].

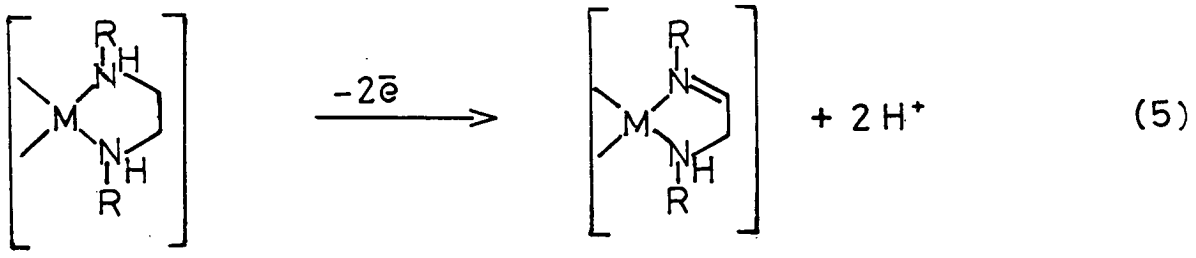

(5)

The approach adopted was based on the synthesis of the mononuclear, octahedral Rh(III) precursor, followed by electrochemical reduction of this complex to the corresponding d^7 Rh(II) species.

Ligand Synthesis

$[14]aneN_4$, the non-methylated analogue of $Me_4[14]aneN_4$, was first synthesised by Van Alphen [215] and later by Stetter and Mayer [216]. The yields of amine from these routes were rather low. A significantly higher yield (over 65%) can be achieved using the in situ template method later developed by Barefield *et al* [217-219]. This route, summarised in Fig. 7.1, involves a condensation reaction between 1,5,8,12-tetraazadodecane and glyoxal in the presence of nickel(II) ions, followed by reduction using $NaBH_4$ or hydrogen and Raney nickel catalyst. The Ni(II) ion can then be displaced from $[14]aneN_4$ using CN^-. $Me_4[14]aneN_4$ can be obtained in quantitative yield by methylation of free $[14]aneN_4$ using formic acid/formaldehyde [61]. It is

aslo available from a commercial supplier.

A wide variety of macrocyclic tetramines have been obtained by using modifications of this metal ion assisted cyclisation reaction [217-219].

The single crystal X-ray strucure of [14]aneN$_4$ has been determined [220]. This shows two independent molecules per unit cell, each with a crystallographically imposed centre of inversion. Both molecules exhibit very similar endo-conformations, closely resembling the conformations found for the Co(II) and Ni(II) complexes [221,222]. This contrasts with the exodentate conformations characteristic of all of the free thiether crowns (Chapter 6). The endo form identified for free [14]aneN$_4$ is stabilised by H-bonding across the 1,3-diamine links. Thus, unlike its thioether analogues, this ligand is pre-organised with respect to co-ordination of a transition metal within the macrocyclic cavity. Although the structure of free Me$_4$[14]aneN$_4$ has not been reported, the close relationship between the two macrocycles suggests that it should adopt a similar configuration to [14]aneN$_4$, with the N-functions in an endo configuration, with all four methyl groups lying on the same side of the N$_4$ plane [223].

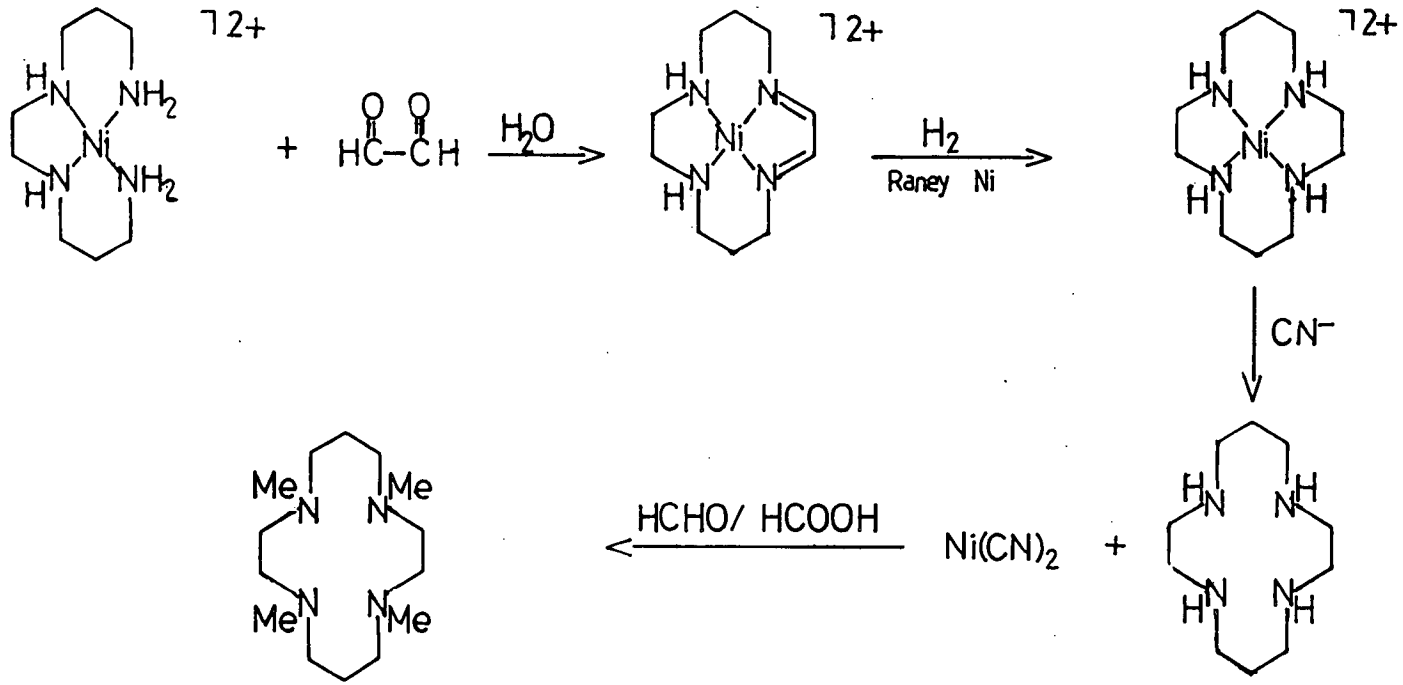

Fig. 7.1: Synthesis of $Me_4[14]aneN_4$

7.2: Results and Discussion

7.2.1: $[RhCl_2(Me_4[14]aneN_4)]^+$

Reaction of $RhCl_3.3H_2O$ with one molar equivalent of $Me_4[14]aneN_4$ in refluxing anhydrous MeOH or EtOH for 1h under N_2 gave a golden yellow solution, (prolonged refluxing resulted in reduction to rhodium metal). Addition of excess NH_4PF_6 afforded a bright yellow product, which was recrystallised from MeCN to yield orange, air-stable crystals. The importance of utilizing anhydrous conditions should be emphasised since in the presence of water, ligand protonation is predominant.

The I.R. spectrum of the complex shows a single peak at $280cm^{-1}$ assigned to a Rh-Cl stretching vibration, (υ(Rh-Cl)). The presence of only one such band suggests that this is a trans-dichloro complex. The UV/vis spectrum of the product shows an intense transition at λ_{max}= 222nm (ε_{max}= 39,900cm^{-1}), which is assigned to a Cl$\longrightarrow$Rh charge-transfer transition. Two d-d transitions are also observed at λ_{max}= 324 (241) and 452 (63). The low extinction coefficients for the d-d bands are consistent with a relatively high degree of molecular symmetry, indicating that the two co-ordinated Cl^- ligands are mutually trans. Similar intensities are reported for a series of analogous complexes, trans-$[RhX_2([14]aneN_4)]^+$ [182,183]. The f.a.b. mass spectrum of the complex shows a peak with the correct isotopic distribution at M^+= 429 assigned to

$[^{103}Rh^{35}Cl_2(Me_4[14]aneN_4)]^+$, with further peaks at M^+ = 394 and 358 corresponding to successive loss of chloride ligand giving $[^{103}Rh^{35}Cl(Me_4[14]aneN_4)]^+$ and $[^{103}Rh(Me_4[14]aneN_4\text{-}H)]^+$ respectively. Based on this evidence together with microanalytical data, we formulated the complex as trans-$[RhCl_2(Me_4[14]aneN_4)]PF_6$.

It was important to assign the configuration of the N-methyl groups in this complex. When tmc co-ordinates to four equatorial sites of a rhodium(III) atom the subsequent disposition of each of the four methyl groups, either above or below the co-ordination plane, gives rise to sixteen possible arrangements. These reduce to the five energetically distinct geometries shown in Fig. 7.2 [223].

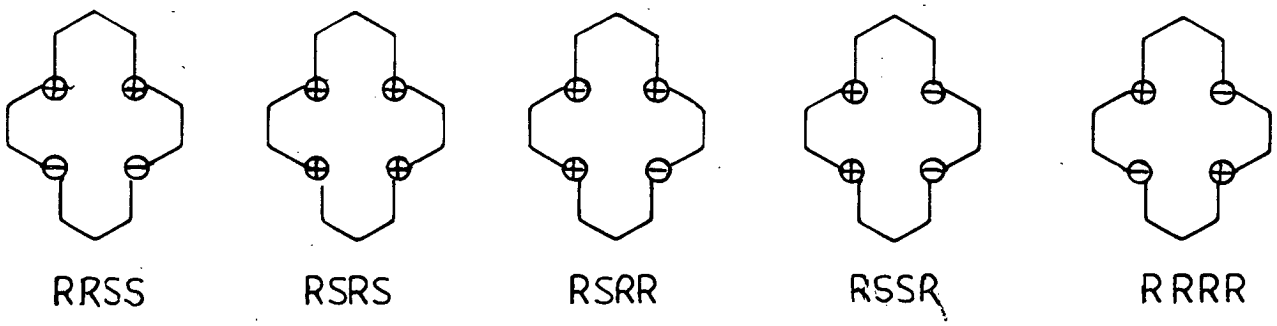

Fig. 7.2: Diagrammatic representation of the five main isomers of $[M(Me_4[14]aneN_4)]^{n+}$, (+ and - refer to the orientation of the Me groups above and below the plane)

Original reports stated that the RRSS isomer was the thermodynamically favoured isomer (since this configuration minimises the steric interactions between the methyl groups) and that the RSRS isomer (the

conformation adopted by the free ligand), was the kinetically favoured conformer [223]. More recently, however, Moore [224] and Lincoln [225] have demonstrated for square panar Ni(II) complexes, that these two isomers can readily interconvert in strongly co-ordinating solvents such as dmso, via the asymmetric RSRR isomer (Fig. 7.3).

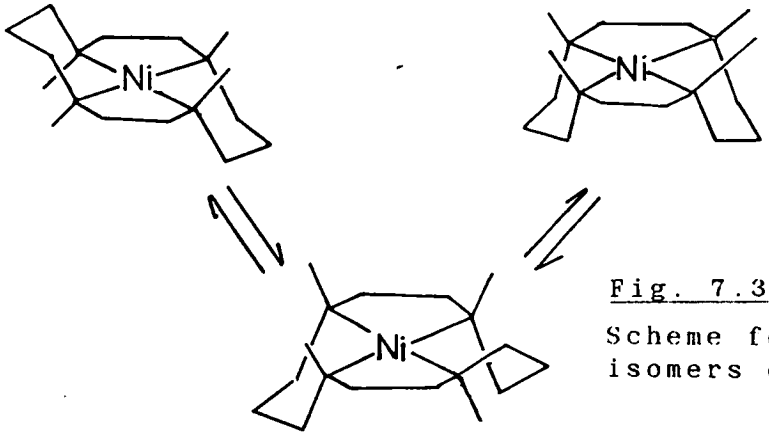

Fig. 7.3:
Scheme for interconversion of isomers of $[Ni(Me_4[14]aneN_4)]^{2+}$

The ^1H n.m.r. spectrum of $[RhCl_2(Me_4[14]aneN_4)]^+$ shows a single resonance at δ= 2.78ppm attributed to four equivalent methyl groups of a symmetric isomer. A further four methyl resonances observed at δ= 2.76, 2.75, 2.67 and 2.51ppm may be assigned to the non-equivalent methyl groups of an asymmetric isomer. ^{13}C DEPT n.m.r. spectroscopy is a particularly useful technique for assisting in the elucidation of the structure of this complex, since it readily distinguishes between CH_3 and CH_2 resonances. The ^{13}C DEPT n.m.r. spectrum of the isolated product measured in CD_3CN, likewise reveals the presence of two isomers in solution (Fig. 7.4). The symmetric isomer shows resonances at δ= 50.69 ($\underline{C}H_3$), 23.86 ($NCH_2\underline{C}H_2$), 61.52 and 63.10ppm ($\underline{C}H_2$ adjacent to N). Fourteen further resonances are apparent in the ^{13}C

n.m.r. spectrum with δ= 47.11, 47.95, 49.87, 53.63ppm for the four methyl carbon centres. From these data, the asymmetric isomer can be assigned tentatively to the species with an RSRR configuration, with three methyl groups above and one methyl group below the RhN_4 co-ordination plane, or to a solvated species which arises from the equilibrium shown in Fig. 7.5. A solvated species of this nature would enable inversion at the N-function as described by Moore et al [224]. Interconversion between the RSRS and RRSS isomers requires cleavage of the Rh-N bond, generating a tridentate $Me_4[14]aneN_4$ intermediate with a solvent molecule occupying the vacant site, followed by N-inversion and chelate ring closure to give the RSRR asymmetric isomer. This would then have to undergo a further chelate ring opening and N-inversion at another site to complete the interconversion. However, this process would be expected to be slow since it involves substitution of Cl^- for a solvent molecule in a low-spin d^6 system. The ratio of the two species present in the ^{13}C n.m.r. spectrum appears to be approximately 50:50.

Fig. 7.5: Proposed mechanism for solvation of $[RhCl_2(Me_4[14]aneN_4)]^+$

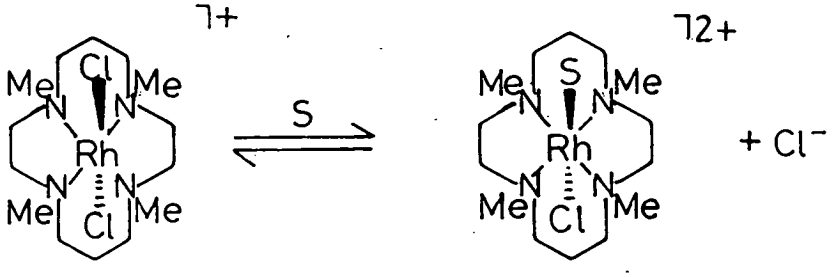

S=solvent

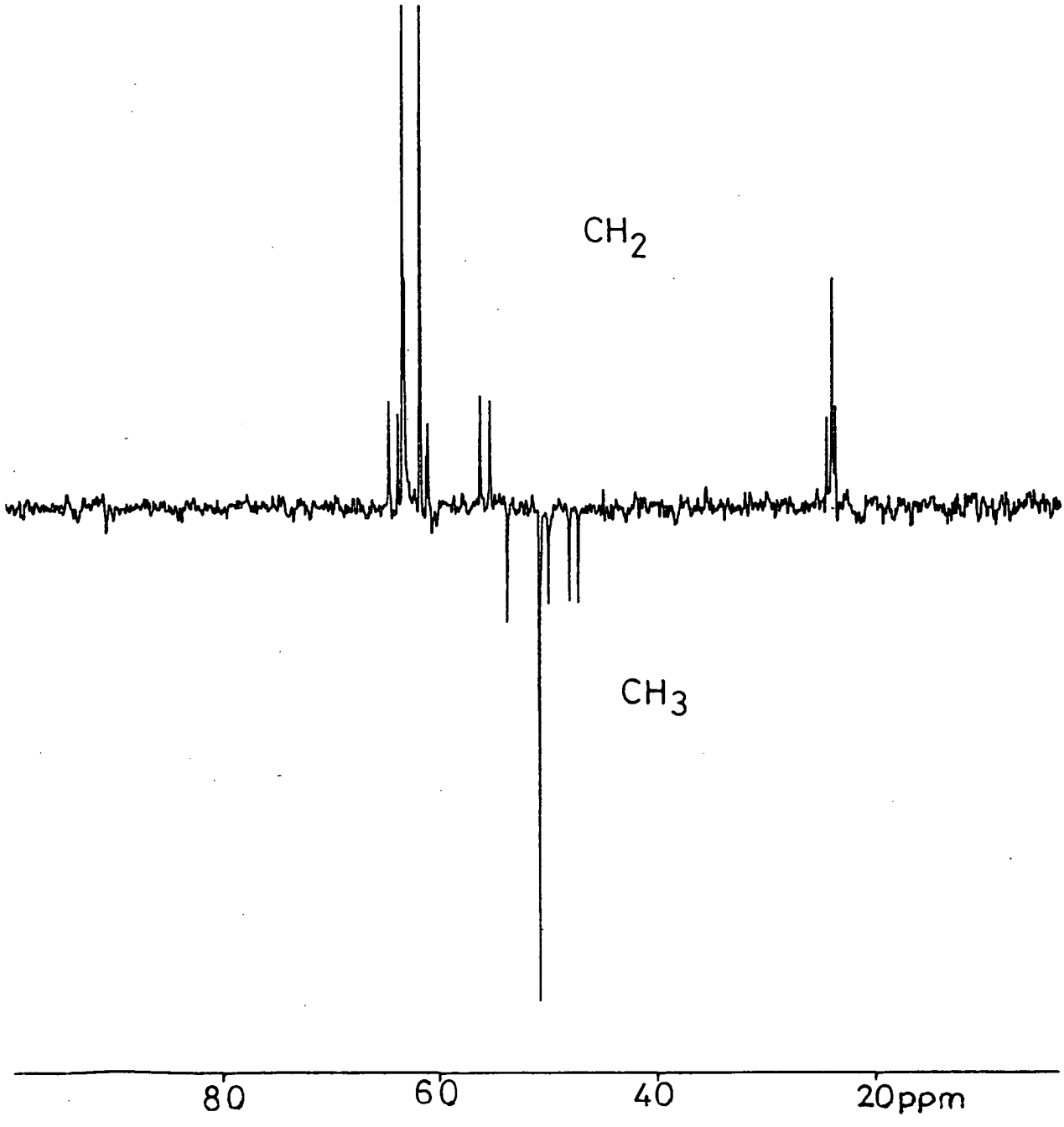

Fig. 7.4: ^{13}C DEPT n.m.r. spectrum of $[RhCl_2(Me_4[14]aneN_4)]^+$ (CD_3CN, 50.32MHz)

It was important to assign a configuration to the symmetric isomer which could be either RRSS or RSRS. In view of the paucity of structurally characterised Rh(III) tetra-aza macrocyclic complexes, a crystallographic study was undertaken.

7.2.2: Single Crystal Structure of

$[RhCl_2(Me_4[14]aneN_4)]PF_6$

Details of the structure solution are given in the Experimental Section. Selected bond lengths are given in Table 7.1 and bond angles in Table 7.2. An ORTEP plot showing the molecular structure of the cation is presented in Figs. 7.6.

During refinement of the structure significant disorder was identified for the cation. This was modelled successfully to give two conformations of the macrocycle in a ratio of approximately 2:1. The disorder is thought to arise due to either the presence of two different isomers or partial rotation of the cations within the crystal lattice. The discussion below refers exclusively to the major component of that disorder.

The X-ray structure reveals four $[RhCl_2(Me_4[14]aneN_4)]^+$ cations and four PF_6^- anions per unit cell, each of which is bisected by a crystallographically imposed mirror plane. The cation, therefore, exhibits m symmetry with the mirror plane passing through the Rh and Cl atoms and through the

central carbon atom of the propyl chains in each of the six-membered chelate rings. Octahedral geometry is achieved for the Rh(III) ion by co-ordination to two mutually trans Cl^- ligands and to a square planar arrangement of the four N-donors of the macrocycle, [Rh-Cl= 2.355(3), 2.362(3), Rh-N= 2.110(8), 2.114(8)Å]. The preference for $Me_4[14]aneN_4$ complexes to adopt transoid configurations has been confirmed from structural studies on trans-$[RuX_2(Me_4[14]aneN_4)]$ (X= Cl, NCO, or NCS) [226], trans-$[Ru(O)_2(Me_4[14]aneN_4)]^{2+/+}$ [210,227,228], RSRR trans-$[Ru(O)Cl(Me_4[14]aneN_4)]^+$ [229] and trans-$[Os(O)_2(Me_4[14]aneN_4)]^{2+/+}$ [210,230].

The structure shows that $[RhCl_2(Me_4[14]aneN_4)]^+$ adopts an RRSS configuration with two methyl groups above and two methyl groups below the RhN_4 co-ordination plane. The Rh atom is displaced by only 0.017Å out of the N_4 plane, confirming that the top and bottom faces of the complex-cation appear almost identical to the co-ordinated Rh atom. This contrasts with the significantly larger displacement of 0.082Å for the Pd(II) atom above the N_4 plane in the RSRS isomer of $[Pd(Me_4[14]aneN_4)]^{2+}$ [231], where all four methyl groups lie on the opposite side of the plane. Calculations indicate that the cavity size of the co-ordinated macrocycle in trans-$[RhCl_2(Me_4[14]aneN_4)]^+$ [N(1)-N(4)= 2.905(11), N(1)-N(1')= 3.146(11) and N(4)-N(4')= 2.983(11)Å] is slightly larger than that of

$[Pd(Me_4[14]aneN_4)]2+$ [N(1)-N(4)= 2.968(15), N(1)-N(1')= 2.860(16) and N(4)-N(4')= 2.946(17)Å] presumably representing the different conformations adopted by the two complexes.

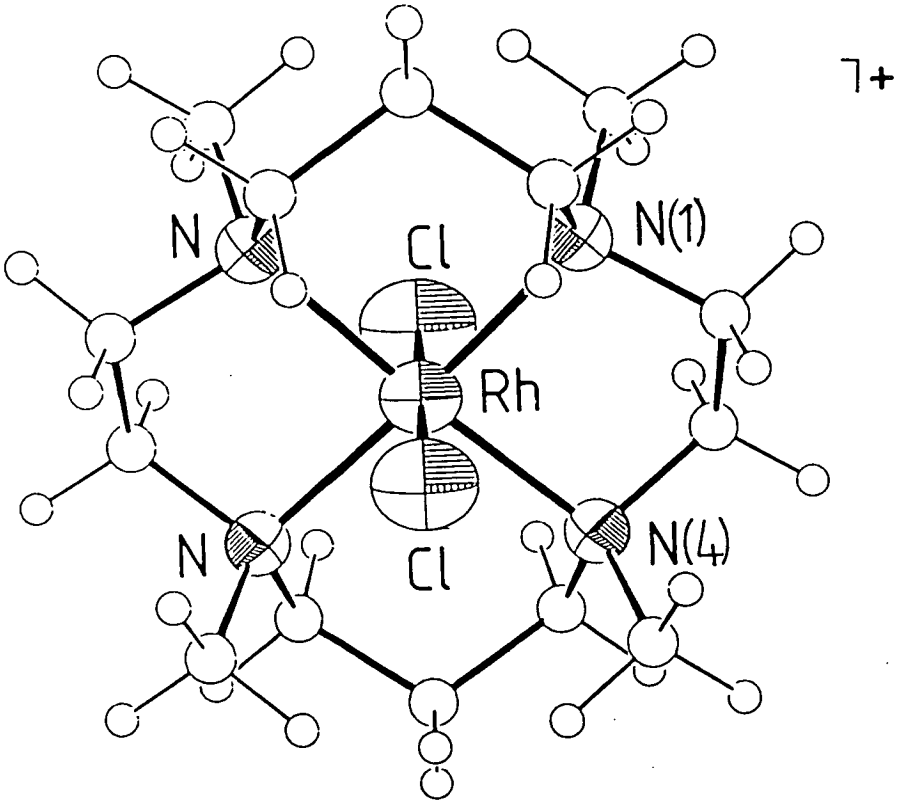

Fig. 7.6: View of the single crystal structure of $[RhCl_2(Me_4[14]aneN_4)]^+$

Single Crystal Structure of

$[RhCl_2(Me_4[14]aneN_4)]PF_6$

Table 7.1: Selected Bond Lengths(Å) with e.s.d.'s

Rh(1) - Cl(1)	2.355(3)	Rh(1) - Cl(2)	2.362(3)
Rh(1) - N(1)	2.110(8)	Rh(1) - N(4)	2.114(8)

Table 7.2: Selected Angles(°) with e.s.d.'s

Rh(1)- N(4)- C(3)	105.1(6)	Rh(1)- N(1)-C(2)	101.6(6)
Rh(1)- N(4)- C(5)	107.2(7)	Rh(1)- N(1)-C(14)	109.4(6)
Rh(1)- N(4)- C(4N)	124.7(9)	Rh(1)- N(1)-C(1N)	119.8(8)
Rh(1)- N(4)- C(3')	105.3(7)	Rh(1)- N(1)-C(2')	100.1(7)
Rh(1)- N(4)- C(5')	108.9(10)	Rh(1)- N(1)-C(14')	116.0(9)
Rh(1)- N(4)- C(4N')	114.0(10)	Rh(1)- N(1)-C(1N')	111.8(9)
Cl(1)-Rh(1)-Cl(2)	178.04(11)	Cl(1)-Rh(1)-N(1)	88.78(23)
Cl(1)-Rh(1)- N(4)	90.33(22)	Cl(2)-Rh(1)-N(1)	89.91(23)
Cl(2)-Rh(1)- N(4)	91.05(22)	N(1)-Rh(1)-N(4)	86.9(3)

Strain-energy minimisation analyses have been performed by Hambley [223] on a series of 4-, 5-, and 6-co-ordinate Ni(II) complexes incorporating $Me_4[14]aneN_4$. The results from this study indicate that four-co-ordinate square planar complexes have a strong preference for the RSRS configuration, whereas six-co-ordinate octahedral complexes exhibit a strong preference for the RRSS configuration. The evidence accummulated from crystallographic studies on $[Pd([14]aneN_4)]^{2+}$ [232,233], $[Pd(Me_4[14]aneN_4)]^{2+}$ [231], $[Pd(Bz_4[14]aneN_4)]^{2+}$ [119] and this study of trans-$[RhCl_2(Me_4[14]aneN_4)]^{+}$ is consistent with these calculations. A similar RRSS configuration for co-ordinated $Me_4[14]aneN_4$ has been observed for several Ni(II) complexes including $[Ni(Me_4[14]aneN_4)(OH_2)_2]Cl_2.2H_2O$ [234], $[Ni(Me_4[14]aneN_4)][CF_3SO_3]_2$ [234], $[\{Ni(Me_4[14]aneN_4)(N_3)\}_2(\mu\text{-}N_3)]^{+}$ [235] and $[Ni(O_2COMe)_2(Me_4[14]aneN_4)]$ [236] as well as $[Ni(Me_4[14]aneN_4)]^{2+}$ when prepared by methylation of $[Ni([14]aneN_4)]^{2+}$ [235]. Examples of Ni(II) complexes adopting the RSRS configuration include $[Ni(O_2COMe)(Me_4[14]aneN_4)]^{+}$ [236], $[Ni(Me_4[14]aneN_4)][CF_3SO_3]_2.Me_2CO.H_2O$ [223] and $[Ni(Me_4[14]aneN_4)(N_3)]^{+}$ [237].

7.3: Electrochemical Study of $[RhCl_2(Me_4[14]aneN_4)]^+$

The aim of this work was to investigate whether $Me_4[14]aneN_4$ can stabilise a monomeric Rh(II) complex.

Trans-$[RhCl_2(Me_4[14]aneN_4)]^+$ exhibits a quasi-reversible reduction at $E_{1/2}$= -0.99V *vs.* Fc/Fc^+ in MeCN (0.1M $NBu^n_4PF_6$) at platinum electrodes (Fig. 7.7). This process is assigned to a Rh(III)/(II) redox couple. Cyclic voltammetry confirmed that loss of Cl^- occurred on reduction of $[RhCl_2(Me_4[14]aneN_4)]^+$, the $Cl^{-/0}$ couple being observed near +1.0V. A daughter product can also be detected near -0.35V. As in the thioether systems described in Chapter 6, we predict that binding of Cl^- to the metal centre would be destabilised on reduction to Rh(II), due to the increase in electron-density centred on the metal. This may lead to formation of five-co-ordinate or solvated product(s) which would account for the daughter product observed in the cyclic voltammogram. This would possibly provide the opportunity of utilizing the reduction of $[RhCl_2(Me_4[14]aneN_4)]^+$ to generate an electron-rich rhodium centre incorporating a vacant co-ordination site for binding and activating small molecule substrates such as CO, O_2 and alkenes. Several attempts have been made to obtain a quantitative measurement of this reduction by coulometry. This consistently gives n>1 electron, and suggests that the process corresponds predominantly to a one-electron reduction generating a Rh(II) species. However, some further decomposition or disproportionation also occurs.

Controlled potential electrolysis of the complex measured in MeCN at a platinum gauze, at -1.1V, afforded a yellow e.s.r. active solution. The e.s.r. spectrum (measured at 77K as an MeCN glass) shows g_1= 2.110, g_2= 2.015 and g_3= 1.996 (Fig. 7.8) and is consistent with the formation of a paramagnetic Rh(II) species[105.107].

The in situ spectroelectrochemistry of $[RhCl_2(Me_4[14]aneN_4)]^+$ (measured in MeCN, 0.1M $NBu^n_4PF_6$ at 248K) was investigated using an O.T.T.L.E. system (Fig. 7.9). Reduction of the Rh(III) precursor at -1.3V results in total collapse of the charge-transfer band at λ_{max}= 222nm. This is accompanied by isosbestic growth of a new charge-transfer band on the edge of the solvent front (λ_{iso}= 206, 285nm). The shift of the band at 222nm to higher energy upon increasing the electon-density on the metal centre, is confirmation that this corresponds to a Cl⟶Rh charge-transfer transition. This species does not reoxidise at 0V, 248K. These results are consistent with the reduction being accompanied by loss of chloride, and the isosbestic nature of the process indicates that chloride loss is rapid relative to the time-scale of the experiment.

Attempts to substitute the Cl^- ligands for PR_3 (R= Et, Ph, OMe) and pyridine, by treatment of a solution of $[RhCl_2(Me_4[14]aneN_4)]PF_6$ in MeCN with $TlPF_6$ and PR_3 or pyridine were unsuccessful. This may be due to the effect of the methyl groups on nitrogen, or the inertness of the low-spin d^6 system towards substitution.

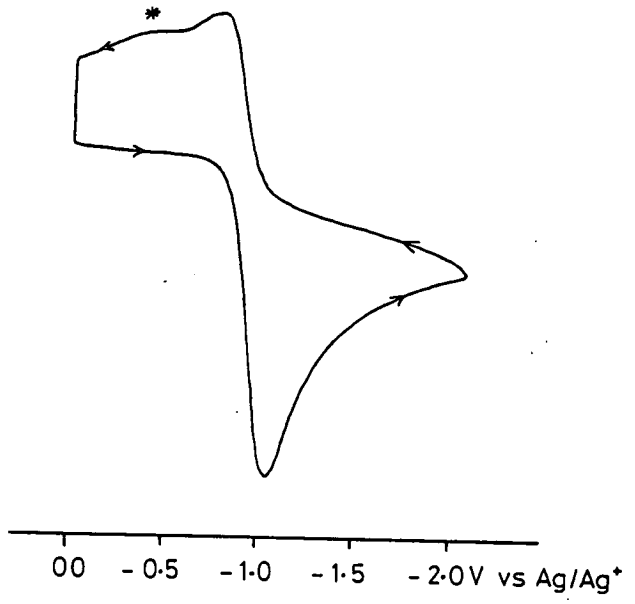

Fig. 7.7: Reductive cyclic voltammogram of $[RhCl_2(Me_4[14]aneN_4)]^+$ ($MeCN/0.1M\ NBu^n_4PF_6$)

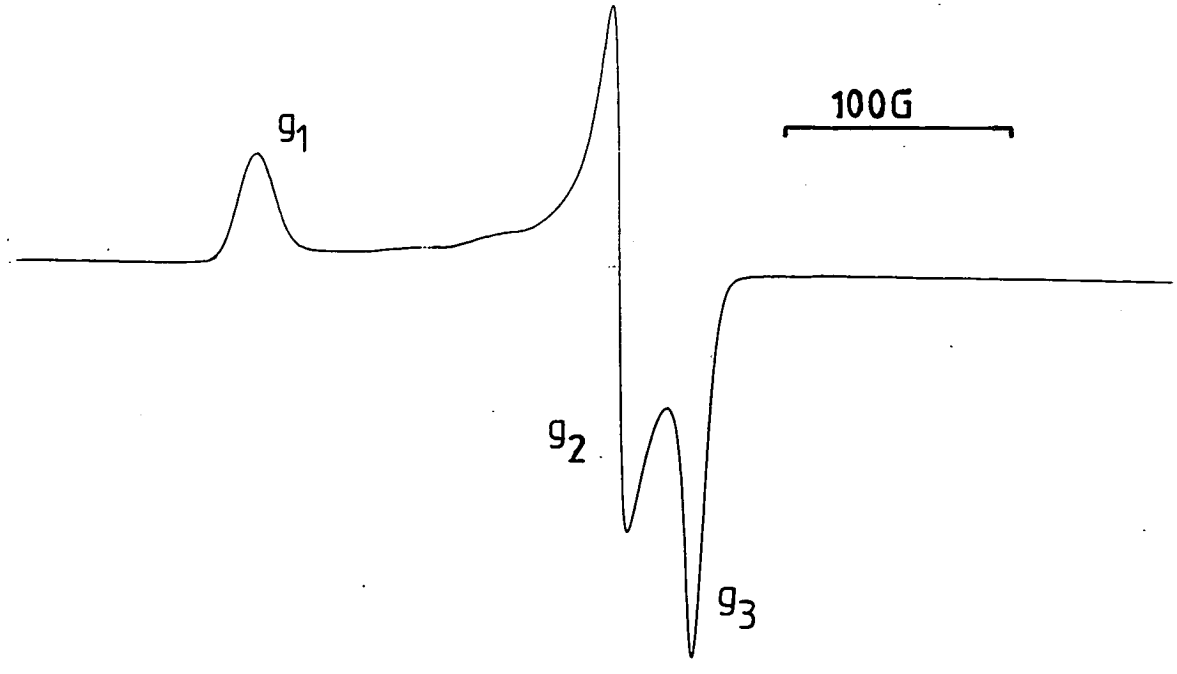

Fig. 7.8: E.s.r. spectrum of product from reduction of $[RhCl_2(Me_4[14]aneN_4)]^+$ ($MeCN/0.1M\ NBu^n_4PF_6$, 77K)

Fig. 7.9: Electronic spectrum showing reduction of $[RhCl_2(Me_4[14]aneN_4)]^+$ ($MeCN/0.1M\ NBu^n_4PF_6$, 248K)

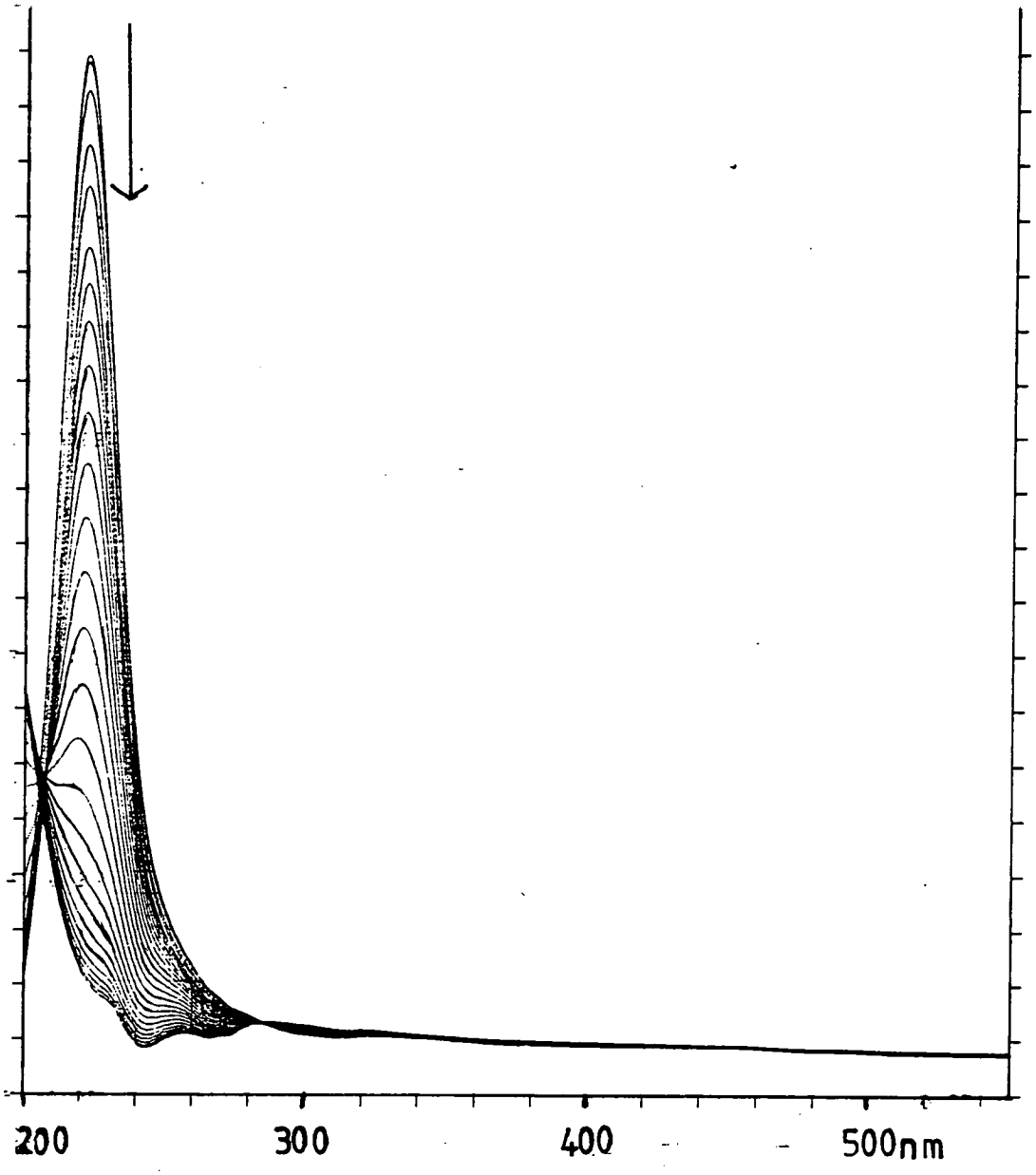

7.4: Conclusions

These results confirm that the 14-membered ring tetra-aza macrocycle, $Me_4[14]aneN_4$, can readily bind Rh(III) to afford $[RhCl_2(Me_4[14]aneN_4)]^+$ as the octahedral trans-dichloro isomer exclusively. This contrasts with the analogous tetrathia system, $[RhCl_2([14]aneS_4)]^+$, which forms only the cis-dichloro isomer (Chapter 6) and reflects the difference in size of sulphur versus the smaller nitrogen-donor atoms. Interestingly, the non-methylated analogue, $[14]aneN_4$, complexes with Rh(III) to give a mixture of cis- and trans-dichloro isomers depending upon the reaction conditions [182-185]. The RRSS configuration identified for the N-Me functions is in accord with predictions from molecular mechanics calculations, and minimises the steric interactions between the methyl groups and the Cl^- ligands.

The electrochemical study of this complex indicates that a monomeric Rh(II) species can be generated, although chloride loss is still apparent. These results show that alkylated tetra-aza macrocycles could be important ligands for the stabilisation of Rh(II) species.

7.5: Experimental

7.5.1: $[RhCl_2(Me_4[14]aneN_4)]PF_6$

$RhCl_3.H_2O$ (150mg, 0.59mmol) was treated $Me_4[14]aneN_4$ (150mg, 0.59mmol) in dry, refluxing methanol (130ml) under N_2 for 1h to give a bright orange solution. Addition of excess NH_4PF_6 yielded a golden microcrystalline product which was collected, recrystallised from MeCN and dried *in vacuo* (Yield: 230mg, 70%). Mol. wt. 575.3. Elemental analysis: found C= 29.0, H= 5.65, N= 9.71%; calculated for $[C_{14}H_{32}N_4Cl_2Rh]PF_6$ C= 29.2, H= 5.61, N= 9.74%. F.a.b. mass spectrum (dmf/glycerol matrix): found M^+= 429, 394, 358: calculated for

$[^{103}Rh^{35}Cl_2(Me_4[14]aneN_4)]^+$ M^+= 429,

$[^{103}Rh^{35}Cl(Me_4[14]aneN_4)]^+$ M^+= 394,

$[^{103}Rh(Me_4[14]aneN_4)]^+$ M^+= 359.

^1H n.m.r. spectrum (200.13MHz, CD_3CN, 293K): δ= 2.78 (s, $C\underline{H}_3$, 12H), 2.2-3.5ppm (m, $C\underline{H}_2$) (symmetric isomer): δ= 2.76, 2.75, 2.67, 2.51ppm (s, $C\underline{H}_3$, 12H), 2.2-3.5ppm (m, $C\underline{H}_2$) (asymmetric isomer). ^{13}C DEPT n.m.r. spectrum (50.32MHz, CD_3CN, 293K): δ= 23.86 ($CH_2\underline{C}H_2CH_2$, 2C), 50.69 ($\underline{C}H_3$, 4C), 61.52 ($N\underline{C}H_2CH_2\underline{C}H_2N$, 4C), 63.10ppm ($N\underline{C}H_2\underline{C}H_2N$, 4C)(symmetric isomer): δ 23.55, 24.36 ($NCH_2\underline{C}H_2CH_2N$, 2C), 47.11, 47.95, 49.87, 53.63 ($\underline{C}H_3$, 4C), 55.21, 56.12, 60.80, 60.94, 62.93 (two overlapping resonances), 63.58, 64.40ppm ($N\underline{C}H_2$, 8C) (asymmetric isomer). UV/vis spectrum (MeCN): λ_{max}= 222nm

(ε_{max} = 39,900$M^{-1}cm^{-1}$), 324 (241), 452 (631). I.R. spectrum (CsI disc): 3000w, 2940w, 1450m, 1380m, 1290m, 1240w, 1200w, 1170m, 1150w, 1110w, 1050w, 1030w, 980w, 920w, 840vs, 750m, 720w, 555v, 280w cm^{-1}.

7.5.2: $[RhCl_2(Me_4[14]aneN_4)]BPh_4$

The BPh_4^- salt was prepared by using $NaBPh_4$ in place of NH_4PF_6 in the above preparation. Mol. wt. 747.46. Elemental analysis: found C= 61.4, H= 7.02, N= 8.08, Cl= 9.89%; calculated for $[C_{10}H_{32}Cl_2N_4Rh](C_{24}H_{20}B)$: C= 60.9, H= 6.99, N= 8.48, Cl= 9.46%. ^1H n.m.r. spectrum (80MHz, CD_3CN, 298K): δ= 2.78 (s, CH_3, 12H), 2.6-3.3 (m, CH_2, 20H), 7.2-7.9ppm (m, BPh_4^-, 20H).

7.5.3: Single Crystal Structure of

$[RhCl_2(Me_4[14]aneN_4)]PF_6$

Recrystallisation of the complex from MeCN yielded orange, rhomboid crystals suitable for a single crystal X-ray structure determination.

Crystal Data:

$[C_{14}H_{32}N_4Cl_2Rh]^+PF_6^-$, M= 575.3. Orthorhombic, space group P_{nma}, a= 14.952(4), b= 10.687(3), c= 13.487(4)Å, V= 2155Å^3 (by least-squares refinement on diffraction angles for 17 centred reflections, λ= 0.71073Å), Z= 4, D_c= 1.773gcm^{-3}. Crystal dimensions 0.79x0.54x0.46mm, μ(Mo-Kα)= 11.09cm^{-1}, F(000)= 1168.

Data Collection and Processing:

Stöe STADI-4 four-circle diffractometer, ω/θ mode with ω scan-width $(1.05-0.347\tan\theta)^{o}$, graphite-monochromated Mo-Kα radiation; 1650 reflections measured ($1.5<\theta<22.5^{o}$, h $0\longrightarrow12$, k $0\longrightarrow15$, l $0\longrightarrow16$) giving 1265 with $\underline{F}>6\sigma(\underline{F})$. No significant crystal decay, no absorption correction.

Structure Analysis and Refinement:

The Rh position was deduced from a Patterson synthesis. Iterative cycles of least-squares refinement and difference Fourier syntheses revealed the positions of all other non-hydrogen atoms. Anisotropic thermal parameters were refined for Rh, Cl, P, F and N. During refinement, some disorder of the macrocyclic ligand became apparent. This could only be modelled successfully by refining the minor component as an idealised rigid group, and, for the major component, constraining all C-C and C-N bonds to be a common value of 1.523(10)Å, and all macrocyclic angles to be tetrahedral. The sum of the site occupancies for the two components were always equal to one. The discussion of the structure refers to the major component (66.3(13)%) of the disorder. We believe that the disorder arises from rotation of one component relative to the other within the crystal lattice, however, the presence of a minor isomer in the solid state cannot be entirely discounted. The weighting scheme

$\underline{w}^{-1} = \sigma^2(\underline{F}) + 0.000811\underline{F}^2$ gave satisfactory agreement analyses. At convergance, $\underline{R}$, $\underline{R}_w = 0.0715$ and 0.1153 respectively, $\underline{S} = 1.369$ for 126 independent parameters, and the final difference Fourier synthesis showed no feature above 1.26 or below $-0.74 e\text{Å}^{-3}$.

CHAPTER 8

Platinum Metal Complexes of Mixed Thia-Oxa Crowns

8.1: Introduction

Macrocyclic ligands incorporating recognition sites capable of binding both hard and soft metal guest ions are of considerable current interest, since they may facilitate electron-transfer studies and serve as models of relevance to biological redox processes [238]. They may also provide effective systems with which to monitor alkali metal concentrations in solution, due to the allosteric effect of binding two metals in close proximity to each other [239,240]. The mixed polythia-oxa-donor macrocycle, [15]aneS_2O_3 has the potential to bind soft transition metal ions via the sulphur-donor atoms, and hard alkali metal ions or polar organic substrates via the oxygen-donor atoms. This Chapter describes the co-ordination chemistry of [15]aneS_2O_3 with platinum metal ions and preliminary investigations on the binding of alkali metal ions to the crown ether receptor sites. As an introduction, a discussion of the synthesis of mixed thia-oxa macrocyclic ligands is included, as well as a brief outline of some related literature.

Ligand Synthesis

The synthesis of a series of mixed polythia-oxa macrocycles has been reported by Bradshaw and co-workers [241]. The general procedure involves a

high-dilution cyclisation of the appropriate oligoethylene glycol dichloride with ethane-1,2-dithiol (Fig. 8.1). Other mixed thia-oxa macrocycles incorporating varying numbers of sulphur and oxygen atoms are also readily prepared [241-243].

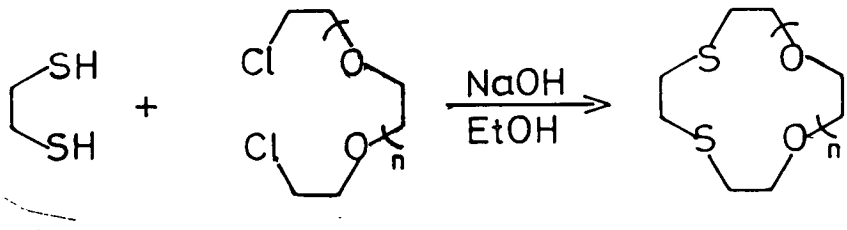

Fig. 8.1: Synthesis of mixed S- and O-donor macrocycles

The single crystal structure of [15]aneS_2O_3 [244] shows the sulphur atoms to be exodentate, with an S-C-C-S torsion angle of $-166.8(3)^{o}$, i.e. anti, placing the two sulphur atoms about 4.5A apart.

Since the discovery of crown ethers by Pederson [245,246], the selectivity of these systems and their derivatives for specific alkali metal cations has received an enormous amount of attention [247,248]. Izatt and co-workers have demonstrated that partial substitution of oxygen-donor atoms for sulphur changes the cation selectivity pattern [249]. Thus the stability of alkali and alkaline earth complexes decreases, while the affinity of the macrocycle for Ag^{+} and Hg^{2+} is enhanced.

The only examples of transition metal complexes incorporating [15]aneS_2O_3 are those of the type $[MCl(arene)([15]aneS_2O_3)]^{+}$, (M= Ru, Os), and

$[M'Cl(C_5Me_5)([15]aneS_2O_3)]^+$, (M'= Rh, Ir), prepared by treatment of $[15]aneS_2O_3$ with the appropriate dimeric chloro-bridged precursor [150]. The single crystal structure of $[RuCl(\underline{p}\text{-cymene})([15]aneS_2O_3)]^+$ shows the Ru(II) ion bound symmetrically to the two adjacent macrocyclic thioether-donors, with a chloride ion and the p-cymene ligand completing the octahedral stereochemistry, [Ru-S(1)= 2.3810(11), Ru-S(4)= 2.3773(11)Å]. The oxygen-donor atoms are oriented away from the metal centre and do not interact. Consequently, these are available for binding to alkali metal ions. The single crystal structure of $[RhCl(C_5Me_5)([15]aneS_2O_3)]^+$ exhibits a very similar stereochemistry, with Rh(III) bound octahedrally to two macrocyclic thioether-donor atoms, one Cl^- ion and the C_5Me_5 ring, [Rh-S(1)= 2.3722(13), Rh-S(4)= 2.3594(12)Å], (Fig. 8.2).

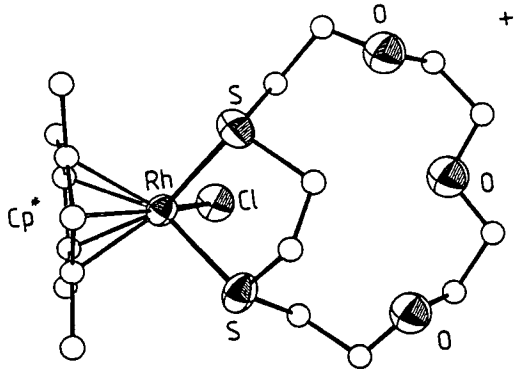

Fig. 8.2:
Single crystal structure of $[RhCl(C_5Me_5)([15]aneS_2O_3)]^+$

Few examples of transition metal complexes incorporating related macrocycles have been reported. The single crystal structure of $[PdCl_2(L)]$, (1), shows Pd(II) bound to a square planar arrangement of the two thia-donors and mutually cis-dichloro ligands, [Pd-S= 2.303(2), Pd-Cl= 2.314(2)Å]. The bidentate

co-ordination of the macrocycle via its two remote sulphur-donors necessitates that it adopts a folded conformation. Thus, the oxygen atom lone-pairs are directed away from the central metal [250].

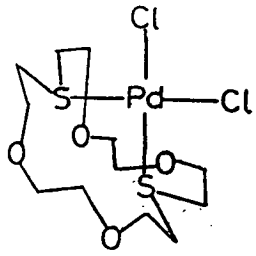

(1)

The multi-site receptor Schiff base bis(crown ether), (2) [251], in the absence of transition metal ions, binds K^+ via two co-facial benzo-15-crown-5 units with the formation of an intermolecular sandwich, to give a 1:1 ligand:K^+ stoicheiometry. Addition of Ag^+ however, generates a tetrahedral complex with Ag(I) co-ordinated to two thioether-donor atoms and two Schiff base functions. Addition of K^+ to this complex affords a 1:1:2 Ag^+:ligand:K^+ stoicheiometry (3). This ligand, (2), also forms a tetragonal complex with Cu^{2+}, and this gives a 1:1:1 Cu^{2+}:ligand^1:K^+ ratio. Thus, the presence of a transition metal imposes some conformational rigidity, and this determines the type of complex formed. More recently, Beer and co-workers have reported a catenate complex incorporating (4), with Cu(I) bound to the two bipyridal units of two interlocking ligands. Ring closure is achieved in this system by complexation of K^+ at the crown ether receptor sites [252].

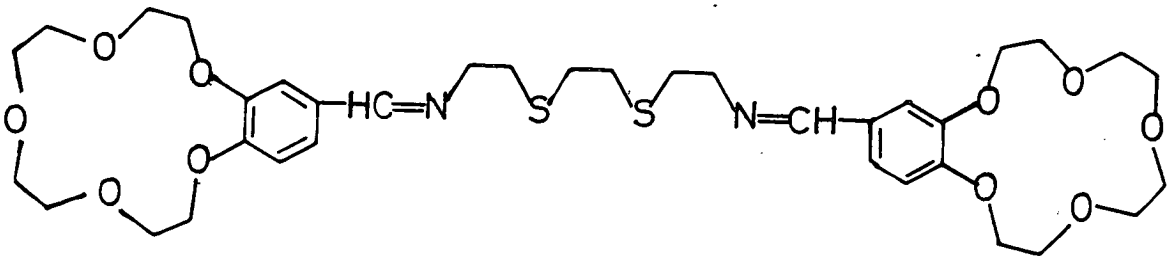

(2)

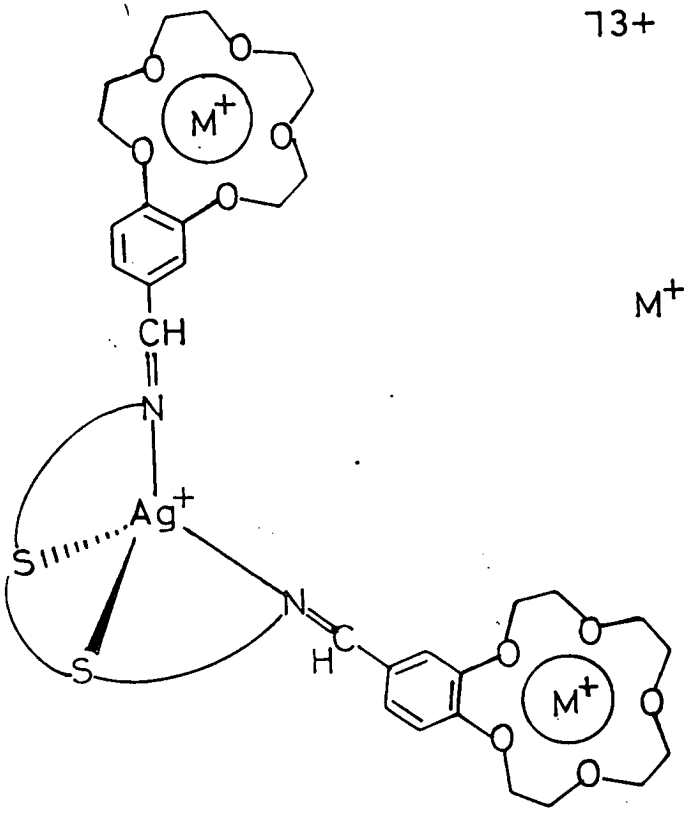

$M^+ = Na^+, K^+$ (3)

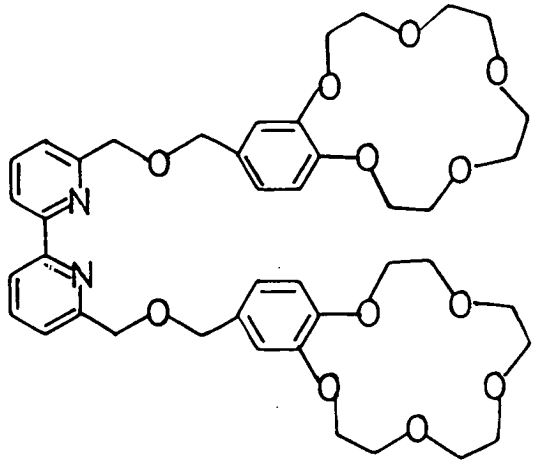

(4)

Another macrocyclic ligand has been shown to bind Ni(II) via the Schiff base and Ba(II) via the crown ether receptor sites, to give the complex-cation, (5) [253].

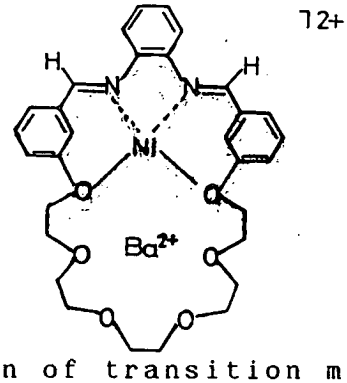

(5)

Co-ordination of transition metal fragments (e.g. $ZnCl_2$, $HgCl_2$, $PdCl_2$, $W(CO)_4$) to the nitrogen atoms of (6), enforces planarity on the bipyridyl unit [254]. Rebek and co-workers have shown that this distorts the crown ether ring so that only four of the five oxa-donors can direct their lone-pairs into the macrocyclic cavity, and this markedly diminishes subsequent binding of alkali metal ions [255]. The allosteric properties of this ligand are apparent from the observation that in the absence of a transition metal fragment this ligand transports Na^+ ions in preference to K^+, whereas binding tungsten at the bipyridyl function reverses this preference [256].

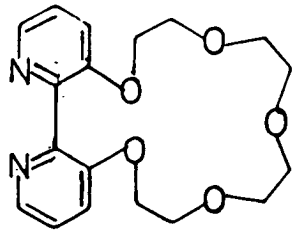

(6)

8.2: Results and Discussion

The objective of this work was to synthesise a series of platinum metal complexes incorporating [15]aneS_2O_3. Particular interest lay in the elucidation of the structures adopted by these systems, and the conformation of the co-ordinated macrocycle. Subsequently, and assessment of the possibility of binding alkali metal ions to the crown ether functions is discussed.

The macrocyclic ligand, [15]aneS_2O_3, was prepared by the method of Bradshaw and co-workers [241], and the resulting white crystalline product was fully characterised prior to use. Details of this synthesis are given in the Experimental Section.

8.2.1: Palladium

Treatment of $PdCl_2$ with one molar equivalent of [15]aneS_2O_3 in refluxing $MeOH/H_2O$ afforded a bright yellow solution. Evaporation of the solvent and recrystallisation from MeCN gave the product as an orange crystalline solid.

The f.a.b. mass spectrum of the product shows a molecular ion peak with the correct isotopic distribution at M^+= 357, corresponding to $[^{106}Pd([15]aneS_2O_3-H)]^+$. The ^1H n.m.r. spectrum shows a complex second order multiplet in the region δ= 2.28-4.18ppm, while ^{13}C DEPT n.m.r. spectroscopy shows five distinct methylene carbon

resonances at δ= 71.07, 70.33, 69.38 all $\underline{C}H_2$'s adjacent to O), 37.64 and 35.73ppm ($\underline{C}H_2$'s adjacent to S). The UV/vis spectrum of the product reveals absorption bands at λ_{max}= 394nm (ε_{max}= 975$M^{-1}cm^{-1}$) and 262 (8,820). The magnitude of these extinction coefficients suggest that the former corresponds to a d-d transition in a cis-dichloro complex, while the latter corresponds to a S$\longrightarrow$Pd or Cl$\longrightarrow$Pd charge-transfer transition. This, together with microanalytical and I.R. spectroscopic data, confirms the product as cis-[$PdCl_2$([15]aneS_2O_3)].

We were particularly interested to investigate the ability of this macrocycle to function as a receptor for both hard and soft metal ions. We proposed that binding an alkali metal ion would require more ether functions, and therefore undertook the synthesis of the bis-complex. $[Pd([15]aneS_2O_3)_2]^{2+}$.

Treatment of $PdCl_2$ with two molar equivalents of [15]aneS_2O_3 in refluxing $MeOH/H_2O$ afforded a bright yellow solution. Addition of excess NH_4PF_6 gave a yellow precipitate which was recrystallised from $MeNO_2$. The corresponding BPh_4^- salt could be isolated by replacing NH_4PF_6 with $NaBPh_4$ in the above preparation. However, recrystallisation of this salt from Me_2CO, MeCN, $MeNO_2$ or dmso resulted in rapid decomposition, giving a black material which could not be characterised. This occurred for all BPh_4^- salts incorporating this macrocycle.

The f.a.b. mass spectrum of the product reveals molecular ion peaks with the correct isotopic

distributions at M^+= 610 and 358, corresponding to $[^{106}Pd([15]aneS_2O_3)_2]^+$ and $[^{106}Pd([15]aneS_2O_3)]^+$ respectively. The ^1H n.m.r. spectrum of the complex exhibits a second order ABCD pattern at δ= 3.33-3.98ppm. The ^{13}C DEPT n.m.r. spectrum shows methylene carbon resonances at δ= 69.99, 68.84, 68.15 (all $\underline{C}H_2$'s adjacent to O) and 37.11ppm (two overlapping resonances due to $\underline{C}H_2$'s adjacent to S), indicating that the two macrocycles adopt the same conformation in solution. This, combined with microanalytical, I.R. and UV/vis spectral data, confirms the formulation $[Pd([15]aneS_2O_3)_2](PF_6)_2$. In order to elucidate the stereochemistry around the Pd ion, and to determine the conformation of the complex, a single crystal X-ray structural determination was undertaken.

8.2.2: Single Crystal Structure of

$[Pd([15]aneS_2O_3)_2](PF_6)_2$

Details of the structure solution and refinement are given in the Experimental Section. Tables of relevant bond lengths, angles and torsions are given in Tables 8.1, 8.2 and 8.3 respectively. Two ORTEP plots revealing the geometry of the cation are presented in Figs. 8.3 and 8.4.

The single crystal structure of the complex shows the Pd(II) ion sitting on a crystallographic inversion centre, and bound to a precisely co-planar arrangement of the four macrocyclic thioether-donor atoms, [Pd-S(1)= 2.3149(10), Pd-S(4)= 2.3017(10)Å], with the

angles around the Pd(II) ion being very close to 90^{o}. Notably all of the oxygen-donor atoms are directed away from the central metal ion and do not interact. The donor atoms of the two macrocycles form a near planar arrangement, but the methylene carbons make the overall conformation rather twisted. Furthermore, the conformation of the co-ordinated macrocycle in this complex is almost identical to that found for $[MCl(arene)([15]aneS_2O_3)]^+$, (M= Ir, Ru)[150].

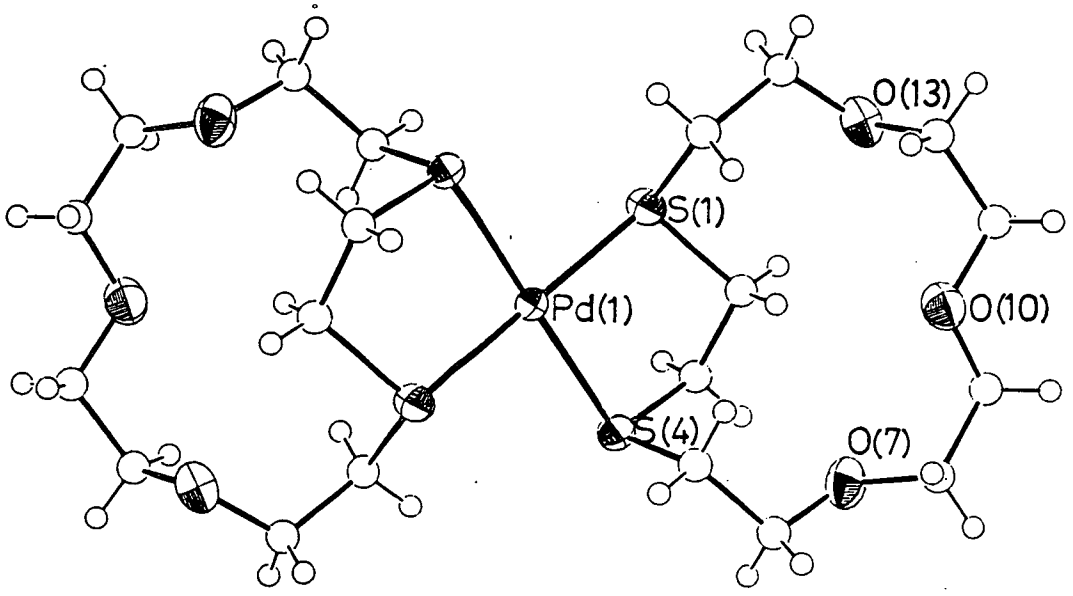

Fig. 8.3: View of the single crystal structure of $[Pd([15]aneS_2O_3)_2]^{2+}$

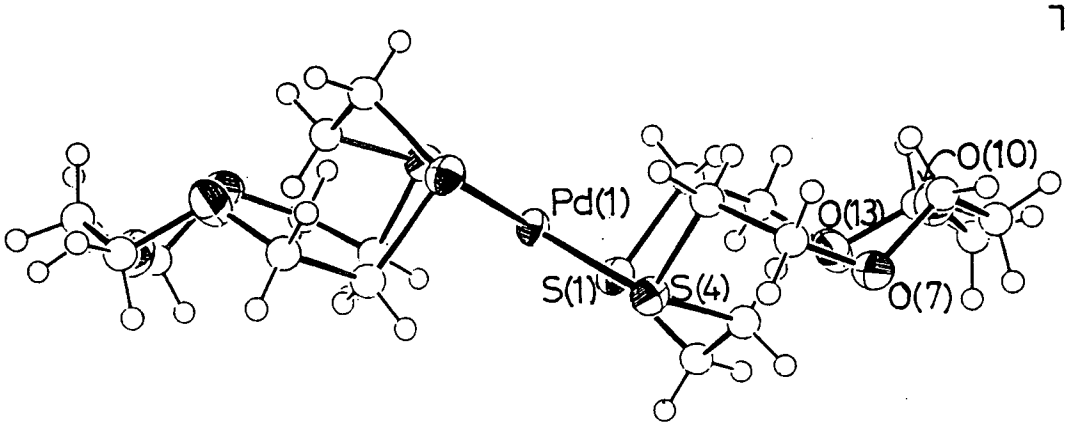

Fig. 8.4: Alternative view of the single crystal structure of $[Pd([15]aneS_2O_3)_2]^{2+}$

Single Crystal Structure of

$[Pd([15]aneS_2O_3)_2](PF_6)_2$

Table 8.1: Selected Bond Lengths(Å) with e.s.d.'s

Pd(1) - S(1)	2.3149(10)	O(7) - C(8)	1.417(6)
Pd(1) - S(4)	2.3017(10)	C(8) - C(9)	1.492(7)
S(1) - C(2)	1.818(4)	C(9) -O(10)	1.403(6)
S(1) -C(15)	1.819(5)	O(10) -C(11)	1.418(6)
C(2) - C(3)	1.507(5)	C(11) -C(12)	1.478(7)
C(3) - S(4)	1.813(4)	C(12) -O(13)	1.441(6)
S(4) - C(5)	1.821(4)	O(13) -C(14)	1.413(5)
C(5) - C(6)	1.502(7)	C(14) -C(15)	1.522(6)
C(6) - O(7)	1.406(6)		

Table 8.2: Selected Angles(°) with e.s.d.'s

S(1)-Pd(1) - S(4)	89.78(4)	C(5) - C(6) - O(7)	111.1(4)
Pd(1)- S(1) - C(2)	101.99(13)	C(6) - O(7) - C(8)	116.3(4)
Pd(1)- S(1) -C(15)	108.40(15)	O(7) - C(8) - C(9)	109.7(4)
C(2)- S(1) -C(15)	102.48(19)	C(8) - C(9) -O(10)	110.1(4)
S(1)- C(2) - C(3)	108.7(3)	C(9) -O(10) -C(11)	113.3(3)
C(2)- C(3) - S(4)	112.3(3)	O(10) -C(11) -C(12)	109.6(4)
Pd(1)- S(4) - C(3)	100.01(13)	C(11) -C(12) -O(13)	109.8(4)
Pd(1)- S(4) - C(5)	103.16(14)	C(12) -O(13) -C(14)	114.8(3)
C(3)- S(4) - C(5)	104.81(19)	O(13) -C(14) -C(15)	112.9(4)
S(4)- C(5) - C(6)	110.9(3)	S(1) -C(15) -C(14)	111.4(3)

Table 8.3: Selected Torsion Angles(^{o}) with e.s.d.'s

C(15)	- S(1)	- C(2)	- C(3)	-153.4(3)
O(7)	- C(8)	- C(9)	-O(10)	-72.9(5)
C(2)	- S(1)	-C(15)	-C(14)	-71.0(3)
C(8)	- C(9)	-O(10)	-C(11)	-171.1(4)
S(1)	- C(2)	- C(3)	- S(4)	60.1(3)
C(9)	-O(10)	-C(11)	-C(12)	-171.7(4)
C(2)	- C(3)	- S(4)	- C(5)	61.1(3)
O(10)	-C(11)	-C(12)	-O(13)	77.4(5)
C(3)	- S(4)	- C(5)	- C(6)	61.0(3)
C(11)	-C(12)	-O(13)	-C(14)	-156.3(4)
S(4)	- C(5)	- C(6)	- O(7)	-76.7(4)
C(12)	-O(13)	-C(14)	-C(15)	87.3(4)
C(5)	- C(6)	- O(7)	- C(8)	-109.8(4)
O(13)	-C(14)	-C(15)	- S(1)	69.5(4)
C(6)	- O(7)	- C(8)	- C(9)	152.3(4)

8.2.3: Platinum

The analogous Pt(II)-mono(macrocycle) and -bis(macrocycle) complexes, $[PtCl_2([15]aneS_2O_3)]$ and $[Pt([15]aneS_2O_3)_2]^{2+}$, were prepared successfully by similar methods to the Pd(II) systems.

The f.a.b. mass spectrum of $[PtCl_2([15]aneS_2O_3)]$ reveals molecular ion peaks at M^+= 483 and 447, corresponding to

$[^{195}Pt^{35}Cl([15]aneS_2O_3+H)]^+$ and

$[^{195}Pt([15]aneS_2O_3)]^+$ respectively.

The ^1H n.m.r. spectrum of this species exhibits a complex multiplet in the range δ= 2.83-4.30ppm due to the macrocyclic methylene protons, while the ^{13}C DEPT n.m.r. spectrum shows five methylene carbon resonances at δ= 70.17, 69.33, 69.00 (all due to $\underline{C}H_2$'s adjacent to O), 37.57 and 36.86ppm (two different $\underline{C}H_2$'s adjacent to S). This evidence, together with microanalytical, I.R. and UV/vis spectroscopic data, confirms that the product is cis-$[PtCl_2([15]aneS_2O_3)]$, (ν(Pt-Cl)= 330, 310cm^{-1}).

The f.a.b. mass spectrum of $[Pt([15]aneS_2O_3)_2](PF_6)_2$ exhibits molecular ion peaks with the correct isotopic distributions at M^+= 699 and 446, corresponding to

$[^{195}Pt([15]aneS_2O_3)_2]^+$ and

$[^{195}Pt([15]aneS_2O_3-H)]^+$ respectively.

The ^1H n.m.r. spectrum, [m, δ= 3.2-4.2ppm], and ^{13}C DEPT n.m.r. spectrum of this complex, [δ= 70.17, 69.33, 69.00 ($O\underline{C}H_2$), 37.57 and 36.86ppm ($S\underline{C}H_2$)] are consistent with

this assignment. This evidence, together with microanalytical, I.R. and UV/vis spectral data, confirms the formulation $[Pt([15]aneS_2O_3)_2](PF_6)_2$. Furthermore, it is likely that the cation adopts a very similar structure to its Pd(II) analogue, with square planar co-ordination of Pt(II) to the four sulphur-donor atoms, with the O-donor atoms directed away from the central metal and not interacting.

8.2.4: Rhodium

Treatment of $RhCl_3$ with two molar equivalents of $[15]aneS_2O_3$ in refluxing MeOH gave a bright yellow solution. Addition of excess NH_4PF_6 yielded an orange precipitate, which was recrystallised from $MeNO_2$ giving orange crystals.

The I.R. spectrum of this material shows a single peak at $350cm^{-1}$, attributed to a Rh-Cl stretching vibration (υ(Rh-Cl)), suggesting a trans-dichloro complex. F.a.b. mass spectrometry shows molecular ion peaks at M^+= 667 and 642. The isotopic distributions indicate that these correspond to

$[^{103}Rh^{35}Cl_2([15]aneS_2O_3)_2]^+$ and

$[^{103}Rh^{35}Cl([15]aneS_2O_3)_2]^+$ respectively.

The ^1H n.m.r. spectrum of this complex shows a second order multiplet at δ= 2.67-4.30ppm due to the methylene protons, and the ^{13}C DEPT n.m.r. spectrum shows five distinct methylene carbon resonances at δ= 69.55, 69.40, 67.85 ($\underline{C}H_2$'s adjacent to O), 36.59 and 33.53ppm ($\underline{C}H_2$'s

adjacent to S), consistent with the presence of only one isomer in solution, in which the macrocyclic ligands adopt a common conformation. It is likely that this is the same as that identified in the Pd(II) and Pt(II) complexes discussed above. Two absorption bands at λ_{max}= 435nm (ε_{max}= 132$M^{-1}cm^{-1}$) and 283 (32,970) are apparent in the UV/vis spectrum of the complex. The former corresponds to a d-d transition, and furthermore, the magnitude of the extinction coefficient is comparable to that measured for trans-$[RhCl_2([16]aneS_4)]^+$ (Chapter 6), suggesting a trans-dichloro isomer. All of these data, as well as microanalyses, are consistent with the formulation trans-$[RhCl_2([15]aneS_2O_3)_2]PF_6$.

8.2.5: Iridium

The analogous iridium(III) complex was prepared by a similar method to that employed for rhodium(III).

The f.a.b. mass spectrum of the complex shows molecular ion peaks at M^+= 767, 733, 696 and 444. The isotopic distributions based on ^{193}Ir are consistent with

$[Ir^{35}Cl_2([15]aneS_2O_3)_2]^+$,

$[Ir^{35}Cl([15]aneS_2O_3)_2+H)]^+$,

$[Ir([15]aneS_2O_3)_2-H]^+$ and

$[Ir([15]aneS_2O_3)-H]^+$ respectively.

The ^1H n.m.r. [m, δ= 3.3-4.2ppm, $C\underline{H}_2$] and ^{13}C DEPT n.m.r. spectra [δ= 69.68, 69.54, 67.57 ($OC\underline{H}_2$), 35.76 and 32.60ppm ($SC\underline{H}_2$)] both confirm the presence of one symmetrical isomer in solution, as identified for each

previous [15]aneS$_2$O$_3$ complex. All of these data, together with microanalytical, I.R. and UV/vis spectral data, are consistent with the formulation trans-[IrCl$_2$([15]aneS$_2$O$_3$)$_2$]PF$_6$.

8.2.6: Ruthenium

Treatment of RuCl$_2$(PPh$_3$)$_3$ with two molar equivalents of [15]aneS$_2$O$_3$ in refluxing MeOH yielded a yellow solution. Addition of excess NH$_4$PF$_6$ gave a yellow precipitate, which was recrystallised from CH$_2$Cl$_2$.

The f.a.b. mass spectrum of this product exhibits molecular ion peaks with the correct isotopic distributions based on ^{101}Ru and ^{35}Cl, at M$^+$= 1047, 904, 650 and 640. These correspond to

[RuCl(PPh$_3$)([15]aneS$_2$O$_3$)$_2$PF$_6$]$^+$,

[RuCl(PPh$_3$)([15]aneS$_2$O$_3$)$_2$+2H]$^+$,

[RuCl(PPh$_3$)([15]aneS$_2$O$_3$)]$^+$ and

[RuCl([15]aneS$_2$O$_3$)$_2$]$^+$ respectively.

The ^{1}H n.m.r. spectrum of this species shows a multiplet at δ= 7.3-8.0ppm corresponding to the aromatic protons of PPh$_3$. A further complex multiplet is evident at δ= 2.0-4.3ppm due to the macrocyclic protons. A 1:2 PPh$_3$:[15]aneS$_2$O$_3$ stoicheiometry is observed. The ^{13}C DEPT n.m.r. spectrum shows, in addition to a series of CH resonances at around 130ppm (due to the phenyl rings), five distinct macrocyclic methylene carbon resonances at δ= 69.35, 68.55, 68.41 (O<u>C</u>H$_2$), 32.08 and 30.84ppm (S<u>C</u>H$_2$). This evidence, together with microanalytical and I.R.

spectral data, enabled formulation of the complex as $[RuCl(PPh_3)([15]aneS_2O_3)_2]PF_6$. Only one isomer exists in solution, and the two macrocyclic ligands are symmetrical, adopting the same conformation.

Recently it has been shown that the binding of Li^+ to aza-15-crown-5 linked ferrocene, (7), results in a shift in the ferrocene oxidation wave to more positive potentials [257]. Also, Green and co-workers have demonstrated that addition of Na^+, K^+ or Li^+ to the tungsten(IV) complex, (8), results in significant changes in both the $E_{1/2}$ values and the peak separations [258]. This is attributed to binding of the alkali metal ions to the crown ether ligands. Thus, having prepared a series of platinum metal complexes incorporating $[15]aneS_2O_3$ we were interested to determine whether the crown ether units would bind alkali metal cations, and, if so, whether this would have any effect upon the redox characteristics of the complex. Initially therefore, an electrochemical study of the bis(macrocycle) complexes was undertaken.

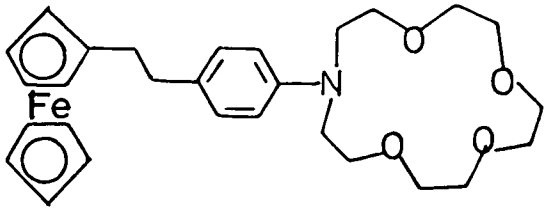

(7)

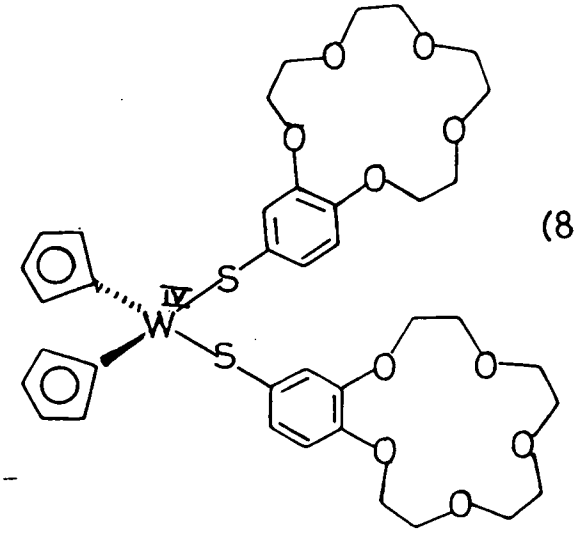

(8)

Cyclic voltammetry of $[Pd([15]aneS_2O_3)_2](PF_6)_2$ measured in MeCN (0.1M $NBu^n_4PF_6$ supporting electrolyte) at platinum electrodes shows two irreversible reductions at E_{pc}= -0.75 and 1.20V *vs.* Fc/Fc^+ (at a scan-rate of $200mVs^{-1}$. No oxidative activity is observed within the range of the solvent (0 to +2.0V). These results suggest that this complex would not be particularly useful to monitor the binding of alkali metal ions since E_{pc} varies considerably with both temperature and scan-rate.

Cyclic voltammetry of $[RuCl(PPh_3)([15]aneS_2O_3)_2]PF_6$ under similar conditions shows a fully reversible oxidation at $E_{1/2}$= +0.85V *vs.* Fc/Fc^+ (ΔE_p= 80mV at a scan-rate of $180mVs^{-1}$), assigned to a Ru(II)/(III) redox couple. This system may therefore be better suited for monitoring any shifts in $E_{1/2}$ upon addition of alkali metal ions. However, no peak shift was observed on addition of Na^+ ions.

In order to assess whether $[15]aneS_2O_3$ would bind alkali metal ions, an n.m.r. study was undertaken. ^{13}C DEPT n.m.r. spectra of $[15]aneS_2O_3$ in the presence of differing quantities of Na^+ (varying from 0.2 to 2.2 equivalents) were recorded, and compared with free $[15]aneS_2O_3$. No significant shifts in the positions of the resonances were apparent. Thus it was concluded that $[15]aneS_2O_3$ does not bind Na^+. The reason may be that this particular macrocycle incorporates too few oxa-donor atoms, and because the two soft thioether-donors will

tend to destabilise binding of alkali metal ions. Time did not permit investigation of the binding of other alkali metal ions or the effect of increasing the concentrations.

Addition of two equivalents of glycine to a solution of $[Pd([15]aneS_2O_3)_2](PF_6)_2$ has no effect upon the positions of the $\underline{C}H_2$ resonances, suggesting that organic substrates do not bind to $[15]aneS_2O_3$, presumably for the same reasons.

8.3: Conclusions

These results show that the mixed thia/oxa-donor macrocycle, [15]aneS_2O_3, co-ordinates readily to a range of platinum group metals to give both mono- and bis-macrocyclic complexes. In each case binding is via the two adjacent sulphur-donor atoms, leaving the non-interacting oxa-donors directed away from the metal.

Preliminary attempts to bind alkali metal ions via the crown ether functions proved unsuccessful. This is attributed to the number of O-donor atoms being too few, as well as incorporation of soft S-donors within the macrocyclic ring, which are not optimal for binding hard alkali metal ions. It is likely that the larger macrocycles [21]aneS_2O_5 (9) and [24]aneS_2O_6 (10) may be better suited to accommodate both transition metal and alkali metal ions.

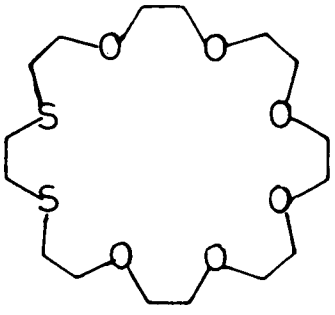

(9)

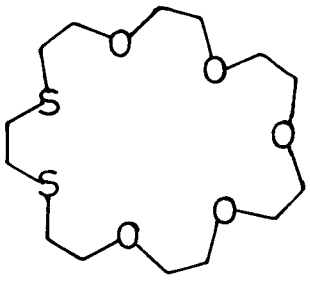

(10)

8.4: Experimental

8.4.1: [15]aneS_2O_3

A.: Preparation of 1,11-dichloro-3,6,9-trioxaundecane [259]

Tetraethylene glycol (0.692mol) and pyridine (1.54mol) were added to a flask containing benzene (550ml). The reaction mixture was heated to reflux, and $SOCl_2$ (1.54mol) was added dropwise over a period of 1h. Refluxing for a further 16h gave a brown solution and precipitate. After cooling, 15ml conc. HCl diluted with 50ml H_2O was added dropwise over 10mins. The aqueous layer was then removed and the organic layer was dried over $MgSO_4$. Removal of benzene gave a brown oil which was distilled at 96°C/0.4mmHg to afford a light yellow oil (Yield: 121.3ml, 76%). Mol. wt. 321.12. Elemental analysis: found C= 41.4, H= 6.98, Cl= 31.4%; calculated for $C_8H_{16}Cl_2O_3$: C= 41.6, H= 6.98, Cl= 30.7%. E.I. mass spectrum: found M^+= 230; calculated for $C_8H_{16}Cl_2O_3$ M^+= 230. ^1H n.m.r. spectrum (80.13MHz, $(CD_3)_2CO$, 298K): δ= 3.62 (s, $OC\underline{H}_2C\underline{H}_2O$, 8H), 3.73-3.67ppm (m, $ClC\underline{H}_2C\underline{H}_2O$, 8H).

B.: Cyclisation

1,11-Dichloro-3,6,9-trioxaundecane (121g, 0.524mol) and ethane-1,2-dithiol (49.4g, 0.524mol) were added dropwise, at the same rate, over a period of 6h, with stirring, to a refluxing solution of NaOH (44g) in dry EtOH (800ml). The resulting mixture was refluxed for a further 5h. After cooling, the excess base was

neutralised with HCl, and the precipitate filtered. After removing the EtOH, the orange oil was extracted with 3x300ml portions of diethyl ether. The combined ether extract was then dried ($MgSO_4$) and the ether removed. The resulting orange oil was then distilled via Kugeröre at 147°C/0.1mmHg to give a pale yellow oil. Recrystallisation from 50:50 benzene:hexane afforded the product as a white crystalline solid (Yield: 23.4g, 18%). Mol. wt. 252.39. Elemental analysis: found C= 47.6, H= 8.02, S= 25.1%; calculated for $C_{10}H_{20}O_3S_2$; C= 47.6, H= 7.94, S= 25.4%. M.Pt.= 49-51°C. E.I. mass spectrum: found M^+= 252; calculated for $C_{10}H_{20}O_3S_2$ M^+= 252. ^1H n.m.r. spectrum (80.13MHz, $CDCl_3$, 298K): δ= 2.72 (t, $SC\underline{H}_2CH_2O$, 4H), 2.87 (s, $SC\underline{H}_2C\underline{H}_2S$, 4H), 3.64 (s, $OC\underline{H}_2C\underline{H}_2O$, 8H), 3.75ppm (t, $OC\underline{H}_2CH_2S$, 4H). ^{13}C DEPT n.m.r. spectrum (50.32MHz, $CDCl_3$, 298K): δ= 72.69, 71.22, 70.09 (3x$O\underline{C}H_2$), 33.00, 31.62ppm (2x$S\underline{C}H_2$).

8.4.2: $[PdCl_2([15]aneS_2O_3)]$

Treatment of $PdCl_2$ (40mg, 0.226mmol) with $[15]aneS_2O_3$ (57mg, 0.226mmol) in refluxing $MeOH/H_2O$ (1:1v.v., 35ml) for 2h under N_2 afforded a bright yellow solution. Removal of solvent yielded an orange precipitate which was recrystallised from EtOH (Yield: 97mg, 83%). Mol. wt. 429.69. Elemental analysis: found C= 27.7, H= 4.68, Cl= 16.3%; calculated for $[C_{10}H_{20}Cl_2O_3S_2Pd]$: C= 28.0, H= 4.69, Cl= 16.5%. F.a.b. mass spectrum (3-NOBA matrix): found M^+= 357. Calculated

for $[^{106}Pd([15]aneS_2O_3)]^+$ M^+= 358. ^1H n.m.r. spectrum (200.13MHz, CD_3CN, 298K): δ= 2.28-4.18ppm (m, 20H). ^{13}C DEPT n.m.r. spectrum (50.32MHz, CD_3CN, 298K): δ= 71.07, 70.33, 69.38 (3xOCH_2), 37.64, 35.73ppm (2xSCH_2). UV/vis spectrum (MeCN): λ_{max}= 394nm (ε_{max}= 975$M^{-1}cm^{-1}$), 262 (8,820). I.R. spectrum (KBr disc): 3000w, 2920m, 2860m, 1480w, 1460m, 1440w, 1385m, 1360m, 1350w, 1315m, 1290w, 1260w, 1250m, 1195w, 1130m, 1105vs, 1080m, 1060w, 1040w, 1020w, 990m, 940w, 910m, 900m, 870w, 840m, 820m, 790w, 780w, 615w, 560w, 520w, 360w, 340m, 320m, 300m cm^{-1}.

8.4.3: $[PtCl_2([15]aneS_2O_3)]$

Method as for 8.4.2 using $PtCl_2$ (29mg, 0.113mmol) and $[15]aneS_2O_3$ (30mg, 0.113mmol). The product was isolated as a yellow solid (Yield: 33mg, 56%). Mol. wt. 518.29. Elemental analysis: found C= 22.8, H= 3.81, Cl= 14.1, S= 11.9%; calculated for $[C_{10}H_{20}Cl_2O_3S_2Pt]$: C= 23.2, H= 3.89, Cl= 13.7, S= 12.4%. F.a.b. mass spectrum (3-NOBA matrix): found M^+= 483 and 447. Calculated for

$[^{195}Pt^{35}Cl([15]aneS_2O_3)]^+$ M^+= 482,

$[^{195}Pt([15]aneS_2O_3)]^+$ M^+= 447.

^1H n.m.r. spectrum (200.13MHz, CD_3NO_2, 298K): δ= 2.83-4.30ppm (m, 20H). ^{13}C DEPT n.m.r. spectrum (50.32MHz, CD_3NO_2, 333K): δ= 70.70, 70.59, 69.60 (3xOCH_2), 37.85, 35.86ppm (2xSCH_2). UV/vis spectrum (MeCN): λ_{max}= 310nm (ε_{max}= 778$M^{-1}cm^{-1}$), 204 (10,780).

I.R. spectrum (KBr disc): 3000w, 2980w, 2920m, 2860m, 1480w, 1460m, 1440m, 1385vs, 1360m, 1350w, 1310m, 1290w, 1245m, 1190m, 1130vs, 1105vs, 1080vs, 1040m, 1020vs, 985m, 970m, 940m, 910m, 900m, 870w, 840m, 820m, 790w, 655w, 615w, 560w, 520m, 490w, 480w, 450w, 440w, 380w, 360w, 330m, 310m cm^{-1}.

8.4.4: $[Pd([15]aneS_2O_3)_2](PF_6)_2$

$PdCl_2$ (30mg, 0.169mmol) was added to a solution of $[15]aneS_2O_3$ (86mg, 0.338mmol) in $MeOH/H_2O$ (1:1v.v., 30ml). The reaction mixture was refluxed for 2h under N_2, yielding a bright yellow solution. Addition of excess NH_4PF_6 gave a yellow precipitate which was collected and recrystallised from $MeNO_2$ (Yield: 110mg, 73%). Mol. wt. 901.09. Elemental analysis: found C= 26.4, H= 4.43, S= 15.2%; calculated for $[C_{20}H_{40}O_6S_4Pd](PF_6)_2$: C= 26.7, H= 4.47, S= 14.3%. F.a.b. mass spectrum (3-NOBA matrix): found M^+= 610 and 358. Calculated for

$[^{106}Pd([15]aneS_2O_3)_2]^+$ M^+= 610,

$[^{106}Pd([15]aneS_2O_3)]^+$ M^+= 358.

^1H n.m.r. spectrum (200.13MHz, $(CD_3)_2CO$, 298K): ABCD pattern, δ= 3.33-3.98ppm (m, 40H). ^{13}C DEPT n.m.r. spectrum (50.32MHz, CD_3CN, 298K): δ= 69.99, 68.84, 68.15 ($3xO\underline{C}H_2$), 37.11ppm ($S\underline{C}H_2$, two overlapping resonances). UV/vis spectrum (MeCN): λ_{max}= 305nm (ε_{max}= 32,790$M^{-1}cm^{-1}$). I.R. spectrum (KBr disc): 2980w, 2920m, 2860m, 1470m, 1455m, 1395m, 1365m, 1300m, 1260w, 1200w, 1180w, 1120vs, 1090vs, 1040m, 1020w, 965w, 930m,

840vs, 780m, 740w, 555vs, 480w cm^{-1}.

8.4.5: Single Crystal Structure of

$[Pd([15]aneS_2O_3)_2](PF_6)_2$

Orange plates of suitable quality for a single crystal X-ray structure determination were obtained by vapour diffusion of diethyl ether into a solution of the complex in MeCN.

Crystal Data:

$[C_{20}H_{40}O_6S_4Pd](PF_6)_2$. Mol. wt. 901.09. Monoclinic, space group $P2_1/c$, a= 10.394(4), b= 14.003(4), c= 11.675(5)Å, β= 104.22°, V= 1647Å^3 (by least-squares refinement on diffraction angles for 25 centred reflections, λ= 0.71073Å), Z= 2, D_c= 1.82gcm^{-3}. Crystal dimensions 0.10x0.75x0.10mm, μ(Mo-Kα)= 9.07cm^{-1}, F(000)= 912.

Data Collection and Processing:

Stöe STADI-4 four-circle diffractometer, $\omega/2\theta$ mode with ω scan-width $(1.2+0.34\tan\theta)^\circ$, graphite-monochromated Mo-Kα radiation: 2808 unique reflections measured (2θ= 45°, h -12→12, k 0→16, l 0→12) giving 2402 with $F>6\sigma(F)$. No significant crystal decay.

Structure Analysis and Refinement:

Intensity statistics strongly implied the

location of the Pd ion at (1/2,1/2,1/2). This was input into DIRDIF which located all other non-H atoms. The structure was developed by iterative cycles of least-squares refinement and difference Fourier synthesis. At isotropic convergence, correction for absorption was made using DIFABS (maximum transmission factor= 1.290, minimum= 0.875). Anisotropic thermal parameters were refined for all non-H atoms. H atoms were included at fixed, calculated positions. The weighting scheme $\underline{w}^{-1} = \sigma^2(\underline{F}) + 0.000187\underline{F}^2$ gave satisfactory agreement analyses. At final convergence, $\underline{R}$, $\underline{R}_w$= 0.0394 and 0.0537 respectuvely, $\underline{S}$= 1.195 for 205 independent parameters, and the final difference Fourier synthesis showed no feature above +0.67 or below -0.51e$\mathring{A}^3$.

8.4.6: $[Pt([15]aneS_2O_3)_2](PF_6)_2$

Method as for 8.4.4, using $PtCl_2$ (40mg, 0.150mmol) and $[15]aneS_2O_3$ (76mg, 0.301mmol). The product was isolated as a cream-coloured solid (Yield: 74mg, 50%). Mol. wt. 989.69. Elemental analysis: found C= 24.2, H= 4.10, S= 13.4%; calculated for $[C_{20}H_{40}O_6S_4Pt](PF_6)_2$: C= 24.3, H= 4.07, S= 13.0%. F.a.b. mass spectrum (3-NOBA matrix): found M^+= 699 and 446. Calculated for

$[^{195}Pt([15]aneS_2O_3)_2]^+$ M^+= 699,

$[^{195}Pt([15]aneS_2O_3)]^+$ M^+= 447.

^1H n.m.r. spectrum (80.13MHz, CD_3CN, 298K): δ= 3.2-4.2ppm (m, 40H). ^{13}C DEPT n.m.r. spectrum (50.32MHz, CD_3CN,

298K): δ= 70.17, 69.33, 69.00 (3xO$\underline{C}H_2$), 37.57, 36.86ppm (S$\underline{C}H_2$). UV/vis spectrum (MeCN): λ_{max}= 326nm (ε_{max}= 158$M^{-1}cm^{-1}$), 249 (9,150). I.R. spectrum (KBr disc): 3020w, 2920m, 2860w, 1475m, 1455m, 1415m, 1400m, 1365m, 1350w, 1300m, 1260w, 1245w, 1195m, 1180w, 1120vs, 1090m, 1065w, 1040m, 1020w, 965w, 930m, 840vs, 775m, 740w, 660w, 610w, 555vs, 480w cm^{-1}.

8.4.7: $[RhCl_2([15]aneS_2O_3)_2]PF_6$

$RhCl_3.3H_2O$ (30mg, 0.114mmol) was added to a refluxing solution of $[15]aneS_2O_3$ (57mg, 0.228mmol) in MeOH (30ml). The reaction mixture was refluxed for 4h under N_2, yielding a bright yellow solution. Addition of excess NH_4PF_6 gave an orange precipitate which was collected and recrystallised from $MeNO_2$ (Yield: 85mg, 91%). Mol. wt. 823.63. Elemental analysis: found C= 28.5, H= 4.84, Cl= 8.77, S= 16.6%; calculated for $[C_{20}H_{40}Cl_2O_6S_4Rh]PF_6$: C= 29.2, H= 4.89, Cl= 8.61, S= 15.6%. F.a.b. mass spectrum (3-NOBA matrix): found M^+= 677 and 642. Calculated for

$[^{103}Rh^{35}Cl_2([15]aneS_2O_3)_2]^+$ M^+= 677,

$[^{103}Rh^{35}Cl([15]aneS_2O_3)_2]^+$ M^+= 642.

^1H n.m.r. spectrum (200.13MHz, CD_3CN, 298K): δ= 2.67-4.30ppm (m, 40H). ^{13}C DEPT n.m.r. spectrum (50.32MHz, CD_3CN, 298K): δ= 69.55, 69.40, 67.85 (3xO$\underline{C}H_2$), 38.59, 33.53ppm (2xS$\underline{C}H_2$). UV/vis spectrum (MeCN): λ_{max}= 435nm (ε_{max}= 132$M^{-1}cm^{-1}$), 283 (32,970). I.R. spectrum (KBr disc): 3000w, 2900m, 2860m, 1535m, 1460m,

1420w, 1400m, 1360m, 1345w, 1290vs, 1240m, 1210w, 1195m, 1170m, 1140vs, 1100vs, 1080vs, 1050m, 1020m, 1005w, 935m, 920m, 895m, 875m, 840vs, 775m, 665m, 555vs, 485m, 470m, 450w, 350m cm^{-1}.

8.4.8: $[IrCl_2([15]aneS_2O_3)_2]PF_6$

Method as for 8.4.7, using $IrCl_3.3H_2O$ (75mg, 0.213mmol) and $[15]aneS_2O_3$ (108mg, 0.425mmol). The product was isolated as a pale yellow solid (Yield: 55mg, 28%). Mol. wt. 912.84. Elemental analysis: found C= 26.0, H= 4.27, S= 13.2%; calculated for $[C_{20}H_{40}Cl_2O_6S_4Ir]PF_6$: C= 26.3, H= 4.42, S= 14.0%. F.a.b. mass spectrum (3-NOBA matrix): found M^+= 767, 733, 696 and 444. Calculated for

$[^{193}Ir^{35}Cl_2([15]aneS_2O_3)_2]^+$ M^+= 767,

$[^{193}Ir^{35}Cl([15]aneS_2O_3)_2]^+$ M^+= 732,

$[^{193}Ir([15]aneS_2O_3)_2]^+$ M^+= 697,

$[^{193}Ir([15]aneS_2O_3)]^+$ M^+= 445.

^1H n.m.r. spectrum (80.13MHz, CD_3CN, 298K): δ= 3.3-4.2ppm (m, 40H). ^{13}C DEPT n.m.r. spectrum (50.32MHz, CD_3CN, 298K): δ= 69.68, 69.54, 67.67 (3xOCH_2), 35.76, 32.60ppm (2xSCH_2). UV/vis spectrum (MeCN): λ_{max}= 236nm (ε_{max}= 24,860$M^{-1}cm^{-1}$). I.R. spectrum (KBr disc): 3000w, 2900m, 2860m, 1460m, 1405m, 1360m, 1350w, 1290m, 1240w, 1205w, 1135m, 1110m, 1100m, 1070m, 1050w, 1015w, 1000w, 935m, 895w, 840vs, 740w, 555vs, 485w, 470w, 330m, 315m, 300m cm^{-1}.

8.4.9: $[RuCl(PPh_3)([15]aneS_2O_3)_2]PF_6$

Treatment of $RuCl_2(PPh_3)_3$ (100mg, 0.104mmol) with $[15]aneS_2O_3$ (53mg, 0.208mmol) in refluxing MeOH (30ml) for 2h afforded a yellow solution. Addition of excess NH_4PF_6 gave a yellow precipitate which was recrystallised from CH_2Cl_2 (Yield: 100mg, 92%). Mol. wt. 1021.48. Elemental analysis: found C= 44.1, H= 5.35%; calculated for $[C_{38}H_{55}ClO_6PS_4Ru]PF_6$: C= 44.7, H= 5.43%. F.a.b. mass spectrum (3-NOBA matrix): found M^+= 1047, 904, 650 and 640. Calculated for

$[^{101}Ru^{35}Cl(PPh_3)([15]aneS_2O_3)_2PF_6]^+$ M^+= 1047,

$[^{101}Ru^{35}Cl(PPh_3)([15]aneS_2O_3)_2]^+$ M^+= 902,

$[^{101}Ru^{35}Cl(PPh_3)([15]aneS_2O_3)]^+$ M^+= 650,

$[^{101}Ru^{35}Cl([15]aneS_2O_3)_2]^+$ M^+= 640.

^1H n.m.r. spectrum (80.13MHz, $(CD_3NO_2$, 298K): δ= 7.3-8.0 (m, Ph, 15H), 2.0-4.3ppm (m, $C\underline{H}_2$, 40H). ^{13}C DEPT n.m.r. spectrum (50.32MHz, CD_3NO_2, 298K): δ= 134.12, 133.97, 133.28, 133.08, 132.90, 129.57, 127.48, 127.34, 127.15 ($\underline{C}H$ of phenyl rings), 69.35, 68.55, 68.41 ($3xO\underline{C}H_2$), 32.08, 30.84ppm ($2xS\underline{C}H_2$). I.R. spectrum (KBr disc): 3040w, 2920m, 2860m, 1585w, 1570w, 1480m, 1455w, 1430m, 1410m, 1360m, 1290m, 1240w, 1190w, 1130m, 1110m, 1090m, 1000w, 840vs, 750m, 700vs, 555vs, 530vs, 515m, 505w, 465w cm^{-1}.

APPENDIX

Experimental Techniques

Reagents:

All solvents were purified according to standard procedures [260]. Commercial $RuCl_3$, $RhCl_3$, $IrCl_3$, $PdCl_2$, $PtCl_2$, $K_2[PdCl_4]$ and $K_2[PtCl_4]$ (Johnson Matthey plc) were used as supplied.

$NBu^n_4PF_6$ was prepared from 40% $[NBu^n_4]OH$ (Aldrich) and 65% HPF_6 (Strem) and recrystallised from MeOH. "Dried, distilled" grade MeCN (Fisons) was used without further purification.

The ligands:-

1,4,7,10-tetrathia-7,16-diazacyclooctadecane ([18]aneN$_2$S$_4$) (Lancaster Synthesis),

1,4,7,10-tetrathiacyclododecane, ([12]aneS$_4$).

1,4,8,11-tetrathiacyclotetradecane, ([14]aneS$_4$),

1,5,9,13-tetrathiacyclohexadecane, ([16]aneS$_4$),

1,4,8,11,15,18,22,25-octathiacyclooctacosane, ([28]aneS$_8$),

1,4,7,10,13-pentathiacyclopentadecane, ([15]aneS$_5$).

1,4,7,10,13,16-hexathiacyclooctadecane, ([18]aneS$_6$) (Aldrich) and

1,4,8,11-tetramethyl-1,4,8,11-tetraazacyclotetradecane, (Me_4[14]aneN$_4$) (Strem) were used as supplied.

1,4-Dithia-7,10,13-trioxacyclopentadecane, ([15]aneS$_2$O$_3$) was prepared by the method of Bradshaw and co-workers [241].

Infra-red spectra (4000-200cm^{-1}) were recorded on a Perkin-Elmer 598 spectrometer using the KBr or CsI

method. ^{1}H n.m.r.spectra were measured on Brucker WP80, Brucker WP200 and WH360 instruments operating at 80.13MHz, 200.13MHz and 360.13MHz respectively. ^{13}C DEPT n.m.r. spectra were run on a Brucker WP200 or WH360 operating at 50.32MHz and 90.56MHz respectively. Fast atom bombardment (f.a.b.) mass spectra were run on a Kratos MS 50TC spectrometer using 3-nitrobenzyl alcohol (3-NOBA) matrix unless otherwise stated. Electronic spectra were run on a Pye-Unican SP8-400 UV/vis or a Lambda-9 UV/vis/NIR spectrophotometer using quartz cells.

Electrochemical measurements were recorded on a Brucker 310 Universal Modular Polarograph. Cyclic voltammetric studies were undertaken using a three electrode potentiostat system in MeCN with 0.1M tetrabutylammonium hexafluorophosphate ($NBu^{n}_{4}PF_{6}$) supporting electrolyte (unless otherwise stated). Platinum button microelectrodes were employed as auxiliary and working electrodes with a Ag/AgCl reference electrode, and the test solutions were purged with a stream of dry argon gas prior to their study. All potentials are quoted versus Fc/Fc^{+} unless otherwise stated. Controlled potential electrolysis and coulometry were carried out in a three-compartment cell, also using a three electrode system, with a Pt basket and Pt gauze as the respective working and auxiliary electrodes.

The electrogenerated species were transferred via syringe, with rigorous exclusion of air, to pre-cooled e.s.r. tubes, which were then closed with a tap. The

transferred solutions were immediately frozen in liquid nitrogen.

X-band electron spin resonance (e.s.r.) spectra were recorded using a Brucker ER-200D spectrometer employing 100KHz field modulation. All e.s.r. spectra were measured as glasses in MeCN at 77K.

Fast scan voltammograms ($>500mVs^{-1}$) were monitored using the same electrode configuration as employed for cyclic voltammetry, using a Physical Data Inc. model 512A digital transient store in conjunction with a Telequipment model D66A oscilloscope, with subsequent playback to a Bryans Gould Series 50,000 X-Y recorder. Low temperature studies were carried out in a jacketed cell cooled by a Haake F3Q refrigerated circulation unit.

The Optically Transparent Thin Layer Electrode (O.T.T.L.E.) cell used for monitoring in situ UV/vis spectra was designed and built in the Department of Chemistry, University of Edinburgh, in accordance with the original principles of Murray and co-workers [261], and consisted of a fine Pt gauze working electrode (transparency c.a. 40%) fitted into a standard Infrasil quartz, UV/vis/near i.r. cell of 0.05cm pathlength. A quartz extension fitted to the top of the cell functioned as a reservoir and contains a Pt wire auxiliary electrode and Ag/Ag^{+} reference electrode, both protected from the bulk solution by a porous glass frit. This assembly was fitted into a PTFE cell block (Fig. A). Temperature

control, monitored by a thermocouple/digital thermometer was maintained by the passage of dry, pre-cooled nitrogen gas around the assembly.

Solutions of the test species were purged with dry N_2 gas and then electrolysed at the Pt minigrid working electrode of the O.T.T.L.E. cell which was placed directly in the beam of the Lambda-9 UV/vis/NIR spectrophotometer. The progress of the electrolysis was monitored both spectroscopically and by decay of the current to a constant residual value. The potential was then reversed to monitor regeneration of the precursor solution to ensure that the process was chemically revrsible and to confirm that decomposition was minimal.

Key to Fig. A:

A. Counter electrode

B. Reference electrode

C. Working electrode connection protected from bulk solution by PTFE sleeve

D. PTFE cell cap

E. Test solution, deoxygenated with N_2

F. 0.05cm Infrasil Quartz cell containing Pt grid working electrode

G. Pt grid working electrode

H. PTFE cell block

I. Variable temperature N_2 inlet ports

J. Dry N_2 inlet ports

K. Infrasil Quartz cell block windows

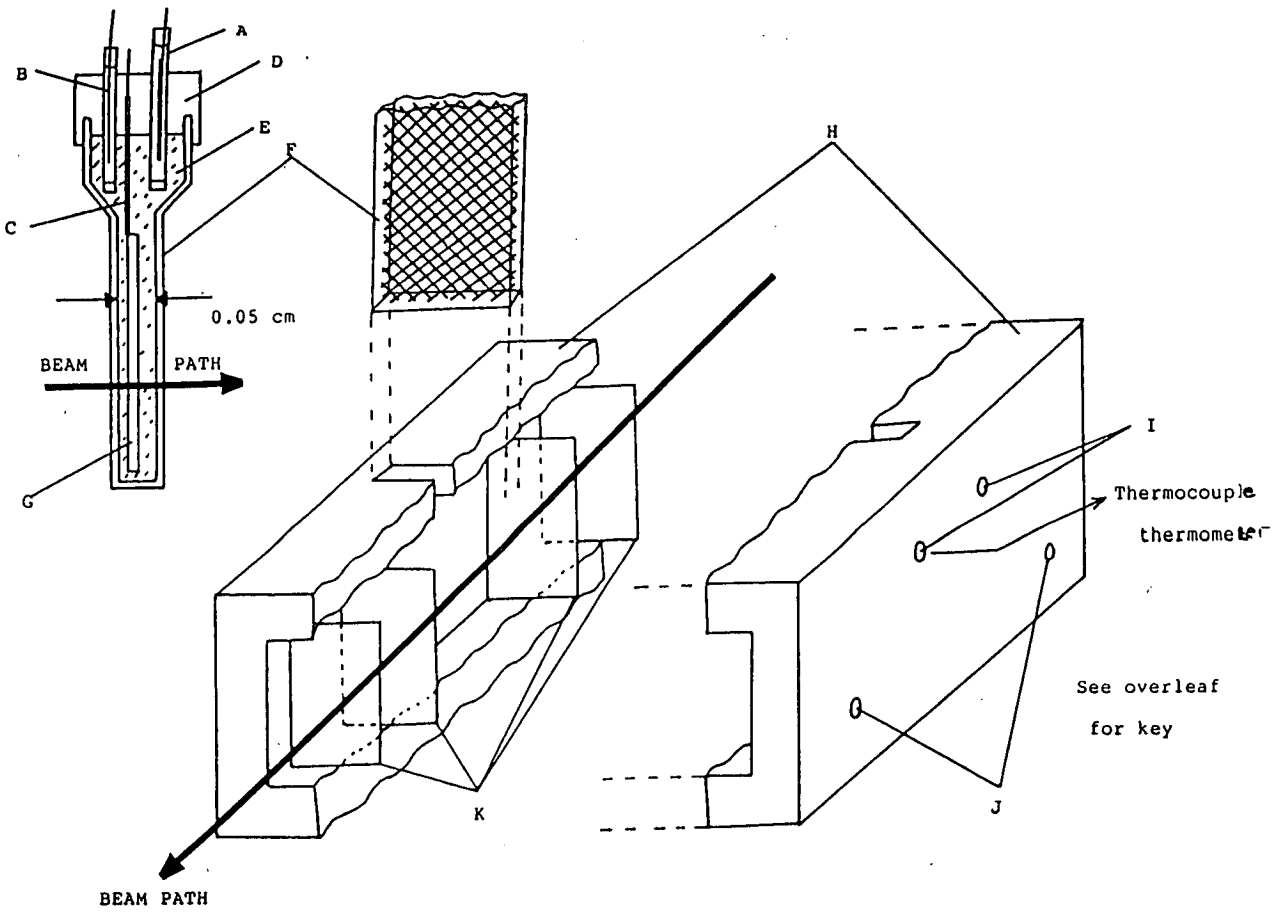

Fig. A: Design of the Optically Transparent Thin Layer Electrode

REFERENCES

References

1. see for example "Co-ordination Chemistry of Macrocyclic Compounds", Ed. G.A. Melson, Plenum, New York 1979.

2. D.K. Cabbiness and D.W. Margerum, J.Am.Chem.Soc., 91, 6540 (1969).

3. J.F. Endicott and B. Durham in "Co-ordination Chemistry of Macrocyclic Compounds", pp.408-415 and references within.

4. M. Schröder, Pure and Appl.Chem., 60, 517 (1988).

5. N. Sutin and P. Gutlich, Comm.Inorg.Chem., 237 (1988).

6. M. Kodama and E. Kimura, J.Chem.Soc.,Chem.Comm., 326 (1975).

7. D.K. Cabbiness and D.W. Margerum, J.Am.Chem.Soc., 92, 2151 (1970).

8. D.H. Busch, K. Farmery, V. Goedken, V. Katovic, A.C. Melnyk, C.R. Sperati and N. Tokel, Advan.Chem.Ser., 100, 44 (1971).

9. F.P. Hinz and D.W. Margerum, Inorg.Chem., 13, 2941 (1988).

10. J.D. Lamb, R.M. Izatt, J.J. Christensen and D.J. Eatough, in "Co-ordination Chemistry of Macrocyclic Compounds", pp.166-169, and references within.

11. G.F. Smith and D.W. Margerum, J.Chem.Soc.,Chem.Comm., 807 (1975).

12. R.E. DeSimone and M.D. Glick, J.Am.Chem.Soc., 98, 762 (1976).

13. R.E. Wolf, J.A.R. Hartman, J.M.E. Storey, B.M. Foxman and S.R. Cooper, J.Am.Chem.Soc., 109, 4328 (1987).

14. R.S. Glass, G.S. Wilson and W.N. Setzer, J.Am.Chem.Soc., 102, 5086 (1980).

15. S.M. Peng and V.L. Goedken, in "Co-ordination Chemistry of Macrocyclic Compounds", p.237.

16. J.M. Rifkind, in "Inorganic Biochemistry", Ed. G.L. Eichhorn, Elsevier, Amsterdam, Ch.25, "Haemoglobin and Myoglobin", pp.832-902.

17. J.J. Katz, in "Inorganic Biochemistry", Ch.29, "Chlorophyll", pp.1022-1066.

18. H.A.O. Hill, in "Inorganic Biochemistry", Ch.30, "Corrinoids", pp1067-1136.

19. D.G. Brown, in "The Chemistry of Vitamin B_{12} and Related Inorganic Systems", Prog.Inorg.Chem., 18, 177 (1973).

20. V.L. Goedken, in "Co-ordination Chemistry of Macrocyclic Compounds", Ch.10, "Natural Product Model Systems", pp.603-654, and references within.

21. J.W. van der Zwaan, "On the Active Site of Nickel Hydrogenases", Ph.D. Thesis, University of Amsterdam (1987).

22. S.P.J. Albracht, A. Kroger, J.W. van der Zwaan, G. Under, R. Bocher, H. Mell and R.D. Fontijn,

Biochim. et Biophys.Acta., 874, 116 (1986).

23. P.M. Collman, H.C. Freeman, J.M. Guss, M. Murata, V.A. Norro, J.A.M. Ramshaw and M.P. Venkatappa, Nature, 272, 319 (1978).

24. B. Fischer and R. Eisenberg, J.Am.Chem.Soc., 102, 7361 (1980).

25. S. Meshitsuka, M. Ichikawa and K.Tamura, J.Chem.Soc.,Chem.Comm., 158 (1974).

26. M. Beley, J.P. Collin, R. Ruppert and J.P. Sauvage, J.Chem.Soc.,Chem.Comm., 1315 (1984).

27. M. Beley, J.P. Collin, R. Ruppert and J.P. Sauvage, J.Am.Chem.Soc., 108, 7461 (1986).

28. D.A. Gangi and R.R. Durand, J.Chem.Soc.,Chem.Comm., 697 (1986).

29. J.P. Collin and K. Kim, J.Am.Chem.Soc., 108, 7847 (1986).

30. Y. LeMest, M. L'Her, J. Courtot-Coupez, J.P. Collman, E.R. Evitt and C.S. Benscosme, J.Chem.Soc.,Chem.Comm., 1286 (1983).

31. J.P. Collman, P. Denisevich, M. Marrocco, C. Koval and F.C. Anson, J.Am.Chem.Soc., 102, 6027 (1980).

32. B.B. Wayland and A.R. Newman, Inorg.Chem., 20, 3093 (1981).

33. D. Pletcher and D.J. Pearce, J.Electroanal.Chem., 197, 317 (1986).

34. M.J. Camenzind, D. Dolphin and B.R. James, J.Chem.Soc.,Chem.Comm., 1137 (1986).

35. I. Taniguchi, N. Nakashima and K. Yasukouchi, J.Chem.Soc.,Chem.Comm., 1814 (1986).

36. J.Y. Becker, B. Vainas, R. Eger and L. Kaufman, J.Chem.Soc.,Chem.Comm.,1471 (1985).

37. P.J. Brothers and J.P. Collman, Acc.Chem.Res., 19, 209 (1986) and references within.

38. B.B. Wayland and H.W. Bosch, J.Chem.Soc.,Chem.Comm., 900 (1986).

39. J.P. Collman, J.I. Brauman and A.M. Madonik, Organometallics, 5, 311 (1986).

40. D.H. Busch, W.D. Lemke, K.E. Travis and N.E. Tokvoryan, Adv.Chem.Ser., 150, 358 (1977).

41. D. Pletcher, R. Rosas, J.Y. Becker and J.B. Kerr, J.Electroanal.Chem., 117, 87 (1981).

42. S.G. Murray and F.R. Hartley, Chem.Rev., 81, 365 (1981).

43. R.W. Hay, in "Inorgnaic Biochemistry", Ellis Horwood, 1984, Ch.4-9, and references within.

44. J.P. Collman, P.J. Brothers, E. Rose, L.J. Wright and L. McElwee-White, J.Am.Chem.Soc., 107, 4570 (1985).

45. see for example "Comprehensive Co-ordination Chemistry", Ed. G. Wilkinson, Pergamon, New York, 4, Ch.48, p.930, Ch49, p.1120.

46. see for example "Comprehensive Co-ordination Chemistry", 5, ch.52. p.353, Ch.51, p.1103.

47. A.J. Blake, R.O. Gould, T.I. Hyde and M. Schröder, J.Chem.Soc.,Chem.Comm., 431 (1987).

48. R.H. Crabtree, Chem.Rev., 85, 245 (1986) and references within.

49. D.St.C. Black and I.A. McLean, J.Chem.Soc.,Chem.Comm., 1004 (1968).

50. D.St.C. Black and I.A. McLean, Tetrahedron Lett., 3961 (1969).

51. D.St.C. Black and I.A. McLean, Aust.J.Chem., 24, 1401 (1971).

52. L.F. Lindoy and D.H. Busch, J.Chem.Soc.,Chem.Comm., 1598 (1968).

53. A.J. Blake, A.J. Holder and M. Schröder, unpublished results.

54. A.J. Blake, A.J. Holder, T.I. Hyde and M. Schröder, J.Chem.Soc.,Chem.Comm., in press.

55. S.R. Cooper, S.C. Rawle, J.A.R. Hartman, E.J. Hintsa and G.A. Adams, Inorg.Chem., 27, 1209 (1988).

56. J.A.R. Hartman and S.R. Cooper, J.Am.Chem.Soc., 108, 1202 (1986).

57. J.A.R. Hartman, E.J. Hintsa and S.R. Cooper, J.Am.Chem.Soc., 108, 1208 (1986).

58. S.C. Rawle, J.A.R. Hartman, D.J. Watkin and S.R. Cooper, J.Chem.Soc.,Chem.Comm., 1083 (1986).

59. B. Dietrich, J.M. Lehn and J.P. Sauvage, J.Chem.Soc.,Chem.Comm.,1055 (1970).

60. H.L. Ammon, K. Chandrasekhar and S.K. Bhattacharjee, Acta.Cryst.C, 40, 2061 (1984).

61. R.N. Icke, B.B. Wisegarver and G.A. Alles, in "Organic Synthesis", Wiley, New York, 1955.

Collected Volumes 111, p.723.

62. P. Moore, N.W. Alcock and K.F. Mok, J.Chem.Soc.,Perkin II, 1186 (1980).

63. A.H. Alberts, R. Annumziata and J.M. Lehn, J.Am.Chem.Soc., 99, 8502 (1977).

64. O. Katin, I. Mogenstern-Badarau, J.P. Audiere, J.M. Lehn and S.A. Sullivan, J.Am.Chem.Soc., 102, 5935 (1980).

65. T.E. Jones, D.B. Rorabacher and L.A. Ochrymowycz, J.Am.Chem.Soc., 97, 7485 (1975).

66. M.D. Glick, D.P. Gavel, L.L. Diaddario and D.B. Rorabacher, Inorg.Chem., 15, 1190 (1976).

67. E.R. Dokal, T.E. Jones, W.S. Sokol, R.J. Engerer, D.B. Rorabacher and L.A. Ochrymowycz, J.Am.Chem.Soc., 98, 4322 (1976).

68. D.B. Rorabacher, J.Am.Chem.Soc., 107, 2399 (1985).

69. R. Malkin, in "Inorganic Biochemistry", 2, Ed. G.L. Eichhorn, Elsevier, New York, 1973, p.689.

70. V. Moskowski, S.P.W. Tang, T.G. Spiro, E. Shapiro and T.H. Moss, Biochemistry, 14, 1244 (1975).

71. N. Atkinson, M.G.B. Drew, G. Forsyth, A.J. Lavery, G. Reid and M. Schröder, J. Chem.Soc.,Chem.Comm., in press.

72. R.O. Gould, A.J. Lavery and M. Schröder, J.Chem.Soc.,Chem.Comm.,1492 (1985).

73. M.G.B. Drew and G. Forsyth, personal communication.

74. R. Yang and L. Zompa, Inorg.Chem., 15, 1499 (1976).

75. A. Bencine, L. Fabbrizzi and A. Poggi, Inorg.Chem.,

20, 2544 (1981).

76. S.R. Cooper, S.C. Rawle, J.A.R. Hartman, E.J. Hintsa and G.A. Admans, Inorg.Chem., 27, 1209 (1988).

77. A.J. Blake, T.I. Hyde and M. Schröder, personal communication.

78. "Monovalent, Trivalent and Tetravalent Nickel", A. Chakravarty and K. Nag, Co-ord.Chem.Rev., 33, 77 (1981).

79. A.H. Maki, N. Edelstein, A. Davidson and R.H. Holm, J.Am.Chem.Soc., 86, 4580 (1964).

80. A.J. Holder, Ph.D. Thesis, University of Edinburgh (1987).

81. R.D. Shannon, Acta.Cryst.A, 32, 751 (1976).

82. G.M. Sheldrick, SHELX76, Program for Crystal Structure Refinement, University of Cambridge (1976).

83. G.M. Sheldrick, SHELX86, Programs for Crystal Structure Determination, University of Göttingen (1986).

84. R.O. Gould and P. Taylor, CALC, Interactive Molecular Geometry Program, University of Edinburgh (1985).

85. P.T. Beurskens, W.P. Bosman, H.M. Doesbury, T.E.M. van der Hark, P.A.J. Prick, J.H. Noordik, G. Beurskens, R.O. Gould and V. Parthasarathai, DIRDIF, Applications of Direct Methods to Difference Structure Factors, University of Nijmegan, The Netherlands (1983).

86. N. Walker and D. Stuart, Acta.Cryst.A, 39, 158 (1983).

87. W. Clegg, Acta.Cryst.A, 37, 22 (1981).

88. International Tables for X-Ray Crystallography, 4, Kynoch Press, Birmingham (1974).

89. P.D. Mallinson and K.W. Muir, ORTEP, J.Appl.Cryst., 18, 51 (1985).

90. W.D.S. Motherwell, PLUTO, University of Cambridge (1976).

91. R.R. Schrock, J.Am.Chem.Soc., 98, 2134 (1976).

92. R.R. Schrock, J.Am.Chem.Soc., 98, 2143 (1976).

93. F.H. Jardine, Prog.Inorg.Chem., 28, 63 (1981).

94. P.G. Gassman, T.J. Atkins and J.T. Lamb, J.Am.Chem.Soc., 94, 7757 (1972).

95. K.B.Wiberg and K.C. Bishop, Tetrahedron Lett., 2727 (1973).

96. K.C. Bishop, Chem.Rev., 76, 461 (1976).

97. J.W. Kaig, R. Moseley and P.M. Maitlis, J.Am.Chem.Soc., 91, 5970 (1969).

98. "Advanced Inorganic Chemistry", Ed. F.A. Cotton and G. Wilkinson, 5th Edn., p.729-732.

99. K. Wieghardt, H.J. Kuppers and J. Wiess, Inorg.Chem., 24, 3067 (1985).

100. K. Wieghardt, W. Schmidt, W. Herrmann and H.J. Kuppers, Inorg.Chem., 22, 2953 (1983).

101. L.R. Gahan, T.W. Hambley, A.M. Sargeson and M.R. Snow, Inorg.Chem., 21, 2699 (1982).

102. W.N. Setzer, C.A. Ogle, G.S. Wilson

and R.S. Glass, Inorg.Chem., 22, 266 (1983).

103. R.W. Hay, B. Jeragh, S.F. Lincoln and G.H. Searle, Inorg.Nucl.Chem.Letts, 14, 435 (1978).

104. see for example "Advanced Inorganic Chemistry", 5th Edn., pp.729-732.

105. A.J. Blake, R.O. Gould, A.J. Holder, T.I. Hyde and M. Schröder, J.Chem.Soc.,Dalton Trans., 1861 (1988).

106. A.J. Blake, T.I. Hyde and M. Schröder, unpublished results.

107. S.C. Rawle, R. Yagbasan and S.R. Cooper, J.Am.Chem.Soc., 109, 6181 (1987).

108. T.I. Hyde and M. Schröder, unpublished results.

109. T. Yoshida and T. Ueda, J.Chem.Soc.,Chem.Comm., 1137 (1985).

110. W.D. Lemke, K.E. Travis, N.E. Takvoryan and D.H. Busch, Adv.Chem.Ser., 358 (1977).

111. T.I. Hyde and M. Schröder, unpublished results.

112. R. Uson, J. Fornies, M. Tomas, B. Menjon, K. Sunkel and R. Bau, J.Chem.Soc.,Chem.Comm., 751 (1981).

113. H. Endres, H.J. Keller, H. van der Sand and V. Dong, Z.Naturforsch, Teil B, 33, 843 (1978).

114. H.A. Boucher, G.A. Lawrence, P.A. Lay, A.M. Sargeson, A.M. Bond, D.F. Sangster and J.C. Sullivan, J.Am.Chem.Soc., 105, 4652 (1983).

115. A.J. Blake, A.J. Holder, T.I. Hyde and M. Schröder, J.Chem.Soc.,Chem.Comm., 987 (1987).

116. R. Kirmse, J. Stach, W. Dietzch, G. Steimecke and E. Hoyer, Inorg.Chem., 19, 2679 (1980).

117. K. Broadley, G.A. Lane, N.G. Connelly and W.E. Geiger, J.Am.Chem.Soc., 105, 2486 (1983).

118. G.A. Lane, W.E. Geiger, J.Am. Chem.Soc., 109, 402 (1987).

119. A.J. Blake, R.O. Gould, T.I. Hyde and M. Schröder, J.Chem.Soc.,Chem.Comm., 1730 (1987).

120. A.J. Blake, A.J. Holder, T.I. Hyde, A.J. Lavery, Y.V. Roberts and M. Schröder, J.Organomet.Chem., 323, 261 (1987).

121. A.J. Blake, L.M. Gordon, A.J. Holder, T.I. Hyde, G. Reid and M. Schröder, J.Chem.Soc.,Chem.Comm., 1452 (1988).

122. A.J. Blake, R.O. Gould, A.J. Holder, T.I. Hyde, A.J. Lavery, M.O. Odulate and M. Schröder, J.Chem.Soc.,Chem.Comm., 118 (1987).

123. A.J. Blake, A.J. Holder, T.I. Hyde and M. Schröder, J.Chem.Soc.,Chem.Comm., in press.

124. D. Parker, J.M. Lehn and J. Rimmer, J.Chem.Soc.,Dalton Trans., 1517 (1985).

125. J.M. Csavas, M.R. Taylor and K.P. Wainwright, J.Chem.Soc.,Dalton Trans., 2573 (1988).

126. A.J. Blake, R.O. Gould, A.J. Lavery and M. Schröder, Angew.Chem.,Int.Ed.Eng., 25, 274 (1986).

127. R.C. Eachus and R.E. Groves, J.Chem.Phys., 65, 5445 (1976).

128. A. Tressaud, S. Khairoun, J.M. Dance, J. Grannec,

G. Demazau and P. Hagenmuller, C.R.Acad.Sci.,Ser.B, 295, 183 (1982).

129. E.P. Talsi, V.P. Babenko, V.A. Nekipelov and V.D. Chinakov, J.Chem.Soc.,Chem.Comm., 1768 (1985).

130. P.Arrizabalaga, G. Bernardinelli, M. Geoffroy, P. Castan and F. Dahan, Chem.Phys.Lett., 124, 549 (1986).

131. V.L. Goedken, in "Co-ordination Chemistry of Macrocyclic Compounds", Ch.10, p.639.

132. J.P. Sauvage, C.O. Dietrich-Buchecher and J.M. Kern, J.Chem.Soc.,Chem.Comm., 760 (1985).

133. N.B. Tucker and E.E. Reid, J.Am.Chem.Soc., 55, 775 (1933).

134. W. Rosen and D.H. Busch, J.Am.Chem.Soc., 91, 4694 (1969).

135. W. Rosen and D.H. Busch, J.Chem.Soc.,Chem.Comm., 148 (1969).

136. L.A. Ochrymowycz, C.P. Mak and J.D. Michna, J.Org.Chem., 39, 2099 (1974).

137. D. Sellman and L. Zapf, Angew.Chem.,Int.Ed.Eng., 23, 808 (1984).

138. J. Buter and R.M. Kellogg, J.Org.Chem., 46, 4481 (1981).

139. S. Ahrland, J. Chatt and N.R. Davis, Quart.Rev., 12, 265 (1958).

140. C.J. Pedersen, J.Am.Chem.Soc., 89, 2495 (1967).

141. C.J. Pedersen, J.Am.Chem.Soc., 89, 7017 (1967).

142. C.J. Pedersen, J.Am.Chem.Soc., 92, 391 (1970).

143. G.W. Gokel, D.J. Cram, C.L. Liotta, H.P. Harris and F.L. Cook, J.Org.Chem., 39, 2445 (1974).

144. G.W. Gokel and H.D. Durst, Synthesis, 168 (1976), and references within.

145. R.E. DeSimone and M.D. Glick, J.Am.Chem.Soc., 97, 942 (1975).

146. N.W. Alcock, N. Herron and P. Moore, J.Chem.Soc.,Chem.Comm., 886 (1976).

147. G.H. Robinson, H. Zhang and J.L. Atwood, Organomet, 6, 887 (1987).

148. D.J. Brauen and G.D. Stucky, J.Am.Chem.Soc., 91, 5462 (1969).

149. R. Shakir, M.J. Zaworotko and J.L. Atwood, J.Organomet.Chem., 171, 9 (1979).

150. M.N. Bell, Ph.D. Thesis, University of Edinburgh (1987).

151. P.H. Davis, K.L. White and R.L. Bedford, Inorg.Chem., 14, 1753 (1975).

152. P.W. Mak and C.K. Poon, Inorg.Chem., 15, 1949 (1976).

153. M.D. Glick, D.P. Gavel, L.L. Diaddario and D.B. Rorabacher, Inorg.Chem., 15, 1190 (1976).

154. M.N. Bell, A.J. Blake, R.O. Gould, A.J. Holder, T.I. Hyde, A.J. Lavery, G. Reid and M. Schröder, J.Incl.Phen., 5, 169 (1987).

155. E.R. Dokal, L.L. Diaddario, M.D. Glick and D.B. Rorabacher, J.Am.Chem.Soc., 99, 4530 (1977).

156. T.F. Lai and C.K. Poon, J.Chem.Soc.,Dalton Trans.,

1465 (1982).

157. W. Rosen and D.H. Busch, Inorg.Chem., 9, 262(1970).

158. A.J. Blake, M. Halcrow and M. Schroder, unpublished results.

159. E.W. Abel, P.D. Beer, I. Moss, K.G. Orrell and V. Sik, J.Organomet.Chem., 341, 559 (1988).

160. J. Craigel, V.B. Petts, M.D. Glick and R.E. DeSimone, Inorg.Chem., 17, 2885 (1978).

161. R.E. DeSimone and M.D. Glick, Inorg.Chem., 17, 3574 (1978).

162. T. Yoshida, T. Adachi, T. Ueda, M. Wanatabe, M. Kaminaka and T. Higuchi, Angew.Chem.,Int.Ed.Eng., 26, 1171 (1987).

163. K. Travis and D.H. Busch, J.Chem.Soc.,Chem.Comm., 1041 (1970).

164. A.J. Holder, Ph.D. Thesis, University of Edinburgh (1987).

165. J.P. Collman, C.E. Barnes, T.J. Collins and P.J. Brothers, J.Am.Chem.Soc., 103, 7030 (1981).

166. J.P. Collman, C.E. Barnes, P.N. Swepston and J.A. Ibers, J.Am.Chem.Soc., 106, 3500 (1984).

167. J.P. Collman, P.J. Brothers, L. McElwee-White, E. Rose and L.J. Wright, J.Am.Chem.Soc., 107, 4570 (1985).

168. B.B. Wayland and A.R. Newman, Inorg.Chem., 20, 3093 (1981).

169. K.J. Del Rossi and B.B. Wayland,

J.Chem.Soc.,Chem.Comm., 1653 (1986).

170. A.W. Addison, B. Watts and M. Wicholas, Inorg.Chem., 23, 813 (1984).

171. L.F. Warren and V.L. Goedken, J.Chem.Soc.,Chem.Comm., 909 (1978).

172. D.J. Doonan, A.L. Balch, S.Z. Goldberg, R. Eisenberg and J.S. Miller, J.Am.Chem.Soc., 97, 1961 (1975).

173. S.Z. Goldberg and R. Eisenberg, Inorg.Chem., 15, 535 (1977).

174. B. Messbauer, H. Meyer, B. Walther, M.J. Heeg, A.F. Maqsudor Raman and J.P. Oliver, Inorg.Chem., 22, 272 (1983).

175. B. Walther, B. Messbauer and H. Meyer, Inorg.Chim.Acta., 37, L525 (1979).

176. A.L. Balch, L.S. Benner and M.M. Olmstead, Inorg.Chem., 18, 2996 (1979).

177. J.R. Boem and A.L. Balch, Inorg.Chem., 18, 778 (1977).

178. M.M. Olmstead, H. Hope, L.S. Benner and A.L. Balch, J.Am.Chem.Soc., 99, 5502 (1977).

179. L.S. Benner, M.M. Olmstead, H. Hole and A.L. Balch, J.Organomet.Chem., 151, C31 (1978).

180. T.D. Miller, M.A.St. Clair, M.K. Reinking and C.P. Kublak, Organomet, 2, 767 (1983).

181. K. Travis and D.H. Busch, Inorg.Chem., 13, 2591 (1974).

182. E.J. Bounsall and S.R. Koprich, Can.J.Chem.,

44, 1481 (1970).

183. P.K. Bhattacharya, J.Chem.Soc.,Dalton Trans., 810 (1980).

184. M.E. Sosa and M.L. Tobe, J.Chem.Soc.,Dalton Trans., 427 (1986).

185. M.J. Rosales, M.E. Sosa and M.L. Tobe, J.Co-ord.Chem., 16, 59 (1987).

186. A.J. Blake, T.I. Hyde, R.S.E. Smith and M. Schröder, J.Chem.Soc.,Chem.Comm., 334 (1986).

187. A.J. Blake, T.I. Hyde and M. Schröder, J.Chem.Soc.,Dalton Trans., 1165 (1988).

188. C.K. Poon, T.W. Tang and C.M. Che, J.Chem.Soc.,Dalton Trans.1697 (1981).

189. C.K. Poon, T.W. Tang and C.M. Che, J.Chem.Soc.,Dalton Trans., 1647 (1983).

190. J.MacB. Harrowfield, A.J. Herit, P.A. Lay, A.M. Sargeson, A.M. Bond, W.A. Mulac and J.C. Sullivan, J.Am.Chem.Soc., 105, 5503 (1983).

191. B.B. Wayland and A.R. Newman, J.Am.Chem.Soc., 101, 6472 (1979).

192. K.M. Kadish, C.L. Yao, J.E. Anderson and P. Cocolios, Inorg.Chem., 24, 4515 (1985).

193. J.E. Anderson, C.L. Yao and K.M. Kadish, Inorg.Chem., 25, 718 (1986).

194. J.E. Anderson, C.L. Yao and K.M. Kadish, J.Am.Chem.Soc., 109, 1106 (1987).

195. T.R. Felthouse, Prog.Inorg.Chem., 29, 74 (1982).

196. E. Billig, S.I. Shupack, J.H. Waters, R. Williams

and H.B. Gray, J.Am.Chem.Soc., 86, 926 (1964).

197. M.A. Bennett and R.A. Longstaff, J.Am.Chem.Soc., 91, 6266 (1969).

198. C. Masters and B.L. Shaw, J.Chem.Soc.,A, 3679 (1971).

199. B.R. James, F.T.T. Ng and E. Ochiai, Can.J.Chem., 50, 590 (1972).

200. G.Valentini, G. Braca, G. Sbrana and A. Colligiani, Inorg.Chim.Acta., 69, 211 (1983).

201. N.V. Vugman and W.O. Franco, J.Chem.Phys., 78, 2099 (1983).

202. N.V. Vugman and N.M. Pinhal, Mol.Phys., 49, 1315 (1983).

203. N.G. Connelly and G. Garcia, J.Chem.Soc.,Chem.Comm., 246 (1987).

204. G. Hunter, A. McAuley and T.W. Whitcombe, Inorg.Chem., 27, 2635 (1988).

105. T. Yoshida, T. Ueda, T. Adachi, K. Yamamoto and T. Higuchi, J.Chem.Soc.,Chem.Comm., 1137 (1985).

206. J. Dale, Acta.Chem.Scand., 27, 1115 (1973).

207. P.W.R. Corfield, C. Ceccarelli, M.D. Glick, I.W.Y. Moy, L.A. Ochrymowycz and D.B. Rorabacher, J.Am.Chem.Soc., 107, 2399 (1985).

208. A.J. Blake, T.I. Hyde and M. Schröder, unpublished results.

209. "Co-ordination Chemistry of Macrocyclic Compounds", and references within.

210. C.M. Che and W.K. Cheng, J.Am.Chem.Soc.,

108, 4644 (1986).

211. C.K. Poon, C.M. Che and K.Y. Wong, Inorg.Chem., 24, 1797 (1985).

212. D. Meyerstein, Y. Koresh, H. Cohen and N. Jubran, J.Chem.Soc.,Chem.Comm., 1683 (1984).

213. D. Meyerstein, G. Ginzberg, H. Cohen and N. Jubran, J.Chem.Soc.,Chem.Comm., 517 (1982).

214. D. Meyerstein, G. Ginzberg, H. Cohen and N. Jubran, Inorg.Chem., 24, 251 (1985).

215. J. Van Alphen, Rec.Trav.Chim.Pays-Bas, 55, 835 (1936).

216. H. Stetter and K.H. Mayer, Chem.Ber., 94, 1410 (1961).

217. E.K. Barefield, Inorg.Chem., 11, 2273 (1972).

218. E.K. Barefield, F. Wagner, A.W. Herlinger and A.R. Dahl, Inorg.Synth., 16, 220 (1976).

219. E.K. Barefield, F. Wagner and K.D. Hodges, Inorg.Chem., 15, 1370 (1976).

220. S.M. Peng and V.L. Goedken, in "Co-ordination Chemistry of Macrocyclic Compounds", Ch.4, p.237.

221. J.F. Endicott, J. Lilie, J.M. Kuszaj, B.S. Ramaswamy, W.G. Schmansees, M.G. Simic, M.D. Glick and D.P. Rillema, J.Am.Chem.Soc., 99, 429 (1977).

222. B. Bosnich, R. Mason, P.J. Pauling, G.B. Robertson and M.L. Tobe, J.Chem.Soc.,Chem.Comm., 97 (1965).

223. T.W. Hambley, J.Chem.Soc.,Dalton Trans., 565 (1986).

224. P. Moore, J. Sachinides and G.R. Willey,

J.Chem.Soc.,Chem.Comm., 522 (1983).

225. S.F. Lincoln, J.H. Coates, D.A. Hadi and D.L. Pisaniello, Inorg.Chim.Acta., 81, L9 (1984).

226. C.M. Che, S.S. Kwong and C.K. Poon, Inorg.Chem., 24, 1601 (1985).

227. C.M. Che, T.W. Tang and C.K. Poon, J.Chem.Soc.,Chem.Comm., 641 (1984).

228. C.M. Che, S.S. Kwong and C.K. Poon, J.Chem.Soc.,Chem.Comm.,986 (1985).

229. C.M. Che, K.Y. Wong and T.C.W. Mak, J.Chem.Soc.,Chem.Comm., 988 (1985).

230. C.M. Che and W.K. Cheng, J.Chem.Soc.,Chem.Comm., 1519 (1986).

231. A.J. Blake, R.O. Gould, T.I. Hyde and M. Schröder, J.Chem.Soc.,Chem.Comm., 431 (1987).

232. M. Yamashita, H. Ito, K. Toriumi and T. Ito, Inorg.Chem., 22, 1566 (1983).

233. K. Toriumim M. Yamashita, H. Ito and T. Ito, Acta.Cryst.,C, 42, 963 (1986).

234. E.K. Barefield, G.M. Freeman and D.G. Van Derveer, Inorg.Chem., 25, 552 (1986).

235. F. Wagner, M.T. Mocella, M.J. D'Aniello, A.H.J. Wang and E.K. Barefield, J.Am.Chem.Soc., 96, 2625 (1974).

236. M. Kato and T. Ito, Bull.Chem.Soc.Jpn., 59, 285 (1986).

237. M.J. D'Aniello, M.T. Mocella, F. Wagner, E.K. Barefield and I.C. Paul, J.Am.Chem.Soc., 97, 192 (1975).

238. P.D. Beer, J.Chem.Soc.,Chem.Comm., 1678 (1986).

239. D.E. Koshland, "Enzymes", 3rd Edn, 1, 341 (1970).

240. J. Rebek, Acc.Chem.Res., 17, 258 (1984).

241. J.S. Bradshaw, J.Y. Hui, B.L. Haymore, J.J. Christensen and R.M. Izatt, J.Heterocyclic Chem., 10, 1 (1973).

242. J.S. Bradshaw, R.A. Reeder, M.D. Thompson and J.J. Christensen, J.Org.Chem., 41, 134 (1976).

243. J.S. Bradshaw, J.Y. Hui, Y. Chan, B.L. Haymore, R.M. Izatt and J.J. Christensen, J.Heterocyclic Chem., 11, 45 (1974).

244. N.K. Dalley, S.B. Larson, J.S. Smith, K.L. Matheson, R.M. Izatt and J.J. Christensen, J.Heterocyclic Chem., 18, 463 (1981).

245. C.J. Pedersen, J.Am.Chem.Soc., 89, 1080 (1967).

246. C.J. Pedersen, J.Am.Chem.Soc., 89, 7017 (1967).

247. see for example "Synthetic Multidentate Macrocyclic Compounds", Ed. R.M. Izatt and J.J. Christensen, Academic Press, New York (1978).

248. D.J. Cram, Angew.Chem.,Int.Ed.Eng., 27, 1009 (1988).

249. R.M. Izatt, R.E. Terry, L.D. Hansen, A.G. Avondet, J.S. Bradshaw, N.K. Dalley, T.E. Jensen and B.L. Haymore, Inorg.Chim.Acta., 30, 1 (1978).

250. B. Metz, D. Moras and R. Weiss, J.Inorg.Nucl.Chem., 36, 785 (1974).

251. P.D. Beer, J.Chem.Soc.,Chem.Comm., 1678 (1986).

252. P.D. Beer, Polyhedron, 8, 1251 (1989).

253. C.J. van Staveren, D.N. Reinhoudt, J. van Eerden and S. Harkema, J.Chem.Soc.,Chem.Comm., 974 (1987).

254. J. Rebek, Acc.Chem.Res., 17, 258 (1984).

255. J. Rebek, J.E. Trend, R.V. Whattley and S. Chakravor, J.Am.Chem.Soc., 101, 4333 (1979).

256. J. Rebek and L. Marshall, J.Am.Chem.Soc., 105, 6668 (1983).

257. M.P. Andrews, C. Blackburn, J.F. McAleer and V.D. Patel, J.Chem.Soc.,Chem.Comm., 1122 (1987).

258. E. Fu, M.L.H. Green, V.J. Lowe and S.R. Marder, J.Organomet.Chem., C39, 341 (1988).

259. C.J. Pedersen, J.Am.Chem.Soc., 89, 7017 (1967).

260. D.D. Perrin, D.R. Perrin and W.L.F. Arma, in "Purification of Laboratory Chemicals", 2nd Ed., Pergamon.

261. W.R. Heinemann, R.W. Murray and G.W. O'Dom, Anal.Chem., 39, 1666 (1967).

Abbreviations

ap	apical
Bz	benzyl
DEPT	distortionless enhancement by polarisation transfer
dmf	dimethylformamide
dmso	dimethylsulphoxide
dppm	diphenylphosphinomethane
E.I.	electron impact
eq	equatorial
e.s.r	electron spin resonance
e.s.d	estimated standard deviation
Et	ethyl
EtOH	ethanol
f.a.b.	fast atom bombardment
Fc/Fc^+	ferrocene/ferrocenium
h	hour(s)
Hz	hertz
I.R.	infra red
M	molecular weight
M^+	molecular ion peak
Me	methyl
MeCN	acetonitrile
Me_2CO	acetone
$MeNO_2$	nitromethane
MeOH	methanol

MHz	megahertz
ml	millilitre(s)
mol.wt.	molecular weight
M.Pt.	melting point
n.m.r.	nuclear magnetic resonance
3-NOBA	3-nitrobenzylalcohol
Ph	phenyl
ppm	parts per million
sh	shoulder
UV/vis	ultra violet/visible
vis	visible

Lecture Courses and Meetings Attended

Lecture Courses

1. Electrochemistry

   Dr. L.J. Yellowlees, University of Edinburgh

2. Catalysis

   Drs. D.A. Whan, M.S. Spencer and J.P.Candlin,

   I.C.I Staff

3. Solving and Refining Crystal Structures

   Drs. A.J. Blake and R.O. Gould,

   University of Edinburgh

4. Modern Methods of N.M.R.

   Dr. I.H. Sadler, University of Edinburgh

5. Mass Spectrometry

   Prof. K.R. Jennings, University of Warwick

6. Electro-analytical Methods

   Dr. G.A. Heath, University of Edinburgh

7. Heavy Metals

   Dr. M. Schröder, University of Edinburgh

9. X-Ray Crystallography

   Drs. A.J. Blake and R.O. Gould,

   University of Edinburgh

Meetings

Departmental Inorganic Colloquia and Friday Discussion Group (3 years).

Platinum Group Metals Conference, Sheffield (1987).

British Crystallographic Association Spring Meeting, Heriot-Watt (1987), Warwick (1988)

U.K. One-Day Macrocyclic Symposium, Birmingham (1988), Durham (1989)

13th International Symposium of Macrocyclic Chemistry, Hamburg (1988)

R.S.C. Scottish Dalton Group Meeting, St. Andrews (1988)

University of Strathclyde Inorganic Club Conference, (1988)

Butler Postgraduate Electrochemistry Meeting, Edinburgh (1987, 1988, 1989)

Course on X-Ray Crystallography, Aston, (1989)

Stereochemical and Redox Properties of Palladium Complexes of 1,4,10,13-Tetrathia-7,16-diazacyclo-octadecane

Gillian Reid, Alexander J. Blake, Timothy I. Hyde, and Martin Schröder*

Department of Chemistry, University of Edinburgh, West Mains Road, Edinburgh EH9 3JJ, Scotland

The square planar S_4 donor complex $[Pd(L^1)]^{2+}$ (L^1 = 7,16-dimethyl-1,4,10,13-tetrathia-7,16-diazacyclo-octadecane) shows a reversible $Pd^{II/I}$ redox couple at $E_{\frac{1}{2}}$ −0.74 V *vs.* Fc/Fc^+; in contrast, the complex $[Pd(L^2)]^{2+}$ (L^2 = 1,4,10,13-tetrathia-7,16-diazacyclo-octadecane) shows distorted octahedral $N_2S_2 + S_2$ co-ordination, and a reversible $Pd^{II/III}$ couple at $E_{\frac{1}{2}}$ +0.57 V *vs.* Fc/Fc^+ (ferrocene/ferrocinium).

Reprinted from the Journal of The Chemical Society
Chemical Communications 1988

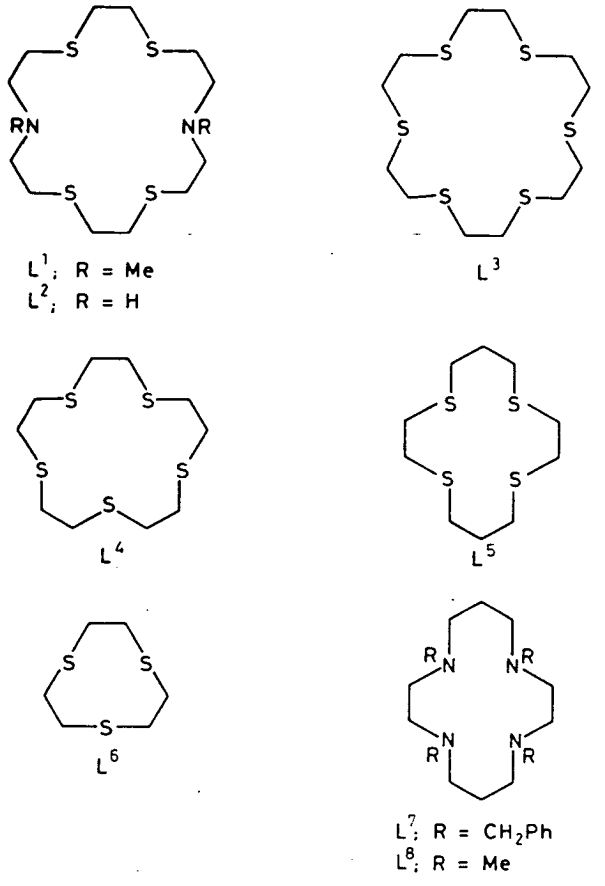

tuted HN-donors; space-filling models of $[Pd(L^1)]^{2+}$ indicate that meridional binding of L^1 is inhibited due to the greater steric bulk of the NMe groups.

The stereochemical differences between these complexes are also reflected in their redox properties. Cyclic voltammetry of $[Pd(L^1)]^{2+}$ in MeCN (0.1 M Bu_4NPF_6) at platinum electrodes shows a reversible reduction at −0.74 V *vs.* Fc/Fc$^+$ (Fc/Fc$^+$ = ferrocene/ferrocinium). ΔE_p 72 mV at a scan rate of 100 mV s^{-1}. Coulometry confirms the reduction to be a one-electron process. The e.s.r. spectrum (77 K; MeCN glass) of the reduced product, generated by controlled potential electrolysis at −0.90 V in MeCN at a Pt gauze, is anisotropic ($g_\parallel$ 2.155, $g_\perp$ 2.049) with hyperfine coupling to ^{105}Pd (I = 5/2, 22.2%) with $A_\parallel$ 48 and $A_\perp$ 34 G (Figure 3), consistent with the formation of a mononuclear d^9 palladium(I) species.[5,6] Electrochemical conversion of $[Pd(L^1)]^{2+}$ [$\lambda_{max.}$ 373 nm ($\varepsilon_{max.}$ 2 175 mol^{-1} dm^3 cm^{-1}), 298(14 460), 232(15 070)] to $[Pd(L^1)]^+$ [$\lambda_{max.}$ 345 nm ($\varepsilon_{max.}$ 2 100 mol^{-1} dm^3 cm^{-1}, sh.), 289(8 700), 236(10 300)] occurs reversibly and isosbestically ($\lambda_{iso.}$ 275,225 nm). The related homoleptic thioether Pd^{II} complexes, $[Pd(L)]^{2+}$ (L = L^3—L^5) and $[Pd(L^6)_2]^{2+}$ show irreversible reductions at E_p −0.73 → −0.875 V *vs.* Fc Fc$^+$ in MeCN at 293 K, although more reversible couples are observed for $[Pd(L^5)]^{2+}$ and $[Pd(L^6)_2]^{2+}$ at reduced temperatures (233 K).[7] Most importantly, $[Pd(L^1)]^{2+}$ is the only thioether complex we have studied which shows a reversible Pd^{III} couple at 293 K. This couple occurs at a particularly anodic potential compared to the tetra-aza analogues $[Pd(L^7)]^{2+}$ ($E_{\frac{1}{2}}$ −1.27 V) and $[Pd(L^8)]^{2+}$ (−1.53 V *vs.* Fc Fc$^+$).[6] These differences may be ascribed to the greater π-acidity of thioether donors, and to the ability of the larger and more flexible ring system of L^1 to accommodate the large Pd^I centre. In contrast, the tetra-aza complexes afford more reactive and transient paramagnetic species, with significant de-metallation occurring over a period of time. Sauvage and co-workers have shown[8] that tetrahedral catenand ligands stabilise d^9 Ni^I centres, and therefore, it seems likely that L^1 undergoes a tetrahedral distortion in the reduced complex $[Pd(L^1)]^+$.

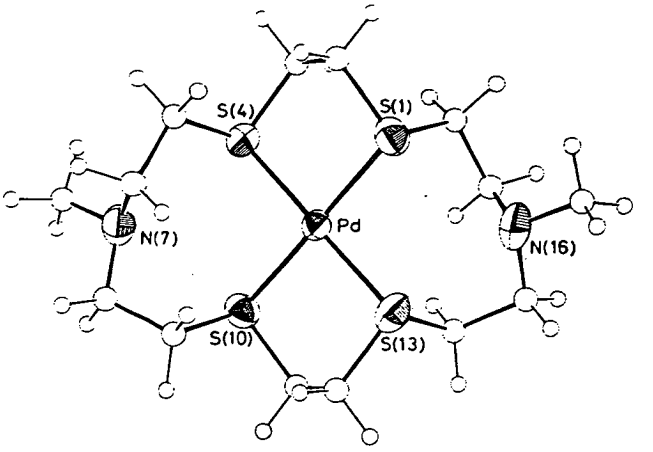

Figure 1. View of the structure of the $[Pd(L^1)]^{2+}$ cation showing the numbering scheme adopted.

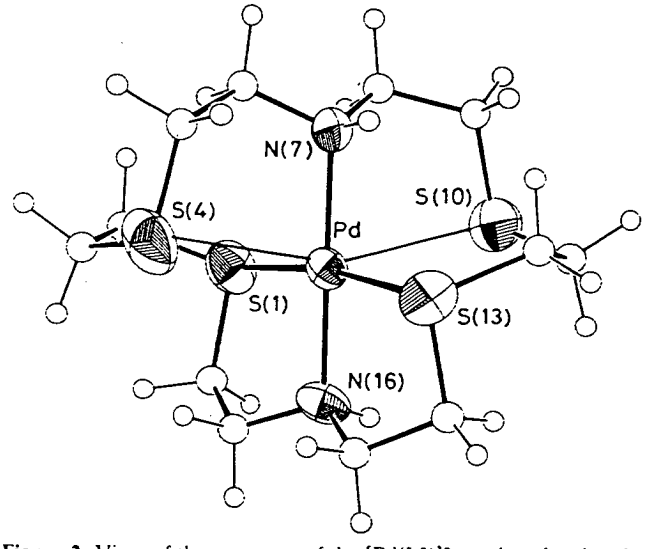

Figure 2. View of the structure of the $[Pd(L^2)]^{2+}$ cation showing the numbering scheme adopted.

In contrast to $[Pd(L^1)]^{2+}$, $[Pd(L^2)]^{2+}$ shows a chemically reversible oxidation at $E_{\frac{1}{2}}$ +0.57 V *vs.* Fc/Fc$^+$, ΔE_p 195 mV at a scan rate of 150 mV s^{-1}, indicative of a large stereochemical change occurring at the metal centre on oxidation. A totally irreversible reduction is observed at E_p −1.03 V at 293 K. Coulometry confirms the oxidation to be a one-electron process to form a bright red paramagnetic species which shows an anisotropic e.s.r. spectrum (77 K, MeCN; g_1 2.064, g_2 2.052, g_3 2.019) (Figure 4), assigned to the formation of a mononuclear d^7 palladium(III) species.[9,10] Electrochemical conversion of $[Pd(L^2)]^{2+}$ [$\lambda_{max.}$ 514 nm ($\varepsilon_{max.}$ 124 mol^{-1} dm^3 cm^{-1}), 332 (4 250), 266 (10 000), 233 (10 850)] to $[Pd(L^2)]^{3+}$ [$\lambda_{max.}$ 488 nm ($\varepsilon_{max.}$ 3 180 mol^{-1} dm^3 cm^{-1}), 341 (5 890), 264 (11 170)] occurs reversibly and isosbestically [$\lambda_{iso.}$ 241 nm].

The generation of Pd^{III} from the 4 + 2 co-ordinate $[Pd(L^2)]^{2+}$ is consistent with the availability of a distorted octahedral stereochemistry in this system. These results

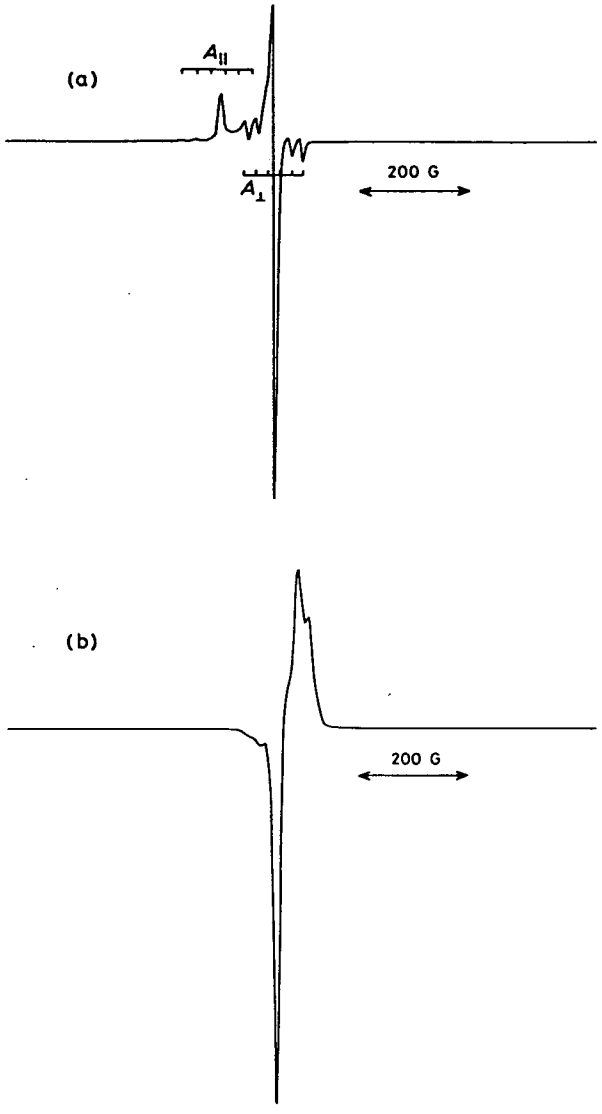

Figure 3. *X*-Band e.s.r. spectrum of (a) $[Pd(L^1)]^+$ and (b) $[Pd(L^2)]^{3+}$, both generated electrochemically; measured at 77 K in MeCN glass in the presence of 0.1 M $Bu^n_4NPF_6$. 1 G = 10^{-4} T.

suggest that there may be a significant kinetic/conformational barrier at room temperature to the formation of the corresponding Pd^{III} complex of L^3 (ref. 4).

We thank the S.E.R.C. (U.K.) for support, and Johnson Matthey p.l.c. for generous loans of platinum metals.

Received, 18th May 1988; Com. 8/01973H

References

1 D. St. C. Black and I. A. McLean, *J. Chem. Soc., Chem. Commun.*, 1968, 1004; *Tetrahedron Lett.* 1969, 3961; *Aust. J. Chem.*, 1971, **24**, 1401.
2 B. Dietrich, J.-M. Lehn, and J.-P. Sauvage, *J. Chem. Soc., Chem. Commun.*, 1970, 1055; A. A. Alberts, R. Annunziata, and J.-M. Lehn, *J. Am. Chem. Soc.*, 1977, **99**, 8502.
3 M. Schröder, *Pure Appl. Chem.*, 1988, **60**, 517.
4 A. J. Blake, R. O. Gould, A. J. Lavery, and M. Schröder, *Angew. Chem.*, 1986, **98**, 282; *Angew. Chem., Int. Ed. Engl.*, 1986, **25**, 274.
5 K. Broadley, G. A. Lane, N. G. Connelly, and W. E. Geiger, *J. Am. Chem. Soc.*, 1983, **105**, 2486; E. P. Talsi, V. P. Babenko, V. A. Likholobov, V. M. Nekipelov, and V. D. Chinakov, *J. Chem. Soc., Chem. Commun.*, 1985, 1768; P. Arrizabalaga, G. Bernardinelli, M. Geoffroy, P. Castan, and F. Dahan, *Chem. Phys. Lett.*, 1986, **124**, 549; G. A. Lane, W. E. Geiger, and N. G. Connelly, *J. Am. Chem. Soc.*, 1987, **109**, 402, and references therein.
6 A. J. Blake, R. O. Gould, T. I. Hyde, and M. Schröder, *J. Chem. Soc., Chem. Commun.*, 1987, 431 and 1730.
7 A. J. Blake, R. O. Gould, A. J. Holder, T. I. Hyde, A. J. Lavery, G. Reid, and M. Schröder, unpublished results.
8 J. P. Sauvage, C. O. Dietrich-Buchecher, and J. M. Kern, *J. Chem. Soc., Chem. Commun.*, 1985, 760.
9 R. C. Eachus and R. E. Groves, *J. Chem. Phys.*, 1976, **65**, 5445; R. Kirmse, J. Stach, W. Dietzsch, G. Steimecke, and E. Hoyer, *Inorg. Chem.*, 1980, **19**, 2679; A. Tressaud, S. Khairoun, J.-M. Dance, J. Grannec, G. Demazeau, and P. Hagenmuller, *C. R. Acad. Sci., Ser. B*, 1982, **295**, 183.
10 A. J. Blake, A. J. Holder, T. I. Hyde, and M. Schröder, *J. Chem. Soc., Chem. Commun.*, 1987, 987; A. J. Blake, A. J. Holder, T. I. Hyde, Y. V. Roberts, A. J. Lavery, and M. Schröder, *J. Organomet. Chem.*, 1987, **323**, 261.
11 W. Clegg, *Acta Crystallogr., Sect. A*, 1981, **37**, 22.
12 DIRDIF, P. T. Beurskens, W. P. Bosman, H. M. Doesbury, Th. E. M. van den Hark, P. A. J. Prick, J. H. Noordik, G. Beurskens, R. O. Gould, and V. Parthasarathia, 'Applications of Direct Methods to Difference Structure Factors,' University of Nijmegen, Netherlands, 1983.

Stereochemical and Electronic Control of the Copper(II)/(I) Couple by N_2S_4-Donor Macrocycles

Nigel Atkinson,[a] Alexander J. Blake,[b] Michael G. B. Drew,[c] George Forsyth,[c] Aidan J. Lavery,[a] Gillian Reid,[b] and Martin Schröder[b]

[a] *Department of Chemical and Physical Sciences, The Polytechnic, Queensgate, Huddersfield HD1 3DH, England*
[b] *Department of Chemistry, University of Edinburgh, West Mains Road, Edinburgh EH9 3JJ, Scotland*
[c] *Department of Chemistry, The University, Whiteknights, PO Box 224, Reading RG6 2AD, England*

The N_2S_4 donor complex $[Cu(L^1)]^{2+}$ (L^1 = 1,4,10,13-tetrathia-7,16-diazacyclo-octadecane) shows a chemically reversible copper(II)/(I) couple at $E_{\frac{1}{2}}$ −0.31 V *vs.* Fc/Fc$^+$ (ferrocene/ferrocenium), whereas the methylated analogue, $[Cu(L^2)]^{2+}$ (L^2 = 7,16-dimethyl-1,4,10,13-tetrathia-7,16-diazacyclo-octadecane) shows a more anodic copper(II)/(I) couple at $E_{\frac{1}{2}}$ +0.06 V *vs.* Fc/Fc$^+$; these differences in redox potential can be related to the stereochemical features of the copper(II) complexes, the crystal structures of which have been determined for $[Cu(L^1)]^{2+}$ and $[Cu_2(L^2)(NCMe)_2]^{2+}$.

The co-ordination chemistry of the mixed N_2S_4 donor macrocycles L^1 (L^1 = 1,4,10,13-tetrathia-7,16-diazacyclo-octadecane) and L^2 (L^2 = 7,16-dimethyl-1,4,10,13-tetrathia-7,16-diazacyclo-octadecane) are of particular interest since these ligands incorporate both hard and soft donor atoms in a co-ordinatively restricted environment.[1] Very little has been reported on the stereochemical characteristics of transition metal complexes of these ligands[1—3], although Black and co-workers have defined[1] the possibilities of *meso* and *rac* isomers for octahedral complexes of the type $[M(L^1)]^{x+}$. We were interested in the stereochemical preferences of d^9 Cu^{II} with these N_2S_4 donor ligands, and report herein structural and redox data for these Cu^{II} species.

Reaction of $Cu(ClO_4)_2$ with one equivalent of L (L = L^1 or L^2) in refluxing EtOH for 3 h afforded green solutions from which the complexes $[Cu(L)](ClO_4)_2$ could be isolated as green products. Crystals of $[Cu(L^1)](ClO_4)_2 \cdot H_2O$ were grown from aqueous solution. The single crystal *X*-ray structure of

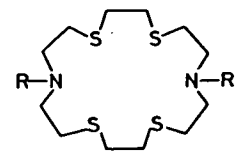

L^1 : R = H
L^2 : R = Me

Pd^{II} with L^1 and L^2, we propose that the cation $[Cu(L^2)]^{2+}$ would adopt a *meso* configuration. This would allow closer approach of the four soft thioether donors to the metal centre, and thus provide greater stability of the Cu^I species, as observed experimentally.

The net stabilisation of Cu^I by L^2 is reflected in the isolation of the stable binuclear species $[Cu_2(L^2)(NCMe)_2]^{2+}$. The single crystal *X*-ray structure of $[Cu_2(L^2)(NCMe)_2](PF_6)_2$ shows† (Figure 2) a centrosymmetric structure with each Cu^I centre bound tetrahedrally to two S-donors and one N-donor of L^2 [Cu–S(4) 2.317(4), Cu–S(10) 2.286(4), Cu–N(7) 2.165(7) Å], and one MeCN molecule [Cu–N(1S) 1.924(9) Å]. The Cu · · · Cu separation is 4.283(2) Å with each Cu^I ion bound by an N_2S_2 donor set similar to that found in the Type 1 copper proteins.[7]

We thank the S.E.R.C. for support.

Received, 25th January 1989; Com. 9/00417C

References

1 D. St. C. Black and I. A. McLean, *Chem. Commun.*, 1968, 1004; *Tetrahedron Lett.*, 1969, 3961; *Austr. J. Chem.*, 1971, **24**, 1401.
2 B. Dietrich, J.-M. Lehn, and J.-P Sauvage, *Chem. Commun.*, 1970, 1055; A. A. Alberts, R. Annunziata, and J.-M. Lehn, *J. Am. Chem. Soc.*, 1977, **99**, 8502.
3 G. Reid, A. J. Blake, T. I. Hyde, and M. Schröder, *J. Chem. Soc., Chem. Commun.*, 1988, 1397.
4 J. R. Hartman and S. R. Cooper, *J. Am. Chem. Soc.*, 1986, **108**, 1202.
5 P. W. R. Corfield, C. Ceccarelli, M. D. Glick, I. W.-Y. Moy, L. A. Ochrymowycz, and D. B. Rorabacher, *J. Am. Chem. Soc.*, 1985, **107**, 2399.
6 W. N. Setzer, C. A. Ogle, G. S. Wilson, and R. S. Glass, *Inorg. Chem.*, 1983, **22**, 266.
7 H. C. Freeman, in 'Co-ordination Chemistry,' vol. 21, ed. J. P. Laurent, Pergamon Press, Oxford, 1981, p. 29.
8 SHELX76, Program for Crystal Structure Determination, G. M. Sheldrick, University of Cambridge, 1976.

Palladium(II)/(III) Complexes of Triaza Macrocycles: Synthesis and Single Crystal *X*-Ray Structures of $[Pd^{III}(tacn)_2]^{3+}$ and $[Pd^{II}(tacn)(tacnH)]^{3+}$ (tacn = 1,4,7-triazacyclononane)

Alexander J. Blake, Linda M. Gordon, Alan J. Holder, Timothy I. Hyde, Gillian Reid, and Martin Schröder*

Department of Chemistry, University of Edinburgh, West Mains Road, Edinburgh EH9 3JJ, Scotland

The complex cation $[Pd(tacn)_2]^{2+}$ (tacn = 1,4,7-triazacyclononane) shows a one-electron oxidation at $E_{\frac{1}{2}} = +0.07$ V *vs.* Fc/Fc^+ (ferrocene/ferrocinium) to afford the stable mononuclear Pd^{III} species $[Pd(tacn)_2]^{3+}$, which has a tetragonally-distorted octahedral structure with Pd–N(1) = 2.180(9), Pd–N(4) = 2.118(9), Pd–N(7) = 2.111(9) Å.

Reprinted from the Journal of The Chemical Society
Chemical Communications 1988

Palladium(II)/(III) Complexes of Triaza Macrocycles: Synthesis and Single Crystal *X*-Ray Structures of $[Pd^{III}(tacn)_2]^{3+}$ and $[Pd^{II}(tacn)(tacnH)]^{3+}$ (tacn = 1,4,7-triazacyclononane)

Alexander J. Blake, Linda M. Gordon, Alan J. Holder, Timothy I. Hyde, Gillian Reid, and Martin Schröder*

Department of Chemistry, University of Edinburgh, West Mains Road, Edinburgh EH9 3JJ, Scotland

The complex cation $[Pd(tacn)_2]^{2+}$ (tacn = 1,4,7-triazacyclononane) shows a one-electron oxidation at $E_{\frac{1}{2}}$ = +0.07 V *vs.* Fc/Fc$^+$ (ferrocene/ferrocinium) to afford the stable mononuclear Pd^{III} species $[Pd(tacn)_2]^{3+}$, which has a tetragonally-distorted octahedral structure with Pd–N(1) = 2.180(9), Pd–N(4) = 2.118(9), Pd–N(7) = 2.111(9) Å.

We have been investigating the stereochemical and redox properties of tridentate macrocyclic ligands with Pd^{II} and Pt^{II}.[1] The stabilisation of M^{III} species by 1,4,7-trithiacyclononane (ttcn) in the complexes $[M(ttcn)_2]^{3+}$ (M = Pd, Pt)[2,3] has prompted us to study the analogous chemistry with the triaza analogue 1,4,7-triazacyclononane (tacn).[4]

Reaction of K_2PdCl_4 with two molar equiv. of tacn.$3HNO_3$ in water in the presence of NaOH affords an orange solution from which the complex $[Pd(tacn)_2](PF_6)_2$† can be isolated by addition of excess of NH_4PF_6. In addition, by controlling the pH of the reaction solution, the protonated complex cation $[Pd(tacn)(tacnH)]^{3+}$† can be isolated. Single crystals of $[Pd(tacn)(tacnH)](PF_6)_2(NO_3).H_2O$ were grown from

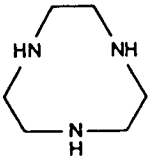

tacn

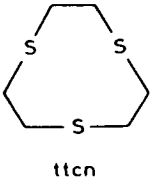

ttcn

† All complexes have been characterised by spectroscopic and analytical methods.

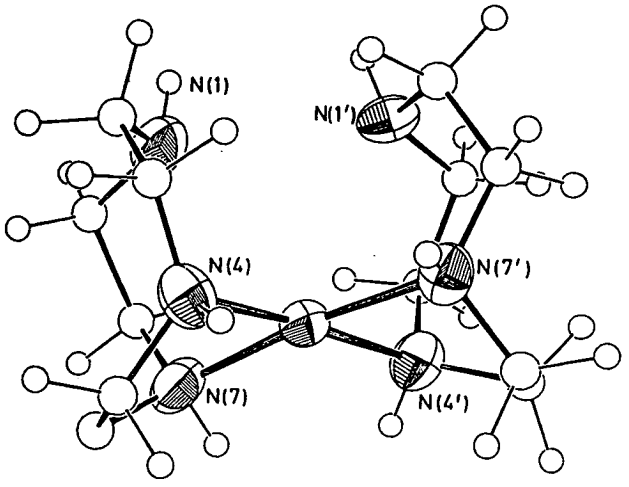

Figure 1. Single crystal *X*-Ray structure of $[Pd(tacn)(tacnH)]^{3+}$ with numbering scheme adopted.

aqueous solution and the single crystal *X*-ray structure of the complex was determined.

Figure 1 shows the structure of the $[Pd(tacn)(tacnH)]^{3+}$ cation.‡ The triaza ligands are each co-ordinated *via* two N-donors to the Pd^{II} centre to give a square planar complex, Pd–N(4) = 2.017(14), Pd–N(7) = 2.087(14), Pd–N(4') = 2.051(12), Pd–N(7') = 2.067(13) Å. The unusual feature of the structure is that the two non-bonding N-donors, N(1) and N(1'), lie on the same side of the PdN_4 plane to give a *syn* configuration for the complex, Pd–N(1) = 2.982(11), Pd–N(1') = 3.079(11) Å. The N(1) · · · N(1') distance is 2.954(15) Å. This structure contrasts with that of the Pt^{II} analogue $[Pt(tacn)_2]^{2+}$ in which the two non-bonding N-donors lie on opposite sides of the PtN_4 plane to give an *anti* configuration of macrocyclic ligands.[5] Extensive H-bonding occurs in the Pd^{II} complex between the cation and the NO_3^- and H_2O molecules. This may explain the net stabilisation of the *syn* over the *anti* isomer for this species, and suggests that H-bonding may be used to control the configuration of co-ordinated polyaza macrocycles. In the absence of H-bonding, we would expect the complex cation $[Pd(tacn)_2]^{2+}$ to adopt an *anti* configuration, and be isostructural with its Pt^{II} analogue.§

Cyclic voltammetry of $[Pd(tacn)_2](PF_6)_2$ in MeCN (0.1 M, $Bu^n_4NPF_6$) at platinum electrodes shows a chemically reversible oxidation at $E_{\frac{1}{2}}$ = +0.07 V *vs.* Fc/Fc$^+$ (ferrocene/ferrocinium).[6] A more sluggish, second oxidation is observed at +0.45 V. Coulometry confirms both these oxidations to be one-electron processes. Since the triaza ligand is redox-inactive within this potential range, these oxidations are

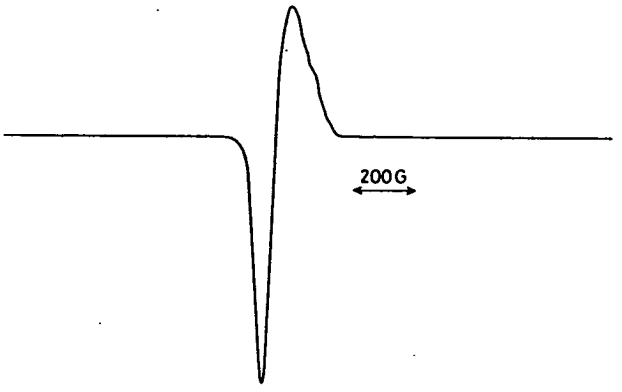

Figure 2. *X*-Band e.s.r. spectrum of $[Pd(tacn)_2]^{3+}$ measured at 77 K (MeCN glass).

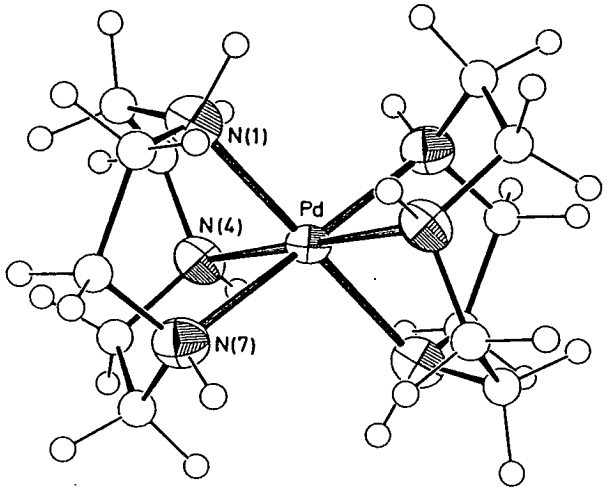

Figure 3. Single crystal *X*-ray structure of $[Pd(tacn)_2]^{2+}$ with numbering scheme adopted.

‡ *Crystal data* for $C_{12}H_{31}N_6Pd^{2+}.NO_3^-.2PF_6^-.H_2O$: A yellow columnar crystal (0.10 × 0.14 × 0.55 mm) was mounted on a Stöe–Siemens AED2 four-circle diffractometer. Orthorhombic, space group $P2_12_12_1$, a = 8.4574(15), b = 16.2641(27), c = 18.756(4) Å, U = 2579.9 Å^3 (by least-squares refinement on diffractometer angles for 11 reflections with 15 <θ <17°, λ = 1.54184 Å), M = 735.62, D_c = 1.894 g cm^{-3}, Z = 4, μ(Cu-K_α) = 83.10 cm^{-1}. Data collection using Cu-K_α *X*-radiation yielded 2155 unique reflections ($2\theta_{max}$.120°, h 0→9, k 0→18, l 0→21). These were corrected for absorption using ψ scans, and 1663 with $F > 6\sigma(F)$ were used in all calculations. After location of the Pd atom from a Patterson synthesis, its position was used in DIRDIF[11] to develop the structure. Using this method, followed by iterative cycles of least-squares refinement and difference Fourier synthesis,[12] all non-H atoms were found. With the exception of a carbon atom in one of the ligands, for which disorder had to be modelled, all non-H atoms were refined anisotropically. H atoms were included in fixed, calculated positions. At final convergence, R = 0.0492, R_w = 0.0674, S = 1.112 for 338 parameters and the final difference map showed no feature above +1.04 or below −0.72 eÅ^{-3}.

For $C_{12}H_{30}N_6Pd^{3+}.3PF_6^-$: A yellow plate (0.40 × 0.45 × 0.025 mm) was mounted on a Stöe–Siemens AED2 four-circle diffractometer. Triclinic, space group $P\bar{1}$, with a = 9.3663(22), b = 9.3853(24), c = 17.314(5) Å, α = 80.661(13), β = 79.832(13), γ = 61.199(10)°, U = 1307.5 Å^3 [from 2θ values of 18 reflections measured at ±ω (24 <2θ <25°, λ = 0.71073 Å)], M = 799.70, D_c = 2.03 g cm^{-3}, Z = 2, μ(Mo-K_α) = 9.69 cm^{-1}, T = 298 K. Data collection using Mo-K_α *X*-radiation gave 3415 unique reflections ($2\theta_{max}$.45°, h −9→10, k −9→10, l 0→18) of which 2452 with $F > 2\sigma(F)$ were used in all calculations. A Patterson synthesis located two Pd atoms on inversion centres. DIRDIF[11] found all non-H atoms. The structure was developed by least-squares refinement and difference Fourier synthesis.[12] The Pd, C, N, P, and F atoms were refined anisotropically. H Atoms were included in fixed calculated positions. One cation was significantly better determined than the other; all parameters quoted in the text refer to the former. At final convergence, R = 0.0594, R_w = 0.0828, S = 1.050 for 364 parameters and the final difference map showed no feature above +1.7 or below −0.48 e Å^{-3}. Atomic co-ordinates, bond lengths and angles, and thermal parameters have been deposited at the Cambridge Crystallographic Data Centre. See Notice to Authors, Issue No. 1.

§ Since the submission of this paper, McAuley *et al.*[13] have reported the crystal structure of $[Pd(tacn)_2]^{2+}$ with the two ligands in an *anti* configuration.[13]

therefore assigned to $Pd^{II/III}$ and $Pd^{III/IV}$ couples, respectively. Controlled potential electrolysis of $[Pd(tacn)_2]^{2+}$ at +0.3 V affords the bright yellow Pd^{III} complex, the e.s.r. spectrum of which (77 K, MeCN glass) shows a strong, broad, near-isotropic signal with, $g_\perp = 2.123$, $g_\parallel = 2.007$ (Figure 2). Super-hyperfine coupling to two N-donors (1:2:3:2:1 quintet) is more apparent in the second derivative spectrum with $A_{II} = 27$ G (1G = 10^{-4} T). Similar coupling to two N-donors has been observed for octahedral Ni^{III} tetra-aza macrocyclic complexes with a d_{z^2} ground state.[7] Further oxidation at +0.7 V leads to the formation of a product which is e.s.r. silent and is therefore assigned to the octahedral Pd^{IV} species $[Pd(tacn)_2]^{4+}$. The reversible interconversion of the $Pd^{II/III/IV}$ complexes was confirmed by *in situ* electronic spectral measurements using an optically transparent thin layer electrode (OTTLE) system.

The complex $[Pd(tacn)_2](PF_6)_3$† was isolated by careful addition of diethyl ether to an electrolysed solution. Crystals of the complex were grown from MeCN/diethyl ether and the single crystal *X*-ray structure determined. The structure of $[Pd(tacn)_2](PF_6)_3$‡ (Figure 3) shows tetragonally distorted N_6 co-ordination around the Pd^{III} centre with Pd–N(1) = 2.180(9), Pd–N(4) = 2.118(9), Pd–N(7) = 2.111(9) Å, consistent with a Jahn–Teller distorted d^7 complex. The structure of $[Pd(tacn)_2]^{3+}$ is therefore related to that of $[Pd(ttcn)_2]^{3+}$ which is the only other reported crystal structure of a mononuclear Pd^{III} species.[2] However, the trithia complex $[Pd(ttcn)_2]^{3+}$ is generated at a higher anodic potential ($E_{\frac{1}{2}}$ = 0.605 V *vs.* Fc/Fc$^+$), and is also much less stable than the triaza analogue in the solid state and in solution. $[Pd(tacn)_2]^{3+}$ is stable indefinitely in MeCN and $MeNO_2$ and may be manipulated readily in non-reducing solvents; in contrast, $[Pd(ttcn)_2]^{3+}$ decomposes slowly in these solvents, and is stabilised indefinitely only in acidic media. Interestingly, the solid state structure of $[Ni(tacn)_2]^{3+}$ shows a greater tetragonal distortion than the Pd^{III} complex, Ni–N = 1.964(5), 1.985(5), 1.970(5), 1.965(5) Å and 2.107(5), 2.111(5) Å.[8] This may reflect the greater size of Pd^{III} *vs.* Ni^{III}, with the cavity generated by two tacn ligands being too large for Ni^{III}.[8,9]

The stabilisation of Pd^{III} by the triaza macrocycle (tacn) contrasts with the redox properties of square planar Pd^{II} tetra-aza complexes which, in general, do not show $Pd^{II/III}$ couples.[1,10] This difference can be ascribed to the availability of distorted octahedral stereochemistry in the complexes of tacn.

We thank the S.E.R.C. for support, and Johnson Matthey Plc for generous loans of platinum metals.

Received, 6th June 1988; Com. 8/02253D

References

1 M. Schröder, *Pure Appl. Chem.*, 1988, **60**, 517, and references therein.
2 A. J. Blake, A. J. Holder, T. I. Hyde, and M. Schröder, *J. Chem. Soc., Chem. Commun.*, 1987, 987; A. J. Blake, A. J. Holder, T. I. Hyde, Y. V. Roberts, A. J. Lavery, and M. Schröder, *J. Organomet. Chem.*, 1987, **323**, 261.
3 A. J. Blake, R. O. Gould, A. J. Holder, T. I. Hyde, M. O. Odulate, A. J. Lavery, and M. Schröder, *J. Chem. Soc., Chem. Commun.*, 1987, 118.
4 K. Wieghardt and P. Chaudhuri, 'Progress in Inorganic Chemistry,' **35**, pp. 329—436, ed. S. J. Lippard, 1987.
5 K. Wieghardt, M. Köppen, W. Swiridoff, and J. Weiss, *J. Chem. Soc., Dalton Trans.*, 1983, 1869.
6 D. Fortier, A. McAuley, S. Subramanian, and T. W. Whitcombe, 30th. International Congress of Pure and Applied Chemistry, Manchester, U.K., September 1985.
7 F. V. Lovecchio, E. S. Gore, and D. H. Busch, *J. Am. Chem. Soc.*, 1974, **96**, 3109.
8 K. Wieghardt, W. Walz, B. Nuber, J. Weiss, A. Ozarowski, H. Stratemeier, and D. Reinen, *Inorg. Chem.*, 1986, **25**, 1650.
9 V. J. Thöm, J. C. A. Boeyens, G. J. McDougall, and R. D. Hancock, *J. Am. Chem. Soc.*, 1984, **106**, 3198.
10 A. J. Blake, R. O. Gould, T. I. Hyde, and M. Schröder, *J. Chem. Soc., Chem. Commun.*, 1987, 431.
11 P. T. Beurskens, W. P. Bosman, H. M. Doesbury, Th. E. M. van den Hark, P. A. J. Prick, J. H. Noordik, G. Beurskens, R. O. Gould, and V. Parthasarathia, DIRDIF, Applications of Direct Methods to Difference Structure Factors, University of Nijmegen, Netherlands, 1983.
12 G. M. Sheldrick, SHELX76, Program for Crystal Structure Determination, University of Cambridge, U.K., 1976.
13 A. McAuley, T. W. Whitcombe, and G. Hunter, *Inorg. Chem.*, 1988, **27**, 2634.

Synthesis and Single-crystal *X*-Ray Structure Determination of *trans*-[$RhCl_2$(tmc)]PF_6 (tmc = 1,4,8,11-tetramethyl-1,4,8,11-tetra-azacyclotetradecane)†

Alexander J. Blake, Gillian Reid, and Martin Schröder*
Department of Chemistry, University of Edinburgh, West Mains Road, Edinburgh EH9 3JJ

Reaction of $RhCl_3 \cdot 3H_2O$ with one molar equivalent of tmc (1,4,8,11-tetramethyl-1,4,8,11-tetra-azacyclotetradecane) in refluxing MeOH affords the complex cation $[RhCl_2(tmc)]^+$. The complex $[RhCl_2(tmc)]PF_6$ crystallises in the orthorhombic space group *Pnma*, with each anion and each cation lying on a crystallographic mirror plane. The single-crystal *X*-ray structure of the octahedral complex shows the chloride ions mutually *trans* to one another, Rh–Cl 2.355(3) and 2.362(3) Å, with the tetra-aza macrocycle adopting an *RRSS* conformation with two methyl groups lying above, and two methyl groups lying below the RhN_4 plane [Rh–N 2.110(8) and 2.114(8) Å]. *trans*-$[RhCl_2(tmc)]^+$ shows a quasi-reversible Rh^{III}–Rh^{II} redox couple at $E_{\frac{1}{2}} = -0.99$ V *vs.* $[Fe(\eta\text{-}C_5H_5)_2]$–$[Fe(\eta\text{-}C_5H_5)_2]^+$ in MeCN; slow loss of chloride occurs on electrochemical reduction of the complex.

We have been investigating the synthesis and redox activation of macrocyclic complexes of the platinum group metals.[1] As part of this study, we have reported recently the stabilisation of Pt^{III} [2] and Pd^{III} [3,4] centres by polythia macrocycles, and the generation of Pd^{I} bound to tetra-aza ionophores.[5] We wished to extend this work to the complexation of Rh^{III} by N- and S-donor macrocyclic ligands, and to monitor their ability to stabilise d^7 Rh^{II} centres.[2,3] Our approach was based on the synthesis of mononuclear, octahedral Rh^{III} precursors incorporating redox-inactive tetra-aza ligands. On reduction, such complexes would therefore show potential metal-based redox activity, and could give the corresponding Jahn-Teller distorted mononuclear Rh^{II} species. The generation of univalent Cu,[6] Ni,[7] and Pd[5] complexes of tmc [tmc = 1,4,8,11-tetramethyl-1,4,8,11-tetra-azacyclotetradecane (tetramethylcyclam)] has been reported previously. We reasoned that the stabilisation of reduced Rh centres might therefore be achieved using the same macrocyclic ligand system. A further impetus for this work has been the reported generation of mononuclear Rh^{II} porphyrin intermediates,[8] and the stabilisation of Rh^{II} by homoleptic hexathia co-ordination in $[Rh(L^1)_2]^{2+}$ (L^1 = 1,4,7-trithiacyclononane).[2,3,9]

We report herein the synthesis, single-crystal *X*-ray structure determination, and preliminary redox data on the Rh^{III} macrocyclic complex $[RhCl_2(tmc)]^+$.

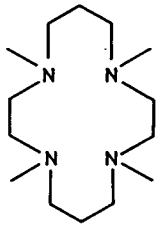

tmc

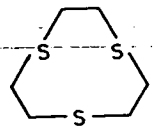

L^1

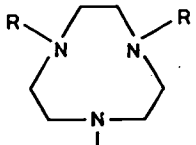

L^2 : R = Me

L^3 : R = H

Results and Discussion

Reaction of $RhCl_3 \cdot 3H_2O$ with one molar equivalent of tmc in refluxing MeOH for 1 h under N_2 affords a yellow solution. Addition of excess of NH_4PF_6 gave a yellow precipitate which could be recrystallised from MeCN. The i.r. spectrum of the product shows a single band at 280 cm^{-1} assigned to a rhodium–chloride stretching vibration, ν(Rh–Cl), in addition to bands assignable to co-ordinated tmc, and PF_6^- counter ion. The u.v.–visible spectrum shows absorbances at $\lambda_{max.}$ 227 (ε 39 900), 324 (241), and 452 nm (63 dm^3 mol^{-1} cm^{-1}); the low absorption coefficients for the *d–d* transitions at 324 and 452 nm are consistent with a *trans*-dichloro system as observed for a series of analogous complexes *trans*-$[RhX_2(cyclam)]^+$ (cyclam = 1,4,8,11-tetra-azacyclotetradecane).[10] The absorbance at 227 nm is assigned to a Cl→Rh ligand-to-metal charge-transfer transition. The fast-atom bombardment (f.a.b.) mass spectrum of the complex shows a peak with the correct isotopic distribution at $M^+ = 429$ assigned to $[^{103}Rh^{35}Cl_2(tmc)]^+$, with peaks at $M^+ = 394$ and 358 corresponding to $[^{103}Rh^{35}Cl(tmc)]^+$ and $[^{103}Rh(tmc - H)]^+$ respectively. This, together with analytical data, suggested the complex cation to be *trans*-$[RhCl_2(tmc)]^+$. The ^1H n.m.r. spectrum of the product in CD_3CN showed a single resonance at δ 2.78 p.p.m. assigned to four equivalent methyl groups of a symmetric isomer. A further four methyl resonances observed at δ 2.76, 2.75, 2.67, and 2.51 p.p.m. may be assigned to the methyl groups of an asymmetric isomer.[11] The ^{13}C DEPT n.m.r. spectrum of the isolated product likewise showed the presence of two isomers in solution. The symmetric isomer showed resonances at δ 50.69 (CH_3), 23.86, 61.52, and 63.10 p.p.m. (three types of CH_2). Fourteen further resonances were observed in the ^{13}C n.m.r. spectrum with δ 47.11, 47.95, 49.87, 53.63 p.p.m. for the four methyl carbon centres. From these data, the asymmetric isomer can be

† *trans*-Dichloro(1,4,8,11-tetramethyl-1,4,8,11-tetra-azacyclotetradecane-*NN'N''N'''*)rhodium(III) hexafluorophosphate.

Supplementary data available: see Instructions for Authors, *J. Chem. Soc., Dalton Trans.*, 1988, Issue 1, pp. xvii—xx.

Table 1. Selected bond lengths (Å) and angles (°) with estimated standard deviations in parentheses for $[RhCl_2(tmc)]PF_6$

Rh(1)–Cl(1)	2.355(3)	P(1)–F(1)	1.569(12)
Rh(1)–Cl(2)	2.362(3)	P(1)–F(2)	1.551(11)
Rh(1)–N(1)	2.110(8)	P(1)–F(3)	1.608(12)
Rh(1)–N(4)	2.114(8)	P(1)–F(4)	1.582(14)
Rh(1)–N(4)–C(3)	105.1(6)	Rh(1)–N(1)–C(2)	101.6(6)
Rh(1)–N(4)–C(5)	107.2(7)	Rh(1)–N(1)–C(14)	109.4(6)
Rh(1)–N(4)–C(4N)	124.7(9)	Rh(1)–N(1)–C(1N)	119.8(8)
Rh(1)–N(4)–C(3′)	105.3(7)	Rh(1)–N(1)–C(2′)	100.1(7)
Rh(1)–N(4)–C(5′)	108.9(10)	Rh(1)–N(1)–C(14′)	116.0(9)
Rh(1)–N(4)–C(4N′)	114.0(10)	Rh(1)–N(1)–C(1N′)	111.8(9)
Cl(1)–Rh(1)–Cl(2)	178.04(11)	F(1)–P(1)–F(2)	89.6(6)
Cl(1)–Rh(1)–N(1)	88.78(23)	F(1)–P(1)–F(3)	89.1(6)
Cl(1)–Rh(1)–N(4)	90.33(22)	F(1)–P(1)–F(4)	178.4(7)
Cl(2)–Rh(1)–N(1)	89.91(23)	F(2)–P(1)–F(3)	175.5(6)
Cl(2)–Rh(1)–N(4)	91.05(22)	F(2)–P(1)–F(4)	91.4(7)
N(1)–Rh(1)–N(4)	86.9(3)	F(3)–P(1)–F(4)	89.7(7)

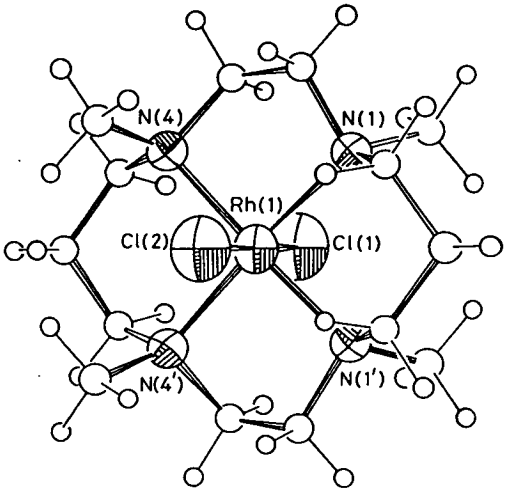

Figure. Structure of the $[RhCl_2(tmc)]^+$ cation with atomic numbering scheme adopted

assigned tentatively to a species with an *RSRR* configuration with three methyl groups above, and one methyl group below the RhN_4 plane, or to a solvated species. The ratio of the two isomers in solution appears to be near 50:50.

It was important to assign a configuration to the symmetric isomer which could be either *RRSS* (two methyls up, two methyls down) or *RSRS* (all methyls up). In view of the fact that no structural studies on Rh^{III} tetra-aza macrocyclic complexes have been previously reported, a crystallographic study was undertaken.

The complex was recrystallised from MeCN to yield orange rhomboid crystals of $[RhCl_2(tmc)]PF_6$. The cation is markedly disordered and the following discussion refers to the major component of that disorder. The *X*-ray structure shows four $[RhCl_2(tmc)]^+$ cations and four PF_6^- anions per unit cell, each bisected by a crystallographically-imposed mirror plane. The cation (see Figure) therefore possesses *m* symmetry with the mirror plane passing through the Rh and Cl atoms and through the central carbon atom of each propyl chain. The octahedral Rh^{III} atom is co-ordinated to two mutually *trans* Cl^- ligands and by a planar arrangement of four N-donors, Rh–Cl 2.355(3) and 2.362(3), Rh–N 2.110(8) and 2.114(8) Å. The structure shows the complex adopting an *RRSS* configuration (or *trans*-III in the notation used by Bosnich *et al.*[12]) with two methyl groups above, and two methyl groups below the RhN_4 co-ordination plane. The Rh atom is displaced by only 0.017 Å out of the N_4 plane confirming that the top and bottom faces of the complex appear identical to the co-ordinated Rh atom. This contrasts with the displacement of 0.082 Å of the Pd atom in the *RSRS* isomer of $[Pd(tmc)]^{2+}$.[5] Calculations indicate that the cavity size of the co-ordinated macrocycle in *trans*-$[RhCl_2(tmc)]^+$ [N(1)–N(4) 2.905(11), N(1)–N(1′) 3.146(11), and N(4)–N(4′) 2.983(11) Å] is slightly larger than that of $[Pd(tmc)]^{2+}$ [N(1)–N(4) 2.968(15), N(1)–N(1′) 2.860(16), and N(4)–N(4′) 2.946(17) Å].[5] Other platinum metal complexes of tmc that have been reported include *trans*-$[RuX_2(tmc)]^+$ (X = Cl, NCO, or NCS),[13] *trans*-$[Ru(O)_2(tmc)]^{2+/+}$,[14] *RSRR trans*-$[Ru(O)Cl(tmc)]^+$,[15] *RSRS trans*-$[Ru(O)(NCMe)(tmc)]^{2+}$,[16] and *trans*-$[Os(O)_2(tmc)]^{2+/+}$.[17] An *RRSS* configuration for co-ordinated tmc has been observed for $[Ni(tmc)(OH_2)_2]Cl_2 \cdot 2H_2O$, $[Ni(tmc)][CF_3SO_3]_2$,[18] $[\{Ni(tmc)(N_3)\}_2(\mu\text{-}N_3)]^+$,[19] and $[Ni(O_2COMe)_2(tmc)]$,[20] while the *RSRS* configuration has been found in $[Ni(O_2COMe)(tmc)]^+$,[20] $[Ni(tmc)][CF_3SO_3]_2 \cdot Me_2CO \cdot H_2O$,[21] and $[Ni(N_3)(tmc)]^+$.[22] Strain-energy minimisation analyses on Ni^{II} complexes by Hambley[21] suggest that the *RSRS* and *RRSS* conformations are preferred by four-co-ordinate square-planar and by six-co-ordinate octahedral complexes of tmc respectively. Our crystallographic studies on $[Pd(tmc)]^{2+}$,[5] $[Pd(tbc)]^{2+}$ [tbc = 1,4,8,11-tetrabenzyl-1,4,8,11-tetra-azacyclotetradecane (tetrabenzylcyclam)],[1,23] and *trans*-$[RhCl_2(tmc)]^+$ are in accord with these calculations.

trans-$[RhCl_2(tmc)]^+$ shows a quasi-reversible reduction at $E_{\frac{1}{2}} = -0.99$ V *vs.* $[Fe(\eta\text{-}C_5H_5)_2]$–$[Fe(\eta\text{-}C_5H_5)_2]^+$ in MeCN (0.1 mol dm^{-3} $NBu^n_4PF_6$) at platinum electrodes assigned tentatively to a Rh^{III}–Rh^{II} couple. Cyclic voltammetry confirmed that loss of Cl^- occurred on reduction of $[RhCl_2(tmc)]^+$, the $Cl^{-/0}$ couple being observed near +1.0 V, with a daughter product being detected near −0.35 V. Binding of Cl^- to the metal centre would be expected to be destabilised on reduction of rhodium(III) to rhodium(II), leading to the formation of five-co-ordinate or solvated product(s). This opens up the possibility of utilising the reduction of $[RhCl_2(tmc)]^+$ to generate an electron-rich rhodium centre which, on loss of Cl^-, has a vacant co-ordination site for binding of substrates such as CO, O_2, or alkene. More importantly, these results show that simple alkylated tetra-aza macrocycles could be important ligands for the stabilisation of rhodium(II) [and rhodium(I)] species.

Relatively few examples of mononuclear, rhodium(II) species have been reported in the literature.[8,9,24–26] An important example is [Rh(L′)] [L′ = porphyrinate(2−)] which readily dimerises to $[\{Rh(L')\}_2]$ involving a direct Rh–Rh bond.[8] Other examples include $[Rh(sep)]^{2+}$ [sep = 1,3,6,8,10,13,16,19-octa-azabicyclo[6.6.6]icosane (sepulchrate)] which shows[25] a Rh^{II} couple at $E_{\frac{1}{2}} = -0.71$ V *vs.* $[Fe(\eta\text{-}C_5H_5)_2]$–$[Fe(\eta\text{-}C_5H_5)_2]^+$. The related mixed-sandwich species $[Rh(\eta\text{-}C_5Me_5)(L)]^{2+}$ (L = L^1—L^3) likewise show reversible or quasi-reversible reductions on the cyclic voltammetric time-scale; the reduction products derived from these complexes are however unstable during the electrogeneration experiments at 293 K.[27]

Current work is aimed at the full electrochemical characterisation of the redox and chemical processes (ligand dissociation, dimerisation, O_2 binding) occurring in the Rh systems described herein, and the synthesis of the related complexes $[RhY_2(tmc)]^{3+}$ (Y = pyridine or PR_3).

Experimental

Infrared spectra were measured as Nujol mulls, KBr and CsI discs using a Perkin-Elmer 598 spectrometer over the range 200—4 000 cm^{-1}. U.v.–visible spectra were measured in

quartz cells using a Pye Unicam SP8-400 spectrophotometer. Microanalyses were performed by the Edinburgh University Chemistry Department Microanalytical Service. Electrochemical measurements were performed on a Bruker E310 Universal Modular polarograph. All readings were taken using a three-electrode potentiostatic system in acetonitrile containing 0.1 mol dm^{-3} $NBu^n_4PF_6$ or $NBu^n_4BF_4$ as supporting electrolyte. Cyclic voltammetric measurements were carried out using a double platinum electrode and a Ag–AgCl reference electrode. Mass spectra were run by electron impact on a Kratos MS 902 and by fast-atom bombardment on a Kratos MS 50TC spectrometer.

Synthesis of trans-$[RhCl_2(tmc)]PF_6$.—$RhCl_3 \cdot 3H_2O$ (0.15 g, 0.5 mmol) was treated with one molar equivalent of tmc (0.15 g, 0.59 mmol) in refluxing MeOH under N_2 for 1 h. Addition of excess of NH_4PF_6 gave a golden microcrystalline product which was collected, recrystallised from MeCN, and dried *in vacuo*. Yield: 230 mg, 70% (Found: C, 29.0; H, 5.7; N, 9.7. Calc. for $C_{14}H_{32}Cl_2F_6N_4PRh$: C, 29.2; H, 5.6; N, 9.7%). I.r. spectrum: 3 000, 2 940, 1 450, 1 380, 1 290, 1 260, 1 240, 1 200, 1 170, 1 150, 1 110, 1 050, 1 030, 980, 920, 840, 800, 790, 750, 720, 555, and 280 cm^{-1}. U.v.–visible spectrum: $\lambda_{max.}$ 227 (ε 39 900), 324 (241), and 452 nm (63 dm^3 mol^{-1} cm^{-1}). F.a.b. mass spectrum: found M^+ 429, calc. for $[^{103}Rh^{35}Cl_2(tmc)]^+$ M^+ 429; found M^+ 394, calc. for $[^{103}Rh^{35}Cl(tmc)]^+$ M^+ 394; found M^+ 358, calc. for $[^{103}Rh(tmc - H)]^+$ M^+ 358. ^1H N.m.r. spectrum (CD_3CN, 293 K, 200 MHz): δ 2.78 (s, CH_3, 12 H) and 2.2—3.5 p.p.m. (m, CH_2, 20 H) (symmetric isomer); δ 2.76, 2.75, 2.67, 2.51 (s, CH_3, 12 H) and 2.2—3.5 p.p.m. (m, CH_2, 20 H) (asymmetric isomer). ^{13}C DEPT n.m.r. (CD_3CN, 293 K, 50.32 MHz): δ 23.86 ($CH_2CH_2CH_2$, 2 C), 50.69 (CH_3, 4 C), 61.52 ($NCH_2CH_2CH_2N$, 4 C), 63.10 p.p.m. (NCH_2CH_2N, 4 C) (symmetric isomer); δ 23.55, 24.36 ($NCH_2CH_2CH_2N$, 2 C), 47.11, 47.95, 49.87, 53.63 (CH_3, 4 C), 55.21, 56.12, 60.80, 60.94, 62.93 (two overlapping resonances), 63.58, 64.40 p.p.m. (NCH_2, 8 C) (asymmetric isomer).

Addition of $NaBPh_4$ in place of NH_4PF_6 afforded the BPh_4^- salt $[RhCl_2(tmc)]BPh_4$ (Found: C, 61.4; H, 7.0; N, 8.1. Calc. for $C_{38}H_{52}BCl_2N_4Rh$: C, 60.9; H, 7.0; N, 7.5%).

Single-crystal X-*Ray Structure of trans*-$[RhCl_2(tmc)]PF_6$.—Recrystallisation from MeCN yielded orange, rhomboid crystals suitable for a crystallographic study.

Crystal data. $C_{14}H_{32}Cl_2F_6N_4PRh$, M = 575.3, orthorhombic, space group *Pnma*, a = 14.952(4), b = 10.687(3), c = 13.487(4) Å, U = 2 155 $Å^3$ (by least-squares refinement on diffraction angles for 17 centred reflections), Z = 4, λ = 0.710 73 Å, D_c = 1.773 g cm^{-3}. Crystal dimensions 0.79 × 0.54 × 0.46 mm, $F(000)$ = 1 168, μ(Mo-K_α) = 11.09 cm^{-1}.

Data collection and processing. Stoe-Siemens AED2 four-circle diffractometer, ω–θ mode, 1 650 data ($+h, k, l$) measured to $2\theta = 45°$, giving 1 265 with $F \geqslant 6\sigma(F)$. No significant crystal decay, no absorption correction.

Structure analysis and refinement. The Rh position was deduced from a Patterson synthesis and the remaining non-hydrogen atoms from iterative rounds of least-squares refinement and difference Fourier synthesis.[28] Anisotropic thermal parameters were refined for Rh, Cl, P, F, and N. During refinement, some disorder of the macrocyclic ligand became obvious and could only be modelled by refining the minor isomer as an idealised, rigid group and, for the major isomer, constraining all C–C and C–N bonds to a common value of 1.523(20) Å and all macrocyclic angles to be tetrahedral. The discussion of the structure refers to the major component [66.3(13)%] of the disorder. We believe that the disorder arises from rotation of one component relative to the other, although the presence of a minor isomer in the solid state cannot be entirely discounted. At convergence, R, R' = 0.0715, 0.1153 respectively, S = 1.369 for 126 parameters, and the final difference Fourier synthesis showed no feature above 1.26 or below −0.74 e $Å^{-3}$. The weighting scheme $w^{-1} = \sigma^2(F) + 0.000\,811F^2$ gave satisfactory agreement analyses. Illustrations were prepared using ORTEP,[29] molecular geometry calculations utilised CALC,[30] and scattering factor data were inlaid [28] or taken from ref. 31. Fractional atomic co-ordinates are given in Table 2.

Table 2. Fractional atomic co-ordinates with estimated standard deviations in parentheses for $[RhCl_2(tmc)]PF_6$

Atom	x	y	z
Rh(1)	0.150 94(6)	0.25	0.125 14(7)
Cl(1)	0.024 92(22)	0.25	0.020 41(25)
Cl(2)	0.274 05(25)	0.25	0.234 9(3)
N(1)	0.092 2(5)	0.102 8(7)	0.206 5(7)
N(4)	0.211 7(5)	0.110 4(7)	0.036 8(5)
C(2)	0.155 9(8)	−0.004 9(15)	0.184 5(7)
C(3)	0.172 1(11)	−0.012 6(13)	0.073 1(7)
C(5)	0.182 8(14)	0.133 7(4)	−0.069 9(10)
C(6)	0.229 6(18)	0.25	−0.109 4(11)
C(13)	0.039 4(14)	0.25	0.336 8(12)
C(14)	0.095 4(12)	0.133 7(4)	0.316 7(9)
C(4N)	0.310 7(7)	0.077 4(24)	0.039 2(15)
C(1N)	−0.003 3(6)	0.062 5(15)	0.183 7(16)
C(2′)	0.089 5(7)	0.001 4(17)	0.127 2(9)
C(3′)	0.182 2(9)	−0.013 5(12)	0.081 8(12)
C(5′)	0.312 9(7)	0.122 8(19)	0.045(3)
C(6′)	0.341 7(10)	0.25	0.005(4)
C(13′)	−0.004 1(17)	0.25	0.301 4(25)
C(14′)	−0.002 1(7)	0.126 6(20)	0.245 0(18)
C(1N′)	0.151 7(16)	0.060 3(20)	0.291 7(13)
C(4N′)	0.184 5(22)	0.114 8(25)	−0.072 0(10)
P(1)	0.571 4(4)	0.25	0.864 0(4)
F(1)	0.650 4(8)	0.25	0.940 7(11)
F(2)	0.526 4(7)	0.141 8(8)	0.922 2(7)
F(3)	0.623 7(8)	0.354 3(10)	0.800 6(8)
F(4)	0.493 8(11)	0.25	0.784 3(12)

Additional material available from the Cambridge Crystallographic Data Centre comprises thermal parameters, remaining bond lengths and angles, H-atom co-ordinates.

Acknowledgements

We thank the S.E.R.C. for support and Johnson Matthey plc for generous loans of platinum metals.

References

1 M. Schröder, *Pure Appl. Chem.*, 1988, **60**, 517.
2 A. J. Blake, R. O. Gould, A. J. Holder, T. I. Hyde, M. O. Odulate, A. J. Lavery, and M. Schröder, *J. Chem. Soc., Chem. Commun.*, 1987, 118.
3 A. J. Blake, A. J. Holder, T. I. Hyde, and M. Schröder, *J. Chem. Soc., Chem. Commun.*, 1987, 987.
4 A. J. Blake, A. J. Holder, T. I. Hyde, Y. V. Roberts, A. J. Lavery, and M. Schröder, *J. Organomet. Chem.*, 1987, **323**, 261.
5 A. J. Blake, R. O. Gould, T. I. Hyde, and M. Schröder, *J. Chem. Soc., Chem. Commun.*, 1987, 431.
6 N. Jubran, H. Cohen, Y. Koresh, and D. Meyerstein, *J. Chem. Soc., Chem. Commun.*, 1984, 1683.
7 N. Jubran, G. Ginzberg, H. Cohen, and D. Meyerstein, *J. Chem. Soc., Chem. Commun.*, 1982, 517; *Inorg. Chem.*, 1985, **24**, 251.
8 B. B. Wayland and A. R. Newman, *J. Am. Chem. Soc.*, 1979, **101**, 6472; *Inorg. Chem.*, 1981, **20**, 3093; K. M. Kadish, C-L. Yao, J. E. Anderson, and P. Cocolios, *ibid.*, 1985, **24**, 4515; J. E. Anderson, C-L. Yao, and K. M. Kadish, *ibid.*, 1986, **25**, 718; *J. Am. Chem Soc.*, 1987, **109**, 1106.

9 A. J. Blake, R. O. Gould, A. J. Holder, T. I. Hyde, and M. Schröder, *J. Chem. Soc., Dalton Trans.*, in the press.
10 E. J. Bounsall and S. R. Koprich, *Can. J. Chem.*, 1970, **44**, 1481.
11 P. Moore, J. Sachinidis, and G. R. Willey, *J. Chem. Soc., Chem. Commun.*, 1983, 522.
12 B. Bosnich, C. K. Poon, and M. L. Tobe, *Inorg. Chem.*, 1965, **4**, 1102.
13 C-M. Che, S. S. Kwong, and C. K. Poon, *Inorg. Chem.*, 1985, **24**, 1601.
14 C-M. Che, T-W. Tang, and C-K. Poon, *J. Chem. Soc., Chem Commun.*, 1984, 641; C-M. Che, S-S. Kwong, and C-K. Poon, *ibid.*, 1985, 986; C-N. Che and K. Y. Wong, *ibid.*, 1986, 229.
15 C-M. Che, K-Y. Wong, and T. C. M. Mak, *J. Chem. Soc., Chem. Commun.*, 1985, 988.
16 C-M. Che, K-Y. Wong, and T. C. W. Mak, *J. Chem. Soc., Chem. Commun.*, 1985, 546; K-Y. Wong, C-M. Che, and F. C. Anson, *Inorg. Chem.*, 1987, **26**, 737.
17 C-M. Che and W-K. Cheng, *J. Chem. Soc., Chem. Commun.*, 1986, 1519; *J. Am. Chem. Soc.*, 1986, **108**, 4644.
18 E. K. Barefield, G. M. Freeman, and D. G. Van Derveer, *Inorg. Chem.*, 1986, **25**, 552.
19 F. Wagner, M. T. Mocella, M. J. D'Aniello jun., A. H. J. Wang, and E. K. Barefield, *J. Am. Chem. Soc.*, 1974, **96**, 2625.
20 M. Kato and T. Ito, *Bull. Chem. Soc. Jpn.*, 1986, **59**, 285.
21 T. W. Hambley, *J. Chem. Soc., Dalton Trans.*, 1986, 565.
22 M. J. D'Aniello, M. T. Mocella, F. Wagner, E. K. Barefield, and I. C. Paul, *J. Am. Chem. Soc.*, 1975, **97**, 192.
23 A. J. Blake, R. O. Gould, T. I. Hyde, and M. Schröder, *J. Chem. Soc., Chem Commun.*, 1987, 1730.
24 T. R. Felthouse, *Prog. Inorg. Chem.*, 1982, **29**, 74.
25 J. MacB. Harrowfield, A. J. Herit, P. A. Lay, A. M. Sargeson, A. M. Bond, W. A. Mulac, and J. C. Sullivan, *J. Am. Chem. Soc.*, 1983, **105**, 5503.
26 E. Billig, S. I. Shupack, J. H. Waters, R. Williams, and H. B. Gray, *J. Am. Chem. Soc.*, 1964, **86**, 926; M. A. Bennett and R. A. Longstaff, *ibid.*, 1969, **91**, 6266; C. Masters and B. L. Shaw, *J. Chem. Soc. A*, 1971, 3679; B. R. James, F. T. T. Ng, and E. Ochiai, *Can. J. Chem.*, 1972, **50**, 590; G. Valentini, G. Braca, G. Sbrana, and A. Colligiani, *Inorg. Chim. Acta*, 1983, **69**, 211; N. V. Vugman and W. O. Franco, *J. Chem. Phys.*, 1983, **78**, 2099; N. V. Vugman and N. M. Pinhal, *Mol. Phys.*, 1983, **49**, 1315; N. G. Connelly and G. Garcia, *J. Chem. Soc., Chem. Commun.*, 1987, 246.
27 M. N. Bell, A. J. Blake, M. Schröder, and T. A. Stephenson, *J. Chem. Soc., Chem. Commun.*, 1986, 471; M. N. Bell, A. J. Blake, and M. Schröder, unpublished work.
28 G. M. Sheldrick, SHELX 76, Program for Crystal Structure Determination, University of Cambridge, 1976.
29 P. D. Mallinson and K. W. Muir, ORTEP II, interactive version, *J. Appl. Crystallogr.*, 1985, **18**, 51.
30 R. O. Gould and P. Taylor, CALC, FORTRAN77 version, University of Edinburgh, 1985.
31 D. T. Cromer and J. L. Mann, *Acta Crystallogr., Sect. A*, 1968, **24**, 321.

Received 24*th June* 1987; *Paper* 7/1136

Journal of Organometallic Chemistry, 356 (1988) 389–396
Elsevier Sequoia S.A., Lausanne – Printed in The Netherlands

Platinum metal thioether macrocyclic complexes: synthesis and single crystal X-ray structure of *cis*-$[IrCl_2(L)]BPh_4$ (L = 1,4,8,11-tetrathiacyclotetradecane)

Alexander J. Blake, Robert O. Gould, Gillian Reid and Martin Schröder *

Department of Chemistry, University of Edinburgh, West Mains Road, Edinburgh EH9 3JJ (Great Britain)

(Received April 27th, 1988)

Abstract

Reaction of $IrCl_3$ with 1,4,8,11-tetrathiacyclotetradecane (L) in refluxing $EtOH/H_2O$ gives the complex cation $[IrCl_2(L)]^+$. Crystals of $[IrCl_2(L)]BPh_4$ are monoclinic, space group $P2_1$, with *a* 12.6927(14), *b* 12.1361(20), *c* 14.4912(18) Å, β 111.813(13)°, *V* 2072.4 Å^3, D_c 1.363 g cm^{-3}, $Z = 2$. The single crystal X-ray structure of $[IrCl_2(L)]BPh_4$ shows a distorted octahedral stereochemistry around Ir^{III}, with mutually *cis* Cl^- ligands, Ir–Cl(1) 2.389(5), Ir–Cl(2) 2.385(5) Å, angle Cl(1)IrCl(2) 91.02(16)°. The tetrathia macrocycle is coordinated to the metal centre via all four S-donors (Ir–S(1) 2.277(4), Ir–S(4) 2.287(5), Ir–S(8) 2.268(4), Ir–S(11) 2.343(5) Å) with S(1), S(4), and S(8) *trans* to Cl(2), S(11), and Cl(1) respectively.

Introduction

We have been investigating the synthesis, structure and redox properties of platinum metal complexes of polydentate thioether macrocycles [1,2]. The fourteen-membered ring, tetrathia ligand 1,4,8,11-tetrathiacyclotetradecane (L), the sulphur-donor analogue of cyclam, has been found to bind effectively to a range of second and third row transition metal centres including Hg^{II} [3,4], Nb^{V} [5], Ru^{II} [6], Rh^{I} [7,8], Rh^{III} [8], Pd^{II} [1], while ligands of larger hole size have been found to complex with Mo^0, Mo^{II} [9] and Mo^{IV} [10]. This contrasts with the poor binding properties of non-cyclic thioether ligands to transition metal ions [11]. Very few non-porphyrin macrocyclic complexes of Ir have been reported previously [1,12], and no examples of Ir complexation by L have been described. We report here the synthesis and crystal structure of the Ir^{III} species *cis*-$[IrCl_2(L)]BPh_4$.

0022-328X/88/$03.50

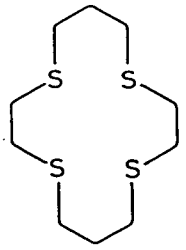

(L)

Results and discussion

$IrCl_3 \cdot 3H_2O$ was treated with one molar equivalent of L in refluxing $EtOH/H_2O$ under N_2 for 14 h in the presence of an excess of $NaBPh_4$. On cooling, the yellow/brown precipitate was collected and recrystallised from CH_3NO_2 to afford a cream-coloured product. The IR spectrum of this complex showed, in addition to bands due to coordinated L and BPh_4^-, two bands at 310 and 305 cm^{-1} assigned to Ir–Cl stretching vibrations, ν(Ir–Cl), suggesting the formation of a *cis*-dichloro complex. The electronic spectrum of the complex showed absorptions at 348 and 297 nm tentatively assigned to *d–d* transitions. The magnitudes of the extinction coefficients, 113 and 1,400 M^{-1} cm^{-1} respectively, for these absorptions are indicative of a *cis* configuration at the metal centre; *d–d* transitions in d^6 metal complexes have been shown previously to have larger extinction coefficients for *cis* than for *trans*-configurations owing to the lower symmetry of *cis*-isomers, e.g. *cis*- and *trans*-$[Rh(X)_2(cyclam)]^+$ [13–15]. The fast-atom bombardment mass spectrum of the complex shows the main molecular ion peak at $M^+ = 531$ corresponding to $[^{193}Ir^{35}Cl_2(L)]^+$, with the correct isotopic distribution. Daughter peaks at $M^+ = 496$ and 461 correspond to $[^{193}Ir^{35}Cl(L)]^+$ and $[^{193}Ir(L)]^+$ respectively, formed by successive loss of Cl. These data together with analytical data suggest that the complex isolated was *cis*-$[IrCl_2(L)]^+BPh_4^-$.

In order to confirm the structure of the complex and the connectivity and conformation of the macrocyclic ligand, a single crystal X-ray structural determination was undertaken. Crystals of *cis*-$[IrCl_2(L)]BPh_4$ were grown from CH_3NO_2/Et_2O. Figure 1 gives views of the complex cation. The structure analysis confirms the *cis* configuration of the Cl^- ligands, with Ir–Cl(1) 2.389(5), Ir–Cl(2) 2.385(5) Å. The macrocycle is coordinated to the Ir^{III} centre as a tetradentate ligand, Ir–S(1) 2.277(4), Ir–S(4) 2.287(5), Ir–S(8) 2.268(4), Ir–S(11) 2.343(5) Å, and adopts a folded conformation with Cl(1) and Cl(2) lying *trans* to S(8) and S(1) respectively. The conformation of the coordinated ligand in this complex is similar to that in *cis*-$[RuCl_2(L)]$ [6] and indicates a general tendency of L to bind to larger metal ions to give *cis* octahedral complexes. In contrast, cyclam binds to Rh^{III} to give both *cis*- and *trans*-dichloro complexes [12,15], while only a *trans* isomer has been isolated for the cation $[RhCl_2(tmc)]^+$ (tmc = 1,4,8,11-tetramethyl-1,4,8,11-tetraazacyclotetradecane) [16]. The ^{13}C NMR spectrum of *cis*-$[IrCl_2(L)]^+$ in CD_3NO_2 shows five resonances at δ 37.99, 29.52, 28.96, 28.39, 23.90 ppm for the secondary carbon centres of the coordinated macrocycle (L), confirming the presence of only one isomer and retention of the *cis* configuration in solution. The metal–sulphur

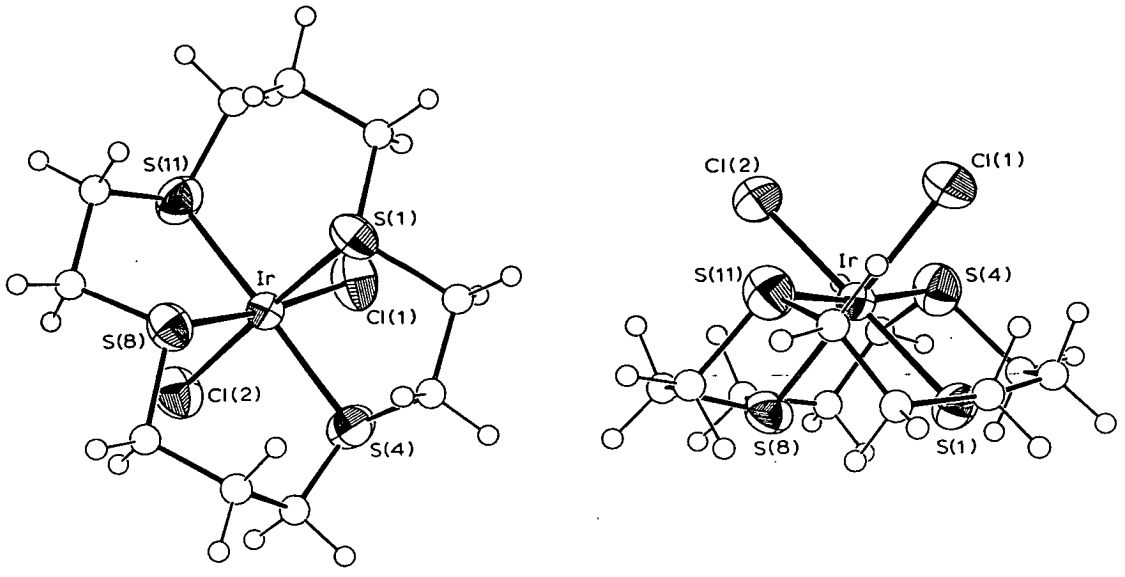

Fig. 1. Two views of the single crystal X-ray structure of *cis*-$[IrCl_2(L)]BPh_4$ with numbering scheme used.

bond lengths in *cis*-$[IrCl_2(L)]^+$ follow the same pattern as found for *cis*-$[RuCl_2(L)]^+$ [6]. For the Ru^{II} complex, it was noted that the metal–sulphur bond distances *trans* to Cl^- (2.262(1) Å) were shorter than those *trans* to S (2.333(1) Å). This is attributed to greater Ru → S(π) back-donation to the thioether donors *trans* to Cl^- [6]. For *cis*-$[IrCl_2(L)]^+$, the same general pattern in bond lengths is observed, with Ir–S 2.277(4), 2.268(4) Å (*trans* to Cl^-) and 2.287(5) 2.343(5) Å (*trans* to S).

Cyclic voltammetry of *cis*-$[IrCl_2(L)]PF_6$ in CH_3CN (0.1 *M* $^nBu_4NPF_6$) at platinum electrodes shows no oxidation in the range 0 → +2.0 V vs. Fc/Fc^+. The complex undergoes an irreversible reduction at $E_p = -1.82$ V vs. Fc/Fc^+ at a scan rate of 200 mV s^{-1}, presumably corresponding to the formation of an Ir^I species of type $[Ir(L)]^+$ via loss of Cl^-. This occurs at a considerably more cathodic potential than that for the analogous tetra-aza complex *trans*-$[RhCl_2(tmc)]^+$ which shows a quasi-reversible $Rh^{III/II}$ couple at $E_{1/2}$ −0.99 V vs. Fc/Fc^+ in CH_3CN [16]. Larger thioether ring systems may be more likely to give *trans*-dichloro complexes, and to stabilise lower valent, electron-rich Ir centres [7].

Experimental

Infrared spectra were recorded as Nujol mulls or as KBr or CsI discs on a Perkin–Elmer 598 spectrometer over the range 200–4000 cm^{-1}. UV-visible spectra were recorded for solutions in quartz cells using a Pye Unicam SP8-400 spectrophotometer. Microanalyses were performed by the Edinburgh University Chemistry Department microanalytical service. Electron impact mass spectra were obtained on a Kratos MS 902 and fast atom bombardment mass spectra on a Kratos MS 50TC spectrometer. Electrochemical measurements were performed with a Bruker E310 Universal Modular Polarograph; for all readings a three-electrode potentiostatic system in acetonitrile containing 0.1 *M* $^nBu_4NPF_6$ as supporting electrolyte was used. Cyclic voltammetric measurements were carried out with a double platinum electrode and a Ag/AgCl reference electrode. Potentials are quoted versus ferro-

cene/ferrocinium, Fc/Fc^+. ^1H and ^{13}C NMR spectra were recorded at 200 and 50.32 MHz, respectively, on Bruker a WP200 spectrometer.

1,4,8,11-Tetrathiacyclotetradecane was purchased from Aldrich Chemicals.

Synthesis of $[IrCl_2(L)]BPh_4$

To a solution of 1,4,8,11-tetrathiacyclotetradecane (0.04 g, 1.49×10^{-4} mol) in refluxing EtOH (50 cm^3) containing an excess of $NaBPh_4$ (0.075 g, 2.19×10^{-4} mol) was added a solution of $IrCl_3 \cdot 3H_2O$ (0.052 g, 1.47×10^{-4} mol) in water (5 cm^3). The mixture was refluxed under N_2 for 14 h then allowed to cool, and the yellow/brown precipitate collected. The product was dissolved in hot $MeNO_2$ and filtered to remove insoluble chloro-bridged polymers. The filtrate was cooled to afford a cream precipitate of $[IrCl_2(L)]BPh_4$, which was collected and dried in vacuo. Yield 0.042 g, 33%. Elemental analysis: found C, 47.4; H, 4.8% calculated for $[IrCl_2(L)]BPh_4$ C, 48.0; H, 4.7%. Infrared spectrum (CsI disc): (L): 2910(m), 1430(vs), 1270(m) cm^{-1}, BPh_4^-: 3060, 2980, 1580, 1480, 1430, 860, 840, 810, 610, 530 cm^{-1}, (Ir–Cl): 310, 305 cm^{-1}. Mass spectrum (FAB) in dmf/glycerol matrix: M^+ (found) = 531, 496, 461; M^+ (calculated) = 531 for $[^{193}Ir^{35}Cl_2(L)]^+$, 496 for $[^{193}Ir^{35}Cl(L)]^+$, 461 for $[^{193}Ir(L)]^+$. UV-VIS (MeCN): λ_{max} 348 (113), 297 (1, 400), 275 (2, 760), 267 (3, 370), 216 nm (ϵ_{max} 29,400 M^{-1} cm^{-1}).

Synthesis of $[IrCl_2(L)]PF_6$

The PF_6^- salt was prepared by using NH_4PF_6 in place of $NaBPh_4$ in the above preparation. Elemental analysis: Found C, 18.1; H, 3.0; S, 18.8. $[IrCl_2(L)]PF_6$ calcd.: C, 17.8; H, 3.0; S, 18.9%. ^1H NMR (CD_3NO_2, 293 K, 200 MHz): δ 2.5–3.5 ppm (m, CH_2). ^{13}C NMR (CD_3NO_2, 293 K, 50.32 MHz): δ 37.99, 29.52, 28.96, 28.39, 23.90 ppm.

X-Ray structure determination of $[IrCl_2(L)]BPh_4$

A colourless crystal ($0.46 \times 0.15 \times 0.15$ mm) suitable for an X-ray diffraction study was obtained by diffusion of Et_2O vapour into a solution of the complex in CH_3NO_2.

Crystal data. $C_{34}H_{40}BCl_2IrS_4$, $M = 850.85$, monoclinic, space group $P2_1$, with a 12.6927(14), b 12.1361(20), c 14.4912(18) Å, β 111.813(13)°, V 2072.4 Å^3 (From θ values of 20 reflections measured at $\pm\omega$, $19 < 2\theta < 30°$, λ 0.71073 Å), $Z = 2$, D_c 1.363 g cm^{-3}, μ 35.18 cm^{-1}, $F(000) = 848$.

Table 1

Bond lengths (Å) with standard deviations

Ir(1)–S(1)	2.277(4)	S(8)–C(7)	1.772(21)
Ir(1)–S(4)	2.287(5)	S(8)–C(9)	1.775(20)
Ir(1)–S(8)	2.268(4)	S(11)–C(10)	1.851(23)
Ir(1)–S(11)	2.343(5)	S(11)–C(12)	1.811(21)
Ir(1)–Cl(1)	2.389(5)	C(2)–C(3)	1.55(3)
Ir(1)–Cl(2)	2.385(5)	C(5)–C(6)	1.46(3)
S(1)–C(2)	1.855(21)	C(6)–C(7)	1.58(3)
S(1)–C(14)	1.809(17)	C(9)–C(10)	1.59(3)
S(4)–C(3)	1.781(20)	C(12)–C(13)	1.48(3)
S(4)–C(5)	1.755(24)	C(13)–C(14)	1.57(3)

Table 2

Angles (degrees) with standard deviations

S(1)–Ir(1)–S(4)	88.10(15)	Ir(1)–S(4)–C(5)	111.3(8)
S(1)–Ir(1)–S(8)	86.42(15)	C(3)–S(4)–C(5)	102.1(10)
S(1)–Ir(1)–S(11)	97.65(15)	Ir(1)–S(8)–C(7)	110.1(7)
S(1)–Ir(1)–Cl(1)	91.29(16)	Ir(1)–S(8)–C(9)	103.5(6)
S(1)–Ir(1)–Cl(2)	176.15(15)	C(7)–S(8)–C(9)	103.7(9)
S(4)–Ir(1)–S(8)	98.93(16)	Ir(1)–S(11)–C(10)	103.1(7)
S(4)–Ir(1)–S(11)	172.26(16)	Ir(1)–S(11)–C(12)	111.0(7)
S(4)–Ir(1)–Cl(1)	86.72(16)	C(10)–S(11)–C(12)	100.2(10)
S(4)–Ir(1)–Cl(2)	88.96(16)	S(1)–C(2)–C(3)	103.5(13)
S(8)–Ir(1)–S(11)	86.64(16)	S(4)–C(3)–C(2)	109.0(14)
S(8)–Ir(1)–Cl(1)	173.81(16)	S(4)–C(5)–C(6)	118.5(18)
S(8)–Ir(1)–Cl(2)	91.58(15)	C(5)–C(6)–C(7)	118.7(20)
S(11)–Ir(1)–Cl(1)	87.97(16)	S(8)–C(7)–C(6)	108.0(15)
S(11)–Ir(1)–Cl(2)	85.51(16)	S(8)–C(9)–C(10)	105.0(13)
Cl(1)–Ir(1)–Cl(2)	91.02(16)	S(11)–C(10)–C(9)	107.4(14)
Ir(1)–S(1)–C(2)	99.9(7)	S(11)–C(12)–C(13)	120.4(15)
Ir(1)–S(1)–C(14)	110.0(6)	C(12)–C(13)–C(14)	116.3(17)
C(2)–S(1)–C(14)	104.8(9)	S(1)–C(14)–C(13)	106.5(12)
Ir(1)–S(4)–C(3)	103.4(7)		

Table 3

Torsion angles (degrees) with standard deviations

S(4)–Ir(1)–S(1)–C(2)	25.7(7)	S(1)–Ir(1)–S(11)–C(12)	23.7(7)
S(4)–Ir(1)–S(1)–C(14)	135.5(6)	S(4)–Ir(1)–S(11)–C(10)	139.5(13)
S(8)–Ir(1)–S(1)–C(2)	124.8(7)	S(4)–Ir(1)–S(11)–C(12)	−114.0(13)
S(8)–Ir(1)–S(1)–C(14)	−125.4(6)	S(8)–Ir(1)–S(11)–C(10)	3.1(7)
S(11)–Ir(1)–S(1)–C(2)	−149.1(7)	S(8)–Ir(1)–S(11)–C(12)	109.6(7)
S(11)–Ir(1)–S(1)–C(14)	− 39.3(6)	Cl(1)–Ir(1)–S(11)–C(10)	−173.8(7)
Cl(1)–Ir(1)–S(1)–C(2)	− 61.0(7)	Cl(1)–Ir(1)–S(11)–C(12)	− 67.3(7)
Cl(1)–Ir(1)–S(1)–C(14)	48.8(6)	Cl(2)–Ir(1)–S(11)–C(10)	95.0(7)
Cl(2)–Ir(1)–S(1)–C(2)	66.0(24)	Cl(2)–Ir(1)–S(11)–C(12)	−158.5(7)
Cl(2)–Ir(1)–S(1)–C(14)	175.8(22)	Ir(1)–S(1)–C(2)–C(3)	− 55.6(13)
S(1)–Ir(1)–S(4)–C(3)	3.7(7)	C(14)–S(1)–C(2)–C(3)	−169.5(12)
S(1)–Ir(1)–S(4)–C(5)	112.6(9)	Ir(1)–S(1)–C(14)–C(13)	67.0(12)
S(8)—Ir(1)–S(4)–C(3)	− 82.4(7)	C(2)–S(1)–C(14)–C(13)	173.6(12)
S(8)–Ir(1)–S(4)–C(5)	26.5(9)	Ir(1)–S(4)–C(3)–C(2)	− 40.6(14)
S(11)–Ir(1)–S(4)–C(3)	141.9(13)	C(5)–S(4)–C(3)–C(2)	−156.3(14)
S(11)–Ir(1)–S(4)–C(5)	−109.3(14)	Ir(1)–S(4)–C(5)–C(6)	− 41.8(20)
Cl(1)–Ir(1)–S(4)–C(3)	95.1(7)	C(3)–S(4)–C(5)–C(6)	67.9(20)
Cl(1)–Ir(1)–S(4)–C(5)	−156.0(9)	Ir(1)–S(8)–C(7)–C(6)	60.6(15)
Cl(2)–Ir(1)–S(4)–C(3)	−173.8(7)	C(9)–S(8)–C(7)–C(6)	170.7(14)
Cl(2)–Ir(1)–S(4)–C(5)	− 64.9(9)	Ir(1)–S(8)–C(9)–C(10)	− 56.7(13)
S(1)–Ir(1)–S(8)–C(7)	−125.0(7)	C(7)–S(8)–C(9)–C(10)	−171.7(13)
S(1)–Ir(1)–S(8)–C(9)	124.7(7)	Ir(1)–S(11)–C(10)–C(9)	− 37.2(14)
S(4)–Ir(1)–S(8)–C(7)	− 37.5(7)	C(12)–S(11)–C(10)–C(9)	−151.8(14)
S(4)–Ir(1)–S(8)–C(9)	−147.8(7)	Ir(1)–S(11)–C(12)–C(13)	− 37.5(18)
S(11)–Ir(1)–S(8)–C(7)	137.1(7)	C(10)–S(11)–C(12)–C(13)	70.9(18)
S(11)–Ir(1)–S(8)–C(9)	26.8(7)	S(1)–C(2)–C(3)–S(4)	64.7(14)
Cl(1)–Ir(1)–S(8)–C(7)	166.5(16)	S(4)–C(5)–C(6)–C(7)	72.1(25)
Cl(1)–Ir(1)–S(8)–C(9)	56.3(17)	C(5)–C(6)–C(7)–C(8)	− 81.6(22)
Cl(2)–Ir(1)–S(8)–C(7)	51.7(7)	S(8)–C(9)–C(10)–S(11)	62.1(15)
Cl(2)–Ir(1)–S(8)–C(9)	− 58.6(7)	S(11)–C(12)–C(13)–C(14)	70.0(22)
S(1)–Ir(1)–S(11)–C(10)	− 82.8(7)	C(12)–C(13)–C(14)–S(1)	− 84.5(18)

Table 4

Atomic coordinates with esds

	x	y	z	U_{iso}
Ir(1)	−0.13020(4)	0.0000	−0.16511(3)	0.0389(3)
S(1)	−0.3025(3)	−0.0714(4)	−0.2598(3)	0.0541(24)
S(4)	−0.0928(4)	−0.1606(4)	−0.0762(3)	0.062(3)
S(8)	−0.0728(4)	−0.0509(4)	−0.2896(3)	0.0557(25)
S(11)	−0.1573(4)	0.1766(4)	−0.2355(3)	0.068(3)
Cl(1)	−0.2034(4)	0.0680(4)	−0.0461(3)	0.078(3)
Cl(2)	0.0556(3)	0.0628(4)	−0.0661(3)	0.069(3)
C(2)	−0.3221(16)	−0.1701(16)	−0.1698(15)	0.083(13)
C(3)	−0.2142(15)	−0.2433(15)	−0.1396(15)	0.074(12)
C(5)	0.0160(18)	−0.2353(18)	−0.0949(18)	0.096(7)
C(6)	0.0163(20)	−0.2421(17)	−0.1955(19)	0.106(18)
C(7)	0.0491(16)	−0.1359(16)	−0.2423(16)	0.083(14)
C(9)	−0.0203(15)	0.0734(15)	−0.3208(13)	0.075(13)
C(10)	−0.1231(16)	0.1579(19)	−0.3481(16)	0.094(16)
C(12)	−0.3068(17)	0.2095(16)	−0.2922(14)	0.084(14)
C(13)	−0.3900(15)	0.1239(19)	−0.3451(14)	0.084(14)
C(14)	−0.4121(12)	0.0311(13)	−0.2789(13)	0.071(13)
B(1)	−0.7682(12)	0.0237(13)	−0.5127(10)	0.044(4)
C(1′)	−0.6589(5)	0.0257(10)	−0.6377(5)	0.054(4)
C(2′)	−0.6517(5)	0.0128(10)	−0.7309(5)	0.064(4)
C(3′)	−0.7481(5)	−0.0152(10)	−0.8130(5)	0.076(5)
C(4′)	−0.8517(5)	−0.0304(10)	−0.8019(5)	0.055(4)
C(5′)	−0.8589(5)	−0.0175(10)	−0.7087(5)	0.054(4)
C(6′)	−0.7625(5)	0.0105(10)	−0.6267(5)	0.043(3)
C(7′)	−0.9666(6)	−0.0705(5)	−0.5299(7)	0.042(3)
C(8′)	−1.0838(6)	−0.0678(5)	−0.5545(7)	0.058(4)
C(9′)	−1.1419(6)	0.0322(5)	−0.5778(7)	0.057(4)
C(10′)	−1.0828(6)	0.1295(5)	−0.5765(7)	0.056(4)
C(11′)	−0.9657(6)	0.1268(5)	−0.5519(7)	0.045(3)
C(12′)	−0.9076(6)	0.0268(5)	−0.5286(7)	0.043(3)
C(13′)	−0.6310(9)	−0.1535(9)	−0.4643(6)	0.059(4)
C(14′)	−0.5816(9)	−0.2434(9)	−0.4038(6)	0.064(4)
C(15′)	−0.6062(9)	−0.2644(9)	−0.3193(6)	0.063(4)
C(16′)	−0.6802(9)	−0.1954(9)	−0.2953(6)	0.072(5)
C(17′)	−0.7296(9)	−0.1054(9)	−0.3559(6)	0.060(4)
C(18′)	−0.7050(9)	−0.0845(9)	−0.4404(6)	0.046(3)
C(19′)	−0.6820(9)	0.1565(7)	−0.3568(6)	0.064(4)
C(20′)	−0.6334(9)	0.2549(7)	−0.3108(6)	0.069(5)
C(21′)	−0.6144(9)	0.3405(7)	−0.3669(6)	0.067(4)
C(22′)	−0.6439(9)	0.3277(7)	−0.4692(6)	0.072(5)
C(23′)	−0.6925(9)	0.2293(7)	−0.5152(6)	0.059(4)
C(24′)	−0.7116(9)	0.1437(7)	−0.4590(6)	0.045(3)

Data collection and processing. Stoe-Siemens AED2 four-circle diffractometer, graphite-monochromated Mo-K_α X-radiation, ω–θ scans with ω scan width $(1.4 + 0.35 \tan\theta)°$, 2882 reflections measured ($2\theta_{max}$ 45°, h $-13 \rightarrow 12$, k $0 \rightarrow 13$, l $0 \rightarrow 14$), giving 2508 with $F \geqslant 6\sigma(F)$ for use in subsequent calculations. No significant crystal decay was observed.

Structure analysis and refinement. The Ir position was located from a Patterson synthesis and input to DIRDIF [17], which located the Cl and S atoms. Iterative

least-squares refinements and difference Fourier syntheses [18] located all other non-H atoms. At isotropic convergence, final correction for absorption was made using DIFABS [19]. (An initial absorption correction was made using 48 Ψ scans (max. transmission factor = 0.2382, min. = 0.2022)). Anisotropic thermal parameters were refined for Ir, S, Cl, and C atoms of the cation. H atoms were included at calculated positions [18]. Phenyl groups of the BPh_4^- counter-ions were refined as rigid groups. The absolute configuration of the structure was not easy to establish with certainty as both hands refined well to essentially the same R-factors. The 20 reflections were selected with the greatest discrimination factor, defined as $D = |F_1F_2|\sin^2(\phi_1 - \phi_2)/|F_o|$ where subscripts 1 and 2 refer to structure factors calculated for the Ir atoms and for the other atoms respectively. For the fully refined data sets, these 20 data gave $R = 0.032$ for the hand chosen, and 0.049 for the opposite hand. More strikingly, bond lengths to Ir are much less consistent in the less favoured hand, the Ir–S lengths being more divergent, and the Ir–Cl lengths being much shorter. The weighting scheme $w^{-1} = \sigma^2(F) + 0.002572F^2$ gave satisfactory analyses. At convergence, $R, R_w = 0.0363$ and 0.0509 respectively for 205 parameters, $S = 1.137$. The maximum and minimum residues in the final ΔF syntheses were +0.67 and −0.64 eÅ^{-3} respectively. Illustrations were prepared by use of ORTEP [20] and molecular geometry calculations by use of CALC [21], scattering factor data were taken from ref. 22. Bond lengths, angles, torsion angles and fractional coordinates are given in Tables 1–4.

Acknowledgements

We thank the SERC for support and Johnson–Matthey Plc for generous loans of platinum metals.

References

1 M. Schröder, Pure Appl. Chem., 60 (1988) 517.
2 M.N. Bell, A.J. Blake, R.O. Gould, A.J. Holder, T.I. Hyde, A.J. Lavery, G. Reid and M. Schröder, J. Inclusion Phenomena, 5 (1987) 169.
3 N.W. Alcock, N. Herron and P. Moore, J. Chem. Soc., Chem. Commun., (1976) 886.
4 N.W. Alcock, N. Herron and P. Moore, J. Chem. Soc., Dalton Trans., (1978) 394.
5 R.E. DeSimone and M.D. Glick, J. Am. Chem. Soc., 97 (1974) 942.
6 T.F. Lai and C.K. Poon, J. Chem. Soc., Dalton Trans., 1982, 1465.
7 T. Yoshida, T. Ueda, T. Adachi, K. Yamamoto and T. Higuchi, J. Chem. Soc., Chem. Commun., 1985, 1137.
8 W.D. Lemke, K.E. Travis, N.E. Takvoryan and D.H. Busch, Adv. Chem. Ser., 150 (1977) 358. See also: K. Travis and D.H. Busch, Inorg. Chem., 13 (1974) 2591.
9 T. Yoshida, T. Adachi, T. Ueda, M. Watanabe, M. Kaminaka and T. Higuchi, Angew. Chem., 99 (1987) 1182; Angew. Chem. Int. Ed. Engl., 26 (1987) 1171.
10 J. Cragel, V.B. Petts, M.D. Glick and R.E. DeSimone, Inorg. Chem., 17 (1978) 2885; R.E. DeSimone and M.D. Glick, ibid., 17 (1978) 3574.
11 S.G. Murray and F.R. Hartley, Chem. Rev., 81 (1981) 365.
12 C.-K. Poon, T.-W. Tang and C.-M. Che, J. Chem. Soc., Dalton Trans., (1981) 1697; C.-K. Poon, T-W Tang and C-M. Che, J. Chem. Soc., Dalton Trans., (1983) 1647; J. MacB. Harrowfield, A.J. Herit, P.A. Lay, A.M. Sargeson, A.M. Bond, W.A. Mulac and J.C. Sullivan, J. Am. Chem. Soc., 105 (1983) 5503; A.J. Blake, T.I. Hyde, R.S.E. Smith and M. Schröder, J. Chem. Soc., Chem. Commun., (1986) 334; A.J. Blake, T.I. Hyde, and M. Schröder, J. Chem. Soc., Dalton Trans., (1988) 1165.
13 E.J. Bounsall and S.R. Koprich, Can. J. Chem., 44 (1970) 1481.

14 P.K. Bhattacharya, J. Chem. Soc., Dalton Trans., (1980) 810.
15 M.E. Sosa and M.L. Tobe, J. Chem. Soc., Dalton Trans., (1986) 427; M.J. Rosales, M.E. Sosa and M.L. Tobe, J. Coord. Chem., 16 (1987) 59.
16 A.J. Blake, G. Reid and M. Schröder, J. Chem. Soc., Dalton Trans., (1988) 1561.
17 DIRDIF, P.T. Beurskens, W.P. Bosman, H.M. Doesbury, Th. E.M. van den Hark, P.A.J. Prick, J.H. Noordik, G. Beurskens, R.O. Gould and V. Parthasarathia, Applications of Direct Methods to Difference Structure Factors, University of Nijmegen, Netherlands, 1983.
18 SHELX76, Program for Crystal Structure Determination, G.M. Sheldrick, University of Cambridge, 1976.
19 DIFABS, Program for Empirical Absorption Corrections, N. Walker and D. Stuart, Acta Crystallogr. A, 39 (1983) 158.
20 ORTEPII, interactive version. P.D. Mallinson and K.W. Muir, J. Appl. Cryst., 18 (1985) 51.
21 CALC, Fortran77 version. R.O. Gould and P. Taylor, University of Edinburgh, 1985.
22 D.T. Cromer and J.L. Mann, Acta Crystallogr. A, 24 (1968) 321.

Journal of Organometallic Chemistry, 359 (1989) 371–378
Elsevier Sequoia S.A., Lausanne – Printed in The Netherlands

Organometallic macrocyclic complexes: the synthesis, electrochemistry and single crystal X-ray structure of $[Fe(C_5H_5)(L)]^+$ (L = 1,4,7-trithiacyclononane)

Alexander J. Blake, Rhona D. Crofts, Gillian Reid and Martin Schröder *

Department of Chemistry, University of Edinburgh, West Mains Road, Edinburgh EH9 3JJ (Scotland)

(Received May 27th, 1988)

Abstract

Reaction of $[Fe(C_5H_5)I(CO)_2]$ with one molar equivalent of L (L = 1,4,7-trithiacyclononane) affords the complex cation $[Fe(C_5H_5)(L)]^+$ in high yield. Crystals of $[Fe(C_5H_5)(L)]BPh_4$ are monoclinic, space group $P2_1/c$, with a 15.0461(14), b 10.5866(12), c 19.8032(18) Å, β 100.205(9)°, V 3104.48 Å^3, D_c 1.327 g cm^{-3}, $Z = 4$. The single crystal X-ray structure of the complex shows octahedral Fe^{II} with the carbocyclic and macrocyclic ligands bound facially to the metal centre, Fe–S(1) 2.2100(18), Fe–S(4) 2.2053(19), Fe–S(7) 2.2078(19), Fe–C 2.007(12)–2.112(12) Å. Two orientations of the C_5H_5 ring are observed. $[Fe(C_5H_5)(L)]PF_6$ shows a reversible one-electron $Fe^{II/III}$ couple at $E_{1/2} = +0.44$ V vs. Fc/Fc^+ in CH_3CN at platinum electrodes. Coulometry confirms that the oxidation is a one-electron process. The Fe^{III} complex has been characterised by ESR and UV-visible spectroscopy.

Introduction

Coordination complexes of thioether macrocyclic ligands are the subject of particular current interest in view of their unusual stereochemical, electronic and redox properties [1–7]. We are particularly interested in developing the coordination chemistry of small ring tridentate macrocycles, such as 1,4,7-trithiacyclononane (L), 1,4,7-triazacyclononane and 1,4,7-trimethyl-1,4,7-triazacyclononane towards the synthesis of redox-active piano-stool complexes of the type $[M(L)(X)(Y)(Z)]^{x+}$ (X,Y,Z = neutral or anionic ligands) [1]. As a start to this study, we report herein the synthesis, structure and electrochemistry of the mixed-sandwich complex cation $[Fe(C_5H_5)(L)]^+$.

To date the only reported Fe complexes of 1,4,7-trithiacyclononane (L) are the bis-sandwich species $[Fe(L)_2]^{2+/3+}$ and $[Fe(L)(L^1)]^{2+/3+}$ (L^1 = 1,4,7-trithiacyclononane-1-oxide) [8,9]. The low-spin complex $[Fe(L)_2]^{2+}$ shows a particularly anodic

0022-328X/89/$03.50

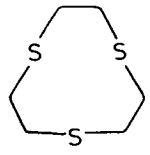

(L)

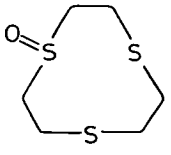

(L')

$Fe^{II/III}$ couple ($E_{1/2}$ +0.98 V vs. Fc/Fc^+) [8,9]; a similar stabilisation of the d^6 M^{II} centre has also been noted for the Ru^{II} analogue $[Ru(L)_2]^{2+}$ ($E_{1/2}$ +1.41 V vs. Fc/Fc^+) [10,11]. We were particularly interested in assessing the stereochemical analogy between carbocyclic moieties such as aryl and cyclopentadienyl ligands and the nine-membered ring tridentate macrocyles; the ability of these ligand systems to bind facially to octahedral metal centres is well documented [1]. We have initiated this study by investigating mixed-sandwich complexes incorporating both carbocyclic and macrocyclic ligands.

Results and discussion

Reaction of $[Fe(C_5H_5)I(CO)_2]$ with one molar equivalent of 1,4,7-trithiacyclononane (L) in refluxing CH_3CN under N_2 affords the complex cation $[Fe(C_5H_5)(L)]^+$. The ^1H NMR spectrum of $[Fe(C_5H_5)(L)]BPh_4$ confirms a $Cp : L : BPh_4^-$ ratio of 1 : 1 : 1, with the proton resonances of the methylene protons giving a complex ABCD pattern centred at 2.45 ppm (Fig. 1). The ^{13}C NMR spectrum of the product showed only two resonances, at δ 35.61 and 74.34 ppm, assigned to the carbon centres of the coordinated thioether and carbocycle, respectively, indicating symmetrical coordination of these moieties to Fe^{II}. The fast atom bombardment mass spectrum of the complex shows a positive ion peak at $M^+ = 301$, with the correct isotopic distribution, corresponding to $[Fe(C_5H_5)(L)]^+$. No other peaks were observed at higher mass units. These data, together with elemental analyses, confirmed the formation of $[Fe(C_5H_5)(L)]^+$.

In order to monitor the stereochemical and conformational features of the complex we undertook a crystallographic study. Single crystals of $[Fe(C_5H_5)(L)]BPh_4$ were grown by diffusion of Et_2O vapour into a solution of the complex in CH_3CN. A view of the cation is shown in Fig. 2. The single crystal X-ray structure confirms

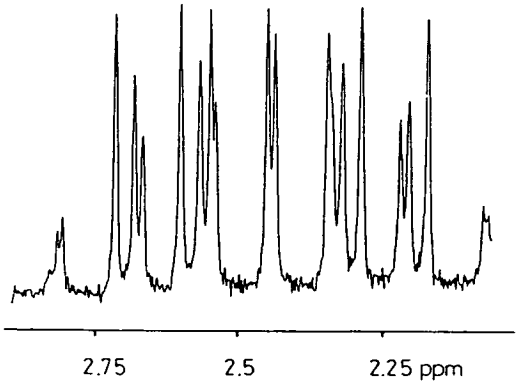

Fig. 1. ^1H NMR spectrum (80 MHz, CD_3NO_2, 293 K) of $[Fe(C_5H_5)(L)]^+$.

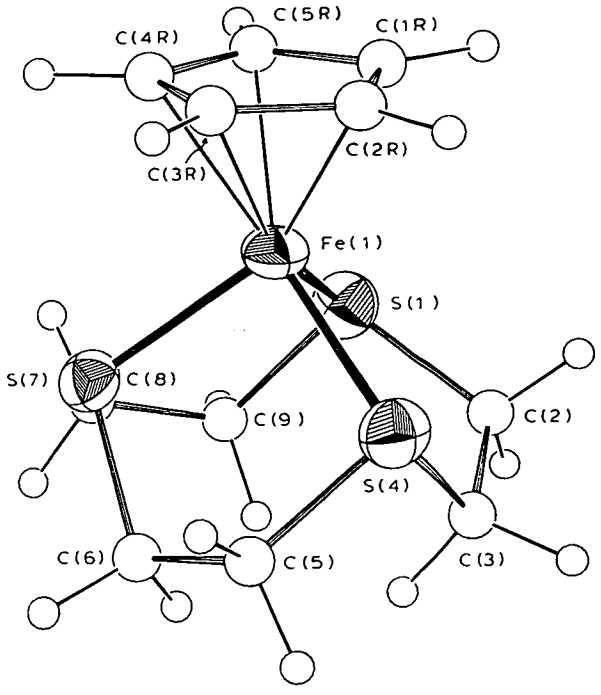

Fig. 2. Single crystal X-ray structure of $[Fe(C_5H_5)(L)]BPh_4$ with numbering scheme adopted. Only one of the two C_5H_5 ring orientations is shown.

the facial coordination of the thioether and carbocyclic ligands to Fe^{II}, Fe–S(1) 2.2100(18), Fe–S(4) 2.2053(19), Fe–S(7) 2.2078(19) Å. Interestingly, the planar cyclopentadienyl moiety is disordered over two equally populated orientations: the two C_5 rings are essentially coplanar but are twisted by 6.18° with respect to each other. This is reminiscent of the disorder observed for the cyclopentadienyl rings in the high temperature solid-state structure of ferrocene [12]. An angle of ca. 3.15° is observed between the S(1)–S(4)–S(7) and C_5 planes in both orientations of the C_5H_5 ligand in the $[Fe(C_5H_5)(L)]^+$ cation.

Cyclic voltammetry of $[Fe(C_5H_5)(L)]PF_6$ shows a reversible one-electron $Fe^{II/III}$ couple at $E_{1/2}$ +0.44 V. vs. Fc/Fc^+, ΔE_p 63 mV. in CH_3CN at platinum electrodes (Fig. 3). Coulometry confirms that the reduction is a one-electron process. The value for this redox process is intermediate between that of $[Fe(L)_2]^{2+}$ [8,9] and ferrocene itself, and reflects the destabilisation of the Fe^{III} oxidation state by (L) relative to the cyclopentadienyl ligand.

Controlled potential electrolysis of $[Fe(C_5H_5)(L)]^+$ at +0.67 V in CH_3CN at a platinum gauze affords the Fe^{III} complex $[Fe(C_5H_5)(L)]^{2+}$, the ESR spectrum of which (measured at 77 K as a CH_3CN glass) shows an anisotropic signal with $g_1 = 2.177$, $g_2 = 2.023$, $g_3 = 1.972$. The UV-vis spectrum of $[Fe(C_5H_5)(L)]^+$ in CH_3CN shows absorption bands at λ_{max} 456 nm (ϵ_{max} 263 M^{-1} cm^{-1}), 371 (351), 266 (9,620) and 222 (18,120). Conversion of Fe^{II} into Fe^{III} can be seen to occur isosbestically (λ_{iso} 290 nm) when an optically transparent thin layer electrode system is used; this is accompanied by a decrease in intensity of the band at 266 nm to ϵ_{max} 7,930 M^{-1} cm^{-1}, and the growth of a shoulder at λ_{max} 312 nm. These results suggest that the absorption band at 266 nm is predominantly a metal-to-ligand charge transfer transition.

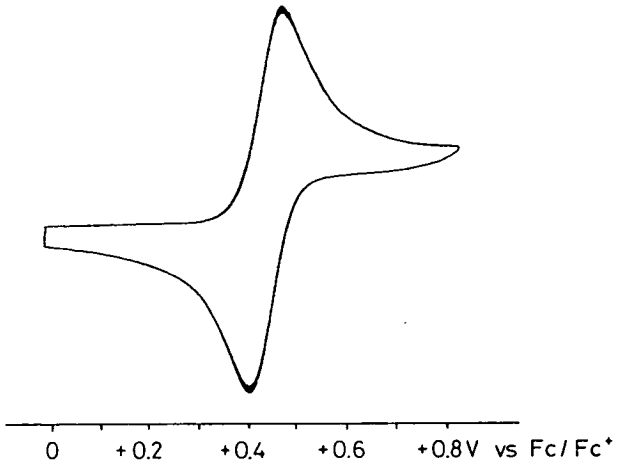

Fig. 3. Cyclic voltammogram of $[Fe(C_5H_5)(L)]PF_6$ in CH_3CN (0.1 *M* $^nBu_4NPF_6$) at platinum electrodes at 273 K.

Current work is aimed at the development of organometallic alkyl and hydrido complexes of Fe^{II} and Ru^{II} with L.

Experimental

Infrared spectra were recorded as Nujol mulls, KBr and CsI discs on a Perkin–Elmer 598 spectrometer over the range 200–4000 cm^{-1}. UV-visible spectra were measured in quartz cells using Perkin–Elmer Lambda 9 and Pye Unicam SP8-400 spectrophotometers. Microanalyses were performed by the Edinburgh University Chemistry Department microanalytical service. ESR spectra were recorded as solids or as frozen glasses down to 77 K using a Bruker ER200D X-band spectrometer. Electrochemical measurements were performed on a Bruker E310 Universal Modular Polarograph. All readings were taken with a three-electrode potentiostatic system in acetonitrile containing 0.1 *M* $^nBu_4NPF_6$ or $^nBu_4BF_4$ as supporting electrolyte. Cyclic voltammetric measurements were carried out with a double platinum electrode and a Ag/AgCl reference electrode. All potentials are quoted versus ferrocene/ferrocinium, Fc/Fc^+. Electron impact mass spectra were recorded on a Kratos MS 902, and FAB spectra on a Kratos MS 50TC spectrometer.

Table 1

Bond lengths (Å) with standard deviations

Fe(1)–S(1)	2.2100(18)	Fe(1)–C(9R)	2.079(11)
Fe(1)–S(4)	2.2053(19)	Fe(1)–C(10R)	2.091(11)
Fe(1)–S(7)	2.2078(19)	S(1)–C(2)	1.826(7)
Fe(1)–C(1R)	2.100(12)	S(1)–C(9)	1.830(6)
Fe(1)–C(2R)	2.112(12)	S(4)–C(3)	1.835(7)
Fe(1)–C(3R)	2.069(12)	S(4)–C(5)	1.832(7)
Fe(1)–C(4R)	2.042(12)	S(7)–C(6)	1.842(7)
Fe(1)–C(5R)	2.007(12)	S(7)–C(8)	1.826(7)
Fe(1)–C(6R)	2.077(11)	C(2)–C(3)	1.498(9)
Fe(1)–C(7R)	2.051(11)	C(5)–C(6)	1.512(10)
Fe(1)–C(8R)	2.024(11)	C(8)–C(9)	1.501(9)

Table 2

Angles (degrees) with standard deviations

S(1)–Fe(1)–S(4)	90.47(7)	Fe(1)–S(7)–C(6)	106.32(23)
S(1)–Fe(1)–S(7)	90.50(7)	Fe(1)–S(7)–C(8)	103.54(22)
S(4)–Fe(1)–S(7)	90.84(7)	C(6)–S(7)–C(8)	100.9(3)
Fe(1)–S(1)–C(2)	103.69(21)	S(1)–C(2)–C(3)	112.5(5)
Fe(1)–S(1)–C(9)	105.97(21)	S(4)–C(3)–C(2)	111.1(5)
C(2)–S(1)–C(9)	99.5(3)	S(4)–C(5)–C(6)	112.9(5)
Fe(1)–S(4)–C(3)	106.06(22)	S(7)–C(6)–C(5)	110.1(5)
Fe(1)–S(4)–C(5)	102.91(24)	S(7)–C(8)–C(9)	112.5(5)
C(3)–S(4)–C(5)	101.1(3)	S(1)–C(9)–C(8)	111.0(4)

Synthesis of [Fe(C_5H_5)(L)]PF_6

Reaction of [Fe(C_5H_5)I(CO)$_2$] (0.067 g, 2.22×10^{-4} mol) with one molar equivalent of L (0.04 g, 2.22×10^{-4} mol) in refluxing CH_3CN under N_2 for 5 h afforded a deep red solution. The solvent was removed in vacuo and the solid product, [Fe(C_5H_5)(L)]I, redissolved in MeOH. Addition of excess of NH_4PF_6 afforded a red precipitate, which was collected and recrystallised from CH_3NO_2 to give [Fe(C_5H_5)(L)]PF_6 (0.065 g, 66%).

Elemental analysis: found: C, 29.7; H, 3.9; S, 22.1. [Fe(C_5H_5)(L)]PF_6 calcd.: C, 29.6; H, 3.8; S, 21.6%. Infrared spectrum (KBr disc): 3120, 1415, 1000, 440 cm^{-1} (C_5H_5); 2960, 2940, 1445, 1415, 1290, 1170, 1120, 955, 910, 670, 410cm^{-1} (L); 840, 555cm^{-1} (PF_6^-). UV-vis spectrum (MeCN): λ_{max} 456 nm (ϵ_{max} 263 M^{-1} cm^{-1}), 371 (351), 266 (9,620), 222 (18,120). ^{13}C NMR spectrum (CD_3CN, 293 K, 50.32 MHz): δ 74.34 (*C*H, C_5H_5), 35.61 ppm (*C*H_2, L). Elemental analysis: found: C, 30.2; H, 4.1. [Fe(C_5H_5)(L)]I calcd.: C, 30.9; H, 4.0%.

Synthesis of [Fe(C_5H_5)(L)]BPh_4

Replacement of NH_4PF_6 by $NaBPh_4$ in the above preparation afforded the corresponding BPh_4^- salt. FAB mass spectrum: found $M^+ = 301$; calculated for [Fe(C_5H_5)(L)]$^+$ $M^+ = 301$ (with correct isotropic distribution). ^1H NMR spectrum (CD_3CN, 298 K, 200 MHz): δ 6.8–7.4 (B*Ph*$_4$, 20H, m), 4.8 (C_5H_5, 5H, s), 2.45ppm (C*H*$_2$, 12H, m).

Table 3

Torsion angles (degrees) of the trithia ligand with standard deviations

C(9)–S(1)–C(2)–C(3)	−69.8(5)
C(3)–S(4)–C(5)–C(6)	−68.2(5)
C(8)–S(7)–C(6)–C(5)	134.5(5)
C(2)–S(1)–C(9)–C(8)	135.6(5)
C(6)–S(7)–C(8)–C(9)	−70.2(5)
S(1)–C(2)–C(3)–S(4)	−44.6(6)
S(4)–C(5)–C(6)–S(7)	−45.0(6)
S(7)–C(8)–C(9)–S(1)	−45.0(6)
C(5)–S(4)–C(3)–C(2)	135.2(5)

X-Ray structure determination of $[Fe(C_5H_5)(L)]BPh_4$

A red crystal (0.46 × 0.46 × 0.35 mm) suitable for X-ray analysis was obtained by isothermal distillation of Et_2O into a solution of the complex in CH_3CN.

Crystal data. $C_{35}H_{37}BFeS_3$, monoclinic, $M = 620.51$, space group $P2_1/c$, with a 15.0461(14), b 10.5866(12), c 19.8032(18) Å, β 100.205(9)°, V 3104.48 Å^3 (from 2θ

Table 4

Fractional coordinates of atoms with standard deviations

	x	y	z	U_{eq}
Fe(1)	0.66556(5)	0.25728(8)	0.06238(4)	0.0387(5)
S(1)	0.80945(10)	0.27927(15)	0.05457(8)	0.0398(9)
S(4)	0.69806(11)	0.28926(17)	0.17408(8)	0.0477(10)
S(7)	0.68452(11)	0.05177(16)	0.07753(9)	0.0458(10)
C(2)	0.8588(4)	0.3555(6)	0.1352(3)	0.048(4)
C(3)	0.8213(4)	0.3050(7)	0.1951(3)	0.053(4)
C(5)	0.6819(5)	0.1327(7)	0.2094(4)	0.062(5)
C(6)	0.7183(5)	0.0272(6)	0.1706(3)	0.055(5)
C(8)	0.7910(4)	0.0207(6)	0.0484(4)	0.052(5)
C(9)	0.8598(4)	0.1222(6)	0.0698(3)	0.044(4)
C(1R)	0.5294(8)	0.2304(11)	0.0182(7)	0.049(5)
C(2R)	0.5800(8)	0.2269(11)	−0.0329(7)	0.042(5)
C(3R)	0.6247(8)	0.3399(11)	−0.0327(7)	0.045(5)
C(4R)	0.6008(8)	0.4139(11)	0.0180(7)	0.065(5)
C(5R)	0.5453(8)	0.3442(11)	0.0517(7)	0.075(9)
C(6R)	0.6311(6)	0.4068(12)	−0.0051(6)	0.049(4)
C(7R)	0.6017(6)	0.2948(12)	−0.0359(6)	0.056(4)
C(8R)	0.5431(6)	0.2406(12)	0.0014(6)	0.069(5)
C(9R)	0.5335(6)	0.3219(12)	0.0538(6)	0.047(6)
C(10R)	0.5892(6)	0.4235(12)	0.0504(5)	0.049(4)
B(1)	0.7788(4)	0.7415(7)	0.3565(3)	0.032(4)
C(1′)	0.78237(25)	0.7785(4)	0.43962(14)	0.037(4)
C(2′)	0.70570(25)	0.7574(4)	0.46866(14)	0.043(4)
C(3′)	0.70930(25)	0.7755(4)	0.53888(14)	0.050(4)
C(4′)	0.78959(25)	0.8145(4)	0.58006(14)	0.059(5)
C(5′)	0.86626(25)	0.8356(4)	0.55102(14)	0.054(5)
C(6′)	0.86265(25)	0.8175(4)	0.48081(14)	0.046(4)
C(7′)	0.80405(25)	0.5869(3)	0.36145(19)	0.035(4)
C(8′)	0.73732(25)	0.4940(3)	0.34974(19)	0.043(4)
C(9′)	0.76012(25)	0.3675(3)	0.36262(19)	0.059(5)
C(10′)	0.84964(25)	0.3338(3)	0.38723(19)	0.066(5)
C(11′)	0.91637(25)	0.4267(3)	0.39894(19)	0.060(5)
C(12′)	0.89357(25)	0.5532(3)	0.38606(19)	0.044(4)
C(13′)	0.85276(23)	0.8251(3)	0.32009(17)	0.032(4)
C(14′)	0.88915(23)	0.7713(3)	0.26673(17)	0.036(4)
C(15′)	0.94320(23)	0.8436(3)	0.23119(17)	0.046(4)
C(16′)	0.96086(23)	0.9698(3)	0.24899(17)	0.044(4)
C(17′)	0.92447(23)	1.0236(3)	0.30235(17)	0.044(4)
C(18′)	0.87042(23)	0.9513(3)	0.33789(17)	0.041(4)
C(19′)	0.67958(21)	0.7741(4)	0.30644(17)	0.037(4)
C(20′)	0.65231(21)	0.7067(4)	0.24580(17)	0.047(4)
C(21′)	0.57296(21)	0.7399(4)	0.20155(17)	0.060(5)
C(22′)	0.52089(21)	0.8406(4)	0.21795(17)	0.067(6)
C(23′)	0.54817(21)	0.9081(4)	0.27859(17)	0.061(5)
C(24′)	0.62752(21)	0.8748(4)	0.32283(17)	0.048(4)

values of 36 reflections measured at $\pm\omega$ (2θ 24–26°, $\bar{\lambda} = 0.71073$ Å)], D_c 1.327 g cm^{-3}, $Z = 4$; $F(000) = 1304$, μ 6.70 cm^{-1}.

Data collection and processing. Stoe–Siemens AED2 four-circle diffractometer, Mo-K_α X-radiation, ω–2θ scans with ω scan width $(0.80 + 0.347 \tan\theta)°$, 4138 reflections measured to 2θ 45°, giving 2519 with $F \geqslant 6\sigma(F)$. No significant crystal decay, no absorption correction.

Structure analysis and refinement. The Fe and S atoms were located by direct methods [13] followed by iterative least-squares refinement and difference Fourier synthesis [14] to locate all other non-H atoms. Anisotropic thermal parameters were refined for all Fe, S, B and C atoms except those of the disordered cyclopentadienyl ring: two orientations of this ring were modelled successfully by refinement as planar rigid groups with C–C distances of 1.373 Å and C–C–C angles of 108°. H atoms on the macrocycle, on the BPh_4^- counter-ion and on both orientations of the cyclopentadienyl ring were included in fixed, calculated positions [14]. The weighting scheme $w^{-1} = \sigma^2(F) + 0.00058F^2$ gave satisfactory analyses. At convergence, $R, R_w = 0.0484$ and 0.0598 respectively for 291 parameters, $S = 1.166$. The maximum and minimum residues in the final ΔF syntheses were 0.39 and -0.38 eÅ^{-3} respectively. Illustrations were prepared using ORTEP [15], molecular geometry calculations utilised CALC [16], and scattering factor data were taken from ref. 17. Bond lengths, angles, torsion angles and fractional coordinates are given in Tables 1–4. Lists of thermal parameters, hydrogen atom coordinates, and observed and calculated structure factors are available from the author.

Acknowledgements

We thank SERC for support.

References

1 M. Schröder, Pure Appl. Chem., 60 (1988) 517 and ref. therein.
2 H.-J. Küppers, A. Neves, C. Pomp, D. Ventur, K. Wieghardt, B. Nuber and J. Weiss, Inorg. Chem., 25 (1986) 2400.
3 M.T. Ashby and D.L. Lichtenberger, Inorg. Chem., 24 (1985) 636.
4 R.S. Glass, W.N. Setzer, C.A. Ogle and G.S. Wilson, Inorg. Chem., 22 (1983) 266; G.S. Wilson, D.D. Swanson and R.S. Glass, ibid., 25 (1986) 3827.
5 E.W. Abel, P.D. Beer, I. Moss, K.G. Orrell, V. Šik, P.A. Bates and M.B. Hursthouse, J. Chem. Soc., Chem. Commun., (1987) 978; E.W. Abel, P.D. Beer, I. Moss, K.G. Orrell, V. Šik, P.A. Bates and M.B. Hursthouse, J. Organomet. Chem., 341 (1988) 559.
6 D. Sellmann and P. Frank, Angew. Chem., 98 (1986) 1115; Angew. Chem. Int. Ed. Engl., 25 (1986) 1107.
7 J.R. Hartman and S.R. Cooper, J. Am. Chem. Soc., 108 (1986) 1202; J.R. Hartman, and S.R. Cooper, ibid., 108 (1986) 1208.
8 K. Wieghardt, H.-J. Küppers and J. Weiss. Inorg. Chem., 24 (1985) 3067.
9 H.-J. Küppers, K. Wieghardt, B. Nuber, J. Weiss, E. Bill and A.X. Trautwein, Inorg. Chem., 26 (1987) 3762.
10 M.N. Bell, A.J. Blake, H.-J. Küppers, M. Schröder and K. Wieghardt, Angew. Chem., 99 (1987) 253; Angew. Chem. Int. Ed. Engl., 26 (1987) 250.
11 S.C. Rawle, T.J. Sewell and S.R. Cooper, J. Chem. Soc., Chem. Commun., (1987) 308; S.C. Rawle, T.J. Sewell and S.R. Cooper, Inorg. Chem., 26 (1987) 3769.
12 P. Seiler and J. Dunitz, Acta Crystallogr., B, 35 (1979) 1068. For discussion see: E.A.V. Ebsworth, D.W.H. Rankin and S. Cradock (Eds.), Structural Methods in Inorganic Chemistry, p. 375–378, Blackwell Scientific Publications, Oxford, 1987.

13 SHELX86, Program for Crystal Structure Solution, G.M. Sheldrick, University of Göttingen, 1986.
14 SHELX76, Program for Crystal Structure Determination, G.M. Sheldrick, University of Cambridge, 1976.
15 ORTEPII, interactive version. P.D. Mallinson and K.W. Muir, J. Appl. Cryst., 18 (1985) 51.
16 CALC, Fortran77 version. R.O. Gould and P. Taylor, University of Edinburgh, 1985.
17 D.T. Cromer and J.L. Mann, Acta Crystallogr., A, 24 (1968) 321.

RESULTS AND DISCUSSION

Reaction of $HgSO_4$ with 2 molar equivalents of [9]aneS$_3$ in refluxing H_2O–MeOH (1 : 1 v/v) for 1 h gave a colourless solution. Addition of NH_4PF_6 afforded a white product which was recrystallized from H_2O. On the basis of elemental analysis and spectroscopic data the complex was assigned as $[Hg([9]aneS_3)_2](PF_6)_2$. The ^1H NMR spectrum of $[Hg([9]aneS_3)_2](PF_6)_2$ showed a characteristic ABCD pattern for the methylene protons of the macrocyclic ligands (Fig. 1). The ^{13}C NMR spectrum of $[Hg([9]aneS_3)_2]^{2+}$ showed a single resonance at $\delta = 26.6$ ppm assigned to the methylene carbon atoms of [9]aneS$_3$. These data indicated the presence of a single product in solution, with two equivalent [9]aneS$_3$ ligands bound facially to the mercury(II) centre. A single crystal X-ray structure determination was undertaken to confirm the stereochemistry of the complex cation.

Crystals of $[Hg([9]aneS_3)_2](PF_6)_2$ were obtained from H_2O. A view of the cation is shown in Fig. 2. The single crystal X-ray structure of the complex shows a centrosymmetric complex cation : the mercury(II) cation occupies a crystallographic inversion centre with all six thioether donors coordinated to it. Interestingly, the Hg—S distances are not identical: two are significantly shorter (Hg—S(4) = 2.638(3) Å) than the remaining four (Hg—S(1) = 2.728(3), Hg—S(7) = 2.712(3) Å, ∠S(1)Hg S(4) = 82.64(9), ∠S(1)HgS(7) = 81.01(8), ∠S(4)Hg S(7) = 82.86(9)°), indicating a small but significant

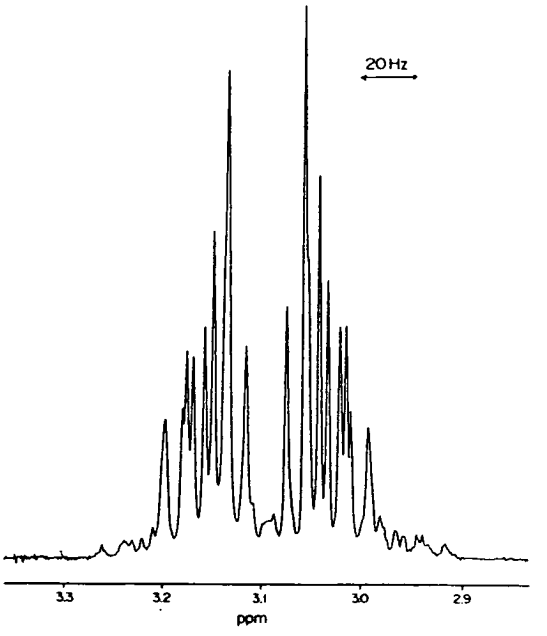

Fig. 1. ^1H NMR spectrum (360 MHz, CD_3CN, 298 K) of $[Hg([9]aneS_3)_2]^{2+}$.

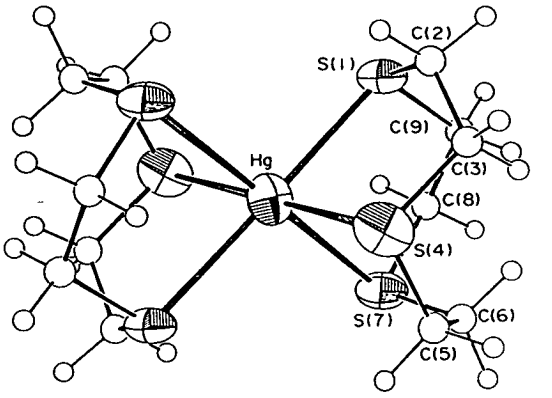

Fig. 2. Single crystal X-ray structure of $[Hg([9]aneS_3)_2]^{2+}$ with numbering scheme adopted.

tetragonal compression for the cation. The related d^{10} complex, $[Ag([9]aneS_3)]^+$, also shows hexathia coordination, with Ag—S bond lengths varying from 2.6665(12) to 2.7813(10) Å, ∠SAgS = 80.35(3), 77.43(3)°.[11] The mercury(II) and silver(I) complexes, therefore, show similar structural features, with the silver(I) species incorporating slightly longer M—S bond lengths reflecting the larger ionic radius of silver(I) over mercury(II) (1.15 vs 1.02 Å[16]). The structural features for these silver(I) and mercury(II) complexes may be interpreted as a compromise between the tendency of second- and particularly third-row d^{10} metal ions to adopt linear coordination, and the preference of [9]aneS$_3$ for facial binding : in the case of mercury(II) and silver(I) the latter appears to dominate.

Interestingly, d^{10} gold(I), which has a particularly strong preference for linear coordination, only binds four thioether donors in $[Au([9]aneS_3)_2]^+$, (Au—S = 2.302(6), 2.350(7), 2.733(8), 2.825(8) Å) to give a structure that is a combination of linear and tetrahedral coordination at gold(I).[5] This contrasts with the recently reported structure of $[Zn([9]aneS_3)_2]^{2+}$ where there is no significant variation in Zn—S bond lengths :[10] these occupy a narrow range (2.491(3)–2.497(3) Å) consistent with the tight coordinative fit of octahedral zinc(II) with facially binding [9]aneS$_3$.

Cyclic voltammetry of $[Hg([9]aneS_3)_2]^{2+}$ shows a chemically reversible reduction at $E_{1/2} = -0.15$ V ($\Delta E_p = 80$ mV) vs Fc/Fc^+ at a scan rate of 90 mV s^{-1} (Fig. 3). Coulometry at 298 K in CH_3CN (0.1 M $^nBuN_4PF_6$) at platinum electrodes shows the reduction to be a two-electron process. However, no stable mercury(I) or mercury(0) species could be isolated under these conditions, with decomposition of the reduction products occurring in solution. The parent mercury(II) complex could not be regenerated from the reduced solution.

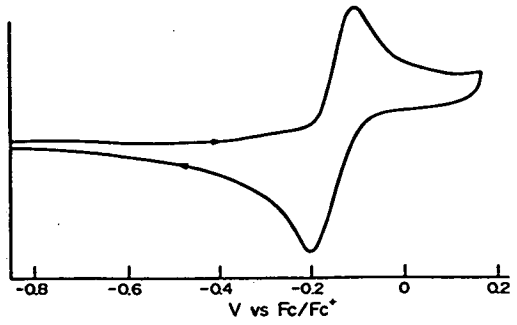

Fig. 3. Cyclic voltammogram of $[Hg([9]aneS_3)_2](PF_6)_2$ in CH_3CN (0.1 M $^nBu_4NPF_6$) at platinum electrodes. Scan rate = 90 mV s^{-1}, 298 K.

We can only speculate at the binding characteristics of $[9]aneS_3$ with $d^{10}s^1$ mercury(I) and/or $d^{10}s^2$ mercury(0). Our previous work has shown that $[9]aneS_3$ binds to gold(I) rather weakly, with the complex $[Au([9]aneS_3)_2]^+$ being highly labile and reactive in solution. Binding of $[9]aneS_3$ to mercury(I) and mercury(0) would be expected to be weaker than with gold(I), explaining the ready decomposition of these low valent mercury complexes in solution. Work is underway to try to stabilize these species at lower temperatures and in alternative solvents.

EXPERIMENTAL

IR spectra were measured as Nujol mulls, KBr and CsI discs using a Perkin–Elmer 598 spectrometer over the range 200–4000 cm^{-1}. UV–vis spectra were measured in quartz cells using Perkin–Elmer Lambda 9 and Pye Unicam SP8-400 spectrophotometers. Microanalyses were performed by the Edinburgh University Chemistry Department microanalytical service. ESR spectra were recorded as solids or as frozen glasses down to 77 K using a Bruker ER200D X-band spectrometer. Electrochemical measurements were performed on a Bruker E310 Universal Modular Polarograph. All readings were taken using a three-electrode potentiostatic system in acetonitrile containing 0.1 M $^nBu_4NPF_6$ or $^nBu_4NBF_4$ as the supporting electrolyte. Cyclic voltammetric measurements were carried out using a double platinum electrode and an Ag/AgCl reference electrode. All potentials are quoted versus ferrocene/ferrocinium (Fc/Fc^+). Mass spectra were obtained by electron impact on a Kratos MS 902 and by fast atom bombardment on a Kratos MS 50TC spectrometer. ^1H NMR spectra were recorded at 200 and 360 MHz on Bruker WP200 and WH360 spectrometers respectively. ^{13}C NMR spectra were recorded at 50.32 MHz on a Bruker WP200 spectrometer.

Synthesis of $[Hg([9]aneS_3)_2](PF_6)_2$

$HgSO_4$ (0.1 g, 0.34 mmol) was treated with $[9]aneS_3$ (0.13 g, 0.72 mmol) in H_2O–MeOH (30 cm^3, 1:1 v/v) under reflux for 1 h. Addition of excess NH_4PF_6 to the resulting solution afforded a white precipitate, which was collected and recrystallized from water to give $[Hg([9]aneS_3)_2](PF_6)_2$ (0.18 g, 62% yield). Found: C, 16.7; H, 2.91. Calc. for $[Hg([9]aneS_3)_2](PF_6)_2$: C, 16.8; H, 2.90%. ^1H NMR spectrum (360 MHz, CD_3CN, 293 K): $\delta = 3.06$ ppm (CH_2, m). ^{13}C NMR spectrum (50.32 MHz, CD_3CN, 293 K): $\delta = 26.6$ ppm (CH_2).

X-ray structure determination of $[Hg([9]aneS_3)_2](PF_6)_2 \cdot \frac{1}{3}H_2O$

A colourless lath (1.00 × 0.173 × 0.078 mm) suitable for X-ray analysis was obtained by recrystallization from hot water.

Crystal data. $C_{12}H_{24}S_6Hg^{2+} \cdot 2PF_6^- \cdot \frac{1}{3}H_2O$, monoclinic, space group $I2/a$ (a non-standard setting of $C2/c$, No. 15), $M = 857.2$, with $a = 11.8667(10)$, $b = 15.1631(23)$, $c = 14.454(4)$ Å, $\beta = 90.224(19)°$, $V = 2600.7$ Å^3, $D_c = 2.18$ g cm^{-3}, [from 2θ values of 20 reflections measured at $\pm\omega$ ($2\theta = 30 \rightarrow 32°$, $\bar{\lambda} = 0.71073$ Å)], $Z = 4$; $F(000) = 1647$, $\mu(Mo\text{-}K_\alpha) = 65.37$ cm^{-1}.

Data collection and processing. Stoë STADI-4 four-circle diffractometer, ω–2θ scans with ω scan width $(1.40 + 0.347 \tan\theta)°$, 1722 unique reflections measured ($2\theta_{max} = 45°$, h $-12 \rightarrow 12$, k $0 \rightarrow 14$, l $0 \rightarrow 15$) giving 1236 with $F \geqslant 6\sigma(F)$. Initial absorption correction based on 72Ψ scans (minimum and maximum transmission factors: 0.1036 and 0.1644, respectively). Correction for linear, isotropic crystal decay (*ca* 25%) applied during data reduction.

Structure analysis and refinement. The mercury atom was located from a Patterson synthesis. Iterative rounds of least-squares refinement and difference Fourier synthesis[17] located all other non-hydrogen atoms. At isotropic convergence, final corrections for absorption were made using DIFABS.[18] Anisotropic thermal parameters were refined for mercury, sulphur, phosphorus and the carbon atoms of the cation, and for the two fully occupied fluorine atoms of the disordered PF_6^- ions. Partial occupancies were refined for all other fluorine atoms using fixed isotropic thermal parameters ($U_{iso} = 0.10/0.15$). Hydrogen atoms were included in fixed, calculated positions.[17] The weighting scheme $w^{-1} = \sigma^2(F) + 0.000331F^2$ gave satisfactory agreement analyses. At convergence, R, $R_w = 0.0421$ and 0.0539, respectively, for 156

Table 1. Bond lengths (Å) with standard deviations

Hg—S(1)	2.728(3)	C(3)—S(4)	1.821(13)
Hg—S(4)	2.638(3)	S(4)—C(5)	1.814(12)
Hg—S(7)	2.712(3)	C(5)—C(6)	1.516(16)
S(1)—C(2)	1.790(12)	C(6)—S(7)	1.792(11)
S(1)—C(9)	1.815(11)	S(7)—C(8)	1.799(11)
C(2)—C(3)	1.523(17)	C(8)—C(9)	1.533(15)

Table 2. Angles (°) with standard deviations

S(1)—Hg—S(4)	82.64(9)	Hg—S(4)—C(5)	102.4(4)
S(1)—Hg—S(7)	81.01(8)	C(3)—S(4)—C(5)	104.6(6)
S(4)—Hg—S(7)	82.86(9)	S(4)—C(5)—C(6)	115.5(8)
Hg—S(1)—C(2)	101.0(4)	C(5)—C(6)—S(7)	118.4(8)
Hg—S(1)—C(9)	97.1(4)	Hg—S(7)—C(6)	95.1(4)
C(2)—S(1)—C(9)	103.9(5)	Hg—S(7)—C(8)	104.1(4)
S(1)—C(2)—C(3)	116.7(8)	C(6)—S(7)—C(8)	104.0(5)
C(2)—C(3)—S(4)	117.5(9)	S(7)—C(8)—C(9)	113.5(7)
Hg—S(4)—C(3)	97.6(4)	S(1)—C(9)—C(8)	118.8(8)

Table 3. Selected torsion angles (°) with standard deviations

C(9)—S(1)—C(2)—C(3)	128.4(9)	S(4)—C(5)—C(6)—S(7)	−60.4(11)
C(2)—S(1)—C(9)—C(8)	−51.7(9)	C(5)—C(6)—S(7)—C(8)	−53.0(10)
S(1)—C(2)—C(3)—S(4)	−59.3(11)	C(6)—S(7)—C(8)—C(9)	129.6(18)
C(2)—C(3)—S(4)—C(5)	−53.7(10)	S(7)—C(8)—C(9)—S(1)	−61.1(10)
C(3)—S(4)—C(5)—C(6)	128.2(9)		

parameters, $S = 1.191$. The maximum and minimum residues in the final ΔF syntheses were 0.80 and -0.80 eÅ^{-3}, respectively. The illustration was prepared using ORTEP,[19] molecular geometry calculations utilized CALC,[20] and scattering factor data were taken from ref. 21. Bond lengths and angles are given in Tables 1–3. Atomic positional and thermal parameters, together with F_o/F_c values have been deposited as supplementary data with the Editor, from whom copies are available on request. Atomic coordinates have also been deposited with the Cambridge Crystallographic Data Centre.

Acknowledgement—We thank the SERC for support.

REFERENCES

1. M. Schröder, *Pure Appl. Chem.* 1988, **60**, 517.
2. S. R. Cooper, *Accts Chem. Res.* 1988, **21**, 141.
3. M. N. Bell, A. J. Blake, H-J. Küppers, M. Schröder and K. Wieghardt, *Angew. Chem.* 1987, **99**, 253; *Angew. Chem. Int. Ed. Engl.* 1987, **26**, 250.
4. A. J. Blake, R. O. Gould, A. J. Holder, T. I. Hyde, M. O. Odulate, A. J. Lavery and M. Schröder, *J. Chem. Soc., Chem. Commun.* 1987, 118.
5. A. J. Blake, R. O. Gould, J. A. Greig, A. J. Holder, T. I. Hyde and M. Schröder, *J. Chem. Soc., Chem. Commun.* 1989, in press.
6. M. N. Bell, A. J. Blake, A. J. Holder, T. I. Hyde, A. J. Lavery, G. Reid and M. Schröder, *J. Incl. Phenom.* 1987, **5**, 169; A. J. Blake, A. J. Holder, T. I. Hyde and M. Schröder, *J. Chem. Soc., Chem. Commun.* 1987, 987; A. J. Blake, A. J. Holder, T. I. Hyde, Y. V. Roberts, A. J. Lavery and M. Schröder, *J. Organomet. Chem.* 1987, **323**, 261; A. J. Holder, M. Schröder and T. A. Stephenson, *Polyhedron* 1987, **6**, 461; A. J. Blake, R. O. Gould, A. J. Holder, T. I. Hyde and M. Schröder, *J. Chem. Soc., Dalton Trans.* 1988, 1861.
7. For example see: C-K. Poon, T-W. Tang and C-M. Che, *J. Chem. Soc., Dalton Trans.* 1981, 1697; *J. Chem. Soc., Dalton Trans.* 1983, 1647: J. MacB. Harrowfield, A. J. Herit, P. A. Lay, A. M. Sargeson, A. M. Bond, W. A. Mulac and J. C. Sullivan, *J. Am. Chem. Soc.* 1983, **105**, 5503; A. J. Blake, T. I. Hyde, R. S. E. Smith and M. Schröder, *J. Chem. Soc., Chem. Commun.* 1986, 334; E. Kimura, Y. Lin, R. Machida and H. Zenda, *J. Chem. Soc., Chem. Commun.* 1986, 1020; A. J. Blake, J. A. Greig and M. Schröder, *J. Chem. Soc., Dalton Trans.* 1988, 2645; C. Pomp, S. Drueke, H-J. Küppers, K. Wieg-

hardt, C. Krüger, B. Nuber and J. Weiss, *Z. Naturfor.* 1988, **43B**, 299 and refs therein.
8. R. S. Glass, G. S. Wilson and W. N. Setzer, *J. Am. Chem. Soc.* 1980, **102**, 5068.
9. R. S. Glass, W. N. Setzer, C. A. Ogle and G. S. Wilson, *Inorg. Chem.* 1983, **22**, 266; W. N. Setzer, B. R. Coleman, G. S. Wilson and R. S. Glass, *Tetrahedron Lett.* 1981, **37**, 2743.
10. H-J. Küppers, K. Wieghardt, B. Nuber and J. Weiss, *Z. Anorg. Allg. Chem.*, in press.
11. H-J. Küppers, K. Wieghardt, Y-H. Tsay, C. Krüger, B. Nuber and J. Weiss, *Angew. Chem.* 1987, **99**, 583; *Angew. Chem. Int. Ed. Engl.* 1987, **26**, 575.
12. J. Clarkson, R. Yagbasan, P. J. Blower, S. C. Rawle and S. R. Cooper, *J. Chem. Soc., Chem. Commun.* 1987, 950.
13. A. J. Blake, R. O. Gould, A. J. Holder, T. I. Hyde and M. Schröder, *Polyhedron* 1989, **8**, 513.
14. D. Sevdic and H. Meider, *J. Inorg. Nucl. Chem.* 1977, **39**, 1403 and 1409; D. Sevdic, L. Fekete and H. Meider, *J. Inorg. Nucl. Chem.* 1980, **42**, 885; D. Sevdic and H. Meider, *J. Inorg. Nucl. Chem.* 1981, **43**, 153 and refs therein.
15. N. W. Alcock, N. Herron and P. Moore, *J. Chem. Soc., Chem. Commun.* 1976, 886.
16. R. D. Shannon, *Acta Cryst.* 1976, **A32**, 751.
17. G. M. Sheldrick, SHELX76, Program for crystal structure determination. University of Cambridge, U.K. (1976).
18. N. Walker and D. Stuart, DIFABS, Program for empirical absorption corrections, *Acta Cryst.* 1983, **A39**, 158.
19. P. D. Mallinson and K. W. Muir, ORTEPII, interactive version, *J. Appl. Cryst.* 1985, **18**, 51.
20. R. O. Gould and P. Taylor, CALC, Fortran77 version. University of Edinburgh, Scotland (1985).
21. D. T. Cromer and J. L. Mann, *Acta Cryst.* 1968, **A24**, 321.

Journal of Inclusion Phenomena 5 (1987), 169–172.

TRANSITION METAL COMPLEXES OF HOMOLEPTIC POLYTHIA CROWNS

M.N. Bell, A.J. Blake, R.O. Gould, A.J. Holder, T.I. Hyde, A.J. Lavery, G. Reid and M. Schröder*
Department of Chemistry,
University of Edinburgh,
West Mains Road,
Edinburgh EH9 3JJ,
Scotland.

The binding of transition metal ions to polydentate macrocyclic ligands to give mono-, bi- and poly-nuclear complexes is well known. We have been investigating the complexation of transition metal ions, particularly those of the platinum group metals, by the homoleptic polythia crown ligands 1,4,7,10,13,16-hexathiacyclooctadecane (L^1), 1,4,8,11-tetrathiacyclotetradecane (L^2) and 1,4,7-trithiacyclononane (L^3). These ligands were attractive since they would be expected to bind effectively to the relatively soft second and third row metal ions and lead to the formation of complexes exhibiting unusual stereochemical, electronic and redox properties.

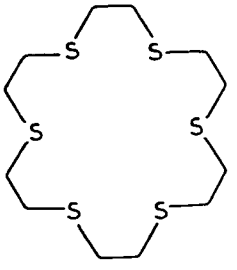

(L^1)

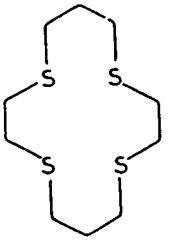

(L^2)

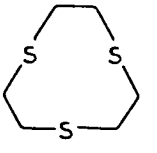

(L^3)

It was shown originally by Black and coworkers (*Tet. Lett.* 1969, 3961) that the potentially hexadentate ligand (L^1) (the thia analogue of 18-crown[6]) could readily encapsulate first row transition metal ions such as Ni^{2+} and Co^{2+} in an octahedral manner. The ability of (L^1) to act as a binucleating ligand had not however been demonstrated. We therefore initiated a study on the reactivity of (L^1) with a variety of metal substrates with a view to investigating its coordination to polymetallic centres.

Reaction of (L^1) with two molar equivalents of $[Cu(NCCH_3)_4]^+$ gave the di-copper(I) complex $[Cu_2(L^1)(NCCH_3)_2]^{2+}$ (1); the single crystal X-ray structure of (1) shows each tetrahedral copper(I) ion bound to *three* thia donors of (L^1), Cu-S = 2.32-2.34Å, and one molecule of CH_3CN, Cu-N = 1.94Å, with a Cu..Cu distance of 4.25Å.

Treatment of the isoelectronic, carbocyclic dimers $[M(cp^*)Cl_2]_2$ (M = Rh, Ir) and $[MCl_2(arene)]_2$ (M = Ru, Os; arene = p-cymene, hexamethylbenzene, benzene) with (L^1) affords the binuclear species $[M_2(cp^*)_2Cl_2(L^1)]^{2+}$ and $[M_2Cl_2(arene)_2(L^1)]^{2+}$ respectively. The single crystal X-ray structure of the di-rhodium(III) product $[Rh_2(cp^*)_2Cl_2(L^1)]^{2+}$ (2) shows the metal ions bound to only *two* of the thia donors of (L^1) with Rh-S = 2.377, 2.365, Rh-Cl = 2.387, Rh-C = 2.161-2.188Å.

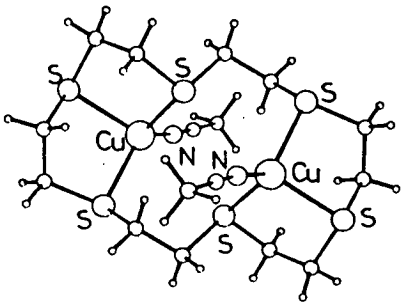

(1)

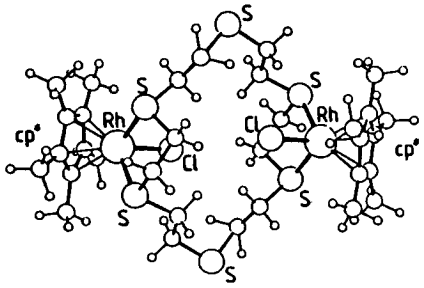

(2)

A series of mononuclear platinum metal complexes have also been prepared.

Reaction of $PdCl_2$ or $PtCl_2$ with (L^1) gave 1:1 complexes $[M(L^1)]^{2+}$ (M = Pd, Pt) (3). The crystal structure analyses of these complexes confirm square planar coordination of the metal ions to *four* thia donors of (L^1) (Pd-S = 2.309, Pt-S = 2.296Å) with the two remaining sulphur donors of (L^1) being essentially non-bonded (Pd-S' = 3.273, Pt-S' = 3.380Å; <S'PdS = 75.1°, 104.9°, <S'PtS = 74.2°, 104.8°). The dangling thia donors S' are therefore unable to complete octahedral coordination around Pd(II) and Pt(II) due to the relatively large radii of these metal ions.

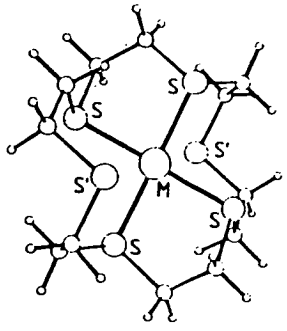

(3)

The small ring trithia macrocycle (L^3) has been shown to bind to first row transition metal ions in a facial manner. Thus *bis*-macrocyclic species of type $[M(L^3)_2]^{2+}$ (M = Co(II), Ni(II), Cu(II)) have been generated previously and shown to have octahedral MS_6 stereochemistries (Glass and coworkers, *Inorg. Chem.*, 1983, 22, 266). Reaction of (L^3) with $PdCl_2$ and $PtCl_2$ in a 2:1 molar ratio yielded complex cations of stoichiometry $[M(L^3)_2]^{2+}$; their structural and redox properties were assessed.

The single crystal X-ray structure of $[Pt(L^3)_2]^{2+}$ (4) shows the complex to have an unusual square-based pyramidal stereochemistry. The Pt(II) ion is coordinated by four thia donors in a square plane, Pt-S = 2.25-2.30Å, with one of the remaining sulphur ligands bound apically Pt-S' = 2.88Å, <SPtS' = 84.0-97.2°. The sixth thia donor is not coordinated to the metal centre, Pt...S'' = 4.04Å. In contrast to the yellow Pt(II) complex (4), the isoelectronic Pd(II) species $[Pd(L^3)_2]^{2+}$ (5) is green and not isostructural. The crystal structure of (5) shows the centrosymmetric cation to have an unexpected distorted octahedral stereochemistry around Pd(II) with $Pd\text{-}S_{equ}$ = 2.332, 2.311 and $Pd\text{-}S'_{ax}$ = 2.952Å.

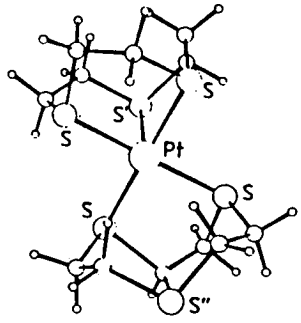

(4)

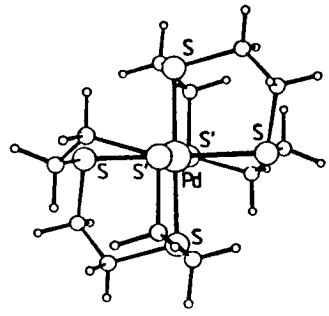

(5)

The complexes (4) and (5) each show, by cyclic voltammetry, one, one electron oxidation at $E_{½}$ = +0.39V. ΔE_p = 145mV. and $E_{½}$ = +0.605V. ΔE_p = 84mV. vs. Fc/Fc^+ respectively in CH_3CN at platinum electrodes. Controlled potential electrolysis of the complexes at +0.5V. and +0.7V. respectively at a platinum gauze affords the corresponding oxidation products $[M(L^3)_2]^{3+}$ which have been identified by esr spectroscopy as formally metal(III) species; $g_{\parallel}$ = 1.987, $g_{\perp}$ = 2.044, $A_{\parallel}$ = 85G, $A_{\perp}$ = 30G (^{195}Pt, I=½, 33.8%) for $[Pt(L^3)_2]^{3+}$, $g_{\parallel}$ = 2.009, $g_{\perp}$ = 2.049, $A_{\parallel}$ = 5G, $A_{\perp}$ = 20G (^{105}Pd, I=$\frac{5}{2}$, 22.2%) for $[Pd(L^3)_2]^{3+}$. Interestingly, the Pd(II) and Pt(II) complexes of (L^1) and (L^2), ((3) and (6)), show no oxidative redox processes by cyclic voltammetry in CH_3CN. The electrochemical inactivity of these latter species may be rationalised by the inability of the macrocycles (L^1) and (L^2) to form octahedral complexes with Pd and Pt centres. The ligand (L^1) may be regarded as being too small to fully encapsulate octahedrally the relatively large Pd(II) and Pt(II) ions. (L^2) would

be expected to bind equatorially to give square planar complexes; this has been confirmed by the single crystal X-ray structure of $[Pd(L^2)]^{2+}$ (6); Pd-S = 2.23-2.33Å. By contrast, coordination of two molecules of (L^3) to Pd(II) and Pt(II) enables a preferred (distorted) octahedral stereochemistry to be achieved on oxidation to the metal(III) species. The coordinative flexibility of (L^3) in this system appears therefore to be crucial in stabilising the d^7 metal centre. In addition, the positive charge in $[M(L^3)_2]^{3+}$ would be expected to be stabilised further by delocalisation onto the thia ligands. The extent of positive charge on the thia donors is currently being assessed.

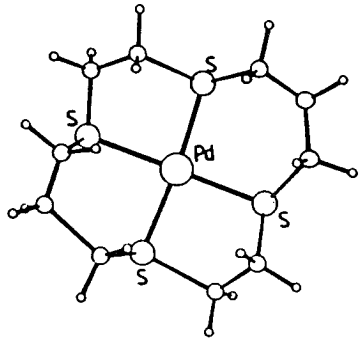

(6)

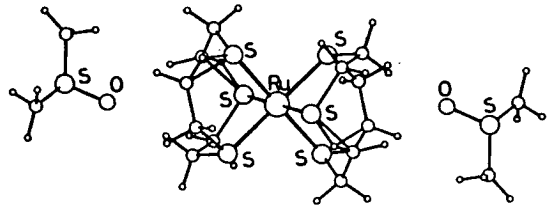

(7)

The homoleptic hexathia complexes $[Rh(L^3)_2]^{3+}$ and $[Ru(L^3)_2]^{2+}$ have also been synthesised. The single crystal X-ray structures of these products confirm their octahedral stereochemistries with Rh-S = 2.330, 2.332; Ru-S = 2.327-2.336Å. An unexpected feature of the structure of $[Ru(L^3)_2](BPh_4)_2.2dmso$ (7) is the approach of the dmso solvate molecules towards the outer face of the coordinated trithia ligands. This occurs via H-bonding of the O-donor of the dmso solvates with the protons of the methylene groups of (L^3), O...H = 2.201, 2.419, 2.790, 3.291Å. This secondary interaction between the dmso molecules with the rear cone/cavity of the coordinated trithia ligand may be regarded as a weak inclusion of solvent; this is supported by the observation that dmso may be replaced by two molecules of other donor solvents such as CH_3CN and CH_3NO_2. The development of related systems incorporating larger and deeper cavities is under investigation.

This is an extended abstract of a poster presented at the *4th. International Symposium on Inclusion Phenomena*, University of Lancaster, 20-25 July 1986.

We thank BP Chemicals and SERC for a CASE Award to (TIH), SERC for support, and Johnson Matthey Plc for generous loans of platinum metals.